UNIVERSITY OF CALIFORNIA
RIVERSIDE

Charged up With *Closo*-Carborane Anions: Chemical Synthesis of Ionic Materials in Ligand Design and Transition Metal Chemistry

A Dissertation submitted in partial satisfaction
of the requirements for the degree of

Doctor of Philosophy

in

Chemistry

by

Steven Paul Fisher

September 2019

Dissertation Committee:

Prof. Vincent Lavallo, Chairperson
Prof. Yinsheng Wang
Prof. William Hill Harman

The Dissertation of Steven Paul Fisher is approved:

Committee Chairperson

University of California, Riverside

Acknowledgements

To the Professors:

I would like to, above all else, thank Prof. Vincent Lavallo for accepting me into his group and giving me the indispensable opportunity to learn and explore chemistry within his research group. During this experience he has helped me in more ways than words could describe, I own much of my success to him. Lastly, I'd like to give him a big-ups for all the extracurricular activities he provided for us, in particular all the camping trips and social events where I meet a lot of great people who I would not likely have met otherwise. Next, I would like to thank all the professors (at UCR and CSUSM) who educated and created the deep fundamental understanding of chemistry I currently hold. In-particular I would like to thank Dr. Eric Reinheimer (CSUSM) for sharing so much knowledge and wisdom with me and seeding the idea of going to graduate school. I also owe a big thanks to Prof. Michael Schmidt (CSUSM) who sparked my interest in chemistry and provided me with my first research opportunity.

To the Visiting Scholars:

I would not have succeeded in graduate school without the help of Dr. Ahmad El-Hellani and Dr. Matt Asay who helped train and fine tune my chemistry skills including many of the air free manipulations and techniques I currently possess. I am greatly indebt to the great ligands left behind by Dr. El-Hellani as well as the experience Dr. Asay provided in synthesizing new ligands leading to my first graduate school publication, thanks for providing me with the skills and ligands I would use throughout my Ph.D career. I would also like to thank Dr. Gregorio Guisado-Barrios for the chemical brain storming that lead to some of the wildest and most fascinating compounds I have created. For Dr. Gregorio Guisado-Barrios I'm sorry we were not able to publish the fascinating borenium chemistry we worked so too hard to create.

To the Staff at UCR:

There are many people I would like to thank who made daily operations much easier. Starting with the staff scientist and undergraduate coordinators; Dr. Dan Borchardt, Dr. Rena Hayashi, Dr. Fook Tham, Dr. Kevin Simpson, Stan Sheldon, Dr. Jie Zhou and Dr. Charlene Tsay. The procurement and financial personal; Prisciliano Saavedra, Tina Enriquez, Natasha Gonzales and Rebecca Ryan. Lastly the graduate student coordinators and affairs personal; Barbara Outzen, Christina Youhas, Jaime Matute, and Jeffery Matute.

To the Lavallo Lab Group Members:

My graduate school experience would not have been the same without the great group of people I have had the pleasure to work with. First and foremost, I have to thank my amazing cohort; Scott McArthur and Sarah Lee. The many experiences I shared with them will never be forgotten. I also have to thank the many group members who passed though during my time; Allen Chan, Jess Estrada, Chris Lugo (Kuchov), Tao Sun, Hoseong Yoo, Sean Quinlivan, Jack Kleinsasser, Micah Eropkin, Anton Tomich (Toemash), Isaac Banda, Sergio Lovera, Varun Tej, David Buttler, Andrew Xiao, Bria Pettway, Nathan Hammes, Javier Fajardo, David Woen, Uday Chauhan, Adam Yu and Rich Thai. I wish the best for all of you and hope to see you again soon.

To My Family and Friends:

Without the support of my family I would not have made it to graduate school and who knows where I would be! I cannot thank them enough for all the support they have provided me. I also have to thank my girlfriend Abby for sticking with me and putting up with my graduate school shenanigans. Of course, I can’t forget all my amazing friends who I haven’t been able to spend as much time with and somehow are still friends with me. Thanks guys for still remembering who I am!

The text, figures, and schemes for the following chapters have been reproduced, in part or in their entirety, from the following published or submitted manuscripts.

Chapter 1: "Non-classical Applications of *closo*-Carborane Anions: from Main Group Chemistry and Catalysis to Energy Storage" S.P. Fisher, A.W. Tomich, S.O. Lovera, J.F. Kleinsasser, J. Guo, M.J. Asay, H.M. Nelson, V. Lavallo, **Chem. Rev.**, 2019, *accepted*, DOI: 10.1021/acs.chemrev.8b00551.

"Teaching an Old Dog New Tricks: New Directions in Fundamental and Applied *closo*-Carborane Anion Chemistry" S.P. Fisher, A.W. Tomich, J. Guo, V. Lavallo, **Chem. Commun**., *2019*, 55, 1684-1701.

Chapter 2: "Synthesis of Unsymmetrical N-Carboranyl NHCs: Directing Effect of the Carborane Anion" M.J. Asay, S.P. Fisher, S.E. Lee, D. Borchardt, F.S. Tham, V. Lavallo, **Chem. Commun.**, *2015*, 51, 5359.

Chapter 3: "Anionic and Zwitterionic Carboranyl N-Heterocyclic Carbene Au(I) Complexes" S.P. Fisher, A. El-Hellani, F.S. Tham, V. Lavallo, **Dalton Trans.**, *2016*, 45, 9762.

Chapter 4: "On the Reactivity of the Carba-*closo*-Dodecaborate Anion with the Trityl Cation" J.F. Kleinsasser, S.P. Fisher, F.S. Tham, V. Lavallo, **Eur. J. Inorg. Chem.**, *2017*, 4417.

ABSTRACT OF THE DISSERTATION

Charged Up With *closo*-Carborane Anions: Chemical Synthesis of Ionic Materials in Ligand Design and Transition Metal Chemistry

by

Steven Paul Fisher

Doctor of Philosophy, Graduate Program in Chemistry
University of California Riverside, September 2019
Dr. Vincent Lavallo, Chairperson

The beginnings of boron rich nanoclusters chemistry are in part due to the pioneering work of Alfred Stock. It was Stock's air sensitive syntheses that paved the road to many pyrophoric borohydrides. Surprisingly some of these pyrophoric borohydrides were found to be useful starting materials for synthesizing the extremely stable *closo*-carborane anions. These polyhedral clusters are composed of mostly boron atoms with at least one carbon atom and are about a nanometer in length. Due to their great stability these anionic clusters have become well known as weakly coordinating anions. This is largely due to the fact that the negative charge is delocalized over the entire polyhedral cluster and that chemist have been able to isolate extremely reactive cations using these anions. However, the applications of these boron rich clusters is not limited to their ability to act as weakly coordinating anions but has extended into the fields of medicine and material sciences.

One field of study is using these materials as anions tethered to ligand scaffolds, with these anionic scaffolds chemist have been able to create metal complexes and, in some cases, even produce state of the art catalyst. A major part of this work is to explore the use of anionic boron rich clusters as ligand substituents in N-heterocyclic carbenes (NHC) ligands. Displayed within is the synthesis of an unsymmetrical NHC bearing one N-bound anionic carborane and one N-bound aryl group. This synthesis proved to be modular accommodating multiple aryl groups. To prove that the anionic NHC salts were viable ligands for coordination chemistry a set of anionic and zwitterionic Au(I) complex were generated. These results showed that these ligands are viable and that the Au(I) complexes are catalytically active for hydroamination chemistry. Envisioning a bimetallic system where the anionic Au(I) complex was coulombically bound to a metal cation lead to the formation of an Au^{-}/Ag^{+} heterobimeallic halide abstracting reagent. Indeed this halide abstracting reagent is capable of chloride abstraction transition metal complexes. As a proof of principle crystal structures were obtained for Au^{-}/Rh^{+} and Au^{-}/Ru^{+} systems. Lastly anionic Au(I) complexes with main group cations is reported.

Table of Contents

List of Figures

List of Schemes

List of Tables

Chapter 1: Introduction

1.1 Background

Since the early 20th century, the unusual chemical bonding and structural motifs of borohydride clusters have intrigued the scientific community. Between 1912-1936 Alfred Stock[1] successfully synthesized a handful of pyrophoric borohydrides[2] including diborane (**B_2H_6**), tetraborane (**B_4H_{10}**), pentaborane (**B_5H_{11}**), hexaborane (**B_6H_{10}**), the notorious "green dragon" **B_5H_9** and the relatively stable decaborane (**$B_{10}H_{14}$**), Figure 1-1.[3] Despite their synthesis, the structure and bonding of these compounds was a complete mystery. For instance, the structure of diborane was argued for years despite Dilthey's report suggesting the correct structure as early as 1921.[4] By 1941 the debate was still ongoing, and in preparation of a review article Schlesinger wrote a personal letter to Linus Pauling asking for his thoughts on the bridging structure of diborane. Pauling responded saying "I do not feel very friendly towards the structure…" and urged Schlesinger to disregard it. Despite Pauling's response, Schlesinger included the structure.[5, 6] The bridged structure began to take hold with the review by Longuet-Higgins and Bell in 1943,[7] and in 1948 Price put an end to the debate by deconvoluting the absorption spectrum of diborane.[8, 9] The structural debate of Stock's borohydrides came to an end in 1950, when the highly debated structure of decaborane (**$B_{10}H_{14}$**)[10] was correctly elucidated by Kasper and coworkers using X-ray diffraction.[11]

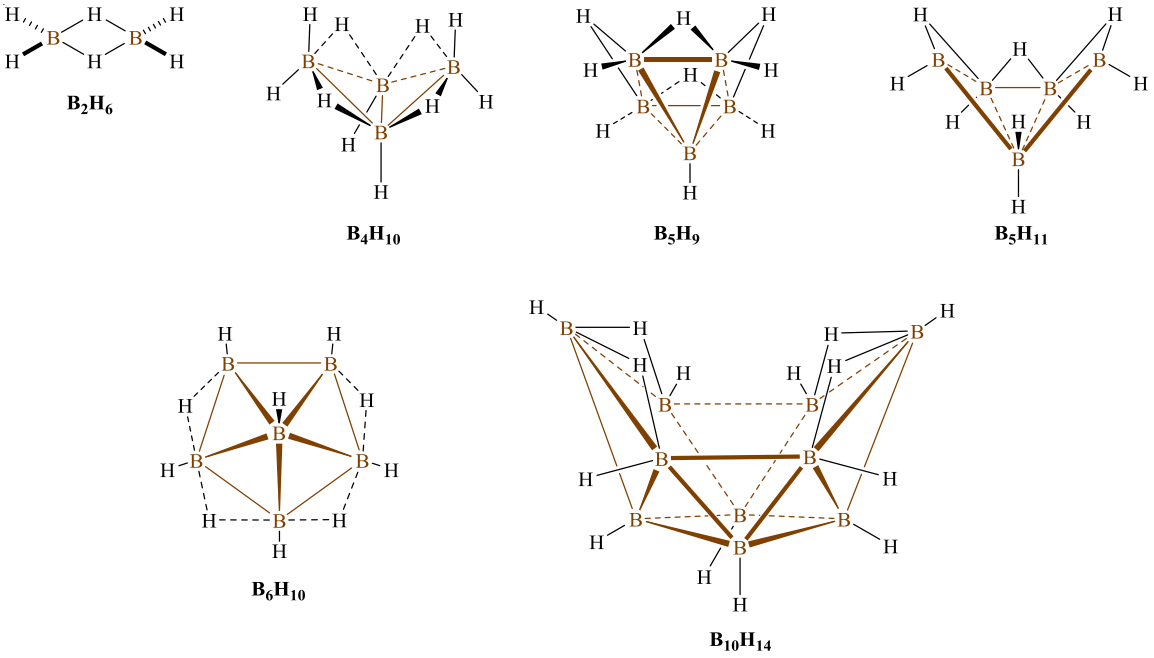

Figure 1-1 Structural representations of the borohydrides discovered by Alfred Stock. B-B bonds are shown in brown and B-H bonds are shown in black.

Just as the structural conundrum was finally solved, the Cold War era reinvigorated the interest in borohydride chemistry. Scientists believed these pyrophoric borohydrides would serve as excellent rocket fuels and that these compounds would surely outperform traditional hydrocarbon-based fuels. Chasing this prediction, the U.S. and Russia spent millions of dollars investigating these compounds as potential fuels in program such as HERMES, ZIP and HEF.[2] As it turns out, the borohydrides were terrible rocket fuels as the particulates formed during combustion caused catastrophic engine failures, toxic exhaust, and made the aircraft easy to spot in the sky. These downfalls led to the abandonment of these programs. However the Cold War era wasn't a total bust for carborane chemistry, during this time borohydride chemistry took an interesting turn.

In 1955, Longuet-Higgins and Roberts predicted that the elusive B_{12} core required two additional electrons to form a stable cluster. Four years later, Hawthorne and Pitochelli successfully synthesized a dianionic B_{12} core in the form of $[B_{12}H_{12}]^{-2}$ (**1**), Figure 1-2.[12-14] That same year Wunderlich and Lipscomb

elucidated the structure of this compound and found that this borohydride had a closed deltahedral structure in the form of an icosahedron. Unlike the smaller pyrophoric borohydrides, the *closo*-$[B_{12}H_{12}]^{-2}$ was found to be extremely stable[15], so much so that one chemist even claimed it as "the most stable molecule known to science".[16] Surprising considering borohydrides were currently being considered as rocket fuels!

Continuing along the path of closed deltahedral structures, in 1963, three reports were simultaneously released by Reaction Motors & Thiokol Chemicals, Olin Mathieson Corporation, and Leonid Zakharkin describing the synthesis of a neutral boron rich cluster that incorporated two carbon atoms into the cluster core forming the molecule $C_2B_{10}H_{12}$.[17-19] This compound is called 1,2-dicarba-*closo*-dodecaborane or *o*-carborane (**2**), Figure 1-2. It is likely that the *o*-carborane was actually discovered years earlier during the Cold War era but was not reported. Four years later in 1967, Knoth at DuPont successfully synthesized two boron rich clusters that contained one carbon atom, these mono anionic compounds were termed the 1-carba-*closo*-dodecaborate **3** and 1-carba-*closo*-decaborate **4**.[20] Going forward the icosahedron **3** and square bicapped antiprism **4** may be referred to as 12-vertex and 10-vertex carborane anions, respectively and the B-H vertices will be unlabeled (Figure 1-2).

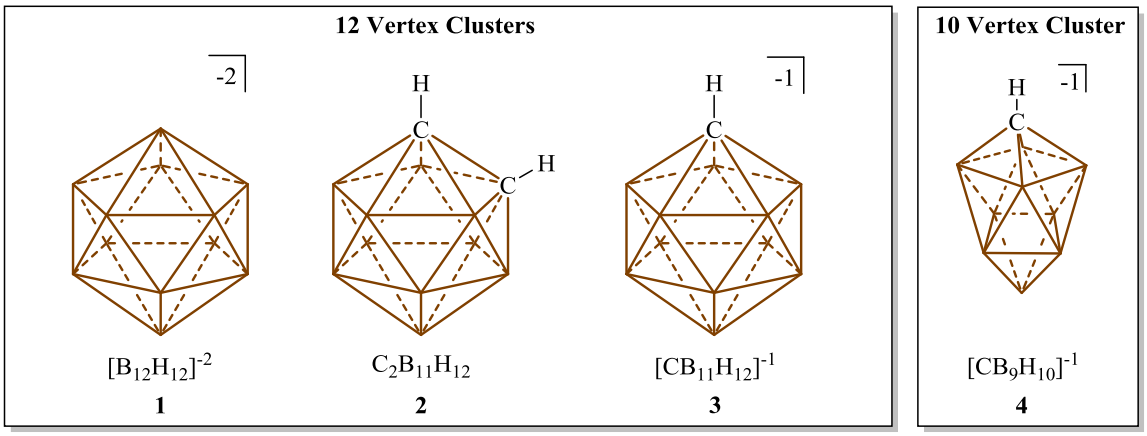

Figure 1-2 Structure of *closo* clusters; 12 vertex $[B_{12}H_{12}]^{-2}$ (**1**), $C_2B_{10}H_{12}$ (**2**), $[CB_{11}H_{12}]^{-1}$ (**3**), and 10 vertex $[CB_9H_{10}]^{-}$ (**4**). Unlabeled vertices = B-H.

Paralleling the reactivity of $[B_{12}H_{12}]^{-2}$ (**1**) the 10 and 12-vertex carborane anions, **3** and **4**, are very thermally, chemically and electrochemically stable species.[15, 21, 22] A vast subset of these species are considered carboranes.[23-32] In a carborane, one or more of the vertices of the boron cluster have been replaced by an atom of carbon. Replacing a boron atom by a carbon atom reduces the overall charge of the cluster by +1. This is because a neutral carbon atom has four valence electrons whereas a neutral boron atom only has three valence electrons. For example, the borane clusters **1** and **2** are dianionic and the carborane clusters **3** and **4** are monoanionic.[20] The aforementioned compounds **3** and **4**, as well as **1** and **2**, are referred to as *closo*-clusters as they have closed shell electronic structures and complete polyhedral shapes.[25] While often referred to as σ-aromatic, these cluster's molecular orbitals are composed of both strongly bonding purely σ and π-type overlaps, resulting in enormous HOMO/LUMO gaps. The number of skeletal electrons for many of the borane and carborane clusters can be calculated using a set of rules called the Jemmis *mno* rules. These rules were first developed by Kenneth Wade in 1971[33] and expanded upon by Michael Mingos in 1972[34] and again in 2001[35] by Eluvathingal Jemmis.[36] The skeletal electron pairs (SEP) represent the number of electron pairs required to fill all the bonding molecular orbitals of a given cluster (SEP = number of bonding molecular orbitals). These powerful rules also dictate which prefix the cluster will carry. For a closed polyhedral structure, the cluster is given the prefix *closo* and has must contain n + 1 SEP or 2[n + 1] skeletal electrons, where n = the number of cluster vertices. If the cluster has n + 2 SEP the prefix *nido* is used. Typically, these clusters are missing one vertex from achieving a closed polyhedral structure. The other two other common prefixes, *arachno* and *hypho*, where the cluster has n + 3 and n + 4 SEP respectively.

The carborane anions **3** and **4** are inherently weakly coordinating as the charge of the cluster is delocalized throughout the entire three dimensional aromatic core.[27, 32] Functionalization of these cluster's surfaces with halogens or alkyl groups through electrophilic aromatic substitution "like" reactions renders these species even more weakly coordinating. While there are many other examples of borohydrides and boron containing clusters that exist, the reader is redirected to Hosmane and Grimes comprehensive books[16, 37] and various review articles.[23, 24, 26-32]

1.2 B-H Functionalization

Functionalization of these clusters can typically be achieved at three distinct positions, using $[CB_{11}H_{12}]^-$ as an example the functionalization starts at the antipodal boron (B12), followed by the lower pentagonal belt (positions B11-B7) and lastly the upper pentagonal belt (positions B6-B2).[38] This functionalization pattern is rationalized by thinking about the cluster as the nucleophile in an electrophilic aromatic substation "like" reaction. The antipodal boron (B12) is farthest from the electronegative carbon vertex and therefore the most susceptible to electrophilic substitution followed by the lower belt and finally the upper belt, Scheme 1-1.[39] It should be noted however that the afromentioned substitution pattern maybe not be the case for fluorination as examples exist were the lower belt is fluorinated before the antipodal boron.

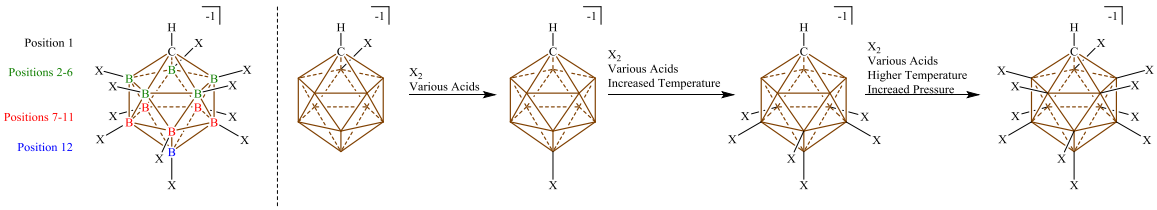

Scheme 1-1 Functionalization positions of $[CB_{11}H_{12}]^-$ and functionalization pathway.

Even though most reagents follow the above stepwise substitution, not all substitution patterns are easily achieved. While iodination gives almost perfect selectivity, other substitutions do not and require precise reaction conditions, scrutinous monitoring over time, or copious purification to remove undesired functionalized products. Despite these potential challenges, the functionalized compounds can be very rewarding. When halogenated, these compounds display enhanced steric bulk which helps screen the negative charge and makes the cluster more chemically inert. While at the University of California Riverside, Professor Christopher Reed demonstrated that the halogenated derivatives of the 12 vertex carborane are exceptionally stable. This allows for isolation of reactive species such as anhydrous H^+, fullerenium cation, benzenium cation, *tert*-butly cation, and the first free silylium ion.[32] Professor Josef

Michl was also able to show that the permethylated (fully methylated at B) cluster $[CB_{11}(CH_3)_{12}]^-$ was capable of being oxidized forming a stable neutral radical.[40]

1.3 C-H Functionalization

Another common functionalization is at the carbon vertex, as seen in the above example with $[CB_{11}(CH_3)_{12}]^-$. The C-H vertex of the carborane is mildly acidic with a pKa of 21.8, the acidity increases with increased B-X functionalization. Removal of the C-H proton by deprotonation with *n*-BuLi followed by the addition of an electrophile, such as an alkyl halide, gives the C alkylated product, Scheme 1-2 (**3Me[Li$^+$]**, **3Et[Li$^+$]** and **3CH$_2$Ph[Li$^+$]**). In the Lavallo group, it is customary to convert the carborane to the trimethylammonium salt, **3[Me$_3$NH$^+$]** then add two equivalents of base. The first equivalent of base removes the trimethylammonium cation, the second equivalent deprotonates the C-H vertex generating **3[2Li$^+$]** which is an isolable dianion. The advantage of using the Me_3NH^+ cation over the Cs^+ cation is that it avoids mixed cations in the product. A plethora of C-functionalizations have been reported and the reader is referred to the Michl review which contains a table of known functionalizations.[27]

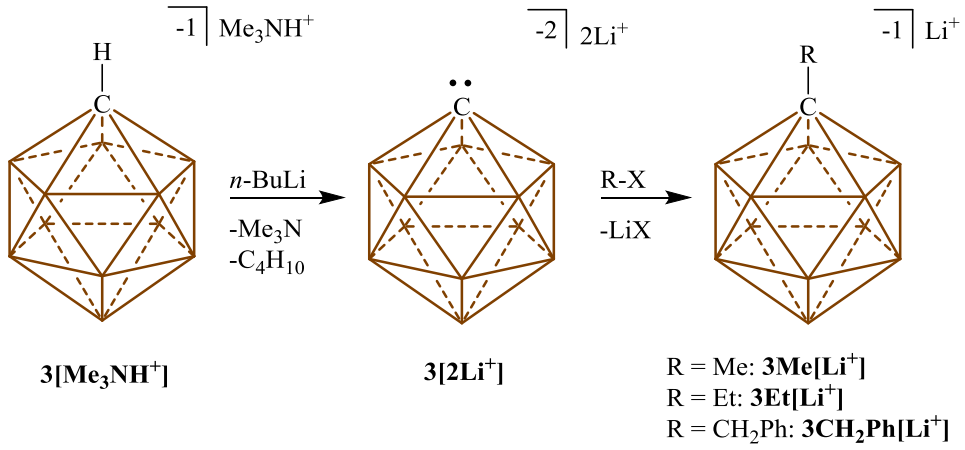

Scheme 1-2 C-H Functionalization of the carborane.

Another method to functionalize the C vertex is to incorporate a C-functionalized component into the carborane framework at an early stage of the cluster synthesis. This method works well for substitutions that are not good candidates for an S_N2 type reactions with **3[2Li$^+$]**. Two methods to do so include; 1) the Brelloch's reaction and 2) cyanide incorporation to decaborane. The first is widely used to create the smaller 10 vertex carborane **4** and is the only named reaction dealing with carboranes. The Brelloch's Reaction removes a B vertex from decaborane and replaces it with a C-H or C-R vertex, where the carbon source is an aldehyde.[41] This reaction proceeds though the hydroxylated species **5** and usually produces a *nido* species, *nido*-[6-R-6-CB_9H_{11}]$^-$ (**6**). However, not all aldehydes generate the same type of product and some aldehydes do not work.[42] For instance, the electron poor aldehyde 4-nitrobenzaldehyde causes decomposition of the cluster, acidic aldehydes such as 4-hydroxybenzaldehyde and 4-carboxybenzaldehyde do not produce the desired addition products and paraformaldehyde and 2-methoxybenzaldehyde produces *arachno* clusters, such as, *arachno*-[6-R-6-CB_9H_{13}]$^-$ (**7**). In the case of 2-methoxybenzaldehyde the *arachno* cluster is believed to be stabilized by intramolecular H-bonding interactions between the methoxy oxygen atom and the *endo*-hydrogen atoms of the cluster. These clusters can readily be closed to the corresponding 10 vertex *closo* cluster.

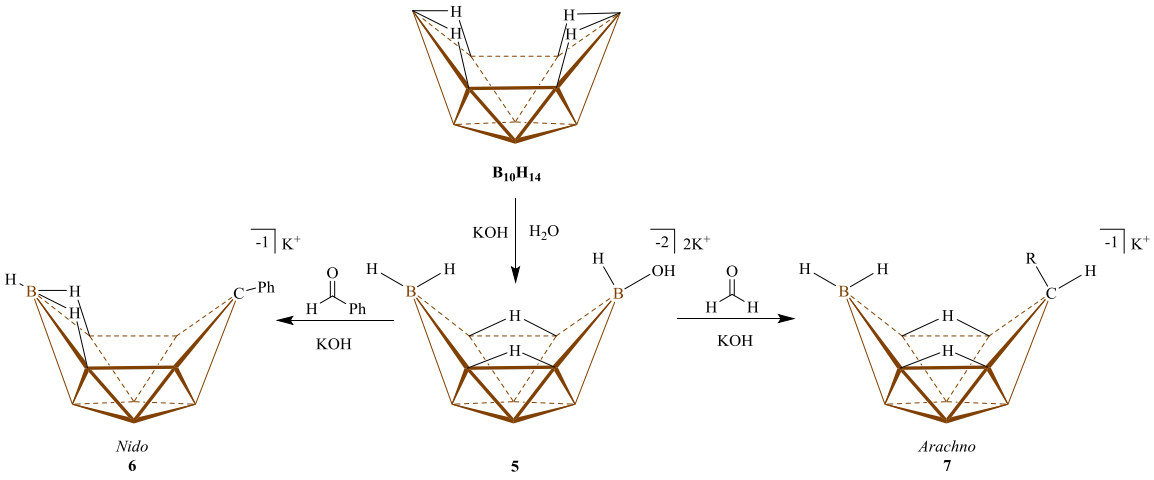

Scheme 1-3 The prototypical Brelloch's Reaction showing both *nido* or *arachno* products.

The second example of this is the amino functionalized carborane, 1-amino-1-carba-*closo*-dodecaborate $[H_2NCB_{11}H_{11}]^-$ (**3NH$_2$**), the synthesis of this compound was released in 1986 by Jelínek and co-workers.[43] However the total synthesis of this compound dates back many years as it is a multistep synthesis that relies on the knowledge of a few intermediate compounds. The total synthesis of the amine is scattered throughout the literature, the next section gives a historical review of the synthesis of the carboranyl amine.

1.4 Historical Synthesis of Carboranyl Amine **3NH$_2$**

The synthesis of the 1-amino-1-carba-*closo*-dodecaborate $[H_2NCB_{11}H_{11}]^-$ (**3NH$_2$**) begins by deportation of decaborane, with a sodium base, giving the mono anionic *nido* cluster that is typically not isolated. This is the $Na^+[B_{10}H_{13}]^-$ (**8[Na$^+$]**) which was first described in 1956 by Guter and Schaeffer[44] and structurally confirmed by X-ray crystallography in 1972.[45] The first isolable intermediate is the *arachno*-$[B_{10}H_{13}CN]^{-2}$ (**9**) first discovered by Knoth and Muetterties in 1961 (Scheme 1-2).[46] In the original publication, the synthesis reacted *nido*-decaborane (**B$_{10}$H$_{14}$**) with 30 equivalents of NaCN producing $2[Na]^+[B_{10}H_{13}CN]^{-2}$ (**9[2Na$^+$]**) which was then crystalized from water as the cesium salt by performing a cation exchange with CsCl and cooling to 5 °C. Plesek and coworkers realized that one equivalent of NaOH and 1 equivalent of NaCN was required to produce **9[2Na+]**,[47] the crystal structure of this compound was elucidated in 1988 and revealed that the CN group occupies the space above the open cluster.[48]

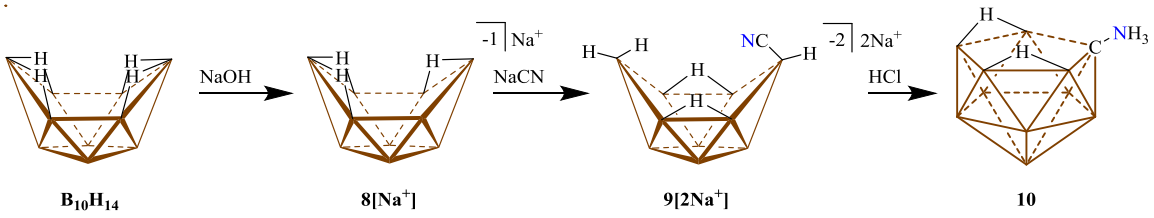

Scheme 1-4 Synthetic pathway to zwitterionic 7-ammonio-7-carba-*nido*-decaborate, **10**.

Once the *arachno*-$[B_{10}H_{13}CN]^{-2}$ (**9[2Na$^+$]**) is prepared, it is treated with HCl producing the zwitterion *nido*-7-H_3N-7-$B_{10}H_{12}$ (**10**). At this point Jelínek and co-workers[43] realized that this open faced *nido* cluster could be closed by treatment of **10** with $NaBH_4$ followed by addition of $Et_3N{\bullet}BH_3$ and heating at 190-200°C for 5 hours. After an extensive workup the 1-amino-1-carba-*closo*-dodecaborate (**3NH$_2$**) was finally obtained in a 65% yield (Scheme 1-3). The pKa of **3NH$_2$** was experientially determined to be 6.0 which is slightly higher than that of aniline, which is 4.6.[43]

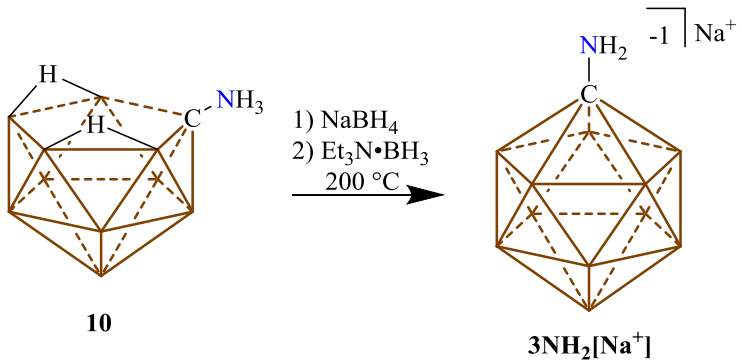

10 **3NH$_2$[Na$^+$]**

Scheme 1-5 Synthetic pathway to 1-amino-1-carba-*closo*-dodecaborate (**3NH$_2$[Na$^+$]**).

Just like the parent carborane, $[CB_{11}H_{12}]^-$, **3NH$_2$** can also be functionalized. Known functionalization include the perfluorinated amine $[1\text{-}NH_2\text{-}CB_{11}F_{11}]^-$, the mono and bis-hydroxylfluoro amine $[1\text{-}NH_2\text{-}6\text{-}(OH)\text{-}CB_{11}F_9]^-$ and $[1\text{-}NH_2\text{-}4,6\text{-}(OH)_2\text{-}CB_{11}F_9]^-$, the periodinated ammonium $[1\text{-}NH_3\text{-}CB_{11}I_{11}]^-$ and hexaiodinated ammonium $[1\text{-}NH_3\text{-}CB_{11}I_6]^-$.[49, 50]

1.5 Experimental

Synthesis of 7-ammonio-7-carba-*nido*-decaborate, 10:

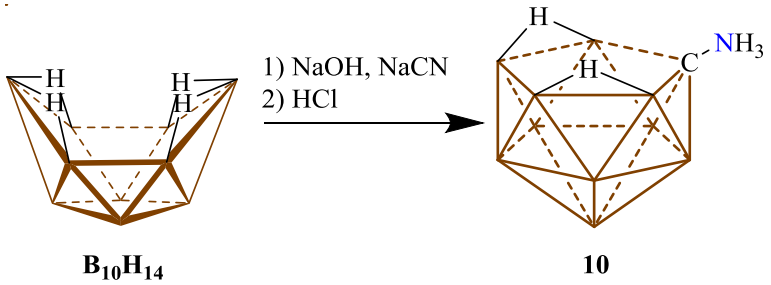

Scheme 1-6 Synthesis of 7-ammonio-7-carba-*nido*-decaborate (**10**).

The synthesis can be performed on a multi-gram scale, reactions as large as 100 grams have been successfully accomplished. Some of the steps are dangerous and should be performed cautiously. Solid **$B_{10}H_{14}$** (70.0 grams, 572 mmol) was crushed to a semi-even powder with a mortar and pestle before being added to 290 mL of ice-cold pentane. The suspension was slowly stirred while an ice-cold solution of NaOH (25.2 grams, 630 mmol) and NaCN (30.9 grams, 630 mmol) in 1145 mL of DI water was slowly added. The flask containing the salts was rinsed with DI water and added to the reaction mixture (*note: NaCN is extremely poisonous and should be handled with care*). The biphasic suspension was vigorously stirred at 0 °C in a well vented fume hood until most of the solid material had dissolved (about 2 hours). **CAUTION: this step could release extremely toxic HCN gas and should be done in a well-ventilated fume hood with the hood sash closed, also be aware of any personnel working on the fume hoods or areas were the fume hoods vent**. A solution of HCl (12 **M**, 287 mL, 3.44 mol) was added dropwise to the ice-cold solution of **9[2Na$^+$]**. After the addition was complete the ice bath was removed, and the reaction stirred at room temperature for one hour. The two layers were separated, and the aqueous layer was extracted with diethyl ether (3 x 1120 mL). The combined organic layers (including the pentane layer) where pumped down to dryness giving a quantitative yield of zwitterion H_3N-$CB_{10}H_{12}$ (**10**). ^{1}H NMR (600 MHz, acetonitrile-d_3, 25°C): δ = 6.63 (2H, N-H), 2.8 to -0.2 (bm, 10H, B-H), 3.48 (2H, bridging B-H-B). ^{1}H[^{11}B] NMR (600 MHz, acetonitrile-d_3, 25°C): δ = 6.63 (t, 2H, N-H), 2.30 (s, B-H), 2.11 (s, B-H), 2.09 (s,

B-H), 1.24 (s, B-H), 1.23 (s, B-H), 1.21 (s, B-H), 0.39 (s, B-H), 3.46 (s, 2H, bridging B-H-B) ppm. $^{11}B[^{1}H]$ NMR (192.5 MHz, acetonitrile-d_3, 25°C): δ = -2.3, -9.7, -11.7, -22.9, -26.6, -33.4 ppm. $^{11}B[^{1}H]$ NMR (96 MHz, acetonitrile-d_3, 25°C) = -2.3, -9.7, -11.7, -22.9, -26.6, -33.4 ppm. ^{11}B NMR (96 MHz, acetonitrile-d_3, 25°C): δ = -2.3 ($^{1}J(H,B)$ = 131.6 Hz), -9.7 ($^{1}J(H,B)$ = 172.6 Hz), -11.7 ($^{1}J(H,B)$ = 131.5 Hz), -22.9 ($^{1}J(H,B)$ = 118.8 Hz), -26.6 ($^{1}J(H,B)$ = 142.2 Hz), -33.4 ($^{1}J(H,B)$ = 142.1 Hz). $^{13}C[^{1}H]$ NMR (151 MHz, acetonitrile-d_3, 25°C) = 56.4 ppm. IR (solid, ATR, 25°C): B-H stretch = 2508 cm^{-1}. HRMS (negative mode ESI/APCI, direct injection) $[M-H]^-$ m/z calc'd = 148.2129 : Found = 148.2135. Melting point > 300°C.

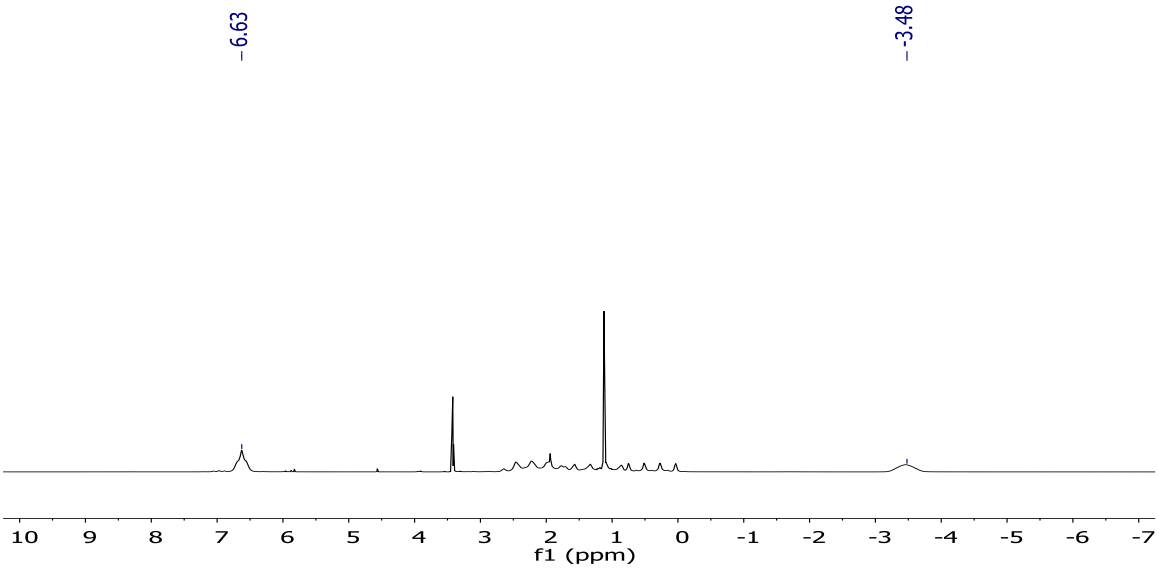

Figure 1-3. ^{1}H-NMR spectrum of zwitterion **10** in acetonitrile-d_3. *Note: diethylether can be seen at 3.4 and 1.2 ppm.*

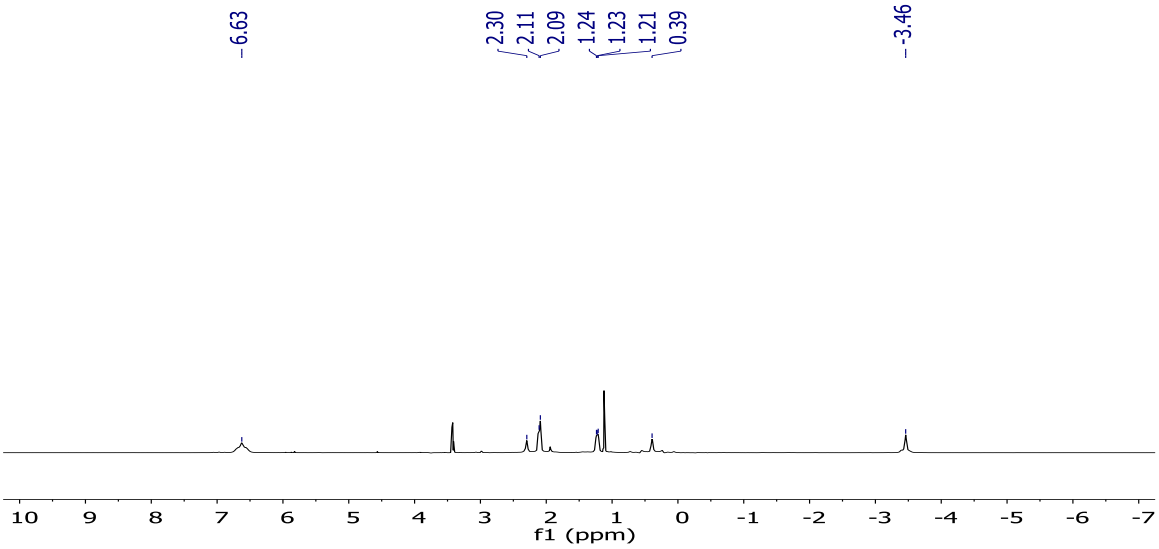

Figure 1-4. $^{1}H[^{11}B]$-NMR spectrum of zwitterion **10** in acetonitrile-d_3. *Note: diethylether can be seen at 3.4 and 1.2 ppm.*

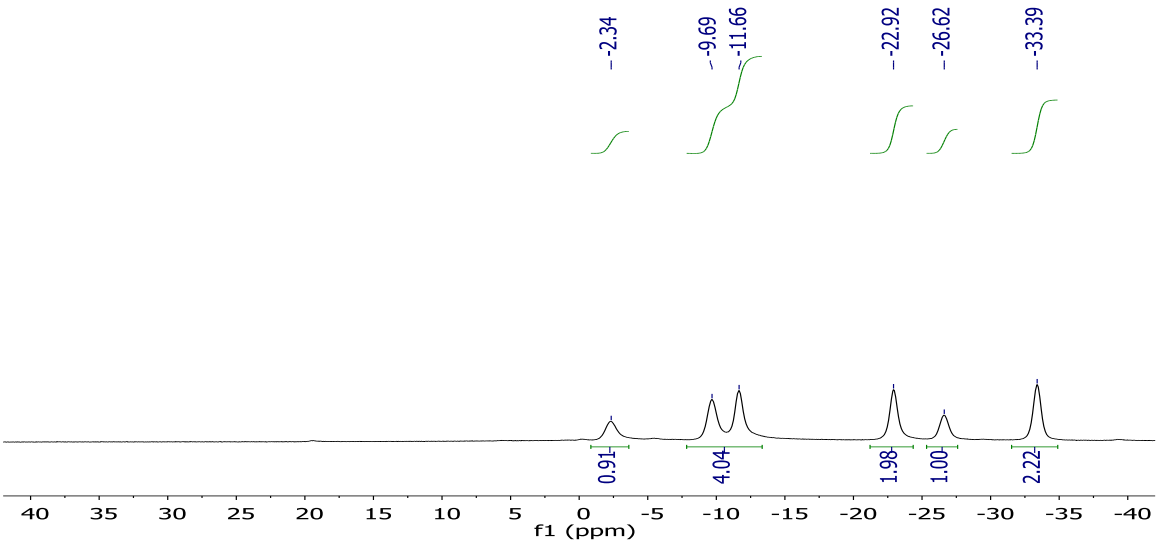

Figure 1-5. $^{11}B[^{1}H]$-NMR spectrum of zwitterion **10** in water-h_2.

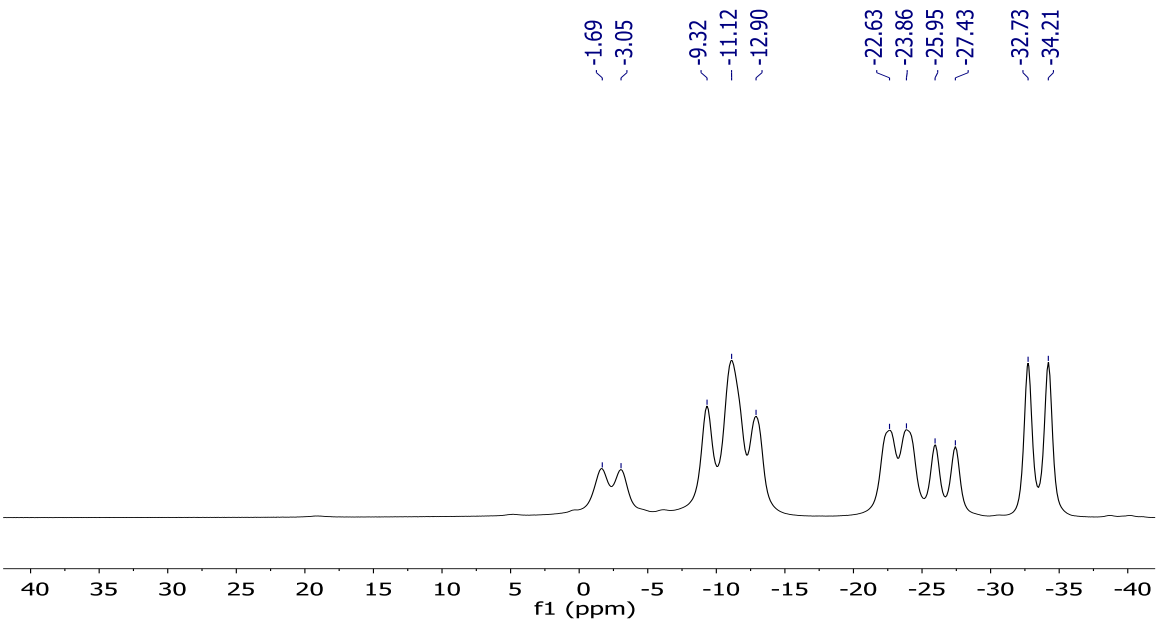

Figure 1-6. ^{11}B-NMR spectrum of zwitterion **10** in acetonitrile-d_3.

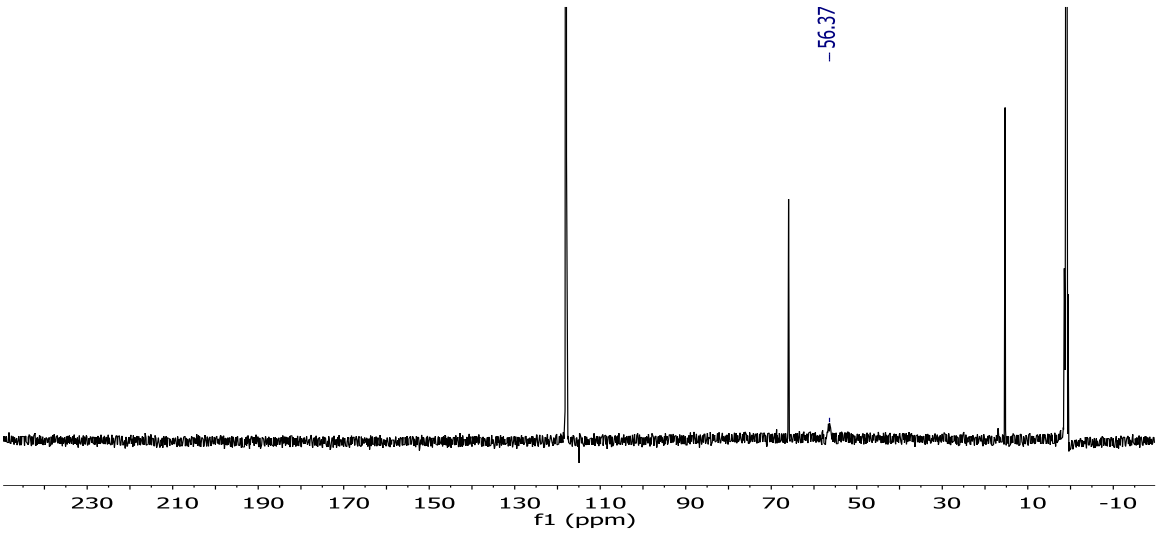

Figure 1-7. ^{13}C[^{1}H]-NMR spectrum of zwitterion **10** in acetonitrile-d_3. *Note: diethylether is present at 66 and 15 ppm.*

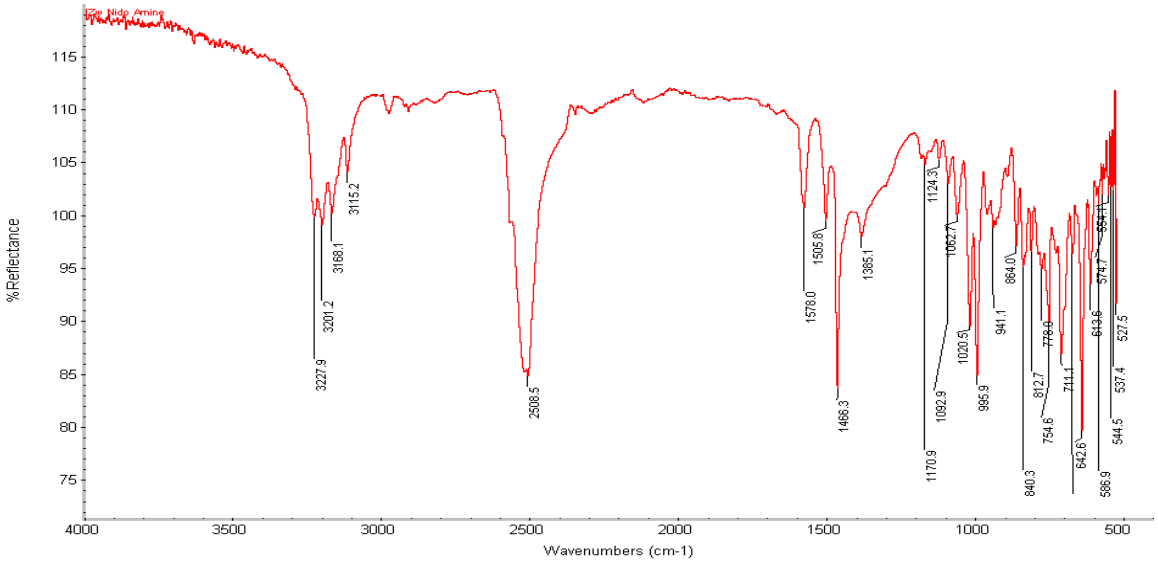

Figure 1-8. IR spectrum of zwitterion **10** showing the B-H stretches at 2508.5 cm.

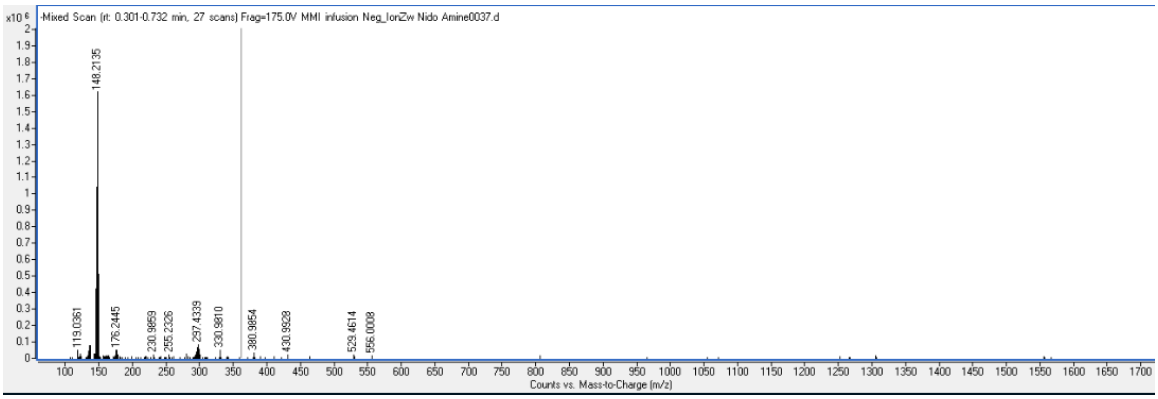

Figure 1-9. Mass spectrum of zwitterion **10**.

Synthesis of 1-amino-1-carba-*closo*-dodecaborate; ($3NH_2[Cs^+]$):

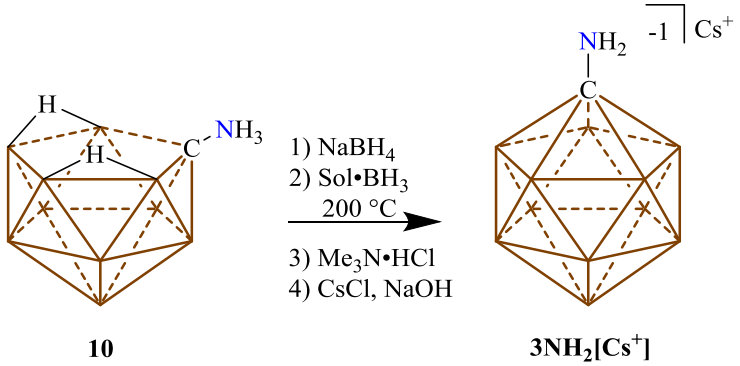

10 **$3NH_2[Cs^+]$**

Scheme 1-7 Synthesis of **$3NH_2[Cs^+]$**. Sol = SMe_2 or THF or Et_3N.

The following considerations were takin into account for the next steps. The reaction was done on a Schlenk line under argon, all glass ware was dried prior to use. Ground glass connections were sealed with Teflon as the borane will remove silicon-based grease.

Zwitterion **10** (15 grams, 0.101 mol) was added to a Schlenk flask containing a stir bar and put under vacuum at 60 °C (at least two hours). In a separate 1000 mL Schlenk flask containing a stir bar, sodium hydride (2.65 grams, 0.111 mol, 1.1 eq) was added and placed under vacuum at 60 °C for one hour. After an hour the flask were backfilled with argon and lifted out of the oil bath. Upon reaching room temperature dry THF (enough to dissolve the material) was added to the flask containing the 7-H_3N-7-$B_{10}H_{12}$, and the sodium hydride powder was suspended in dry THF. The sodium hydride suspension was cooled to 0 °C and upon complete dissolution of **10** the solution was cannula transferred to the sodium hydride slowly under argon. The flask containing **10** was washed with dry THF and transferred as well. After the transfer was complete the slurry was stirred for one hour at room temperature then the THF was stripped off under vacuum forming a white residue, this residue was dried by heating under vacuum at 100 °C overnight.

Under an inert atmosphere, the white cake was broken apart and any solid that had managed to stick to the walls was scraped off and the reaction vessel capped with a rubber septum. Through the septum,

enough solvent (THF, Et_3N) was added to cover the solid and the mixture cooled to 0 °C. Once cooled, dimethylsulfide borane (2 eq, 19 mL) was added under argon. Once any bubbling had ceased the rubber septum was carefully removed and replaced with a dried Allihn condenser. The ice bath was replaced with an oil bath and the mixture heated to 150 °C. During the initial heating it is important to watch the level of refluxing in the Allihn condenser as the refluxing may reach the top of the condenser if it is not long enough. After the refluxing has calmed (about 2 hours) the heat was increased to 200 °C and gently stirred. Periodically the reaction was checked by ^{11}B NMR and if the reaction had not progressed significantly more dimethylsulfide borane was added. The reaction was complete once 7-H_3N-7-$B_{10}H_{12}$ was no longer present in the ^{11}B NMR spectrum. Upon completion of the reaction was cooled to room temperature then cooled to 0 °C and DI water was slowly added to quench the excess NaH/BH_3 (I usually let this stir overnight). If necessary, more DI water was added until the suspension became a solution. At this point trimethylamine hydrochloride (excess of 1 eq., 20 grams) was added inducing a white precipitation. The precipitate was collected and washed with DI water until no boric acid was seen in the ^{11}B NMR spectrum. At this point the white solid is resuspended in DI water and a solution of CsCl (4 eq., 32 grams, 402 mmol) and NaOH (excess of 1 eq., 6 grams, ~150 mmol) was added. The mixture was stirred at 40 °C until most of the white solid had dissolved then the mixture was filtered. The filtrate was concentrated down to about 80 mL of water for every 5 grams of compound and crystalized. The crystals were collected by vacuum filtration then dissolved though the filter using a minimal amount of acetone (if too much wet acetone is used excess CsCl will go through the filter as well). The filtrate was pumped down furnishing the title compound as a white solid. At this point if the ^1H NMR spectrum shows impurities they can likely be removed by washing the crystalline solid in methylene chloride. Typical yields for this process were between 70-90%. *Note: A gooey substance (containing the carborane amine) may appear upon workup. If this happens the goo was refluxed in toluene, then dissolved in minimal acetone and added to a stirring solution of methylene chloride which forms a white precipitate. The precipitate was immediately collected by vacuum filtration (if left stirring for too long the precipitate will turn back into a sticky substance and the acetone trituration has to be repeated). The remaining wash should be checked by ^{11}B NMR as it likely still contains amine, this amine should be saved and reprocessed.* ^1H NMR (300 MHz, acetonitrile-d_3,

25°C): δ = 2.7 - 0.5 (bm, 11H, B-H). $^{1}H[^{11}B]$ NMR (300 MHz, acetonitrile-d_3, 25°C): δ = 1.84 (s, 5H), 1.37 (s, 5H), 1.17 (s, 1H) ppm. $^{11}B[^{1}H]$ NMR (192.5 MHz, acetonitrile-d_3, 25°C): δ = -12.7, -13.3 ppm. $^{11}B[^{1}H]$ NMR (96 MHz, acetonitrile-d_3, 25°C) = -12.8, -14.4 ppm. ^{11}B NMR (96 MHz, acetonitrile-d_3, 25°C): δ = -12.8 ($^{1}J(H,B)$ = 146.3 Hz), -14.4 ($^{1}J(H,B)$ = 146.3 Hz). $^{13}C[^{1}H]$ NMR (192.5 MHz, acetonitrile-d_3, 25°C): δ = 81.5 ppm. IR (solid, ATR, 25°C): B-H stretch = 2522.8 cm^{-1}. HRMS (negative mode ESI/APCI, direct injection) $[M-H]^-$ m/z calc'd = 158.2144 : Found = 158.2151. Melting point > 300°C.

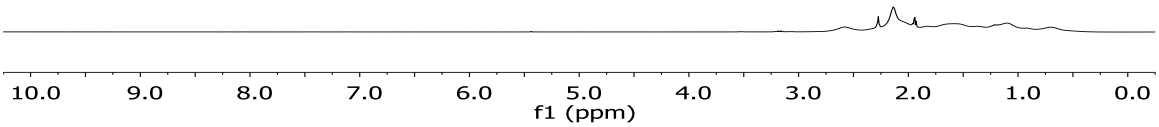

Figure 1-10. 1H-NMR spectrum of **$3NH_2[Cs^+]$** in acetonitrile-d_3, the bump between 0.5 and 2.7 ppm are the B-H protons. *Note: water coordinated to the Cs^+ counter ion can be seen at 2.1 ppm.*

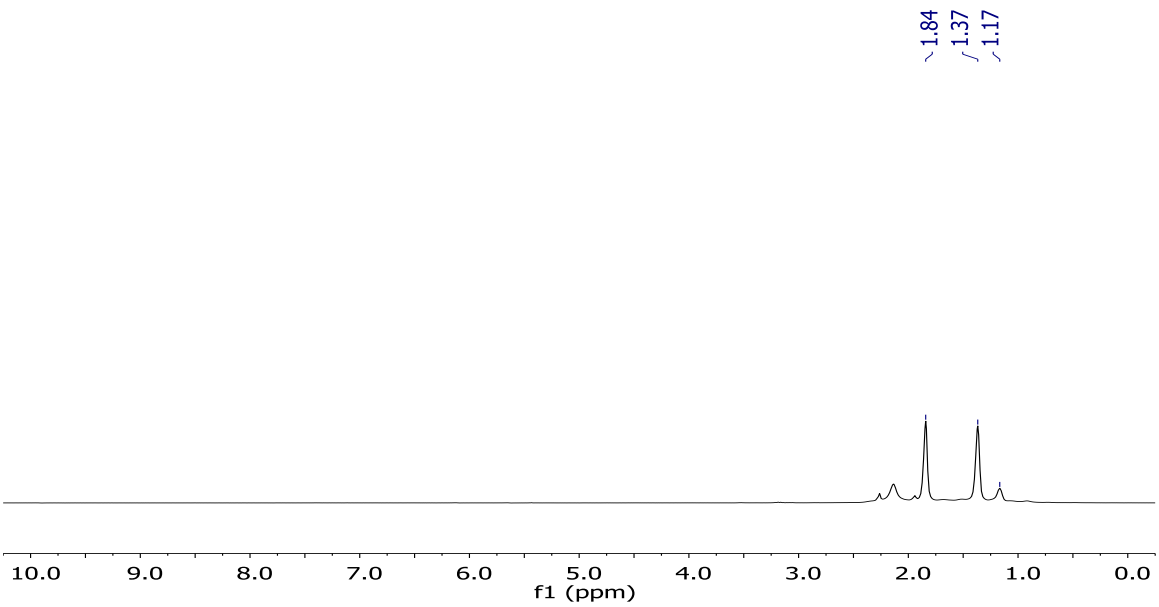

Figure 1-11. ^{1}H-NMR spectrum of **$3NH_2[Cs^+]$** in acetonitrile-d_3. *Note the peak at 2.1 ppm is water coordinated to the Cs^+ counter ion.*

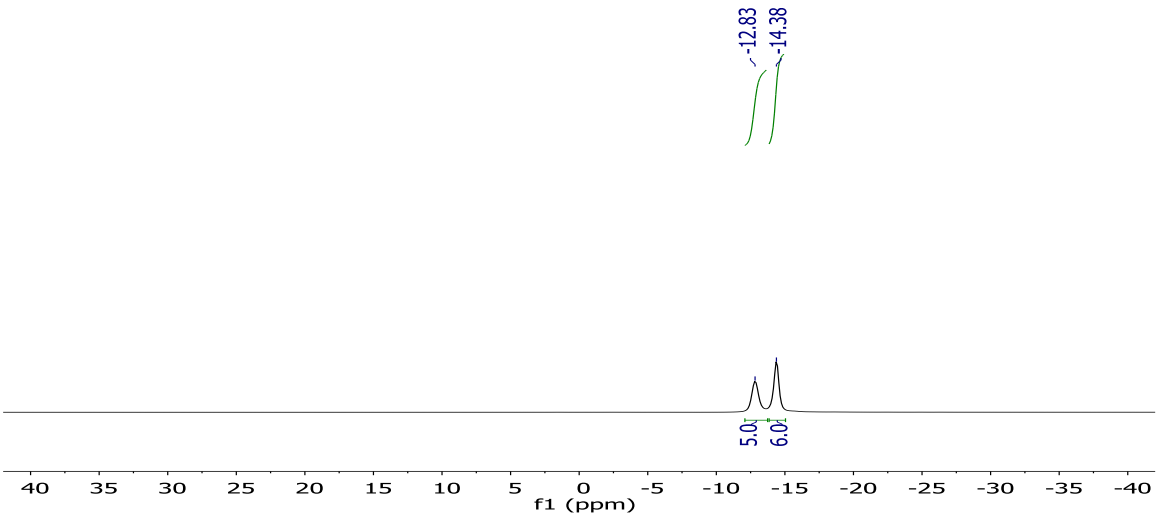

Figure 1-12. ^{11}B[^{1}H]-NMR spectrum of **$3NH_2[Cs^+]$** in acetonitrile-d_3.

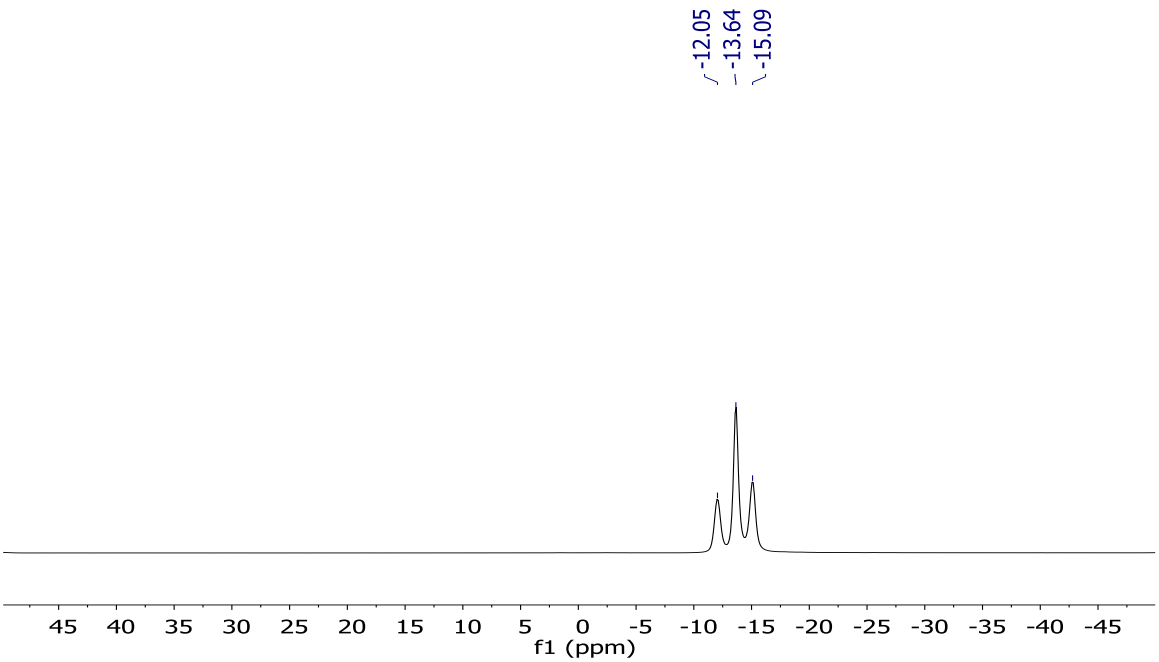

Figure 1-13. ^{11}B-NMR spectrum of **$3NH_2[Cs^+]$** in acetonitrile-d_3.

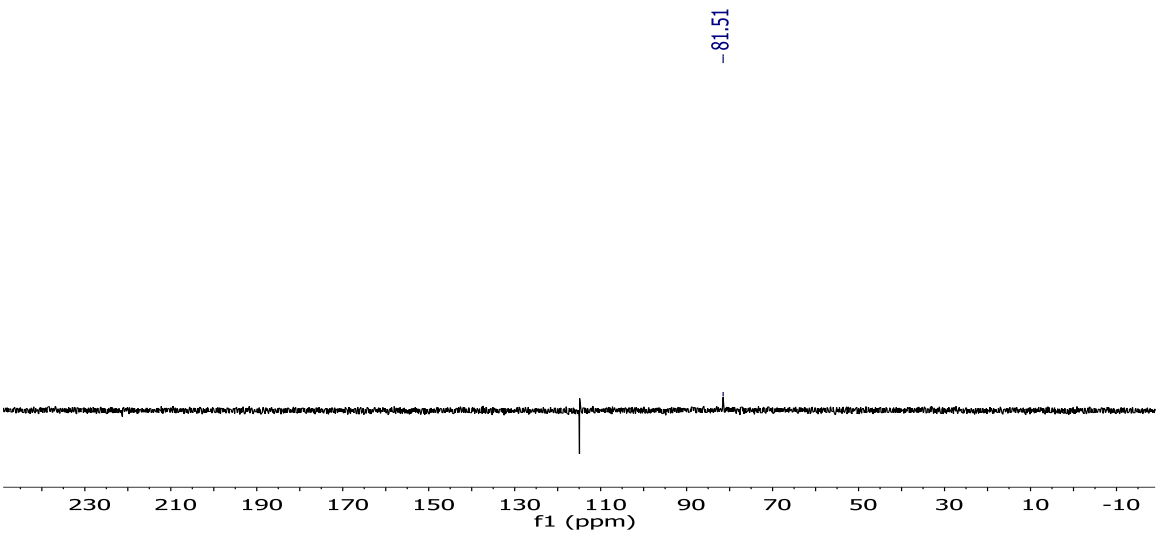

Figure 1-14. ^{13}C[^{1}H]-NMR spectrum of **$3NH_2[Cs^+]$** in water-h_2. *Note: there is an artifact at 115 ppm.*

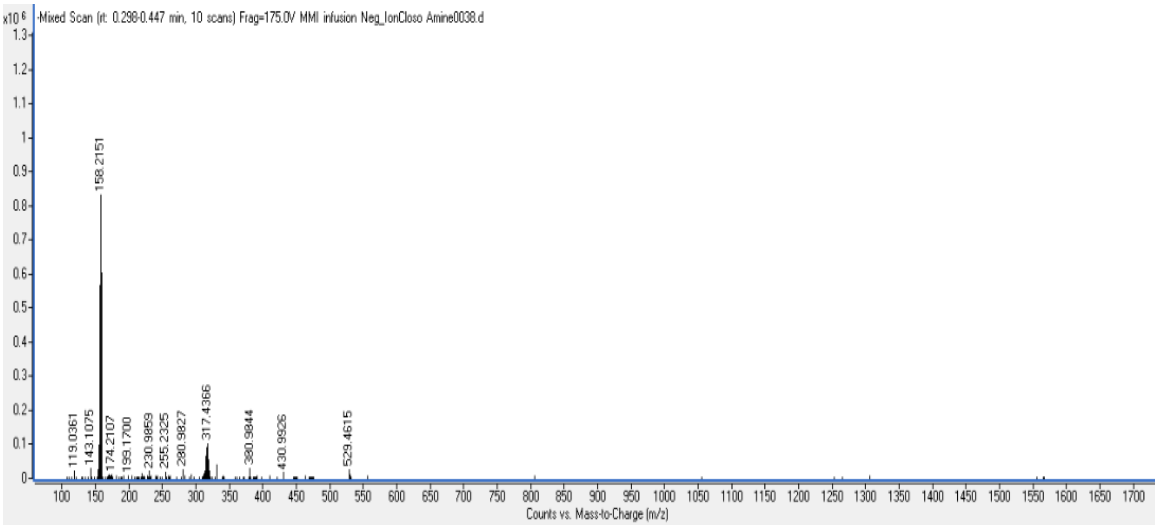

Figure 1-15. Mass spectrum of **$3NH_2[Cs^+]$**.

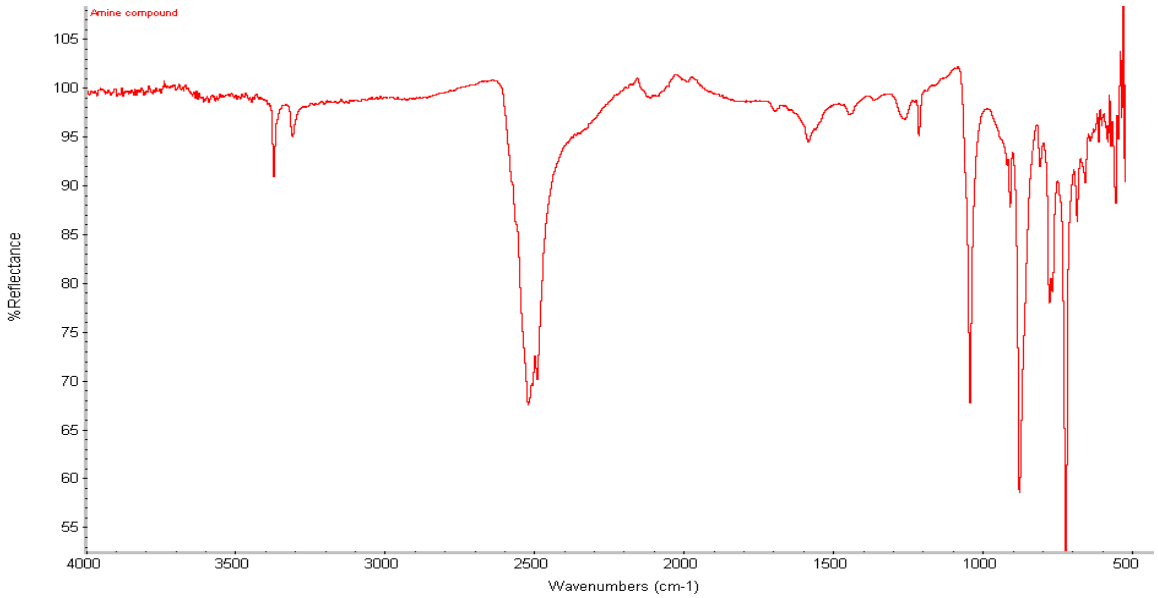

Figure 1-16. IR spectrum of **$3NH_2[Cs^+]$** showing the B-H stretches near 2500 cm^{-1}.

1.6 References

1. A. Stock ,C. Massenez, *Berichte der Deutschen Chemischen Gesellschaft*, 1912, **45**, 3539-3568.
2. A. Dequasie, *The Green Flame : Surviving Government Secrecy*, American Chemical, Society, Washington, D.C., 1991.
3. W. N. Lipscomb, *Boron Hydrides*, Dover Publications, Mineola, New York, 2013.
4. W. Dilthey, *Angewandte Chemie*, 1921, **34**, 596-596.
5. P. Laszlo, *Angewandte Chemie International Edition*, 2000, **39**, 2071-2072.
6. H. I. Schlesinger ,A. B. Burg, *Chemical Reviews*, 1942, **31**, 1-41.
7. H. C. Longuet-Higgins ,R. P. Bell, *Journal of the Chemical Society (Resumed)*, 1943, 250-255.
8. W. C. Price, *The Journal of Chemical Physics*, 1947, **15**, 614-614.
9. W. C. Price, *The Journal of Chemical Physics*, 1948, **16**, 894-902.
10. G. Silbiger ,S. H. Bauer, *Journal of the American Chemical Society*, 1948, **70**, 115-119.
11. J. S. Kasper, C. M. Lucht ,D. Harker, *Acta Crystallographica*, 1950, **3**, 436-455.
12. A. R. Pitochelli ,F. M. Hawthorne, *Journal of the American Chemical Society*, 1960, **82**, 3228-3229.
13. M. F. Hawthorne ,A. R. Pitochelli, *Journal of the American Chemical Society*, 1959, **81**, 5519-5519.
14. H. C. Longuet-Higgins ,M. d. V. Roberts, *Proceedings of the Royal Society of London. Series A. Mathematical and Physical Sciences*, 1955, **230**, 110-119.
15. I. B. Sivaev, V. I. Bregadze ,S. Sjöberg, *Collection of Czechoslovak Chemical Communications*, 2002, **67**, 679-727.
16. R. N. Grimes, *Carboranes*, Academic Press, Burlington, MA, 2011.
17. L. I. Zakharkin, V. I. Stanko, V. A. Brattstev, Y. A. Chapovskii ,Y. T. Struchkov, *Akademii Nauk SSSR, Seriya Khimicheskaya*, 1963, **12**, 1911.
18. T. L. Heying, J. W. Ager, S. L. Clark, D. J. Mangold, H. L. Goldstein, M. Hillman, R. J. Polak ,J. W. Szymanski, *Inorganic Chemistry*, 1963, **2**, 1089-1092.
19. M. M. Fein, J. Bobinski, N. Mayes, N. Schwartz ,M. S. Cohen, *Inorganic Chemistry*, 1963, **2**, 1111-1115.
20. W. H. Knoth, *Journal of the American Chemical Society*, 1967, **89**, 1274-1275.

21. A. Spokoyny, *Pure and Applied Chemistry*, 2013, **85**, 903-919.

22. I. Sivaev, A. V. Prikaznov ,D. Naoufal, *Collection of Czechoslovak Chemical Communications*, 2010, **75**, 1149-1199.

23. S. Duttwyler, *Pure and Applied Chemistry*, 2018, **90**, 733-744.

24. B. J. Eleazer ,D. V. Peryshkov, *Comments on Inorganic Chemistry*, 2018, **38**, 79-109.

25. R. N. Grimes, *Carboranes*, Academic Press, New York, 2016.

26. A. R. Popescu, F. Teixidor ,C. Viñas, *Coordination Chemistry Reviews*, 2014, **269**, 54-84.

27. C. Douvris ,J. Michl, *Chemical Reviews*, 2013, **113**, PR179-PR233.

28. B. Ringstrand ,P. Kaszynski, *Accounts of Chemical Research*, 2013, **46**, 214-225.

29. D. Olid, R. Núñez, C. Viñas ,F. Teixidor, *Chemical Society Reviews*, 2013, **42**, 3318-3336.

30. P. Farràs, E. J. Juárez-Pérez, M. Lepšík, R. Luque, R. Núñez ,F. Teixidor, *Chemical Society Reviews*, 2012, **41**, 3445-3463.

31. M. Scholz ,E. Hey-Hawkins, *Chemical Reviews*, 2011, **111**, 7035-7062.

32. C. A. Reed, *Accounts of Chemical Research*, 2010, **43**, 121-128.

33. K. Wade, *Journal of the Chemical Society D: Chemical Communications*, 1971, 792-793.

34. D. M. P. Mingos, *Nature Physical Science*, 1972, **236**, 99-102.

35. E. D. Jemmis, M. M. Balakrishnarajan ,P. D. Pancharatna, *Journal of the American Chemical Society*, 2001, **123**, 4313-4323.

36. E. D. Jemmis, M. M. Balakrishnarajan ,P. D. Pancharatna, *Chemical Reviews*, 2002, **102**, 93-144.

37. N. S. Hosmane, *Handbook of Boron Science : with Applications in Organometallics, Catalysis, Materials and Medicine*, World Scienific, Hackensack, New Jersey, 2019.

38. T. Jelínek, J. Plešek, F. Mareš, S. Heřmánek ,B. Štíbr, *Polyhedron*, 1987, **6**, 1981-1986.

39. I. Zharov, T.-C. Weng, A. M. Orendt, D. H. Barich, J. Penner-Hahn, D. M. Grant, Z. Havlas ,J. Michl, *Journal of the American Chemical Society*, 2004, **126**, 12033-12046.

40. B. T. King, S. Körbe, P. J. Schreiber, J. Clayton, A. Němcová, Z. Havlas, K. Vyakaranam, M. G. Fete, I. Zharov, J. Ceremuga ,J. Michl, *Journal of the American Chemical Society*, 2007, **129**, 12960-12980.

41. B. Brellochs, J. Bačkovský, B. Štíbr, T. Jelínek, J. Holub, M. Bakardjiev, D. Hnyk, M. Hofmann, I. Císarová ,B. Wrackmeyer, *European Journal of Inorganic Chemistry*, 2004, **2004**, 3605-3611.

42. I. B. Sivaev, Z. A. Starikova, P. V. Petrovskii, V. I. Bregadze ,S. Sjöberg, *Journal of Organometallic Chemistry*, 2005, **690**, 2790-2795.

43. T. Jelínek, J. Plešek, S. Hermanek ,S. Bohumil, *Collection of Czechoslovak Chemical Communications*, 1986, **51**, 819-829.

44. G. A. Guter ,G. W. Schaeffer, *Journal of the American Chemical Society*, 1956, **78**, 3546-3546.

45. L. G. Sneddon, J. C. Huffman, R. O. Schaeffer ,W. E. Streib, *Journal of the Chemical Society, Chemical Communications*, 1972, 474-475.

46. W. H. Knoth ,E. L. Muetterties, *Journal of Inorganic and Nuclear Chemistry*, 1961, **20**, 66-72.

47. J. Plesek, T. Jelínek, E. Drdáková, S. Hermánek ,B. Stibr, *Collection of Czechoslovak Chemical Communications*, 1984, **49**, 1559-1562.

48. K. Baše, N. W. Alcock, O. W. Howarth, H. R. Powell, A. T. Harrison ,M. G. H. Wallbridge, *Journal of the Chemical Society, Chemical Communications*, 1988, 341-342.

49. M. Finze, G. J. Reiss ,M. Zähres, *Inorganic Chemistry*, 2007, **46**, 9873-9883.

50. R. R. Srivastava, D. K. Hamlin ,D. S. Wilbur, *The Journal of Organic Chemistry*, 1996, **61**, 9041-9044.

Chapter 2: Synthesis of Unsymmetrical *N*-carboranyl NHCs: The Directing Effect of the Carborane Anion and Reactivity with Elemental Sulfur

2.1 Introduction

Ancillary ligands are typically constructed with combinations of ubiquitous alkyl and aryl substituents. An interesting alternative to classical alkyl and aryl ligand R-groups are the organomimetic[1] icosahedral carboranes,[2-8] which can be thought of as 3-dimensional analogues[9] of benzene. The most common carboranes used in ligand design are derived from neutral icosahedral dicarbaborane clusters (*o*-carborane). Due to its ready availability, the *ortho*-carborane (*o*-carborane) **3** (Figure 1-2) is the most often implemented. While this cluster offers many distinct characteristics, such as a unique steric profile and the ability to form H-H hydrogen bonds,[8] it exhibits reactivity that is perhaps undesirable for catalysis, such as facile B-H cyclometallation[10] and B-vertex extrusion reactions[11] to afford *nido*-carboranes. The latter reaction has been developed by Teixidor and Viñas to produce novel anionic phosphines and other ligands, featuring *nido*-cluster substituents.[3, 12] Compared to icosahedral dicarbaboranes (*o*-carboarne), the isoelectronic anionic carba-*closo*-dodecaborate clusters (CB_{11}^-)[4] **3** (Figure 1-2) do not undergo vertex extrusion reactions and are more resistant to cyclometallation.[13] Furthermore, clusters **3** are among the weakest coordinating and inert counter anions known and have been applied to the preparation of elusive reactive cations,[14] super acids,[15] and superior systems for silylium catalysis.[16-19]

We recently reported the first utilization of cluster **3** as ligand substituent for a transition metal-based catalyst. Our initial report disclosed the synthesis of a phosphine bearing a perchlorinated carborane anion substituent, which when complex to Au(I) forms one of the most active catalyst ever reported for the alkyne hydroamination reactions.[20] Encouraged by these results, we have begun to develop the synthetic methodology[13, 21, 22] to access a wide range of ligand architectures,[23, 24] which contain covalently linked icosahedral carborane anions, for applications in catalysis.[25-28]

a) Cyclopropantion with dihalocarbenes

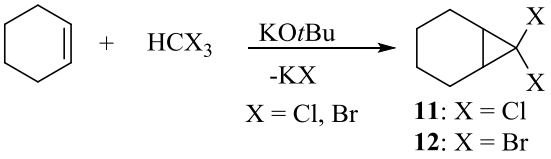

b) Wanzlick Equilibrium

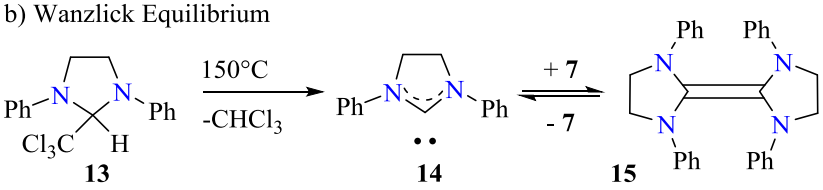

c) Schönherr and Wanzlick work with *in situ* NHC **10**

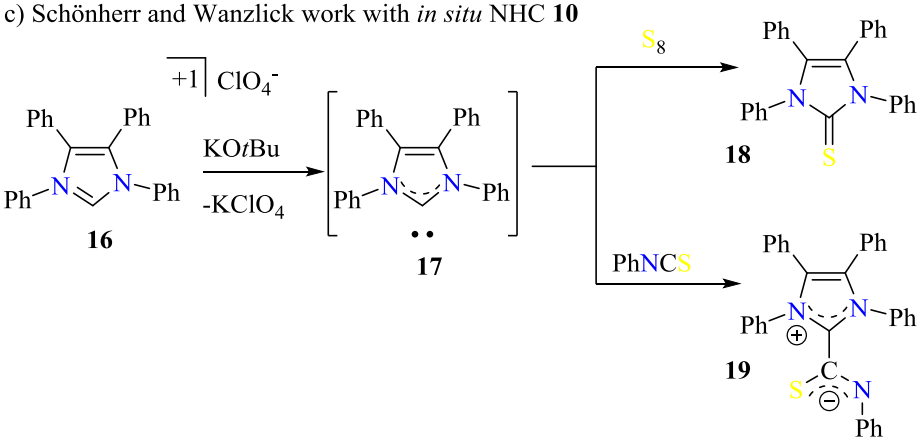

Scheme 2-1 A brief review of historically important non-isolable carbenes and NHCs. Dip = 2,6-diisopropylphenyl.

One avenue of ligand architecture is the ubiquitous carbene ligands with the most notorious carbene ligand being the N-heterocyclic carbene (NHC). The idea of a carbene, or a neutral divalent carbon atom, dates back to the 18th century and is classically credited to Dumas[29] and Regnault[30] who tried to dehydrate methanol with concentrated sulphuric acid or phosphorus pentoxide,[31, 32] however I believe it should be credited to Zers Geuther[33] who suggested the formation of a dichlorocarbene as an intermediate involved in the alkaline hydrolysis of chloroform. Zers Geuther's claim was substantiated in 1954 by Doering and Hoffmann who showed that chloroform (or bromoform) reacted with KO*t*Bu and cyclohexene to form 7,7-dihalobicyclo[4.1.0]heptane (halo = chloro (**11**) or bromo (**12**)), (Scheme 2-1a), which they

proposed proceeded though the formation of a carbene intermediate.[34] Almost 20 years later Schikora and Wanzlick were investigating the thermolysis reaction of imidazolinium **13** and postulated that upon loss of chloroform the carbene **14** was formed, however they were unable to isolate this intermediate and proposed that it dimerized to produce **15** (Scheme 2-1b). About 10 years later in 1970 Schönherr and Wanzlick demonstrated that 1,3,4,5-tetraphenylimidazolium perchlorate (**16**) after reacting with KO*t*Bu displayed chemical reactivity indicative of a carbene intermediate (**17**) but again were unable to isolate the NHC.[35] In their studies they identified the nucleophilic nature of **17** by its reaction with sulfur to form the sulfur adduct, 1,3,4,5-tetraphenylimidazole-2-thione (**18**) as well as the insertion of **17** into phenyl isothiocyanate to form **19** (Scheme 2-1c).

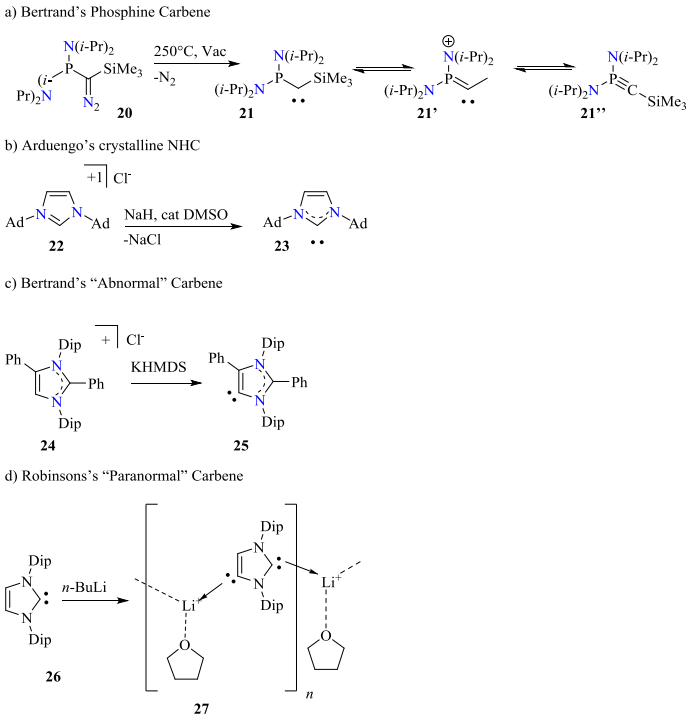

Scheme 2-2 Isolable carbenes and N-heterocyclic carbenes.

In 1988 Guy Bertrand and coworkers published the first isolable carbene utilizing a push-pull tactic, in this sense they sandwiched a diazo carbon with an electron rich phosphazene and an electron poor trialkylsilane. This type of reaction manifested itself with the thermally ejection of N_2 from a diazo-λ^3-

phosphazene, **29**, producing the isolable carbene in the form of a λ^3-phosphinocarbene **21** and its resonance forms **21'** and **21''**, Scheme 2-2a.[36, 37] Closely after this in 1991, Arduengo and coworkers published yet another type of isolable carbene, the push-push carbene. This type of compounds was essentially those which Wanzlick studied but was unable to isolate as a free carbene. The term push-push arises from the two π-donors alpha to the carbene carbon, when the two flanking π-donors are nitrogen atoms the resulting carbenes are known as N-heterocyclic carbenes or NHCs for short. The first isolable, crystalline, NHC was from the reaction of 1,3-bis(adamantly)imidazolium, **22**, with NaH in a catalytic amount of DMSO which furnished the 1,3-bis(adamantly)imidazol-2-ylidene, **23**, Scheme 2-2b.[38] Later in 1998 Arduengo isolated Wanzlick's dream NHC **17** as a colorless crystalline solid.[39] The inability of Schönherr and Wanzlick to isolate **17** is unknown, but it is thought that they may have believed the compound existed as a dimer[40] or was just too reactive to isolate.[41] Other notable NHC derivatives are the "abnormal" NHC first isolated as a free species by Bertrand and coworkers in 2009 (Scheme 2-2c).[42] The authors achieved this by replacing the acidic protons on the imidazolium core, hydrogen atoms at C-2 and C-4, with phenyl rings, **24**. The phenylated imidazolium only contains a single acidic proton, hydrogen atom at C-5, which was deprotonated with potassium bis(trimethylsilyl)amide (KHMDS) giving the abnormal NHC, **25**, Scheme2-2c. In 2010 Robinson and coworkers demonstrated that it was possible to deprotonated both the C-2 and C-5 positions of bis(2,6-diisopropylphenyl)imidazolium, Scheme 2-2d. This was achieved by reacting bis(2,6-diisopropylphenyl)imidazole-2-ylidene **26** with one equivalent of *n*-BuLi which deprotonates one of the imidazol-2-ylidene backbone protons giving the doubly deprotonated C-2/C-5 dicarbene, **27**, otherwise known as a paranormal carbene. This is ends the brief history to NHC molecules and is by no means comprehensive, in particular the classical work done by Fischer[43] and the use of carbenes as organocatalyst[44] has been neglected, there is also a comprehensive book[45].

a) Electronic properties of an NHC

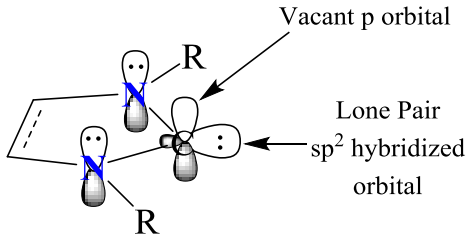

b) Unsaturated and saturated NHCs and isolable cyclic (alkyl)(amino)carbene (**CAAC)**

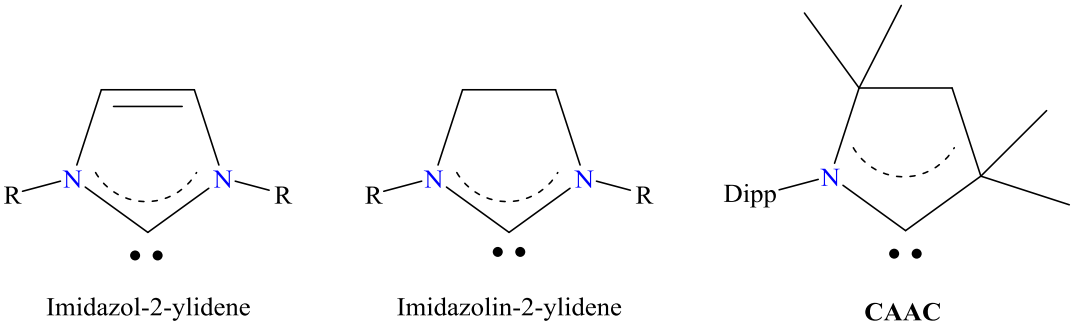

Figure 2-1 a) Electronic properties of NHC, b) Unsaturated, saturated and isolable cyclic (alkyl)(amino)carbene. Dipp = 2,6-diisopropylphenyl.

The stabilization of the N-heterocyclic carbene results from electronic and steric factors. In light of electronic considerations, the NHC is stabilized by π-donation from the alpha nitrogen atoms flanking the carbene center (Figure 2-1a). This effect, along with the cyclic nature, causes the NHC carbene carbon (local C_{2v} symmetry) to take on an sp^2 hybridization which in turn favors the singlet state over the triplet state.[46, 47] Since NHCs favor the singlet state they contain both an "empty" p type orbital and filled sp^2 hybridized orbital, thus these compounds are considered ambiphilic (both nucleophilic and electrophilic). Initially it was though that two neighboring nitrogen atoms were necessary to stabilize the free NHC but this was later reputed by Lavallo and coworkers who demonstrated that only one alpha nitrogen atom was required when they published the cyclic (alkyl)(amino)carbene **CAAC** (Figure 2-1b).[48, 49] For steric considerations, the forward-facing substituents on N help protect the carbene carbon from dimerization, compounds known to dimerize are the imidazolin-2-lyidenes (saturated backbone) such as 1,3-bis(phenyl)imidazoline-2-ylidene and some of its *para* derivatives, a crystal structure for the 1,3-bis(phenyl)imidazoline-2-ylidene dimer is known.[50-52] An excellent article by Dröge and Glorius gives an

overview of the electronic and steric properties of a plethora of carbenes including many of the common NHCs.[53]

2.2 Synthesis of a Symmetrical Imidazolium and Corresponding NHCs

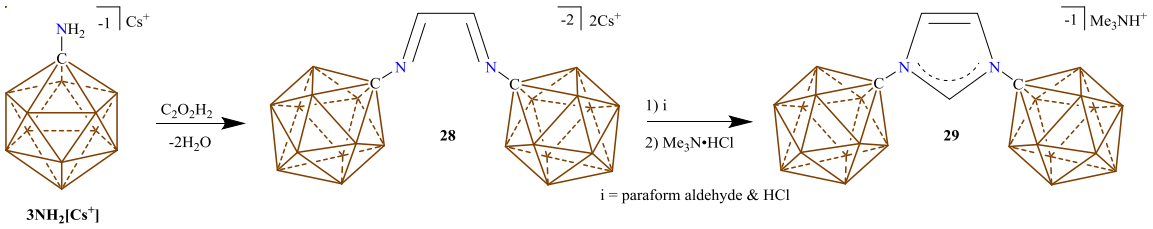

Scheme 2-3 Synthesis of anionic imidazolium **29**.

In 2014 El-Hellani and Lavallo investigated the idea of appending an imidazolium with N-bound anionic carborane substituents and then disclosed the synthesis of polyanionic N-heterocyclic carbene (NHC), featuring two N-bound carborane anions.[23] The anionic imidazolium precursor was synthesized by reacting **$3NH_2[Cs^+]$** with glyoxal giving the dianionic diimine **28** Surprisingly this reaction was the first demonstration of **$3NH_2$** undergoing condensation chemistry since its synthesis in 1968. The pKa of **$3NH_2[Cs^+]$** has been determined experimentally to be 6.0 which is slightly higher than aniline which is 4.6.[54] The diimine, **28**, was then cyclized with paraformaldehyde and acid giving the anionic imidazolium **29** (Scheme 2-3).

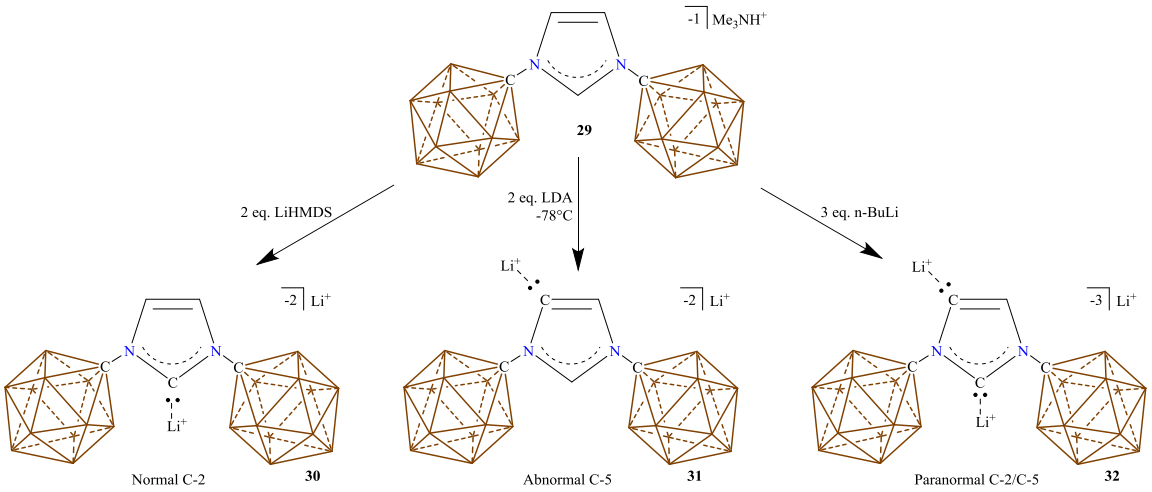

Scheme 2-4 Synthesis of three distinct carbenes from one anionic imidazolium precursor.

What is unique to imidazolium **29** is its ability to form three distinct NHCs salts through judicious choice of base.[46, 55, 56] When using two equivalents of lithium bis(trimethylsilyl)amide (LiHMDS) the normal (C-2 deprotonated) NHC, **30**, is formed (Scheme 2-4). If the reaction is performed at -78°C with lithium bis(diisopropyl)amide (LDA) the abnormal (C-5 deprotonated) NHC, **31**, is the sole product.[42, 57-59] If *n*-BuLi is used the paranormal (C-2/C-5 doubly deprotonated) NHC, **32**, is the only product obtained (Scheme 2-3).[60] Such selectivity of NHC formation has not been achieved in deprotonation reactions of imidazolium salts that contain N-hydrocarbon groups. We became curious to see if it was possible to prepare unsymmetrical NHCs, featuring both carborane and hydrocarbon substituents, and investigate if the same selectivity for NHC formation could be achieved. Here we report the synthesis of an imidazolium zwitterion, featuring mixed carborane and hydrocarbon *N*-substituents, and its deprotonation to form various anionic NHCs.

2.3 Synthesis of an Unsymmetrical Imidazolium and NHCs, The Directing Effect

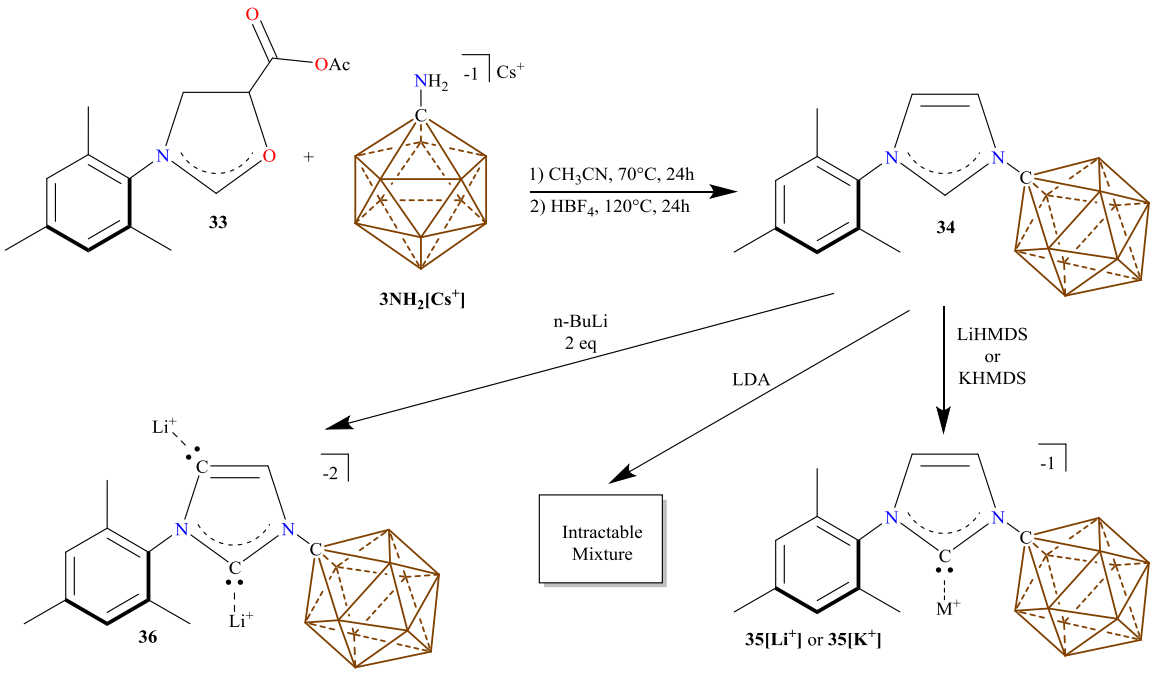

Scheme 2-5 Synthesis of zwitterionic imidazolium **34** and its reaction with different bases to form anionic **35[Li$^+$]**, **35[K$^+$]**, and dianionic **36** NHCs. The second lithiation of **34** with *n*-BuLi occurs with perfect selectivity at the C-5 position to form **36**. M = Li or K, unsubstituted vertices = B-H.

One of the most elegant and versatile methods to synthesize unsymmetrically substituted imidazolium salts has been reported by Fürstner and coworkers[61] and involves the heterocyclic interconversion of oxazolinium salts, *via* reaction with amines. These oxazolinium salts are readily tunable at N and available in three steps from commercial starting materials. By analogy, we envisioned reacting the mesityl substituted oxazolinium cation **33** with anionic carboranyl amine **3NH$_2$[Cs$^+$]**, followed by treatment with acid, would produce the zwitterionic imidazolium species **34** (Scheme 2-5, top).[62]

Indeed, this reaction sequence is effective; affording the imidazolium species **34** in 77% yield based on the carboranyl amine. Since the release of this paper the yield has been increase to >90% by heating the HBF_4 reaction mixture until the reaction is finished, this is monitored by ^{1}H NMR and typically

takes 2-3 days. The zwitterion is soluble in benzene as well as most other common solvents, with the exception of alkanes and H_2O. The ^{1}H NMR spectrum of **34** shows three distinct doublets of doublets for the imidazolium ring protons (8.8 ppm, $^4J_{H\text{-}H}$ = 2.0, 1.8 Hz (C-2); 7.7 pm, $^3J_{H\text{-}H}$ = 2.0 Hz, $^4J_{H\text{-}H}$ = 1.8 Hz, (C-4); 7.3 ppm, $^4J_{H\text{-}H}$ = 2.0 Hz, $^3J_{H\text{-}H}$ = 2.0 Hz, (C-5)). Assignment of the imidazolium backbone protons was determined by NOESY NMR experiments that show coupling between the resonance at 7.7 ppm and the B-H pentagonal belt adjacent to the carborane carbon. In addition, through-space coupling is observed between the signal at 7.3 ppm and the *ortho*-mesityl methyl protons. The ^{13}C NMR spectrum of **34** displays three resonances (142.0, 124.7, 124.8 ppm) for the imidazolium carbons.

Deprotonation of the zwitterionic imidazolium species **34** with LiHMDS dissolved in THF, results in rapid precipitation of a white powder **35[Li$^+$]**. Analysis of the material by ^{1}H NMR shows the disappearance of the low field C-2 proton at 8.8 ppm and the appearance of two doublets (7.4 ppm and 6.8 ppm; d, $^3J_{H\text{-}H}$ = 1.5 Hz), which is consistent with the formation of the normal C-2 NHC. The ^{13}C NMR spectrum of **35[Li$^+$]** displays a broad resonance at 199.9 ppm for the carbene center, which is in the expected range for aryl substituted imidazolylidenes and very close to the lithium complex of NHC **30** (195.0 ppm). Interestingly, deprotonating **34** with KHMDS in lieu of LiHMDS, results in the formation of **35[K$^+$]**, which is very soluble in THF and benzene. The ^{1}H NMR spectrum of **35[K$^+$]** is nearly identical to **35[Li$^+$]**, however the ^{13}C NMR spectrum reveals a downfield shifted carbene resonance (211.1 ppm). The difference in chemical shift compared to **35[Li$^+$]** is likely due to the formation of an NHC Li^+ complex in solution, whereas the K^+ salt **35[K$^+$]** exists as a solvent separated ion pair. The ^{7}Li NMR spectrum of **35[Li$^+$]** shows a broad resonance at 2.3 ppm, which also supports the formation of an NHC Li^+ adduct in solution. Our hypothesis is in line with previous studies[42, 63] that have shown that alkali metal free NHCs are formed when K bases are implemented in lieu of Li reagents.

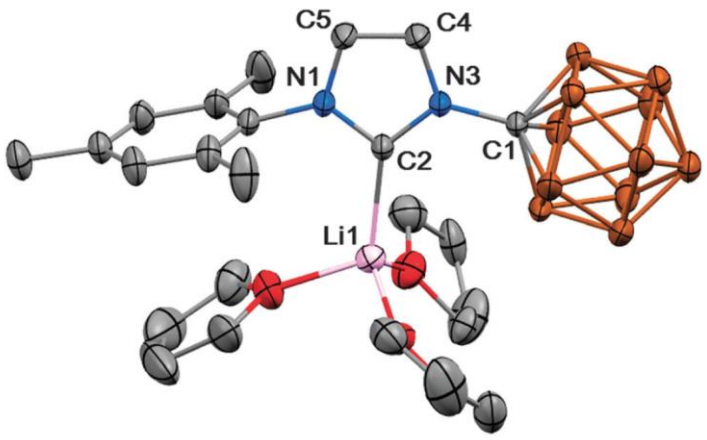

Figure 2-2 Solid state structure of **35[Li$^+$]**. Hydrogens are omitted for clarity. Color code: C = gray, B = brown, N = blue, Li = pink, O = red.

The solid-state structure of **35[Li$^+$]** was unambiguously determined by a single crystal X-ray diffraction study and shows the NHC and three THF molecules coordinated to the Li^+ (Figure 2-2). Both N1 and N3 are planar (sum of CNC angles = 360°), indicating they are both sp^2 hybridized. The nitrogen carbene bond lengths of **35[Li$^+$]** (N1-C2 = 1.3671(17), N3-C2 = 1.3799(17) Å) are in the range reported for standard NHC Li adducts,[63] and comparable to **30**.[23] The carborane-N bond length (N3-C2 = 1.4597(16) Å) and carbon boron distances in the cluster (average C-B distance 1.7724(19) Å) are close to that reported for **30**, and suggest no *exo*-π-conjugation[64] between the carborane substituent and the carbene ring. The carbene-lithium bond length of **35[Li$^+$]** (C2-Li1 = 2.214(3) Å) is in the range reported for standard NHC lithium complexes.[63]

We next explored the possibility of forming an abnormal NHC, analogous to **31**, by reaction of **34** with LDA. All of our attempts to selectively deprotonate the backbone of imidazolium **34** with LDA lead to intractable mixtures of **35[Li$^+$]** and multiple unidentified compounds (Scheme 2-4). These results suggest that it is necessary to have two *N*-carboranyl substituents attached to the imidazolium ring in order to achieve selective backbone deprotonation.

Subsequently, we turned our attention to double deprotonation reactions with *n*-BuLi. In contrast to symmetrical N,N-carboranyl imidazolium salts[23] **34** contains distinct protons at the C-4 and C-5 positions adjacent to the mesityl and carborane anion substituents, respectively. Therefore, we were not only curious if we could isolate a doubly deprotonated species, but would selectively be observed for C-4 or C-5 lithiation? Treatment of a solution of **34** dissolved in diethyl ether with 2 equivalents of *n*-BuLi resulted in the formation of a precipitate (Scheme 2-4). After stirring the mixture for two hours the precipitate was collected and analysed by NMR spectroscopy, which reveals clean formation of a single isomer of the doubly deprotonated dianionic species **36**. Counter intuitively and in contrast to monoanionic **35[Li$^+$]**, dianionic **36** is very soluble in THF. The ^{1}H NMR spectrum displayed a single resonance for the imidazolium ring at 6.6 ppm, which through NOESY NMR analysis we assign to the C-4 proton adjacent to the carborane anion. This data indicates that lithiation of the imidazolium backbone occurs solely at the C-5 position of the ring. We speculate that this directing effect results from a combination of steric and electrostatic effects induced by the carborane anion substituent. The ^{13}C NMR of **36** shows an unsymmetrical imidazolium ring with two low field quaternary resonance at 193.0 and 166.8 ppm that correspond to the C-2 and C-5 deprotonated carbon centers, respectively. The ^{7}Li NMR spectrum of **36** displays two resonance (3.5 and 2.3 ppm), which suggests that both the C-2 and C-5 carbons are coordinated to Li$^+$ ions.

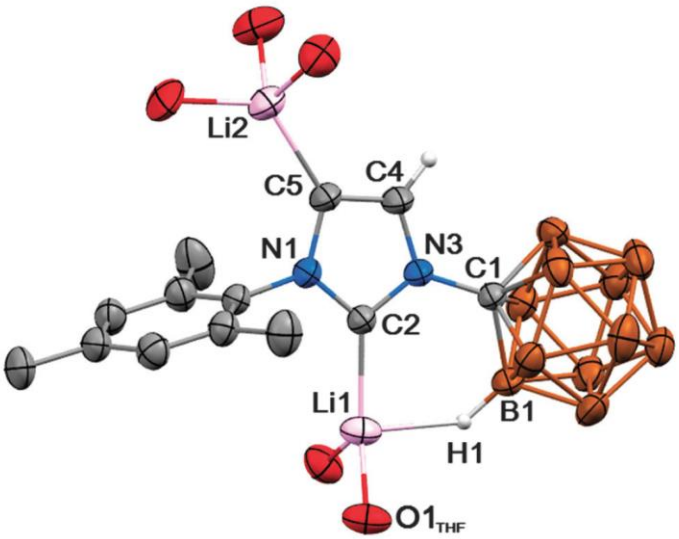

Figure 2-3 Solid state structure of **36**. Carbon rings of THF molecules and most hydrogen atoms (except H1, and C4-H) are omitted for clarity. Color code: C = gray, B = brown, N = blue, Li = pink, O = red.

Single crystal X-ray diffraction study confirms the identity of **36** (Figure 2-3). In contrast to the related trianionic *N*,*N*-dicarboranyl species **36** is monomeric. The central heterocyclic ring bond lengths of **36** (N1-C2 = 1.363(2), N3-N2 = 1.364(2), N1-C5 = 1.426(2), N3–C4 = 1.407(2), C4-C5 = 1.369(3), Å) are similar to those reported for the trianionic species **32** (Figure 2-3),[23] as well as monoanionic hydrocarbon derivatives reported by Robinson (**27**).[60] The carborane nitrogen bond length of (N3-C1 = 1.446(2) Å) and carbon boron distances in the cluster (average C-B distances for carboranes 1.716(1) Å), are only slightly different compared to the normal C-2 dianionic carbene lithium adduct **35[Li$^+$]** A single close B-H contact with the lithium cation bound to C2 (H1-Li1 = 2.14 Å) suggests the occurrence of an agostic-like[65, 66] interaction. The C2-Li2 distance (2.133(4) Å), which is perhaps a result of the B-H-Li bonding interaction that draws the C-2 carbene center closer to the alkali metal cation.

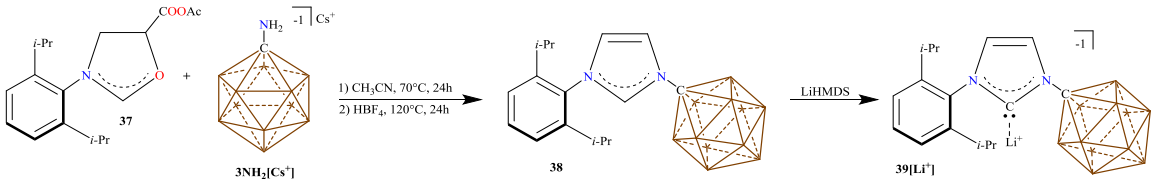

Scheme 2-6 Modular synthesis of DIP zwitterionic imidazolium (**38**) and corresponding NHC **39[Li$^+$]**. *i*-Pr = isopropyl.

Next, we decided to test the tunability of this synthesis by replacing the N-bound mesityl group of the imidazolium with a different aryl substituent. Here we chose 2,6-diisopropylphenyl (Dip) which would lead to a larger steric profile around the C-2 carbon. This synthesis was accomplished by reacting Dip oxazolium **37** with **3NH$_2$[Cs$^+$]** in the same manner as before giving the Dip zwitterionic oxazolium **38**, Scheme 2-6. The ^{1}H NMR spectrum of **38** shows three distinct doublets of doublets for the imidazolium ring protons (8.8 ppm, $^4J_{H\text{-}H}$ = 1.70, 1.7 Hz; 7.8 pm, $^3J_{H\text{-}H}$ = 1.7 Hz, $^4J_{H\text{-}H}$ = 1.7 Hz; 7.7.4 ppm, $^4J_{H\text{-}H}$ = 1.7 Hz, $^3J_{H\text{-}H}$ = 1.7 Hz). This particular imidazolium also contains a characteristic methine resonance at 2.2 ppm and corresponding doublet for the methyl resonances at 1.2 ppm. The ^{13}C NMR spectrum of **38** displays three resonances (146.3, 125.7, 125.5 ppm) for the imidazolium carbons as well as resonance at 30 ppm for the methine carbon and two very close resonances for the *iso*-propyl carbon methyls near 24 ppm. The creation of this compound suggests that our synthetic strategy should be modular with different aryl substituents. Taking this a step further we wanted to see if we could deprotonate the C-2 position of **38**.

Deprotonation of the zwitterionic imidazolium species **38** with LiHMDS dissolved in THF, results in rapid precipitation of a white powder **39**. Analysis of the material by ^{1}H NMR shows the disappearance of the low field C-2 proton at 8.8 ppm and the appearance of two doublets (7.3 ppm and 6.8 ppm; d, $^3J_{H\text{-}H}$ = 1.7 Hz), which is consistent with the formation of the normal C-2 NHC. The ^{13}C NMR spectrum of **39** displays a small resonance at 208.4 ppm for the carbene center, which is in the expected range for aryl substituted imidazolylidenes and close to the lithium complex of NHC **30** (195.0 ppm) and mesityl lithium complex **35[Li$^+$]** (199.9).

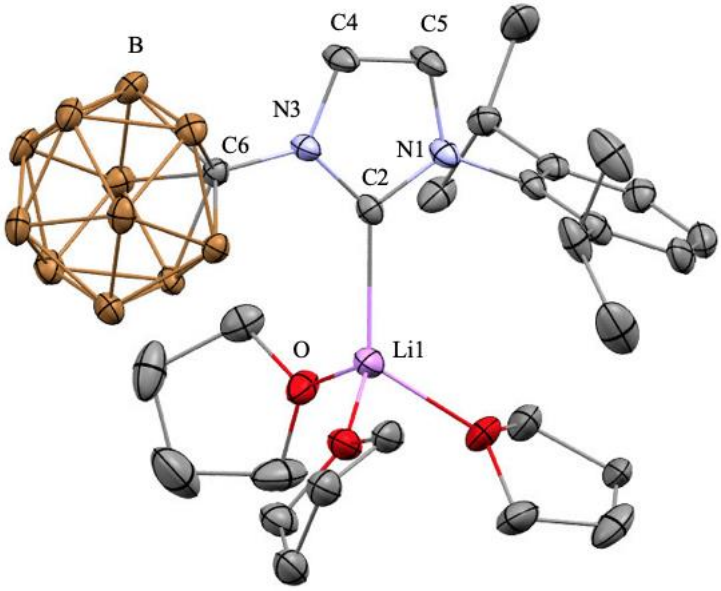

Figure 2-4 Solid state structure of **39**. Hydrogen atoms are omitted for clarity. N = blue, C = black, B = brown, O = red, Li = pink.

The solid-state structure of **39** was unambiguously determined by a single crystal X-ray diffraction study and shows the NHC and three THF molecules coordinated to the Li^+ (Figure 2-4). Both N1 and N3 are planar (sum of CNC angles = 360°), indicating they are both sp^2 hybridized. The nitrogen carbene bond lengths of **39** (N1-C2 = 1.366(3), N3-C2 = 1.379(3) Å) are in the range reported for standard NHC Li adducts,[63] and comparable to **30** and **35[Li$^+$]**.[23] The carborane-N bond length (N3-C6 = 1.459(3) Å) and carbon boron distances in the cluster (average C-B distance 1.717(4) Å) are close to that reported for **30** and **35[Li$^+$]**, and suggest no *exo*-π-conjugation[64] between the carborane substituent and the carbene ring. The carbene-lithium bond length of **39** (C2-Li1 = 2.243(5) Å) is in the range reported for standard NHC lithium complexes.[63]

2.4 Reactivity of NHCs with Elemental Sulfur

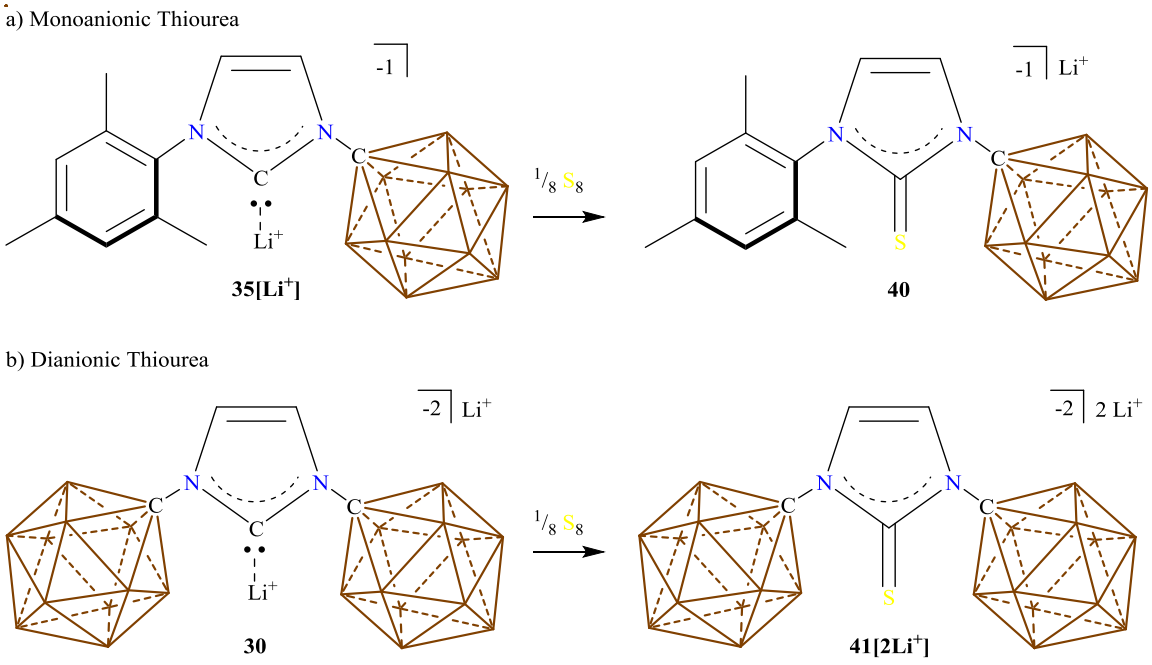

Scheme 2-7 Synthesis of thioureas and their Mg salts.

Since compounds **30** and **35[Li$^+$]** are anionic, we considered testing them as solution phase electrolytes. In order to avoid possible reactivity occurring at the imidazolium C-2 proton we decided to append C-2 with a sulfur which would give a thiourea, Scheme 2-7. Compounds of this type are well known in the literature and are created by reacting the free NHC with an equivalent of elemental sulfur.[67, 68] If we were to make a thiourea from free NHCs **30** and **35[Li$^+$]** we would be generate dianionic and monoanionic products respectively. A potential benefit to these compounds would arise if a pure sulfur cathode was used as it is known that dissolved polysulfides (such as Li_2S) will precipitate from solution depositing on the conductive framework and in turn depleting the cathode.[69] Here we hypothesized that a thiourea may help solubilize the polysulfides avoiding cathode destruction.

To achieve these thioureas we stirred a mixture of NHC and elemental sulfur. The reaction of monoanionic NHC **35[Li$^+$]** with elemental sulfur proceeds smoothly at room temperature producing thiourea **40** in 30 minutes with a 91% yield after workup, Scheme 2-7a. Inspection of the ^{1}H NMR shows the expected three down field resonances, two belonging to the inequivalent imidazolium backbone protons

and the other belonging to the meta hydrogens of the mesityl. The imidazolium backbone protons display two shifts in the ^{1}H NMR spectrum, one proton displays a downfield shift from 7.40 ppm to 7.45 ppm while the other proton shows an up-field shift from 6.79 ppm 6.50 ppm. The ^{11}B NMR displays two resonances at 8.3 and 14.1 ppm, this is due to the upper and lower pentagonal belts overlapping and displaying one large resonance at 14.1 ppm. Mass spectrometry corroborated the presence of sulfur in the molecule and we observe a peak at 359.2770 m/z which correlates well with the calculated value of 359.2756 m/z.

Reaction of dianionic NHC **30** with elemental sulfur at room temperature gave no reaction, however, upon heating the mixture the dianionic thiourea **41[2Li^{+}]** is formed, Scheme 2-7b. Upon inspection of the ^{1}H NMR spectrum there is a down field shift of the backbone proton from 6.96 ppm to 7.08 ppm respectively. Analyzing the mass spectrum, we observed a characteristic peak at 191.1931 m/z (calc: 191.1932) which suggest the presence of a sulfur atom in the molecule. Since the reaction mixture needs to be stirred for extended periods of time there is typically some protonation of **30** back to **29**. Being anionic the protonated imidazolium is difficult to separate from the dianionic thiourea. To avoid this tedious separation potassium tert-butoxide can be added to the reaction mixture along with elemental sulfur driving the reaction to completion.

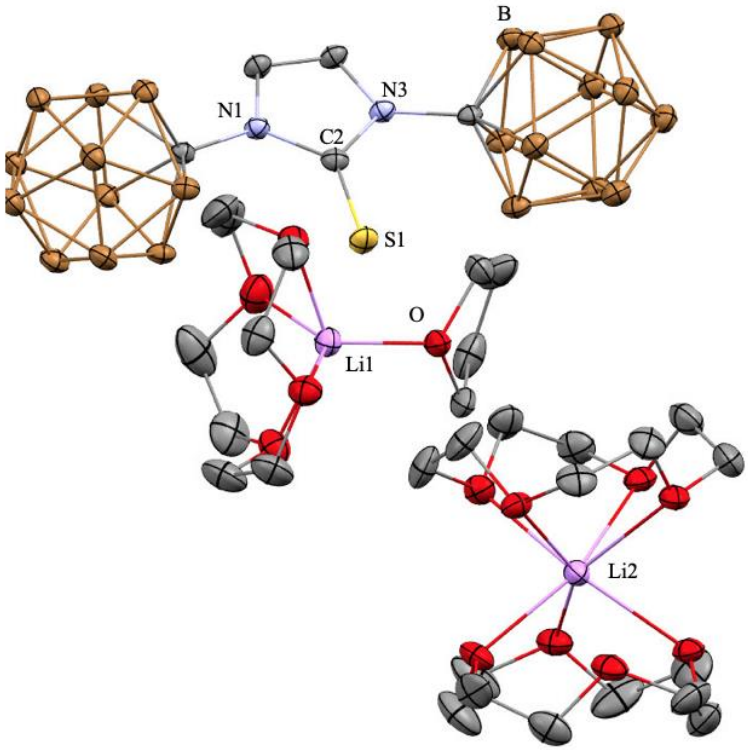

Figure 2-5 Solid state structure of **41[2Li$^+$]**. Hydrogen atoms are omitted for clarity. N = blue, C = black, O = red, Li = pink, S = yellow, B = brown.

Crystals of Thiourea **41[2Li$^+$]** where grown by spiking a THF solution with 12-crown-4. A crystal suitable for single crystal X-ray diffraction study reveals the expected structure with two distant lithium cations, Li1 is coordinated to a molecule of 12-crown-4 and a single molecule of THF and Li2 is coordinated to two molecules of 12-crown-4, Figure 2-5. In the solid both N1 and N3 are planar (sum of CNC angle = 360°), indicating they are both sp^2 hybridized. The sum of the angles around C2 are 360° indicating that the C2 is also sp^2 hybridized. The C2=S1 bond length is 1.666(3) Å is in the reported range of 1.66 to 1.68 Å for standard thiourea.[70-73]

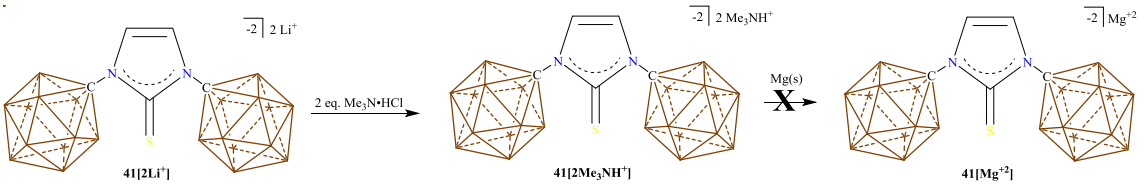

Scheme 2-8 Attempted synthesis of **41[Mg^{+2}]**.

The next step was to create a Mg-ion electrolyte. Since Thiourea **41[2Li^{+}]** was well characterized and carried a -2 charge we thought this would be a better candidate. Our lab has previously reported reduction of trimethylammonium cation with elemental Mg giving a Mg^{+2} counter ion.[74, 75] Using this strategy, we first switched the two-counter ion of Li^{+} for two $HNMe_3^{+}$ ions, Scheme 2-8. Cation exchange was performed by dissolving the **41[2Li^{+}]** in water then adding an excess of two equivalents of trimethylamine hydrochloride which precipitates **41[2Me3NH^{+}]**. The salt is readily collected by filtration and after drying the backbone protons of the imidazolium core can be seen at 7.13 ppm and the methyl protons of Me_3NH^{+} are found at 3.17 ppm.

Next, we reacted **41[Me$_3$NH^{+}]** with elemental Mg. In this reaction we expected the $HNMe_3$ cation to be reduced by the Mg^0 giving NMe_3, H_2 and the thiourea as a magnesium salt **41[Mg^{+2}]**, Scheme 2-8. However, monitoring this reaction by ^{1}H NMR we observed cleavage of the C=S bond and formation imidazolium **29** (see experimental section Figure 2-74 and Figure 2-75). We expect that Mg is a potent enough reducing agent that it is capable of cleaving the C=S bond and forming MgS.

In conclusion we have described the facile synthesis of zwitterionic imidazolium species **34** featuring *N*-hydrocarbon and *N*-carboranyl groups. Deprotonation of this zwitterion with alkali hexamethyl disilazide bases cleanly affords the normal C-2 NHC complexes **35[Li^{+}]** or **35[K^{+}]**. Attempted deprotonation of the zwitterion of **34** with LDA to selectively form an abnormal NHC, leads to an intractable mixture. This result indicates that in order to achieve selective imidazolium backbone deprotonation two anionic *N*-carboranyl groups are required. Double deprotonation reactions of **34** with *n*-BuLi result in the selective formation of C-2/C-5 lithiated species **36**, revealing an unprecedented directing

effect of the anionic icosahedral carborane substituent. We then addressed the aryl group tunability of the imidazolium and created a Dip substituted zwitterionic imidazolium **38**. We were able to selectively deprotonate this imidazolium for the C-2 deprotonated NHC **39**. Lastly we generated thioureas **40** and **41** and tested **41[Mg^{+2}]** as a potential Mg-ion electrolyte but found cleavage of the C=S bond upon reduction of **41[2Me_3NH^+]** with elemental Mg. We are currently investigating the implementation of these novel NHCs in catalysis.

2.5 Experimental

General Considerations:

All manipulations were carried out using standard Schlenk or glovebox techniques under a dinitrogen or argon atmosphere unless otherwise stated. Dry solvents were obtained via distillation under argon from potassium (benzene and toluene), calcium hydride (acetonitrile and methylene chloride), sodium-potassium alloy (diethyl ether), or potassium benzophenone ketyl (tetrahydrofuran). Cesium 1-amino-1-carba-*closo*-undecaborate **3NH_2[Cs^+]** was prepared following the procedure by Jelínek and co-works.[54] The 1-mesityl-3-acetoxyoxazolinium tetrafluoroborate **33** and 1-(2,6-diisopropylphenyl)-3-acetoxyoxazolinium tetrafluoroborate **37** was prepared via the Fürstner synthetic route.[61] Unless specifically stated, reagents were purchased from commercial vendors and used without further purification. Nuclear magnetic resonance (NMR) spectroscopy was carried out using: Bruker Avance 300 MHz, Bruker Avance 600 MHz, Varian Inova 300 MHz, or Varian Inova 400 MHz spectrometers. NMR chemical shifts are reported in parts per million (ppm) with ^{1}H and ^{13}C chemical shifts referenced to the residual non-deutero solvent. The ^{11}B NMR chemical shifts were externally referenced to BF_3•OEt_2. The ^{11}B-^{1}H coupling constants from ^{11}B spectra are reported when possible. The 2D NOESY data were collected using a modified version of the standard Bruker NOESY sequence 'noesygpph'. Decoupling of ^{11}B in the F1 dimension was achieved by inserting a 180 degree ^{11}B pulse midway through the t1 evolution period. Decoupling of ^{11}B in the F2 dimension was achieved by applying broadband GARP ^{11}B decoupling during the acquisition period. Data sets were collected as 1024 x 256 complex point arrays using States-TPPI phase cycling. Sixteen transients were averaged for each t1 increment. Data processing consisted of linear prediction in F1, application of a

90 degree shifted sine bell apodization function in both F1 and F2, and Fourier Transformation with zero filling resulting in a 1024 x 1024 point real array. Two IR instruments were used, PIKE MB3000 and a PerkinElmer Spectrum One. High-resolution mass spectrometry (HRMS) was collected on an Agilent Technologies 6210 (TOF LC/MS) featuring electrospray ionization. Melting points were acquired using a Büchi Melting Point B-545 automatic. Complete crystallographic data for compounds **35[Li$^+$]** and **36** are available free of charge from the Cambridge Crystallographic Data Center under reference numbers 1028440 and 1028443, respectively. These structures can be accessed at : http://www.ccdc.cam.ac.uk/Community/Requestastructure/Pages/DataRequest.aspx.

Synthesis of the Zwitterionic Imidazolium, 23:

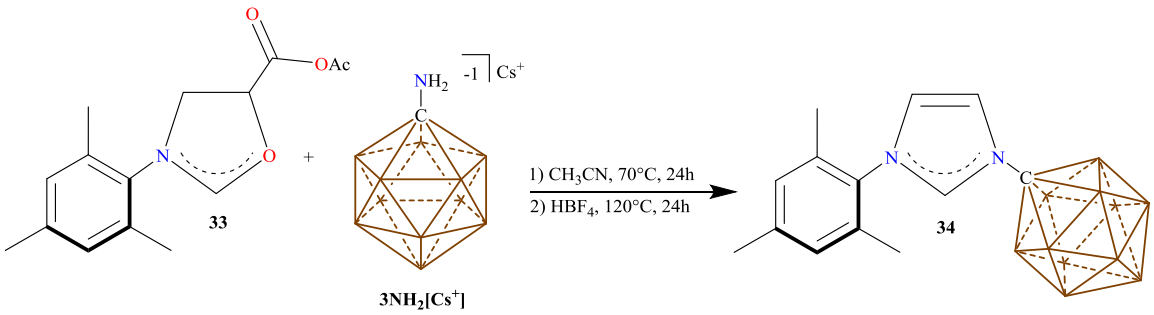

Scheme 2-9 Synthesis of zwitterionic imidazolium, **34**.

A Teflon stoppered Schlenk was equipped with a stir bar and loaded with compound **33** (1.515 g, 4.52 mmol) and cesium 1-amino-1-carba-*closo*-undecaborate **3NH$_2$[Cs$^+$]** (1.45 g, 4.97 mmol). Dry acetonitrile (4 mL) was added to the schlenk which was tightly sealed and heated to 70°C for 24 hours. To the crude reaction mixture tetrafluoroboric acid diethyl ether complex (1.35 mL, 1.61 mmol) was added. The Schlenk was sealed and heated to 110°C for 24 hours (safety note: heating sealed containers is dangerous and was always done in a hood behind a blast shield using a thick-walled Schlenk tube, appropriate precautions should always be taken). The solution was cooled then poured into a beaker

containing sodium bicarbonate (200 mL). Methylene chloride (200 mL) was added and the aqueous phase was further washed with methylene chloride (2 × 100 ml). The organic phase was collected, washed with brine (300 ml) and dried over magnesium sulfate. All volatiles were subsequently removed under vacuum to give a brown solid. This solid was crystallized from a concentrated acetonitrile solution at 5°C to give **34** as light colorless blocks. Further concentration of the supernate led to two further crops of crystals (1.14 g, 77%). ^{1}H NMR (500 MHz, acetonitrile-d_3, 25°C): δ = 8.76 (dd, $^{4}J(H,H)$ = 2.00, 1.75 Hz, 1H), 7.73 (dd, $^{3}J(H,H)$ = 2.00 Hz**,** $^{4}J(H,H)$ = 1.75 Hz, 1H), 7.34 (dd, $^{4}J(H,H)$ = 2.00 Hz, $^{3}J(H,H)$ = 2.00 Hz , 1H), 7.09 (s, 2H), 2.34 (s, 3H), 1.98 (s, 6H), 2.72-1.22 (bm, 11H, B-H). ^{1}H[^{11}B] NMR (192.5 MHz, acetonitrile-d_3, 25°C): δ = 8.76 (1H), 7.73 (1H), 7.34 (1H), 7.09 (2H), 2.34 (3H), 1.98 (6H), 2.14 (5H), 1.68 (6H). ^{13}C[^{1}H] NMR (125 MHz, acetone-d_6, 25°C): δ = 142.0, 137.6, 135.3, 132.0, 130.3, 124.8, 124.7, 76.4, 21.0, 17.2 ppm. ^{11}B[^{1}H] NMR (192.5 MHz, acetonitrile-d_3, 25°C): δ = -8.3, -12.7, -13.3 ppm. ^{11}B[^{1}H] NMR (96 MHz, acetonitrile-d_3, 25°C) = -9.2, -13.5 ppm. ^{11}B NMR (96 MHz, THF-d_8, 25°C): δ = -8.7 ($^{1}J(H,B)$ = 134.4 Hz), -13.4 ($^{1}J(H,B)$ = 137.3 Hz). IR (solid, ATR, 25°C): B-H stretch = 2550 cm^{-1}. HRMS (negative mode ESI/APCI) [M-H]$^{-}$ m/z calc'd = 327.3041 : Found = 327.3041, [M+Cl]$^{-}$ m/z calc'd = 363.2807 : Found = 363.2825. m.p. = 286.8 to 287.7°C.

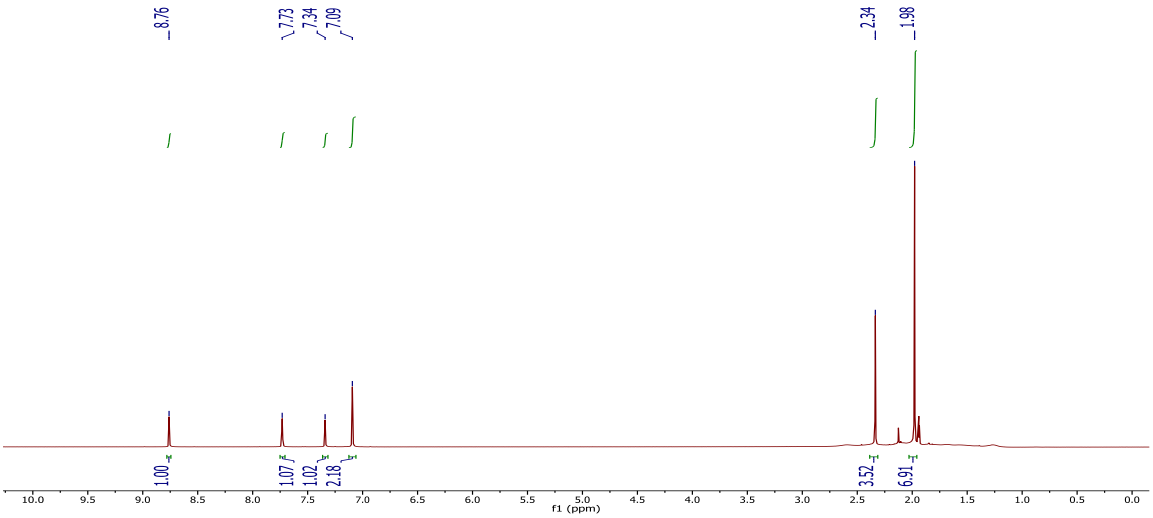

Figure 2-6 ^{1}H-NMR spectrum of **34** in acetonitrile-d_3. The peak at 2.2 ppm is due to water in the deuterated solvent.

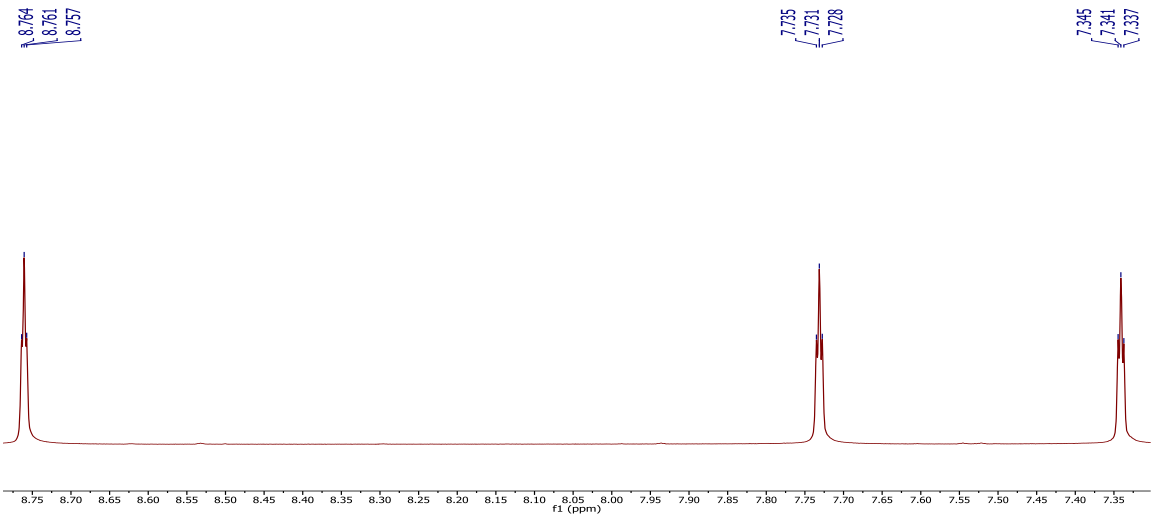

Figure 2-7 An expanded view of the aromatic region of the ^{1}H-NMR of **34** in THF-d_8, showing the small *J*-coupling of the imidazolium protons.

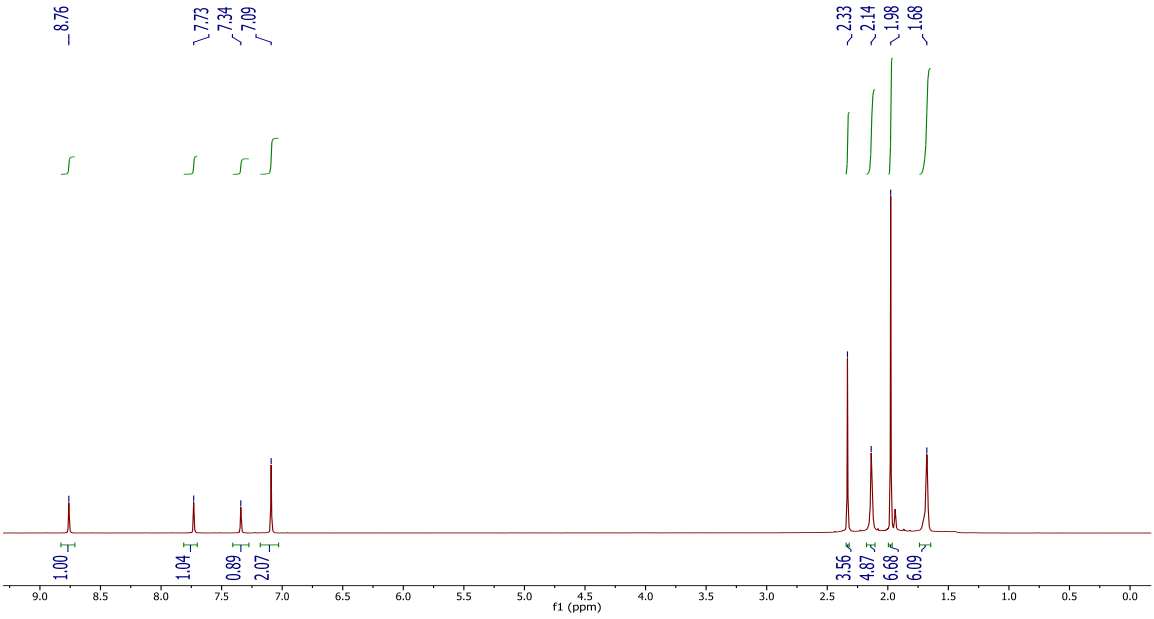

Figure 2-8 ^{1}H[^{11}B] NMR spectrum of **34** in acetonitrile-d_3. The boron hydrides appear at 2.14 and 1.68 ppm.

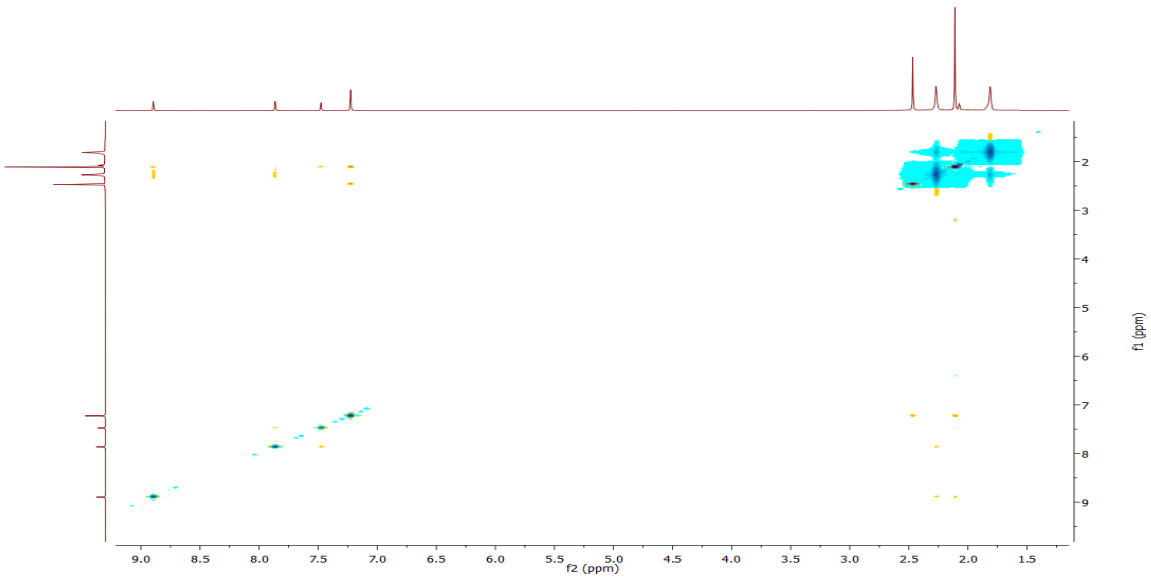

Figure 2-9 $^{1}H[^{11}B]$-NOESY NMR spectrum of **34** in acetonitrile-$d_{3,}$ mixing time = 500 ms.

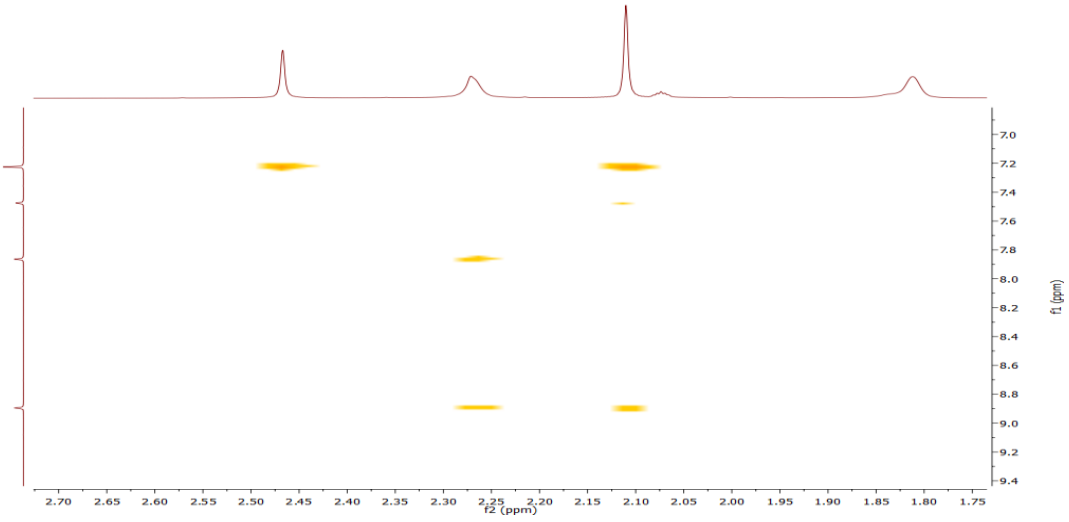

Figure 2-10 $^{1}H[^{11}B]$-NOESY NMR spectrum of **34** with an enlargement of the imidazolium cross-peaks and *ortho* mesityl methyl groups.

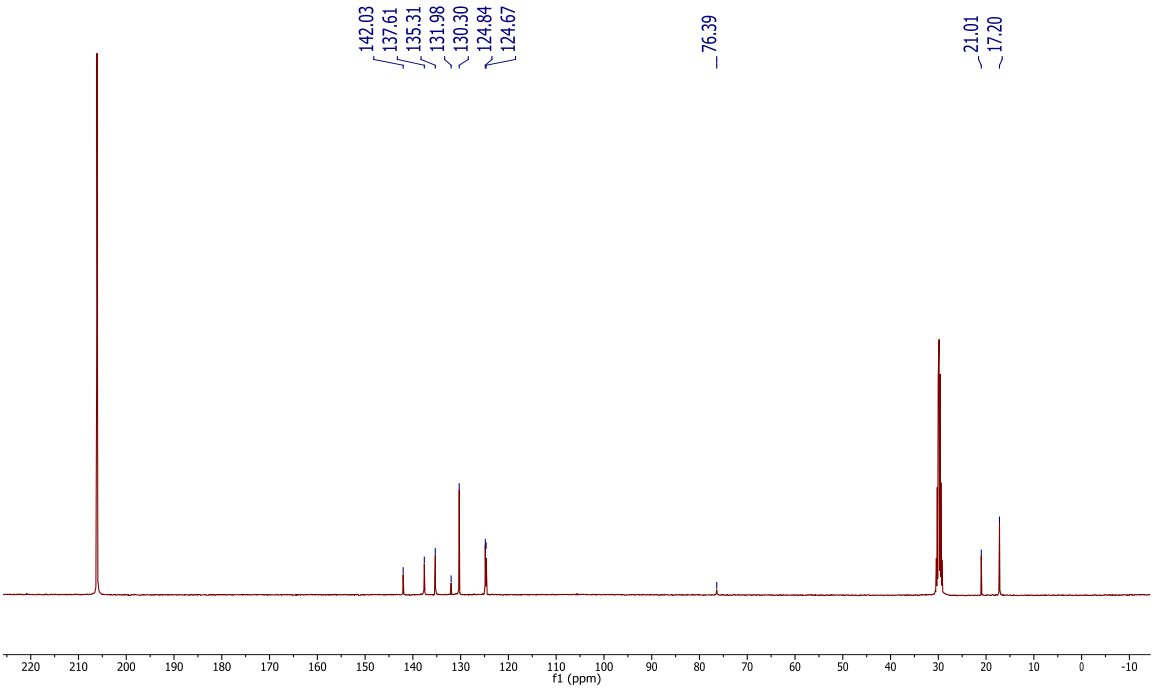

Figure 2-11 $^{13}C[^{1}H]$ NMR of **34** in acetone-d_6. Acetone-d_6 is seen at 206.12 and 29.84 ppm.

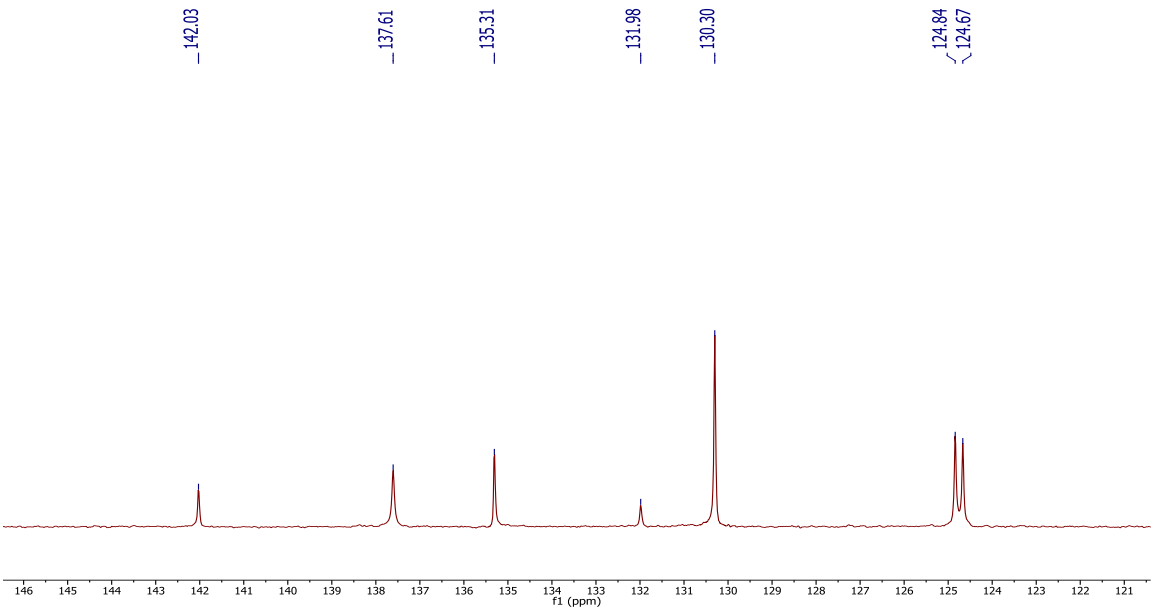

Figure 2-12 Detail of the downfield region of the $^{13}C[^{1}H]$ NMR of **34** in acetone-d_6.

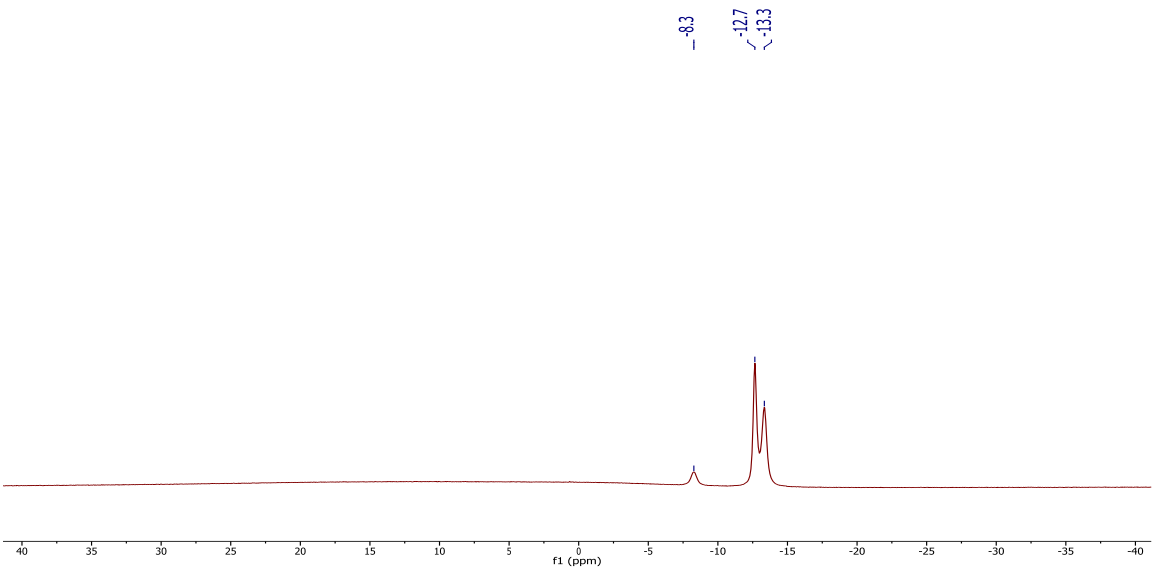

Figure 2-13 $^{11}B[^{1}H]$ NMR spectrum of **34** in acetonitrile-d_3.

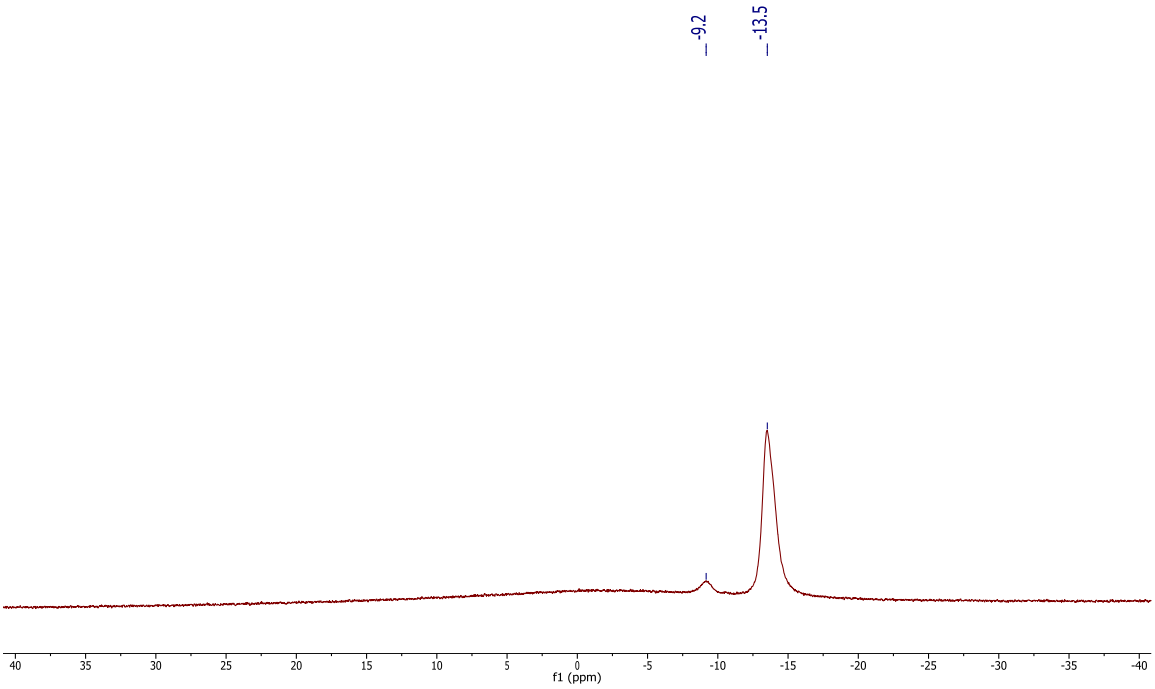

Figure 2-14 $^{11}B[^{1}H]$ NMR spectrum of **34** in acetonitrile-d_3.

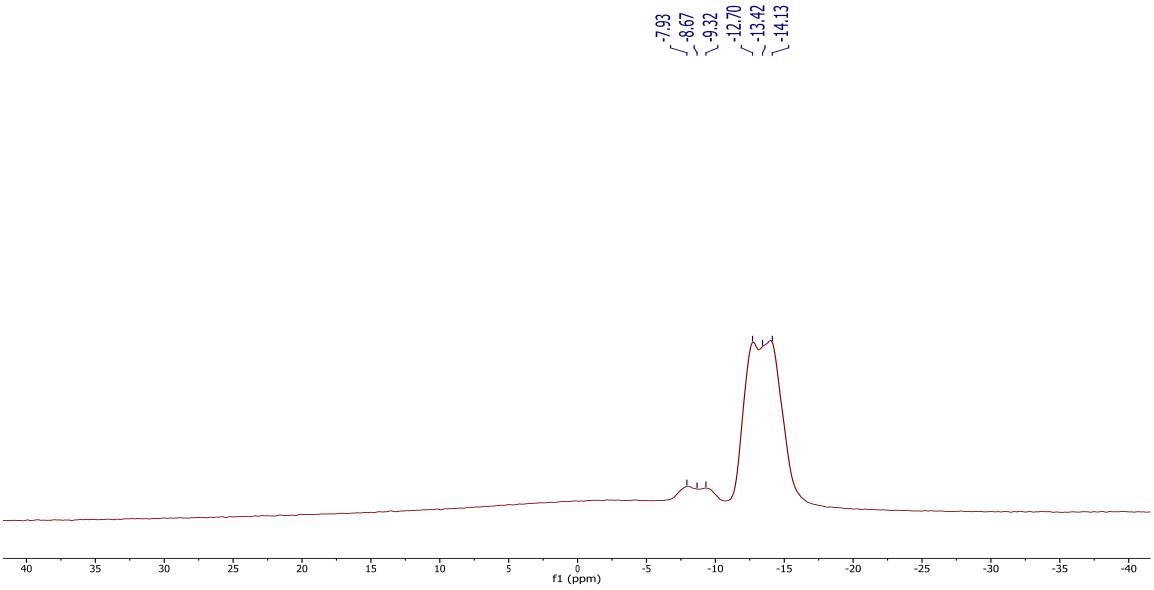

Figure 2-15 ^{11}B NMR of **34** in acetonitrile-d_6 showing the ^{1}J B-H coupling.

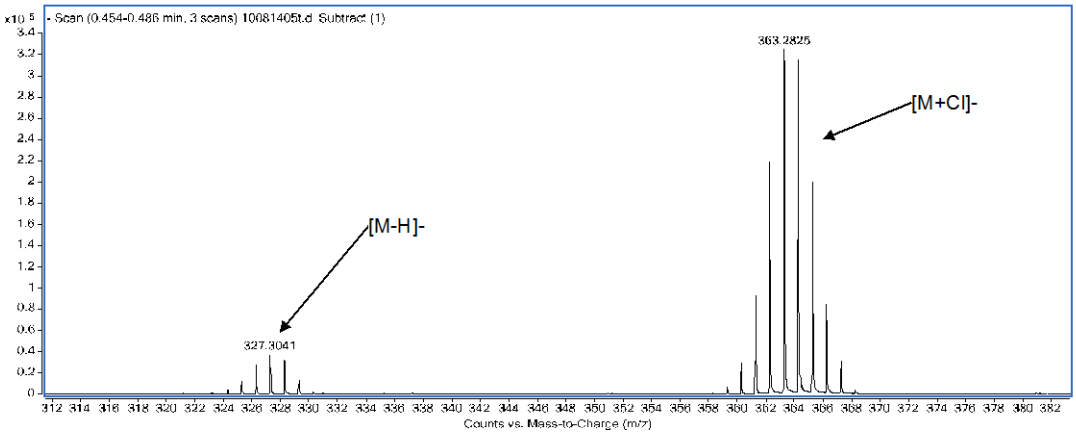

Figure 2-16 Mass spectrum (–ve ESI/APC) of **34**.

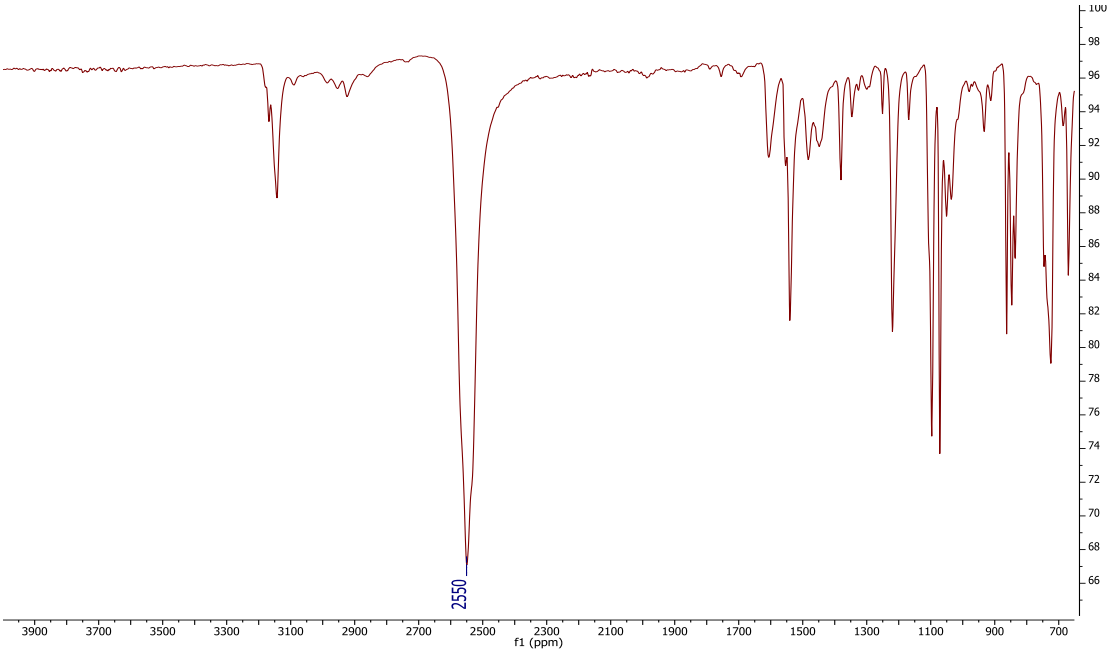

Figure 2-17 IR spectrum of solid **34**. The B-H stretches appear at 2550 cm^{-1}.

Synthesis of the Monoanionic Lithium Carbene, 35[Li^+]:

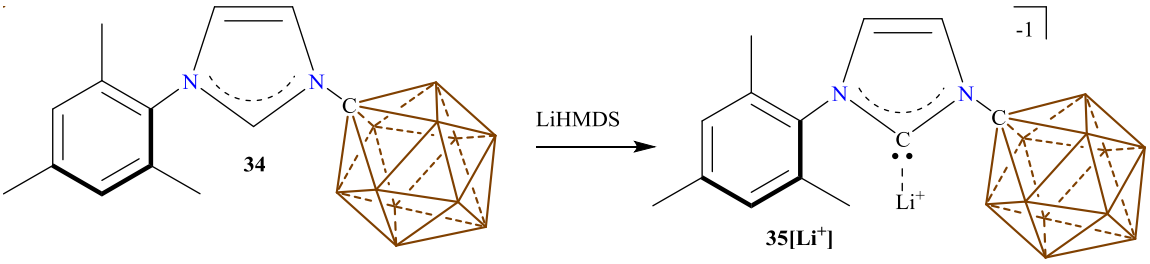

Scheme 2-10 Synthesis of the monoanionic lithium carbene, **35[Li^+]**.

A glass scintillation vial equipped with a stir bar was loaded with **34** (60.0 mg, 0.18 mmol) and lithium hexamethyldisilazide (61.2 mg, 0.37 mmol). THF (1.2 mL) was added to the stirring mixture and allowed to react for one hour. After an hour a yellow-brown precipitate formed and the supernate was carefully removed. The solid was subsequently washed with ether (3 × 3 mL) and dried *in vacuo* to furnish the desired compound, **35[Li^+]** (78.0 mg, 76%). Single crystals of **35[Li^+]** suitable for X-ray diffraction analysis could be obtained as pale yellow plates from a concentrated THF solution. ^{1}H NMR (300 MHz,

THF-d_8, 25°C): δ = 7.40 (d, $^3J(H,H)$ = 1.5 Hz, 1H), 6.98 (s, 2H), 6.79 (d, $^3J(H,H)$ = 1.5 Hz, 1H), 2.30 (s, 3H), 1.95 (s, 6H), 3.00 – 0.72 (bm, 11H, B-H). $^{11}B[^1H]$ NMR (96MHz, THF, 25°C): δ = -10.0, -11.3 ppm. ^7Li NMR (233 MHz, THF, 25°C) = 2.29 ppm. IR (solid, ATR, 25°C): B-H stretch = 2655, 2557, 2523 cm^{-1}.

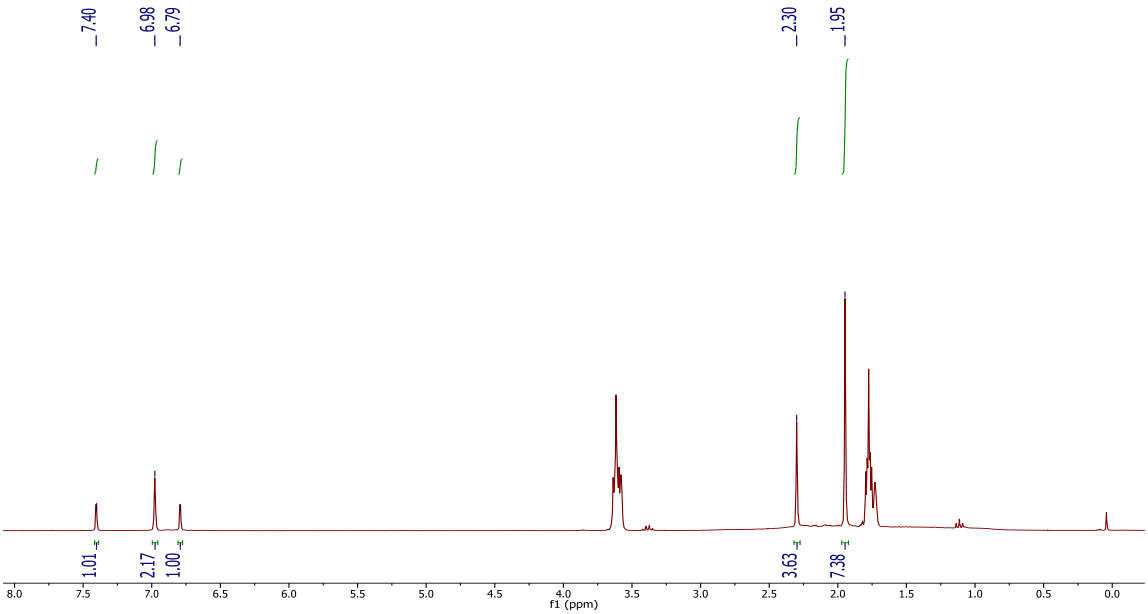

Figure 2-18 ^{1}H-NMR spectrum of **35[Li$^+$]** in THF-d_8. The peak near 0 ppm is due to coordinated HMDS. Traces of diethyl ether can be seen at 3.4 and 1.1 ppm.

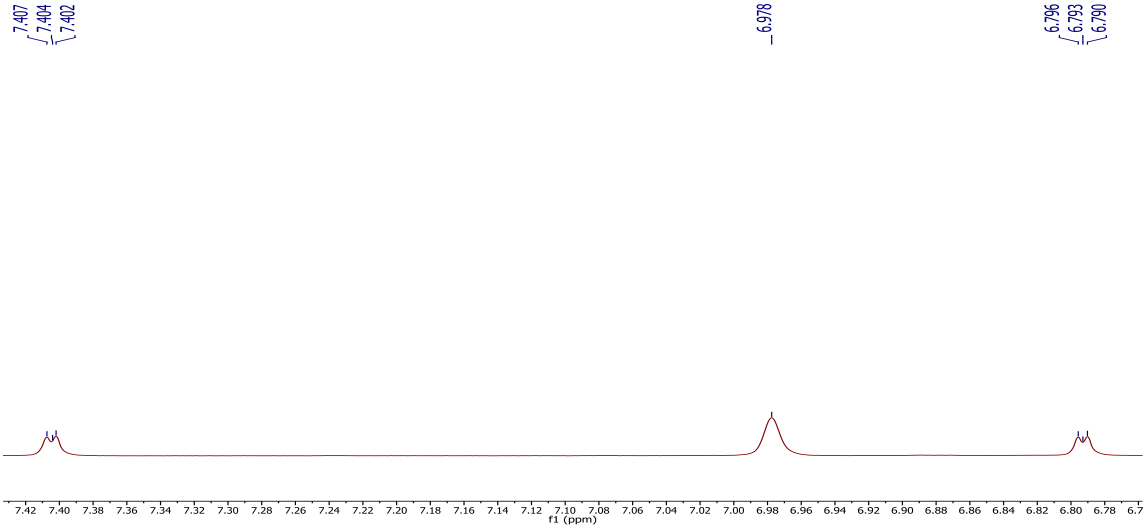

Figure 2-19 An expanded view of the aromatic region of the ^{1}H-NMR of **35[Li$^+$]** in THF-d_8, showing the small ^3J-coupling of the imidazolylidene protons.

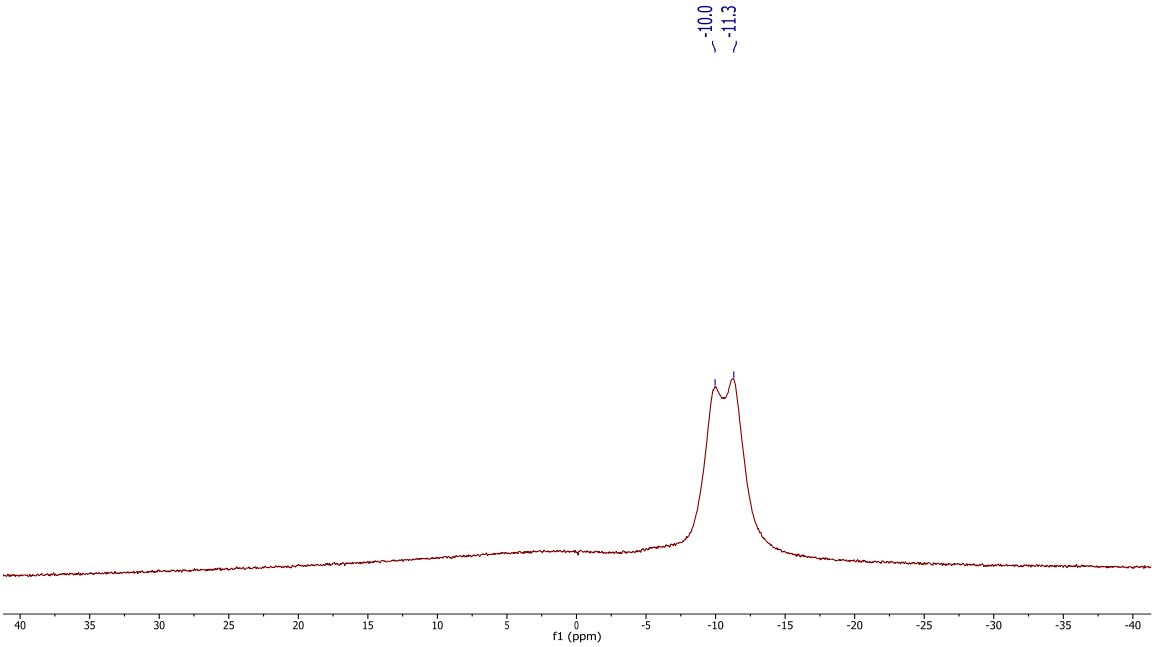

Figure 2-20 $^{11}B[^{1}H]$-NMR spectrum of **35[Li^{+}]** in THF.

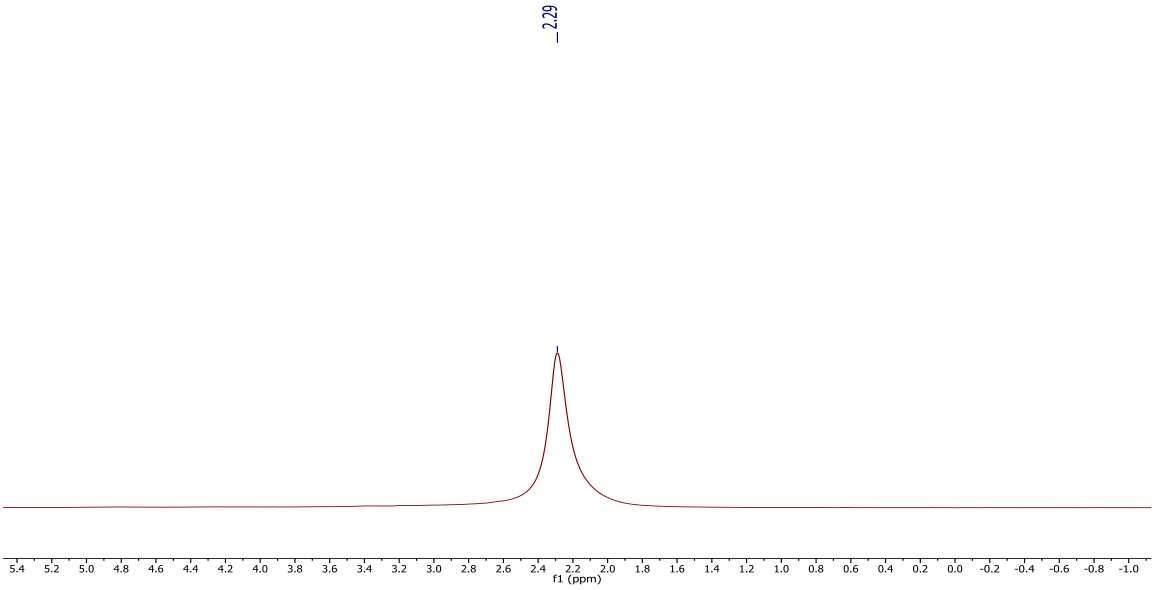

Figure 2-21 ^{7}Li-NMR spectrum of **35[Li^{+}]** in THF.

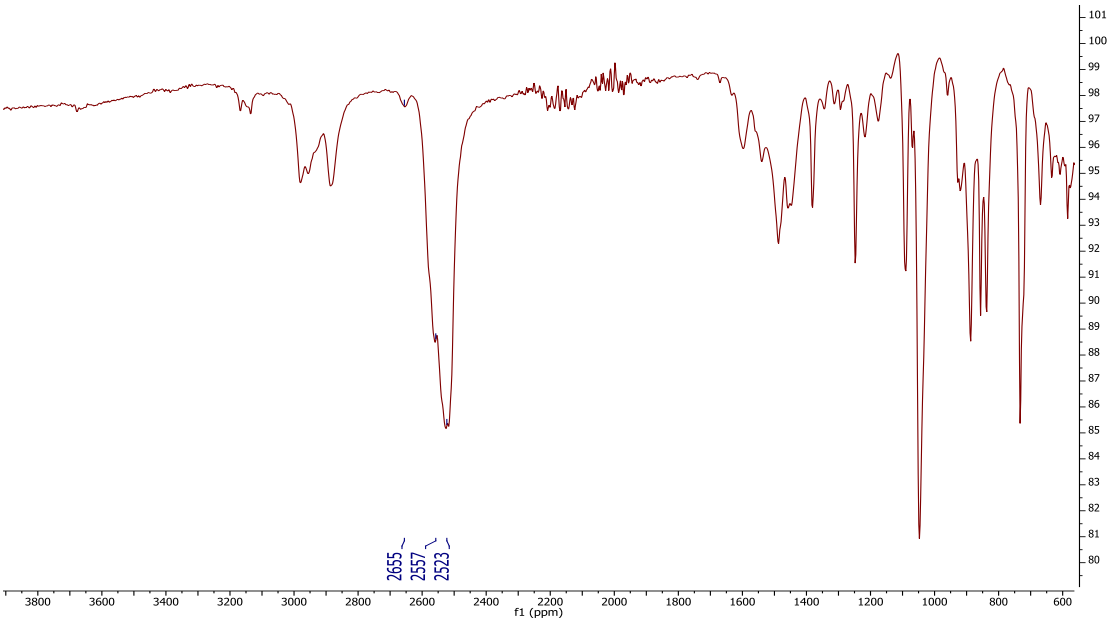

Figure 2-22 IR spectrum of solid **35[Li$^+$]**. The B-H stretches at 2655, 2557 and 2523 cm^{-1}.

Synthesis of the Monoanionic Potassium Carbene, 35[K$^+$]:

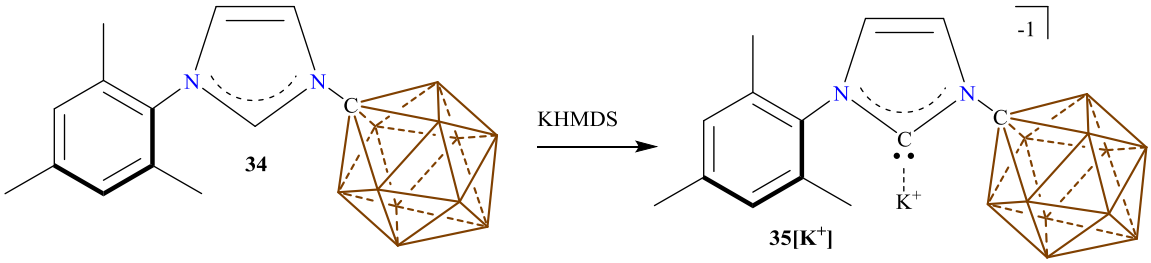

Scheme 2-11 Synthesis of monoanionic potassium carbene, **35[K$^+$]**.

A scintillation glass vial was equipt with a stir bar and loaded with **34** (1.23 g, 3.75 mmol) and KHMDS (0.63 g, 5.61 mmol). A minimal amount of THF (5 mL) was added to dissolve the gently stirring solids. The reaction ran for an hour before the reaction mixture was filtered and crystallized by adding diethyl ether (2 mL) to the THF solution. Light brown cubes of **35[K$^+$]**•$(THF)_{2.5}(ether)_{3.0}$ formed at -30°C. (1.24 g, 61%). ^{1}H NMR (300 MHz, benzene-d_6, 25°C): δ = 7.29 (d, $^3J(H,H)$ = 1.8 Hz, 1H), 6.66 (s, 2H),

5.85 (d, $^{3}J(H,H)$ = 1.8 Hz, 1H), 2.10 (s, 3H), 1.72 (s, 6H), 3.87-1.00 (bm, 11H, B-H). $^{1}H[^{11}B]$ NMR (96 MHz, benzene-d_6, 25°C): δ = 7.29 (1H), 6.65 (2H), 5.85 (1H), 2.75 (5H), 2.34 (5H), 2.10 (3H), 2.01 (5), 1.73 (6H) ppm. ^{1}H NMR (400 MHz, THF-d_8, 25°C): δ = 7.35 (d, $^{3}J(H,H)$ = 1.6 Hz, 1H), 6.96 (s, 2H) ,6.70 (d, $^{3}J(H,H)$ = 1.6 Hz, 1H), 2.29 (s, 3H), 1.94 (s, 6H), 2.88-0.84 (bm, 11H, B-H). $^{1}H[^{11}B]$ NMR (96 MHz, THF-d_8, 25°C): δ = 7.34 (1H), 6.95 (2H), 6.70 (1H), 2.29 (3H), 2.13 (5H), 1.94 (6H), 1.63 (5H) ppm. $^{13}C[^{1}H]$ NMR (100 MHz, THF-d_8, 25°C): δ = 211.3, 139.0, 138.1, 135.7, 129.4, 121.6, 113.0, 82.0, 20.9, 12.6. $^{11}B[^{1}H]$ NMR (96 MHz, THF-d_8, 25°C): δ = -9.9, -13.9 ppm. ^{11}B NMR (96 MHz, THF-d_8, 25°C): δ = -9.4 ($^{1}J(H,B)$ = 129.6 Hz), -13.6 ($^{1}J(H,B)$ = 141.1 Hz) ppm. IR (solid, ATR, 25°C): B-H stretch = 2670, 2567, 2535 cm^{-1}. m.p. = 62.4 to 63.4°C.

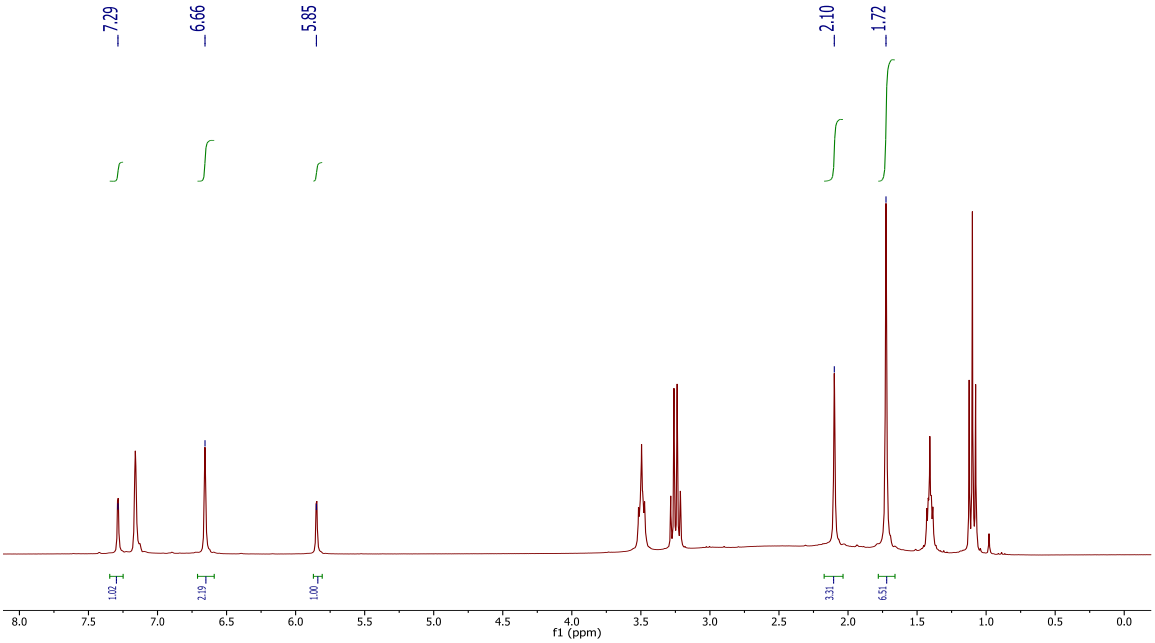

Figure 2-23 ^{1}H-NMR of **35[K^{+}]** in benzene-d_6. Liberated solvents: 2.5 THF molecules and 3.0 Et_2O molecules.

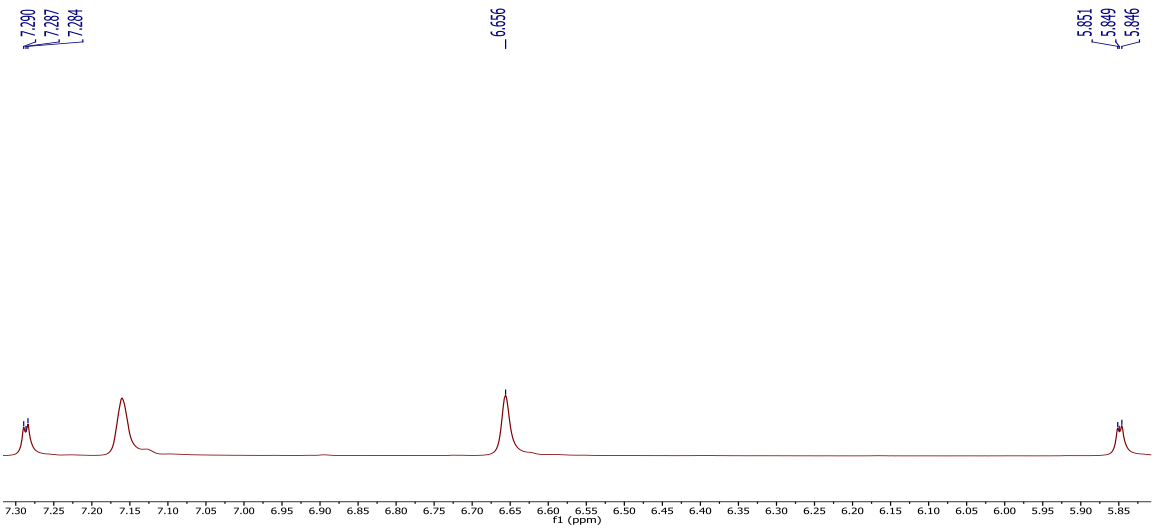

Figure 2-24 An expanded view of the aromatic region of the ^{1}H-NMR of **35[K^{+}]** in benzene-d$_6$, showing the small ^{3}J-coupling of the imidazolylidene protons.

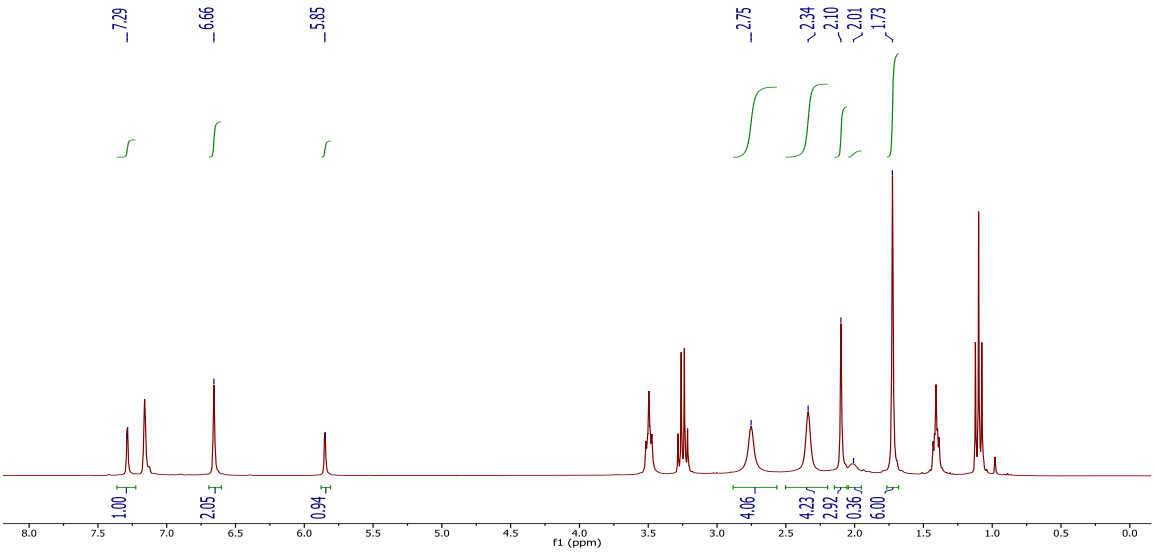

Figure 2-25 ^{1}H[^{11}B]-NMR spectrum of **35[K^{+}]** in benzene-d$_6$. The boron hydrides appear at 2.75, 2.34 and 2.01 ppm.

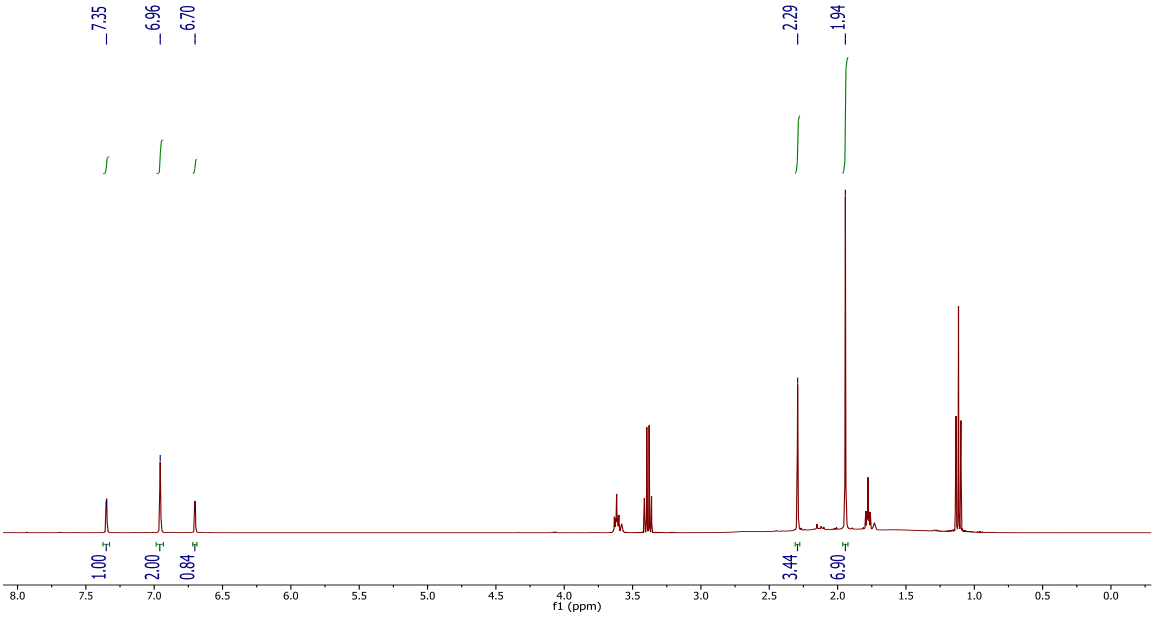

Figure 2-26 ^{1}H-NMR spectrum of **35[K^{+}]** in THF-d_8. Liberated solvents: 1.5 Et_2O molecules.

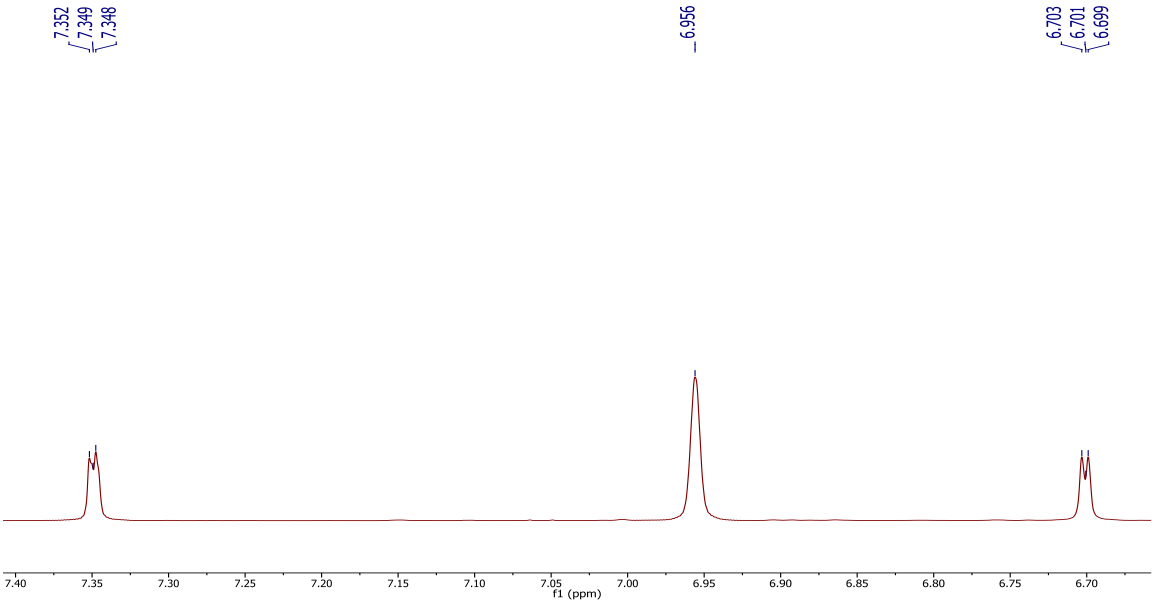

Figure 2-27 An expanded view of the aromatic region of the ^{1}H-NMR of **35[K^{+}]** in THF-d_8, showing the small ^{3}J-coupling of the imidazolylidene protons.

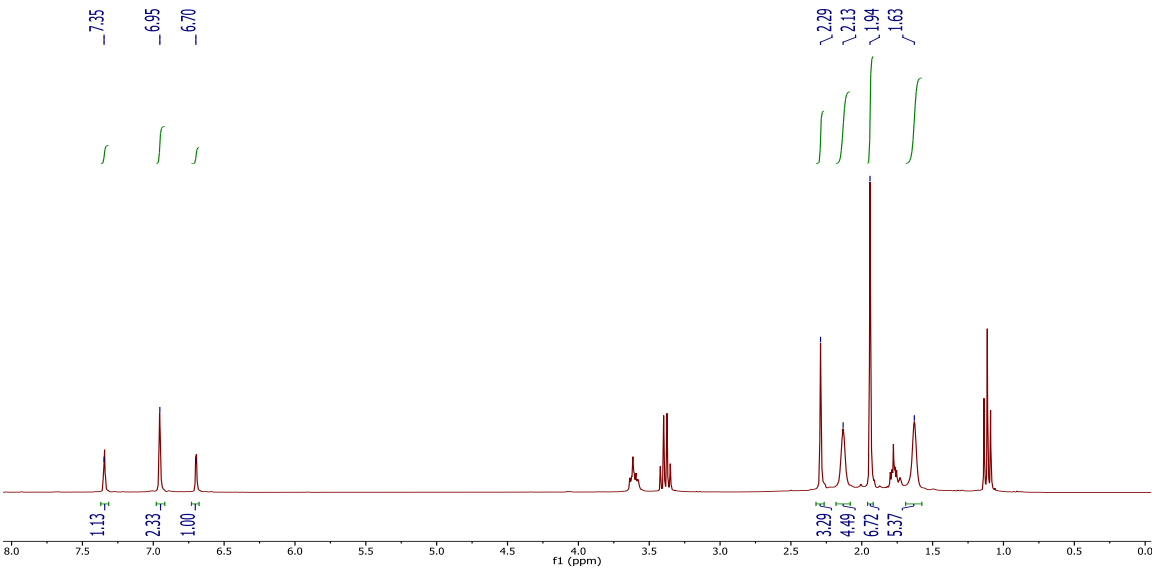

Figure 2-28 $^{1}H[^{11}B]$ NMR spectrum of **35[K^{+}]** in THF-d_8. The boron hydrides appear at 2.13 and 1.63 ppm.

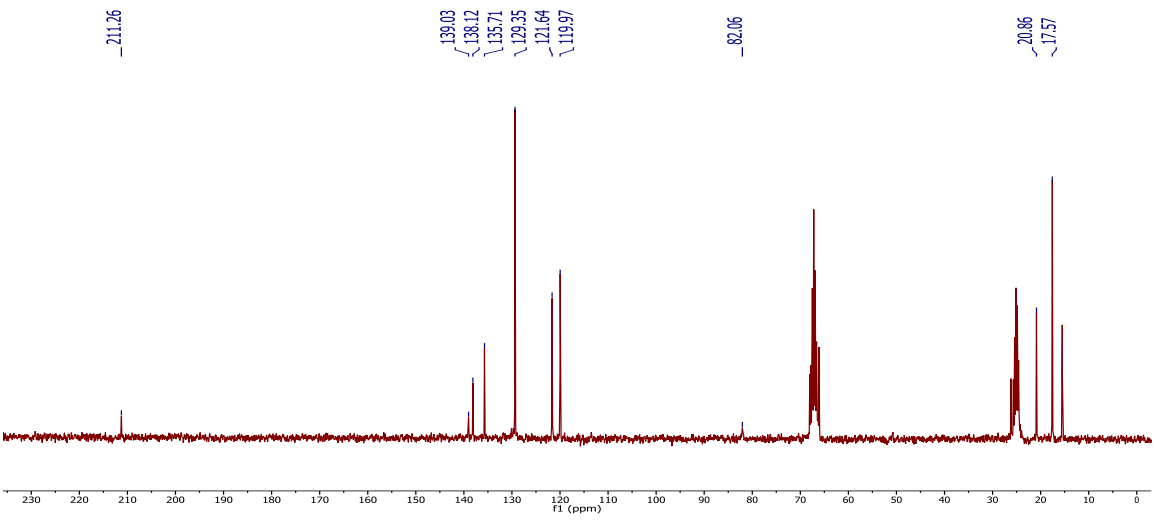

Figure 2-29 $^{13}C[^{1}H]$-NMR of **35[K^{+}]** in THF-d_8. Liberated diethyl ether appears at 15.50 and 66.12 ppm. THF-d_6 is present at 25.17 and 67.21 ppm.

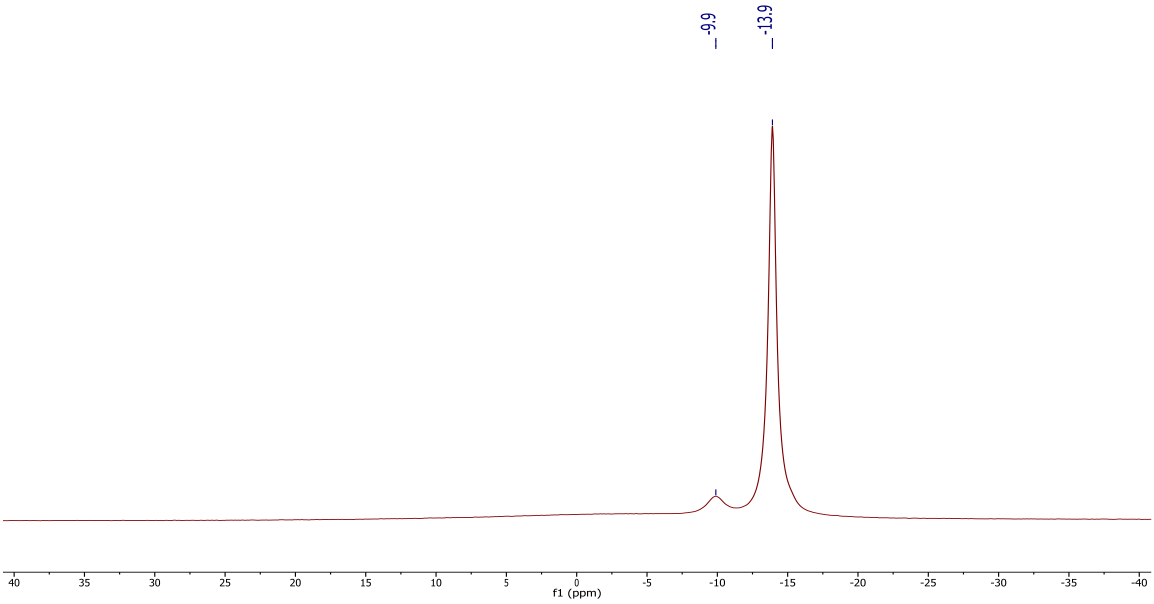

Figure 2-30 $^{11}B[^{1}H]$-NMR of **35[K^{+}]** in THF-d_8.

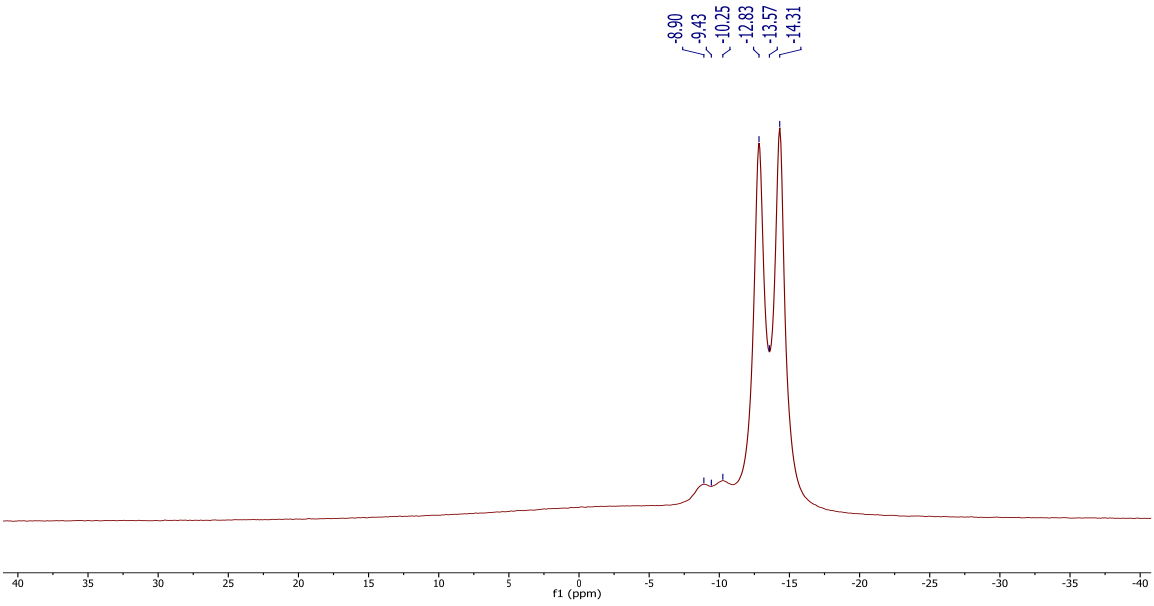

Figure 2-31 ^{11}B NMR of **35[K^{+}]** in THF-d_8 showing the ^{1}J B-H coupling.

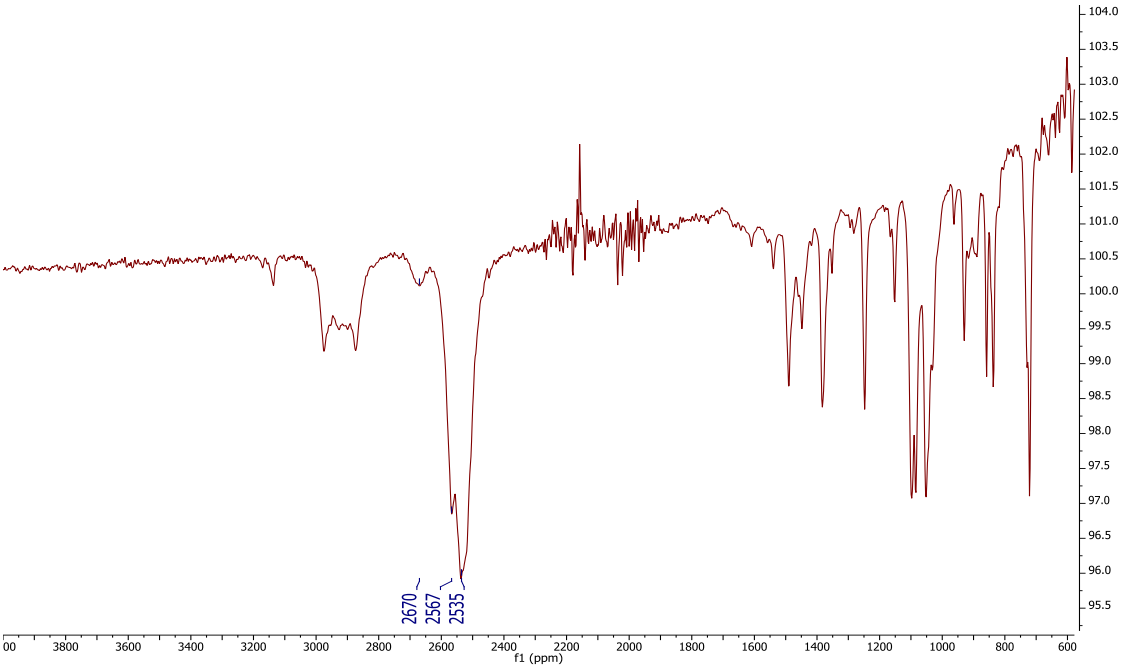

Figure 2-32 IR spectrum of solid **35[K$^+$]**. The B-H stretches at 2670, 2567 and 2535 cm^{-1}.

Synthesis of the Dianionic Lithium Carbene, 36:

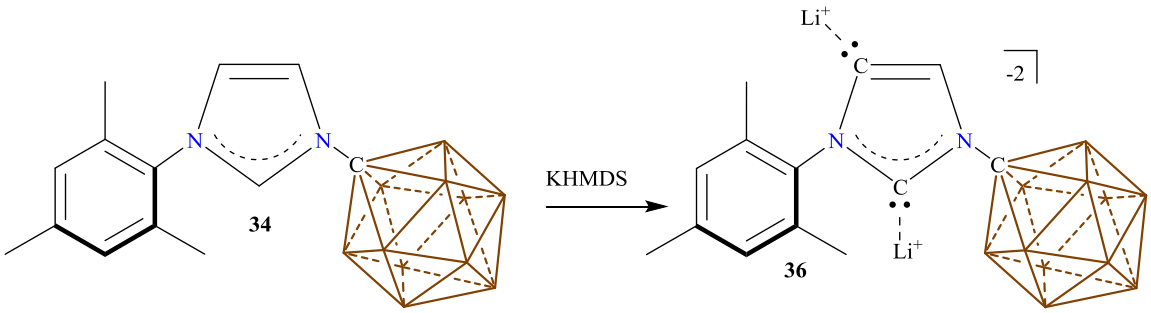

Scheme 2-12 Synthesis of dianionic lithium carbene, **36**.

A scintillation glass vial was equip with a stir bar and loaded with **34** (296.3 mg, 0.90 mmol) and diethyl ether (17 mL). Next, *n*-butyllithium (1.80 mmol) in ether (2 ml) was added to the stirring suspension of **34**. Following the addition of the *n*-butyllithium an oil began to form along the walls of the vial. The reaction mixture was vigorously stirred and scraped with a spatula. This was done periodically

over one hour or until a yellow solid precipitated from the lime-green solution. The reaction was stirred for another hour and then filtered and washed with diethyl ether. The product, **36**•$(Et_2O)_3$, was collected as a yellow solid (487.4 mg, 96%). Single crystals of **36** suitable for X-ray diffraction analysis were grown by layering a concentrated THF solution with diethyl ether. ^{1}H NMR (400 MHz, THF-d_8, 25°C): δ = 6.84 (s, 2H), 6.58 (s, 1H), 2.25 (s, 3H), 1.92 (s, 6H), 2.75-0.76 (bm, 11H, B-H). ^{1}H[^{11}B] NMR (192.5 MHz, THF-d_8, 25°C): δ = 6.84 (2H), 6.58 (1H), 2.25 (3H), 2.05 (4H), 1.92 (6H), 1.58 (5H). ^{13}C[^{1}H] NMR (100 MHz, THF-d_8, 25°C): δ = 193.0, 166.8, 145.6, 135.1, 134.5, 127.6, 127.5, 82.1, 20.0, 17.3. ^{11}B[^{1}H] NMR (96 MHz, THF-d_8, 25°C): δ = -10.5, -10.4 ppm. ^{11}B NMR (96 MHz, THF-d_8, 25°C): δ = -14.2 ($^{1}J(H,B)$ = 130.6 Hz) ppm. ^{7}Li NMR (233 MHz, THF-d_8, 25°C) = 3.54, 2.26 ppm. IR (liquid, THF-d_8, ATR, 25°C): B-H stretch = 2567, 2542 cm^{-1}. m.p. = 171.1 to 173.4 °C.

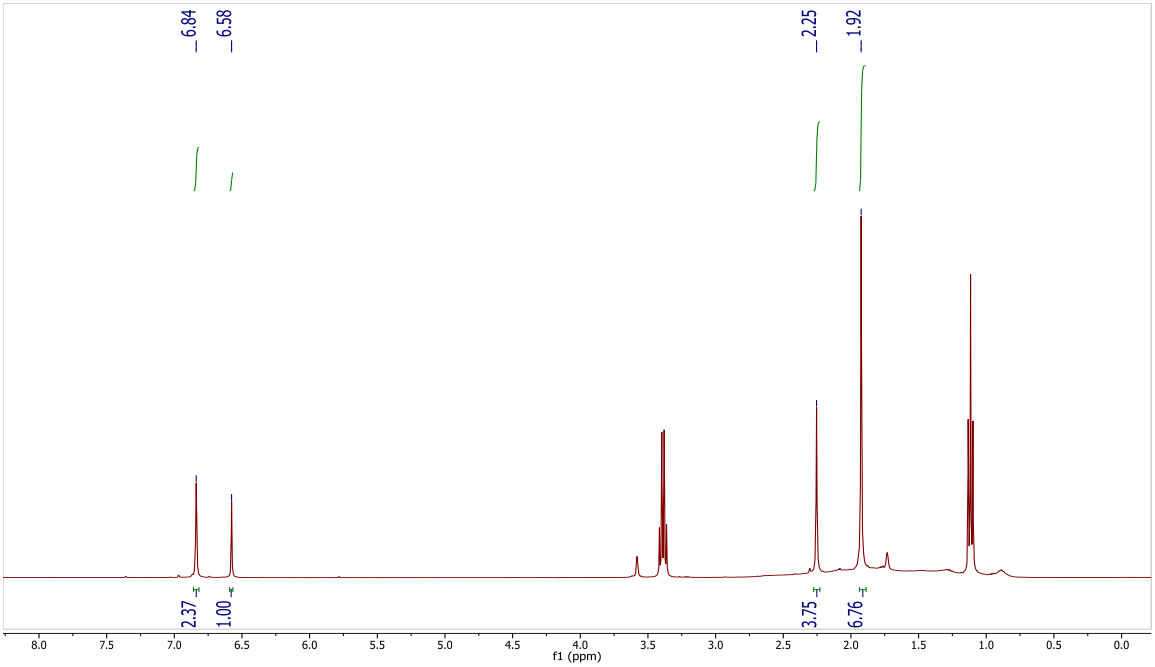

Figure 2-33 ^{1}H-NMR of **36** in THF-d_8. Liberated solvent: 3•Et_2O molecules.

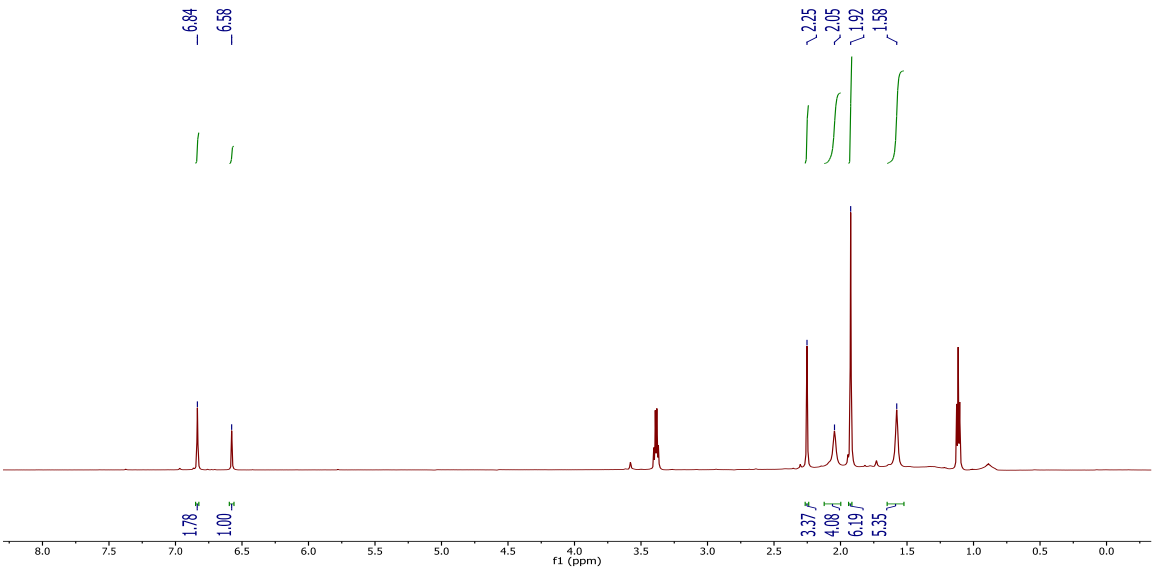

Figure 2-34 $^{1}H[^{11}B]$ NMR of **36** in THF-d_8. The boron hydrides can be seen at 2.05 and 1.58 ppm.

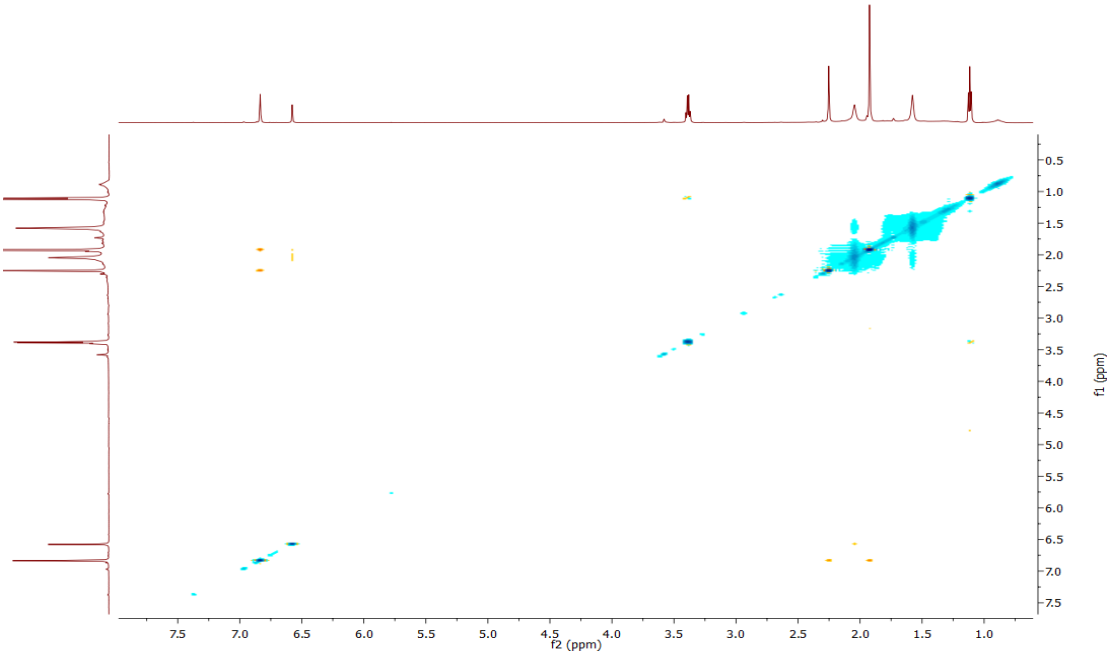

Figure 2-35 $^{1}H[^{11}B]$-NOESY NMR of **36** in THF-d_8, mixing time = 500 ms.

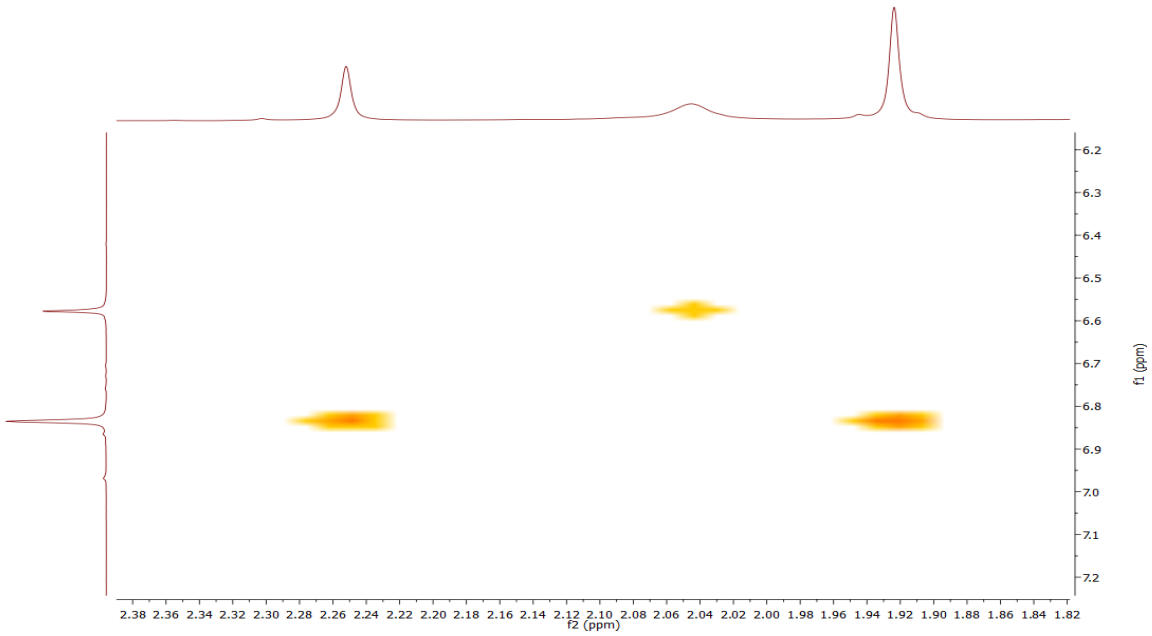

Figure 2-36 $^{1}H[^{11}B]$-NOESY NMR of **36** in THF-d_8, close up of the imidazolylidene cross-peaks.

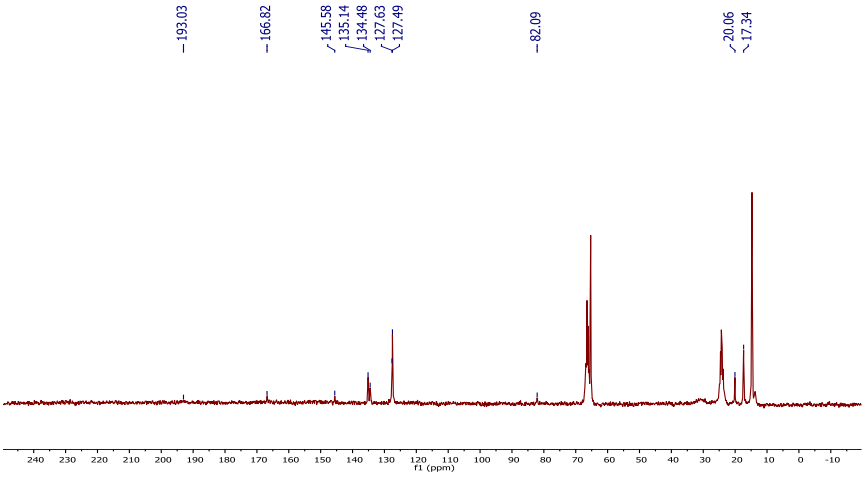

Figure 2-37 $^{13}C[^{1}H]$ NMR of **36** in THF-d_8. Liberated Et_2O appears at 65.31 and 14.70 ppm. THF-d_8 appears at 66.45 and 24.32 ppm.

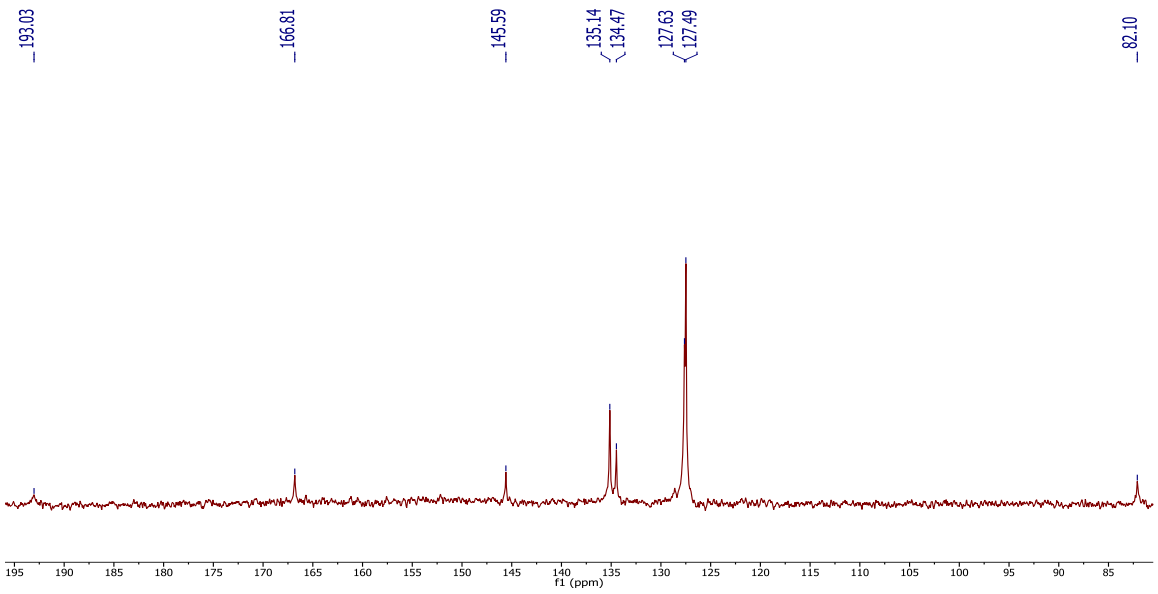

Figure 2-38 An expanded view of the aromatic region of the ^{1}H-NMR of **36** in THF-d_8.

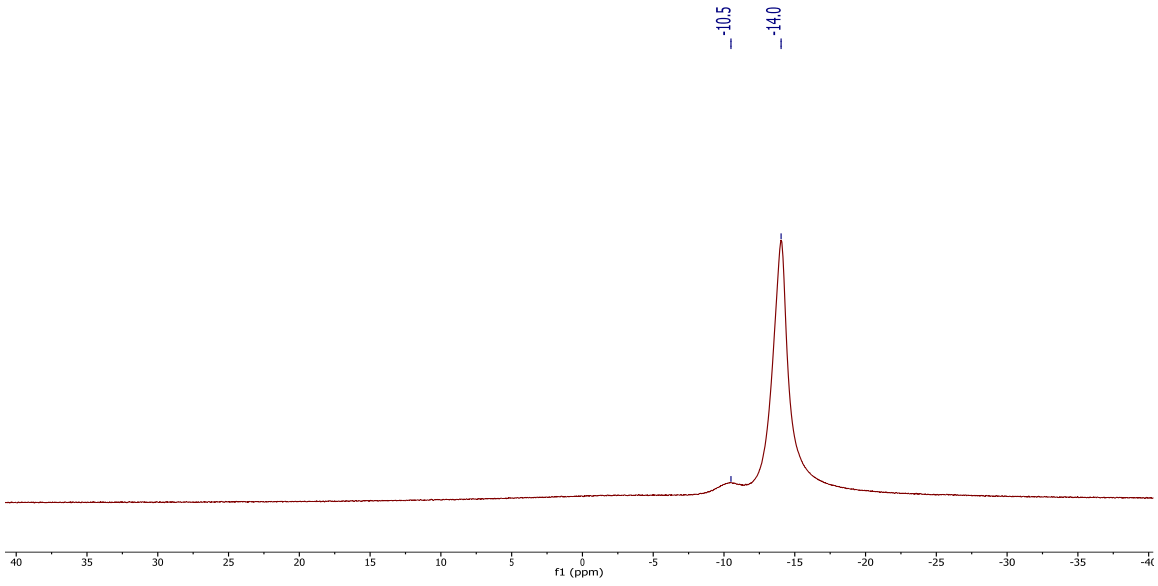

Figure 2-39 ^{11}B[^{1}H] NMR of **36** in THF-d_8.

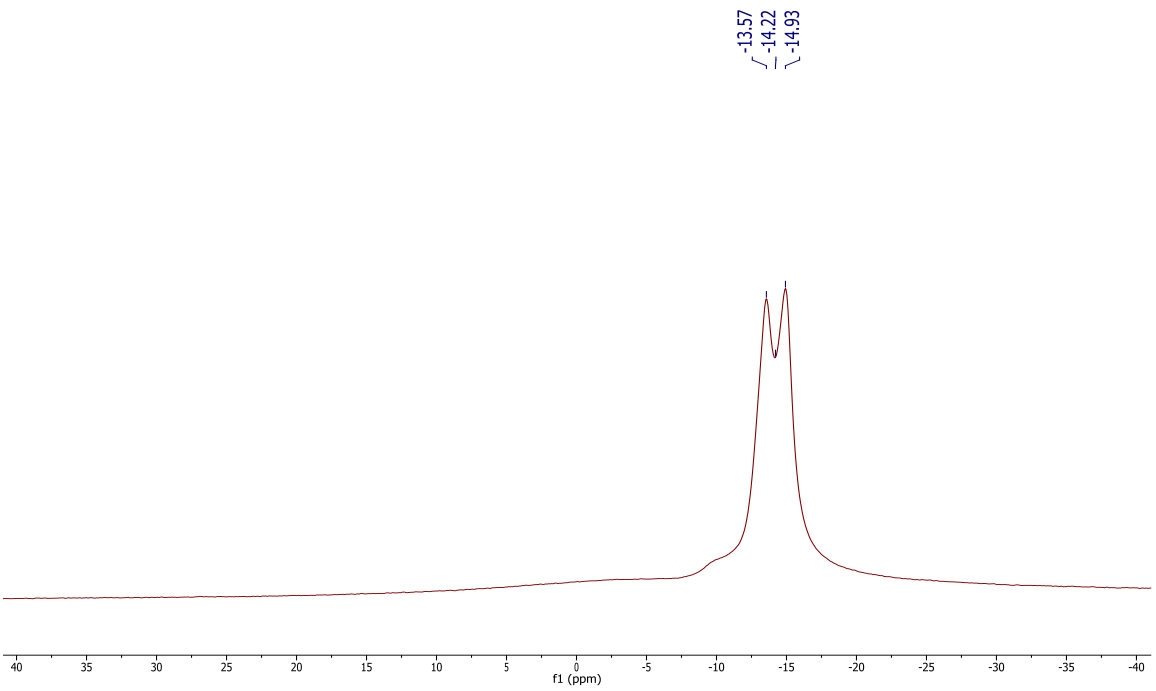

Figure 2-40 ^{11}B NMR of **36** in THF-d_8 showing the ^{1}J B-H coupling.

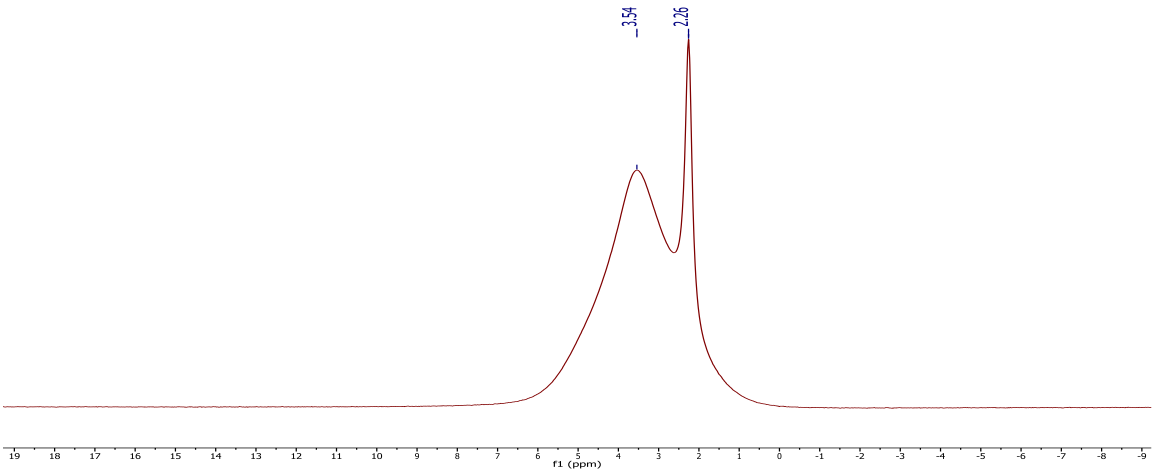

Figure 2-41 ^{7}Li-NMR of **36** in THF-d_8.

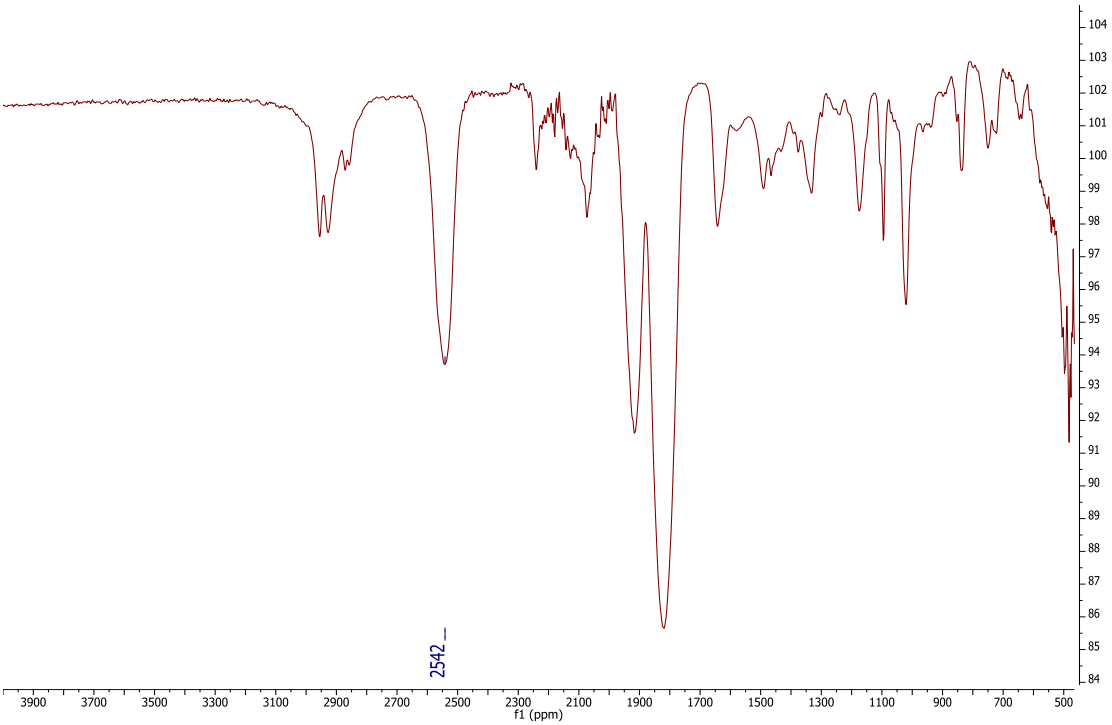

Figure 2-42 IR spectrum of solid **36**. The boron hydrides appear at 2542 and 2567 cm-1.

Synthesis of the zwitterionic imidazolium, 38:

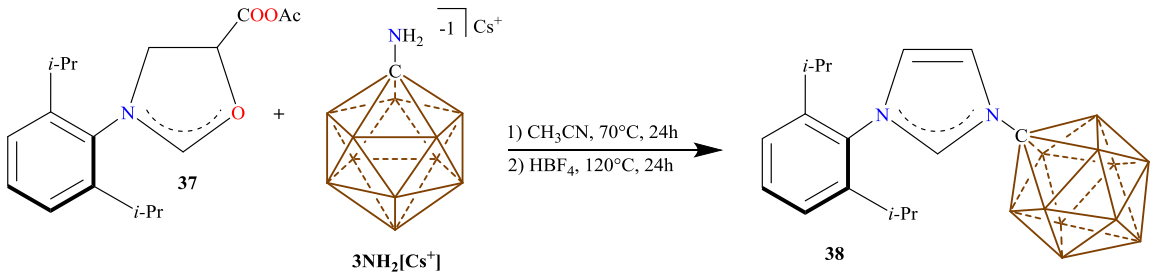

Scheme 2-13 Synthesis of Dip Imidazolium, **38**.

A glass bomb was equipped with a stir bar and loaded with compound **37** (2.383 g, 6.32 mmol) and cesium 1-amino-1-carba-*closo*-undecaborate **$3NH_2[Cs^+]$** (1.84 g, 6.32 mmol). Dry acetonitrile (8 mL) was added to the bomb which was tightly sealed and heated to 80°C for 12 hours. To the crude reaction mixture tetrafluoroboric acid diethyl ether complex (1.5 mL, 1.67 mmol) was added. The Schlenk was

sealed and heated to 120°C for 72 hours (safety note: heating sealed containers is dangerous and was always done in a hood behind a blast shield using a thick-walled Schlenk tube, appropriate precautions should always be taken). The solution was cooled then poured into a beaker containing sodium bicarbonate (200 mL). Methylene chloride (500 mL) was added and the aqueous phase was further washed with methylene chloride (3 × 100 ml). The organic phase was collected, washed with brine (300 ml), run though a plug of silica then dried over magnesium sulfate. All volatiles were subsequently removed under vacuum to give a brown solid. This solid was crystallized from a concentrated acetonitrile solution (8 mL) at 5°C to give **38** as light colorless blocks. ^{1}H NMR (400 MHz, acetonitrile-d_3, 25°C): δ = 8.87 (dd, $^{3}J(H,H)$ = 1.7 Hz, $^{3}J(H,H)$ = 1.70 Hz, 1.7 Hz, 1H), 7.75 (dd, $^{3}J(H,H)$ = 1.7 Hz**,** $^{4}J(H,H)$ = 1.70 Hz, 1H), 7.58 (t, $^{3}J(H,H)$ = 7.6 Hz, 1H), 7.44 (dd, $^{3}J(H,H)$ = 1.7 Hz**,** $^{4}J(H,H)$ = 1.70 Hz, 1H), 7.39 (d, $^{3}J(H,H)$ = 7.6 Hz, 2H), 2.19 (hept, $^{3}J(H,H)$ = 6.8 Hz**,** 2H), 2.9-1.3 (bm, 11H, B-H), 1.15 (d, $^{3}J(H,H)$ = 6.8 Hz**,** 24H) ppm. ^{1}H[^{11}B] NMR (300 MHz, acetonitrile-d_3, 25°C): δ = 8.88 (1H), 7.75 (1H), 7.59 (1H), 7.44 (1H), 7.39 (2H), 2.19 (2H), 2.13 (5H), 1.69 (5H), 1.14 (24H), *note: the antipodal B-H is not observed*. ^{13}C[^{1}H] NMR (101 MHz, acetonitrile-d_3, 25°C): δ = 146.3, 137.5, 132.9, 131.1, 125.7, 125.5, 124.5, 118.2, 76.5, 29.5, 24.1, 23.9 ppm. ^{11}B[^{1}H] NMR (96 MHz, acetonitrile-d_3, 25°C): δ = -5.4, -9.8, -10.3 ppm. ^{11}B NMR (96 MHz, acetonitrile-d_3, 25°C): δ = -5.4 ($^{1}J(H,B)$ = 137.3 Hz), -9.8 ($^{1}J(H,B)$ = 135.4 Hz), -10.3 ($^{1}J(H,B)$ = 152.6 Hz). IR (solid, ATR, 25°C): B-H stretch = 2600 to 2517 cm^{-1}. HRMS (negative mode ESI/APCI) $[M-H]^-$ m/z calc'd = 369.3520 : Found = 369.3509.

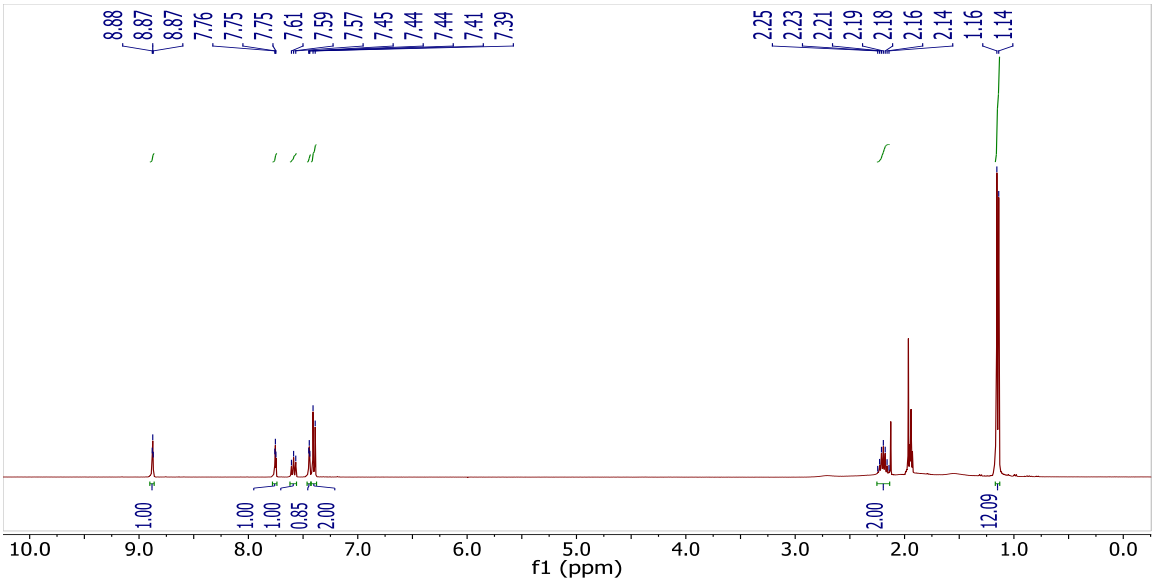

Figure 2-43. ^{1}H-NMR spectrum of **38** in acetonitrile-d_3. The peak at 2.2 ppm is due to water and the peak at 1.96 ppm is due to protio acetonitrile in the deuterated solvent.

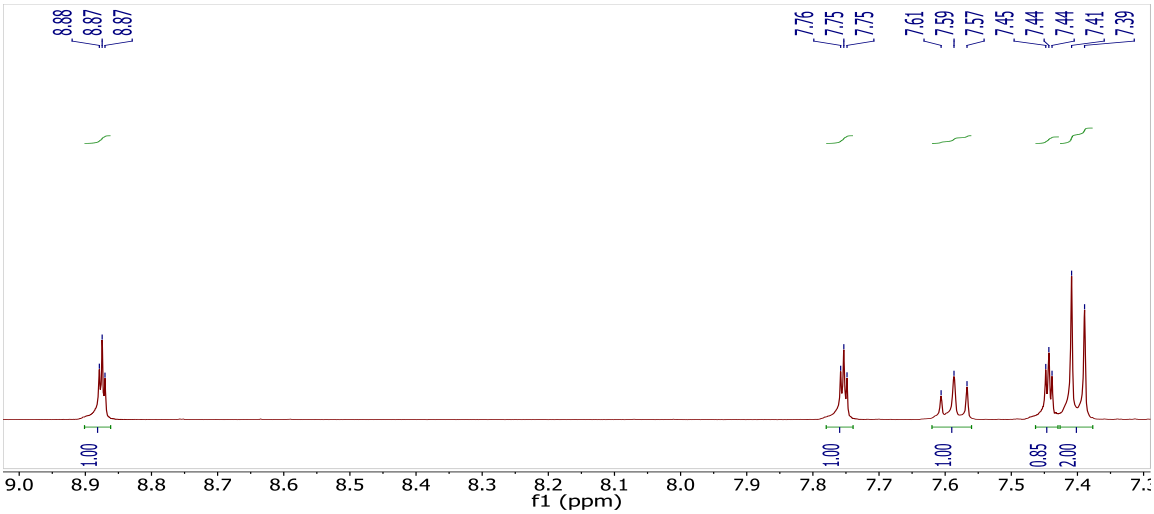

Figure 2-44. An expanded view of the aromatic region of the ^{1}H-NMR of **38** in acetonitrile-d_3, showing the small *J*-coupling of the imidazolium protons.

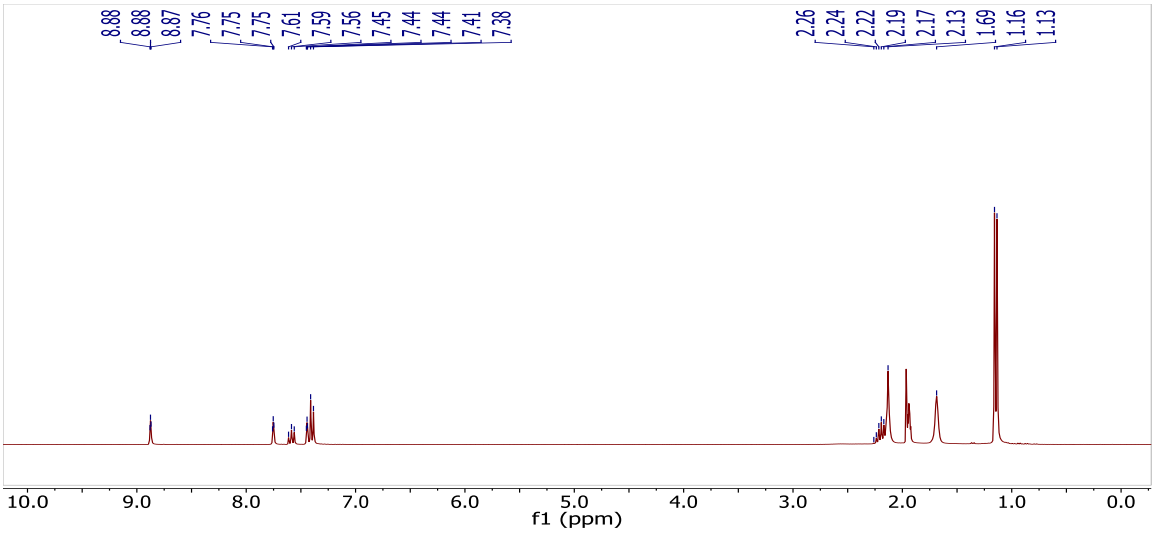

Figure 2-45. $^{1}H[^{11}B]$ NMR spectrum of **38** in acetonitrile-d_3. The boron hydrides appear at 2.13 and 1.69 ppm.

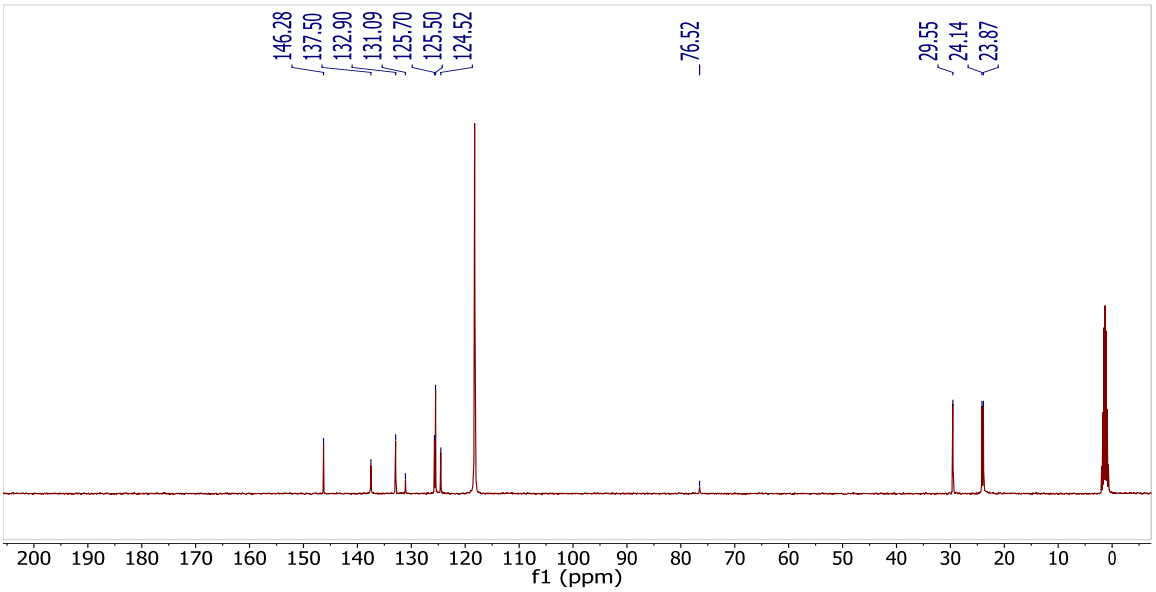

Figure 2-46. $^{13}C[^{1}H]$ NMR of **38** in acetonitrile-d_3. Acetonitrile-d_3 is seen at 118.2 and 1.3 ppm.

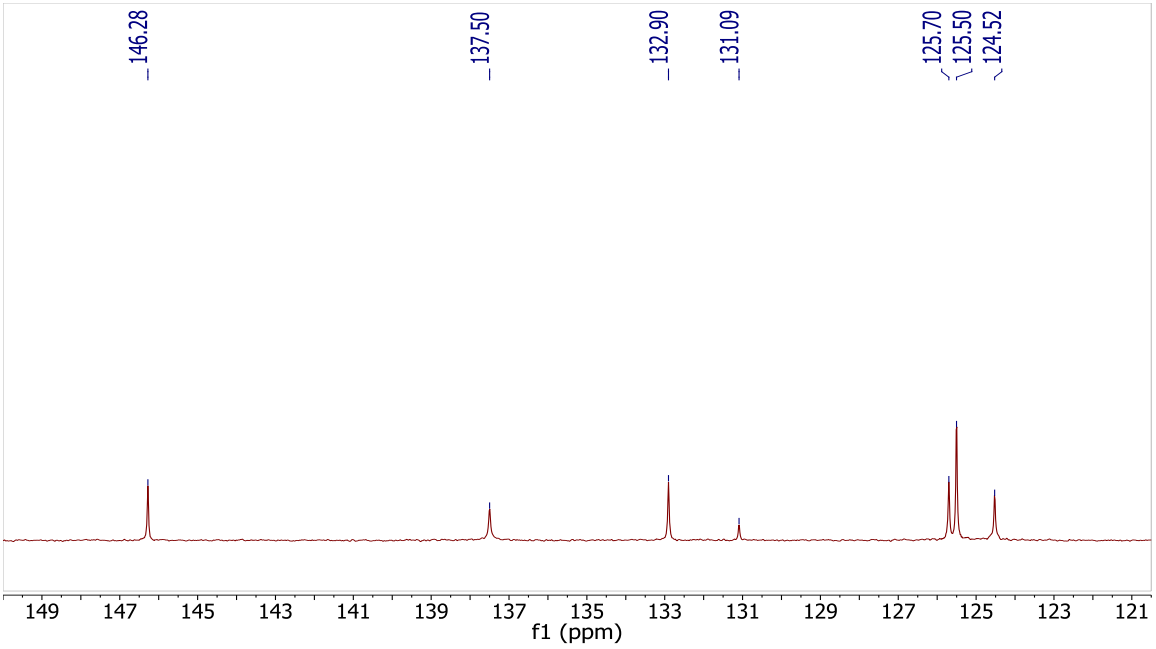

Figure 2-47. Expansion of the downfield region of the $^{13}C[^{1}H]$ NMR of **38** in acetonitrile-d_3.

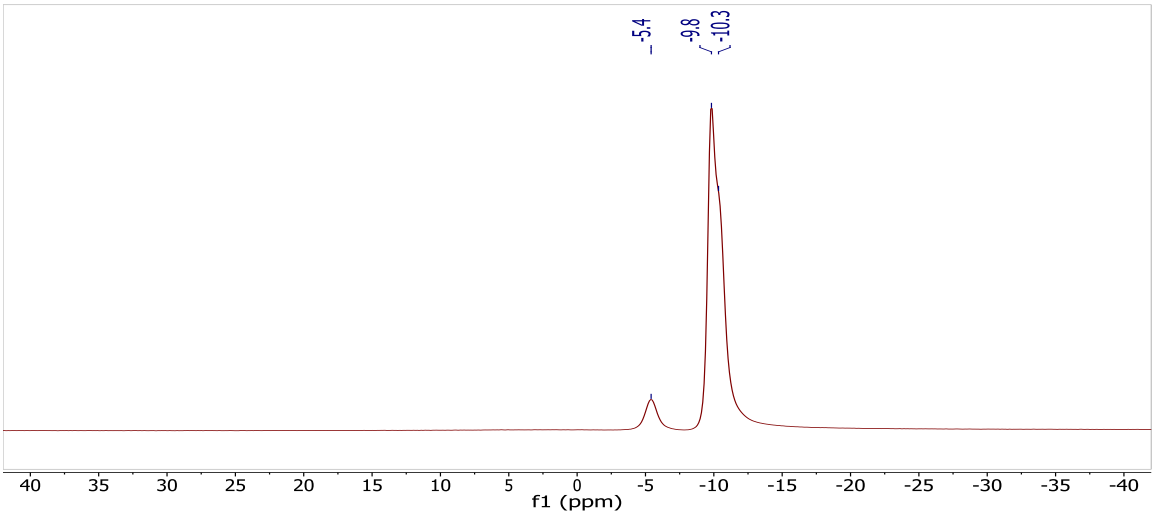

Figure 2-48. $^{11}B[^{1}H]$ NMR spectrum of **38** in acetonitrile-d_3.

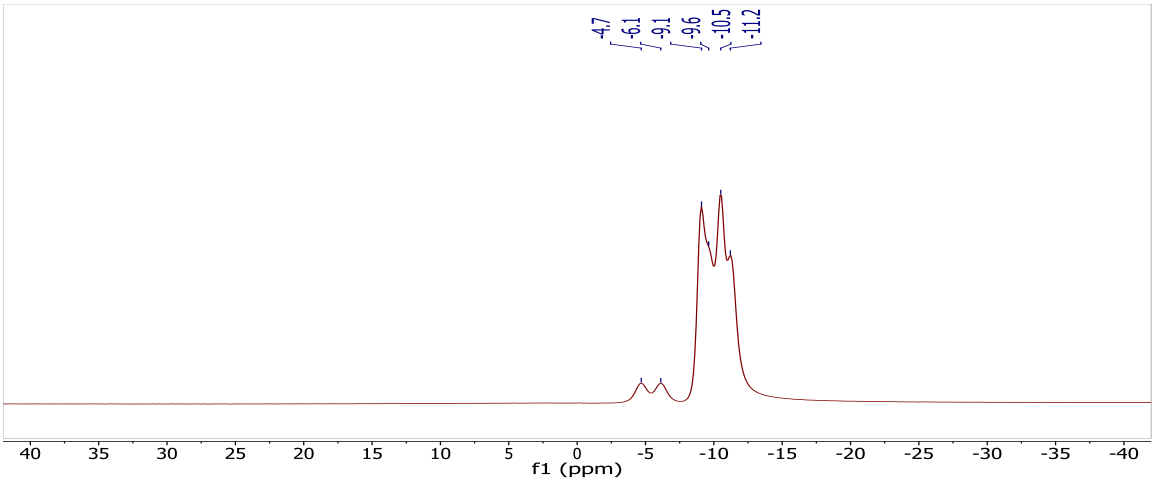

Figure 2-49. ^{11}B NMR of **38** in acetonitrile-d_6 showing the ^{1}J *(H,B)* coupling.

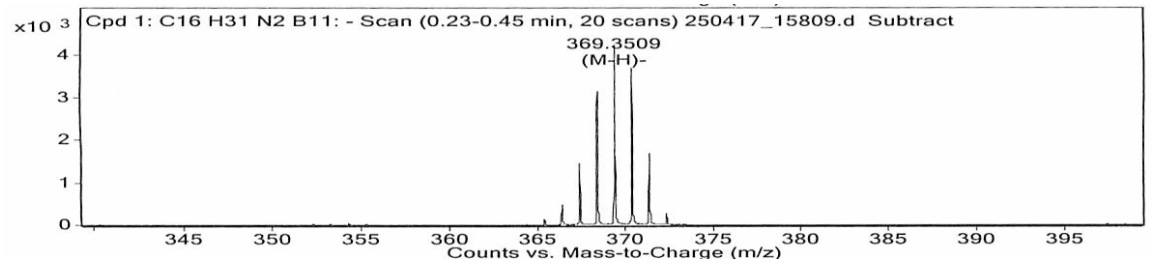

Figure 2-50. Mass spectrum (–ve ESI/APC) of **38**.

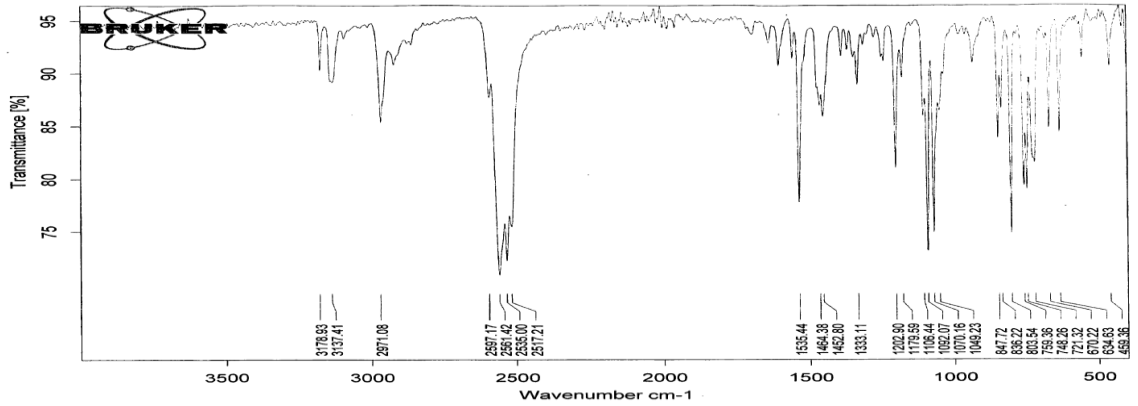

Figure 2-51. IR spectrum of solid **38**. The B-H stretches appear between 2600 and 2500 cm^{-1}.

Synthesis of Dip NHC, 39[Li$^+$]:

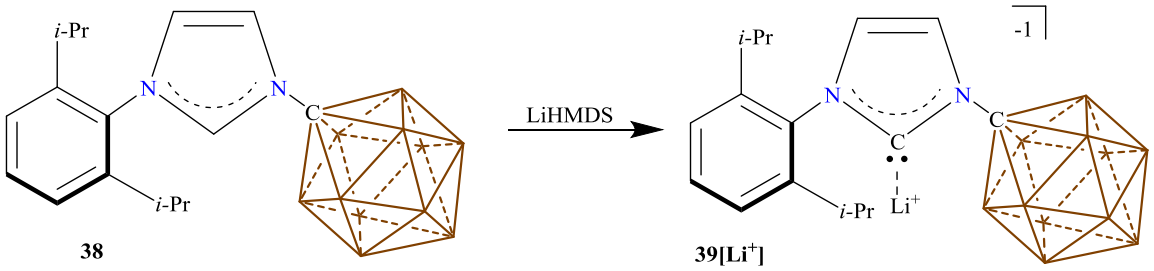

Scheme 2-14 Synthesis of Dip NHC, **39[Li$^+$]**

A glass scintillation vial equipped with a stir bar was loaded with **38** (380.1 mg, 1.03 mmol) and solid was dissolved in THF (2 mL). A solution of lithium hexamethyldisilazide (180.1 mg, 1.07 mmol) in THF (2 mL) was added to the gently stirring imidazolium solution and the reaction stirred for 1 hour at room temperature. During this time a microcrystalline material began to fall out of solution, thus the reaction mixture was cooled to -32°C for 1 hour. The supernate was removed, the solid was washed with diethyl ether (3 × 2 mL) and dried in vacuo to furnish a pristine white solid, 3**9** (350 mg, 90%). Single crystals of $\mathbf{9_{Li}}^+$ suitable for X-ray diffraction where grown from the combined supernate/diethyl ether washes. ^{1}H NMR (400 MHz, THF-d_8, 25°C): δ = 7.35 (t, ^{3}*J(H,H)* = 7.7 Hz, 1H), 7.34 (d, ^{3}*J(H,H)* = 1.7 Hz, 1H), 7.23 (d, ^{3}*J(H,H)* = 7.7 Hz, 2H), 6.82 (d, ^{3}*J(H,H)* = 1.7 Hz, 1H), 2.55 (hept, ^{3}*J(H,H)* = 6.8 Hz, 2H), 1.14 (d, ^{3}*J(H,H)* = 6.8 Hz, 6H), 1.06 (d, ^{3}*J(H,H)* = 6.8 Hz, 6H), 2.8 – 1.2 (bm, 11H, B-H). ^{1}H[^{11}B] NMR (96 MHz, THF-d_8, 25°C): δ = 7.35 (t, 1H), 7.33 (d, 1H), 7.23 (d, 2H), 6.82 (d, 1H), 2.54 (hept, 2H), 2.14 (s, 5H), 1.73 (s, 1H), 1.62 (s, 5H), 1.14 (d, 6H), 1.06 (d, 6H). ^{11}B[^{1}H] NMR (96 MHz, THF-d_8, 25°C): δ = -10.0, -13.9 ppm. 11B NMR (96 MHz, THF-d_8, 25°C): δ = -10.0 (d, ^{1}*J(B,H)* = 128.0 Hz, 1H), -13.9 (d, ^{1}*J(B,H)* = 139.5 Hz, 10H). ^{13}C[^{1}H] NMR (126 MHz, THF-d_8, 25°C): δ = 208.4, 146.9, 139.1, 129.6, 124.2, 122.1, 122.1, 82.2, 28.9, 24.8, 24.0 ppm.

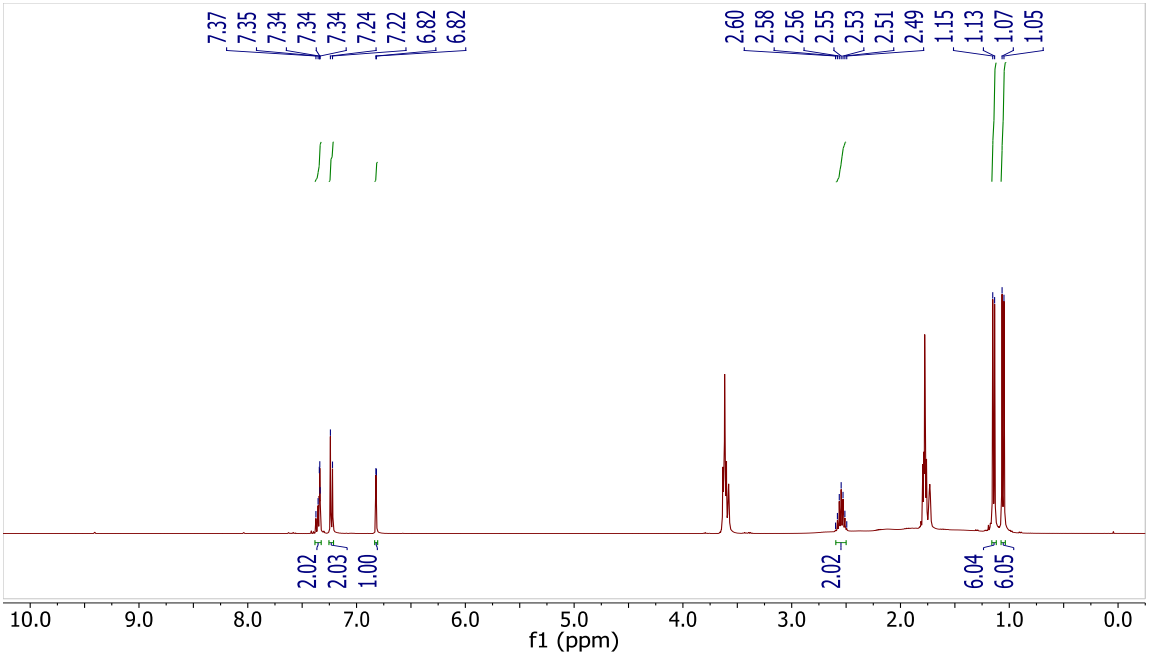

Figure 2-52. ^{1}H-NMR spectrum of **39** in THF-d_8.

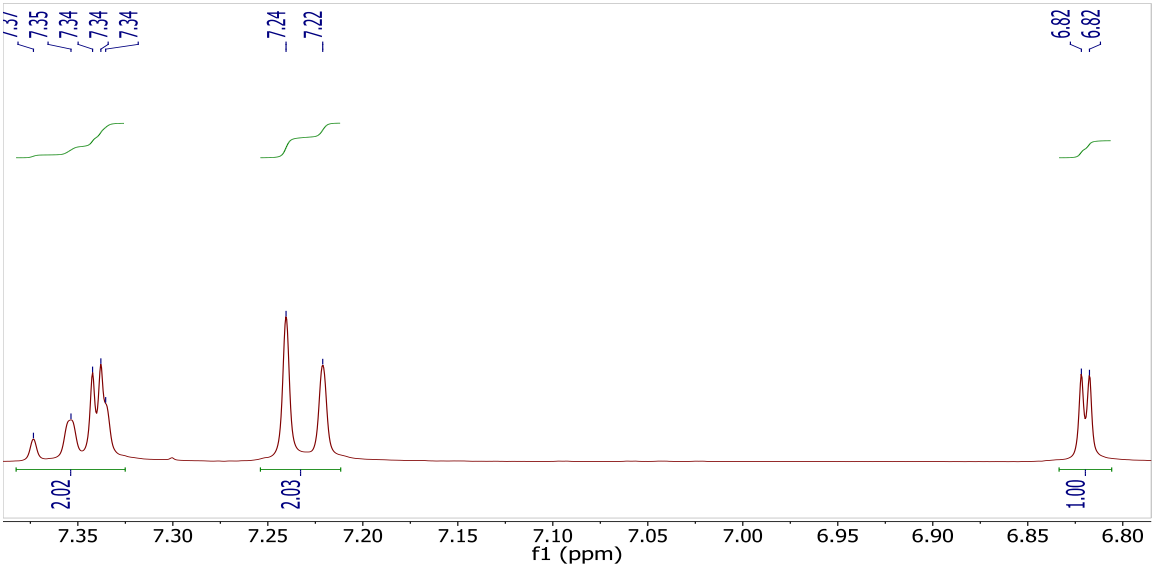

Figure 2-53. An expanded view of the aromatic region of the ^{1}H-NMR of **39** in THF-d_8, showing the small ^{3}J-coupling of the imidazolylidene protons.

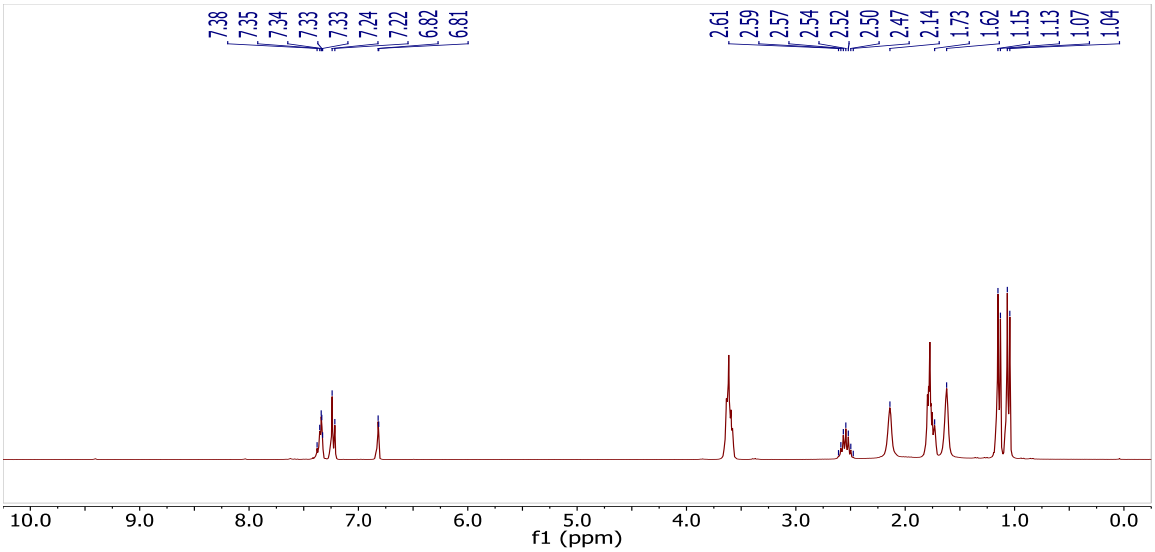

Figure 2-54. $^{1}H[^{11}B]$-NMR spectrum of **39** in THF-d_8. Note: the B-H resonances appear at 2.14, 1.73 and 1.62 ppm.

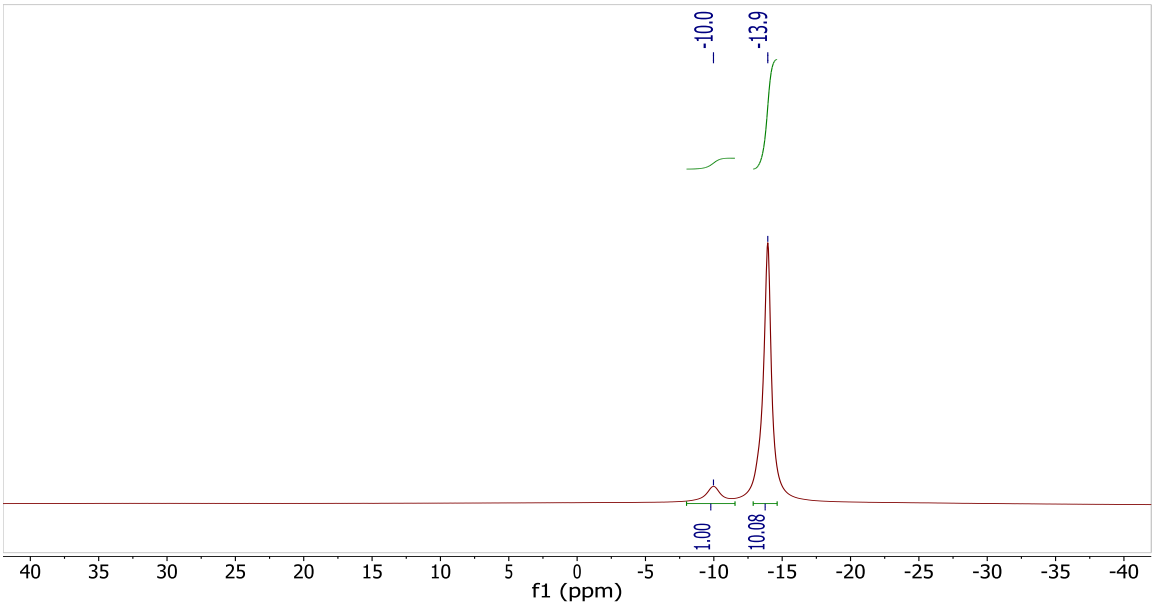

Figure 2-55. $^{11}B[^{1}H]$-NMR spectrum of **39** in THF-d_8.

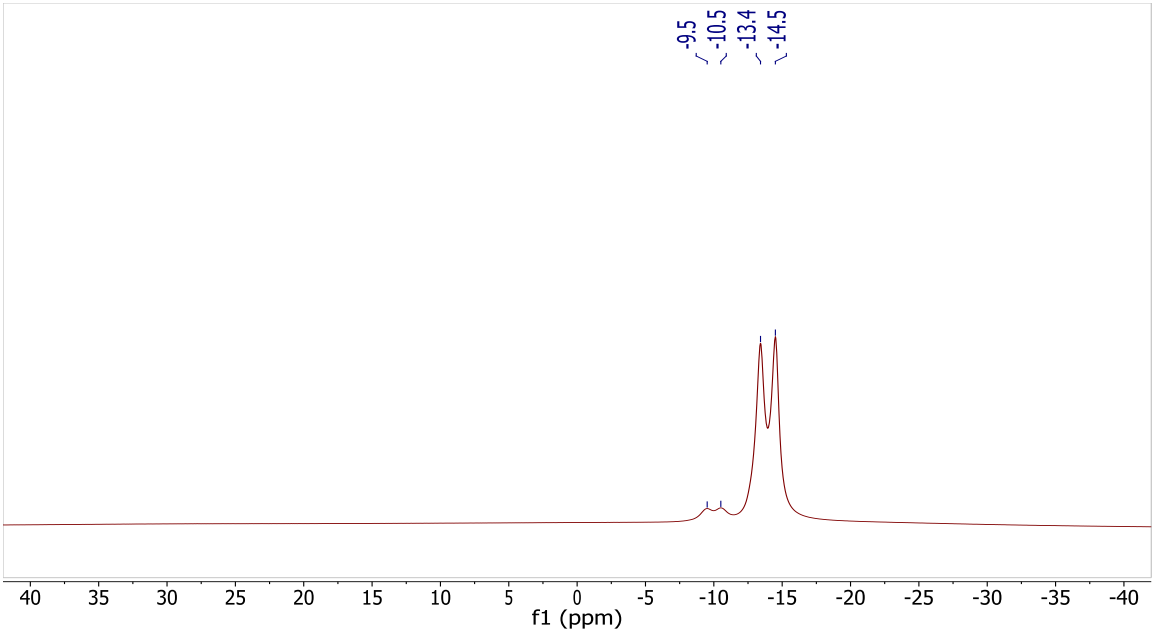

Figure 2-56. ^{11}B-NMR spectrum of **39** in THF-d_8.

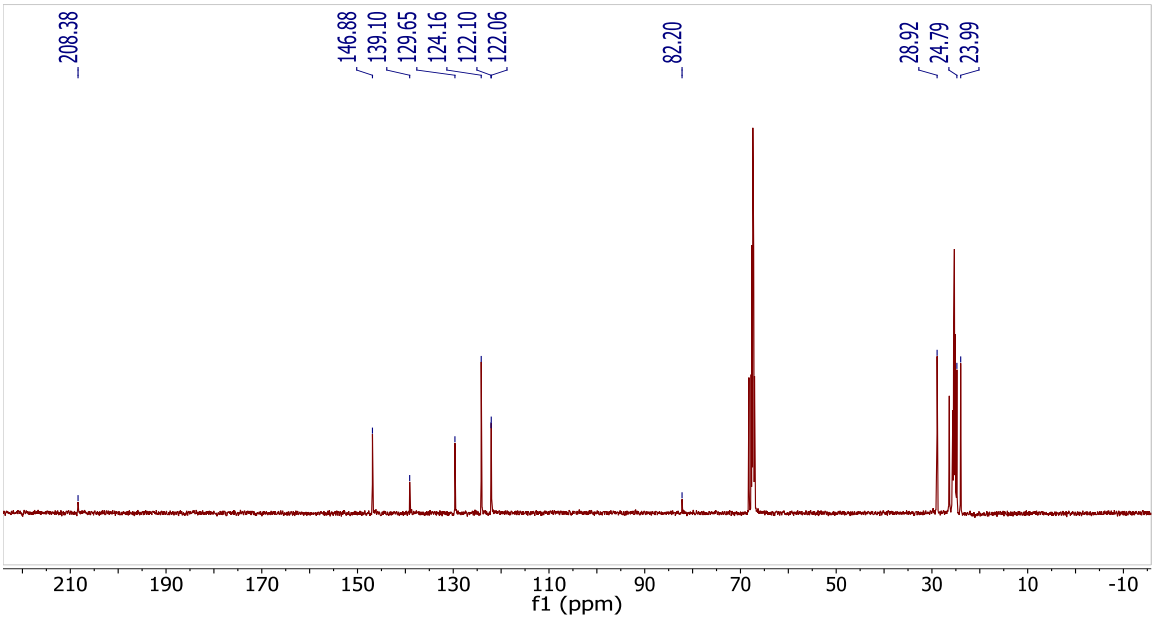

Figure 2-57. ^{13}C[^{1}H]-NMR spectrum of **39** in THF-d_8.

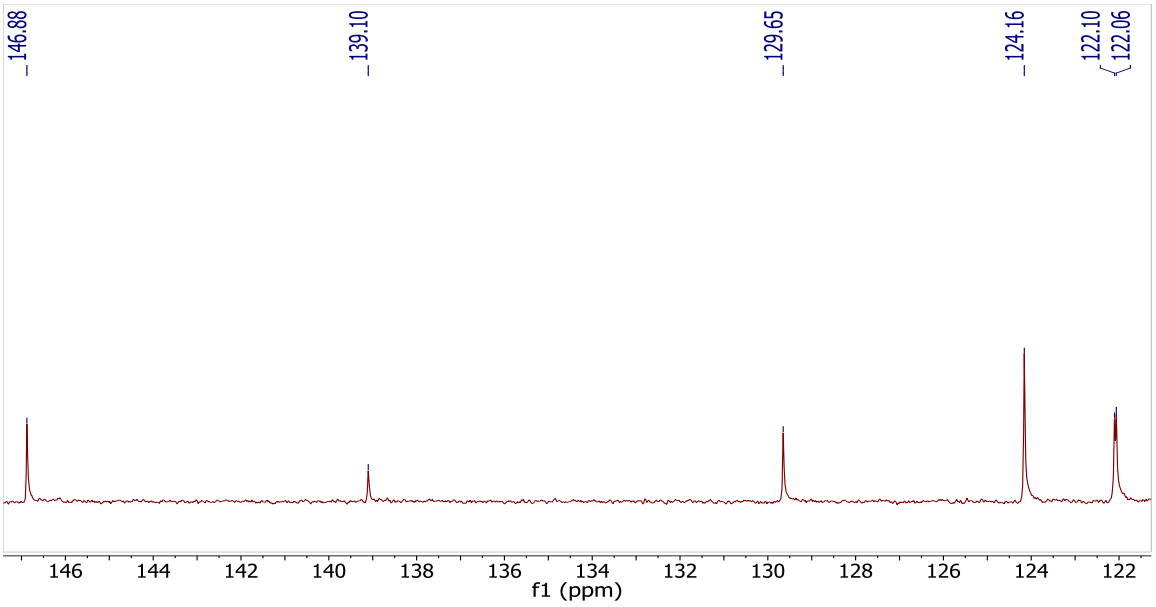

Figure 2-58. An expanded view of the aromatic region of **39** in THF-d_8.

Synthesis of Anionic Thiourea, 40:

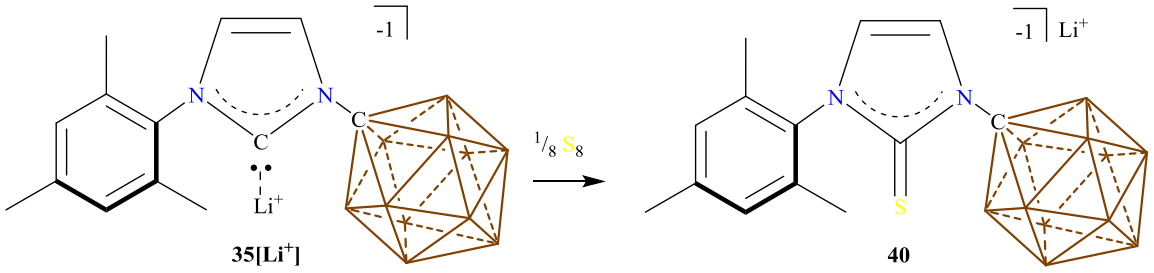

Scheme 2-15 Synthesis of thiourea, **40**.

A scintillation vial was equip with a stir bar and loaded with **25[Li$^+$]** (100 mg, 0.0257 mmol) and elemental sulfur (9.1 mg, 0.283 mmol). The solids were suspended in THF (3 mL) and the reaction stirred for 30 minutes at room temperature. At this point the reaction was filtered and the filtrate pumped down to dryness. The stick solid was dissolved in methylene chloride and added to boiling toluene which precipitated a tan solid. The hot toluene was removed furnishing the title compound in 91% yield (153 mg, 4 coordinated THF molecules to Li$^+$) ^{1}H NMR (300 MHz, methylene chloride-d_2, 25°C): δ = 7.45 (d,

$^{3}J(H,H)$ = 2.6 Hz, 1H), 6.98 (s, 2H), 6.50 (d, $^{3}J(H,H)$ = 2.6 Hz, 1H), 2.35 (s, 3H), 1.97 (s, 6H), 2.4-0.6 (bm, 11H, B-H) ppm. $^{1}H[^{11}B]$ NMR (300 MHz, methylene chloride-d_2, 25°C): δ = 7.45 (d, 1H), 6.98 (s, 2H), 6.50 (d, 1H), 2.59 (s, 5H, B-H), 2.35 (s, 3H), 1.97 (s, 6H), 1.75 (s, 1H, B-H), 1.61 (s, 5H, B-H) ppm. $^{11}B[^{1}H]$ NMR (96 MHz, methylene chloride-d_2, 25°C): δ = -8.3, -14.1 ppm. $^{11}B[^{1}H]$ NMR (96 MHz, methylene chloride-d_2, 25°C): δ = -8.3 ($^{1}J(B,H)$ = 117.3 Hz), -14.1 ($^{3}J(B,H)$ = 134.2 Hz) ppm. IR (solid, ATR, 25°C): B-H stretch = 2533 cm^{-1}. HRMS (negative mode ESI/APCI) $[M]^-$ m/z calc'd = 359.2756: Found = 359.2770.

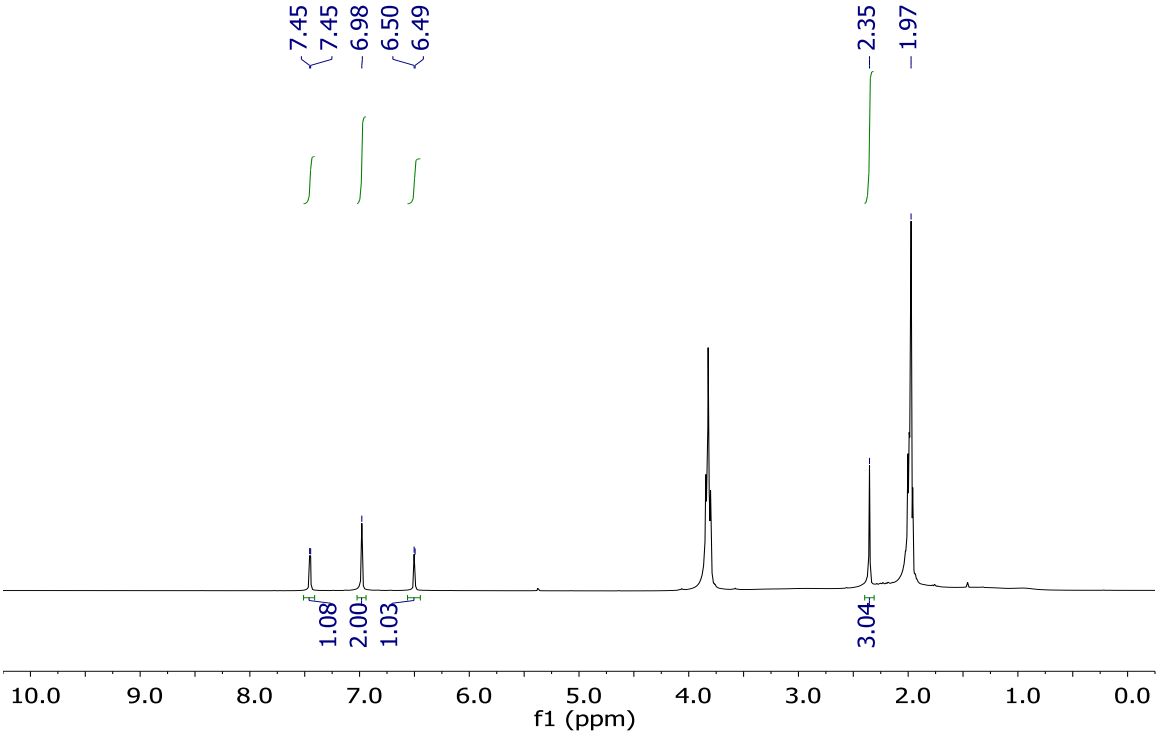

Figure 2-59. ^{1}H-NMR spectrum of **40** in methylene chloride-d_2.

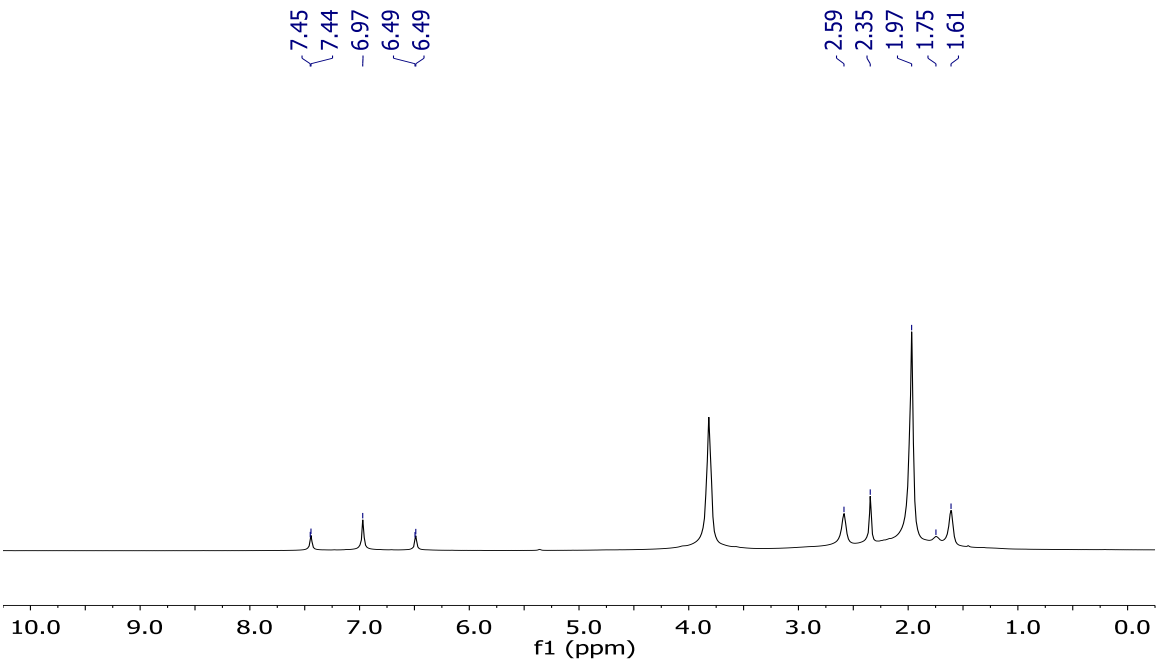

Figure 2-60. $^{1}H[^{11}B]$-NMR spectrum of **40** in methylene chloride-d_2.

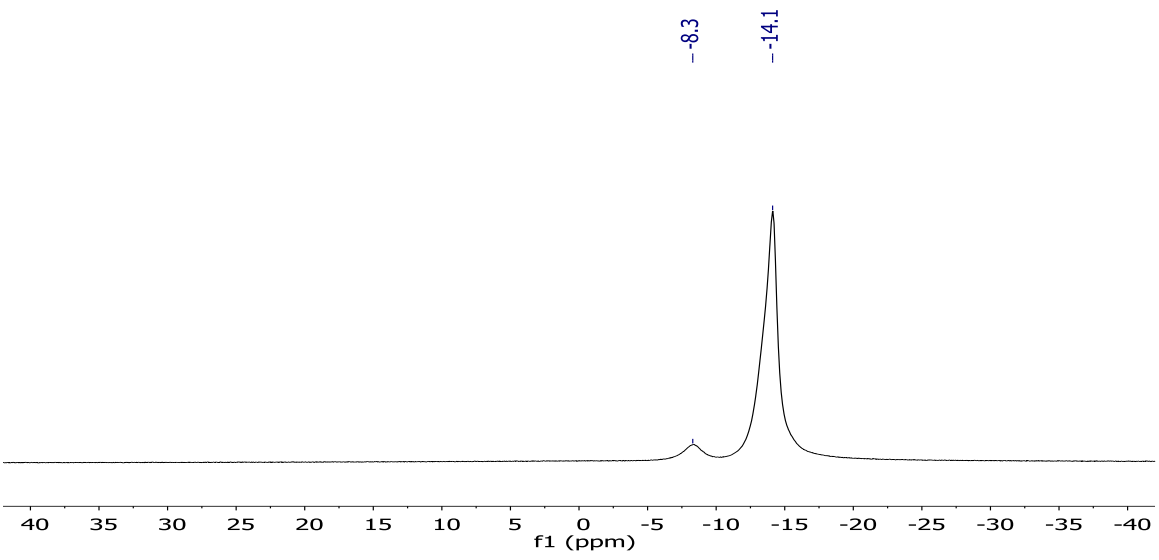

Figure 2-61. $^{11}B[^{1}H]$-NMR spectrum of **40** in methylene chloride-d_2.

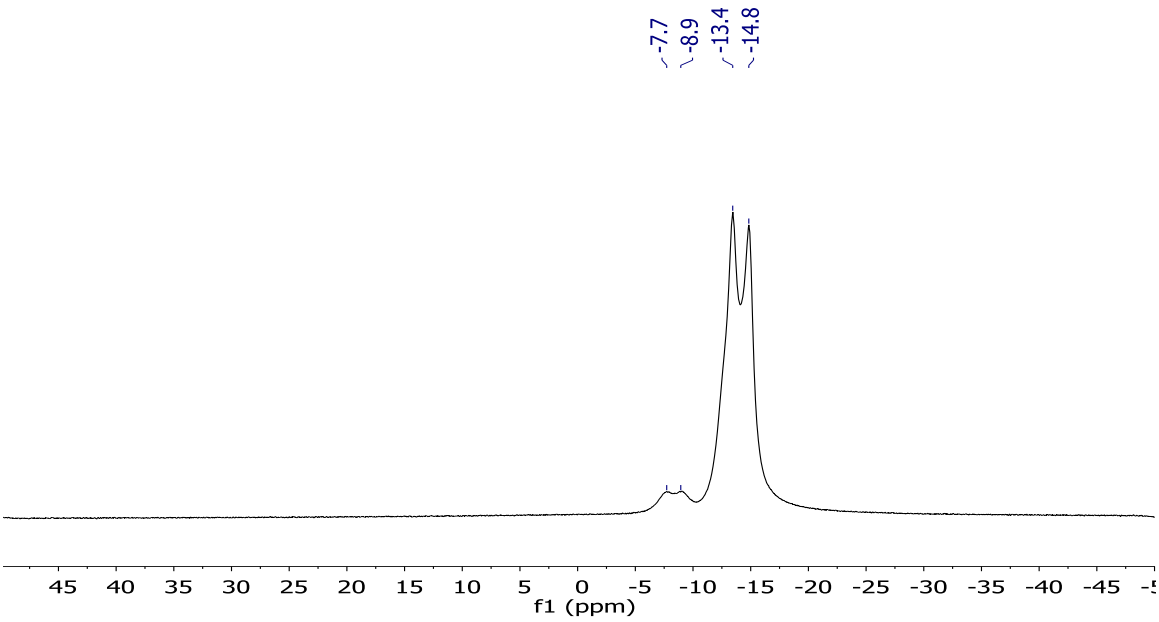

Figure 2-62. ^{11}B-NMR spectrum of **40** in methylene chloride-d_2.

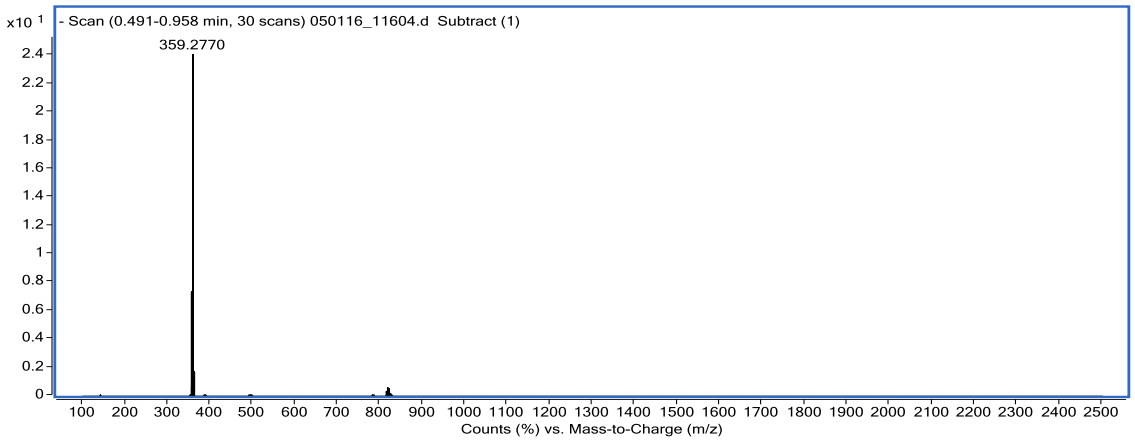

Figure 2-63. Mass spectrum of **40**.

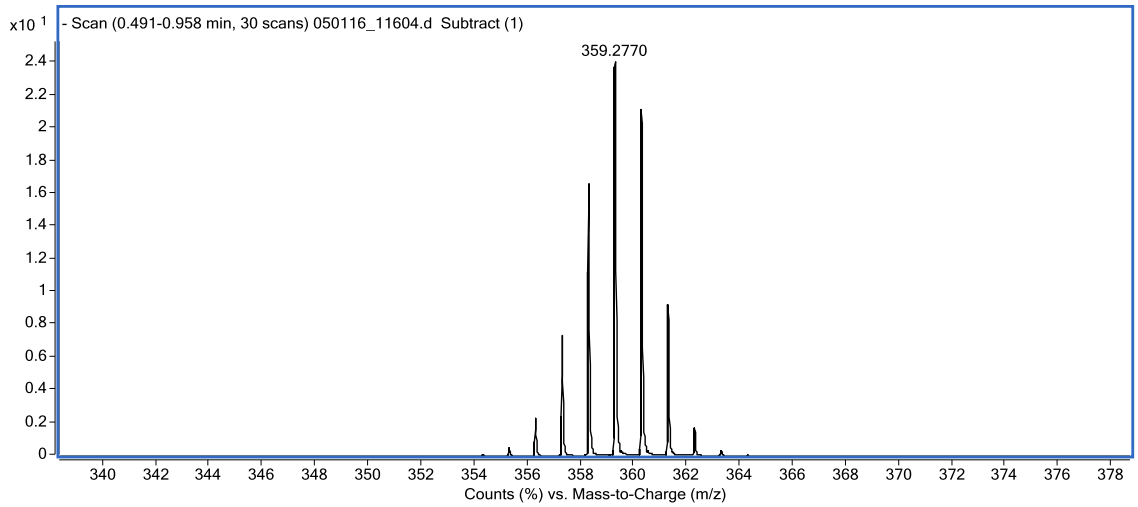

Figure 2-64. Blow up of the Mass spectrum of **40**.

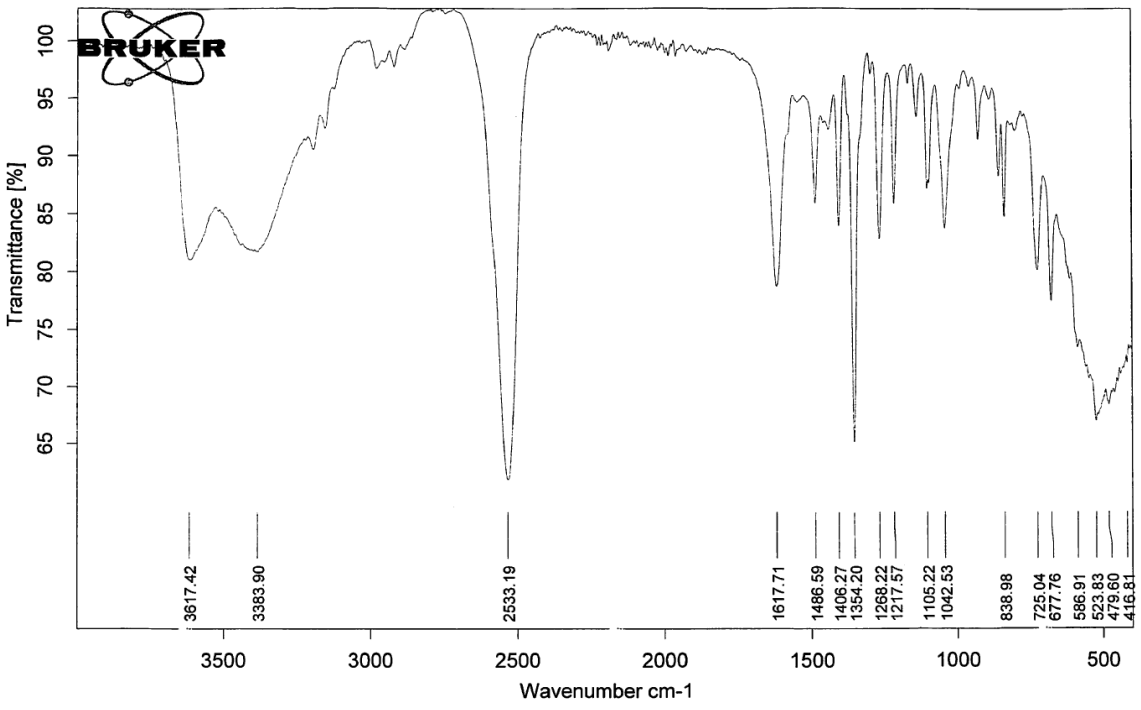

Figure 2-65. IR spectrum of **40** showing the B-H stretches at 2533.19 cm^{-1}.

Synthesis of Dianionic Thiourea 41[2Li$^+$]

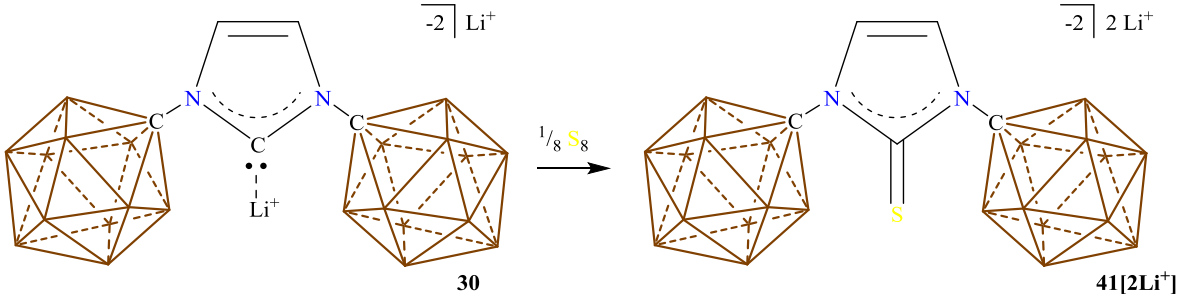

30 **41[2Li$^+$]**

Scheme 2-16 Synthesis of dianionic thiourea **41[2Li$^+$]**.

A flame dried Schlenk was equip with a stir bar and loaded with **30** (200 mg, 251 µmol, six coordinated THF molecules to Li$^+$), elemental sulfur (185 mg, 577 µmol) and THF (3 mL). The reaction was heated to 50°C and stirred for 24 hours.† The reaction was filtered and the filtrate was pumped down to dryness furnishing the title compound, **41[2Li$^+$]**. ^{1}H NMR (300 MHz, acetone-d$_3$, 25°C): δ = 7.08 (s, 2H), 2.5-0.6 (bm, 22H, B-H). ^{11}B[^{1}H] NMR (96 MHz, methylene chloride-d$_2$, 25°C): δ = -7.4, -13.9 ppm. ^{11}B NMR (96 MHz, methylene chloride-d$_2$, 25°C): δ = -7.4 (^{1}*J(H,B)* = 125.6 Hz), -13.9 (^{1}*J(H,B)* = 141.7 Hz) ppm. ^{7}Li NMR (233 MHz, THF-d$_8$, 25°C) = 3.54, 2.26 ppm. IR (solid, ATR, 25°C): B-H stretch = 2519 cm^{-1}. HRMS (negative mode ESI/APCI) [M]$^{-2}$ m/z calc'd = 191.1932 : Found = 191.1931; [M^{-2}+H$^+$]$^-$ m/z calc'd = 383.3931: Found = 383.3941.

† After stirring the reaction mixture was checked by ^{1}H NMR and if protonation was present KOtBu was added. If the reaction mixture showed free NHC more elemental sulfur was added.

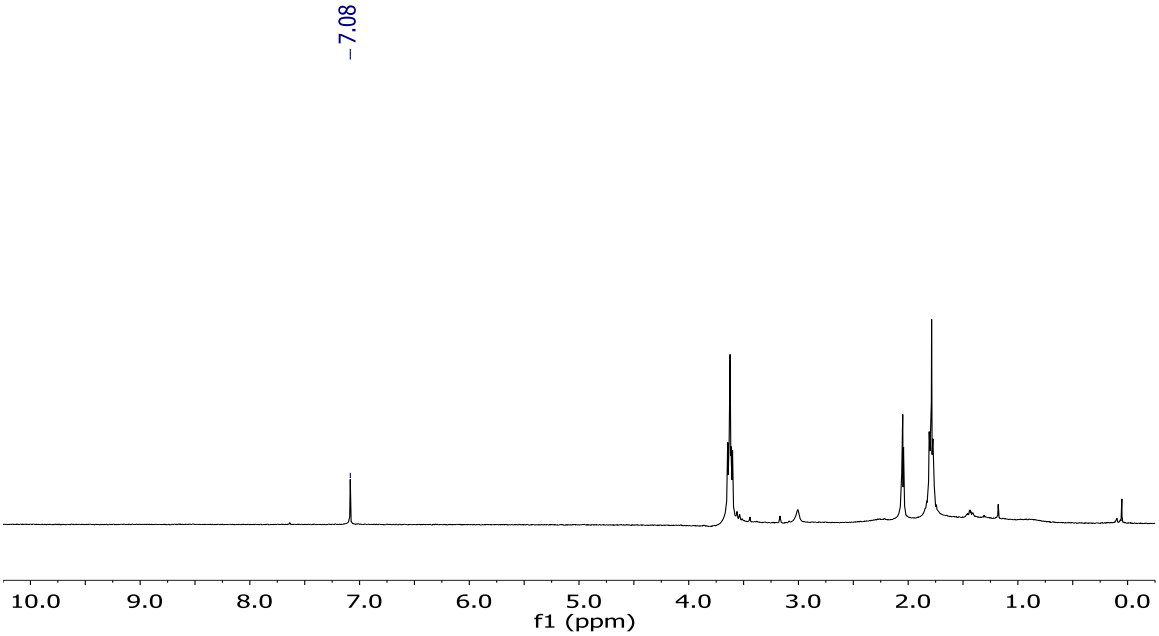

Figure 2-66 ^{1}H NMR-spectrum of **41[2Li^{+}]** in acetone-d_6.

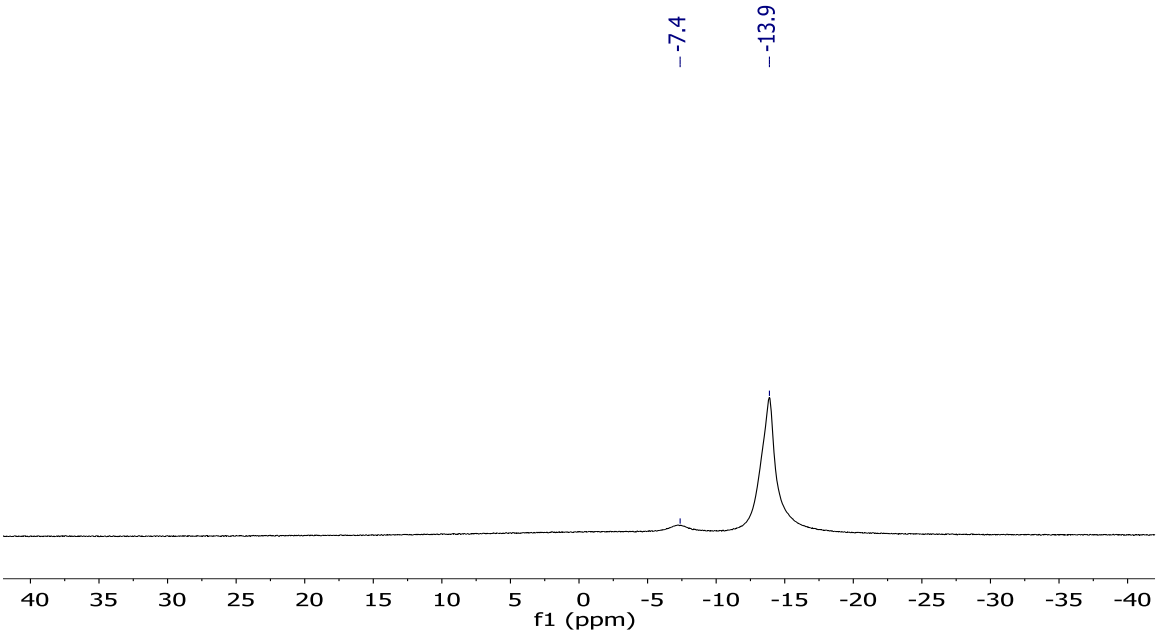

Figure 2-67 ^{11}B[^{1}H] NMR-spectrum of **41[2Li^{+}]** in acetone-d_6.

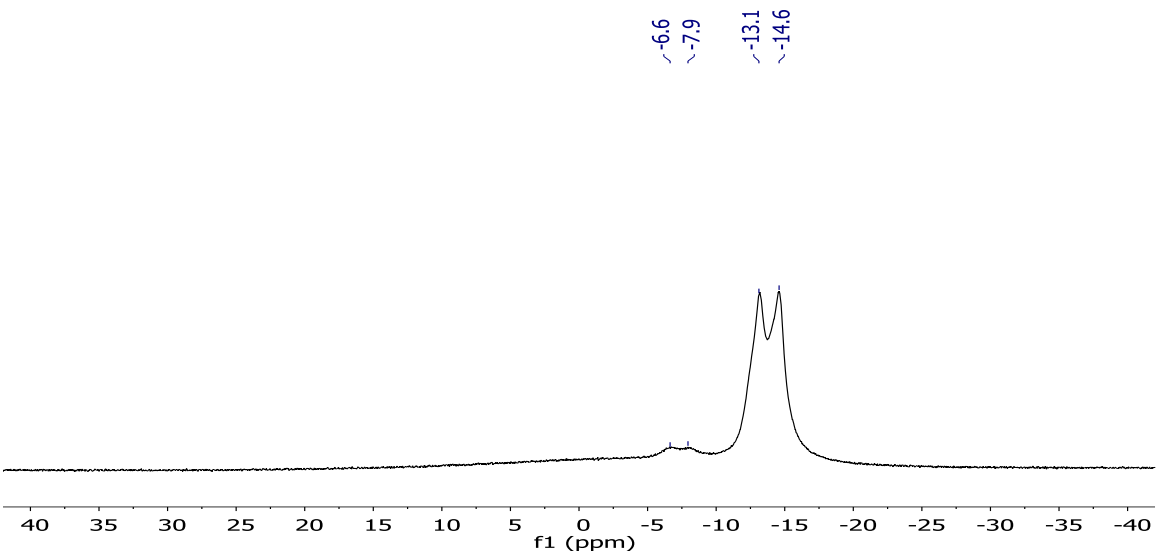

Figure 2-68 ^{11}B NMR-spectrum of **41[2Li$^+$]** in acetone-d_6.

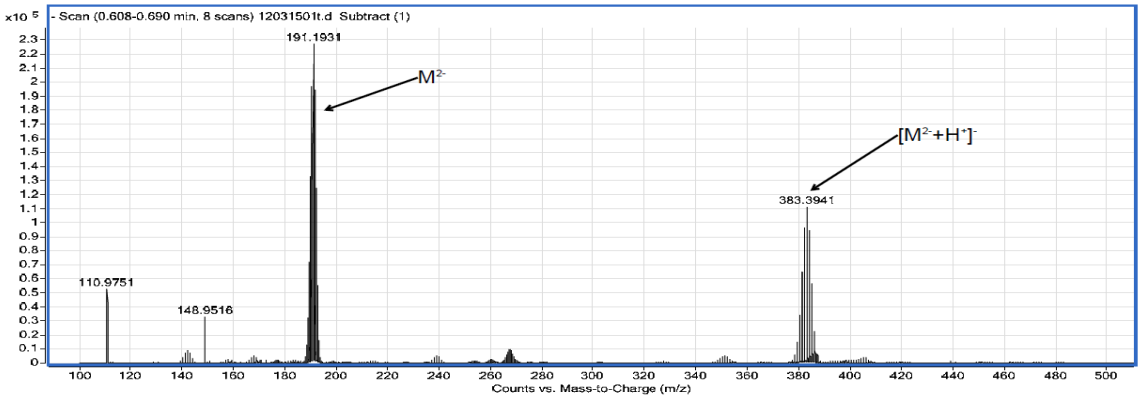

Figure 2-69 Mass spectrum of **41[2Li$^+$]**.

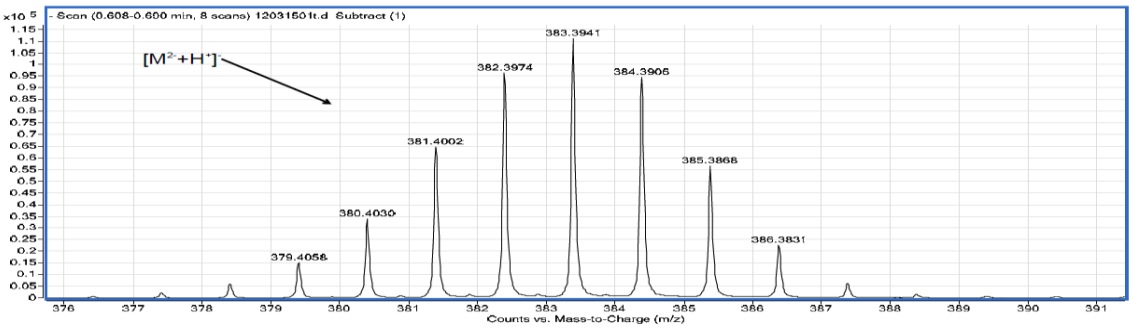

Figure 2-70 Blow up in the mass spectrum of **41[2Li$^+$]** showing the $[M^{-2} + H^+]^-$ ion.

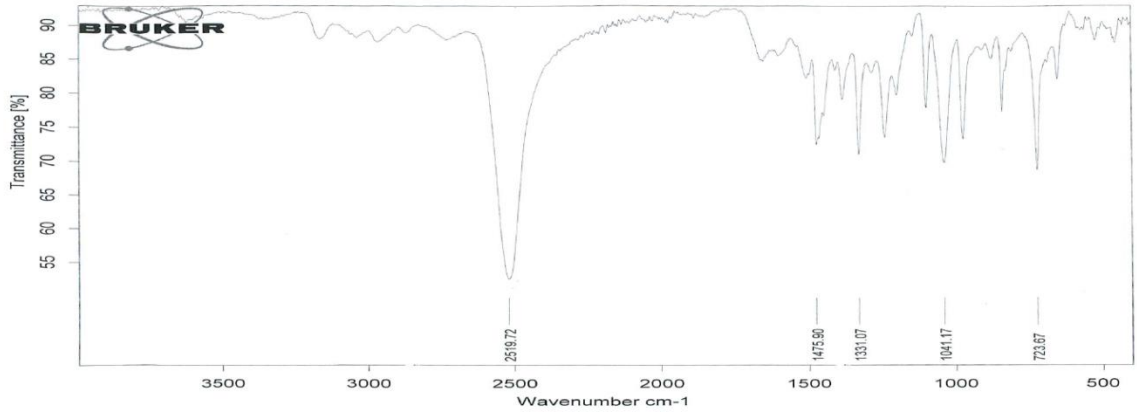

Figure 2-71 IR spectrum of **41[2Li$^+$]** in the solid state. The B-H stretches appear at 2519 cm^{-1}.

Synthesis of Dianionic Thiourea, 41[2Me$_3$NH$^+$]

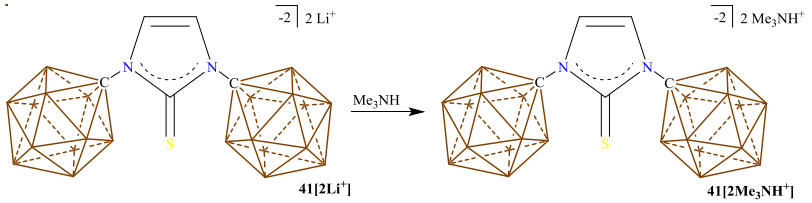

Scheme 2-17 Synthesis of thiourea, **41[2Me$_3$NH$^+$]**.

41[2Li$^+$] was suspended in water and Me$_3$N•HCl (excess of 2 equivalents) was added and the mixture stirred for 2 hours at room temperature. The tan solid was collected by filtration furnishing the title

compound, **41[2Me$_3$NH$^+$]**. ^{1}H NMR (300 MHz, acetone-d$_3$, 25°C): δ = 7.13 (s, 2H), 3.17 (s, 18H), 2.5 – 0.7 (bs, 22H, B-H) ppm. ^{11}B[^{1}H] NMR (96 MHz, acetone-d$_6$, 25°C): δ = -6.9, -12.5, -13.4 ppm.

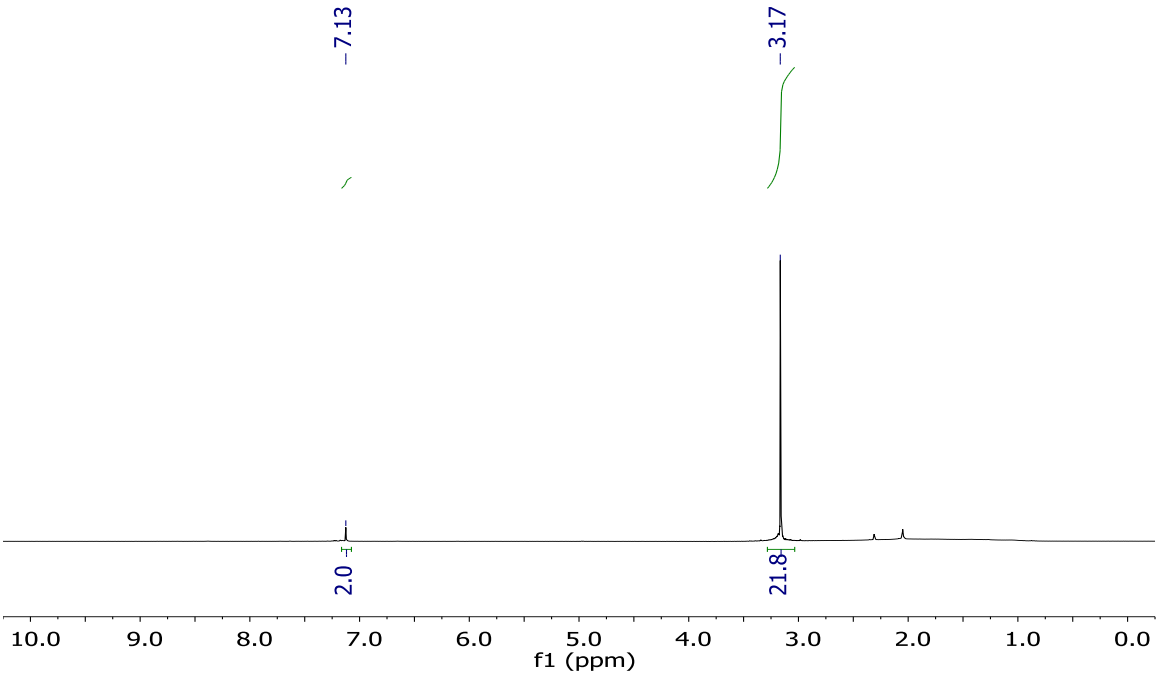

Figure 2-72 ^{1}H NMR-spectrum of **41[2Me3NH$^+$]** in acetone-d$_3$.

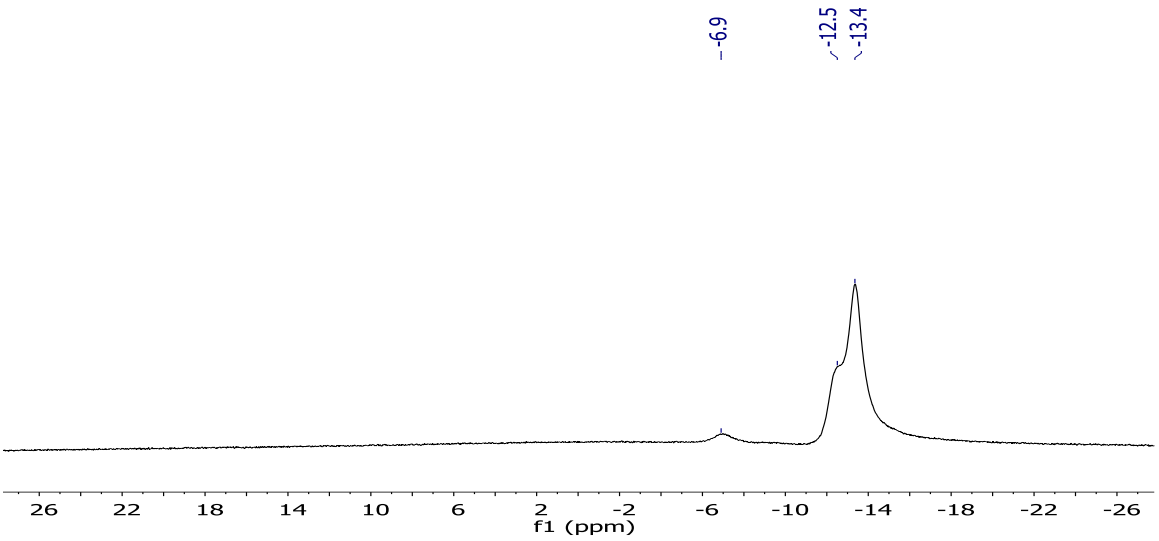

Figure 2-73 ^{11}B[^{1}H] NMR-spectrum of **41[2Me3NH$^+$]** in acetone-d$_3$.

Reaction of 41[2Me$_3$NH$^+$] with elemental Mg:

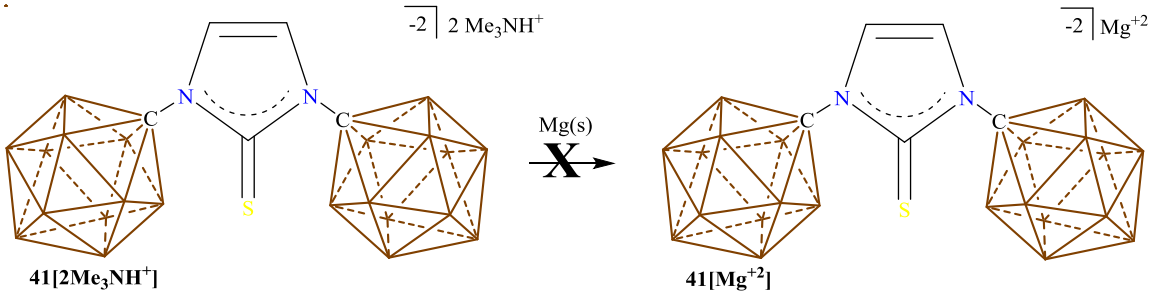

Scheme 2-18 Attempted synthesis of **41[Mg^{+2}]**.

A glass scintillation vial was equip with a stir bar and loaded with **41[2Me$_3$NH$^+$]**, elemental magnesium (excess) and THF. The reaction was stirred and monitored by ^{1}H NMR spectroscopy until reduction occurred. The following NMR shows the reduction.

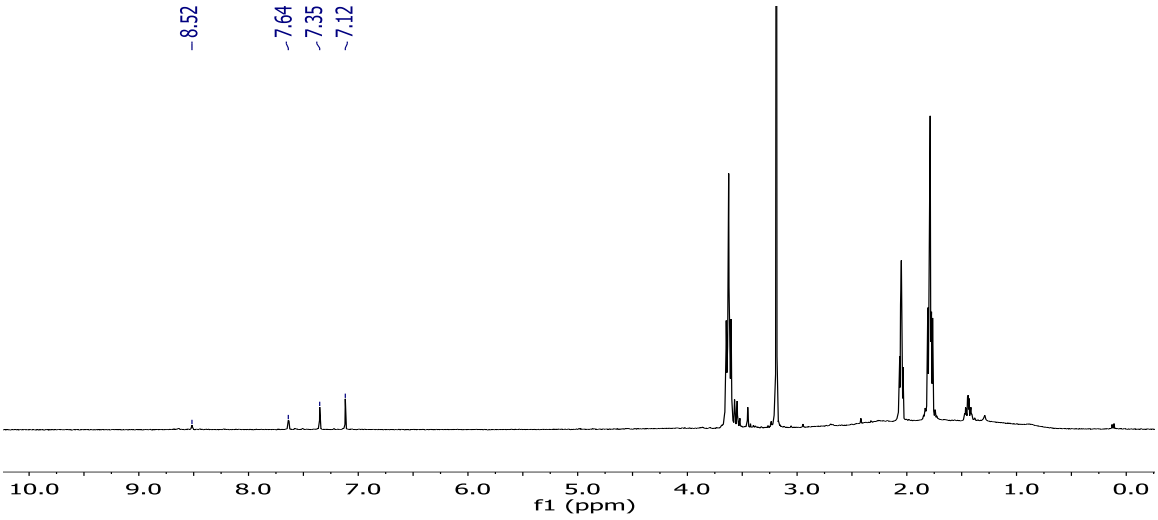

Figure 2-74 ^{1}H NMR-spectrum of the attempted synthesis of **41[Mg^{+2}]** in acetone-d$_6$ showing incomplete reduction of the Me$_3$NH cation.

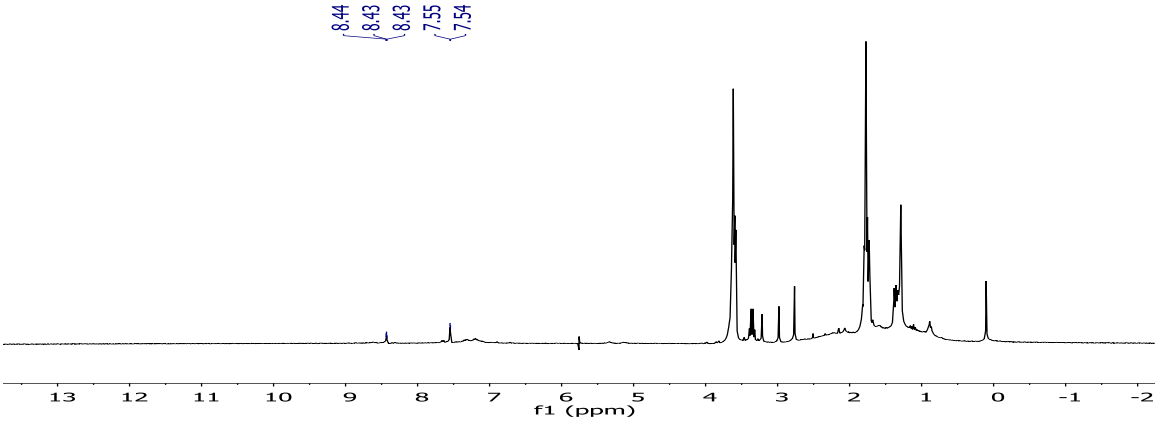

Figure 2-75 ^{1}H NMR-spectrum of the attempted synthesis of **41[Mg^{+2}]** in dry THF-d_8 after reduction had completed. *Note: the presence of imidazolium can be seen at 8.4 and 7.5 ppm.*

X-Ray Structure Determination

Crystal Structure of Monoanionic Lithium Carbene 35[Li^+]:

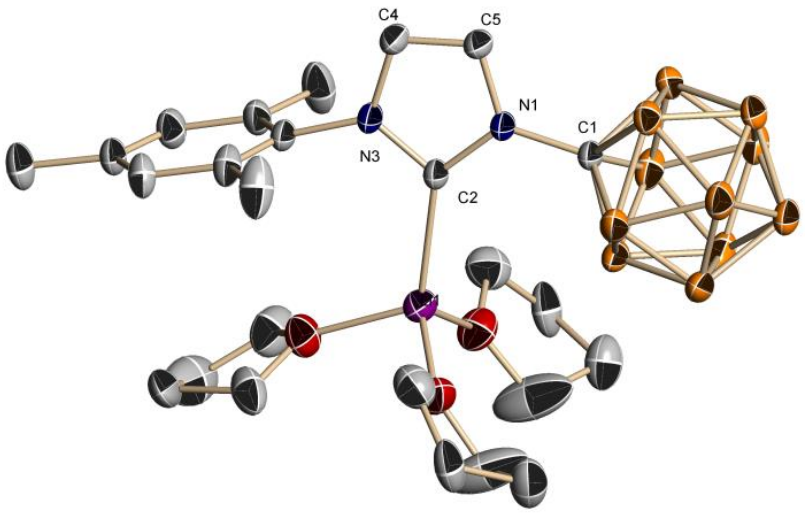

Figure 2-76 Solid state structure of **35[Li^+]**. Hydrogen atoms are omitted for clarity.

A colorless prism fragment (0.532 x 0.455 x 0.379 mm^3) was used for the single crystal x-ray diffraction study of $C_3H_2N_2[CH_{11}B_{11}][C_9H_{11}]Li[C_4H_8O]_3$ (sample vL123MA_0m). The crystal was coated with paratone oil and mounted on to a cryo-loop glass fiber. X-ray intensity data were collected at 163(2) K on a Bruker APEX2 platform-CCD x-ray diffractometer system (fine focus Mo-radiation, λ = 0.71073 Å, 50KV/30mA power). The CCD detector was placed at a distance of 5.0600 cm from the crystal.

A total of 4800 frames were collected for a sphere of reflections (with scan width of 0.3^o in ω and ϕ, starting ω and 2θ angles of –30^o, and ϕ angles of 0^o, 90^o, 120^o, 180^o, 240^o, and 270^o for every 600 frames, and 1200 frames with ϕ-scan from 0-360^o, 10 sec/frame exposure time). The frames were integrated using the Bruker SAINT software package and using a narrow-frame integration algorithm. Based on a monoclinic crystal system, the integrated frames yielded a total of 90725 reflections at a maximum 2θ angle of 61.014^o (0.70 Å resolution), of which 5070 were independent reflections (R_{int} = 0.0355, R_{sig} = 0.0124, redundancy = 17.9, completeness = 100%) and 3960 (78.1%) reflections were greater than 2σ(I). The unit cell parameters were, **a** = 15.1947(4) Å, **b** = 12.6157(3) Å, **c** = 16.6660(4) Å, $\alpha = \beta = \gamma = 90^o$, V = 3194.74(14) Å^3, Z = 4, calculated density D_c = 1.145 g/cm^3. Absorption corrections were applied (absorption coefficient μ = 0.066 mm^{-1}; min/max transmission = 0.966/0.975) to the raw intensity data using the SADABS program.

The Bruker SHELXTL software package was used for phase determination and structure refinement. The distribution of intensities (E^2-1 = 0.997) and systematic absent reflections indicated two possible space groups, Pna2(1) and Pnma. The space group Pnma (#62) was later determined to be correct. Direct methods of phase determination followed by two Fourier cycles of refinement led to an electron density map from which most of the non-hydrogen atoms were identified in the asymmetric unit of the unit cell. With subsequent isotropic refinement, all of the non-hydrogen atoms were identified. There was half a molecule of $C_3H_2N_2[CH_{11}B_{11}][C_9H_{11}]Li[C_4H_8O]_3$ present in the asymmetric unit of the unit cell. All three THF molecules were modeled with disorder (the THF disorder site occupancy ratios were 50%/50%, 56%/44%, and 56%/44%). The molecule was located at the mirror plane perpendicular to the **b**-axis.

Atomic coordinates, isotropic and anisotropic displacement parameters of all the non-hydrogen atoms were refined by means of a full matrix least-squares procedure on F^2. The H-atoms were included in the refinement in calculated positions riding on the atoms to which they were attached. The refinement converged at R1 = 0.0513, wR2 = 0.1426, with intensity I>2σ (I). The largest peak/hole in the final difference map was 0.338/-0.186 e/Å^3. CCDC #1028440 has the complete crystallographic information.

Table 2-1 Crystal data and structure refinement for **35[Li$^+$]**.

Identification code	vL123MA_0m	
Empirical formula	C25 H48 B11 Li N2 O3	
Formula weight	550.50	
Temperature	163(2) K	
Wavelength	0.71073 Å	
Crystal system	Orthorhombic	
Space group	P n m a	
Unit cell dimensions	a = 15.1947(4) Å	α = 90°.
	b = 12.6157(3) Å	β = 90°.
	c = 16.6660(4) Å	γ = 90°.
Volume	3194.74(14) Å^3	
Z	4	
Density (calculated)	1.145 Mg/m^3	
Absorption coefficient	0.066 mm^{-1}	
F(000)	1176	
Crystal size	0.532 x 0.455 x 0.379 mm^3	
Theta range for data collection	1.814 to 30.507°.	
Index ranges	-21<=h<=21, -18<=k<=18, -23<=l<=23	
Reflections collected	90725	

Independent reflections	5070 [R(int) = 0.0355]
Completeness to theta = 25.242°	100.0 %
Absorption correction	Semi-empirical from equivalents
Refinement method	Full-matrix least-squares on F^2
Data / restraints / parameters	5070 / 20 / 261
Goodness-of-fit on F^2	1.037
Final R indices [I>2sigma(I)]	R1 = 0.0513, wR2 = 0.1426
R indices (all data)	R1 = 0.0667, wR2 = 0.1565
Extinction coefficient	n/a
Largest diff. peak and hole	0.338 and -0.186 e.$Å^{-3}$

Crystal Structure of Dianionic Lithium Carbene 36:

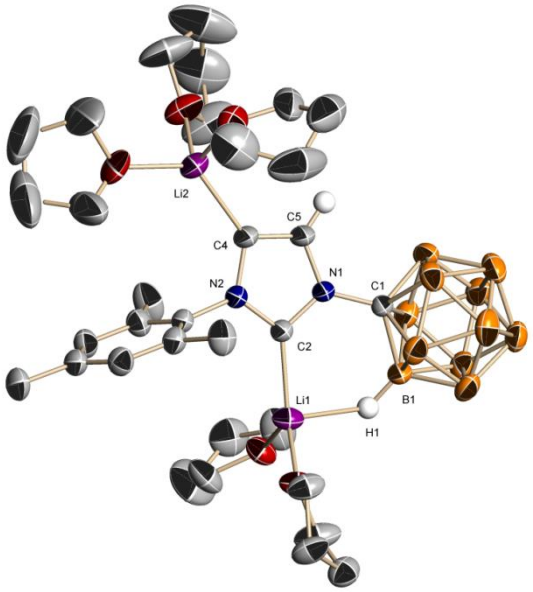

Figure 2-77 Solid state structure of **36**. Hydrogen atoms (except C5-H and H1) are omitted for clarity.

A colorless prism fragment (0.518 x 0.428 x 0.261 mm^3) was used for the single crystal x-ray diffraction study of $C_3HN_2[CH_{11}B_{11}][C_9H_{11}]Li_2[C_4H_8O]_5.[C_4H_8O]_{0.48}$ (sample vL131SF_0m). The crystal was coated with paratone oil and mounted on to a cryo-loop glass fiber. X-ray intensity data were collected at 200(2) K on a Bruker APEX2 platform-CCD x-ray diffractometer system (fine focus Mo-radiation, λ = 0.71073 Å, 50KV/30mA power). The CCD detector was placed at a distance of 5.0600 cm from the crystal.

A total of 3600 frames were collected for a sphere of reflections (with scan width of 0.3^o in ω, starting ω and 2θ angles of -30^o, and ϕ angles of 0^o, 90^o, 120^o, 180^o, 240^o, and 270^o for every 600 frames, 60 sec/frame exposure time). The frames were integrated using the Bruker SAINT software package and using a narrow-frame integration algorithm. Based on a orthorhombic crystal system, the integrated frames yielded a total of 102718 reflections at a maximum 2θ angle of 60.064^o (0.71 Å resolution), of which 13139 were independent reflections (R_{int} = 0.0286, R_{sig} = 0.0155, redundancy = 7.8, completeness = 99.9%) and 11345 (86.3%) reflections were greater than $2\sigma(I)$. The unit cell parameters were, **a** = 15.9089(11) Å, **b** = 26.7369(19) Å, **c** = 10.5610(8) Å, $\alpha = \beta = \gamma = 90^o$, V = 4492.2(6) $Å^3$, Z = 4, calculated density D_c = 1.087

g/cm^3. Absorption corrections were applied (absorption coefficient μ = 0.066 mm^{-1}; min/max transmission = 0.967/0.983) to the raw intensity data using the SADABS program.

The Bruker SHELXTL software package was used for phase determination and structure refinement. The distribution of intensities (E^2-1 = 0.766) and systematic absent reflections indicated two possible space groups, Pnnm and Pnn2. The space group Pnn2 (#34) was later determined to be correct. Direct methods of phase determination followed by two Fourier cycles of refinement led to an electron density map from which most of the non-hydrogen atoms were identified in the asymmetric unit of the unit cell. With subsequent isotropic refinement, all of the non-hydrogen atoms were identified. There was one molecule of $C_3HN_2[CH_{11}B_{11}][C_9H_{11}]Li_2[C_4H_8O]_5$ and one partially occupied [48%] C_4H_8O solvent molecule present in the asymmetric unit of the unit cell. Three of the five THF molecules bonded to the two Li-atoms were modeled with disorder (the THF disorder site occupancy ratios were 50%/50%, 56%/44%, and 56%/44%). The partially occupied THF solvent molecule was located at the 2-fold rotation axis parallel to the **c**-axis. Note that the crystal shattered at about 135K.

Atomic coordinates, isotropic and anisotropic displacement parameters of all the non-hydrogen atoms were refined by means of a full matrix least-squares procedure on F^2. The H-atoms were included in the refinement in calculated positions riding on the atoms to which they were attached. The refinement converged at R1 = 0.0551, wR2 = 0.1520, with intensity I>2σ (I). The largest peak/hole in the final difference map was 0.400/-0.252 e/Å^3. CCDC #1028443 has the complete crystallographic information.

Table 2-2 Crystal data and structure refinement for **36**.

Identification code	vL131SF_0m
Empirical formula	C34.93 H66.85 B11 Li2 N2 O5.48
Formula weight	735.40
Temperature	200(2) K
Wavelength	0.71073 Å

Crystal system	Orthorhombic	
Space group	P n n 2	
Unit cell dimensions	a = 15.9089(11) Å	α = 90°.
	b = 26.7369(19) Å	β = 90°.
	c = 10.5610(8) Å	γ = 90°.
Volume	4492.2(6) $Å^3$	
Z	4	
Density (calculated)	1.087 Mg/m^3	
Absorption coefficient	0.066 mm^{-1}	
F(000)	1581	
Crystal size	0.518 x 0.428 x 0.261 mm^3	
Theta range for data collection	1.489 to 30.032°.	
Index ranges	-22<=h<=22, -37<=k<=37, -14<=l<=14	
Reflections collected	102718	
Independent reflections	13139 [R(int) = 0.0286]	
Completeness to theta = 25.242°	99.9 %	
Absorption correction	Semi-empirical from equivalents	
Refinement method	Full-matrix least-squares on F^2	
Data / restraints / parameters	13139 / 1296 / 804	
Goodness-of-fit on F^2	1.054	

Final R indices [I>2sigma(I)]	R1 = 0.0551, wR2 = 0.1520
R indices (all data)	R1 = 0.0637, wR2 = 0.1624
Absolute structure parameter	-0.03(11)
Extinction coefficient	n/a
Largest diff. peak and hole	0.400 and -0.252 e.Å^{-3}

Crystal Structure of 41[2Li$^+$]

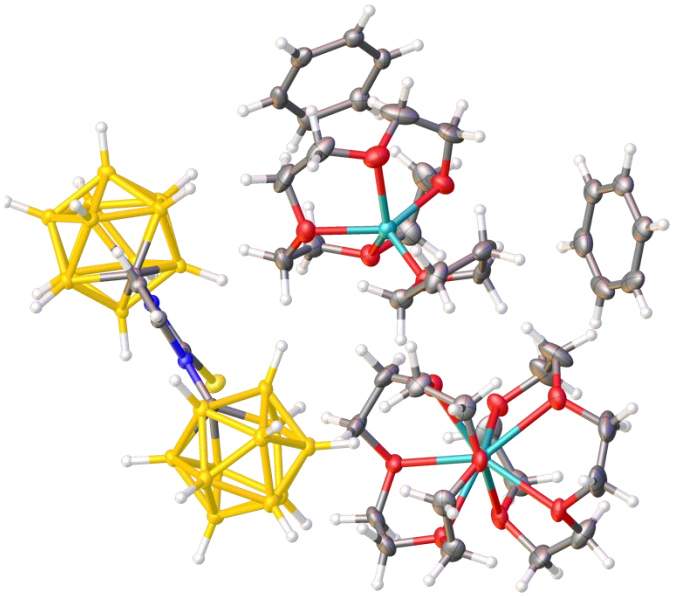

Figure 2-78 Solid state structure of **41[2Li$^+$]**. Color code: H = white, Li = teal, B = yellow N = blue, O = red, S = pale yellow.

Table 2-3 Crystal data and structure refinement for **41[2Li$^+$]**.

Identification code	lavallo27_a	
Empirical formula	C45 H92 B22 Li2 N2 O13 S	
Formula weight	1152.96	
Temperature	100 K	
Wavelength	0.71073 Å	
Crystal system	Monoclinic	
Space group	P 21/n	
Unit cell dimensions	a = 13.1519(6) Å	α= 90°.
	b = 13.6915(7) Å	β= 100.500(2)°.
	c = 35.0702(16) Å	γ = 90°.
Volume	6209.3(5) Å^3	
Z	4	
Density (calculated)	1.233 Mg/m^3	
Absorption coefficient	0.111 mm^{-1}	
F(000)	2448	
Crystal size	0.34 x 0.3 x 0.28 mm^3	
Theta range for data collection	1.899 to 25.394°.	
Index ranges	-15<=h<=15, -16<=k<=16, -42<=l<=40	
Reflections collected	43873	
Independent reflections	11393 [R(int) = 0.0565]	

Completeness to theta = 26.000°	97.3 %
Absorption correction	Semi-empirical from equivalents
Max. and min. transmission	0.2590 and 0.2266
Refinement method	Full-matrix least-squares on F^2
Data / restraints / parameters	11393 / 0 / 766
Goodness-of-fit on F^2	1.028
Final R indices [I>2sigma(I)]	R1 = 0.0653, wR2 = 0.1606
R indices (all data)	R1 = 0.0976, wR2 = 0.1826
Extinction coefficient	n/a
Largest diff. peak and hole	0.903 and -0.405 e.$Å^{-3}$

2.6 References

1. A. Spokoyny, *Pure and Applied Chemistry*, 2013, **85**, 903-919.
2. J. Zhang ,Z. Xie, *Accounts of Chemical Research*, 2014, **47**, 1623-1633.
3. A. R. Popescu, F. Teixidor ,C. Viñas, *Coordination Chemistry Reviews*, 2014, **269**, 54-84.
4. C. Douvris ,J. Michl, *Chemical Reviews*, 2013, **113**, PR179-PR233.
5. D. Olid, R. Núñez, C. Viñas ,F. Teixidor, *Chemical Society Reviews*, 2013, **42**, 3318-3336.
6. Z.-J. Yao ,G.-X. Jin, *Organometallics*, 2012, **31**, 1767-1774.
7. P. Farràs, E. J. Juárez-Pérez, M. Lepšík, R. Luque, R. Núñez ,F. Teixidor, *Chemical Society Reviews*, 2012, **41**, 3445-3463.
8. M. Scholz ,E. Hey-Hawkins, *Chemical Reviews*, 2011, **111**, 7035-7062.
9. P. v. R. Schleyer, C. Maerker, A. Dransfeld, H. Jiao ,N. J. R. van Eikema Hommes, *Journal of the American Chemical Society*, 1996, **118**, 6317-6318.
10. E. L. Hoel ,M. F. Hawthorne, *Journal of the American Chemical Society*, 1975, **97**, 6388-6395.
11. R. A. Wiesboeck ,M. F. Hawthorne, *Journal of the American Chemical Society*, 1964, **86**, 1642-1643.
12. F. Teixidor, M. A. Flores, C. Viñas, R. Kivekäs ,R. Sillanpää, *Organometallics*, 1998, **17**, 4675-4679.
13. A. El-Hellani, C. E. Kefalidis, F. S. Tham, L. Maron ,V. Lavallo, *Organometallics*, 2013, **32**, 6887-6890.
14. S. P. Fisher, A. W. Tomich, S. O. Lovera, J. K. Kleinsasser, J. Guo, M. J. Asay, H. M. Nelson ,V. Lavallo, *Chemical Reviews*, 2019.
15. C. A. Reed, *Accounts of Chemical Research*, 2010, **43**, 121-128.
16. R. Ramírez-Contreras, N. Bhuvanesh, J. Zhou ,O. V. Ozerov, *Angewandte Chemie International Edition*, 2013, **52**, 10313-10315.
17. C. Douvris, C. M. Nagaraja, C.-H. Chen, B. M. Foxman ,O. V. Ozerov, *Journal of the American Chemical Society*, 2010, **132**, 4946-4953.
18. C. Douvris ,O. V. Ozerov, *Science*, 2008, **321**, 1188-1190.
19. K.-C. Kim, C. A. Reed, D. W. Elliott, L. J. Mueller, F. S. Tham, L. Lin ,J. B. Lambert, *Science*, 2002, **297**, 825-827.

20. V. Lavallo, J. H. Wright Ii, F. S. Tham ,S. Quinlivan, *Angewandte Chemie International Edition*, 2013, **52**, 3172-3176.

21. J. Estrada, S. E. Lee, S. G. McArthur, A. El-Hellani, F. S. Tham ,V. Lavallo, *Journal of Organometallic Chemistry*, 2015, **798**, 214-217.

22. J. Estrada, C. A. Lugo, S. G. McArthur ,V. Lavallo, *Chemical Communications*, 2016, **52**, 1824-1826.

23. A. El-Hellani ,V. Lavallo, *Angewandte Chemie International Edition*, 2014, **53**, 4489-4493.

24. J. Estrada ,V. Lavallo, *Angewandte Chemie International Edition*, 2017, **56**, 9906-9909.

25. J. F. Kleinsasser, E. D. Reinhart, J. Estrada, R. F. Jordan ,V. Lavallo, *Organometallics*, 2018, **37**, 4773-4783.

26. J. F. Kleinsasser, S. E. Lee, C. A. Lugo, V. Tej, S. G. McArthur ,V. Lavallo, *Polyhedron*, 2018, **156**, 245-248.

27. A. L. Chan, J. Estrada, C. E. Kefalidis ,V. Lavallo, *Organometallics*, 2016, **35**, 3257-3260.

28. J. Estrada, D. H. Woen, F. S. Tham, G. M. Miyake ,V. Lavallo, *Inorganic Chemistry*, 2015, **54**, 5142-5144.

29. J. B. Dumas, *Ann. Chimie et Phys.*, 1835, **58**, 28.

30. H. V. Regnault, *Ann. Chimie et Phys.*, 1839, **71**, 427.

31. D. Enders, K. Breuer, J. Runsink ,J. Henrique Teles, *Liebigs Annalen*, 1996, **1996**, 2019-2028.

32. W. Kirmse, *Carbene Chemistry*, Academic Press, New York, 1971.

33. Demselben, *Justus Liebigs Annalen der Chemie*, 1862, **123**, 121-122.

34. W. von E. Doering ,A. K. Hoffmann, *Journal of the American Chemical Society*, 1954, **76**, 6162-6165.

35. H.-J. Schönherr ,H.-W. Wanzlick, *Justus Liebigs Annalen der Chemie*, 1970, **731**, 176-179.

36. A. Igau, H. Grutzmacher, A. Baceiredo ,G. Bertrand, *Journal of the American Chemical Society*, 1988, **110**, 6463-6466.

37. A. Igau, A. Baceiredo, G. Trinquier ,G. Bertrand, *Angewandte Chemie International Edition in English*, 1989, **28**, 621-622.

38. A. J. Arduengo, R. L. Harlow ,M. Kline, *Journal of the American Chemical Society*, 1991, **113**, 361-363.

39. A. J. Arduengo Iii, J. R. Goerlich, R. Krafczyk ,W. J. Marshall, *Angewandte Chemie International Edition*, 1998, **37**, 1963-1965.

40. D. M. Lemal, R. A. Lovald ,K. I. Kawano, *Journal of the American Chemical Society*, 1964, **86**, 2518-2519.

41. W. A. Herrmann ,C. Köcher, *Angewandte Chemie International Edition in English*, 1997, **36**, 2162-2187.

42. E. Aldeco-Perez, A. J. Rosenthal, B. Donnadieu, P. Parameswaran, G. Frenking ,G. Bertrand, *Science*, 2009, **326**, 556.

43. K. H. Dötz ,J. Stendel, *Chemical Reviews*, 2009, **109**, 3227-3274.

44. D. M. Flanigan, F. Romanov-Michailidis, N. A. White ,T. Rovis, *Chemical Reviews*, 2015, **115**, 9307-9387.

45. S. P. Nolan, *N-Heterocyclic Carbenes*, Wiley-VCH Verlag GmbH & Co. KGaA, Weinheim, Germany, 2014.

46. M. N. Hopkinson, C. Richter, M. Schedler ,F. Glorius, *Nature*, 2014, **510**, 485.

47. H. V. Huynh, *Chemical Reviews*, 2018, **118**, 9457-9492.

48. V. Lavallo, Y. Canac, C. Präsang, B. Donnadieu ,G. Bertrand, *Angewandte Chemie International Edition*, 2005, **44**, 5705-5709.

49. V. Lavallo, J. Mafhouz, Y. Canac, B. Donnadieu, W. W. Schoeller ,G. Bertrand, *Journal of the American Chemical Society*, 2004, **126**, 8670-8671

50. H. W. Wanzlick ,H. J. Kleiner, *Angewandte Chemie*, 1961, **73**, 493-493.

51. H.-W. Wanzlick, F. Esser ,H.-J. Kleiner, *Chemische Berichte*, 1963, **96**, 1208-1212.

52. P. B. Hitchcock, *Journal of the Chemical Society, Dalton Transactions*, 1979, 1314-1317.

53. T. Dröge ,F. Glorius, *Angewandte Chemie International Edition*, 2010, **49**, 6940-6952.

54. T. Jelínek, J. Plešek, S. Hermanek ,S. Bohumil, *Collection of Czechoslovak Chemical Communications*, 1986, **51**, 819-829.

55. D. Martin, M. Melaimi, M. Soleilhavoup ,G. Bertrand, *Organometallics*, 2011, **30**, 5304-5313.

56. S. Díez-González, N. Marion ,S. P. Nolan, *Chemical Reviews*, 2009, **109**, 3612-3676.

57. S. Gründemann, A. Kovacevic, M. Albrecht, J. W. Faller Robert ,H. Crabtree, *Chemical Communications*, 2001, **0**, 2274-2275.

58. O. Schuster, L. Yang, H. G. Raubenheimer ,M. Albrecht, *Chemical Reviews*, 2009, **109**, 3445-3478.

59. R. H. Crabtree, *Coordination Chemistry Reviews*, 2013, **257**, 755-766.

60. Y. Wang, Y. Xie, M. Y. Abraham, P. Wei, H. F. Schaefer, P. v. R. Schleyer ,G. H. Robinson, *Journal of the American Chemical Society*, 2010, **132**, 14370-14372.

61. A. Fürstner, M. Alcarazo, V. César ,C. W. Lehmann, *Chemical Communications*, 2006, 2176-2178.

62. M. J. Asay, S. P. Fisher, S. E. Lee, F. S. Tham, D. Borchardt ,V. Lavallo, *Chemical Communications*, 2015, **51**, 5359-5362.

63. S. Bellemin-Laponnaz ,S. Dagorne, *Chemical Reviews*, 2014, **114**, 8747-8774.

64. L. A. Boyd, W. Clegg, R. C. B. Copley, M. G. Davidson, M. A. Fox, T. G. Hibbert, J. A. K. Howard, A. Mackinnon, R. J. Peace ,K. Wade, *Dalton Transactions*, 2004, **0**, 2786-2799.

65. M. Etienne ,A. S. Weller, *Chemical Society Reviews*, 2014, **43**, 242-259.

66. M. Brookhart, M. L. H. Green ,G. Parkin, *Proceedings of the National Academy of Sciences*, 2007, **104**, 6908.

67. E. Alvarado, A. C. Badaj, T. G. Larocque ,G. G. Lavoie, *Chemistry – A European Journal*, 2012, **18**, 12112-12121.

68. M. Ruamps, S. Bastin, L. Rechignat, A. Sournia-Saquet, D. A. Valyaev, J.-M. Mouesca, N. Lugan, V. Maurel ,V. César, *Chemical Communications*, 2018, **54**, 7653-7656.

69. X. Fan, W. Sun, F. Meng, A. Xing ,J. Liu, *Green Energy & Environment*, 2018, **3**, 2-19.

70. P. J. Cox, B. Sohal, G. G. Skellern, S. W. Love ,N. Shankland, *Acta Crystallographica Section C*, 1996, **52**, 3152-3154.

71. R. P. Singh, D. Gout ,C. J. Lovely, *European Journal of Organic Chemistry*, 2019, **2019**, 1726-1740.

72. J. Huang, S. Hans-Jörg, E. D. Stevens, S. P. Nolan, K. B. Capps, A. Bauer ,C. D. Hoff, *Inorganic Chemistry*, 2000, **39**, 1042-1045.

73. S.-S. Shen, M.-Y. Lei, Y.-X. Wong, M.-L. Tong, P. L.-Y. Teo, S. Chiba ,K. Narasaka, *Tetrahedron Letters*, 2009, **50**, 3161-3163.

74. S. G. McArthur, R. Jay, L. Geng, J. Guo ,V. Lavallo, *Chemical Communications*, 2017, **53**, 4453-4456.

75. S. G. McArthur, L. Geng, J. Guo ,V. Lavallo, *Inorganic Chemistry Frontiers*, 2015, **2**, 1101-1104.

Chapter 3: Anionic and Zwitterionic Carboranyl N-heterocyclic Carbene Complexes with Coinage Metals (Au and Cu)

3.1 Introduction

N-heterocyclic carbene ligands are ubiquitous motifs in transition metal chemistry and have been utilized in both early and late transition metal complexes. Some of the most well-known examples are Grubb's first- and second-generation olefin metathesis catalysts. The difference between the first and second generation being the replacement of one phosphine ligand with a saturated NHC (imidazolin-2-ylidene) ligand, Figure 3-1. In the second generation catalyst, the NHC gives the catalyst greater activity, enhanced thermal stability, and cross-metathesis selectivity.[1, 2] In fact, metathesis catalysts have found tremendous importance in the chemical industry such as industrial applications. There applications include the processing of 180,000 metric tons of seed oil to olefins, oleochemicals and specialty chemicals,[3] and the medical field. The World Health Organization has deemed Simeprevir, a hepatitis C treatment medication, an essential medicine. One of the steps in the synthesis of this drug requires a Grubb's catalyst to perform a ring closing metathesis of two olefins.[4, 5]

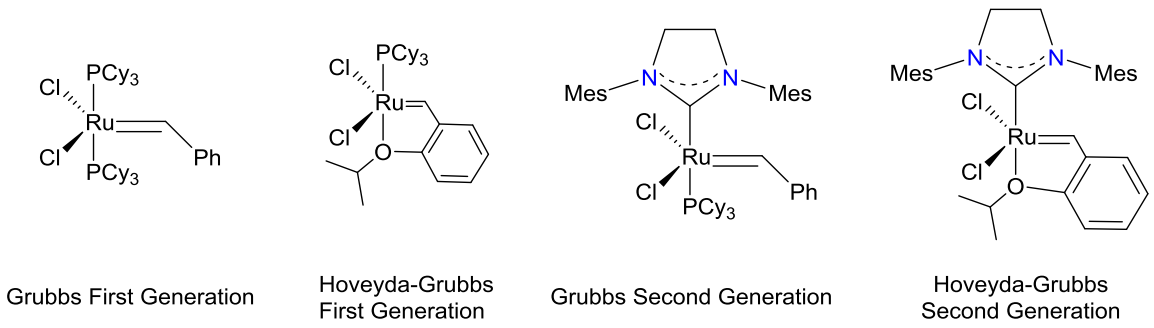

Figure 3-1 Structure of first- and second-generation Grubbs catalyst.

Within the last ten years, Au complexes have grown in remarkable scientific interest and a majority of these complexes bear either a phosphine or NHC ligand with most, if not all of these systems, ligands are designed with pendant alkyl or aryl substituents that can be utilized to manipulate the behavior of the Au center. An alternative to hydrocarbon ligand R-groups are 3-dimensionally aromatic icosahedral carboranes.[6-11] The typical carboranes used in ligand design are derivatives of the icosahedral dicarbaboranes ($H_2C_2B_{10}H_{10}$).[7] Due to its facile synthesis from decaborane,[12, 13] the *ortho*-carborane (**2**) isomer is the most common cluster implemented for these purposes. While this cluster has many intriguing properties, such as a large spherical steric profile, as well as the ability to form H-H hydrogen bonds,[7] it displays chemical reactivity that can be problematic for catalysis, such as facile B-H cyclometallation[14] and cluster opening[9] reactions. The later reactions have been implemented by Teixidor and Viñas to design anionic ligands, featuring *nido*-cluster substituents.[15-18]

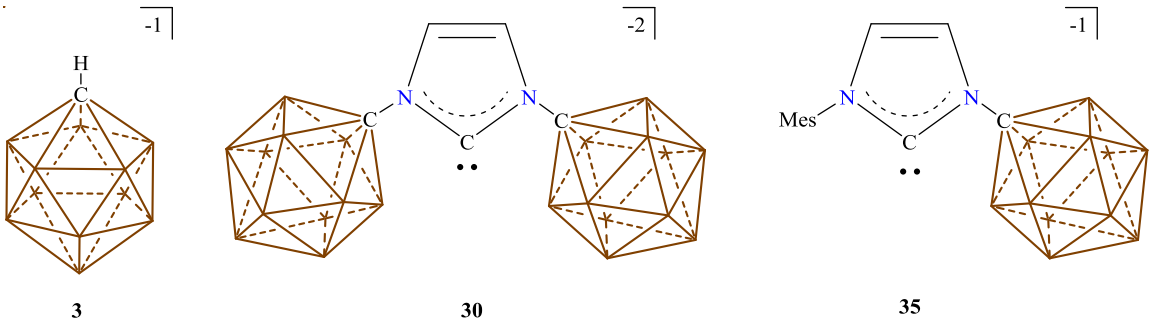

3 **30** **35**

Figure 3-2 The carba-*closo*-dodecaborate anion **3** (left). Symmetrical dianionic carboranyl NHC **30** (center) and unsymmetrical carboranyl NHC **35** (right). Unlabeled cluster vertices = B-H.

In contrast to the neutral C_2B_{10} clusters, the isoelectronic anionic carba-*closo*-dodecaborate cluster **3** ($HCB_{11}H_{11}^-$),[8] Figure 3-2, and its derivatives do not undergo cluster opening reactions and are more resistant to B-H cyclometallation.[19, 20] Additionally, these polyhalogenated clusters are among the weakest coordinating and most robust counter anions known.[21] These properties have been utilized to prepare

isolable versions of highly reactive cations[22-25] and superior systems for silylium[26-29] catalysis. Furthermore, in contrast to *o*-carborane, **3** acts as a strong electron donor, similar to an alkyl group.[30]

We recently reported the first utilization of cluster **3** and its derivatives as ligand substituents for transition metal-based catalysts.[31-35] Notably, it was shown that when complexed to Au(I) a phosphine bearing a perchlorinated carborane anion substituent forms an exceptionally active catalyst for the hydroamination of alkynes.[32] In addition, this system is a single component zwitterionic species that does not require the addition of an acid or Ag initiator. As an extension of this work we have reported the synthesis of symmetrical and unsymmetrical anionic carboranyl N-heterocyclic carbenes[36-44] (NHCs) **30**[45] and **35**[46] (figure 3-2). Depending on the base employed to generate the NHC, such ligands can be prepared as either Li^+, Na^+, or K^+ salts.

Having a van der Waals volume[11] of approximately 141-148 Å cm^{-3}, **3** is an exceptionally large ligand substituent. Coupling these anions to the wing-tips of NHCs should direct the steric bulk of the substituent into the coordination sphere of the ensuing metal center. Considering the size of the anion and the geometry imposed on the rigid NHC 5-membered ring framework, one might question whether these ligands are too large to effectively bind. Herein we show that both carbonranyl NHCs **30** and **35** will readily bind transition metals through the preparation of unusual zwitterionic and anionic Au(I) carbene complexes. These compounds are thoroughly characterized and their structural parameters elucidated by single crystal X-ray diffraction studies as well as percent buried volume ($\%V_{bur}$) [47, 48] calculations.

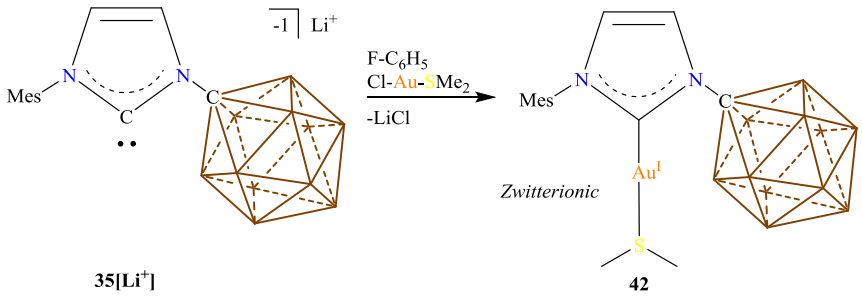

Scheme 3-1 The unsymmetrical carboranyl NHC Li salt **35[Li$^+$]** reacts with ClAuSMe$_2$ to form the corresponding zwitterionic gold complex **42**.

3.2 Synthesis of a Zwitterionic Au(I) Complex

To begin this investigation, we chose to target Au(I) complexes, since they nearly always adopt dicoordinate, linear geometries that are accommodating to large ligands. Moreover, Au(I) complexes are usually thermally stable and easy to handle. This approach was borne out *via* reacting ClAuSMe$_2$ with the lithium carbene **35[Li$^+$]** in a 1:1 ratio with F-C$_6$H$_5$ solvent, Scheme 3-1. Within minutes a white precipitate of LiCl formed and the solution was analyzed by multinuclear NMR spectroscopy. The ^{11}B spectrum shows the expected three resonances (1:5:5 ratio) for the C_{5V} symmetric cluster, indicating that the cluster is intact. Analysis of the ^{1}H spectrum shows the expected downfield shift for the NHC backbone resonances (^{1}H NMR: **35[Li$^+$]** 7.40 and 6.79 ppm; d, $^3J_{H\text{-}H}$ = 1.5 Hz; **42** = 7.71 and 6.83 ppm; d, $^3J_{H\text{-}H}$ = 2.1 Hz), suggesting an NHC Au adduct had formed. In addition, the presence of a bound dimethyl sulfide resonance (free S(Me)$_2$ 2.09 ppm; bound S(Me)$_2$ 2.60 ppm) is consistent with the formation of the zwitterionic gold complex **42**, Scheme 3-1. Furthermore, the ^{13}C spectrum clearly shows a downfield resonance at 175.2 ppm for the bound NHC ligand.

Gold zwitterions that retain a dative thioether ligand are rare but have been observed by our group,[32] as well as Tamm[49] and Bourissou,[50]when weakly coordinating anions are built into the ligand scaffolds. The composition of **42** was confirmed by high resolution mass spectrometry and a single crystal X-ray diffraction study, Figure 3-3. In the solid-state, the complex displays a distorted linear geometry (C1-Au-S angle = 171.7°) which is likely due to the asymmetry of the carboranyl NHC ligand. Interestingly, the

carborane anion is canted away from the cationic gold center, which highlights its weakly coordinating nature. The closest B-H approach to the gold center is 2.81 Å, which is in range for a van der Waals contact but outside the range for cluster B-H agostic bonding.[20, 51, 52] In turn, the mesityl ring is tilted towards the gold center, suggesting a cation-π interaction (Au-C3 distance = 3.168 Å). The NHC Au bond length (2.007(2) Å) falls in the typical range for NHC Au(I) complexes.[36-44] The N-heterocyclic core bond lengths are also in the expected range for standard imidazolyliene Au complexes (bond lengths in Å; C1-N1 = 1.349(3), C1-N2 = 1.353(3), N1-C4 = 1399(3), N2-C5 = 1.382(3), C4-C5 = 1.342(3)). [36-44] In addition, the dative SMe_2 bond length to Au(I) (2.2971(12) is similar to that reported for other zwitterionic gold thioether complexes (2.3026 - 2.456 Å).[32, 49, 50]

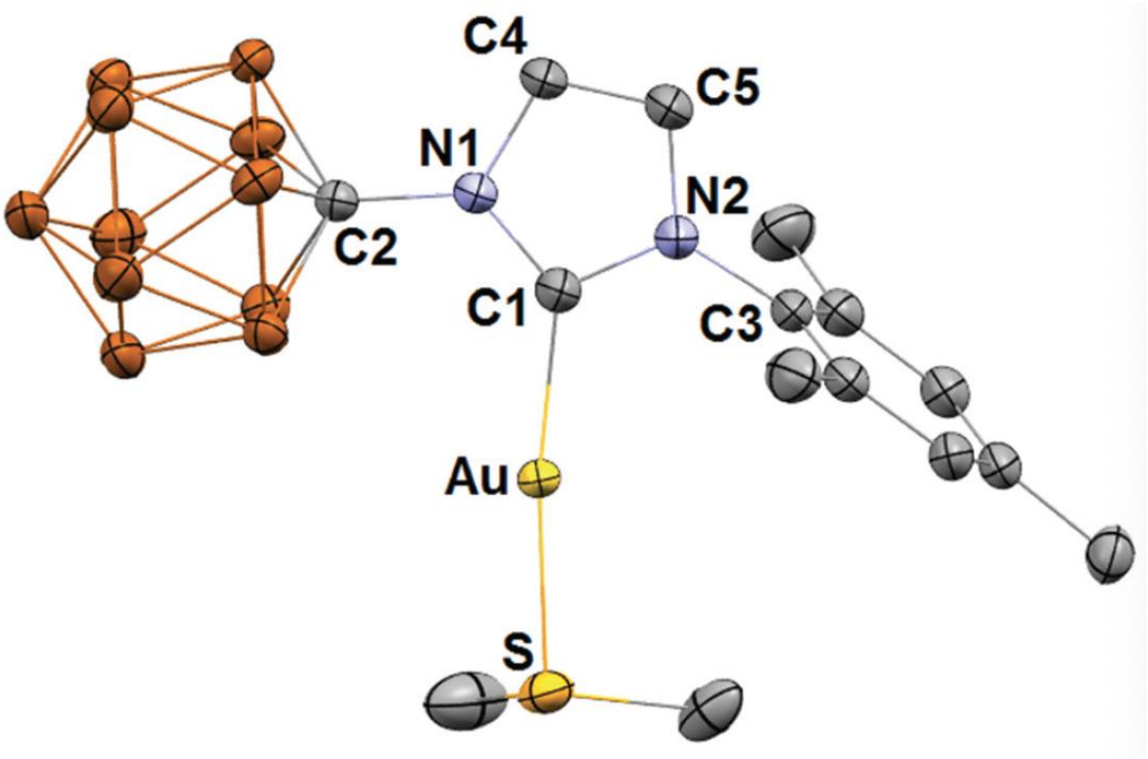

Figure 3-3 Solid state structure of **42**. Hydrogen and a THF solvent molecule of crystallization are omitted for clarity. Color code: C = gray, B = brown, N = blue, Au = orange, S = yellow.

3.3 Synthesis of an Anionic and Dianionic Au(I) complexes

We next turned our attention to the synthesis of an analogous monoanionic complex **43[Li$^+$]**, featuring the symmetrical dianionic carboranyl NHC ligand **30**. Thus, Cl-Au-SMe_2 was reacted with the lithium carbene **30** in a 1:1 ratio with F-C_6H_5 solvent, Scheme 3-2. Copious amounts of oily precipitate rapidly formed in the reaction. Filtration and subsequent concentration of the solution under high vacuum yields the mono anionic Au(I) complex **43[Li$^+$]** in 22% yield and high purity. The identity of **43[Li$^+$]** was corroborated by multinuclear NMR spectroscopy. The ^{11}B spectrum shows the expected three resonances (1:5:5 ratio) for the cluster. The ^{1}H NMR spectrum displays a single downfield shifted resonance for the NHC backbone (^{1}H NMR: [**30** = 6.91; **43[Li$^+$]** = 7.34 ppm] as well as two equivalent methyl groups corresponding to bound dimethyl sulfide and four THF molecules coordinated to the lithium counter cation. The ^{13}C spectrum shows a downfield resonance at 174.3 ppm for the bound NHC ligand.

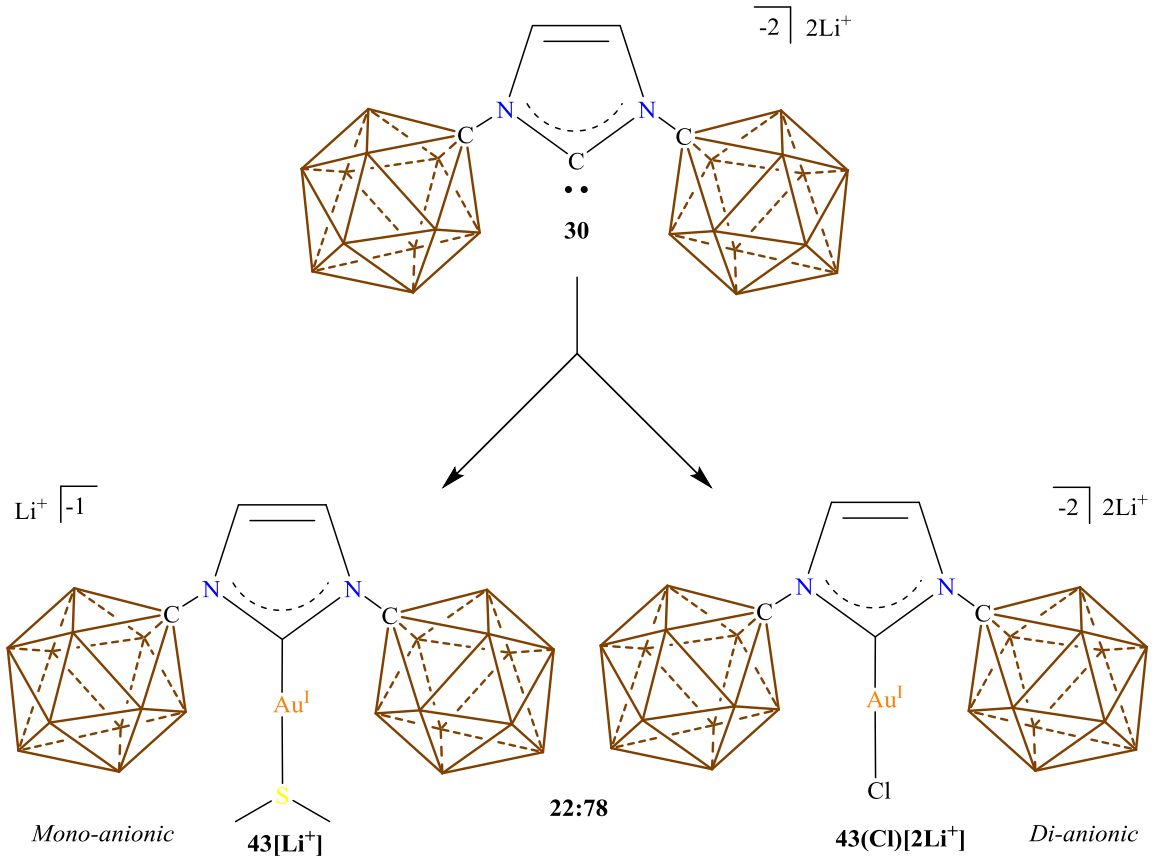

Scheme 3-2 Reaction of dianionic NHC **30** with $ClAuSMe_2$ yields two distinct species **43[Li$^+$]** and **43(Cl)[2Li$^+$]**, which can easily be separated by their differences in solubility.

Puzzled by the low yield of this reaction we postulated that perhaps a distinct species, which is not soluble in F-C_6H_5, precipitated from the reaction and lowered the isolated yield of **43[Li$^+$]**. Indeed, analysis of the residue by multinuclear NMR revealed the formation of a distinct carbene complex that lacks a dimethyl sulfide ligand. The low solubility of this compound in F-C_6H_5 suggest the formation of a more ionic species that we tentatively assign as the dianionic Au(I) complex **43(Cl)[2Li$^+$]** (Scheme 3-2, bottom right). This assignment is also corroborated by high resolution mass spectrometry that shows a molecular ion peak corresponding to **43(Cl)[2Li$^+$]**. Furthermore, **43(Cl)[2Li$^+$]** can be independently synthesized in quantitative yield by performing the analogous reaction in THF solvent instead of F-C_6H_5. In THF, LiCl is completely soluble and therefore, salt metathesis does not occur; instead dimethyl sulfide is liberated. In

addition, **43(Cl)[2Li$^+$]** can be synthesized by reacting **43[Li$^+$]** with a solution of LiCl in THF, which shows the substitutional lability of dimethyl sulfide in the presence of dissolved Cl^- ions. The lability of the dimethyl sulfide ligand of **43[Li$^+$]** compared to **42** is perhaps due to the enhanced steric bulk of the symmetrical dicarboranyl NHC ligand **30** compared to **35[Li$^+$]**. Since the release of this report, the yield for compound **43[Li$^+$]** has been drastically increased (88% vs 22%) via a two-step synthesis instead of a one-step synthesis. The modified synthesis first generates **43(Cl)[2Li$^+$]** selectively (96% yield, step 1) then by reacting **43[Li$^+$]** with dimethylsulfide in dichloromethane generates **43[Li$^+$]** (92% yield, step 2). The product obtained in this method given identical NMR signatures for **43[Li$^+$]** as the direct method which generates the compound in 22% yield.

Seeking data for a comparison with **42** we performed a single crystal X-ray diffraction study of monoanionic complex **43[Li$^+$]**, Figure 3-4. In contrast to **42**, **43[Li$^+$]** is perfectly linear in the solid state (C1-Au-S angle = 179.7°), which is likely due to the symmetric orientation of the two carborane anions about the gold center. The closest B-H contacts with the gold center are 2.61 and 2.57 Å, which are in range for B-H agostic bonding;[20] however, we see no evidence for this kind of interaction by solution NMR studies. Therefore, the close proximity of the carborane anions is likely due to steric effects. The NHC Au bond length (2.030(3) Å) of **43[Li$^+$]** is only slightly elongated compared to **42**. The N-heterocyclic core bond lengths as well as the Au-SMe_2 (bond lengths in Å; C1-N1 = 1.349(3), C1-N2 = 1.353(3), N1-C4 = 1.399(3), N2-C5 = 1.382(3), C4-C5 = 1.342(3); Au-S = 2.2907(10)) are also similar to **42**.

3.4 Percent Buried Volume Calculations of **42** and **43[Li$^+$]**

To gain further insight into the steric parameters that define carboranyl NHC ligands **30** and **35** percent buried volume (%V_{bur}) calculations were performed.[47, 48] We found that ligands **30** and **35** have %V_{bur} volumes of 47.2 and 46.6, respectively. These values are close to the bulkiest known NHCs (51.2 and 47.7).[48] While %V_{bur} is an effective way to calculate the amount of the ligand periphery occupying the coordination sphere it is a function of substituent conformation. Most of the bulkiest NHCs have somewhat flexible R-groups or contain substituted aromatics that change conformations in solution, giving a range of different %V_{bur} values depending on the atomic coordinates utilized. Therefore, the most

informative comparison to make is perhaps between Arduengo's diadamantyl substituted NHC[36-44] (%V_{bur} = 39.8),[48] which due to the substituents spherical shape maintains similar %V_{bur} regardless of the N-adamantyl bond orientation.

3.5 Catalytic Activity of **42** and **43[Li^+]**

In 2013, our group reported a single component hydroamination catalyst that featured a perhalogenated carboranyl phosphine **44**.[32] Catalyst **44** displayed unprecedented catalytic activity and was capable of hydroaminating phenylacetylene and aniline in one hour at room temperature with a catalyst loading of 0.1 mol%, TON >950 (Table 3-1, entry 1). Catalyst **44** performs ever better with bulky amines and electron rich or electron poor alkynes such as 4-fluorophenylacetylene and 4-methoxyphenylacetylene with TON of 95,000 and 92,000 respectively (Table 3-1, entry 2-3). The only other Au complex that has catalytic activity in this range is Malhotra's complex,[53] **45**, which contains a large bulky phosphine ligand and has a reported TON of 31,200 for the hydroamination of phenylactylene and aniline at 50°C over 24 hours (Table 3-1, entry 4).[54] However, this catalyst is not a single component catalyst and requires extra additives such as $H_3PW_{12}O_4$ and $KCTf_3$ as well as a halide abstraction agent (AgOTf) to generate the Au^+ cation.

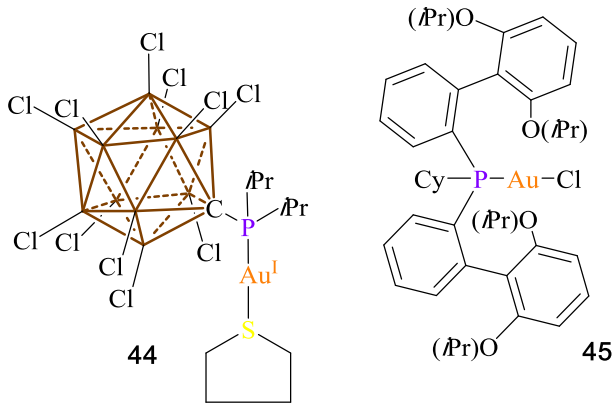

Figure 3-4 Structures of highly active hydroamination catalyst. Lavallo's catalyst **44** and Malhotra's catalyst **45**.

In lieu of these results, we wanted to see if complexes **42** and **43[Li$^+$]** would make a highly active hydroamination catalysts as well. Complexes **42** and **43[Li$^+$]** were catalytically active but did not achieve nearly as high of a TON as Lavallo's or Malhotra's catalyst (Table 3-1, entries 1-4). Both **42** and **43[Li$^+$]** are catalytically active but at 1 mol% loading the catalyst requires 24 hours at room temperature to achieve a TON of >95 for phenylacetylene and aniline (Table 3-1, entries 5-6). The decreased activity of **42** and **43[Li$^+$]** is likely due to the increased steric congestion around the Au center imparted by the forward-facing N-bound substituents of the NHC ligand.

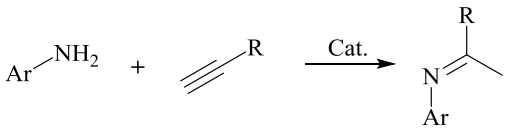

Entry	Catalyst	Catalyst Loading (%)	Ar	R	t (hours)	T (°C)	TON
1	**44**	0.1	Ph	Ph	1	25	>950
2	**44**	0.001	Dipp	4-FC_6H_4	24	50	92,000
3	**44**	0.001	Dipp	4-$MeOC_6H_4$	24	50	>95,000
4	**45**	0.0025	Ph	Ph	24	50	31,200
5	**42**	1	Ph	Ph	24	25	>95
6	**43[Li$^+$]**	1	Ph	Ph	24	25	>95

Table 3-1 Catalytic activity of catalyst **42**, **43[Li$^+$]**, **44** and **45** in the hydroamination reaction. Dipp = 2,6-diisopropylphenyl, Mes = mesityl (2,4,6-trimethylphenyl).

3.6 Synthesis of a Thiourea Au(I) complex

Moving past the catalytic activity of **42** and **43[Li$^+$]** we decided to try and generate a thiourea complex with ligands such as **40**. Thiourea complexes with Au have been reported previously and we were curious to see if thiourea **40** could bind Au in a similar fashion to **30** and **35[Li$^+$]**. Upon reaction with a 1:1 ratio of **40** with $ClAuSMe_2$ in F-C_6H_5 solvent, a white precipitate was observed immediately (Scheme 3-3). An aliquot of the crude reaction mixture was removed and analyzed by multinuclear NMR spectroscopy.

The ^{11}B NMR revealed the typical 1:5:5 pattern suggesting the cluster was intact and retained its C_{5v} symmetry. Analysis of the ^{1}H NMR spectrum revealed a downfield shift of the backbone protons of the imidazolium core (^{1}H NMR: **40** = 7.45 and 6.50 ppm; **46** = 7.84 and 6.75 ppm) and the methyl region displayed the expected three proton resonances at 2.53, 2.37 and 1.96 ppm which we expected to be the 6H of the dimethylsulfide, 3H of the *para* methyls of the mesityl and 6H of the *ortho* methyls of the mesityl, however the integrations were 3:3:3 (**46**) instead of 6:3:6. Upon working up the carobrane containing material it was clear that there was no dimethylsulfide present in the complex (^{1}H NMR of $ClAuSMe_2$ = 2.63 ppm) and instead the peak at 2.53 ppm was one of the methyl resonances of the mesityl which now display three unique resonances instead of two (*ortho* methyls of the mesityl display two unique resonances).

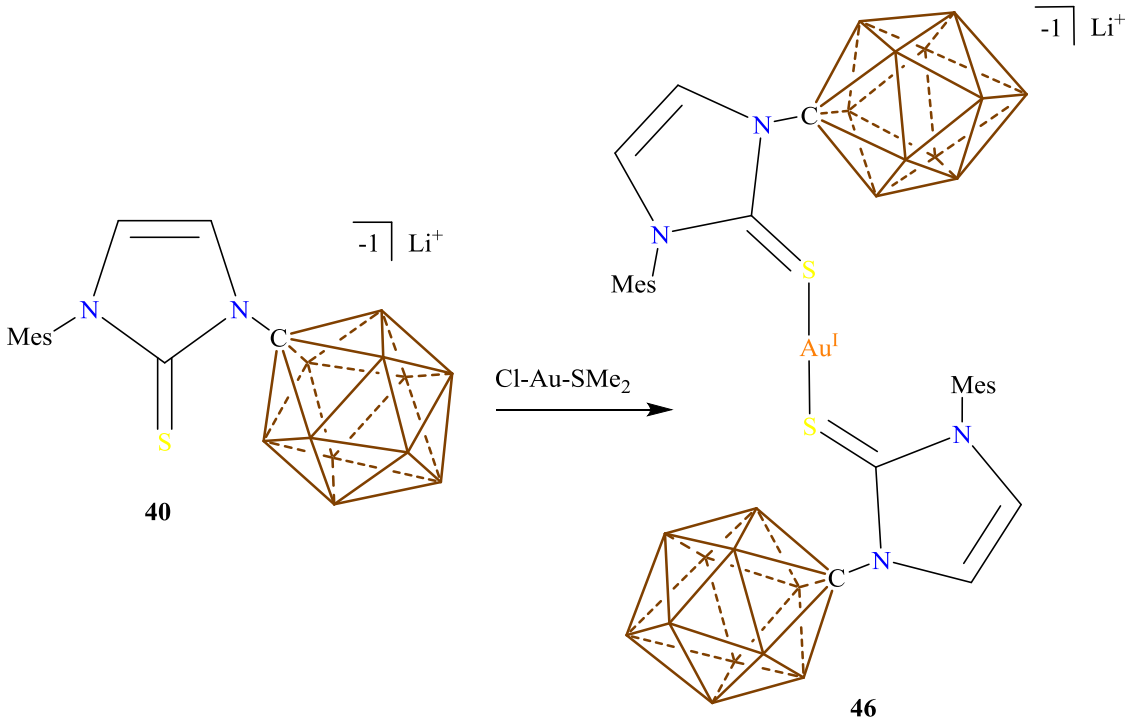

Scheme 3-3 Synthesis of thiourea Au(I) complex, **46**.

The formation of a precipitate and lack of a dimethysulfide resonance in the ^{1}H NMR spectrum suggest the formation of a linear dimeric thiourea Au(I) complex, **46**. To better understand the structure of **46** crystals were grown and a single crystal X-ray diffraction study was performed. Even though the quality of the data was not good enough to accurately discuss bond lengths and angles it was able to confirm the structure of **46**, figure 3-5. As anticipated the unit cell revealed two molecules of thiourea ligand **40**, each thiourea ligand was bound to the Au(I) center though the sulfur atom. Since two thiourea ligands were bound to the Au(I) center the crystal structure also revealed a free Li^{+} ion coordinated by 4 molecules of THF. Since complex **46** did not contain a labile SMe_2 ligand we opted not to test it as a hydroamination catalyst.

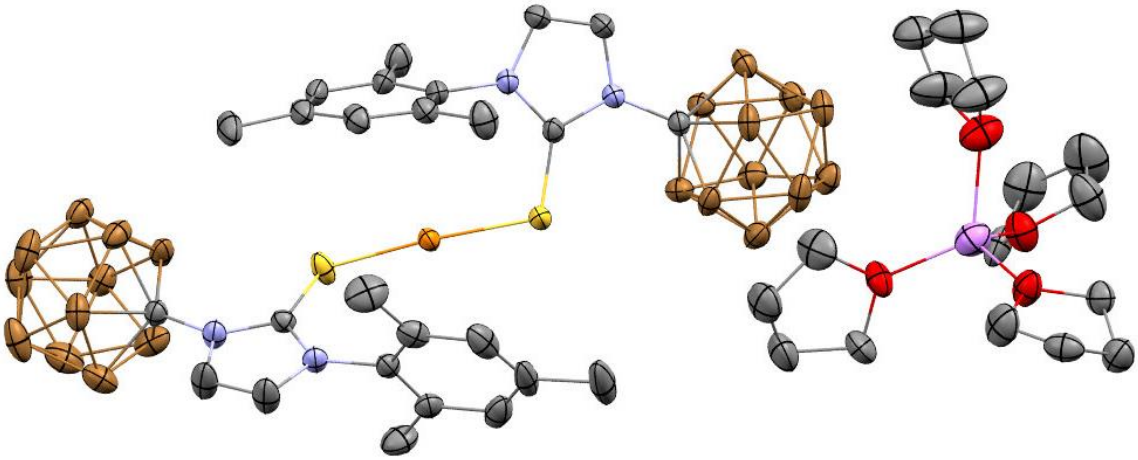

Figure 3-5 Crystal structure of **46**. Hydrogen atoms omitted for clarity. Li = pink, B = brown, C = gray, N = blue, O = red, S = yellow, Au = orange.

3.7 Reactivity of Ligand **30** with Copper

Curious to see if we could generate a copper complex similar to **43[Li^{+}]** we decided to try a 1:1 reaction between CuI and **30**. Indeed when a 1:1 ratio of **30** with CuI is reacted in THF a new downfield resonance at 7.12 ppm is observed in the ^{1}H NMR spectrum corresponding to a shift in the backbone protons of the NHC (free NHC = 6.91 ppm). Analysis of the ^{13}C NMR spectrum reveals an upfield shift of

the C2 carbon from 196.6 ppm (free NHC) to 164.7 ppm suggesting the coordination of NHC to Cu, scheme 3-4. Isolation of this complex was accomplished by concentrating down the crude reaction mixture then preparatively crystalizing the crude at -30°C. *It should be noted that this reaction does not always preparatively crystalize thus the mixture has to be washed with* Et_2O.

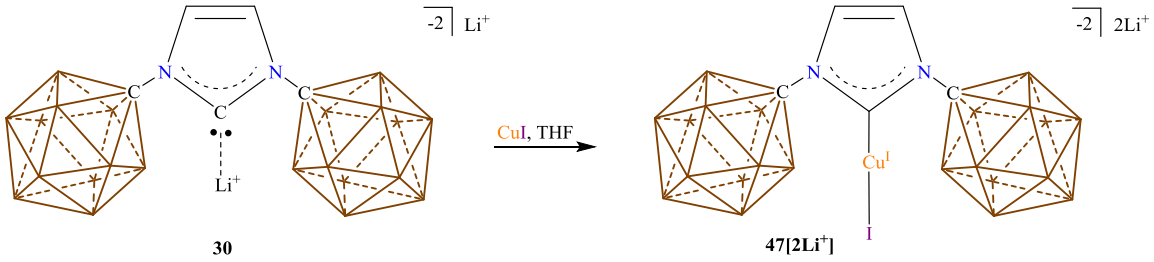

Scheme 3-4 synthesis of **47[2Li$^+$]**.

Using NMR analysis alone it was impossible to determine if the Cu complex that had formed was monomeric in NHC or dimeric in NHC. To help elucidate the structure, a precipitation test with AgBF4 was performed. If the Cu center contained an iodide ligand, one would expect an immediate precipitation of AgI upon addition of $AgBF_4$, if no iodine was present the complex would likely stay in solution. Upon addition of a solution of $AgBF_4$ to a solution of Cu complex an immediate white precipitation was observed suggesting the presence of iodine. To fully determine the structure of the Cu complex a single crystal X-ray diffraction study was undertaken. Even though the data was not of high enough quality to comment on bond lengths and angles the structure was unambiguously determined to be **47[2Li$^+$]**, figure 3-6.

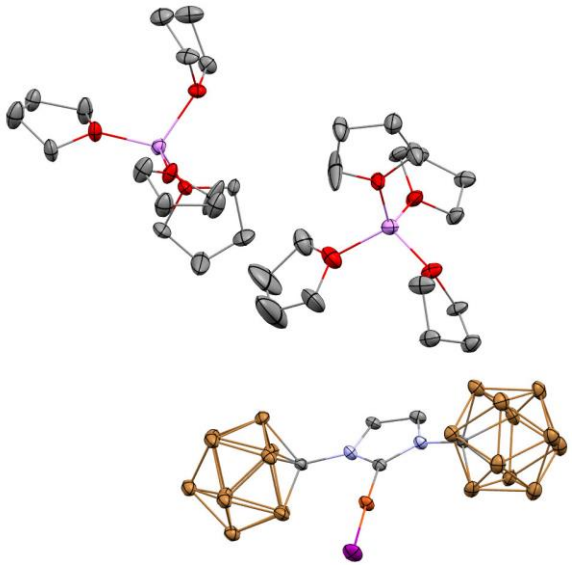

Figure 3-6 Solid state structure of **47[2Li+]**. Li = pink, B = brown, C = gray, N = blue, O = red, Cu = orange, I = purple.

Next, we wanted to see if complex **47[2Li$^+$]** would undergo ligand exchange of I for SMe_2, scheme 3-5. Using identical reaction conditions as **43[Li$^+$]** we found that the reaction mixture contained noticeable amounts of protonated imidazolium **29** as well as the desired dimethylsulfide complex **47[2Li$^+$]** (see experimental section figure 3-36). The lability of the NHC ligand was not desirable and no further reactions with this complex were tested.

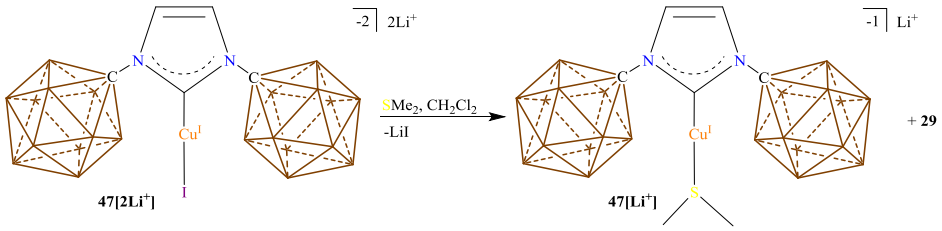

Scheme 3-5 Synthesis of **47[Li$^+$]**.

3.8 Conclusion

This shows that carboranyl NHCs **30** and **35[Li$^+$]** are suitable ligands for transition metals. If we consider **30** as an analogue of Arduengo's carbene, we can conclude that replacement of an adamantyl group by a hydrido substituted icosahedral carborane anion results in a $\%V_{bur}$ increase of 3.7% (($\%V_{bur}$ **43[Li$^+$]** – $\%V_{bur}$ Arduango's diadamantyl NHC)/2 = (47.2% - 39.8%)/2 = 3.7%). We are currently investigating the use of **42** and **43[Li$^+$]** as single component Au catalysts as well as the possibility of preparing polyhalogenated carboranyl NHCs with even larger steric profiles. The Au complex **43[Li$^+$]** is more stable than the corresponding Cu complex **47[Li$^+$]**. The catalytic activity of **42** and **43[Li$^+$]** was measured in terms of a hydroamination reaction between phenylacetylene and aniline. Complexes **42** and **43[Li$^+$]** were found to be competent catalyst with a TON of 95 after 24 hours at room temperature with a catalyst loading of 1 mol%. We also demonstrated that unsymmetrical thiourea **42** was a component ligand by generating a bis(thiourea)Au(I) complex **46**.

3.9 Experimental

General Considerations: All manipulations were carried out using standard Schlenk or glovebox techniques under a dinitrogen atmosphere unless otherwise stated. Dry solvents were obtained via distillation under argon from calcium hydride (acetonitrile), sodium-potassium alloy (diethyl ether), and potassium benzophenone ketyl (tetrahydrofuran). Benzene, methylene chloride and fluorobenzene were collected from a solvent purification system by SG Waters USA, LLC utilizing a fifteen minute argon sparge followed by passage though activated aluminum. Compounds **30** and **35[Li$^+$]** were prepared according to the literature.[45, 46] Unless specifically stated, reagents were purchased from commercial vendors and used without further purification. Nuclear magnetic resonance (NMR) spectroscopy was carried out using: Bruker Avance 300 MHz, Bruker Avance 600 MHz, and Varian Inova 300 MHz. NMR chemical shifts are reported in parts per million (ppm) with ^{1}H and ^{13}C chemical shifts referenced to the residual non-deutero solvent. The ^{11}B-^{1}H coupling constants from ^{11}B spectra are reported when possible. Infrared spectroscopy was recorded on a Bruker ALPHA FTIR Spectrometer. High-resolution mass spectrometry (HRMS) was collected on an Agilent Technologies 6210 (TOF LC/MS) featuring

electrospray ionization. Complete crystallographic data for compounds **42** and **43[Li$^+$]** are available free of charge from the Cambridge Crystallographic Data Center under reference numbers 1449175 and 149174, respectively. These structures can be accessed at: http://www.ccdc.cam.ac.uk/.

Synthesis of 42:

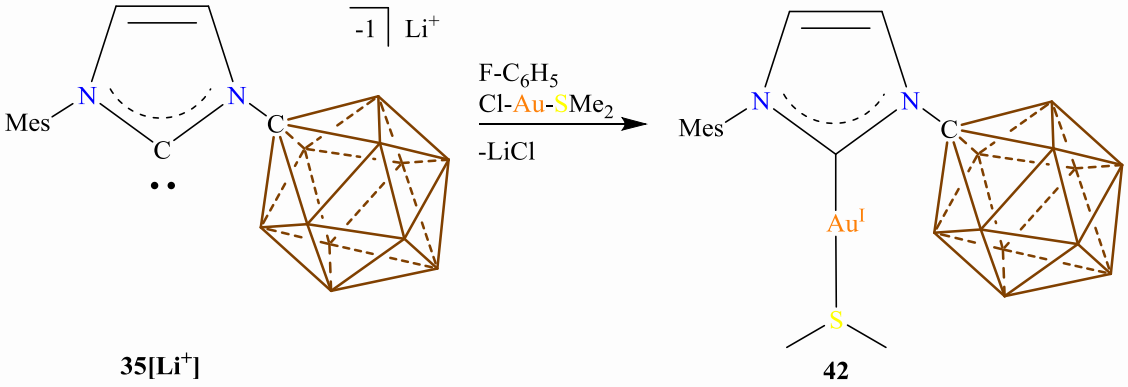

Scheme 3-6 Synthesis of **42**.

A 20 mL scintillation vial was equipped with a stir bar and loaded with **35[Li$^+$]** (50.0 mg, 126 µmol) and $ClAuSMe_2$ (37.9 mg, 126 µmol). The vial was cooled to -40 °C in a cold well before cold (-40 °C) F-C_6H_5 (5 mL) was added and the reaction stirred for 30 minutes at -40 °C. After thirty minutes the reaction mixture was pumped down to dryness, then methylene chloride (7 mL) was added. The mixture was stirred then filtered and the filtrate set aside. Methylene chloride (7mL) was added and the mixture was stirred then filtered. The combined filtrate was pumped down to dryness furnishing **42** (69.4 mg, 82% yield). Single crystals for the X-ray diffraction study were obtained by preparative crystallization from THF and hexane at -30 °C overnight. ^{1}H NMR (300 MHz, methylene chloride-d_2, 25 °C): δ = 7.71 (d, $^3J(H,H)$ = 2.1 Hz, 1H), 6.99 (m, 2H), 6.83 (d, $^3J(H,H)$ = 2.1 Hz, 1H), 2.60 (s, 6H), 2.33 (s, 3H), 1.96 (s, 6H), 3.8 – 0.75 (bm, 11H) ppm. ^{1}H[^{11}B] NMR (192.5 MHz, methylene chloride-d_2, 25 °C): δ = 7.71 (d, 1H), 6.99 (m,

2H), 6.83 (d, 1H), 2.63 (s, 5H, B-H), 2.60 (s, 6H), 2.33 (s, 3H), 1.97 (s, 6H), 1.75 (s, 1H), 1.68 (s, 5H) ppm. $^{13}C[^{1}H]$ (75 MHz, methylene chloride-d_2, 25 °C): δ = 175.2, 140.4, 135.9, 135.1, 129.6, 124.3, 121.6, 78.8, 24.4, 21.3, 17.9 ppm. $^{11}B[^{1}H]$ NMR (96 MHz, methylene chloride-d_2, 25 °C): δ = -8.7, -13.6 ppm. ^{11}B NMR (96 MHz, methylene chloride-d_2, 25 °C): δ = -8.7 ($^{1}J(H,B)$ = 134.4 Hz), -13.6 ($^{1}J(H,B)$ = 144 Hz) ppm. IR (evaporated methylene chloride film, ATR, 25 °C): 2533 (B-H). HRMS (negative mode ESI/APCI) $[M-H]^{1-}$ m/z Calc: $C_{15}H_{29}B_{22}N_2Au_1S_1$ = 585.2828 : Found = 585.2847.

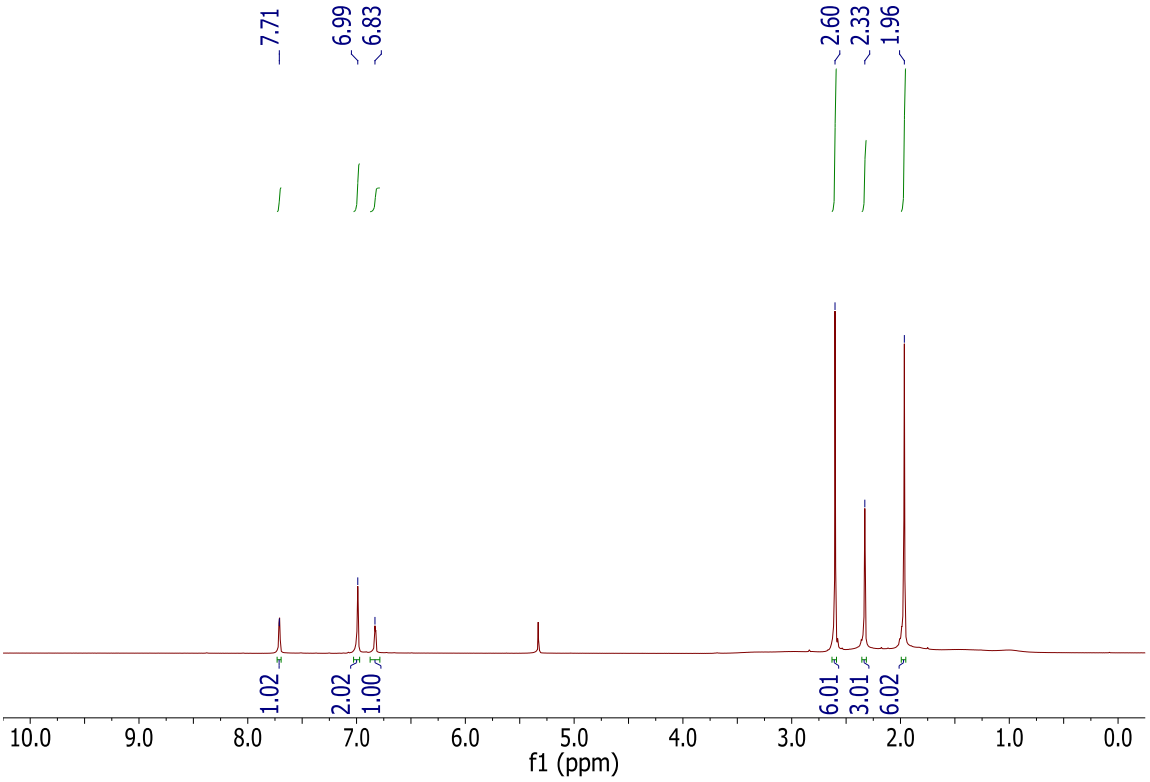

Figure 3-7 ^{1}H-NMR spectrum of **42** in methylene chloride-d_2.

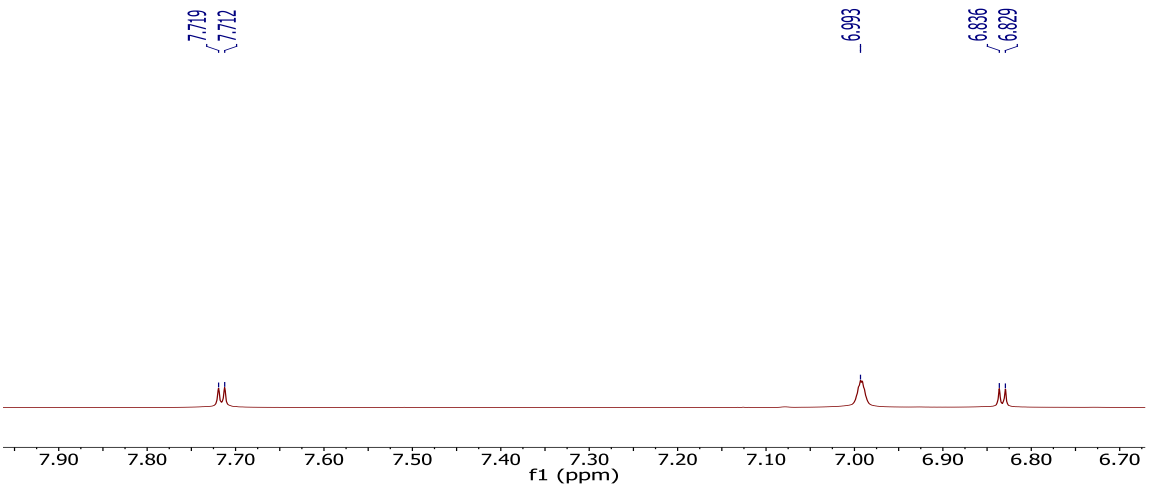

Figure 3-8 An expanded view of the aromatic region of the ^{1}H-NMR spectrum of **42** in methylene chloride-d_2 showing the small $^{3}J(H,H)$ coupling of the imidazolylidene backbone protons.

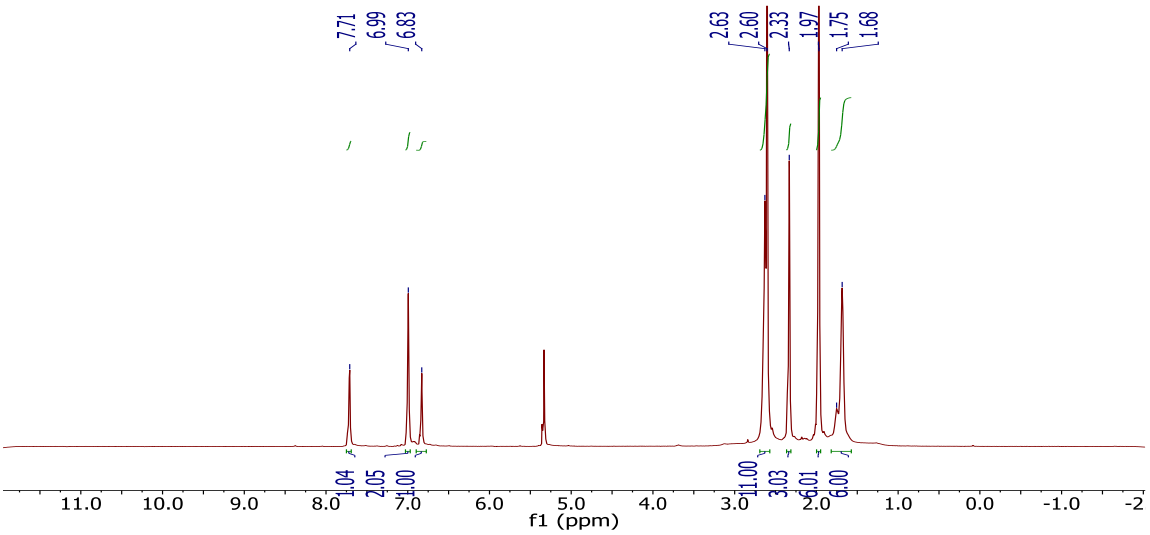

Figure 3-9 ^{1}H[^{11}B]-NMR spectrum of 42 in methylene chloride-d_2. The boron hydrides appear at 2.63, 1.75, and 1.68 ppm.

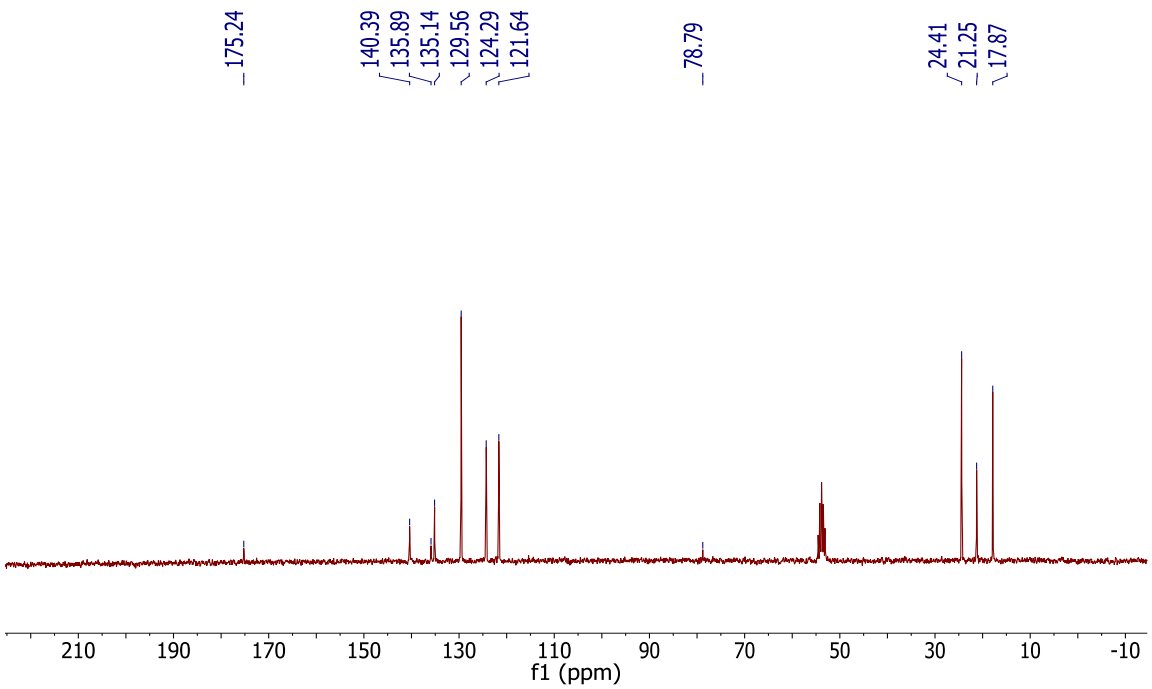

Figure 3-10 $^{13}C[^{1}H]$-NMR spectrum of **42** in methylene chloride-d_2.

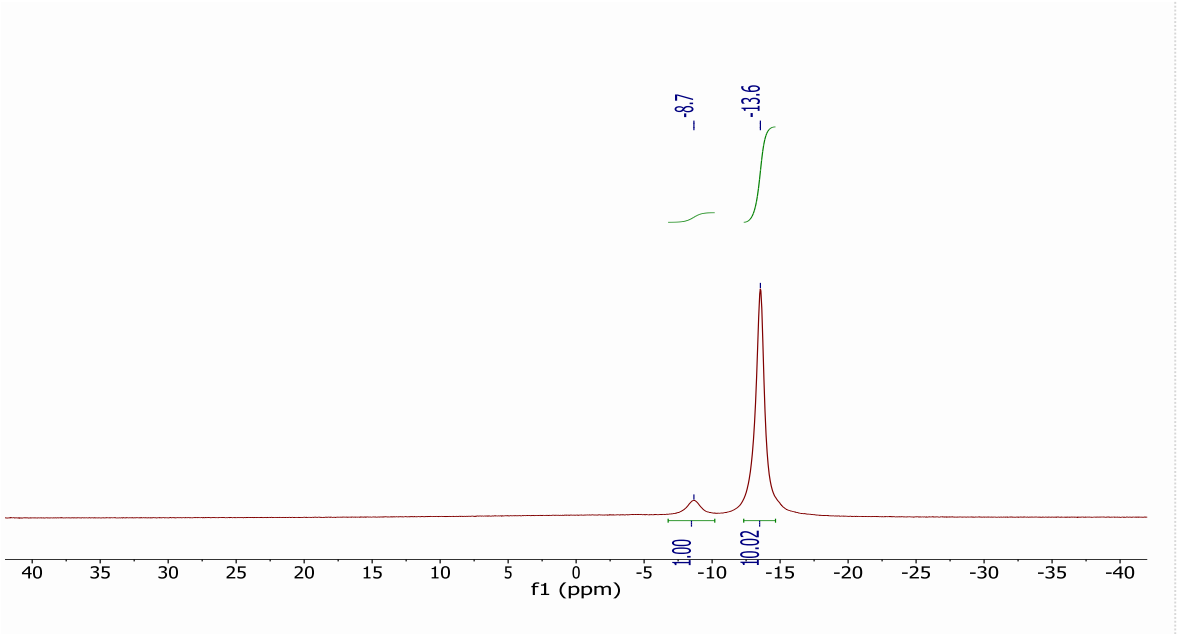

Figure 3-11 $^{11}B[^{1}H]$-NMR spectrum of **42** in methylene chloride-d_2.

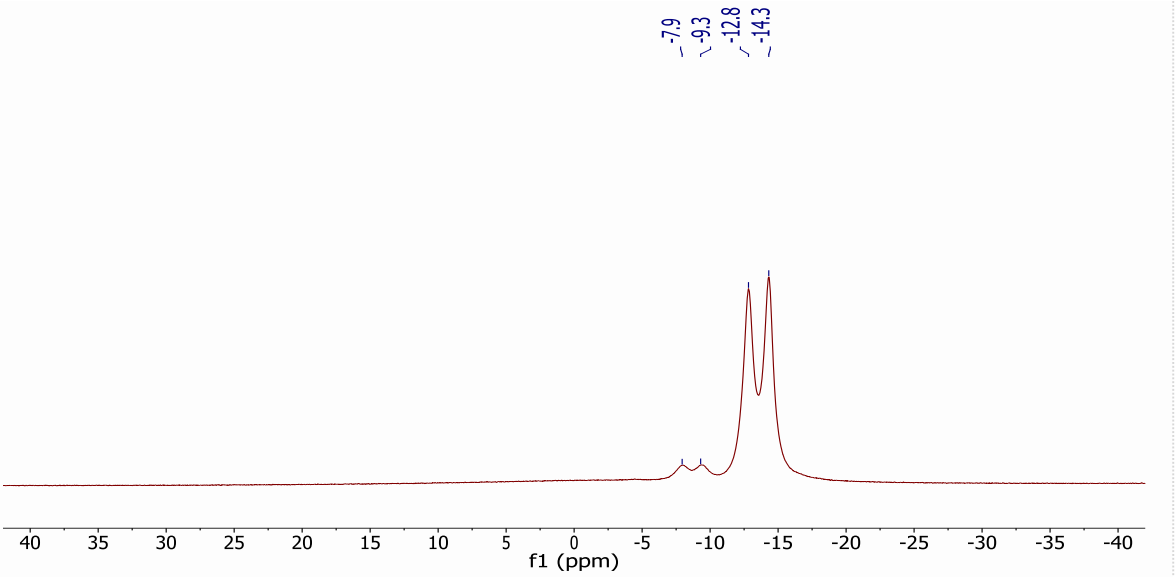

Figure 3-12 ^{11}B-NMR spectrum of 42 in methylene chloride-d_2 showing the $^{1}J(B,H)$ coupling.

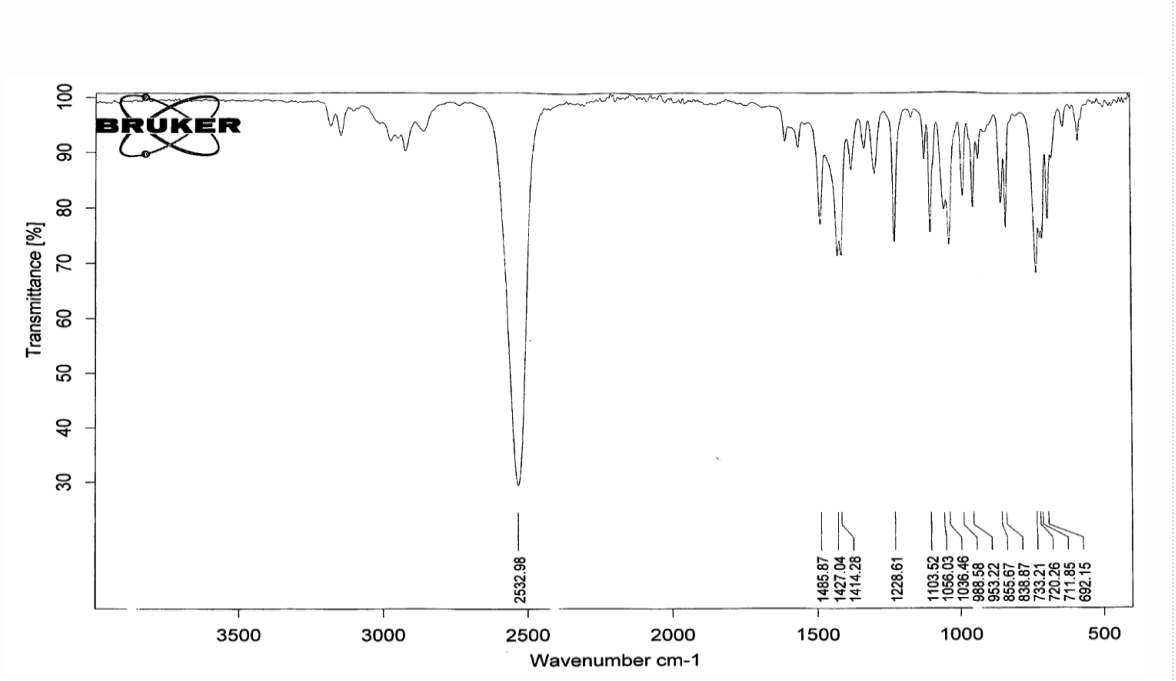

Figure 3-13. IR-spectrum of **42**, the B-H stretches appear at 2532 cm^{-1}.

Synthesis of 43[Li$^+$] and 43(Cl)[2Li$^+$]:

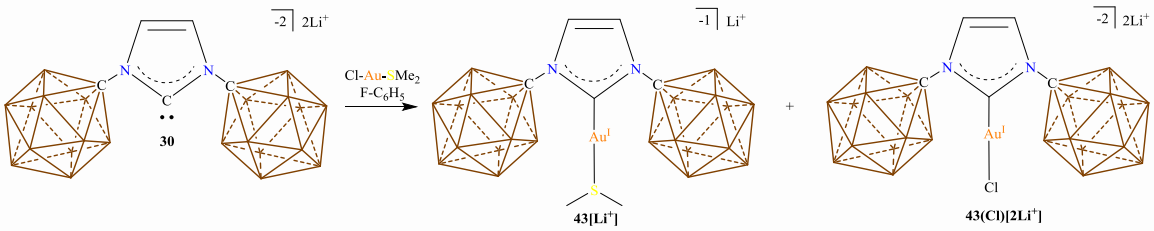

Scheme 3-7 Synthesis of a mixture of **43[Li$^+$]** and **43(Cl)[2Li$^+$]**

A 20 mL glass scintillation vial was equipped with a stir bar and loaded with **30** (50.1 mg, 76 μmol) and $ClAuSMe_2$ (22.6 mg, 76 μmol). The vial was cooled to -40 °C in a cold well and cold (-40 °C) fluorobenzene (5 mL) was added. After 15 minutes any brown solid on the walls of the scintillation vial was scraped down into the reaction mixture and further stirred for 30 minutes at -40 °C. *Note: **30** is not very soluble in F-C_6H_5 and builds up on the vial walls*. More F-C_6H_5 (5 mL) was added to the reaction mixture and the reaction was filtered while cold. The solvent was removed *in vacuo* giving **43[Li$^+$]** as a gold film (15.2 mg, 22% yield). A crystal of **43[Li$^+$]** was grown by cooling a solution of F-C_6H_5 and hexane at -30 °C. ^{1}H NMR (300 MHz, methylene chloride-d_2, 25 °C): δ = 7.34 (s, 2H), 2.78 (s, 6H) 3.38-0.60 (bm, 22H) ppm. ^{1}H[^{11}B] NMR (192.5 MHz, methylene chloride-d_2, 25 °C): δ = 7.34 (s, 2H), 2.78 (s, 6H), 2.58 (s, 5H), 1.68 (s, 1H), 1.60 (s, 5H) ppm. ^{13}C[^{1}H] (150 MHz, methylene chloride-d_2, 25 °C): δ = 174.3, 122.3, 79.9, 25.1 ppm. ^{11}B[^{1}H] NMR (96 MHz, methylene chloride-d_2, 25 °C): δ = -8.8, -13.8 ppm. ^{11}B NMR (96 MHz, methylene chloride-d_2, 25 °C): δ = -8.8 (^{1}*J(H,B)* = 134.4 Hz), -13.8 (^{1}*J(H,B)* = 124.8 Hz) ppm. IR (evaporated methylene chloride film, ATR, 25 °C): 2532 (B-H). HRMS (negative mode ESI/APCI) $[M]^{1-}$ m/z Calc: $C_7H_{30}B_{22}N_2Au_1S_1$ = 609.3999 : Found = 609.3996, $[M\text{-}S(Me)_2]^{1-}$ m/z Calc: $C_5H_{24}B_{22}N_2Au_1$ = 547.3807: Found = 547.3807.

To the insoluble residue, acetonitrile (4 mL) was added and the suspension was filtered. The remaining residue was extracted once more with acetonitrile (2 mL) and again filtered. The combined

filtrate was pumped down to dryness containing **43(Cl)[2Li$^+$]**. ^{1}H NMR (300 MHz, acetonitrile-d_3, 25 °C): δ = 7.35 (s, 2H), 3.5 – 0.65 (bm, 22H, B-H) ppm. ^{1}H[^{11}B] NMR (192.5 MHz, acetonitrile-d_3, 25 °C): δ = 7.34 (s, 2H), 2.57 (bs, 10H), 1.63 (bs, 2H), 1.54 (bs, 10H) ppm. ^{13}C[^{1}H] (150 MHz, acetonitrile-d_3, 25 °C): δ = 172.4, 122.9, 80.9 ppm. ^{11}B[^{1}H] NMR (96 MHz, acetonitrile-d_3, 25 °C): δ = -8.9, -13.9 ppm. ^{11}B NMR (96 MHz, acetonitrile-d_3, 25 °C): δ = -8.9 ($^1J(H,B)$ = 139.2 Hz), -13.9 ($^1J(H,B)$ = 137 Hz) ppm. HRMS (negative mode ESI/APCI) $[M]^{2-}$ m/z Calc: $C_5H_{24}B_{22}N_2Au_1Cl_1$ = 291.1754 : Found = 291.1753.

Spectroscopic Data for 43[Li$^+$]:

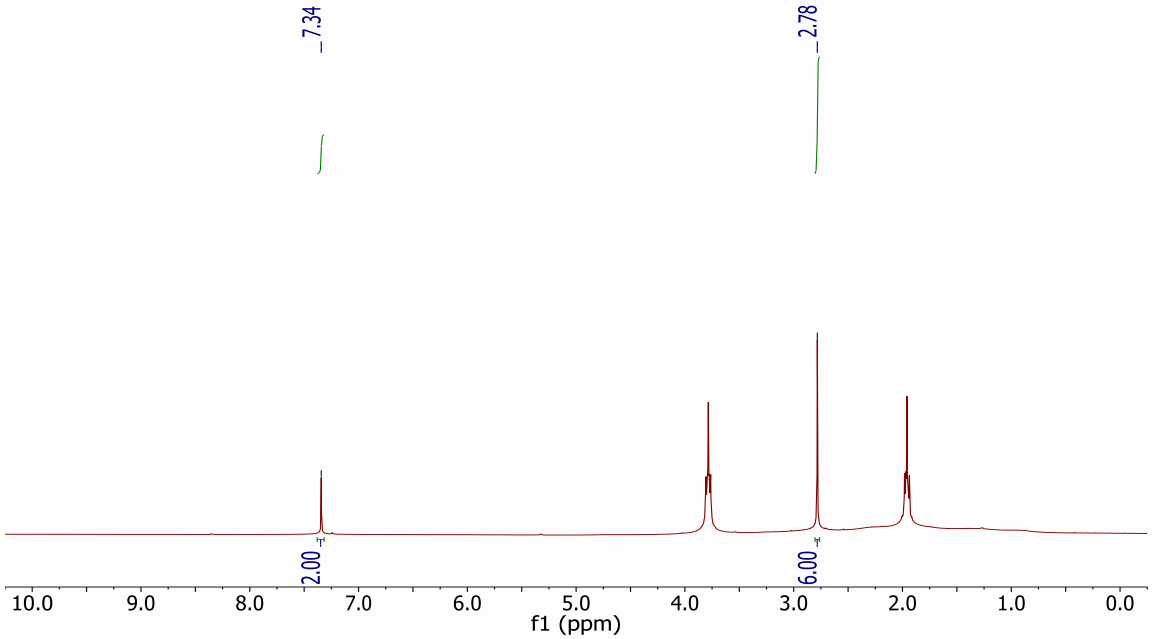

Figure 3-14 ^{1}H-NMR spectrum of **43[Li$^+$]** in methylene chloride-d_2. *Note: THF(3.79 and 1.96 ppm) is coordinated to the lithium cation.*

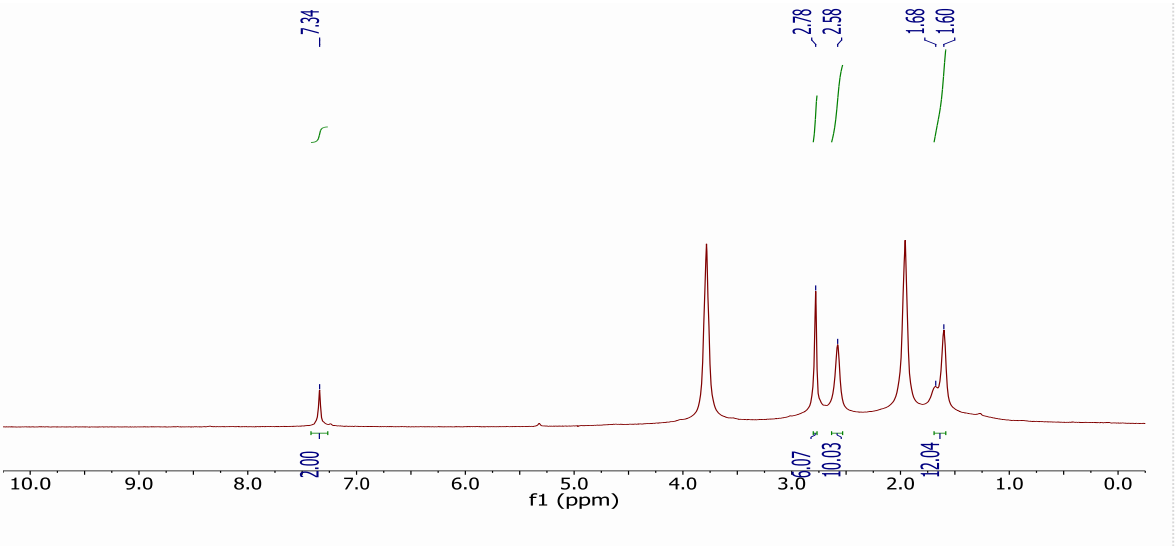

Figure 3-15 $^{1}H[^{11}B]$-NMR spectrum of **43[Li^{+}]** in methylene chloride-d_2. The boron hydrides appear at 2.58, 1.68 and 1.60 ppm.

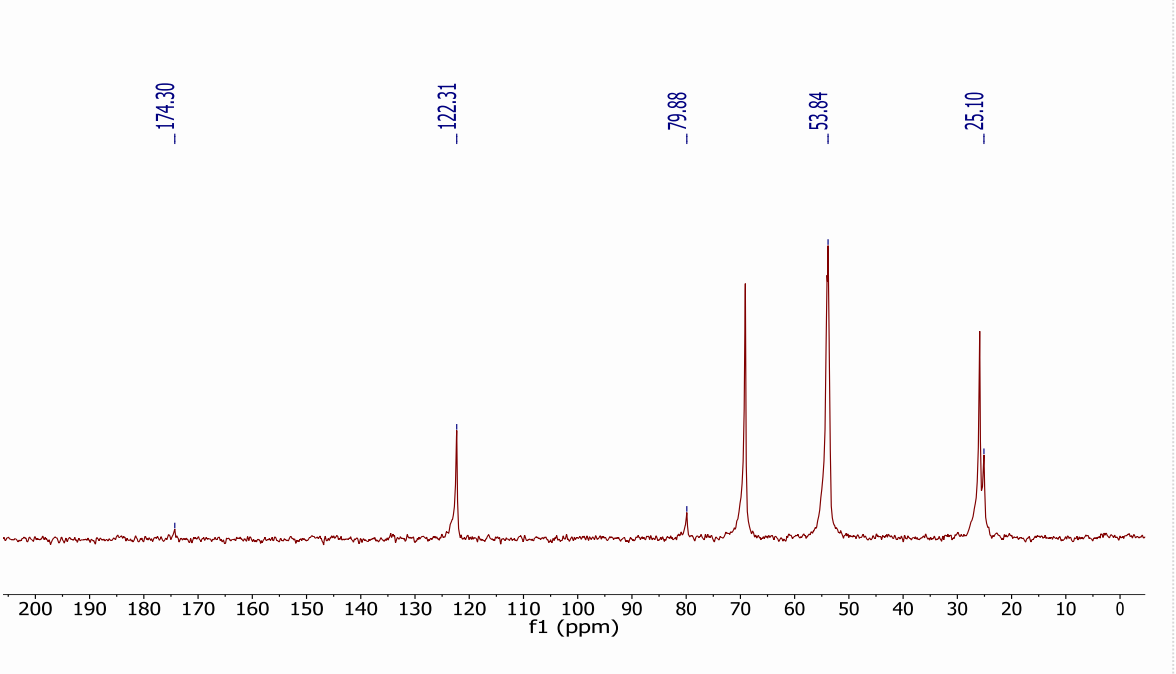

Figure 3-16 $^{13}C[^{1}H]$-NMR spectrum of 43[Li^{+}] in methylene chloride-d_2. *Note: THF (69.09 and 25.88 ppm) is coordinated to the lithium cation.*

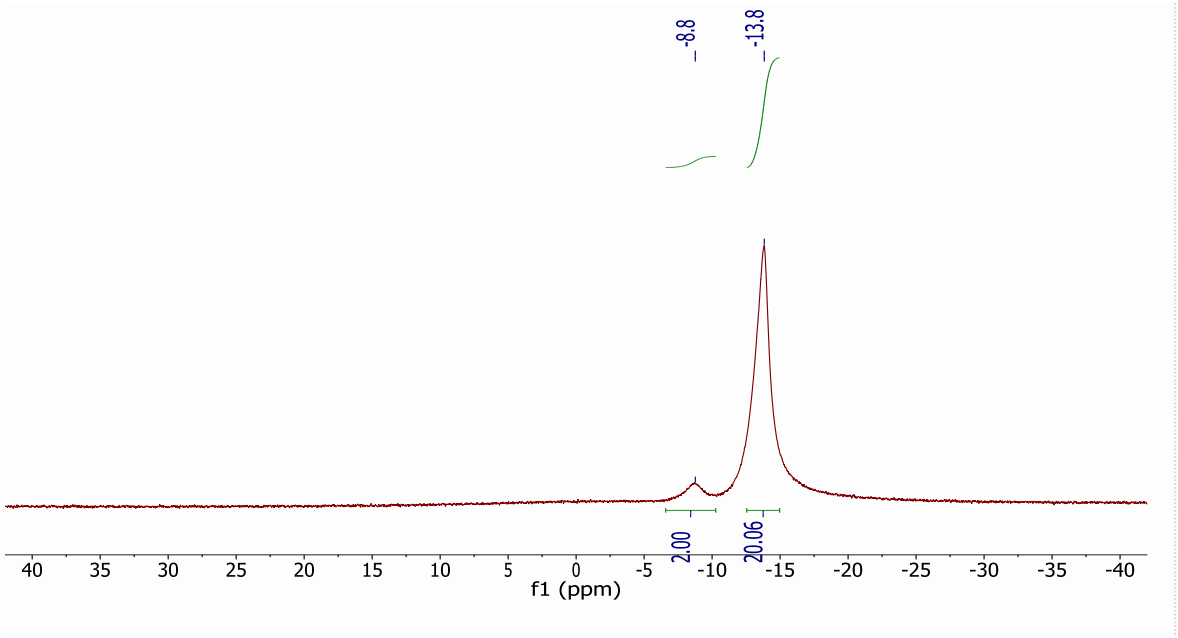

Figure 3-17 $^{11}B[^{1}H]$-NMR spectrum of **43[Li^{+}]**.

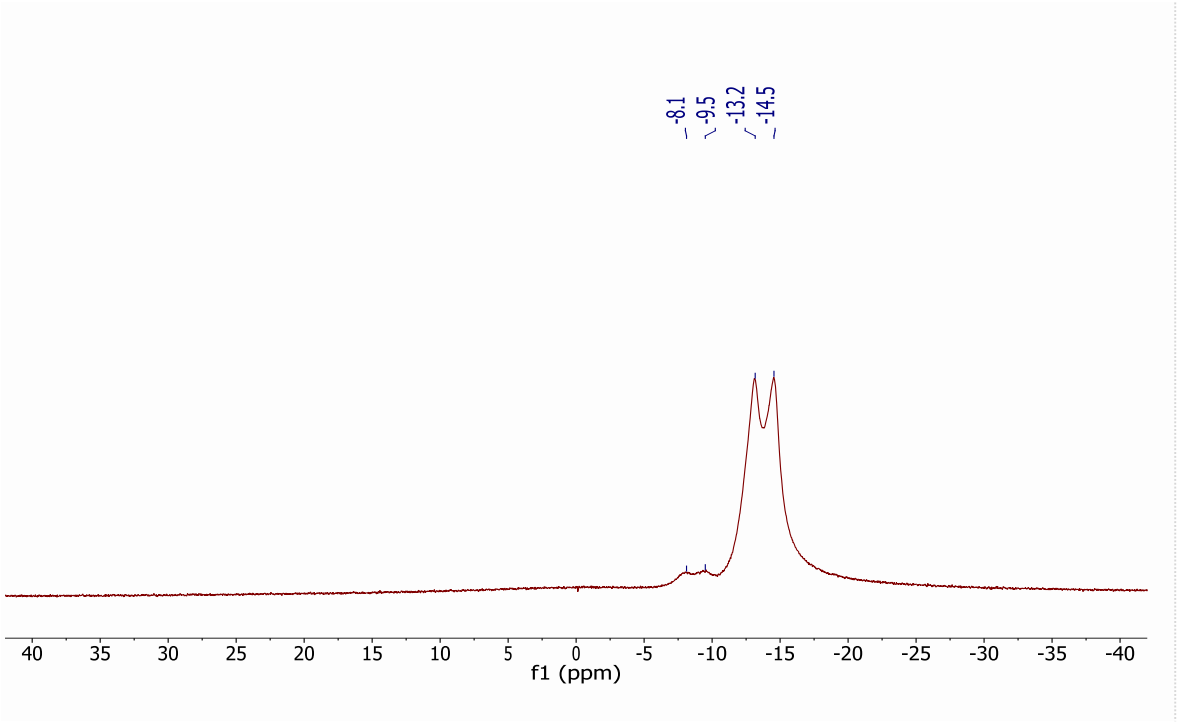

Figure 3-18 ^{11}B-NMR spectrum of **43[Li^{+}]** showing the $^{1}J(B,H)$ coupling.

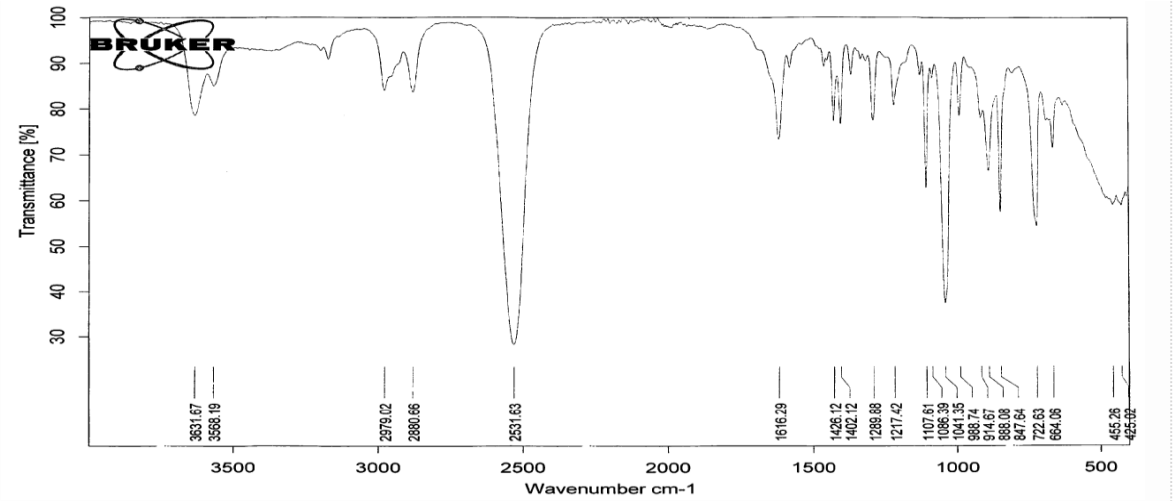

Figure 3-19 IR spectrum **of 43[Li$^+$]**. The B-H stretches appear at 2532 cm^{-1}.

Spectroscopic Data for 43(Cl)[2Li$^+$]:

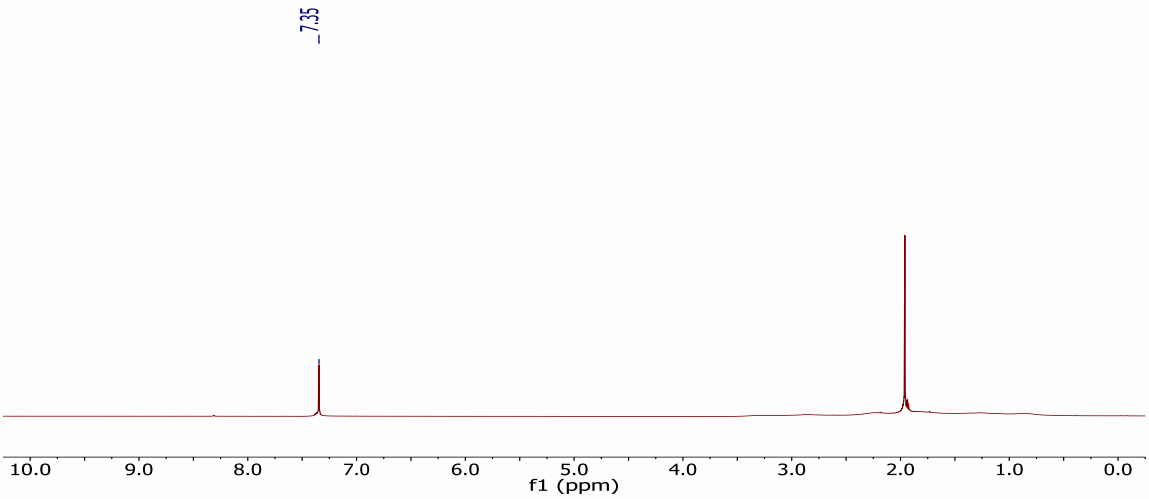

Figure 3-20 ^{1}H-NMR spectrum of the residue **43(Cl)[2Li$^+$]** in acetonitrile-d_3 showing the lack of coordinated dimethylsulfide. *Note: Acetonitrile is coordinated to the lithium cations at 1.96 ppm.*

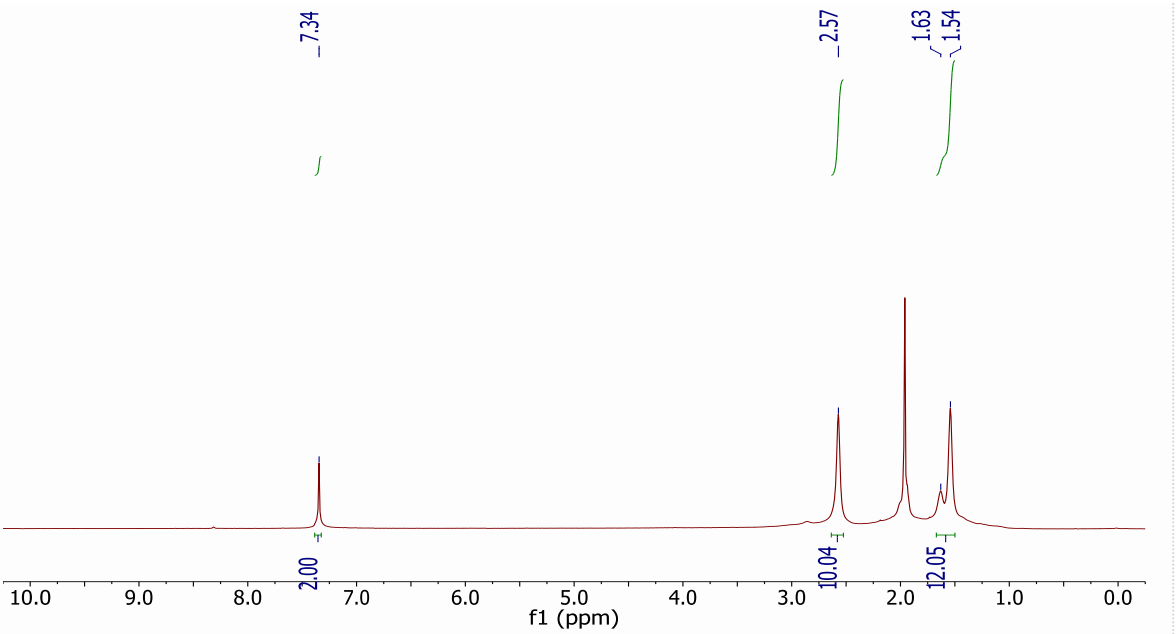

Figure 3-21 $^{1}H[^{11}B]$-NMR spectrum of residue **43(Cl)[2Li^{+}]** in acetonitrile-d_3. The boron hydrides appear at 2.57, 1.63, and 1.54 ppm.

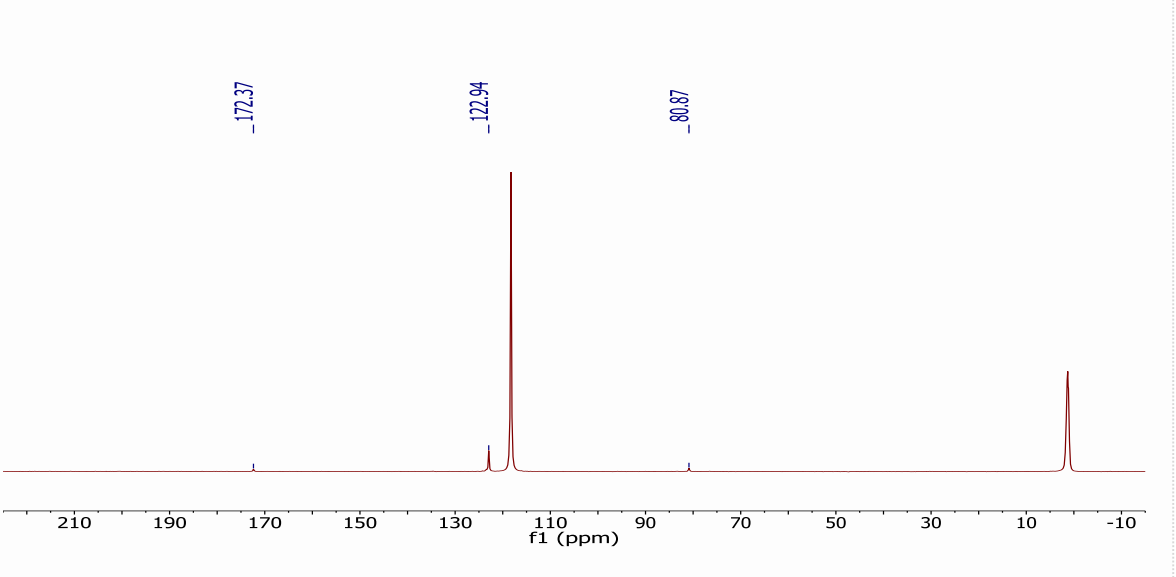

Figure 3-22 $^{13}C[^{1}H]$-NMR spectrum of residue **43(Cl)[2Li^{+}]** in acetonitrile-d_3.

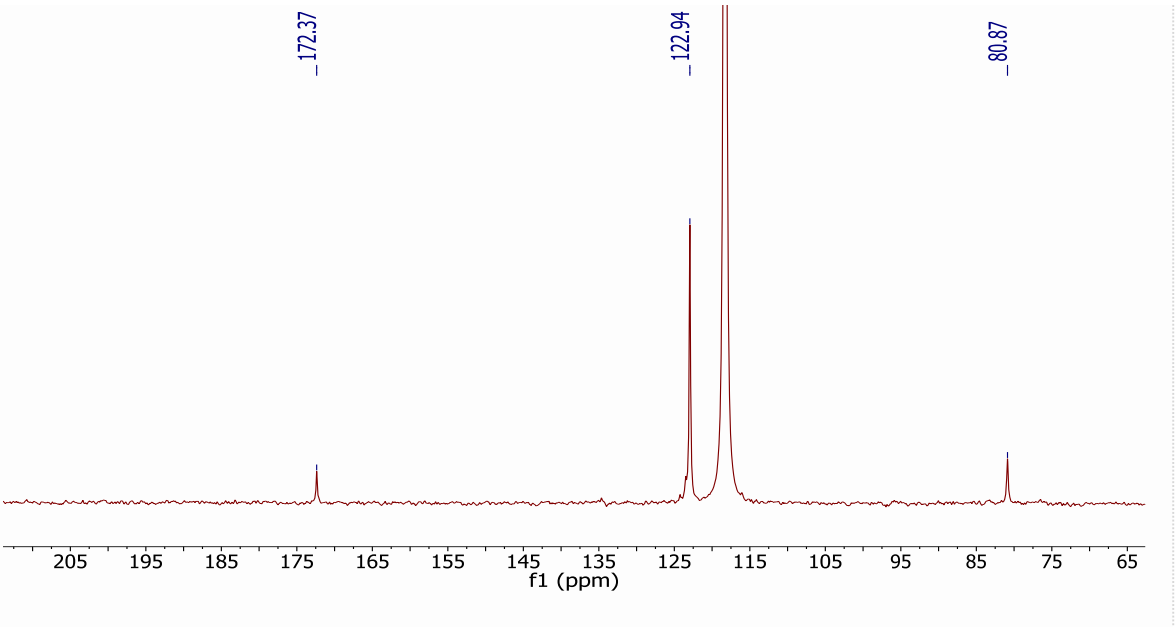

Figure 3-23 A blow up of the $^{13}C[^{1}H]$-NMR spectrum of residue **43(Cl)[2Li^{+}]** in acetonitrile-d_3.

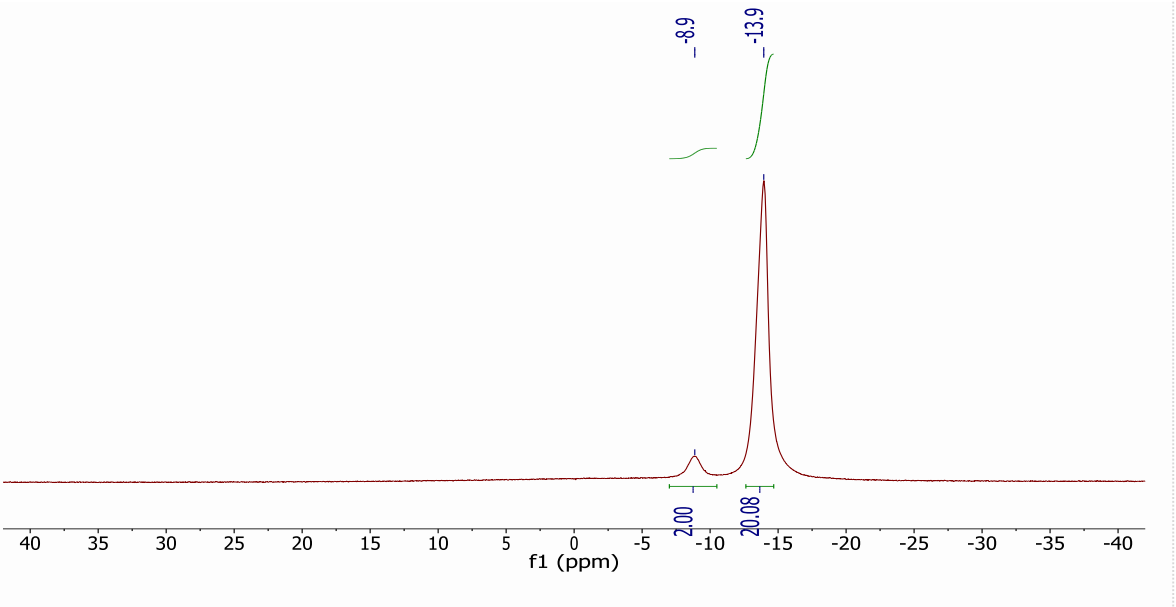

Figure 3-24 $^{11}B[^{1}H]$-NMR spectrum of residue **43(Cl)[2Li^{+}]** in acetonitrile-d_3.

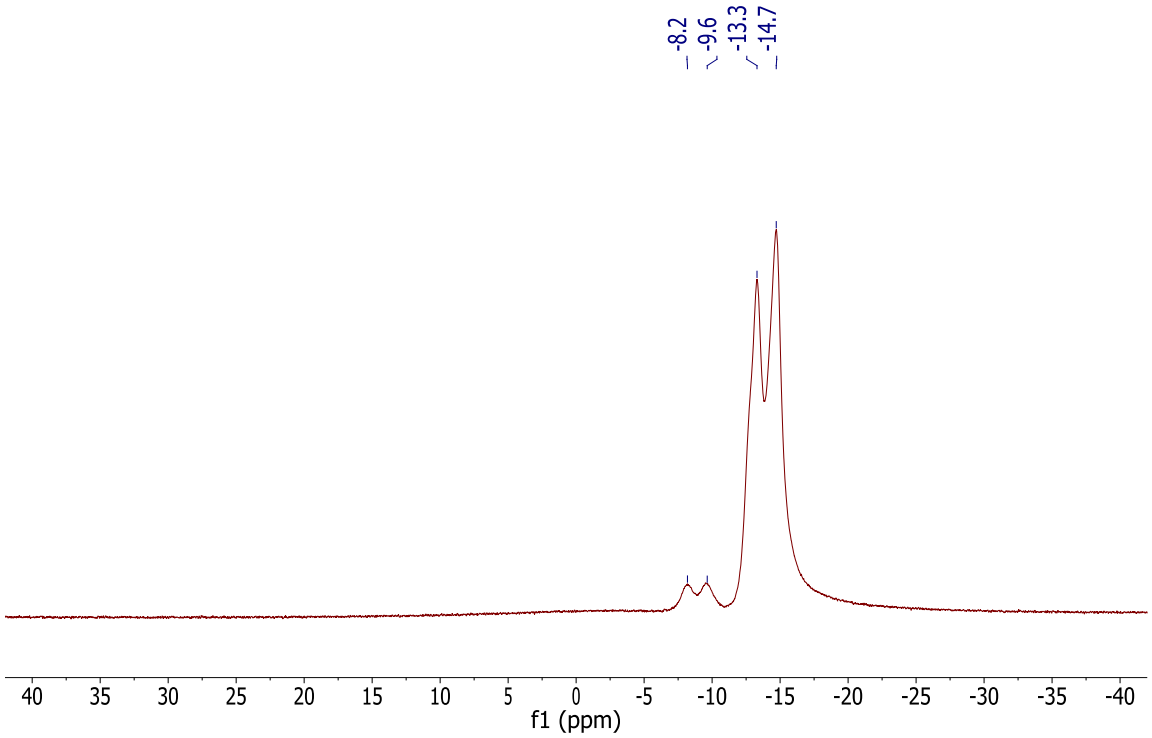

Figure 3-25 ^{11}B-NMR spectrum of residue **43(Cl)[2Li^{+}]** in acetonitrile-d_3 showing the $^{1}J(B,H)$ coupling.

Direct Synthesis of 43(Cl)[2Li$^+$]:

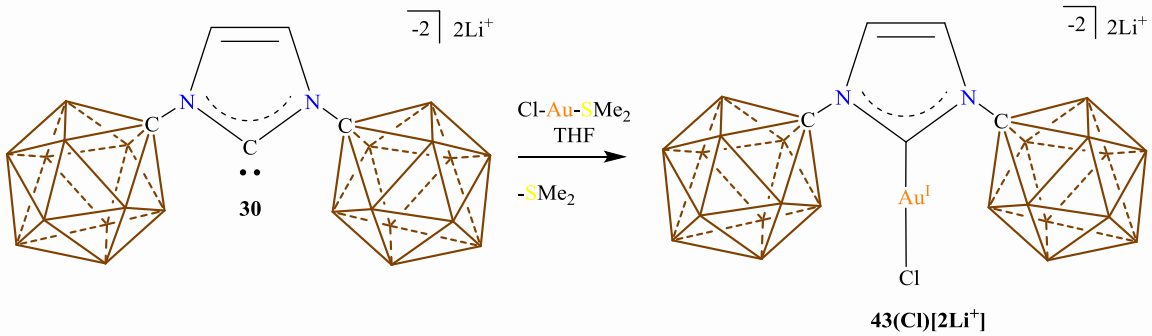

Scheme 3-8 Direct synthesis of **43(Cl)[2Li$^+$]**.

A 20 mL scintillation vial was equipped with a stir bar and loaded with **30** (50.6 mg, 77.3 μmol) and $ClAuSMe_2$ (22.8 mg, 77.3 μmol). The solids were dissolved in THF (2 mL) and the solution was stirred for 2 hours at room temperature, then the high vacuum was applied for three minutes (*removes liquid dimethylsulfide*). After applying vacuum THF (1 mL) was added to the solution and the reaction was stirred for another two hours at room temperature then finally pumped down furnishing the title compound **43(Cl)[2Li$^+$]** quantitatively. The spectroscopic data matches that provided above.

Conversion of 43[Li$^+$] to 43(Cl)[2Li$^+$]:

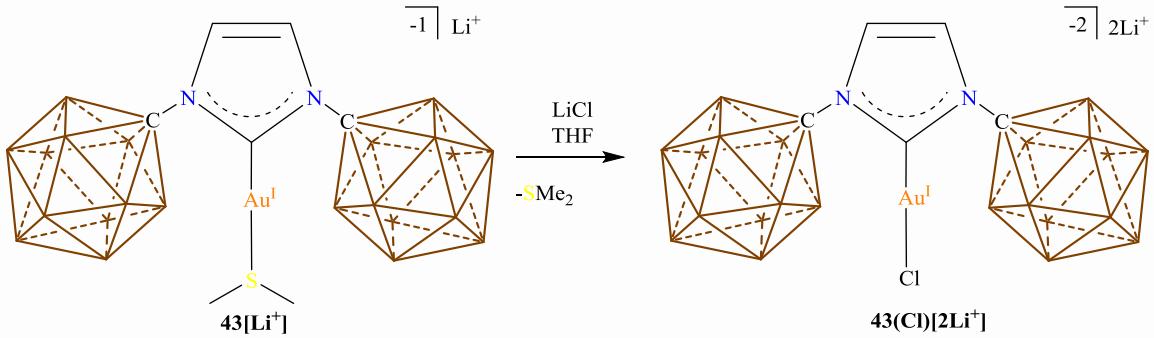

Scheme 3-9 Synthesis of **43(Cl)[2Li$^+$]** from **43[Li$^+$]**.

A 20 mL scintillation vial was equip with a stir bar and **43[Li$^+$]** (34.3 mg) was dissolved in a minimal amount of THF. The THF was then saturated in LiCl and stirred at room temperature for two hours. After two hours the reaction was pumped on via high vacuum (1 minute) then THF (1 mL) was added and stirred for another two hours then pumped down to dryness. Acetonitrile (2 mL) was added and the reaction mixture filtered. The acetonitrile was pumped down giving to quantitatively afford **43(Cl)[2Li$^+$]**. The spectroscopic data matches that provided above.

High Yielding Two Step Synthesis of 43[Li$^+$]:

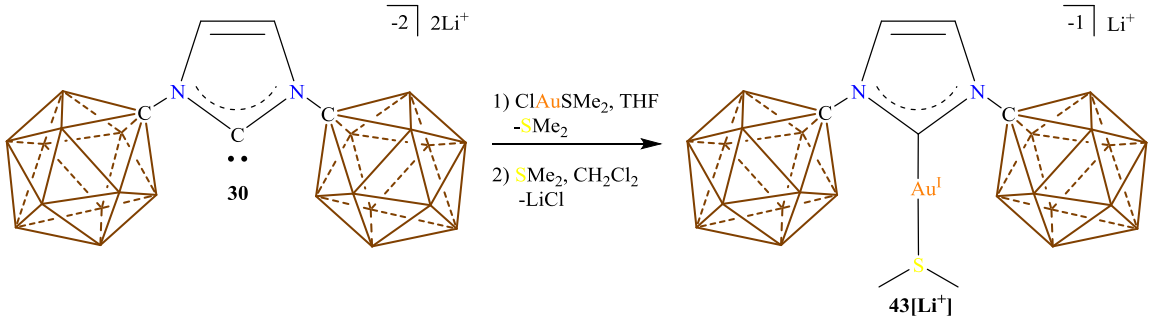

Scheme 3-10 High yielding, two-step synthesis of **43[Li$^+$]**.

A glass scintillation vial was loaded with **30** (two coordinated THF to Li$^+$, 1.00 g, 1.90 mmol) and dissolved in THF (5 mL) and transferred dropwise to a stirring suspension of ClAuSMe$_2$ (561 mg, 1.90 mmol). The vial containing **30** was rinsed with THF (2 x 1 mL) and transferred as well. The reaction was stirred at room temperature for 2 hours before it was filtered through celite. The filtrate was pumped down giving **43(Cl)[2Li$^+$]** in 96% yield (six coordinated THF to Li$^+$, 1.88 g, 1.83 mmol). **43(Cl)[2Li$^+$]** was suspended in methylene chloride (10 mL). To the suspension an excess of dimethylsulfide was added (10 drops from a glass pipette) and the vial stirred for 18 hours. The suspension was filtered and the filtrate concentrated down giving **43[Li$^+$]** with a 95% yield (two coordinated THF to Li$^+$, 1.70g, 1.74 mmol). The compound spectroscopically matched that of above.

Synthesis of 46:

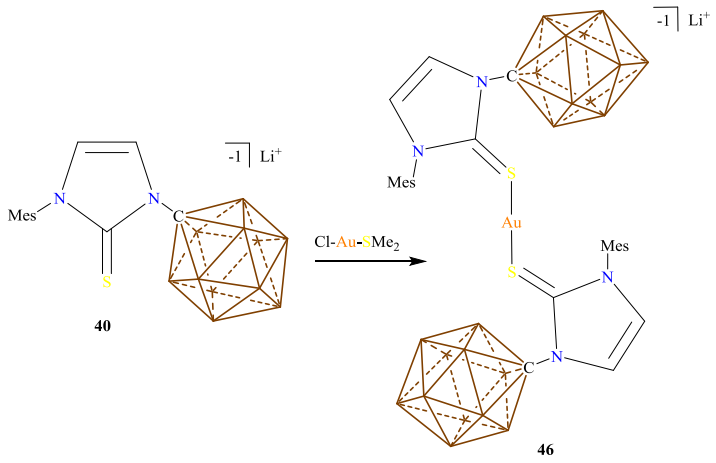

Shceme 3-11 Synthesis of **46**.

A glass scintillation vial was equipt with a stirbar and loaded with unsymmetrical thiourea (85.3 mg, 0.130 mmol) and $ClAuSMe_2$ (38.4 mg, 0.130 mmol). To the solids methylene chloride (3 mL) was added and the suspension stirred for 20 minutes at room temperature. After twenty minutes the reaction was filtered, the vessel was washed twice with methylene chloride (3 mL total) and the wash filtered as well. The filtrates were combined and the liquid removed under reduced pressure. The dried material was then crystalized by dissolving the mixture in THF (2 mL) and adding hexane (few drops) until the solution became cloudy, at this point the cloudy suspension was placed at -30°C overnight furnishing crystals of the title compound. The crystals were crushed and dried under vacuum giving 49.7 mg (one remaining THF), 72% yield (two batches of crystals). ^{1}H NMR (300 MHz, methylene chloride-d_2, 25 °C): δ = 7.84 (s, 2H), 7.07 (s, 2H) 6.75 (s, 2H), 2.9 – 0.7 (bm, 22H), 2.53 (s, 3H), 2.37 (s, 3H), 1.96 (s, 3H) ppm. ^{1}H[^{11}B] NMR (300 MHz, methylene chloride-d_2, 25 °C): δ = 7.82 (s, 2H), 7.05 (s, 2H) 6.74 (s, 2H), 2.53 (s, 3H), 2.53 (s, 10H, B-H), 2.36 (s, 3H), 1.94 (s, 3H), 1.66 (s, 10H), 3H (s, 2H) ppm. ^{11}B[^{1}H] NMR (96 MHz, methylene chloride-d_2, 25 °C): δ = -7.0, -13.0 ppm. ^{11}B NMR (96 MHz, methylene chloride-d_2, 25 °C): δ = -7.0 ($^{1}J(H,B)$ = 140.7 Hz), -13.0 ($^{1}J(H,B)$ = 149.1 Hz) ppm. IR (evaporated methylene chloride film, ATR, 25 °C): 2532 (B-H). HRMS (negative mode ESI/APCI) $[M]^{1-}$ m/z Calc: $C_7H_{30}B_{22}N_2Au_1S_1$ = 609.3999 : Found = 609.3996, $[M\text{-}S(Me)_2]^{1-}$ m/z Calc: $C_5H_{24}B_{22}N_2Au_1$ = 547.3807: Found = 547.3807.

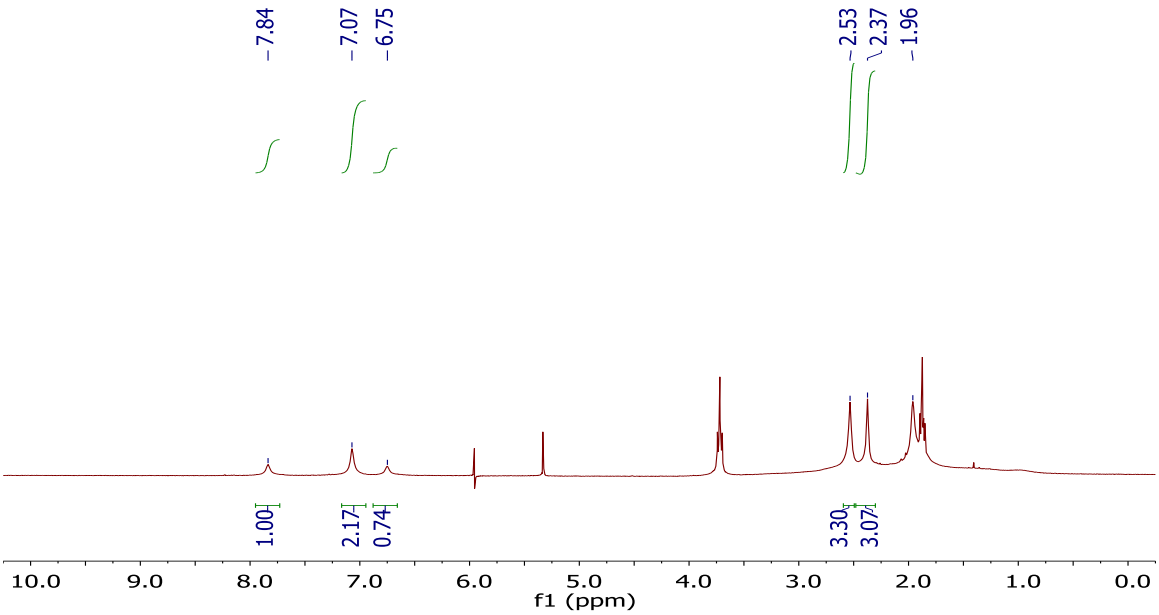

Figure 3-26 ^{1}H-NMR spectrum of **46** in methylene chloride-d_2. *Note: THF coordinated to Li^{+} can be seen at 3.6 and 1.8 ppm and the peak at 6 ppm is an artifact*.

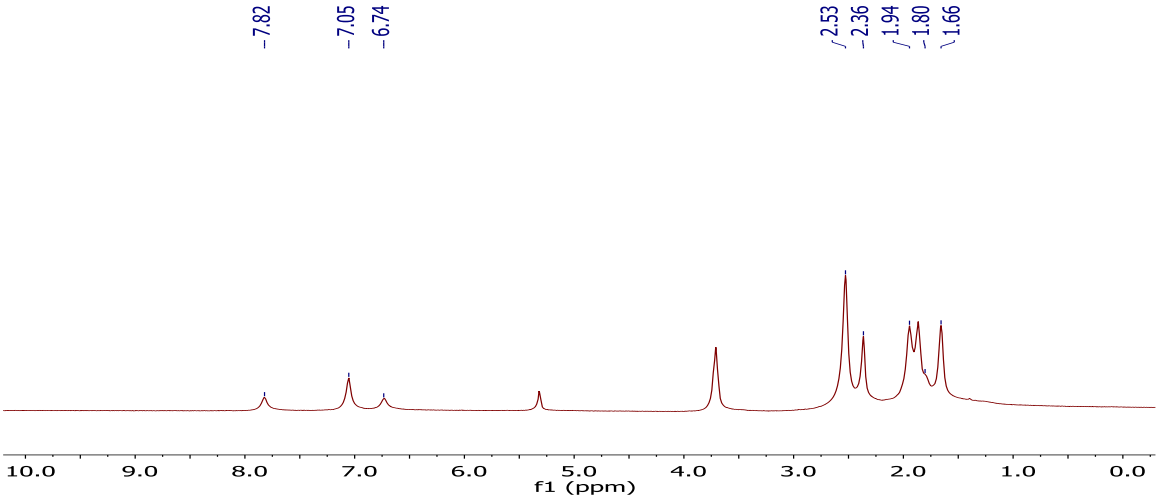

Figure 3-27 ^{1}H[^{11}B]-NMR spectrum of **46** in methylene chloride-d_2. The B-H resonances are at 2.53, 1.66 and 1.80 ppm.

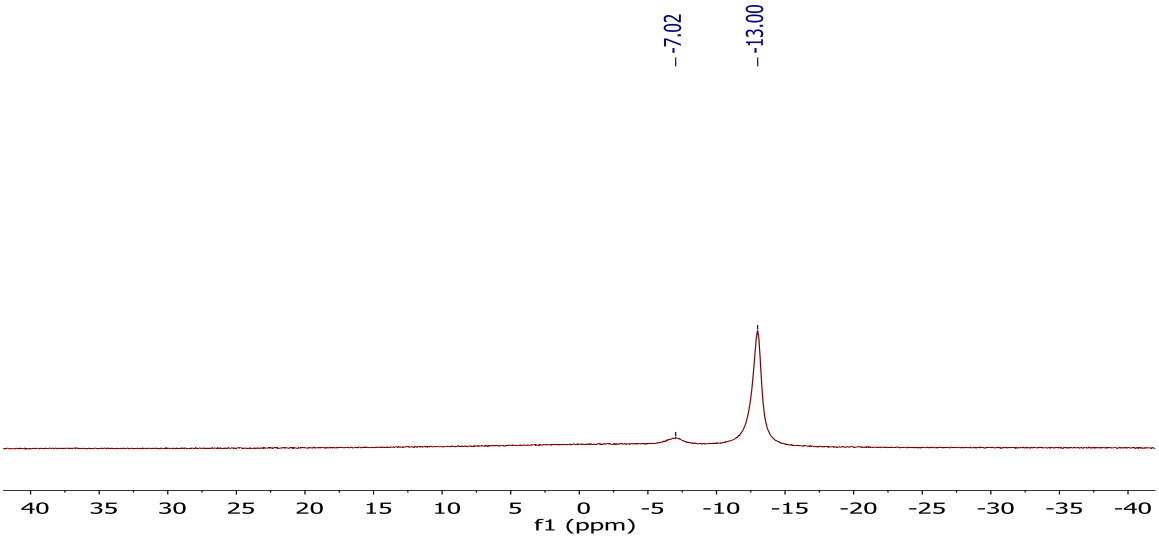

Figure 3-28 $^{11}B[^{1}H]$-NMR spectrum of **46** in methylene chloride-d_2.

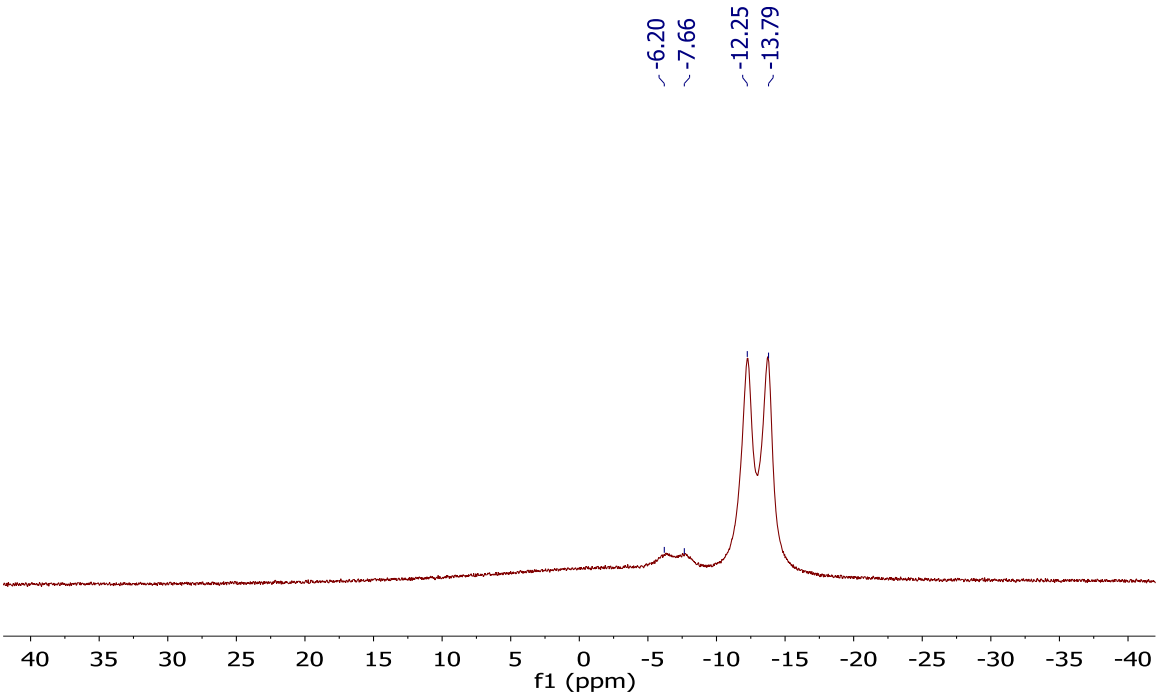

Figure 3-29 ^{11}B-NMR spectrum of **46** in methylene chloride-d_2.

Synthesis of 47[2Li$^+$]:

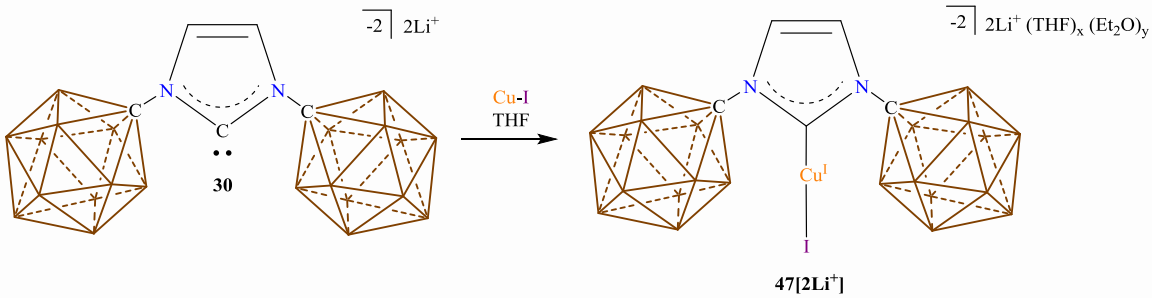

Scheme 3-12 Synthesis of **47[2Li$^+$]**.

A 20 mL glass scintillation vial was equipped with a stir bar and loaded with CuI (270 mg, 1.42 mmol) and suspended in THF (1 mL). The suspension was vigorously stirred while a solution of **30** (720 mg, 1.24 mmol) in THF (4 mL) was added dropwise, after which the vial sealed and the reaction stirred for 2 hours at room temperature. Next the suspension was filtered (removal of excess CuI) and the filtrate was cooled to -30 °C in a freezer for 30 minutes. The pursuing crystals were washed with cold THF (3 x 2 mL, cooled to -30 °C) furnishing **47[2Li$^+$]** (yield from 1st batch of crystals = 780 mg, 87%, x ~ 4, y = 0). Alternatively, the crude reaction mixture could be filtered and washed with diethyl ether to remove trace impurities. After removal of the diethyl ether the title compound is furnished as an off white solid (>90% yield, x ~ 3, y ~ 0.4). ^{1}H NMR (300 MHz, THF-d_8, 25 °C): δ = 7.12 (s, 2H), 3.5 - 0.6 (bm, 22H) ppm. ^{1}H[^{11}B] NMR (600 MHz, acetonitrile-d_3, 25 °C): δ = 7.14 (s, 2H), 2.37 (s, 5H), 1.59 (s, 1H), 1.54 (s, 5H) ppm. ^{13}C[^{1}H] (75 MHz, THF-d_8, 25 °C): δ = 164.7, 120.6, 80.3 ppm. ^{11}B[^{1}H] NMR (192 MHz, acetonitrile-d_3, 25 °C): δ = -9.7, -14.0 ppm. ^{11}B NMR (192 MHz, acetonitrile-d_3, 25 °C): δ = -973 (^{1}*J(H,B)* = 134.1 Hz), -14.0 (^{1}*J(H,B)* = 138.0 Hz) ppm. HRMS (negative mode ESI/APCI) [M]$^-$ m/z Calc: $C_5H_{24}B_{22}N_2Cu_1I_1Li_1$ = 547.2650: Found = 547.2578, [M-(H)]$^-$ m/z Calc: $C_5H_{23}B_{22}N_2Cu_1I_1Li_1$ = 546.2572: Found = 546.2609.

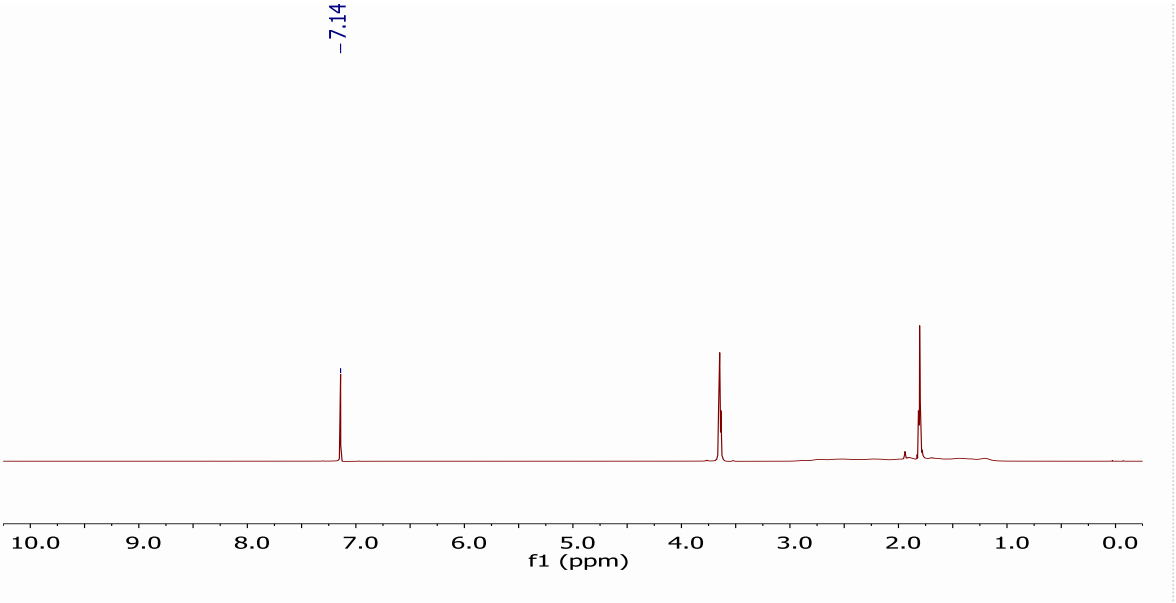

Figure 3-30 ^{1}H-NMR spectrum **of 47[2Li^{+}]** in acetonitrile-d_3 after preparative crystallization. *Note: THF (3.6 and 1.8 ppm) are coordinated to the lithium cation.*

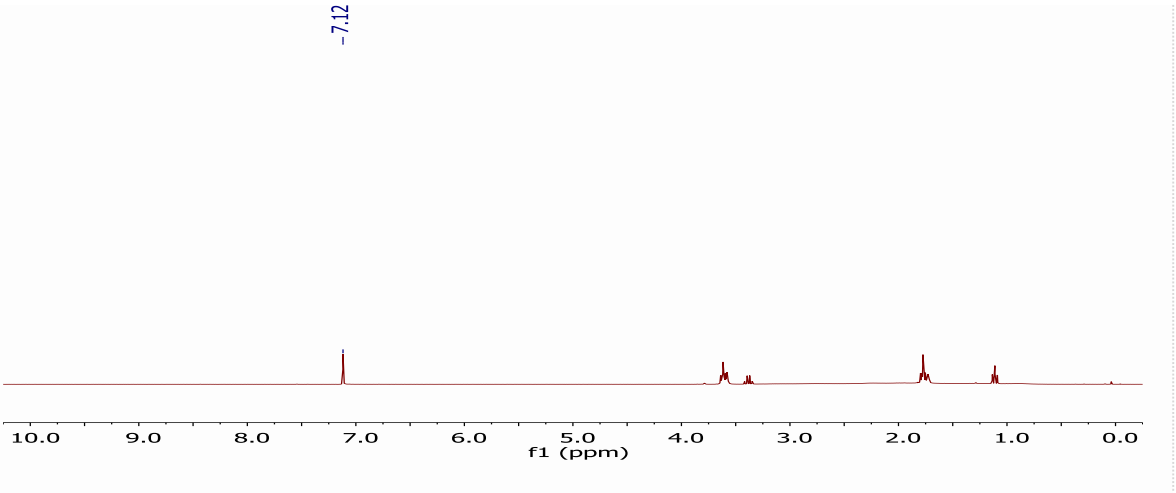

Figure 3-31^{1}H-NMR spectrum **of 47[2Li^{+}]** in THF-d_8 after diethyl ether wash. *Note: THF (3.6 and 1.8 ppm) and Et_2O (3.4 and 1.1 ppm) is coordinated to the lithium cation.*

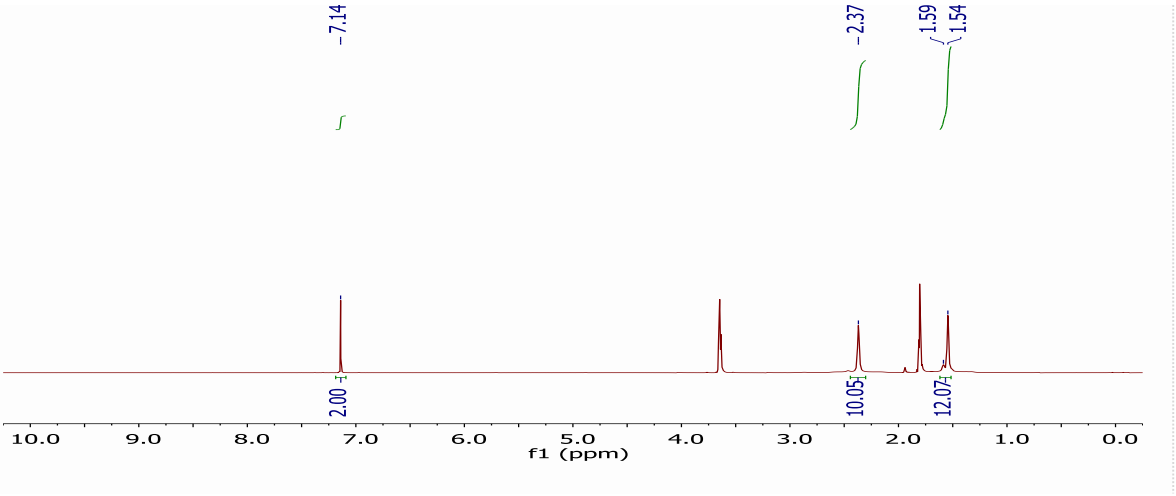

Figure 3-32 $^{1}H[^{11}B]$-NMR spectrum of **47[2Li^{+}]** in acetonitrile-d_3. The boron hydrides appear at 2.37, 1.59 and 1.54 ppm.

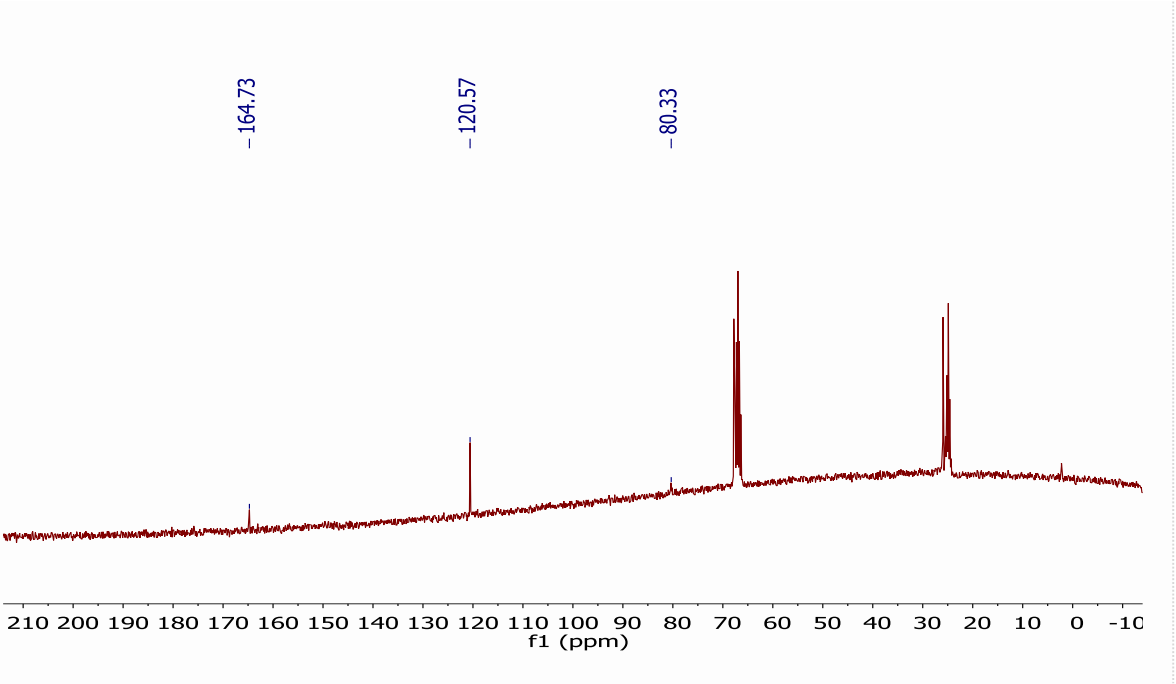

Figure 3-33 $^{13}C[^{1}H]$-NMR spectrum of **47[2Li^{+}]** in THF-d_8. Note: THF(67 and 25 ppm) is coordinated to the lithium cation.

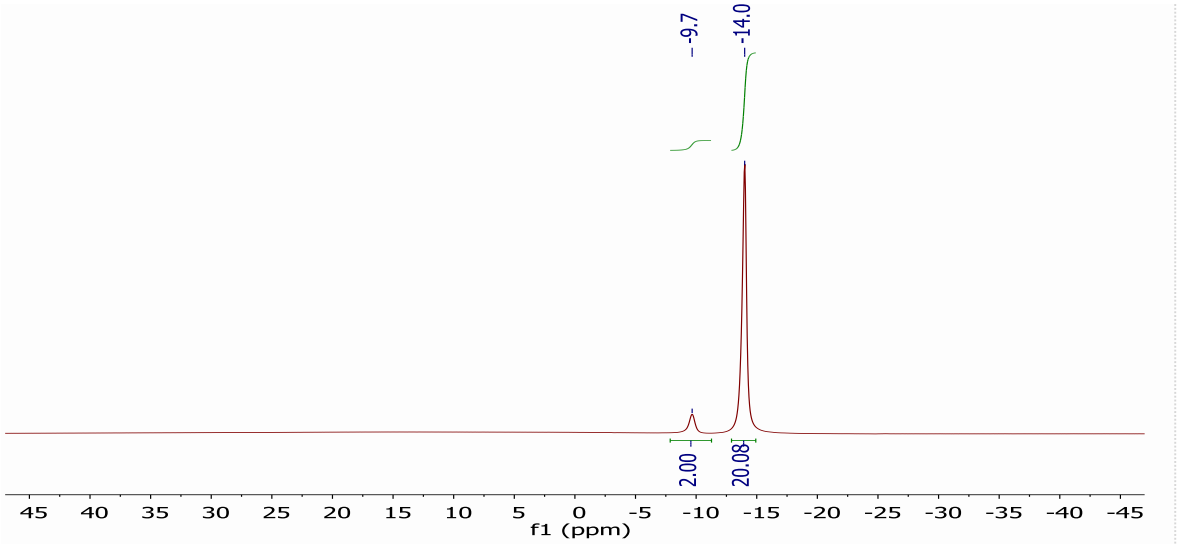

Figure 3-34 $^{11}B[^{1}H]$-NMR spectrum of **47[2Li^{+}]** in acetonitrile-d_3.

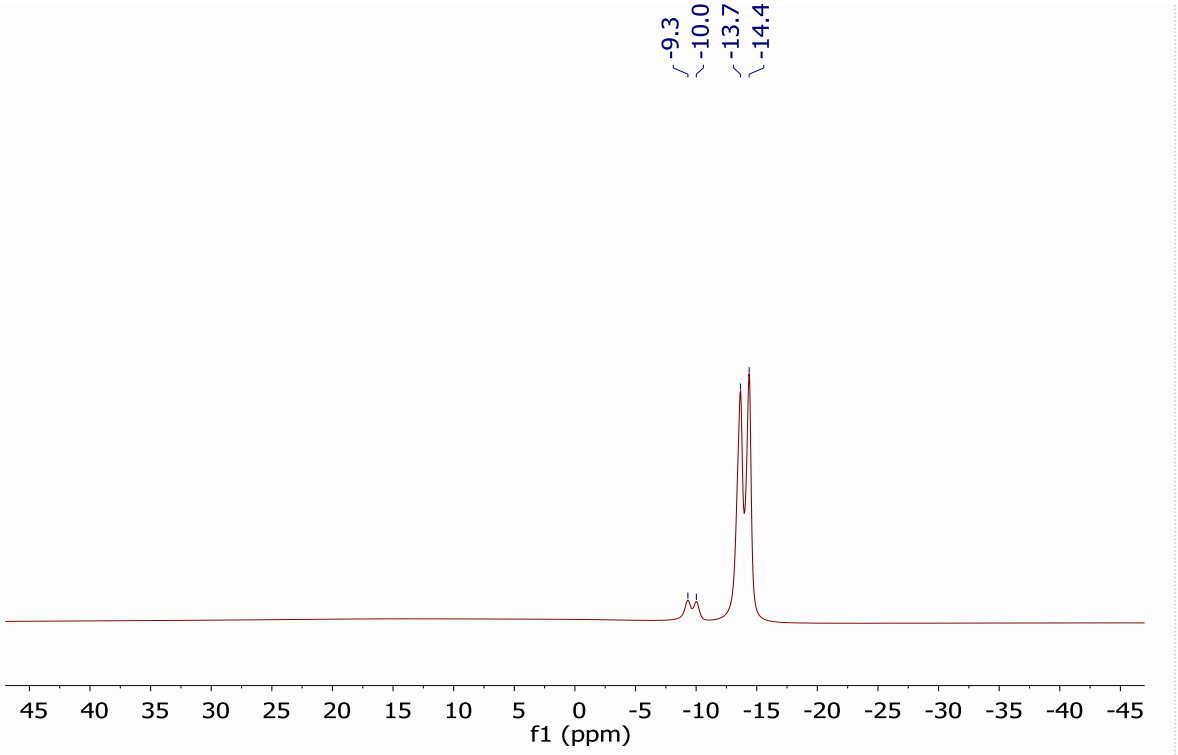

Figure 3-35 ^{11}B-NMR spectrum of **47[2Li^{+}]** in acetonitrile-d_3 showing the $^{1}J(B,H)$ coupling.

Synthesis of 47[Li$^+$] Showing the Presence of Imidazolium 29:

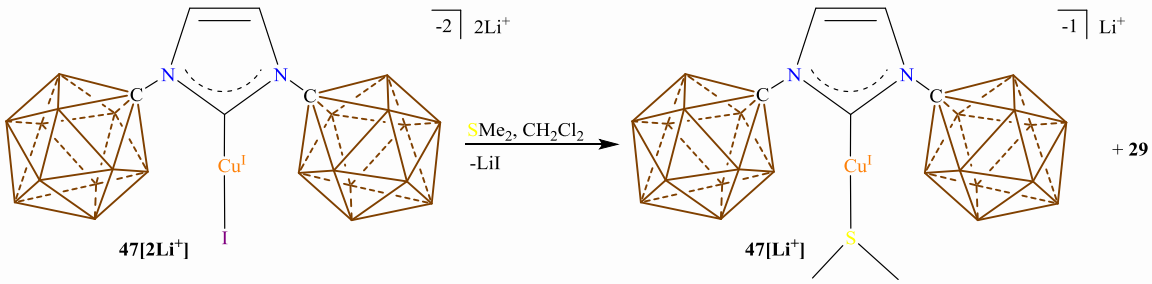

Scheme 3-13 Synthesis of **47[Li$^+$]** contaminated with **29**.

47[2Li$^+$] was suspended in methylene chloride (10 mL). To the suspension an excess of dimethylsulfide was added (10 drops from a glass pipette) and the vial stirred for 18 hours. The suspension was filtered and the filtrate concentrated down giving **47[Li$^+$]** contaminated with **29**. ^{1}H NMR (300 MHz, methylene chloride-d_2, 25 °C): δ = 7.08 (s, 2H), 3.5 - 0.8 (bm, 22H), 2.33 (6H, s) ppm.

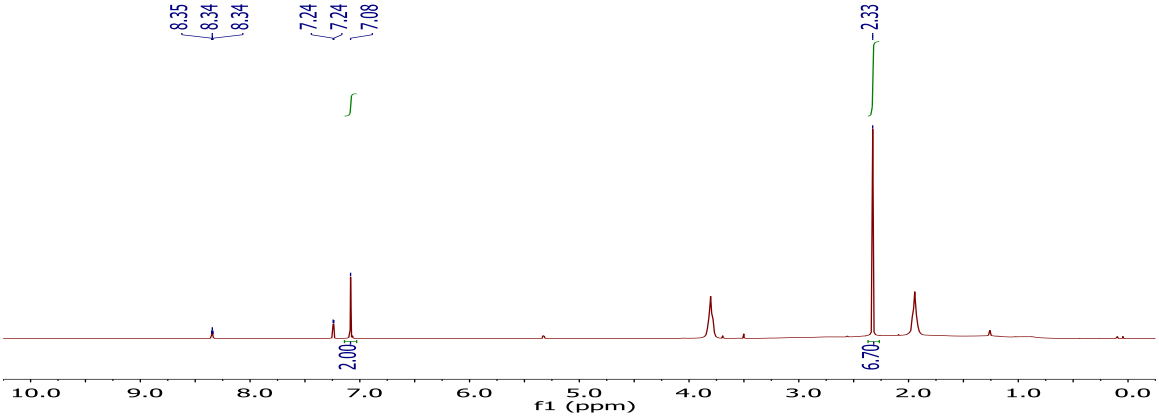

Figure 3-36 ^{1}H-NMR spectrum of **47[Li$^+$]** in methylene chloride-d_2. The peaks at 8.34 and 7.24 ppm represent imidazolium **29**.

X-Ray Structure Determination

Crystal Structure of 42:

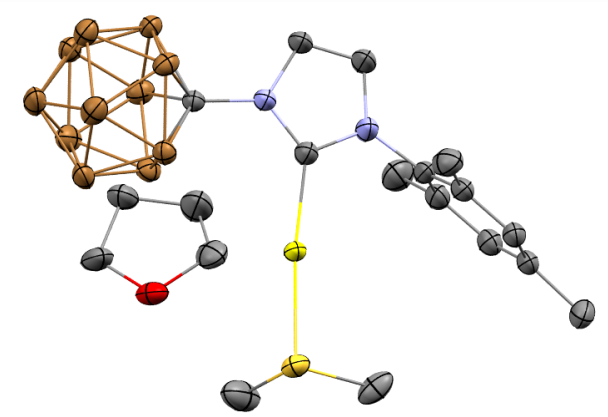

Figure 3-37 Solid state structure of **42**. Hydrogen atoms are omitted for clarity. Color code: Au = yellow, B = brown, C = gray, N = blue, O = red, S = orange.

A brown fragment of a prism (0.325 x 0.288 x 0.168 mm^3) was used for the single crystal x-ray diffraction study of $C_{15}H_{30}N_2B_{11}SAu_{0.88}Cs_{0.12}.C_4H_8O$ (sample vL156SF_0m). The crystal was coated with paratone oil and mounted on to a cryo-loop glass fiber. X-ray intensity data were collected at 100(2) K on a Bruker APEX2 platform-CCD x-ray diffractometer system (fine focus Mo-radiation, λ = 0.71073 Å, 50KV/30mA power). The CCD detector was placed at a distance of 5.0600 cm from the crystal.

A total of 3600 frames were collected for a sphere of reflections (with scan width of 0.3° in ω, starting ω and 2θ angles at –30°, and ϕ angles of 0°, 90°, 120°, 180°, 240°, and 270° for every 600 frames, 10 sec/frame exposure time). The frames were integrated using the Bruker SAINT software package and using a narrow-frame integration algorithm. Based on an orthorhombic crystal system, the integrated frames yielded a total of 96913 reflections at a maximum 2θ angle of 52.728° (0.80 Å resolution), of which 5742 were independent reflections (R_{int} = 0.0304, R_{sig} = 0.0108, redundancy = 16.9, completeness = 100%) and 4992 (86.9%) reflections were greater than 2σ (I). The unit cell parameters were, **a** = 18.8223(7) Å, **b** =

15.7649(6) Å, **c** = 18.9175(7) Å, $\alpha = \beta = \gamma = 90^{o}$, V = 5613.4(4) $Å^3$, Z = 8, calculated density D_c = 1.540 g/cm^3. Absorption corrections were applied (absorption coefficient μ = 4.867 mm^{-1}; max/min transmission = 0.495/0.301) to the raw intensity data using the SADABS program.

The Bruker SHELXTL software package was used for phase determination and structure refinement. The distribution of intensities (E^2-1 = 1.104) and systematic absent reflections indicated one possible space group, Pbca. The space group Pbca (#61) was later determined to be correct. Direct methods of phase determination followed by two Fourier cycles of refinement led to an electron density map from which most of the non-hydrogen atoms were identified in the asymmetric unit of the unit cell. With subsequent isotropic refinement, all of the non-hydrogen atoms were identified. There was one disordered molecule of $C_{15}H_{30}N_2B_{11}SAu$ and one disordered THF solvent present in the asymmetric unit of the unit cell. The Au/Cs and THF disordered site occupancy ratios were 88%/12% and 55%/45%, respectively.

Atomic coordinates, isotropic and anisotropic displacement parameters of all the non-hydrogen atoms were refined by means of a full matrix least-squares procedure on F^2. The H-atoms were included in the refinement in calculated positions riding on the atoms to which they were attached. The refinement converged at R1 = 0.0165, wR2 = 0.0395, with intensity, $I>2\sigma$ (I). The largest peak/hole in the final difference map was 0.524/-0.425 e/$Å^3$

Table 3-2 Crystal data and structure refinement for **42**.

Identification code	vL156SF_0m
Empirical formula	C19 H38 Au0.88 B11 Cs0.12 N2 O S
Formula weight	650.84
Temperature	100(2) K
Wavelength	0.71073 Å
Crystal system	Orthorhombic
Space group	P b c a

Unit cell dimensions	a = 18.8223(7) Å	α = 90°.
	b = 15.7649(6) Å	β = 90°.
	c = 18.9175(7) Å	γ = 90°.
Volume	5613.4(4) $Å^3$	
Z	8	
Density (calculated)	1.540 Mg/m^3	
Absorption coefficient	4.867 mm^{-1}	
F(000)	2569	
Crystal size	0.325 x 0.288 x 0.168 mm^3	
Theta range for data collection	2.000 to 26.364°.	
Index ranges	-23<=h<=23, -19<=k<=19, -23<=l<=23	
Reflections collected	96913	
Independent reflections	5742 [R(int) = 0.0304]	
Completeness to theta = 25.242°	100.0 %	
Absorption correction	Semi-empirical from equivalents	
Refinement method	Full-matrix least-squares on F^2	
Data / restraints / parameters	5742 / 28 / 371	
Goodness-of-fit on F^2	1.035	
Final R indices [I>2sigma(I)]	R1 = 0.0165, wR2 = 0.0395	
R indices (all data)	R1 = 0.0219, wR2 = 0.0420	

Extinction coefficient	n/a
Largest diff. peak and hole	0.524 and -0.425 e.Å^{-3}

Crystal Structure of 43[Li$^+$]:

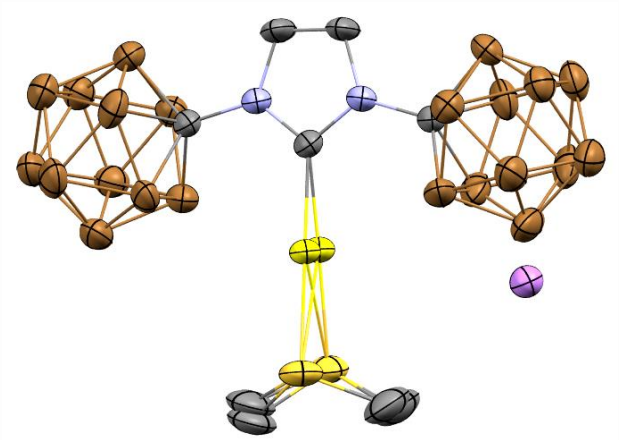

Figure 3-38 Solid state structure **of 43[Li$^+$].** Hydrogen atoms and THFs are omitted for clarity. Color code: Au = yellow, B = brown, C = gray, Li = pink, N = blue, S = orange.

A colorless plate fragment (0.308 x 0.266 x 0.056 mm^3) was used for the single crystal x-ray diffraction study of $Li[C_4H_8O]_2]^+$ $[C_7H_{30}B_{22}N_2SAu]^-$ (sample vL163SF_0m). The crystal was coated with paratone oil and mounted on to a cryo-loop glass fiber. X-ray intensity data were collected at 200(2) K on a Bruker APEX2 platform-CCD x-ray diffractometer system (fine focus Mo-radiation, λ = 0.71073 Å, 50KV/30mA power). The CCD detector was placed at a distance of 5.0600 cm from the crystal.

A total of 3600 frames were collected for a sphere of reflections (with scan width of 0.3^o in ω and ϕ, starting ω and 2θ angles of –30^o, and ϕ angles of 0^o, 90^o, 120^o, 180^o, 240^o, and 270^o for every 600 frames, 30 sec/frame exposure time). The frames were integrated using the Bruker SAINT software package and using a narrow-frame integration algorithm. Based on a monoclinic crystal system, the integrated frames

yielded a total of 98237 reflections at a maximum 2θ angle of 59.142° (0.72 Å resolution), of which 12091 were independent reflections (R_{int} = 0.0477, R_{sig} = 0.0287, redundancy = 8.1, completeness = 100%) and 10308 (85.3%) reflections were greater than 2σ(I). The unit cell parameters were, **a** = 11.1021(7) Å, **b** = 14.8321(10) Å, **c** = 26.1690(17) Å, **β** = 90.0492(12)°, V = 4309.2(5) Å^3, Z = 4, calculated density D_c = 1.394 g/cm^3. Absorption corrections were applied (absorption coefficient μ = 3.495 mm^{-1}; max/min transmission = 0.828/0.412) to the raw intensity data using the SADABS program.

The Bruker SHELXTL software package was used for phase determination and structure refinement. The distribution of intensities (E^2-1 = 0.812) and systematic absent reflections indicated one possible space group, P2(1)/n. The space group P2(1)/n (#14) was later determined to be correct. Direct methods of phase determination followed by two Fourier cycles of refinement led to an electron density map from which most of the non-hydrogen atoms were identified in the asymmetric unit of the unit cell. With subsequent isotropic refinement, all of the non-hydrogen atoms were identified. There was one disordered cation of $[Li[C_4H_8O]_2]^+$ and one disordered anion of $[C_7H_{30}B_{22}N_2SAu]^-$ present in the asymmetric unit of the unit cell. Three of the four THF molecules of the cation were modeled with disorder (disordered site occupancy ratios were 80%/20%, 77%/23%, and 55%/45%). The $AuSC_2H_6$-group of the anion was modeled with disorder (disordered site occupancy ratios were 81%/19%). The structure was refined as a pseudo-merohedral twin (twin law 1 0 0 0 -1 0 0 0 -1, and twin ratio of 59%/41%).

Atomic coordinates, isotropic and anisotropic displacement parameters of all the non-hydrogen atoms were refined by means of a full matrix least-squares procedure on F^2. The H-atoms were included in the refinement in calculated positions riding on the atoms to which they were attached. The refinement converged at R1 = 0.0314, wR2 = 0.0704, with intensity I>2σ (I). The largest peak/hole in the final difference map was 1.080/-0.861 e/Å^3.

Table 3-3 Crystal data and structure refinement for **43[Li^+]**.

Identification code	vL163SF_0m	
Empirical formula	C23 H62 Au B22 Li N2 O4 S	
Formula weight	904.53	
Temperature	200(2) K	
Wavelength	0.71073 Å	
Crystal system	Monoclinic	
Space group	P 21/n	
Unit cell dimensions	a = 11.1021(7) Å	α = 90°.
	b = 14.8321(10) Å	β = 90.0492(12)°.
	c = 26.1690(17) Å	γ = 90°.
Volume	4309.2(5) $Å^3$	
Z	4	
Density (calculated)	1.394 Mg/m^3	
Absorption coefficient	3.495 mm^{-1}	
F(000)	1816	
Crystal size	0.308 x 0.266 x 0.056 mm^3	
Theta range for data collection	1.373 to 29.571°.	
Index ranges	-15<=h<=15, -20<=k<=20, -36<=l<=36	
Reflections collected	98237	
Independent reflections	12091 [R(int) = 0.0477]	

Completeness to theta = 25.242°	100.0 %
Absorption correction	Semi-empirical from equivalents
Refinement method	Full-matrix least-squares on F^2
Data / restraints / parameters	12091 / 405 / 592
Goodness-of-fit on F^2	1.027
Final R indices [I>2sigma(I)]	R1 = 0.0314, wR2 = 0.0704
R indices (all data)	R1 = 0.0419, wR2 = 0.0745
Extinction coefficient	n/a
Largest diff. peak and hole	1.080 and -0.861 e.$Å^{-3}$

3.10 References

1. R. H. Grubbs, E. Khosravi ,E. B. Anderson, *Handbook of Metathesis*, 2015.
2. O. M. Ogba, N. C. Warner, D. J. O'Leary ,R. H. Grubbs, *Chemical Society Reviews*, 2018, **47**, 4510-4544.
3. R. H. Grubbs, *Angewandte Chemie International Edition*, 2006, **45**, 3760-3765.
4. WHO, *WHO Model Lists of Essential Medicines*, https://www.who.int/medicines/publications/essentialmedicines/en/, Accessed February 2, 2019.
5. Å. Rosenquist, B. Samuelsson, P.-O. Johansson, M. D. Cummings, O. Lenz, P. Raboisson, K. Simmen, S. Vendeville, H. de Kock, M. Nilsson, A. Horvath, R. Kalmeijer, G. de la Rosa ,M. Beumont-Mauviel, *Journal of Medicinal Chemistry*, 2014, **57**, 1673-1693.
6. J. Zhang ,Z. Xie, *Accounts of Chemical Research*, 2014, **47**, 1623-1633.
7. A. R. Popescu, F. Teixidor ,C. Viñas, *Coordination Chemistry Reviews*, 2014, **269**, 54-84.
8. C. Douvris ,J. Michl, *Chemical Reviews*, 2013, **113**, PR179-PR233.
9. D. Olid, R. Núñez, C. Viñas ,F. Teixidor, *Chemical Society Reviews*, 2013, **42**, 3318-3336.
10. Z.-J. Yao ,G.-X. Jin, *Coordination Chemistry Reviews*, 2013, **257**, 2522-2535.
11. M. Scholz ,E. Hey-Hawkins, *Chemical Reviews*, 2011, **111**, 7035-7062.
12. Y. Li, P. J. Carroll ,L. G. Sneddon, *Inorganic Chemistry*, 2008, **47**, 9193-9202.
13. U. Kusari, Y. Li, M. G. Bradley ,L. G. Sneddon, *Journal of the American Chemical Society*, 2004, **126**, 8662-8663.
14. E. L. Hoel ,M. F. Hawthorne, *Journal of the American Chemical Society*, 1975, **97**, 6388-6395.
15. F. Teixidor, M. A. Flores, C. Viñas, R. Kivekäs ,R. Sillanpää, *Organometallics*, 1998, **17**, 4675-4679.
16. C. Viñas, R. Nuñez, F. Teixidor, R. Kivekäs ,R. Sillanpää, *Organometallics*, 1996, **15**, 3850-3858.
17. F. Teixidor, J. A. Ayllon, C. Vinas, R. Kivekas, R. Sillanpaa ,J. Casabo, *Inorganic Chemistry*, 1994, **33**, 1756-1761.
18. F. Teixidor, J. Ayllón, C. Viñas, R. Kivekäs, R. Sillanpää ,J. Casabó, *Journal of the Chemical Society, Chemical Communications*, 1992, 1281-1282.
19. J. Estrada, S. E. Lee, S. G. McArthur, A. El-Hellani, F. S. Tham ,V. Lavallo, *Journal of Organometallic Chemistry*, 2015, **798**, 214-217.

20. A. El-Hellani, C. E. Kefalidis, F. S. Tham, L. Maron ,V. Lavallo, *Organometallics*, 2013, **32**, 6887-6890.

21. C. A. Reed, *Accounts of Chemical Research*, 2010, **43**, 121-128.

22. R. T. Boeré, C. Bolli, M. Finze, A. Himmelspach, C. Knapp ,T. L. Roemmele, *Chemistry – A European Journal*, 2013, **19**, 1784-1795.

23. C. Bolli, T. Köchner ,C. Knapp, *Zeitschrift für anorganische und allgemeine Chemie*, 2012, **638**, 559-564.

24. E. Molinos, S. K. Brayshaw, G. Kociok-Köhn ,A. S. Weller, *Dalton Transactions*, 2007, 4829-4844.

25. A. Rifat, G. Kociok-Köhn, J. W. Steed ,A. S. Weller, *Organometallics*, 2004, **23**, 428-432.

26. R. Ramírez-Contreras, N. Bhuvanesh, J. Zhou ,O. V. Ozerov, *Angewandte Chemie International Edition*, 2013, **52**, 10313-10315.

27. C. Douvris, C. M. Nagaraja, C.-H. Chen, B. M. Foxman ,O. V. Ozerov, *Journal of the American Chemical Society*, 2010, **132**, 4946-4953.

28. C. Douvris ,O. V. Ozerov, *Science*, 2008, **321**, 1188-1190.

29. S. P. Fisher, A. W. Tomich, S. O. Lovera, J. K. Kleinsasser, J. Guo, M. J. Asay, H. M. Nelson ,V. Lavallo, *Chemical Reviews*, 2019.

30. J. Estrada, C. A. Lugo, S. G. McArthur ,V. Lavallo, *Chemical Communications*, 2016, **52**, 1824-1826.

31. J. Estrada, D. H. Woen, F. S. Tham, G. M. Miyake ,V. Lavallo, *Inorganic Chemistry*, 2015, **54**, 5142-5144.

32. V. Lavallo, J. H. Wright Ii, F. S. Tham ,S. Quinlivan, *Angewandte Chemie International Edition*, 2013, **52**, 3172-3176.

33. J. F. Kleinsasser, E. D. Reinhart, J. Estrada, R. F. Jordan ,V. Lavallo, *Organometallics*, 2018, **37**, 4773-4783.

34. J. F. Kleinsasser, S. E. Lee, C. A. Lugo, V. Tej, S. G. McArthur ,V. Lavallo, *Polyhedron*, 2018, **156**, 245-248.

35. A. L. Chan, J. Estrada, C. E. Kefalidis ,V. Lavallo, *Organometallics*, 2016, **35**, 3257-3260.

36. F. Izquierdo, S. Manzini ,S. P. Nolan, *Chemical Communications*, 2014, **50**, 14926-14937.

37. M. N. Hopkinson, C. Richter, M. Schedler ,F. Glorius, *Nature*, 2014, **510**, 485.

38. S. Bellemin-Laponnaz ,S. Dagorne, *Chemical Reviews*, 2014, **114**, 8747-8774.

39. D. Martin, M. Melaimi, M. Soleilhavoup ,G. Bertrand, *Organometallics*, 2011, **30**, 5304-5313.

40. S. Díez-González, N. Marion ,S. P. Nolan, *Chemical Reviews*, 2009, **109**, 3612-3676.

41. F. E. Hahn ,M. C. Jahnke, *Angewandte Chemie International Edition*, 2008, **47**, 3122-3172.

42. R. H. Crabtree, *Coordination Chemistry Reviews*, 2013, **257**, 755-766.

43. O. Schuster, L. Yang, H. G. Raubenheimer ,M. Albrecht, *Chemical Reviews*, 2009, **109**, 3445-3478.

44. A. Krüger ,M. Albrecht, *Australian Journal of Chemistry*, 2011, **64**, 1113-1117.

45. A. El-Hellani ,V. Lavallo, *Angewandte Chemie International Edition*, 2014, **53**, 4489-4493.

46. M. J. Asay, S. P. Fisher, S. E. Lee, F. S. Tham, D. Borchardt ,V. Lavallo, *Chemical Communications*, 2015, **51**, 5359-5362.

47. H. Clavier ,S. P. Nolan, *Chemical Communications*, 2010, **46**, 841-861.

48. T. Dröge ,F. Glorius, *Angewandte Chemie International Edition*, 2010, **49**, 6940-6952.

49. S. Kronig, E. Theuergarten, C. G. Daniliuc, P. G. Jones ,M. Tamm, *Angewandte Chemie International Edition*, 2012, **51**, 3240-3244.

50. M. Devillard, E. Nicolas, C. Appelt, J. Backs, S. Mallet-Ladeira, G. Bouhadir, J. C. Slootweg, W. Uhl ,D. Bourissou, *Chemical Communications*, 2014, **50**, 14805-14808.

51. M. Etienne ,A. S. Weller, *Chemical Society Reviews*, 2014, **43**, 242-259.

52. M. Brookhart, M. L. H. Green ,G. Parkin, *Proceedings of the National Academy of Sciences*, 2007, **104**, 6908.

53. D. Malhotra, M. S. Mashuta, G. B. Hammond ,B. Xu, *Angewandte Chemie International Edition*, 2014, **53**, 4456-4459.

54. S. M. Inamdar ,N. T. Patil, *Organic Chemistry Frontiers*, 2015, **2**, 995-998.

Chapter 4: Bimetallic Complexes Featuring an Anionic Au(I) Fragment

4.1 Synthesis of a Heterobimetallic Complex Linked via Ion Pairing

Determined to find a use for our Au(I) complexes **42** and **43[Li$^+$]**, we thought to investigate the anionic nature of complex **43**. Since complex **43[Li$^+$]** contained a lithium counter cation, we wondered if we could switch the Li^+ counter-ion for a cationic transition metal complex. As a simple test, we chose to switch Li^+ for Ag^+. This choice seemed logical as the most common oxidation state for charged Ag is Ag^+. The bimetallic Au/Ag complex would also be a useful halide abstraction reagent which could be used to abstract a halogen from a transition metal halide complex forming a cationic transition metal complex. A brief survey of the literature revealed that complexes of this type had recently been reported in the form of Au/Ag nanoparticles,[1-3] as well as older publications featuring homogeneous Au/Ag clusters,[4, 5] polymers,[6, 7] and ionic $[Au(C_6F_5)_x(CN)_y]^-$ where x = 3, 2 and y = 1, 2, respectively.[8] Perhaps not surprisingly there are a no reports of two coordinate Au(I)/Ag(I) bimetallic complexes. This is likely due to the fact that most Ag^+ containing reagents act as chloride abstraction agents forming active L-Au^+ catalysts.[9, 10]

For us to achieve this transformation we decided to develop a two-component reaction with one being be a solution of **43[Li$^+$]** and the other a solution of an Ag^+ salt. Upon mixing in the Ag^+ salt we wanted to lose the Li^+ salt byproduct as a precipitate and keep the bimetallic Au(I)/Ag(I) complex in solution. Since Ag^+ is a larger cation than Li^+, the carborane anion should favor the Ag^+ ion over the Li^+ ion. In pursuit of this chemistry, a 1:1 ratio of $AgBF_4$ to **43[Li$^+$]** was reacted in F-C_6H_5 solvent. Immediately, a copious amount of solid were seen precipitating from the solution. A ^{11}B NMR analysis was performed on the crude reaction mixture. This NMR revealed no traces of boron indicating that all the products from the reaction had precipitated. Luckily, the reaction mixture was completely soluble in THF which upon ^{11}B NMR analysis revealed the presence of BF_4 anion, singlet at -1.3 ppm, and carborane anion at -9.5, -13.1 and -13.9 ppm (peaks with a 1:5:5 ratio). To better understand what had happened in this reaction, the crude reaction mixture was dissolved in deuterated THF and the solution analyzed by ^1H NMR spectroscopy. The ^1H NMR spectrum revealed a single downfield resonance at 7.46 ppm (NHC backbone

protons) and an upfield resonance at 2.82 ppm (dimethylsulfide methyl protons) suggesting that the anionic Au(I) complex was still intact. As it turns out the THF solution containing the crude reaction mixture slowly turns into a thick jelly after about 45 minutes, indicative of polymerized THF.

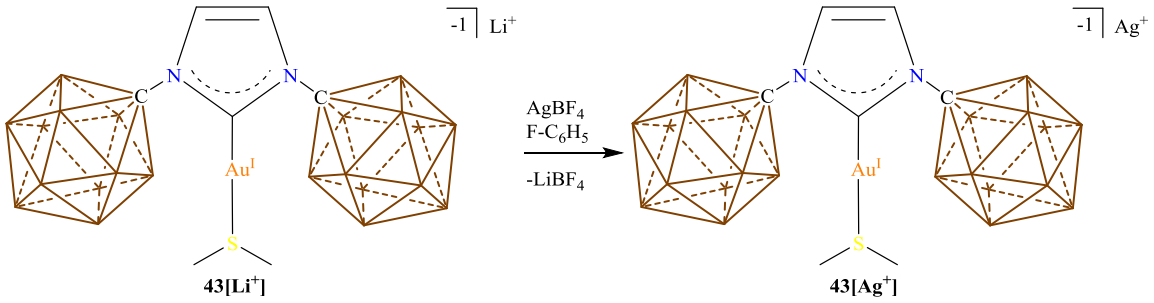

Scheme 4-1 Synthesis of bimetallic complex **43[Ag$^+$]**.

We believed that the desired bimetallic Au(I)/Ag(I) complex, **43[Ag$^+$]**, had precipitated from solution along with $LiBF_4$, as indicated by the peak at -1.3 ppm in the ^{11}B NMR spectrum. To separate bimetallic complex **43[Ag$^+$]** from $LiBF_4$, we decided to wash the solid in diethyl ether. However, this method was not very efficient as after multiple Et_2O washes the solid still contained decent amounts of $LiBF_4$. At this point we decided to try dissolving the solid material in a minimal amount of THF then adding the THF solution to a vigorously stirring solution of Et_2O which should induce precipitation of bimetallic complex **43[Ag$^+$]** while keeping $LiBF_4$ in solution. Indeed, this strategy worked and $LiBF_4$ was successfully removed.

The last remaining challenge was to fully elucidate the structure of **43[Ag$^+$]**, specifically the presence of an Ag^+ counter-ion. To do this we thought to grow crystals of **43[Ag$^+$]** for a single crystal X-ray diffraction study. Upon layering a THF solution with fluorobenzene and storing the crystallization at -30 °C we were able to successfully grow crystals. The crystal structure of **43[Ag$^+$]** revealed that we had switched the Li^+ counter-ion for an Ag^+ counter-ion. In the solid state the structure of **43[Ag$^+$]** displays a stack of two anti-parallel anionic Au(I) fragments held together by bridging Ag^+ counter-ions linked though

neighboring carborane clusters (Figure 4-1). This anti-parallel feature is not caused by Au-S interactions as the Au-S distance (3.59 Å) is outside that of the sum of van der Waals radii (Au-S van der Waals radii = 3.46 Å), nor is this feature caused by S-S interactions as the sum of van der Waals radii for S-S is 3.60 Å and the closest S-S distance in the crystal structure is 4.62 Å. The bridging Ag^+ counter-ions display three coordination features with the B-H bonds of two neighboring carboranes, one carborane interacts with the Ag^+ ion at position B7 and B8 while the other carborane interacts with the Ag^+ ion at B7. Lastly the Ag^+ ion is coordinated to one molecule of THF. Corroborating this result is the ^{7}Li NMR spectrum taken of purified **43[Ag$^+$]** which shows no signals, indicating that no large quantities of Li^+ is present in the solution.

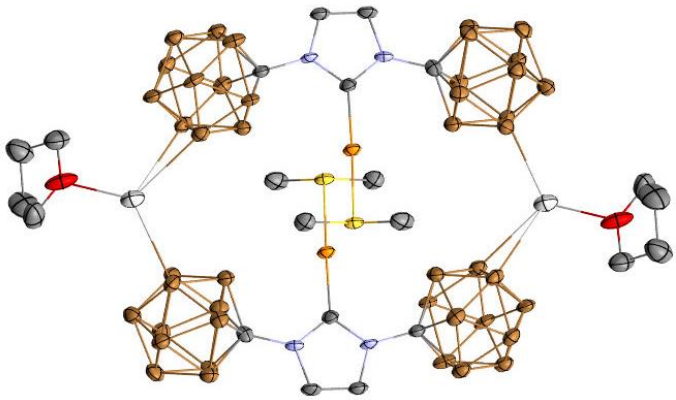

Figure 4-1 Solid state structure of **43[Ag$^+$]**. Hydrogen atoms omitted for clarity. Color code: B = brown, C = gray, N = blue, O = red, S = yellow, Ag = silver, Au = orange.

With bimetallic **43[Ag$^+$]** in hand we wanted to see if we could perform a halide abstraction from a transition metal complex bearing a metal halide bond. A literature search revealed that reactions of this type have never been reported, the reason being there is only a handful of anionic Au complexes,[11-14] excluding tetrahaloaurates[15, 16] and dicyanoaurates,[17, 18] in the literature and only one example of an anion Au(I)/Ag(I) system.[8] Thus we needed to devise a synthetic strategy to access these types of heterobimetallic complexes.

Before pioneering a method to synthesize these bimetallic complexes, we wanted to consider practical bimetallic systems that could perform tandem catalysis. Here we had envisioned a hydroamination

reaction followed by hydrogenation. In this system the hydroamination would be performed by the Au(I) fragment while the hydrogenation would be performed by the M^+ fragment. Our strategy was a shotgun approach where we would try a variety of metal halide candidates and then analyze the crude reaction mixture by ^{1}H NMR spectroscopy. If the crude reaction mixture contained a single major product, we would attempt to crystalize the crude reaction to obtain crystals for X-ray diffraction. Of the candidates we tried we were able to obtain two crystal structure IDs for the reaction of **43[Ag$^+$]** with $[Rh(COD)Cl]_2$ (COD = 1,5-cyclooctadiene) and $[Ru(C_6H_6)Cl_2]_2$.

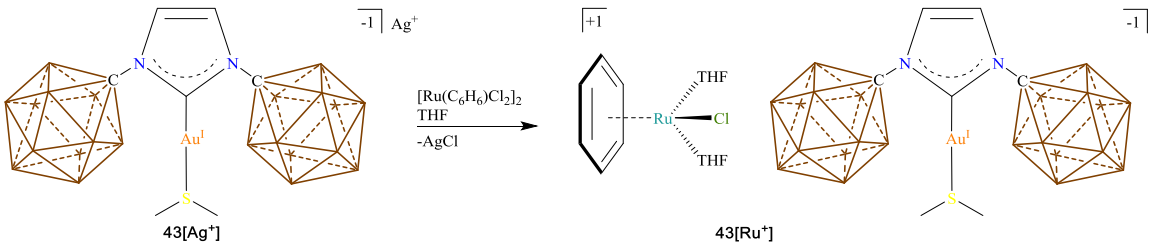

Scheme 4-2 Synthesis of expected **43[Ru$^+$]**. *Note the crystal structure does not support the predicted structure.*

For the reaction of **43[Ag$^+$]** with $[Ru(C_6H_6)Cl_2]_2$ we chose to react 0.5 equivalents of $[Ru(C_6H_6)Cl_2]_2$ with **43[Ag$^+$]** in THF, Scheme 4-2. The crude ^{1}H NMR spectrum of **43[Ru$^+$]** displayed two downfield singlets (7.42 and 5.96 ppm) corresponding to the backbone protons of the NHC core and the six protons of the benzene ring as well as an upfield resonance at 2.81 ppm corresponding to the methyl protons of the Au bound dimethylsulfide ligand. The crude reaction mixture was filtered, and the filtrate prepared for crystallization. The complex we predicted from this reaction was **43[Ru$^+$]**. Vapor diffusion of F-C_6H_5 with hexane produced single crystals suitable of an X-ray diffraction study. To our surprise, the crystal structure revealed a $[Ru_2(C_6H_6)_2Cl_3]^+$ counter ion which did not correspond to the product found in the ^{1}H NMR spectrum as the bound C_6H_6 integrated to six protons not 12 protons (Figure 4-2). However, careful inspection of the ^{1}H NMR spectrum revealed a small singlet at 5.72 ppm that could correspond to

the crystalized product, Figure 4-11. It should be noted that prolonged exposure to THF will irreversibly decompose **43[Ru$^+$]**.

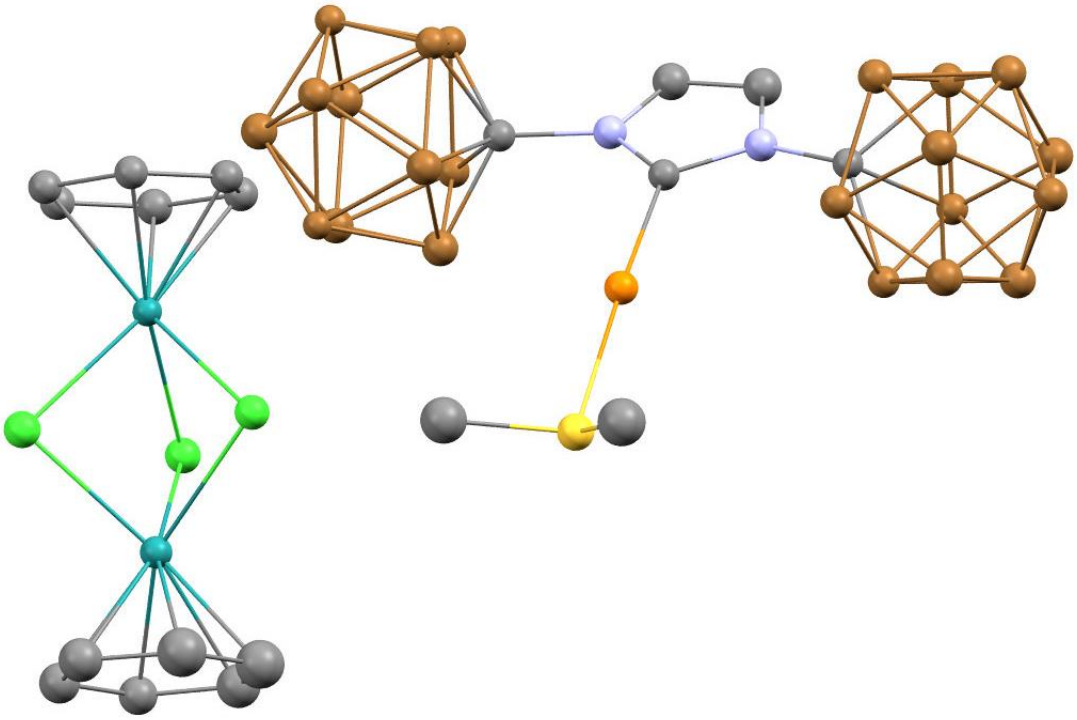

Figure 4-2 Crystal structure of **43[Ru$^+$]** with an $[Ru_2(C_6H_6)_2Cl_3]^+$ counter ion. Hydrogen atoms are omitted for clarity. Color code: B = brown, C = gray, N = blue, S = yellow, Cl = green, Ru = teal, Au = orange.

Concurrent with the above experiment we also obtained crystals from the reaction of **43[Ag$^+$]** with $[Rh(COD)Cl]_2$ (COD = 1,5-cyclooctadiene) in THF, Scheme 4-3. After filtration of AgCl, the reaction mixture was pumped down to dryness and extracted with F-C_6H_5. The extract was concentrated and preparatively crystalized at -30°C. At this point we predicted two possible solid-state structures, if the solvent (THF or F-C_6H_5) was coordinating to the Ru^+ we expected **43[Rh$^+$]**, if the solvent wasn't coordinating we expected to see the Rh^+ counter ion coordinated to one of the carborane anions of the anionic Au(I) fragment, **43**. This prediction was based off the work by Weller and coworkers who demonstrated that if monoanion **1** was crystalized with $[Rh(COD)]^+$ in methylene chloride the Rh fragment

would crystalize to the carborane anion. If the crystallization was performed in THF, the $[Rh(COD)]^+$ fragment coordinated to two molecules of THF.[19]

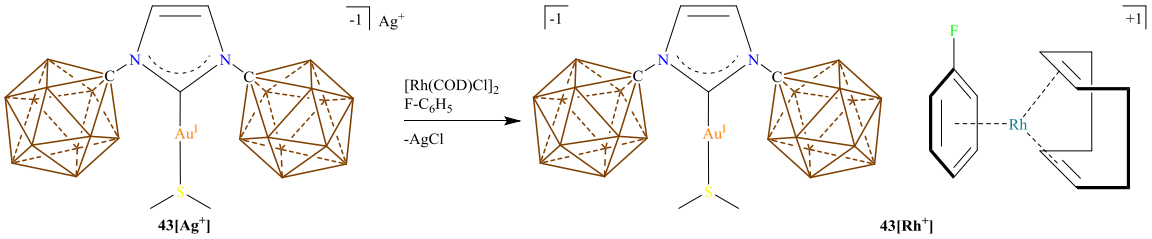

Scheme 4-3 Synthesis of expected **43[Rh$^+$]**.

The single crystal X-ray diffraction study revealed that the Rh^+ ion of **43[Rh$^+$]** was coordinated to a molecule of fluorobenzene, Figure 4-3. However, when the crystals are put under vacuum the F-C_6H_5 ligand is removed and the Rh^+ fragment is coordinated to the carborane anion, indicated by the lack of F-C_6H_5 in the ^{1}H NMR spectrum of **43[Rh$^+$]**, Figure 4-15.

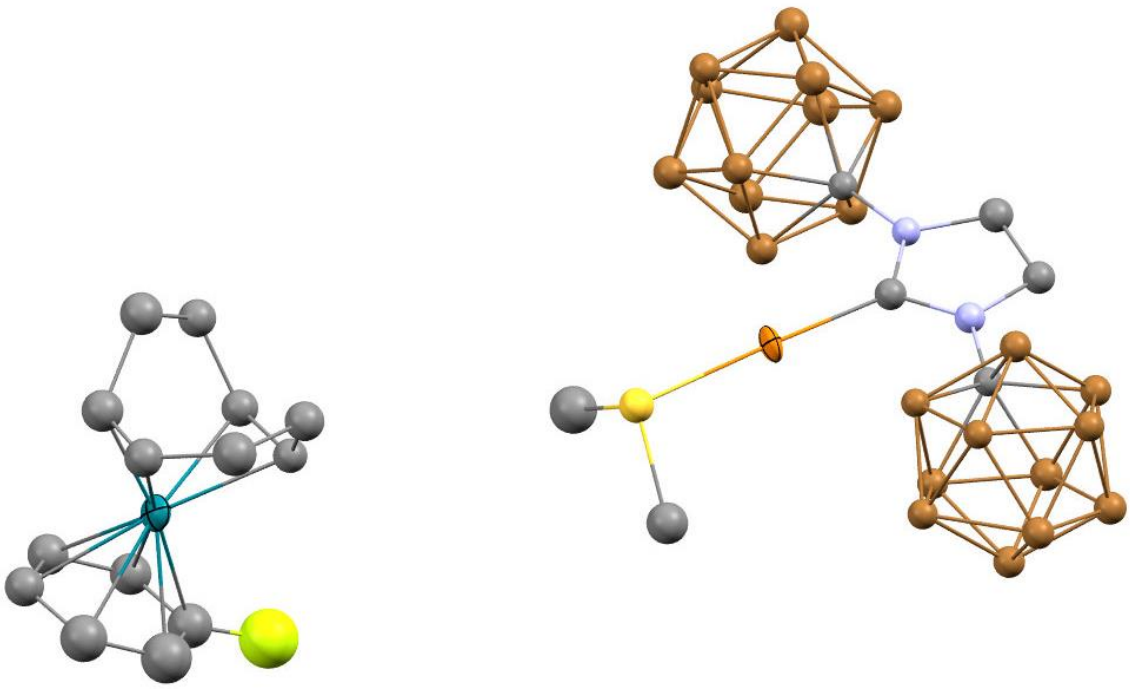

Figure 4-3 Solid-state structure of **43[Rh$^+$]**. Hydrogen atoms have been omitted for clarity. Color code: B = brown, C = gray, N = blue, F = green, S = yellow, Au = orange.

4.2 Tandem Hydroamination and Hydrogenation with **43[Rh$^+$]**

Bimetallic complexes with Au and Rh are rare and only recently have examples in the literature started to emerge.[20-25] One area of interest is the transmetalation of R type ligands from Au to Rh.[20, 21] This first appeared in 2011 when Shi and Blum demonstrated that vinyl or aryl ligands on Au could be transmetalated to Cp*$RhCl_2(PPh_3)$ (Cp* = pentamethylcyclopentadiene), **44** - **46**, Scheme 4-4.[20] In this report, the authors where also able to isolate an Au(I)/Rh(I) bimetallic complex **47** where the Rh^+ is π-coordinated to the face of the benzene ring, Scheme 4-4 inset. This coordination motif is similar to the coordination of Rh^+ in **43[Rh$^+$]**.

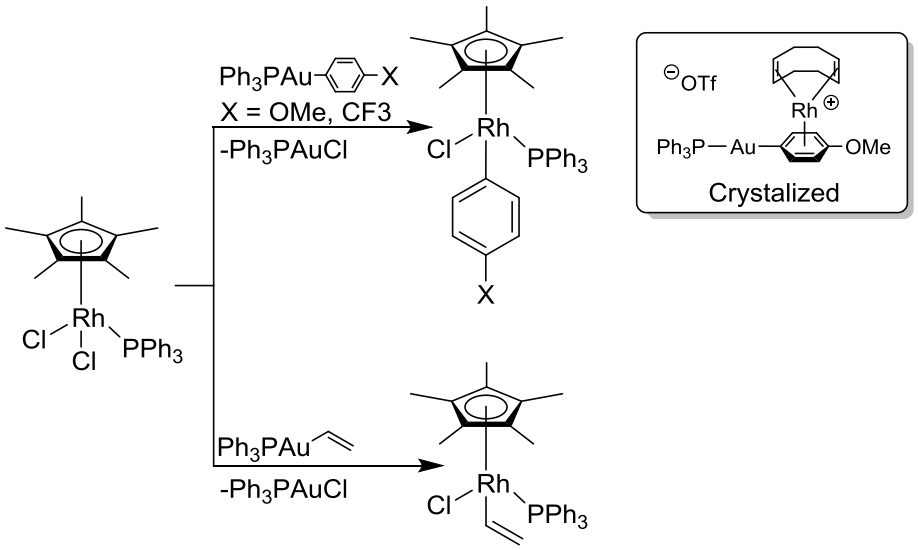

Scheme 4-4 Transmetalation with an Au/Rh system. The inset depicts the crystal structure of an Au/Rh complex obtained by the authors.

In 2013, the first report of a catalytically active Au(I)/Rh(I) system was introduced by Hansmann and coworkers.[22] In this catalytic reaction a racemic propargyl alcohol undergoes a tandem Meyer-Schuster rearrangement followed by an asymmetric 1,4-addition, furnishing ß-disubstituted ketone, Scheme 4-5. During this reaction the Au center catalyzes the Meyer-Schuster rearrangement and the chiral Rh center catalyzes the asymmetric conjugate addition. Even though this represents the first catalytic Au/Rh system it should be noted that the Au and Rh components are completely separate components.

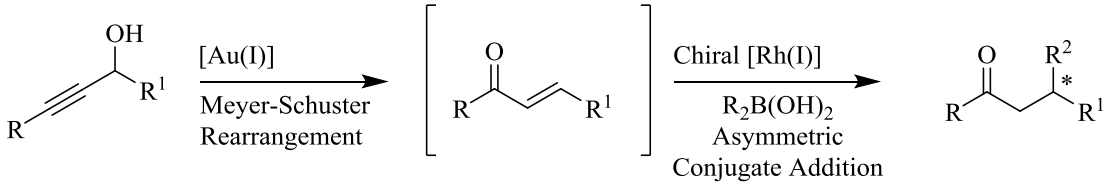

Scheme 4-5 Tandem bimetallic Meyer-Schuster rearrangement followed by asymmetric conjugate addition. The * indicates the chiral center formed during the reaction.

In 2018 the first report of a unimolecular Au/Rh catalytic system was published. In this report by Guisado-Barrios and coworkers, bimetallic Au/Rh systems, **48** and **49**, were proven to couple nitrobenzene

and benzylic alcohols, Table 4-1.[23] They created two unimolecular bimetallic catalyst in which both demonstrated complete conversion of substrates, however they were only mildly selective in product formation. When both Au and Rh were on the same side product II was favored (Table 4-1, Entry 1) but when Au and Rh were on opposite sides product III was favored (Table 4-1, Entry 2).

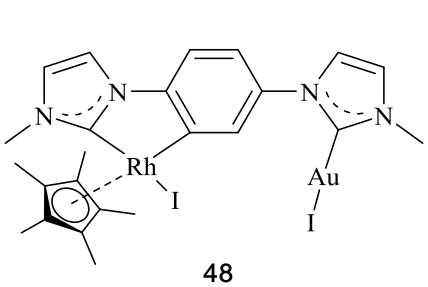

48

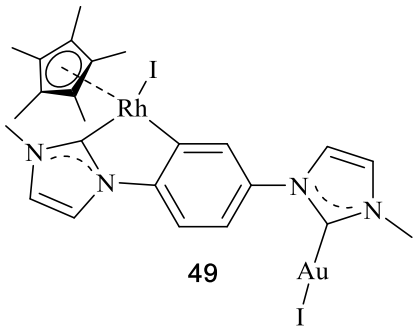

49

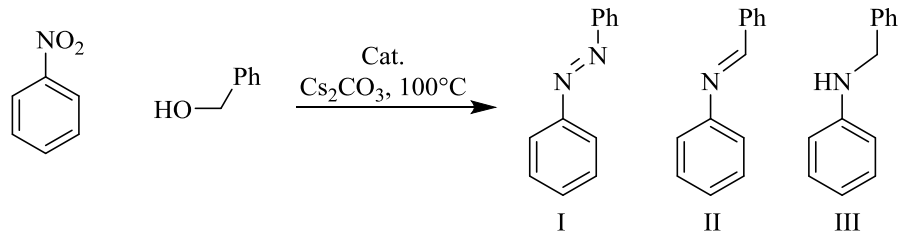

I II III

Entry	Cat.	Conversion %	Yield % I	II	III
1	48	100	25	62	13
2	49	100	18	34	48

Table 4-1 Table showing the coupling reaction of nitrobenzene and benzyl alcohol with bimetallic catalyst **48** and **49**.

To the best of our knowledge no one has attempted a hydroamination followed by a hydrogenation with an Au(I)/Rh(I) system. We decided to attempt a tandem hydroamination hydrogenation experiment with crystalline **43[Rh$^+$]**. In this experiment, a flame dried Schlenk flask was loaded with **43[Rh$^+$]**, alkyne substrate, amine substrate and H_2. As a prototypical experiment we decided to use phenylacetylene as the alkyne substrate and aniline as the amine substrate. Shortly after beginning the reaction a slight color

change was noticed in the crude reaction mixture. To analyze this change an aliquot of the reaction mixture was removed and analyzed by ^{1}H NMR spectroscopy. The ^{1}H NMR spectrum revealed that the alkyne was being consumed but the amine was not. The ^{1}H NMR displayed no signals between 0 and -30 suggesting no long lived Rh-H species indicating the alkyne was not being hydrogenated, nor was there any indication of ethylbenzene in the ^{1}H NMR. The ^{1}H NMR spectrum did contain three new broad signals at 6.94, 6.63, and 5.85 ppm. If more alkyne is added to the reaction the consumption of alkyne continues and the aforementioned peaks increase in intensity. If enough alkyne is added the solution turns in to a waxy solid indicating the presence of a polymer.

Unknown to us at the time of this experiment was the catalytic activity of Rh^{+} with alkynes. Rh^{+} cations are well-known within the literature to act as alkyne polymerization catalyst.[26] Indeed the three signals in the ^{1}H NMR spectrum at 6.94, 6.63 and 5.85 ppm matched that for poly(phenylacetylene).[27, 28] With this result we decided to consider a different direction for this project.

4.3 Experimental

General Considerations:

All manipulations were carried out using standard Schlenk or glovebox techniques under an argon or dinitrogen atmosphere unless otherwise stated. Dry solvents were obtained via distillation under argon from potassium (benzene-d_6), phosphorus pentoxide (fluorobenzene, fluorobenzene-d_5) or calcium hydride (methylene chloride-d_2). Benzene, toluene, pentane and hexane were collected from a solvent purification system by SG Waters USA, LLC utilizing a fifteen minute argon sparge followed by passage though activated aluminum. Cesium 1-amino-1-carba-*closo*-undecaborate **3** was prepared following the procedure by Jelínek and co-workers.[29] The NHC **30** was prepared via the El-Hellani route.[30] Unless specifically stated, reagents were purchased from commercial vendors and used without further purification. Nuclear magnetic resonance (NMR) spectroscopy was carried out using: Bruker Avance 300 MHz, Bruker NEO 400 MHz, Bruker Avance 600 MHz, Varian Inova 300 MHz, Varian Inova 400 MHz or Varian Inova 500 MHz spectrometers. NMR chemical shifts are reported in parts per million (ppm) with ^{1}H and ^{13}C chemical shifts referenced to the residual non-deutero solvent. The ^{11}B NMR chemical shifts were externally

referenced to BF_3•OEt_2. The ^{11}B-^{1}H coupling constants from ^{11}B spectra are reported when possible. High-resolution mass spectrometry (HRMS) was collected on an Agilent Technologies 6210 (TOF LC/MS) featuring a multimode ESI/APCI with direction injection. Fourier transform infrared spectroscopy was recorded on a Bruker ALPHA interferometer in a glove box under an Argon atmosphere.

Synthesis of 4**3[Ag$^+$]:**

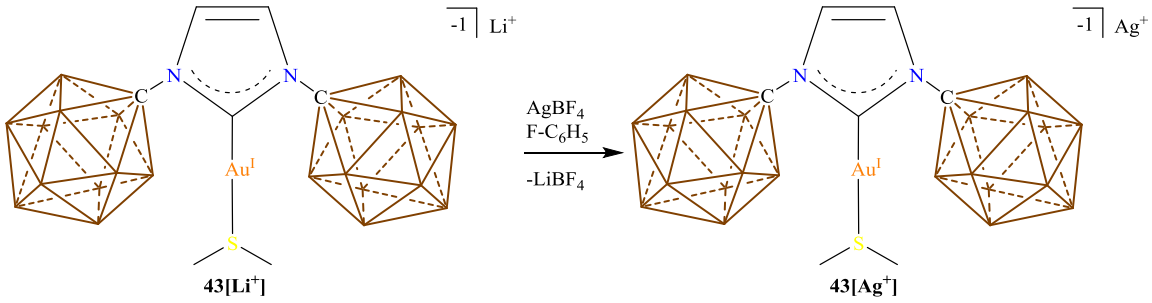

Scheme 4-6 Synthesis of **43[Ag$^+$]**.

A glass scintillation vial equipped with a stir bar was loaded with **43[Li$^+$]** (350 mg, 380 µmol) and dissolved in F-C_6H_5 (4 mL). A solution of $AgBF_4$ (76 mg, 380 µmol) in F-C_6H_5 (3 mL) was added dropwise to the suspension containing **43[Li$^+$]** causing an immediate precipitation. The reaction was stirred overnight at room temperature. The F-C_6H_5 supernatant was removed and the solid washed with diethyl ether (3 x 20 mL). The remaining solid was pumped down to dryness furnishing **43[Ag$^+$]** as a dark solid (200 mg, 70.14% yield, 0.45 coordinated THF to Ag^+). *Note: if there is a signal present in the ^{7}Li NMR spectrum but not the ^{19}F NMR spectrum, there was incomplete conversion from Li^+ to Ag^+ (i.e.* ***43[Li$^+$]*** *is still present) and the $AgBF_4$ step needs to be repeated.* ^{1}H NMR (600 MHz, THF-d_8, 25°C): ∂ = 7.46 (s, 2H), 2.82 (s, 6H), 3.1 – 1.2 (bs, 22H) ppm. $^{1}H[^{11}B]$ NMR (300 MHz, THF-d_8, 25°C): ∂ = 7.46 (s), 2.82 (s), 2.62 (bs, H-B), 1.94 (bs, H-B), 1.73 (bs, B-H) ppm. $^{11}B[^{1}H]$ NMR (96 MHz, THF-d_8, 25°C): ∂ = -9.5, -13.1, -13.9 ppm. ^{11}B NMR (96 MHz, THF-d_8, 25°C): ∂ = -9.5 ($^{1}J(H,B)$ = 119.3 Hz), -13.1, -13.9 ($^{1}J(H,B)$ = 134.0 Hz) ppm. $^{13}C[^{1}H]$ NMR (151 MHz, THF-d_8, 25°C): ∂ = 174.7, 122.8, 80.5, 24.5 ppm.

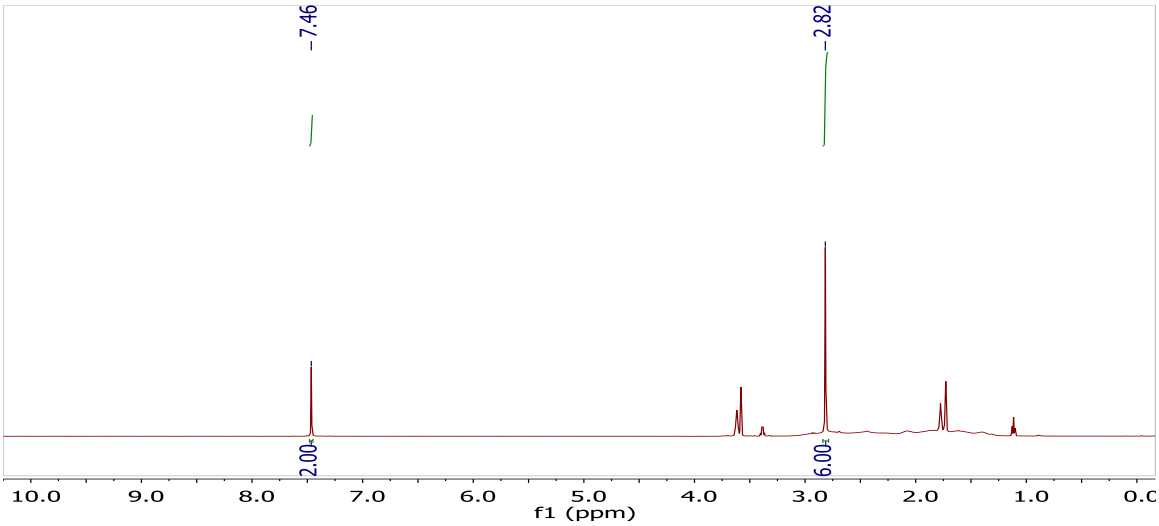

Figure 4-4 ^{1}H-NMR spectrum of **43[Ag^{+}]** in THF-d_8. Note: THF and Et_2O are coordinated to the Ag^{+} counter cation at 3.6 and 1.8 ppm and 3.4 and 1.2 ppm respectively.

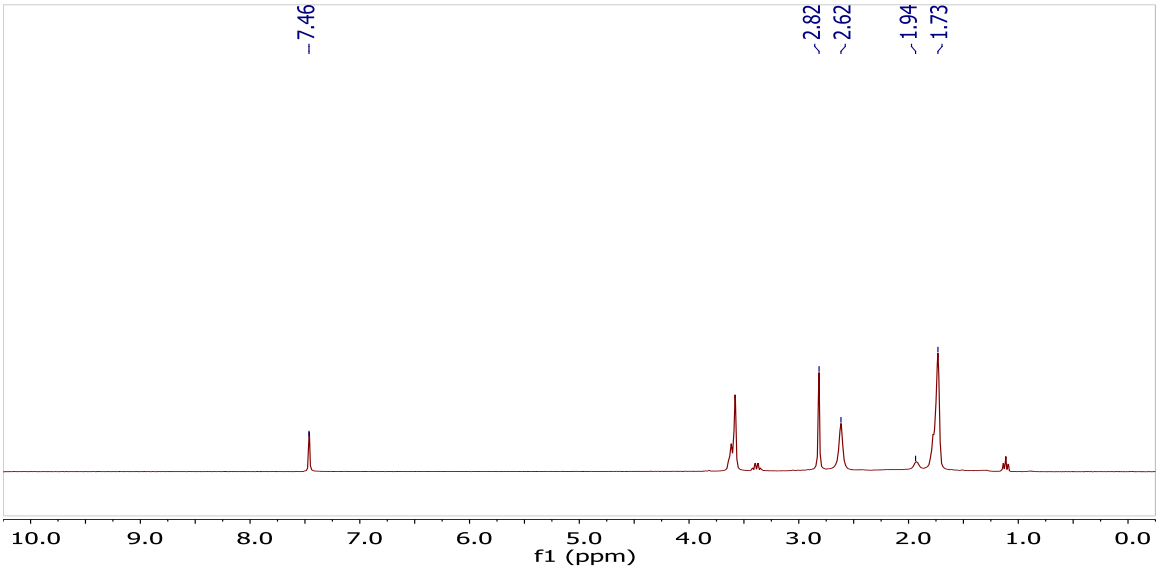

Figure 4-5 ^{1}H[^{11}B]-NMR spectrum of **43[Ag^{+}]** in THF-d_8. Note: the peaks at 2.62, 1.94 and 1.73 ppm correspond to the H-B resonances.

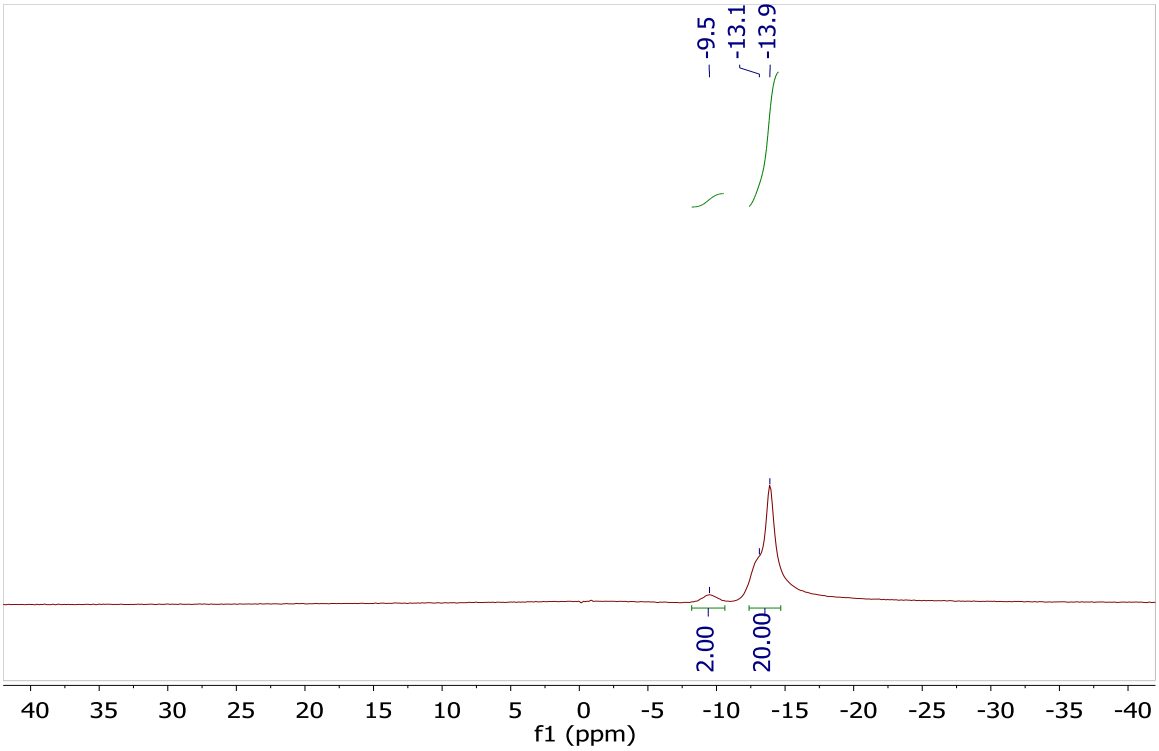

Figure 4-6 $^{11}B[^{1}H]$-NMR spectrum of **43[Ag^{+}]** in THF-d_8.

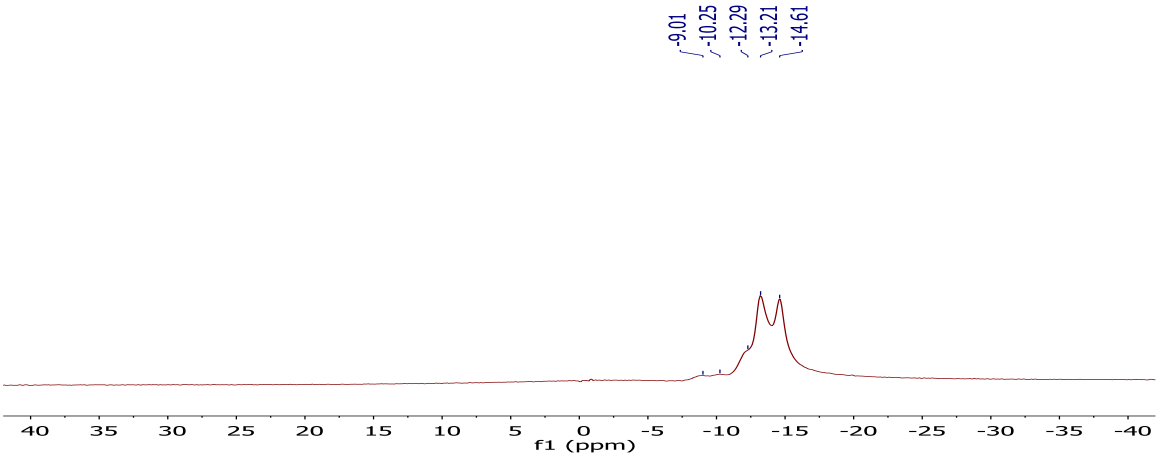

Figure 4-7 ^{11}B-NMR spectrum of **43[Ag^{+}]** in THF-d_8.

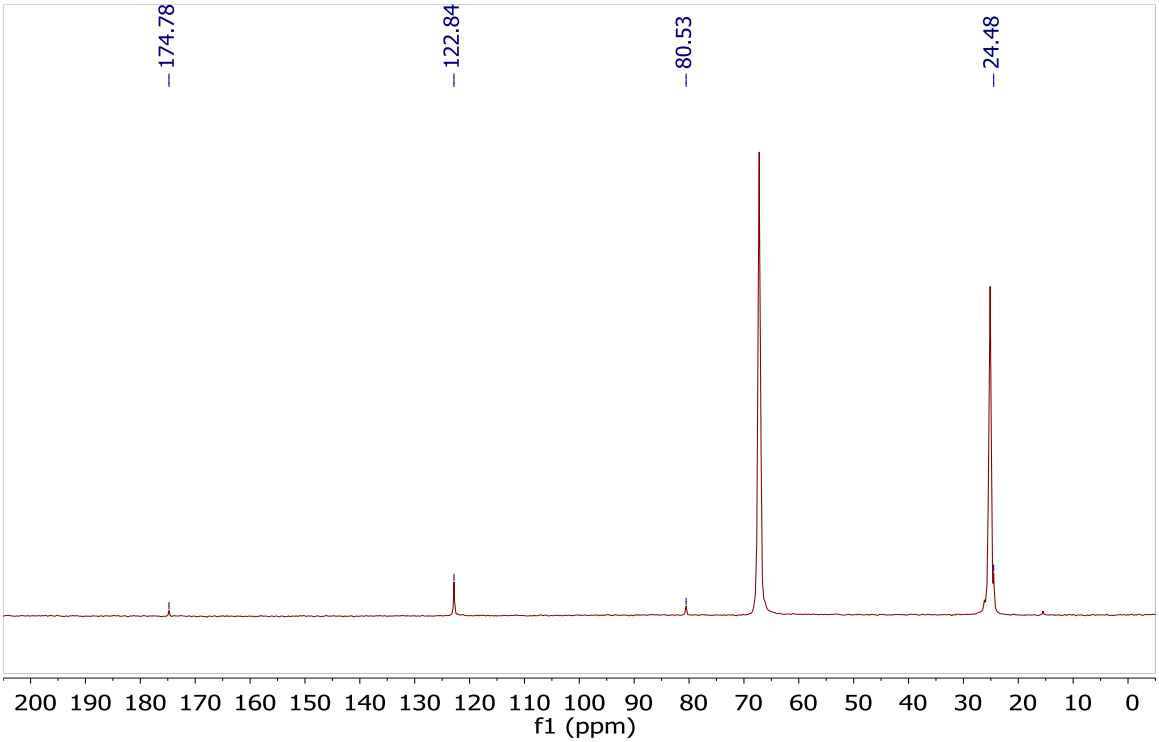

Figure 4-8 $^{13}C[^{1}H]$-NMR spectrum of **43[Ag^{+}]** in THF-d_8.

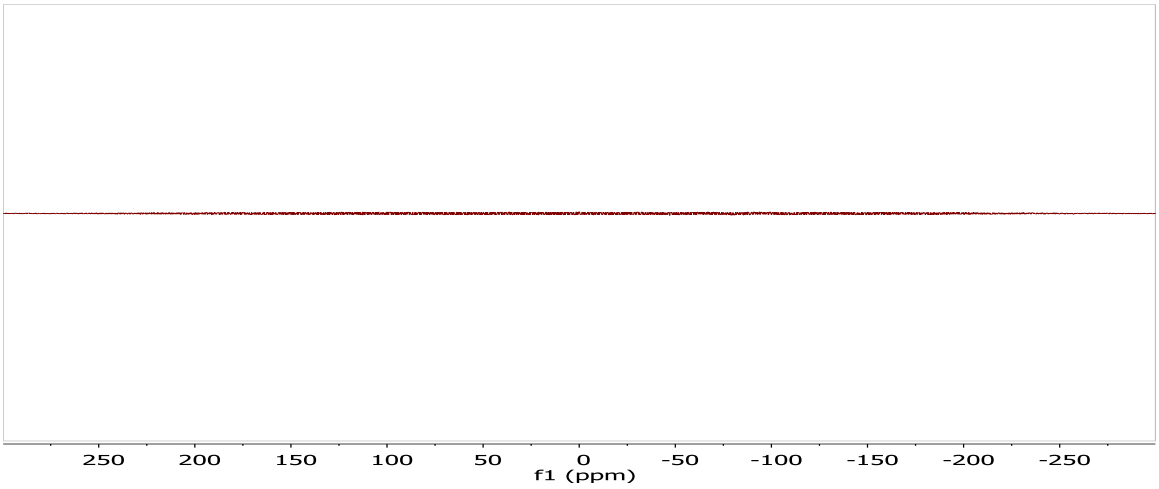

Figure 4-9 ^{19}F-NMR spectrum of **43[Ag^{+}]** in THF-d_8.

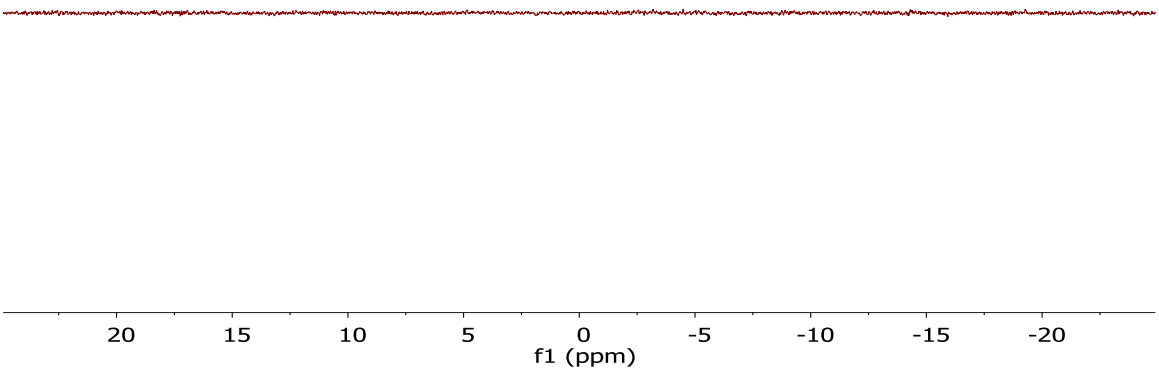

Figure 4-10 ^{7}Li-NMR spectrum of **43[Ag^{+}]** in THF-d_8.

Synthesis of **43[Ru^{+}]**:

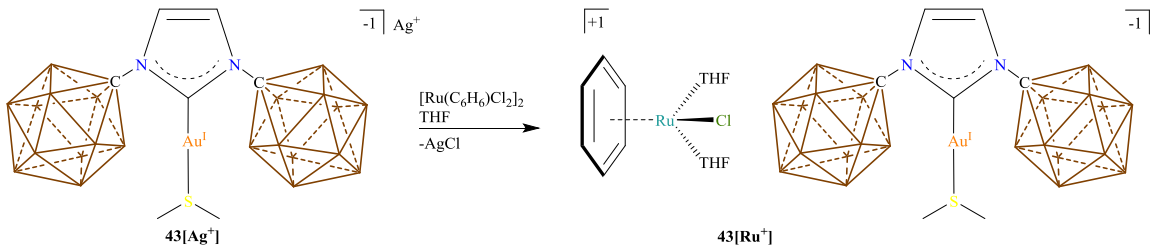

Scheme 4-7 Synthesis of **43[Ru^{+}]**.

A glass scintillation vial was equipped with a stir bar and loaded with **43[Ag^{+}]** (125 mg, 152 µmol) and dissolved in THF (3 mL). A solution of $[Ru(C_6H_6)Cl_2]_2$ (38 mg, 76 µmol) in THF (3 mL) was added dropwise and a precipitate was immediately observed. The reaction was stirred for 30 minutes at room temperature before it was filtered. The filtrate was dried to a dark residue. The residue was extracted with

methylene chloride and all volatiles were removed under vacuum, furnishing the title compound. ^{1}H NMR (600 MHz, THF-d_8, 25°C): ∂ = 7.42 (s, 2H), 5.96 (s, 6H), 2.81 (s, 6H), 2.9 – 0.6 (bs, 22H) ppm. ^{1}H[^{11}B] NMR (600 MHz, THF-d_8, 25°C): ∂ = 7.42 (s), 5.96 (s), 3.36 (bs, H-B), 2.81 (s), 2.54 (bs, H-B), 1.61 (bs, H-B) ppm. ^{11}B[^{1}H] NMR (96 MHz, THF-d_8, 25°C): ∂ = -7.9, -13.2 ppm. ^{11}B NMR (96 MHz, THF-d_8, 25°C): ∂ = -7.9 ($^{1}J(H,B)$ = 121.9 Hz), -13.2 ($^{1}J(H,B)$ = 138.7 Hz) ppm.

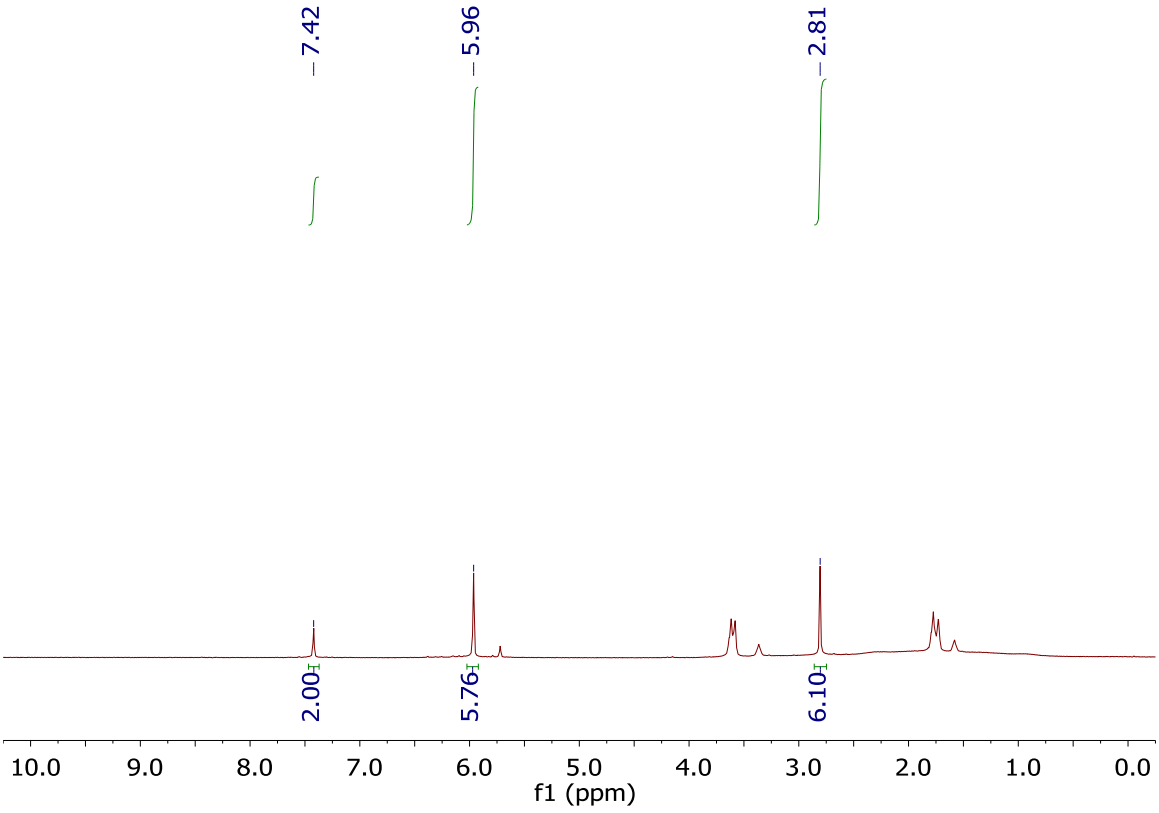

Figure 4-11 ^{1}H-NMR spectrum of **43[Ag^{+}]** in THF-d_8.

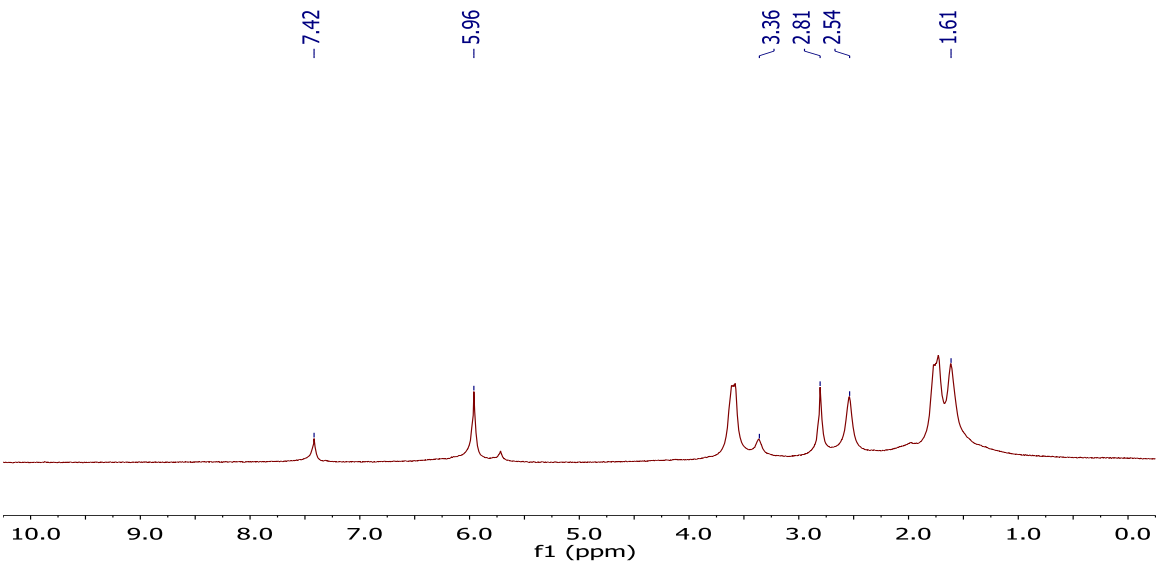

Figure 4-12 $^{1}H[^{11}B]$-NMR spectrum of **43[Ag^{+}]** in THF-d_8. Note: the peaks at 3.36, 2.54 and 1.61 correspond to the H-B resonances.

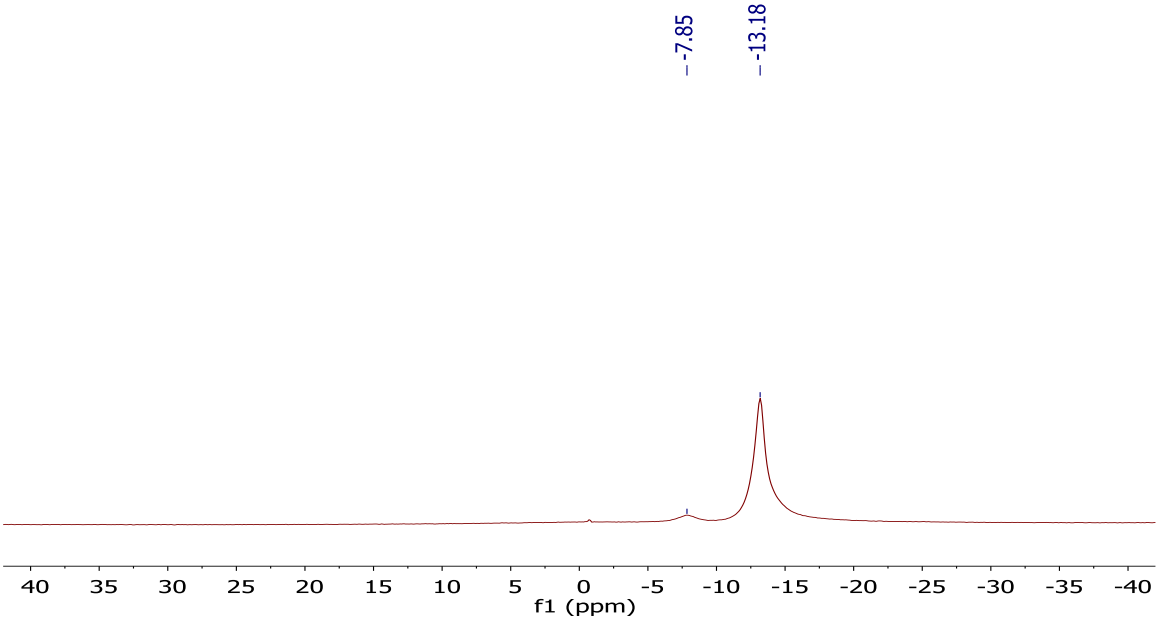

Figure 4-13 $^{11}B[^{1}H]$-NMR spectrum of **43[Ag^{+}]** in THF-d_8.

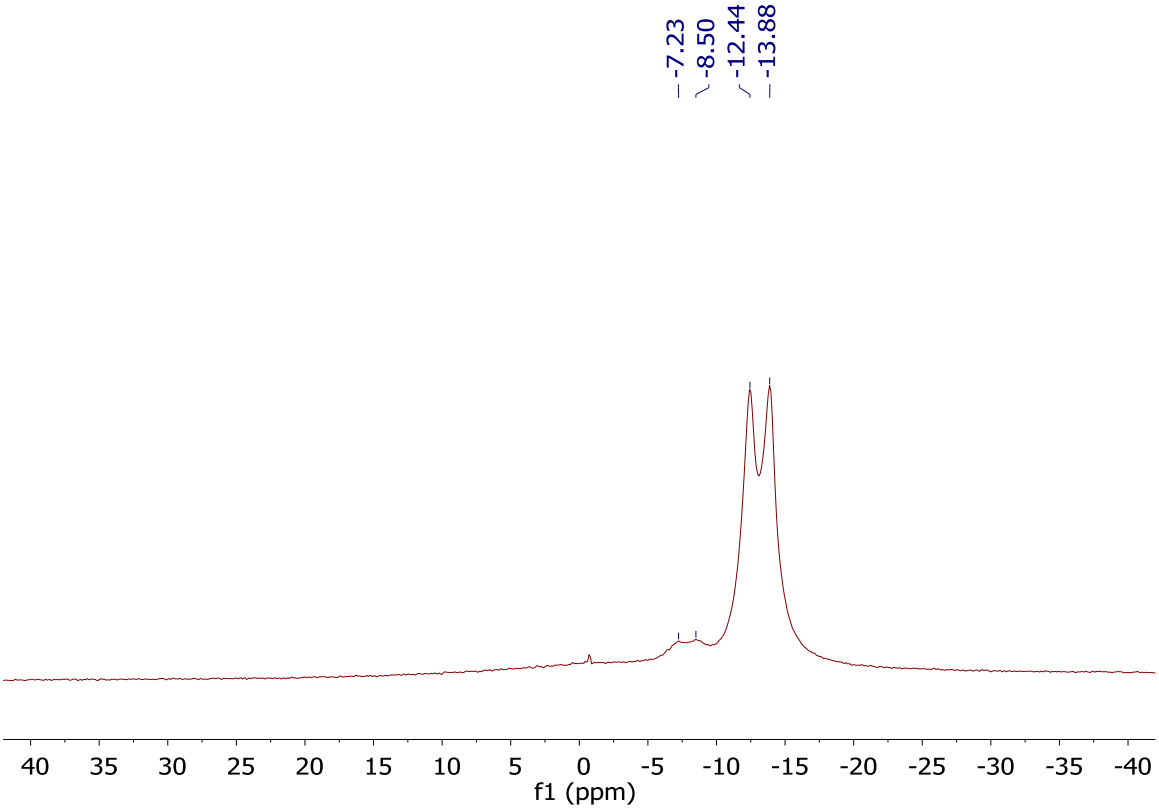

Figure 4-14 ^{11}B-NMR spectrum of **43[Ag$^+$]** in THF-d_8.

Synthesis of **43[Rh$^+$]:**

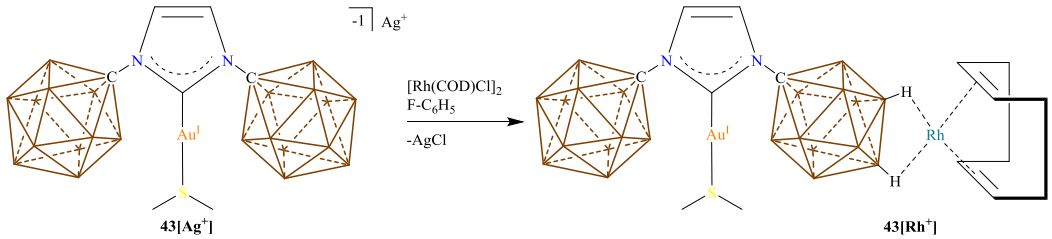

Scheme 4-8 Synthesis of **43[Rh$^+$]**.

A glass scintillation vial wrapped in aluminum foil was equipped with a stir bar and loaded with **43[Ag$^+$]** (259 mg, 328 µmol) in dimethoxyethane (0.5 mL). A solution of $[Rh(COD)Cl]_2$ (81 mg, 164 µmol,

COD = 1,5-cyclooctadiene) in F-C_6H_5 (10 mL) was added dropwise to the stirring DME mixture. The vial containing the $[Rh(COD)Cl]_2$ was washed with F-C_6H_5 (5 mL) and the solution transferred as well. The reaction was stirred for 1 hour at room temperature before it was filtered. The remaining solid on the filter was extracted with dimethoxyethane (1 mL) and the combined filtrates were preparatively crystalized by adding hexane until the solution turned cloudy at which point the turbid mixture was cooled to -30°C. The resulting crystals were washed with cold F-C_6H_5 and placed under vacuum furnishing the title compound (192 mg, 64% yield). ^{1}H NMR (500 MHz, methylene chloride-d_2, 25°C): ∂ = 7.34 (s, 2H), 4.25 (bs, 4H), 2.78 (s, 6H), 2.49 (bs, 4H), 4.25 (bs, 4H) 3.2 – 0.6 (bs, 22H) ppm. ^{11}B[^{1}H] NMR (128 MHz, methylene chloride-d_2): -8.8, -13.9 ppm. ^{11}B NMR (128 Mhz, methylene chloride-d_2, 25°C): ∂ = 8.8 ($^1J(H,H)$ = 131.4 Hz), -13.9 ($^1J(H,H)$ = 133.2 Hz).

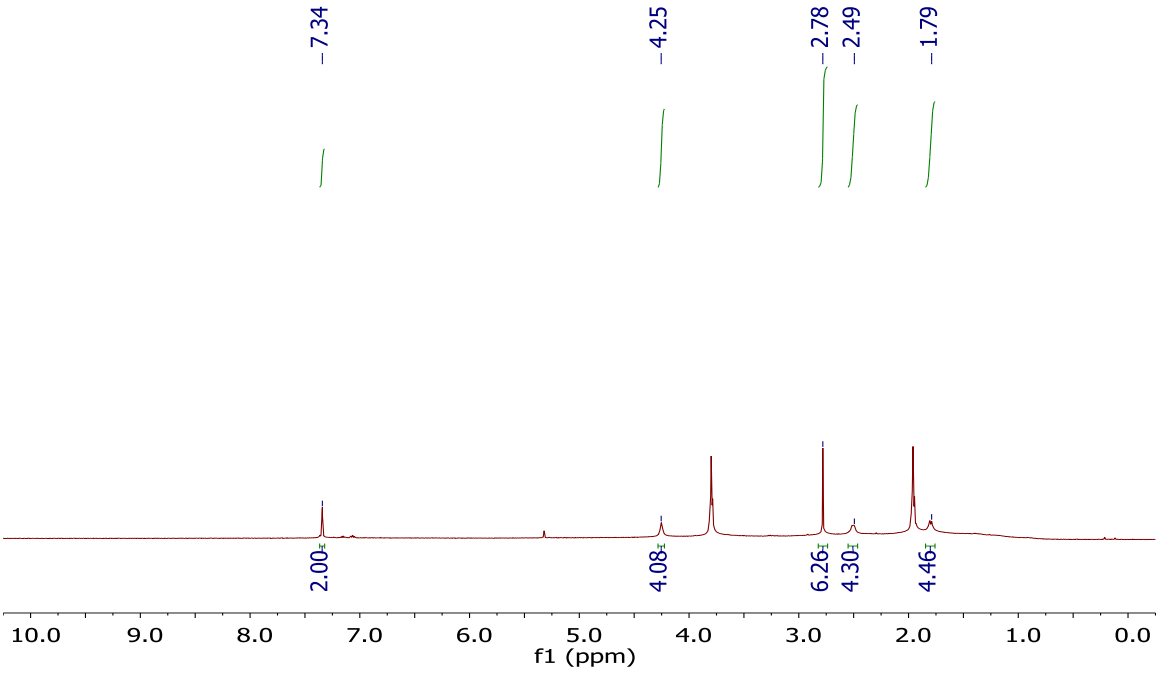

Figure 4-15 ^{1}H-NMR spectrum of **43[Rh$^+$]** in methylene chloride-d_2.

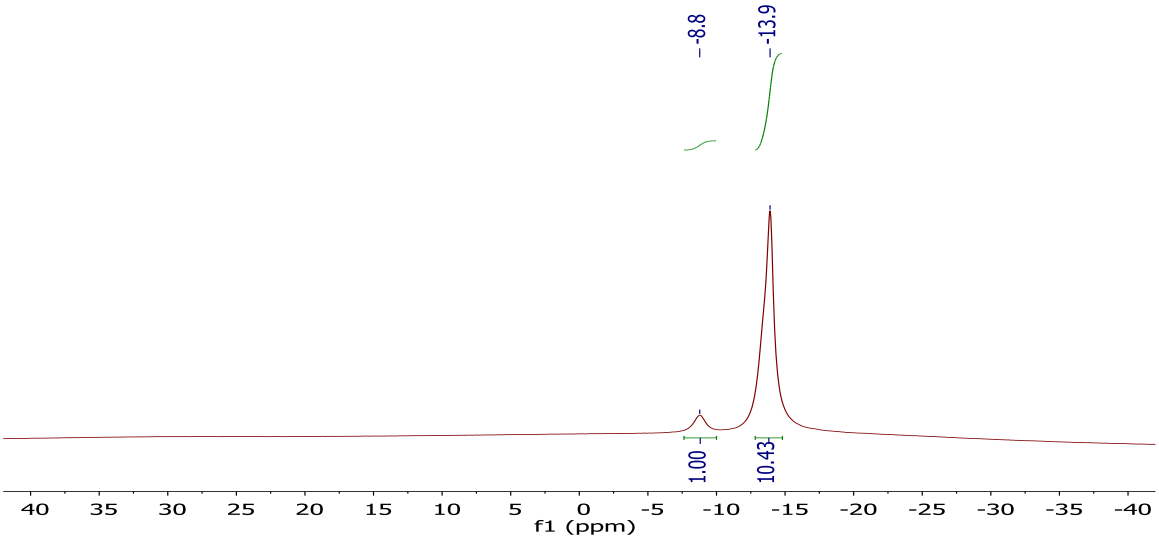

Figure 4-16 $^{11}B[^{1}H]$-NMR spectrum of **43[Rh^{+}]** in methylene chloride-d_2.

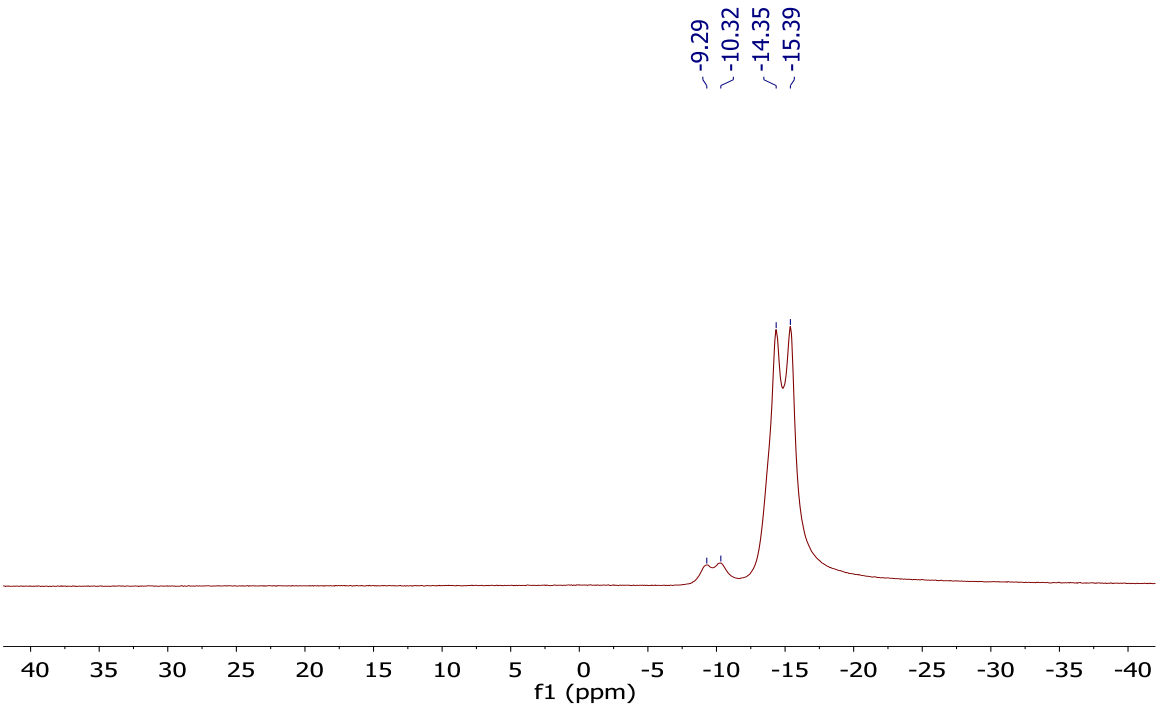

Figure 4-17 ^{11}B-NMR spectrum of **43[Rh^{+}]** in methylene chloride-d_2.

Hydroamination Conditions using 1 mol% **43[Rh$^+$]**:

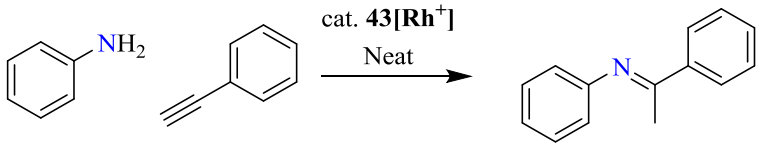

Scheme 4-9 Catalytic hydroamination using **43[Rh$^+$]**.

A preweighed scintillation vial was equipped with a stir bar and loaded with **43[Rh$^+$]** (1 mol%, 10 mg, 11 µmol), aniline (100 µL, 1.1 mmol) and phenylacetylene (121 µL, 1.1 mmol). The sticky reaction mixture was stirred for 10 minutes and then the crude reaction mixture was analyzed by ^{1}H NMR spectroscopy.

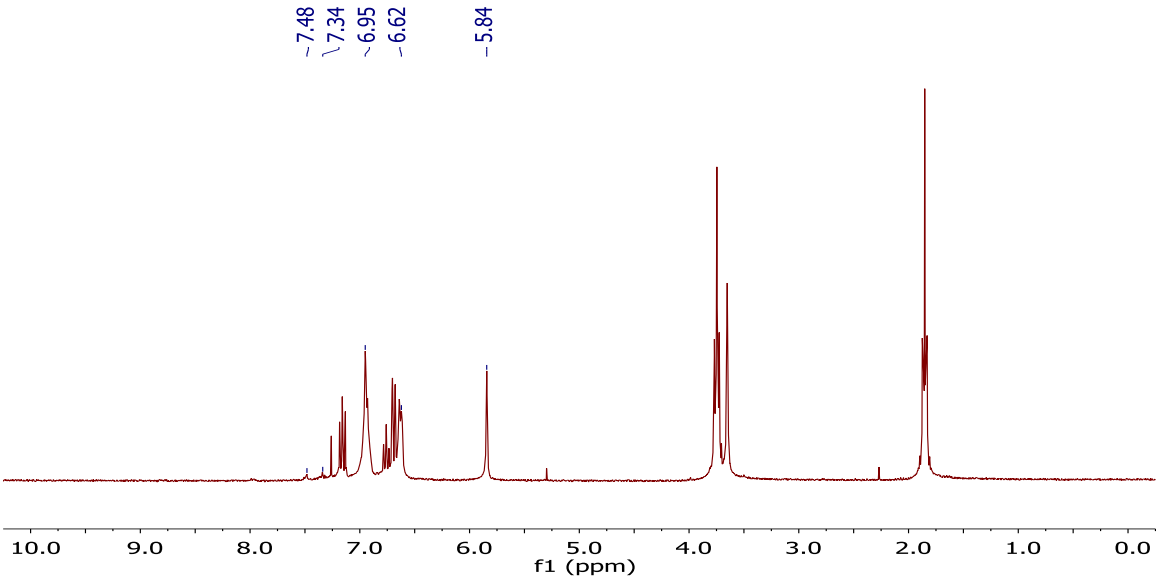

Figure 4-18 ^{1}H-NMR spectrum of the reaction showing almot complete consumption of phenylacetylene after 10 minutes. *Note: the peaks for residual phenylacetylene are at 7.34 and 7.48 ppm. The peaks of the polymer show up at 6.96, 6.62 and 5.84 ppm.*

Hydroamination Conditions using 1 mol% $[Rh(COD)Cl]_2$:

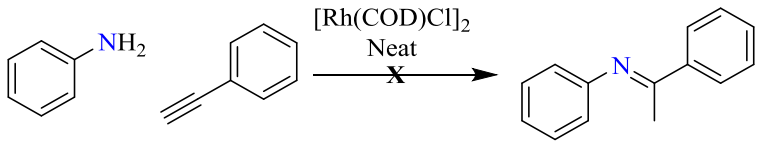

Scheme 4-10 Hydroamination using $[Rh(COD)Cl]_2$. COD = 1,5-cyclooctadiene.

A preweighed scintillation vial was equipped with a stir bar and loaded with $[Rh(COD)Cl]_2$ (1 mol%, 9.7 mg, 20 µmol), aniline (179 µL, 2.0 mmol) and phenylacetylene (216 µL, 2.0 mmol). The neat reaction mixture was stirred and over time aliquots of the reaction mixture were removed and analyzed by NMR.

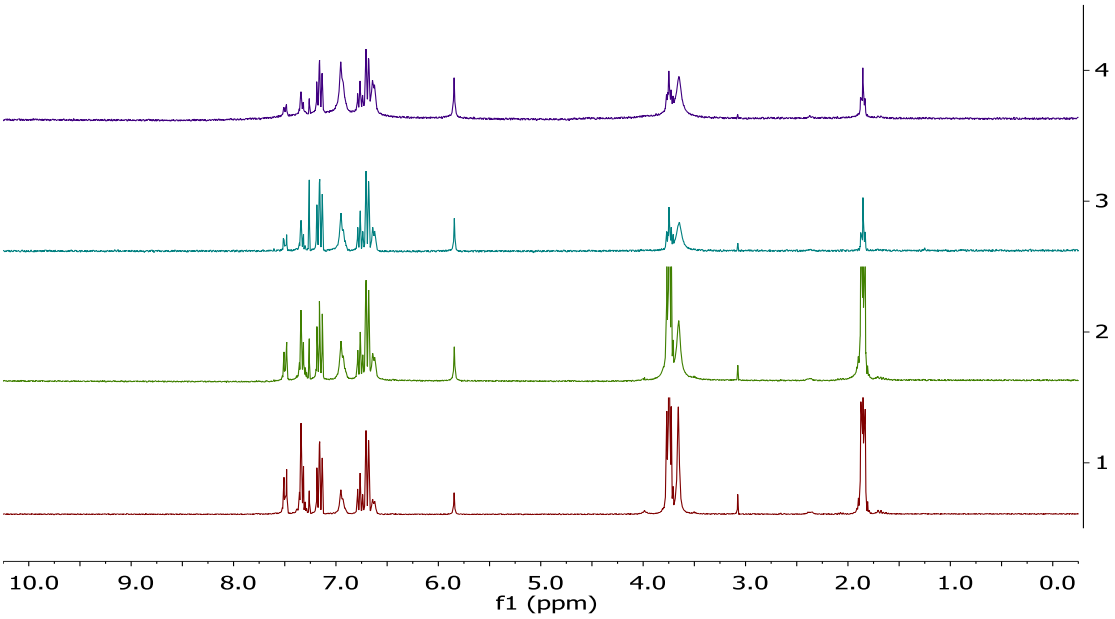

Figure 4-19 Time lapse of ^{1}H-NMR spectrums for the hydroamination using **43[Rh$^+$]** catalyst. Red trace = 6 minutes, green trace = 51 minutes, teal trace = 3 hours and 54 minutes, purple trace = 7 hours and 2 minutes.

Phenylacetylene Polymerization using 1 mol% **43[Rh$^+$]**:

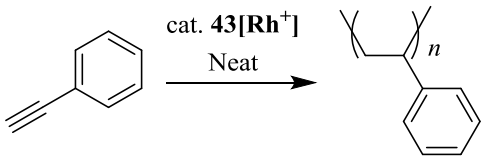

Scheme 4-11 Polymerization of phenylacetylene with **43[Rh$^+$]**.

A preweighed scintillation vial was equipped with a stir bar and loaded with $[Rh(COD)Cl]_2$ (1 mol%, 16 mg, 17 µmol) and phenylacetylene (186 µL, 1.7 mmol). The neat reaction mixture was stirred and over time aliquots of the reaction mixture were removed and analyzed by NMR.

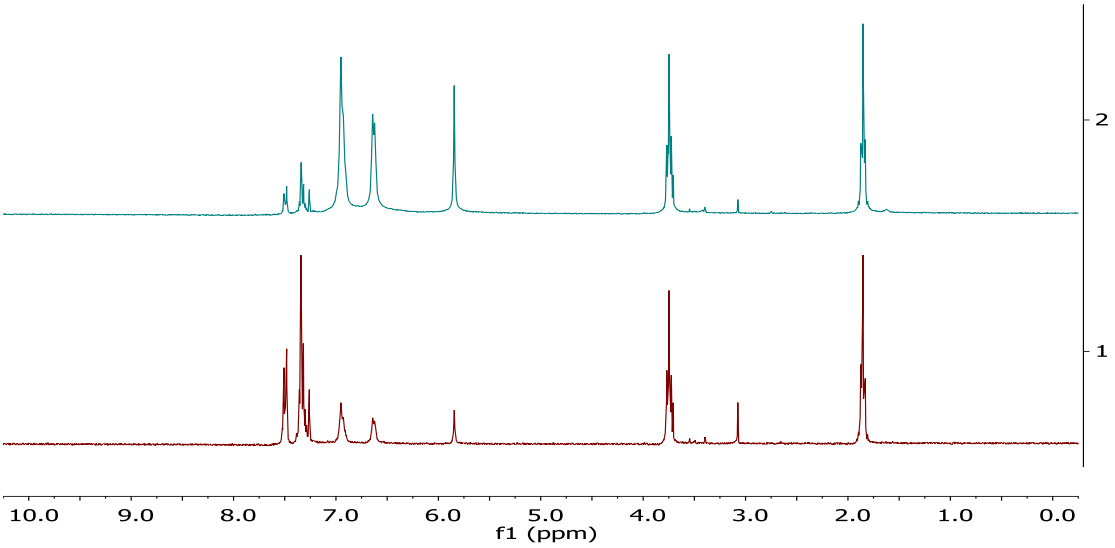

Figure 4-20 Time lapse of ^{1}H-NMR spectrums for the polymerization of phenylacetylene using **43[Rh$^+$]** catalyst. Red trace = 4 minutes, teal trace = 4 hours and 11 minutes.

4.4 References

1. L. Dai, L. Song, Y. Huang, L. Zhang, X. Lu, J. Zhang ,T. Chen, *Langmuir*, 2017, **33**, 5378-5384.

2. Y. Guan, N. Zhao, B. Tang, Q. Jia, X. Xu, H. Liu ,R. I. Boughton, *Chemical Communications*, 2013, **49**, 11524-11526.

3. A. G. Garcia, P. P. Lopes, J. F. Gomes, C. Pires, E. B. Ferreira, R. G. M. Lucena, L. H. S. Gasparotto ,G. Tremiliosi-Filho, *New Journal of Chemistry*, 2014, **38**, 2865-2873.

4. G. van Koten, J. T. B. H. Jastrzebski ,J. G. Noltes, *Journal of the Chemical Society, Chemical Communications*, 1977, 203-204.

5. G. Van Koten, J. T. B. H. Jastrzebski ,J. G. Noltes, *Inorganic Chemistry*, 1977, **16**, 1782-1787.

6. R. Usón, A. Laguna, M. Laguna, B. R. Manzano, P. G. Jones ,G. M. Sheldrick, *Journal of the Chemical Society, Dalton Transactions*, 1984, 285-292.

7. R. Usón, A. Laguna, M. Laguna, P. G. Jones ,G. M. Sheldrick, *Journal of the Chemical Society, Chemical Communications*, 1981, 1097-1098.

8. R. Usón, A. Laguna, P. Brun, M. Laguna ,M. Abad, *Journal of Organometallic Chemistry*, 1981, **218**, 265-273.

9. V. Lavallo, G. D. Frey, S. Kousar, B. Donnadieu ,G. Bertrand, *Proceedings of the National Academy of Sciences*, 2007, **104**, 13569.

10. E. Herrero-Gómez, C. Nieto-Oberhuber, S. López, J. Benet-Buchholz ,A. M. Echavarren, *Angewandte Chemie International Edition*, 2006, **45**, 5455-5459.

11. J. W. Taylor, A. McSkimming, M.-E. Moret ,W. H. Harman, *Angewandte Chemie International Edition*, 2017, **56**, 10413-10417.

12. R. D. Dewhurst, A. F. Hill ,M. K. Smith, *Organometallics*, 2005, **24**, 5576-5580.

13. E. C. Coles, J. D. Jessop, J. P. Camilleri, L. A. Williams, M. J. Plant, M. M. O'Sullivan ,P. A. Lewis, *Rheumatology*, 1998, **37**, 992-1002.

14. R. F. Baggio ,S. Baggio, *Journal of Inorganic and Nuclear Chemistry*, 1973, **35**, 3191-3200.

15. S. A. Westcott, B. D. Sherry, F. D. Toste ,J.-M. Campagne, *Encyclopedia of Reagents for Organic Synthesis*, 2011, **0**, 1-4.

16. E. V. Makotchenko, I. A. Baidina ,I. V. Korol'kov, *Journal of Structural Chemistry*, 2014, **55**, 887-894.

17. R. A. Penneman ,E. Staritzky, *Journal of Inorganic and Nuclear Chemistry*, 1958, **7**, 45-50.

18. A. Rosenzweig ,D. T. Cromer, *Acta Crystallographica*, 1959, **12**, 709-712.

19. A. S. Weller, M. F. Mahon ,J. W. Steed, *Journal of Organometallic Chemistry*, 2000, **614-615**, 113-119.

20. Y. Shi ,S. A. Blum, *Organometallics*, 2011, **30**, 1776-1779.

21. M. N. Peñas-Defrutos, C. Bartolomé, M. García-Melchor ,P. Espinet, *Angewandte Chemie International Edition*, 2019, **58**, 3501-3505.

22. M. M. Hansmann, A. S. K. Hashmi ,M. Lautens, *Organic Letters*, 2013, **15**, 3226-3229.

23. M. Böhmer, F. Kampert, T. T. Y. Tan, G. Guisado-Barrios, E. Peris ,F. E. Hahn, *Organometallics*, 2018, **37**, 4092-4099.

24. Z. Zhu, K. Chen, Q. Xu ,M. Shi, *Advanced Synthesis & Catalysis*, 2015, **357**, 3081-3090.

25. L.-P. Liu ,G. B. Hammond, *Chemical Society Reviews*, 2012, **41**, 3129-3139.

26. M. A. Casado, A. Fazal ,L. A. Oro, *Arabian Journal for Science and Engineering*, 2013, **38**, 1631-1646.

27. I. Saeed, M. Shiotsuki ,T. Masuda, *Macromolecules*, 2006, **39**, 8567-8573.

28. R. J. Kern, *Journal of Polymer Science Part A-1: Polymer Chemistry*, 1969, **7**, 621-631.

29. T. Jelínek, J. Plešek, S. Hermanek ,S. Bohumil, *Collection of Czechoslovak Chemical Communications*, 1986, **51**, 819-829.

30. A. El-Hellani ,V. Lavallo, *Angewandte Chemie International Edition*, 2014, **53**, 4489-4493.

Chapter 5: On the Reactivity of the Carba-*closo*-dodecaborate Anion with the Trityl Cation

5.1 Introduction

Carboranes[1-10] are a class of boron cluster compounds that contain at least one carbon atom in the skeleton. The most thermodynamically and chemically robust carborane clusters are the 12-vertex icosahedral derivatives. Such clusters are neutral if they contain two carbon atoms[7] and mononegatively charged if they contain one carbon atom.[4] The latter family of charged clusters contain a CB_{11} core and are of particular interest as weakly coordinating anions for highly electrophilic cations,[8, 11-22] substituents in ligand design[23-40] and components of ionic conducting materials.[41-43] The parent cluster, specifically the carba-*closo*-dodecaborate anion $[HCB_{11}H_{11}]^-$ **3**, is the basic building block for functionalized derivatives (Scheme 5-1). The B-H vertices of this molecule can undergo electrophilic substitution reactions,[4] most commonly with elemental halogens or alkyl electrophiles, that lead to replacement of hydrides with X or R groups, respectively. The substitution occurs selectively, first at the B-H antipodal to carbon because this position is most electron rich, then at the central and subsequently upper pentagonal belt.

In 1994 elegant and pioneering work by Reed and co-workers[44] showed the synthesis of trityl cations with various polyhalogenated derivatives of **3**. These trityl salts are the basis for the synthesis of Reed's silylium cations and subsequent carborane superacids.[8] Interestingly, they found an incompatibility between the trityl cation and unsubstituted **3**. They reported that when the silver salt of **3**, **3[Ag$^+$]**, was treated with trityl bromide salt metathesis did occur, but the reaction did not lead to the desired trityl carobrane salt **3[Tr$^+$]** (Scheme 5-1). Instead a new unidentified product was observed that retained the local C_{5V} symmetry of the cluster but contained a substituted B-H vertex as indicated by ^{11}B NMR spectroscopy. Based on an early report by Hawthorne[45] on the electrochemical oxidation of the related 10-vertex anion $[HCB_9H_9]^-$ (**4**) which results in the formation of a carborane B-B dimer, they proposed that perhaps the trityl cation abstracted hydrides from the cluster **3** and a similar dimer **50** formed (Figure 5-1). Additionally, under certain reaction conditions they observed the formation of $HC(Ph)_3$, which is supportive of this

reaction pathway. Out of genuine curiosity we decided to reinvestigate this reaction and unambiguously determine its outcome.

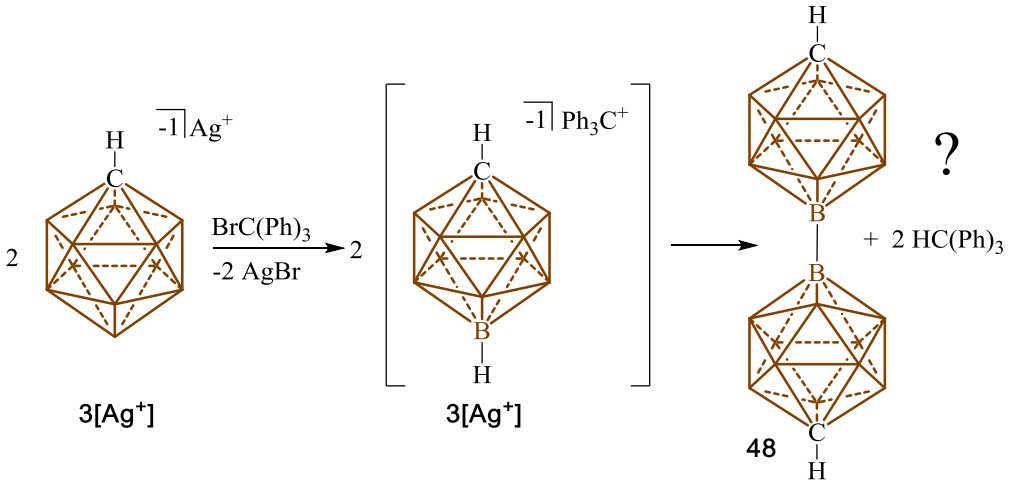

Scheme 5-1 Reed and co-workers previously discovered an incompatibility between the trityl cation and the carborane anion **1**. Hydride abstraction form the carborane followed by dimerization to produce **3** was the proposed decomposition pathway. Unlabeled vertices: B-H

5.2 A Reinvestigation of the Reed's Reaction between **3** and Ph_3C^+

In lieu of preparing **3[Ag$^+$]** which would require an extra synthetic step,[4] we chose to examine the salt metathesis reaction of trityl bromide with the lithium salt **3[Li$^+$]**. As solvent we chose F-C_6H_5, since both reactants are very soluble in this medium and LiBr is not. Thus we performed the reaction, and as expected saw a rapid precipitation of LiBr (Scheme 5-2). The reaction was filtered and subsequently concentrated to dryness under high vacuum. The material was then dissolved in H_2O and for convenience NMe_3•HCl was added to precipitate any carborane containing salts. After drying the precipitate it was analyzed by $^{11}B[^1H]$ NMR spectroscopy. Similar to what Reed reported[44] we observed three resonances (7.0, -8.1, -12.1 ppm) in a 1:5:5 ratio, respectively. Substitution of the antipodal B vertex at 7.0 ppm was corroborated by ^{11}B NMR spectroscopy, which shows this signal as a singlet. We next analyzed the residue by ^1H NMR spectroscopy. The proton NMR spectrum shows a large singlet for the $[HNMe_3]^+$ cation's

methyl groups at 3.10 ppm, a singlet at 5.46 that integrates for 1H relative to $[HNMe_3]^+$, two 2H doublets at 6.82 and 7.33 ppm that are coupled (7.9 Hz), as well as a 10 H multiplet between 7.12 - 7.29 ppm. Importantly (vide infra), a trace (< 5%) of a minor compound with distinct ^1H NMR chemical shifts was observed. An HSQC (^1H-^{13}C correlation experiment) shows that the 1H resonance at 5.46 ppm correlates with a 13C nucleus at 57.5 ppm indicating the formation of a new sp^3 hybridized carbon center. High resolution mass spectrometry (negative ion mode) showed that the new compound has a mass that corresponds to **3** plus $C(Ph)_3$, less 1 proton. All of this data is consistent with the formation of the product **51[$HNMe_3^+$]** (Scheme 5-2).

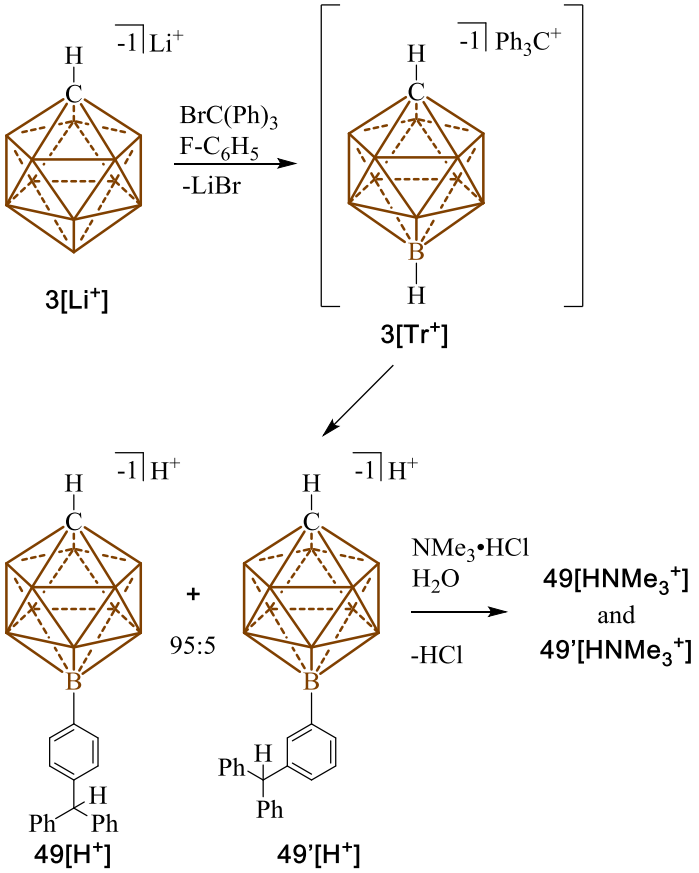

Scheme 5-2 Reaction of **3[Li+]** with BrC(Ph)3 in F-C6H5 solvent leads to electrophilic arylation of the carborane at the B-vertex antipodal to C. The reaction produces a mixture (95:5) of arylated carborane **51** and **51'**. Tr = $(Ph)_3C^+$. Unlabeled vertices = B-H.

Presumably, the reaction proceeds via initial formation of the trityl cation **3[Tr$^+$]** as an intermediate, where subsequently the carobrane acts as nucleophile that attacks the *para*-position of the trityl cation. It should be noted that its is well known that bulky nucleophiles attack the *para*-position of trityl cations if the central carbon is sterically inaccessible. The net reaction is an electrophilic aromatic arylation of the carborane cage to produce the carborane acid **51[H$^+$]**, which upon cation exchange is isolated as the trimethylammonium salt **51[HNMe$_3^+$]** (Scheme 5-2).

A single crystal X-ray diffraction study confirmed the identity of **51[HNMe$_3^+$]** as the arylated carborane, which is substituted at a phenyl *para*-position (Figure 5-1, left). While we were unable to obtain

very high quality crystals that would provide accurate data for bond length and angle analysis (even utilizing a Cs^+ counterion), the connectivity of **51[HNMe$_3^+$]** is unambiguous.

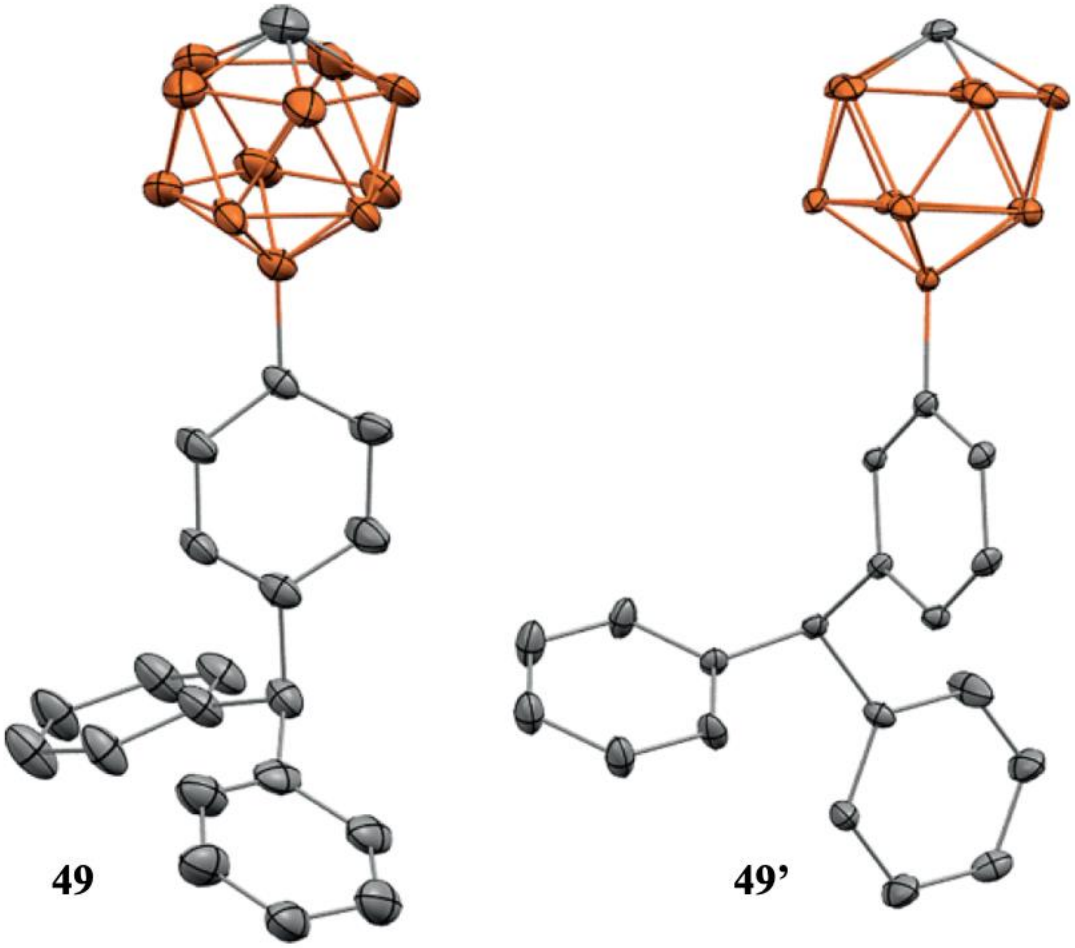

Figure 5-1 Solid state structures of **51[HNMe$_3^+$]**, major crystals (left). Note: [HNMe$_3^+$] cation, hydrogens, and disorder positions omitted for clarity. Portion of the lattice form the minor crystal containing cocrystalized **51** and **51'** (right). Note: [HNMe$_3^+$] cation, hydrogens and disordered positions of **3** omitted for clarity. Color code: B = brown and C = gray.

In the same mass of crystals we found a small amount of morphologically distinct material. Although highly disordered over two positions crystallographic analysis of the material reveals that co-crystallizaiton of two distinct carborane anions, namely the *para*-arylated product **51[HNMe$_3^+$]** and the

meta-arylated product **51'[HNMe$_3^+$]**, in a 7:3 occupancy ratio in the lattice (Figure 5-1, right). We attribute the minor peaks observed in the 1H NMR spectra to that of **51'[HNMR$_3^+$]**.

Given that we chose different reaction conditions than that of reported by Reed an co-workers, we next sought to replicate their exact experimental conditions[44] to unambiguously confirm that the carborane B-B dimer **50** does not form. Thus, **3[Ag$^+$]** was treated with trityl bromide in acetonitrile. As reported an equivalent of AgBr forms, but in our hands we do not observe even trace of HC(Ph)$_3$. After an analogous workup described above we isolated a mixture of **51 [HNMe$_3^+$]** and **51'[HNMe$_3^+$]**, but in this case the ratio of the products was 1:1, *para* to *meta*, respectively.

5.3 Conclusions

This communication unambiguously explains the incompatibility of the carborane anion **3** and the trityl cation. We believe carborane anion **3** is not susceptible to hydride abstraction by C(Ph)$_3^+$, instead it undergoes classical electrophilic substitution chemistry,[4] which shows solvent and countercation dependence on *para* to *meta* selectivity. While we do not fully understand the observed formation of the unusual *meta* product of electrophilic aromatic substitution on a phenyl ring, the result is intriguing and may lead to new approaches to *meta*-directed arene functionalization. Furthermore, all previous B-arylations of **3** have been achieved utilizing transition metal coupling[46-51] or Li$^+$ initiated sigma bond metathesis.[52] Thus, the observed electrophilic arylation of B-H vertex of **3** introduces a new paradigm in the chemical elaboration of this anion.

CCDC 1552016 (for **51[HNMe$_3^+$]**), 1563018 (for **51[Cs$^+$]**) and 1552017 (for **51'[HNMe$_3^+$]**) contain the supplementary crystallographic data for this paper. These data can be obtained free of charge from The Cambridge Crystallographic Data Centre.

5.4 Experimental

General Considerations:

All manipulations were carried out using standard Schlenk or glovebox techniques under a dinitrogen or argon atmosphere unless otherwise stated. Fluorobenzene was distilled from a solvent still

over P_2O_5 and refluxed for several days. Acetonitrile was distilled from a solvent still over CaH_2 and refluxed for several days. Lithium 1-carba-*closo*-undecaborate **3[Li]**$^+$ was prepared from a modified procedure by Uchiyama and co-workers: **1[HNMe$_3$]**$^+$ was deprotonated with LiH in acetonitrile; excess LiH was filtered and **1[Li]**$^+$ was isolated by removing solvent via vacuum.[1] Silver 1-carba-*closo*-undecaborate **1[Ag]**$^+$ was prepared from a procedure by Reed and co-workers.[2] Unless specifically stated, reagents were purchased from commercial vendors and used without further purification. Nuclear magnetic resonance (NMR) spectroscopy was carried out using: Bruker Avance 300 MHz, Bruker Avance 600 MHz, or Varian Inova 300 MHz spectrometers. NMR chemical shifts are reported in parts per million (ppm) with ^{1}H and ^{13}C chemical shifts referenced to the residual non-deutero solvent. High-resolution mass spectrometry (HRMS) was collected on an Agilent Technologies 6210 (TOF LC/MS) multimode-ESI/APCI with direct injection. IR was taken on a PerkinElmer Spectrum One. Crystallographic data for compounds **51[HNMe$_3$]**$^+$, **51[Cs]**$^+$, and **51'[HNMe$_3$]**$^+$ are available free of charge from the Cambridge Crystallographic Data Center under reference numbers 1552016, 1563018, and 1552017, respectively. This structure can be accessed at : http://www.ccdc.cam.ac.uk/Community/Requestastructure/Pages/DataRequest.aspx.

Synthesis of Trityl Carborane, **51[HNMe$_3$]$^+$** and **51'[HNMe$_3$]$^+$:**

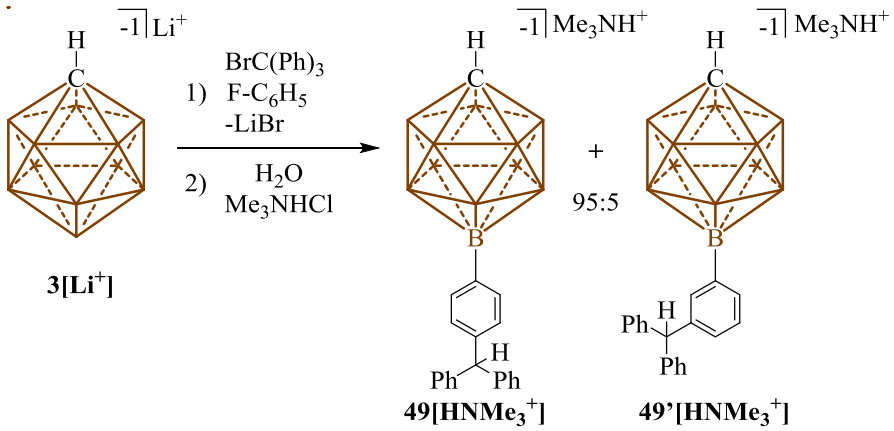

Scheme 5-3 Synthesis of the mixture of **49[HNMe$_3$$^+$]** and **49'[HNMe$_3$$^+$]** using **3[Li$^+$]**.

A glass scintillation vial equipped with a stir bar was loaded with **3[Li]$^+$** (300 mg, 955 μmol) and dry fluorobenzene (2 mL). A separate vial was loaded with a solution of trityl bromide (309 mg, 955 μmol) in fluorobenzene (2 mL). The solution of trityl bromide was transferred to the solution containing **3[Li]$^+$**. The vial that originally contained the trityl bromide was washed with fluorobenzene (2 x 1 mL) and the wash was transferred to the solution of **3[Li]$^+$** as well. The reaction was stirred for 20 minutes at room temperature. After 20 minutes, the reaction was filtered and subsequently concentrated down to a thick oil under vacuum. This oil was then dissolved in 10mL of deionized H_2O. Once fully dissolved, trimethylammonium hydrochloride (100 mg, 1.0 mmol) was added to the aqueous solution producing an off-white precipitate. The precipitate was then washed with deionized H_2O (3 x 4mL) resulting in products, **51[HNMe$_3$]$^+$** and **51'[HNMe$_3$]$^+$** (359 mg, 89% yield). *Note: picks picked are for compound* **51** *only.* ^{1}H NMR (300 MHz, acetone-d$_6$, 25°C): δ = 7.34 (d, ^{3}*J(H,H)* = 7.9 Hz, 2H), 7.29 - 7.12 (m, 10H), 6.82 (d, ^{3}*J(H,H)* = 7.9 Hz, 2H), 5.46 (s, 1H), 3.10 (s, 9H), 2.24 (s, 1H), 2.60 - 0.88 (bm, 10H, B-H) ppm. ^{1}H[^{11}B] NMR (300 MHz, acetone-d$_6$, 25°C): δ = 7.34 – 7.14 (12H), 6.81 (1H), 6.79 (1H), 5.45 (1H), 3.17 (9H), 2.21 (B-H), 1.79 (B-H), 1.76 (B-H) ppm, 1.72 (B-H) ppm. ^{13}C[^{1}H] NMR (75 MHz, acetone-d$_6$, 25°C): δ = 145.7, 140.7, 133.6, 130.1, 128.8, 127.9, 126.7, 57.5, 47.0, 46.0 ppm, *(broad $C_{aromatic}$-B resonance not detected).* ^{11}B[^{1}H] NMR (96 MHz, acetone-d$_6$, 25°C): δ = 7.0, -8.1, -12.1 ppm. ^{11}B NMR (96 MHz,

acetone-d_6, 25°C): δ = 7.0, -8.1 ($^1J(H,B)$ = 136.3 Hz), -12.1 ($^1J(H,B)$ = 149.5 Hz) ppm. IR (Solid, ATR, 25°C): B-H stretch = 2549 and 2512 cm^{-1}. HRMS (negative mode ESI/APCI) $[M]^-$ m/z calc'd = 385.3131 : Found = 385.3154

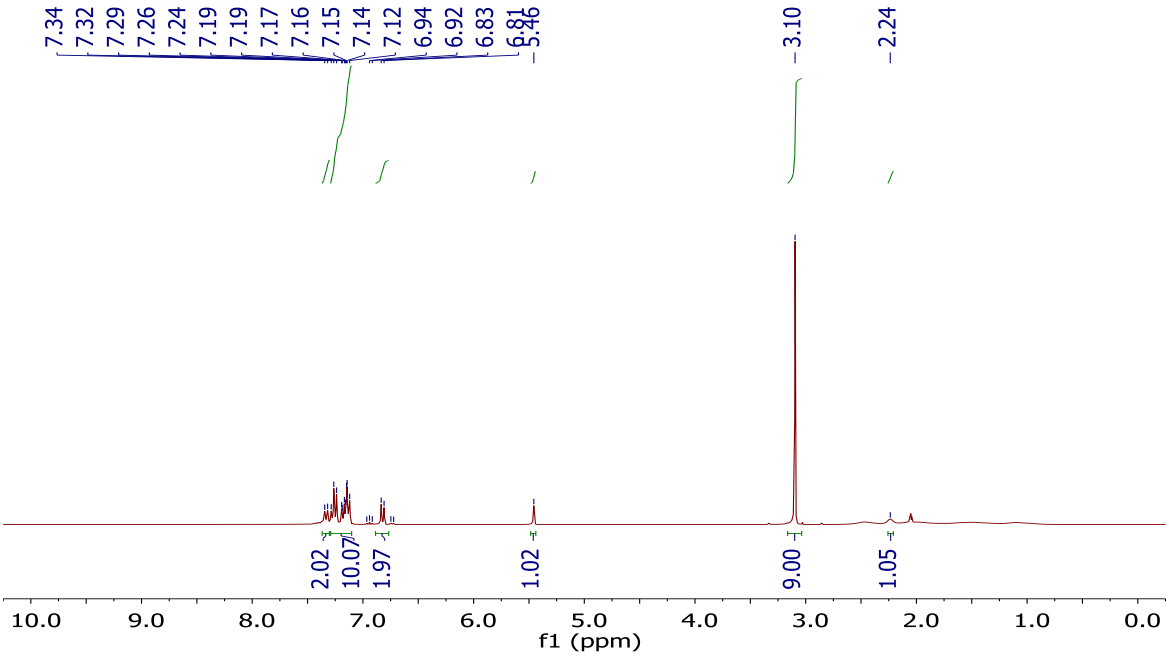

Figure 5-2 ^{1}H-NMR spectrum of **51[HNMe$_3^+$]** in acetone-d_6. *Note:* ***51'[HNMe$_3^+$]*** *is seen at 6.94 and 6.73 ppm.*

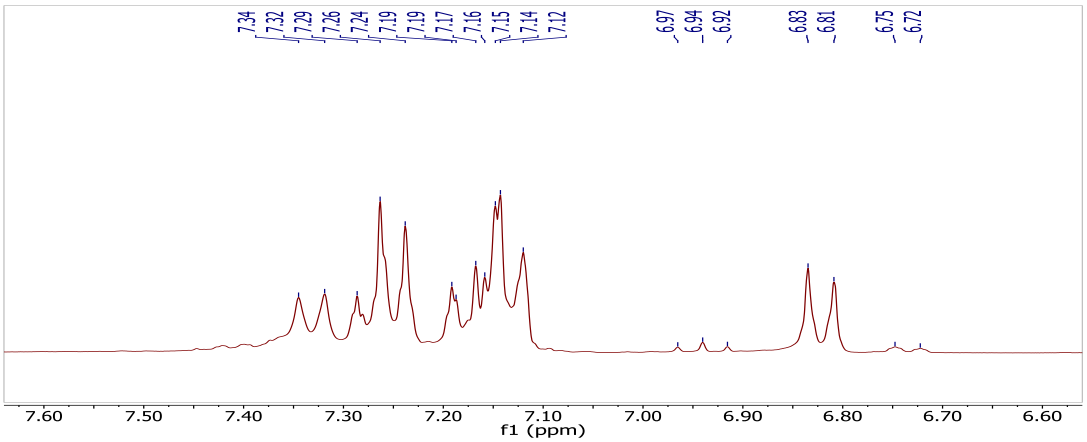

Figure 5-3 An expansion of the aromatic region of ^{1}H-NMR spectrum of **51[HNMe$_3^+$]** in acetone-d_6. *Note:* ***51'[HNMe$_3^+$]*** *can be seen at 6.94 and 6.74 ppm.*

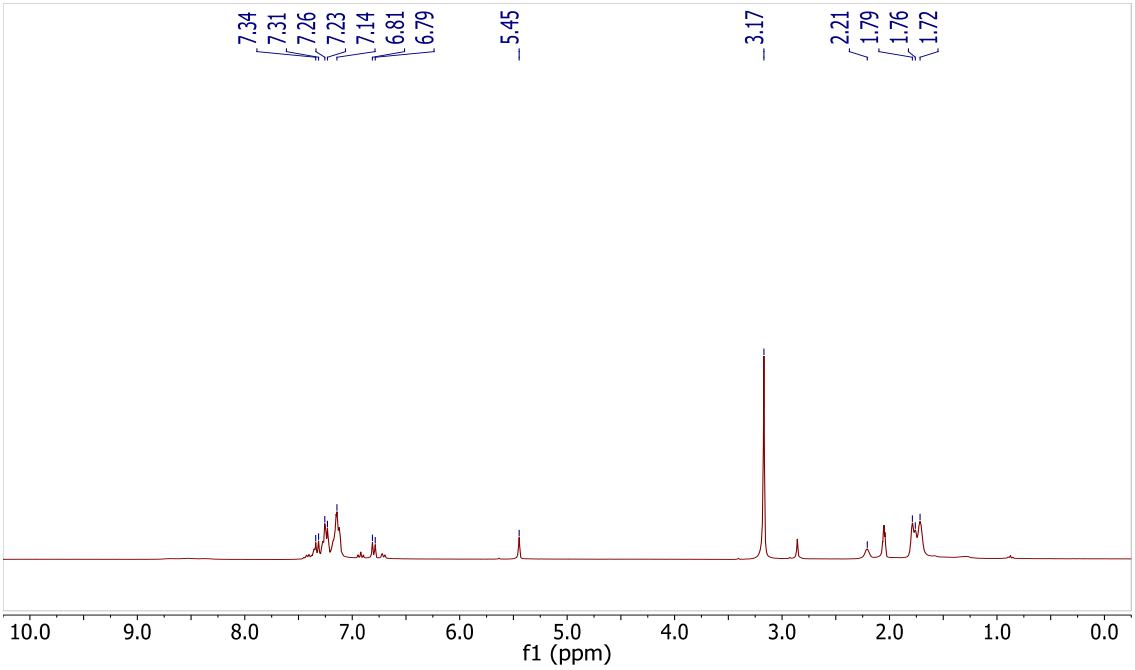

Figure 5-4 $^{1}H[^{11}B]$-NMR spectrum of the mixture containing **51[HNMe$_3^+$]** in acetone-d_6.

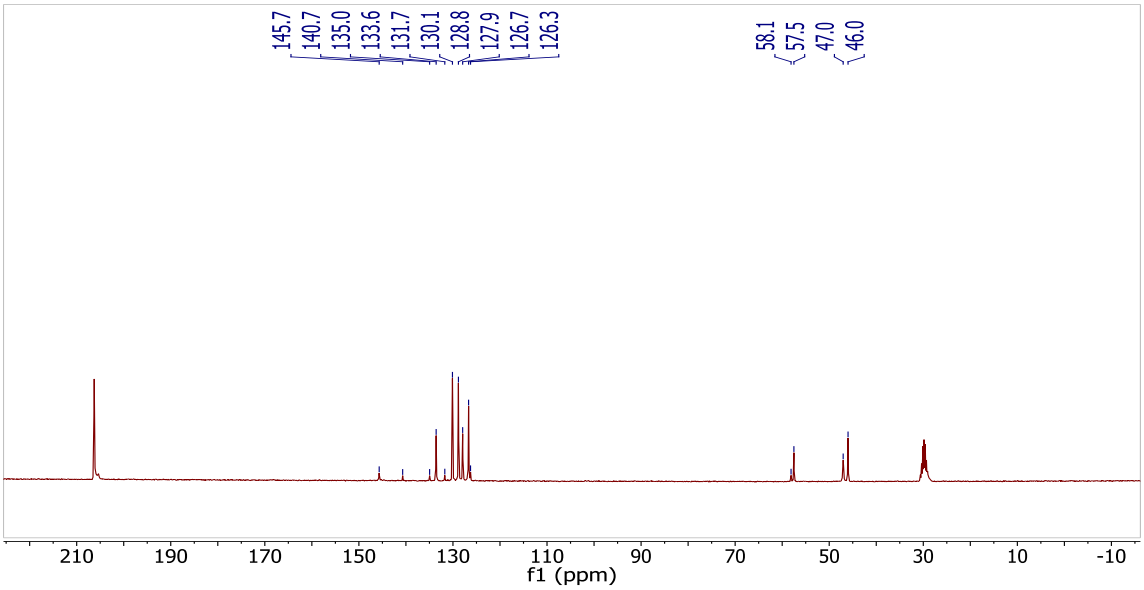

Figure 5-5 $^{13}C[^{1}H]$-NMR spectrum of **51[HNMe$_3^+$]** in acetone-d_6. Note: **51'[HNMe$_3^+$]** is seen at 135.0, 131.7, 126.3, and 58.1 ppm.

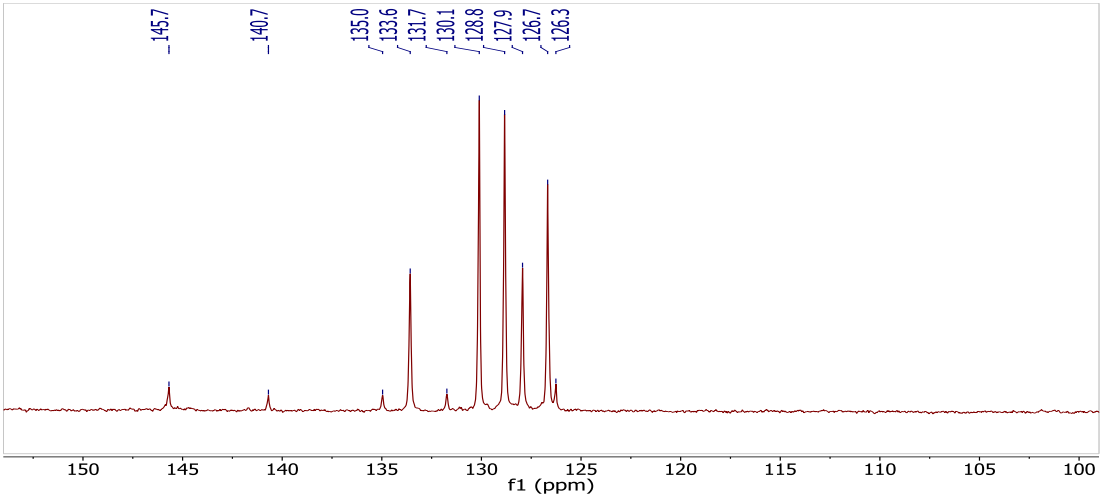

Figure 5-6 An expansion of the aromatic region of the ^{13}C[1H]-NMR spectrum of **51[HNMe$_3^+$]** in acetone-d_6. *Note:* ***51'[HNMe$_3^+$]*** *is seen at 135.0, 131.7, 126.3, and 58.1 ppm.*

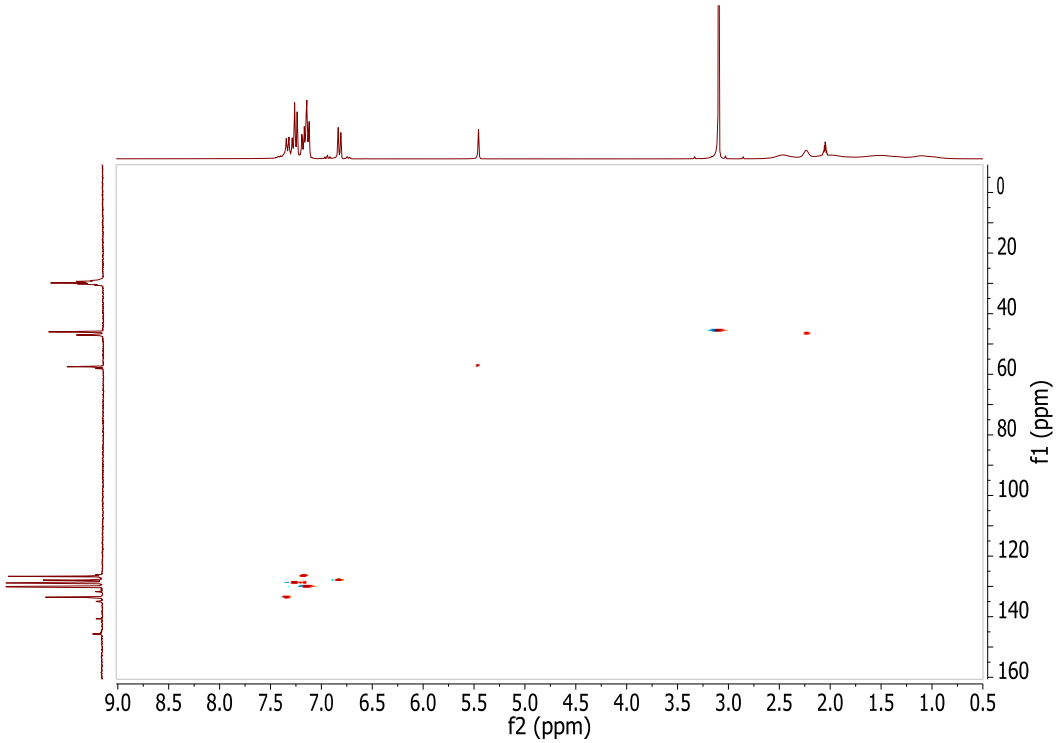

Figure 5-7 HSQC NMR spectrum of **51[HNMe$_3^+$]** in acetone-d_6.

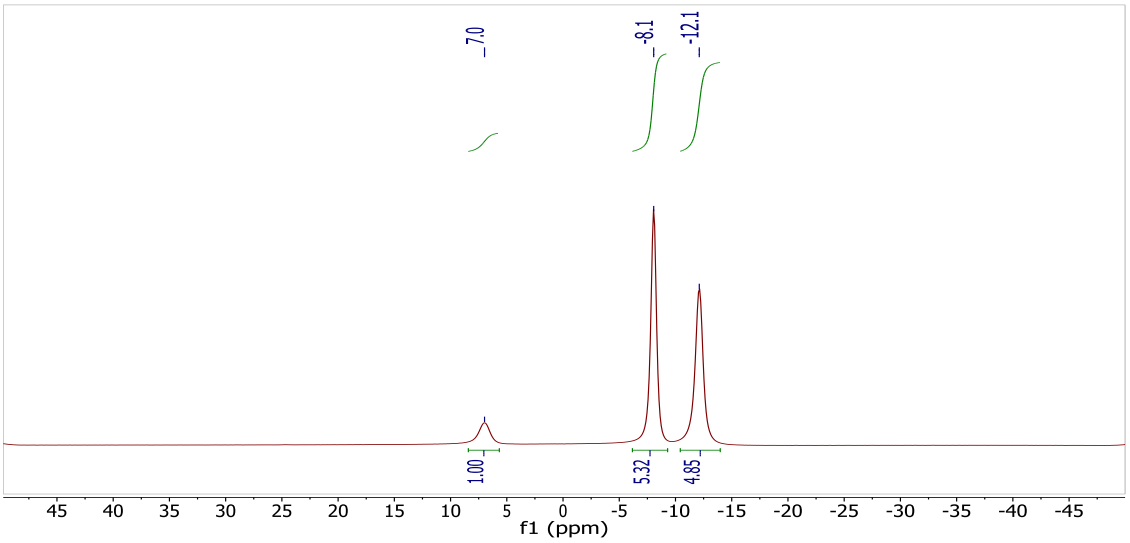

Figure 5-8 $^{11}B[^{1}H]$-NMR spectrum of compound **51[$HNMe_3^+$]** in acetone-d_6.

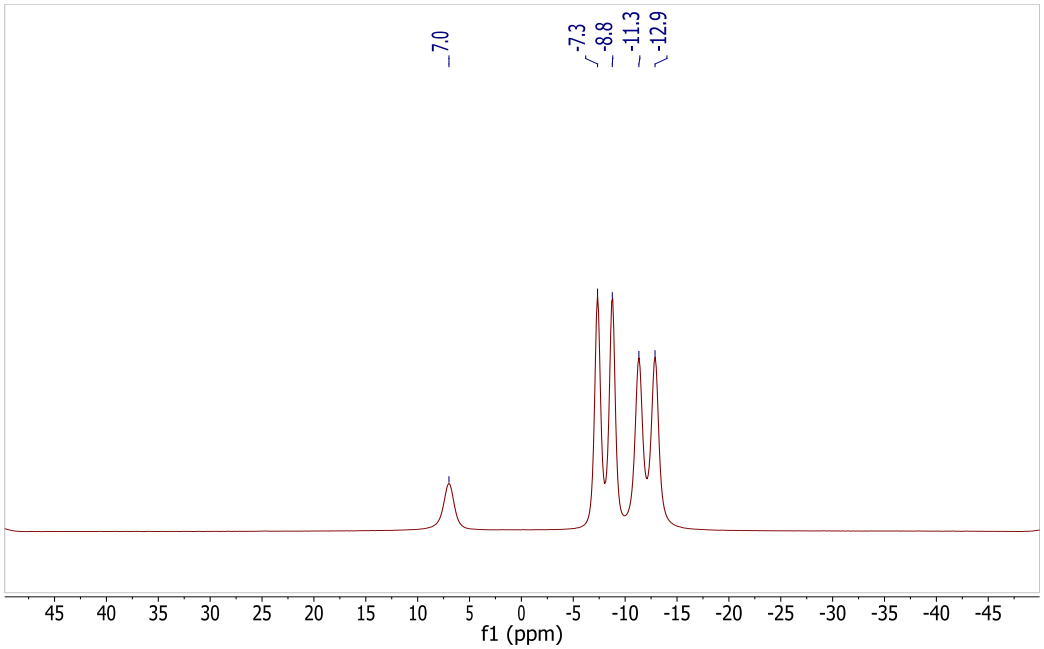

Figure 5-9 ^{11}B-NMR spectrum of compound **51[$HNMe_3^+$]** in acetone-d_6.

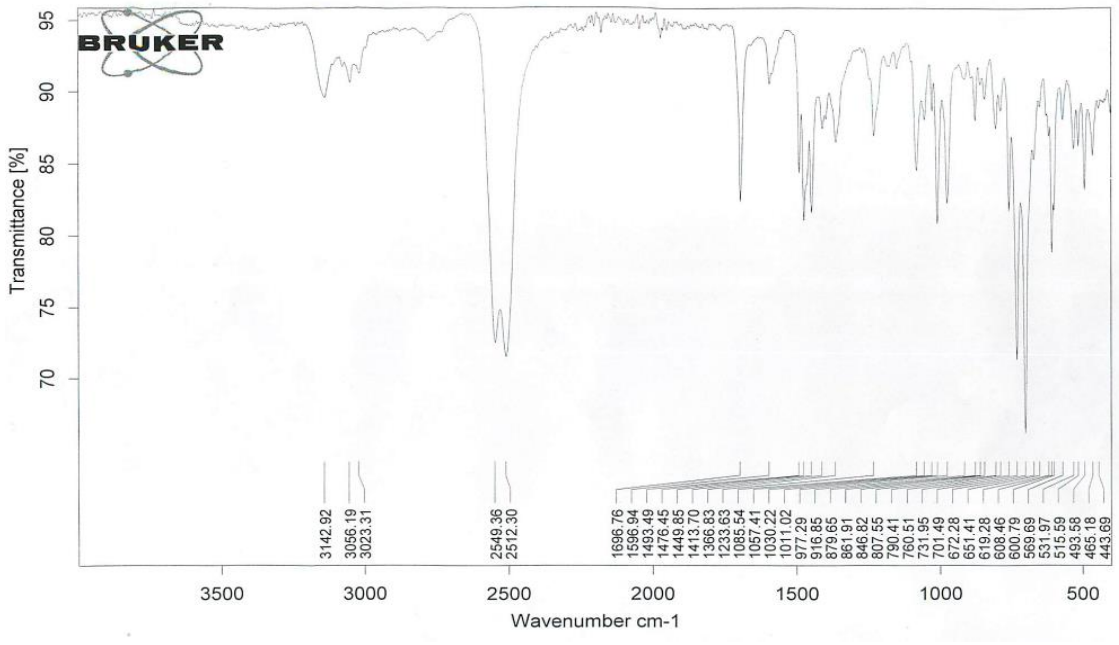

Figure 5-10 IR spectrum of solid **51[HNMe$_3^+$]**. Showing the B-H stretches at 2549 and 2512 cm^{-1}.

Synthesis of Trityl Carborane, **51[HNMe$_3^+$]** and **51'[HNMe$_3^+$]** with the **3[Ag$^+$]** Salt**:**

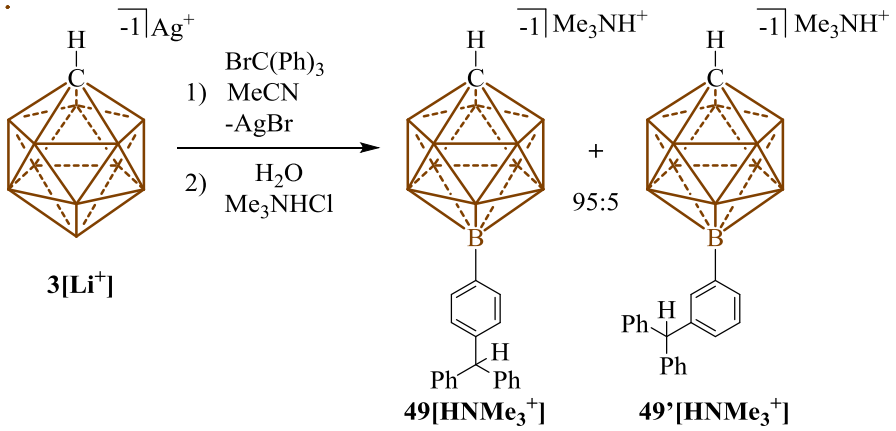

Scheme 5-4 Synthesis of the mixture of **49[HNMe$_3^+$]** and **49'[HNMe$_3^+$]** using **3[Ag$^+$]**.

The following procedure is based on a reaction by Reed and coworkers.[3] A glass scintillation vial equipped with a stir bar was loaded with **3[Ag$^+$]** (100 mg, 399 μmol) and dry acetonitrile (2 mL). A

separate vial was loaded with a solution of trityl bromide (129 mg, 399 μmol) in acetonitrile (2 mL). The solution of trityl bromide was transferred to the solution containing **3[Ag$^+$]**. The vial originally containing the trityl bromide solution was washed with acetonitrile (2 x 1 mL) and transferred to the solution of **3[Ag$^+$]** as well. The reaction was stirred for 20 minutes at room temperature. After 20 minutes, the reaction was filtered and subsequently concentrated down to a thick oil under vacuum. This oil was then dissolved in 10mL of deionized H_2O. Once fully dissolved, trimethylammonium hydrochloride (40 mg, 420 μmol) was added to the aqueous solution producing an off-white precipitate. The precipitate was then washed with deionized H_2O (3 x 4mL) resulting in products, **51[HNMe$_3^+$]** and **51'[HNMe$_3^+$]** (147 mg, 83% yield). *Note: Peaks picked are for compound* **51'[HNMe$_3^+$]** *only.* ^{1}H NMR (300 MHz, acetone-d$_6$, 25°C): δ = 7.35 – 7.11 (m, 12H), 6.91 (dd, $^3J(H,H)$ = 7.4 Hz, $^3J(H,H)$ = 7.4 Hz, 1H), 6.70 (d, $^3J(H,H)$ = 7.4 Hz, 1H), 5.45 (s, 1H), 3.21 (s, 9H), 2.20 (s, 1H), 2.60 - 0.78 (bm, 10H, B-H) ppm. ^{1}H[^{11}B] NMR (300 MHz, acetone-d$_6$, 25°C): δ = 7.38 – 7.13 (12H), 6.95 (1H), 6.75 (1H), 5.46 (1H), 3.01 (9H), 2.24 (1H), 1.80 (B-H), 1.77 (B-H), 1.74 (B-H) ppm. ^{13}C[^{1}H] NMR (75 MHz, acetone-d$_6$, 25°C): δ = 145.8, 134.9, 131.7, 130.1, 129.0, 128.8, 127.0, 126.6, 126.2, 58.1, 47.0, 46.1 ppm, *(broad $C_{aromatic}$-B resonance not detected).* ^{11}B[^{1}H] NMR (96 MHz, acetone-d$_6$, 25°C): δ = 7.0, -8.1, -12.1 ppm. ^{11}B NMR (96 MHz, acetone-d$_6$, 25°C): δ = 7.0, -8.0 ($^1J(H,B)$ = 136.3 Hz), -12.1 ($^1J(H,B)$ = 149.5 Hz) ppm. IR (Solid, ATR, 25°C): B-H stretch = 2545 cm^{-1}. HRMS (negative mode ESI/APCI) [M]$^-$ m/z calc'd = 385.3131 : Found = 385.3147

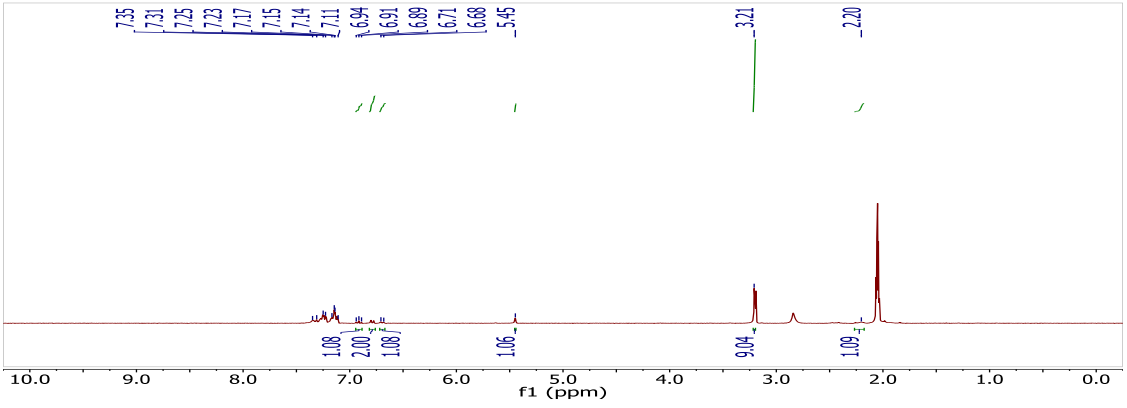

Figure 5-11 ^{1}H-NMR spectrum of the mixture containing **51'[HNMe$_3^+$]** in acetone-d$_6$. Note: Water is seen at 2.84 ppm. Integration of 1.08 to 2.00 shows a 1:1 ratio of **51'[HNMe$_3^+$]** to **51[HNMe$_3^+$]**, respectively.

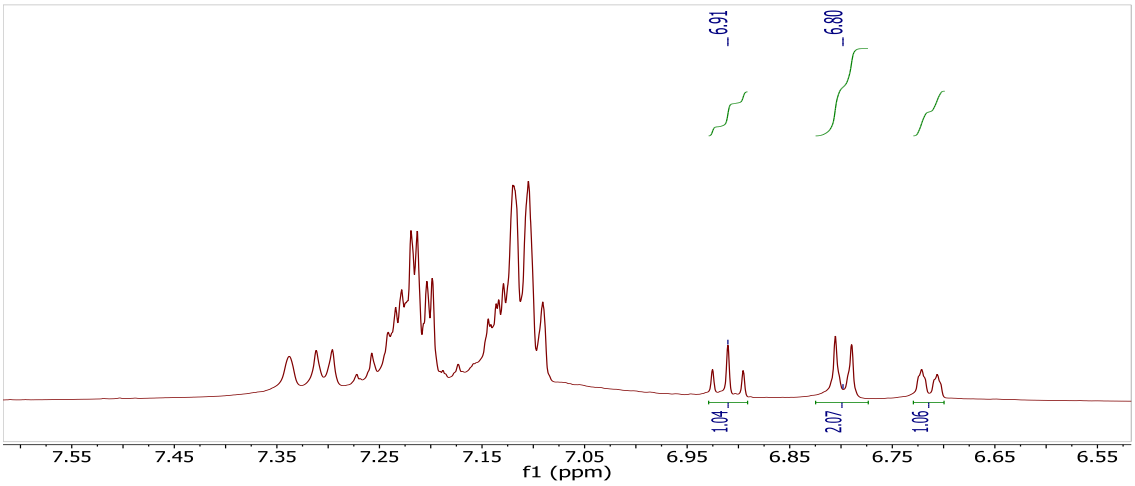

Figure 5-12 An expansion of the 1H-NMR spectrum of the mixture containing **51'[HNMe$_3^+$]** in acetone-d6. *Note: Compound **49'** is seen at 6.91 ppm and **51[HNMe$_3^+$]** is seen at 6.80 ppm.*

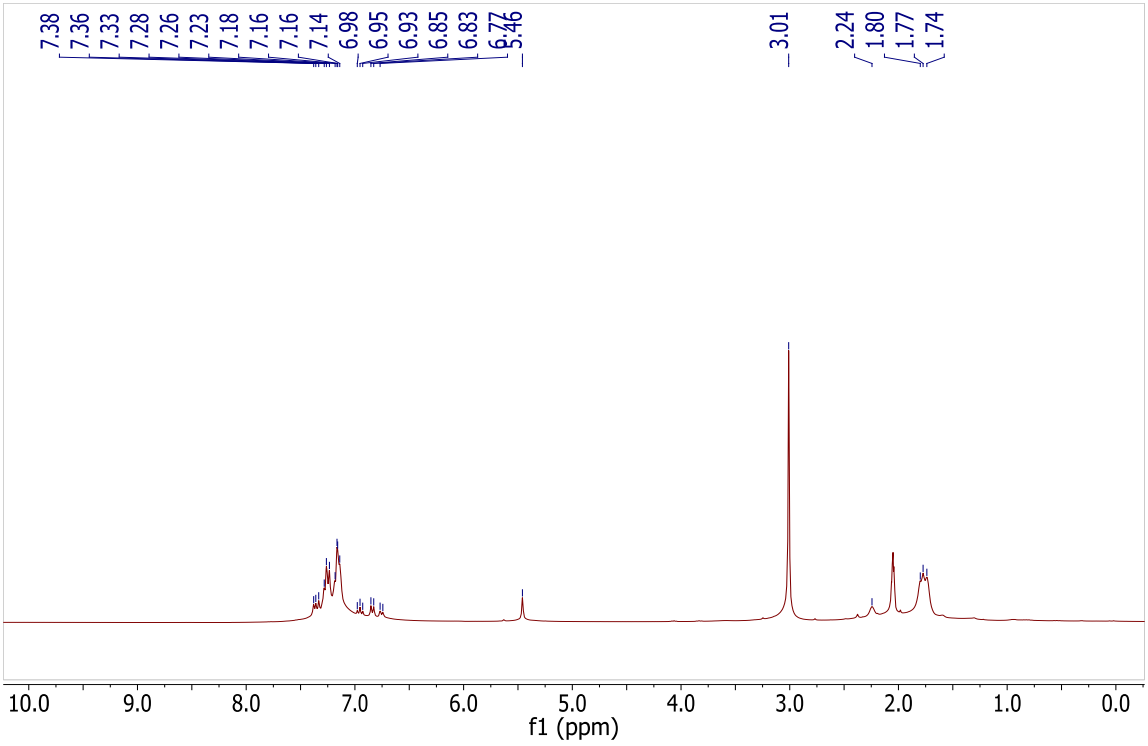

Figure 5-13 ^{1}H[^{11}B]-NMR spectrum of the mixture containing **51'[HNMe$_3^+$]** in acetone-d$_6$.

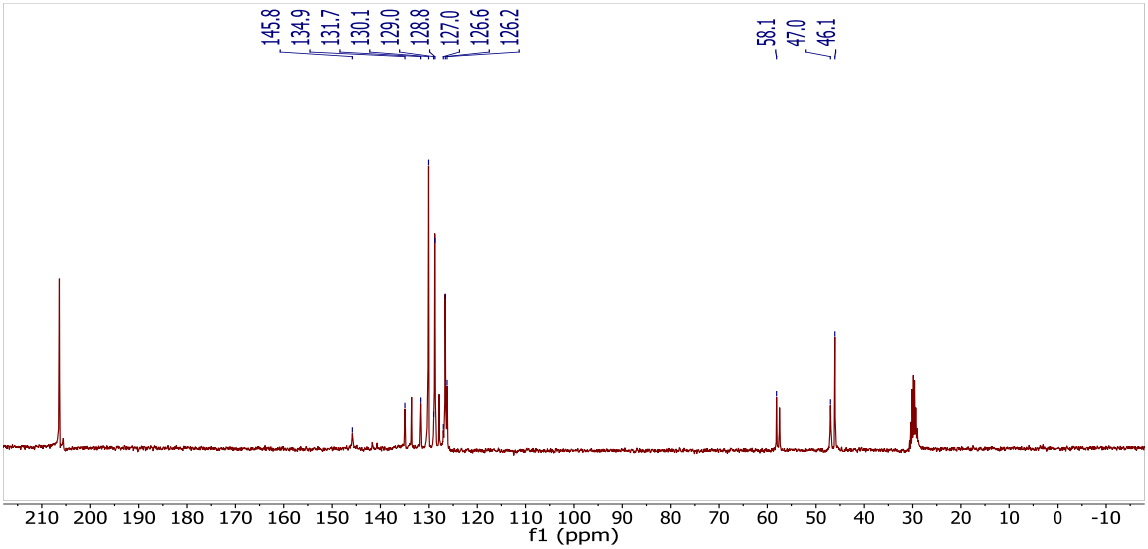

Figure 5-14 $^{13}C[^{1}H]$-NMR spectrum of the mixture containing **51'[HNMe$_3^+$]** in acetone-d_6.

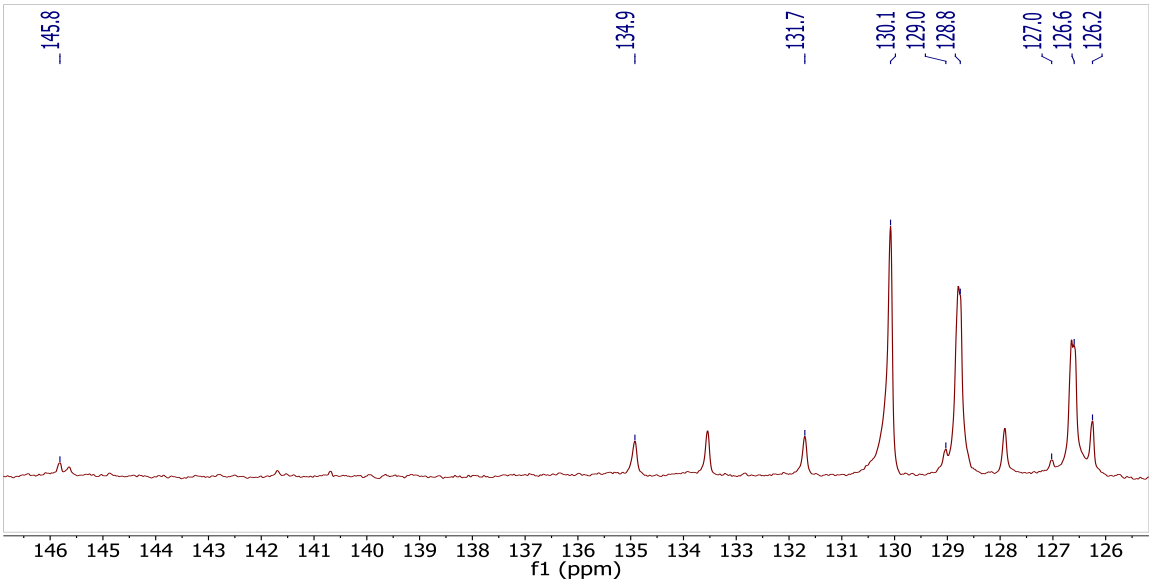

Figure 5-15 An expansion of $^{13}C[^{1}H]$ NMR of the aromatic region of the mixture containing **51'[HNMe$_3^+$]**.

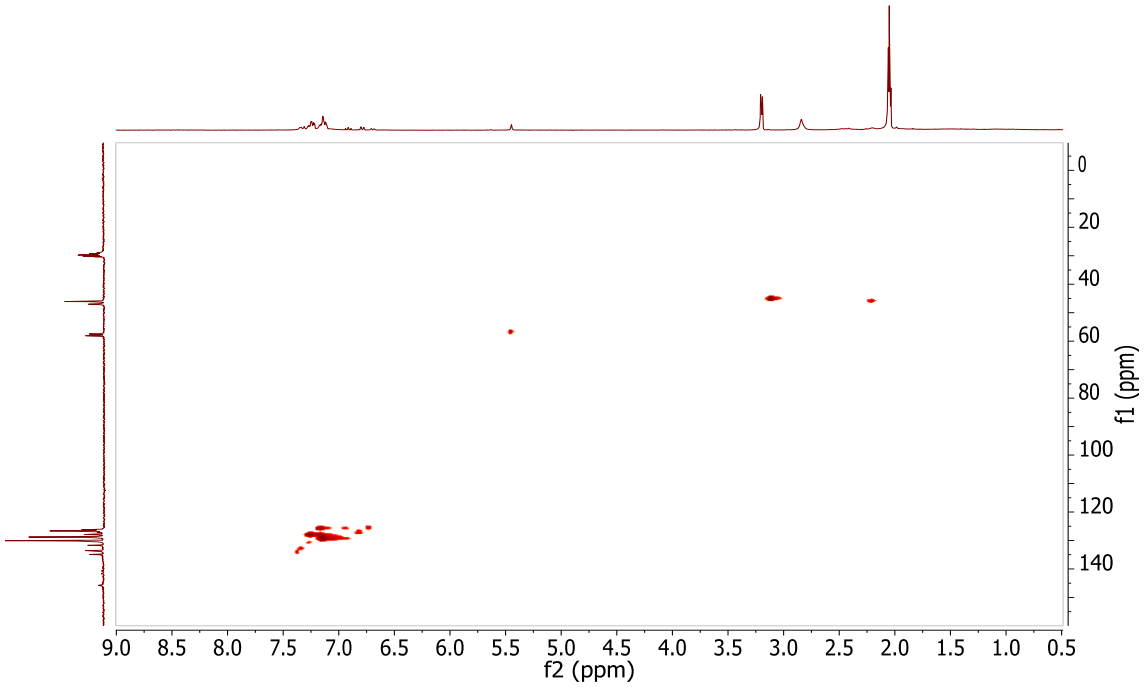

Figure 5-16 HSQC NMR spectrum of the mixture containing **51'[$HNMe_3^+$]** in acetone-d_6.

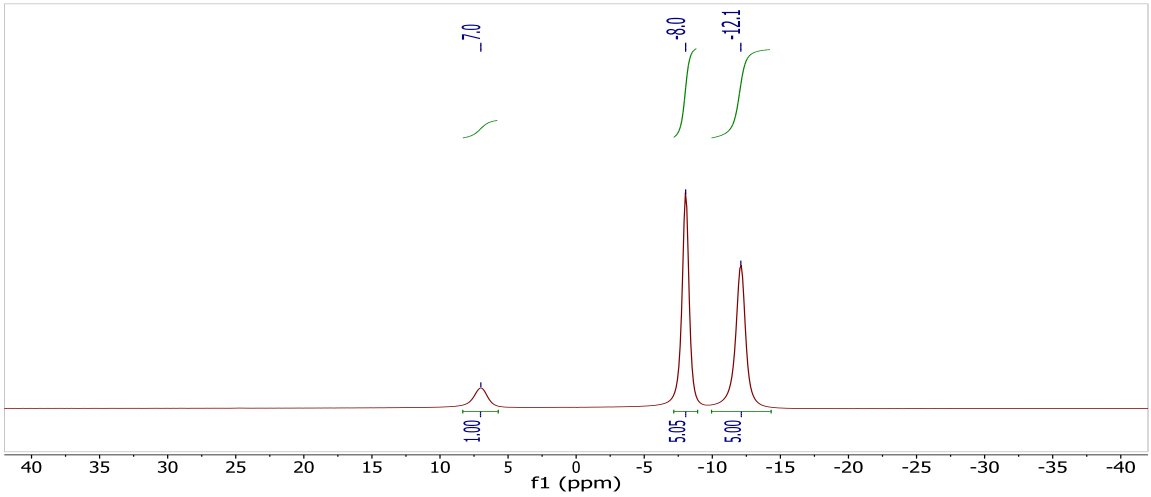

Figure 5-17 $^{11}B[^1H]$-NMR spectrum of the mixture containing **51'[$HNMe_3^+$]** in acetone-d_6.

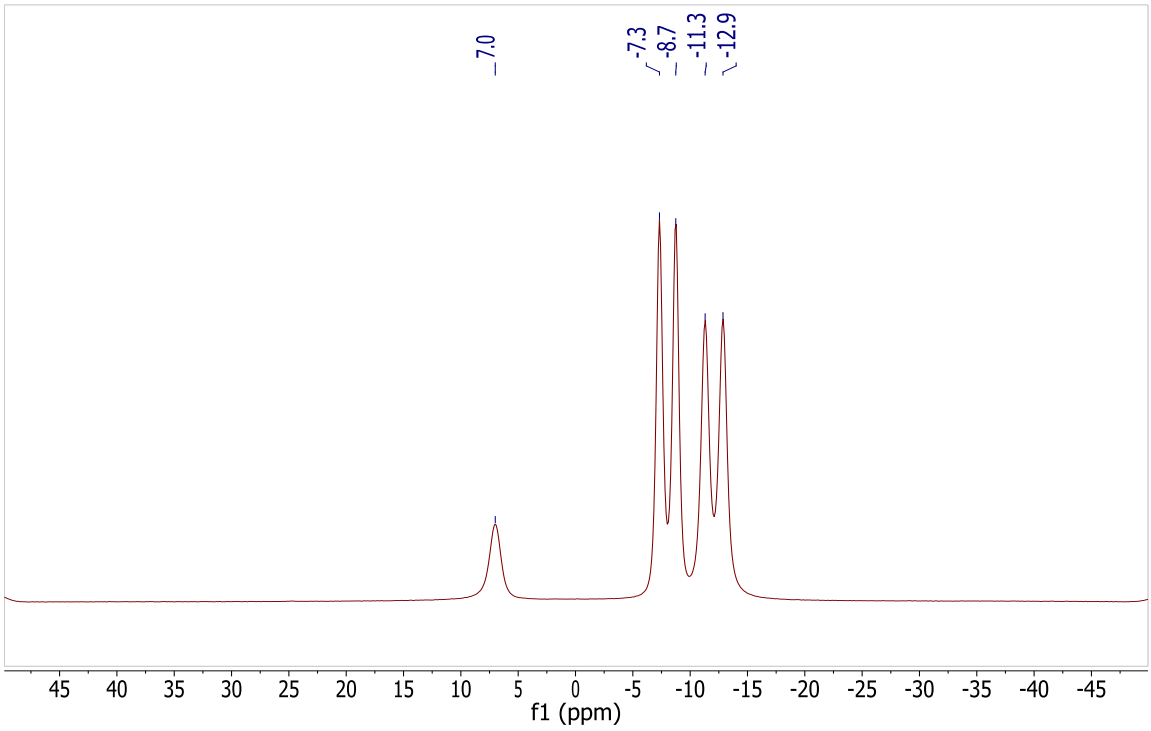

Figure 5-18 $^{11}B[^{1}H]$-NMR spectrum of the mixture containing **51'[HNMe$_3^+$]** in acetone-d_6.

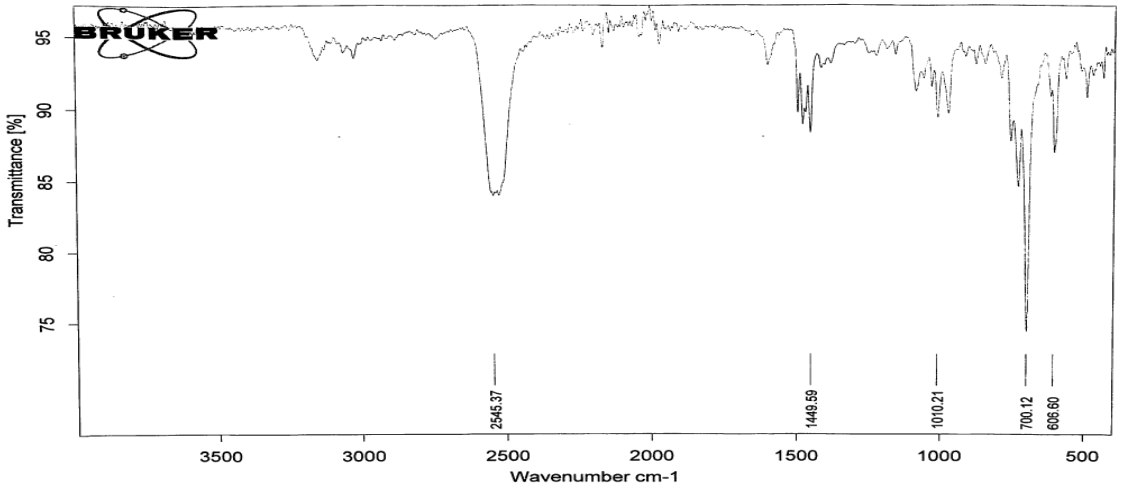

Figure 5-19 IR spectrum of the solid mixture **51[HNMe$_3^+$]** and **51'[HNMe$_3^+$]**. Showing the B-H stretches at 2545 cm^{-1}.

X-Ray Structure Determination

X-Ray Structure of **51[HNMe$_3^+$]:**

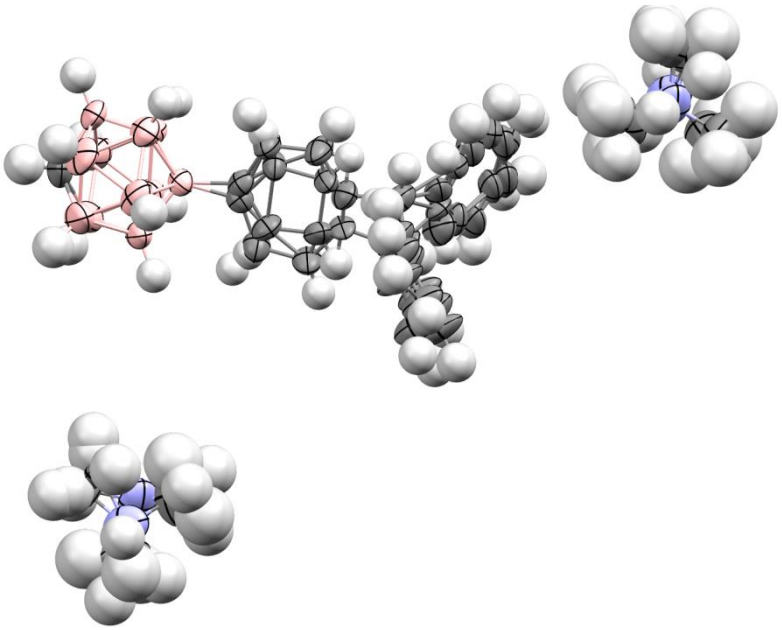

Figure 5-20 Crystal structure of **51[HNMe$_3^+$]**. Color code: H = white, B = pink, C = gray, N = blue.

A colorless prism fragment (0.516 x 0.289 x 0.128 mm^3) was used for the single crystal x-ray diffraction study of $[CH_{11}B_{11}C_{19}H_{15}]^-.[C_3H_{10}N]^+$ (sample vL266JK_0m-5). The crystal was coated with paratone oil and mounted on to a cryo-loop glass fiber. X-ray intensity data were collected at 100(2) K on a Bruker APEX2 platform-CCD x-ray diffractometer system (fine focus Mo-radiation, λ = 0.71073 Å, 50KV/30mA power). The CCD detector was placed at a distance of 5.0600 cm from the crystal.

A total of 3600 frames were collected for a sphere of reflections (with scan width of 0.3^o in ω, starting ω and 2θ angles of –30^o, and ϕ angles of 0^o, 90^o, 120^o, 180^o, 240^o and 270^o for every 600 frames, 120 sec/frame exposure time). The Bruker Cell_Now program was used to obtain the two different

orientation matrices of the rotational twin components (Twin law is 94° rotation about the 0 1 0 real axis). These matrices were imported into the APEX2 program for Bravais lattice determination and initial unit cell refinement. The frames were integrated using the Bruker SAINT software package and using a narrow-frame integration algorithm. Based on a monoclinic I-center crystal system, the integrated frames yielded a total of 2350 unique independent reflections [maximum 2θ = 42.520° (0.98 Å resolution), data completeness = 61.8%] and 1839(78.3%) reflections were greater than $2\sigma(I)$. The unit cell parameters were, **a** = 15.8564(26) Å, **b** = 10.6647(18) Å, **c** = 15.8859(26) Å, **β** = 94.2825(25)°, V = 2678.9(8) Å^3, Z = 4, calculated density D_c = 1.104 g/cm^3. Absorption corrections were applied (absorption coefficient μ = 0.057 mm^{-1}; max/min transmission = 0.993/0.971) to the raw intensity data using the Bruker TWINABS program.

The Bruker SHELXTL software package was used for phase determination and structure refinement. Using the first twin domain HKL 4 intensity data, the distribution of intensities (E^2-1 = 0.734) and systematic absent reflections indicated three possible space groups, I2, I2/m, and Im. The space group I2 (#5) was later determined to be correct. Direct methods of phase determination followed by two Fourier cycles of refinement led to an electron density map from which most of the non-hydrogen atoms were identified in the asymmetry unit of the unit cell. With subsequent isotropic refinement, all of the non-hydrogen atoms were identified. The combined (major and minor components) HKLF 5 intensity dataset was used in the final structure refinement. There were two half disordered-cations of $[C_3H_{10}N]^+$ and one disordered-anion of $[CH_{11}B_{11}C_{19}H_{15}]^-$ present in the asymmetry unit of the unit cell. The two disordered-cations were located at the 2-fold rotation axis parallel to the b-axis, and modeled with 50%/50% site occupancy ratio disorder. The site occupancy ratio of the disordered-anion was 54%/46%. The rotational twin law was 94° rotation about the 0 1 0 real axis. The major/minor twin component ratio was 54%/46%. The alert levels A and B are due to the poor crystal quality with low resolution data diffracting to 0.98 Angstroms at 120 seconds long exposure time. The disorder of the cation and anion further contributed to the poor resolution data. Attempts to obtain bigger and better quality crystal were unsuccessful.

Atomic coordinates, isotropic and anisotropic displacement parameters of all the non-hydrogen atoms were refined by means of a full matrix least-squares procedure on F^2. The H-atoms were included in the refinement in calculated positions riding on the atoms to which they were attached, except the H1 atom bonded to C1A was refined with DFIX restraint. The refinement converged at R1 = 0.0722, wR2 = 0.1857, with intensity, $I>2\sigma(I)$. The largest peak/hole in the final difference map was 0.235/-0.158 e/Å^3.

Table 5-1 Crystal data and structure refinement for **51[$HNMe_3^+$]**.

Identification code	vL266JK_0m-5	
Empirical formula	C23 H36 B11 N	
Formula weight	445.44	
Temperature	100(2) K	
Wavelength	0.71073 Å	
Crystal system	Monoclinic	
Space group	I 2	
Unit cell dimensions	a = 15.856(3) Å	α= 90°.
	b = 10.6647(18) Å	β= 94.283(3)°.
	c = 15.886(3) Å	γ = 90°.
Volume	2678.9(8) Å^3	
Z	4	
Density (calculated)	1.104 Mg/m^3	
Absorption coefficient	0.057 mm^{-1}	
F(000)	944	
Crystal size	0.516 x 0.289 x 0.128 mm^3	
Theta range for data collection	1.750 to 21.260°.	
Index ranges	-16<=h<=16, 0<=k<=10, 0<=l<=16	

Reflections collected	7977
Independent reflections	2350 [R(int) = 0.0357]
Completeness to theta = 25.242°	61.8 %
Absorption correction	Semi-empirical from equivalents
Refinement method	Full-matrix least-squares on F^2
Data / restraints / parameters	2350 / 1085 / 414
Goodness-of-fit on F^2	1.137
Final R indices [I>2sigma(I)]	R1 = 0.0722, wR2 = 0.1857
R indices (all data)	R1 = 0.0940, wR2 = 0.1999
Absolute structure parameter	-9(7)
Extinction coefficient	n/a
Largest diff. peak and hole	0.235 and -0.158 e.$Å^{-3}$

X-Ray Structure of **51[Cs^+]:**

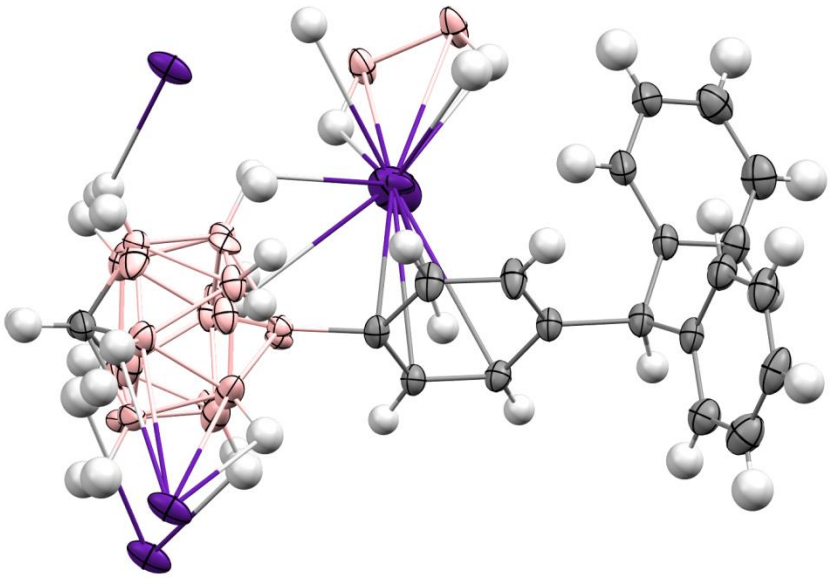

Figure 5-21 Crystal structure of **51[Cs^+]**. Color code = H = white, B = pink, C = gray, Cs = purple.

A colorless prism fragment (0.434 x 0.273 x 0.126 mm^3) was used for the single crystal x-ray diffraction study of $[Cs]^+.[C_{20}H_{26}B_{11}]^-$ (sample vL266JKr2-20_0m). The crystal was coated with paratone oil and mounted on to a cryo-loop glass fiber. X-ray intensity data were collected at 100(2) K on a Bruker APEX2 platform-CCD x-ray diffractometer system (fine focus Mo-radiation, λ = 0.71073 Å, 50KV/30mA power). The CCD detector was placed at a distance of 5.0600 cm from the crystal.

A total of 3600 frames were collected for a sphere of reflections (with scan width of 0.3^o in ω, starting ω and 2θ angles of -30^o, and ϕ angles of 0^o, 90^o, 120^o, 180^o, 240^o, and 270^o for every 600 frames, 20 sec/frame exposure time). The frames were integrated using the Bruker SAINT software package and using a narrow-frame integration algorithm. Based on a monoclinic crystal system, the integrated frames yielded a total of 57635 reflections at a maximum 2θ angle of 63.056^o (0.70 Å resolution), of which 7865 were independent reflections (R_{int} = 0.0234, R_{sig} = 0.0140, redundancy = 7.3, completeness = 99.0%) and

6993 (88.9%) reflections were greater than 2σ(I). The unit cell parameters were, **a** = 13.7371(4) Å, **b** = 10.4955(3) Å, **c** = 17.4166(5) Å, **β** = 108.6604(5)°, V =2379.08(12) $Å^3$, Z = 4, calculated density D_c = 1.447 g/cm^3. Absorption corrections were applied (absorption coefficient μ = 1.563 mm^{-1}; max/min transmission = 0.827/0.550) to the raw intensity data using the SADABS program.

The Bruker SHELXTL software package was used for phase determination and structure refinement. The distribution of intensities (E^2-1 = 0.946) and systematic absent reflections indicated one possible space group, P2(1)/n. The space group P2(1)/n (#14) was later determined to be correct. Direct methods of phase determination followed by two Fourier cycles of refinement led to an electron density map from which most of the non-hydrogen atoms were identified in the asymmetric unit of the unit cell. With subsequent isotropic refinement, all of the non-hydrogen atoms were identified. There was one disordered cation of $[Cs]^+$ and one disordered anion of $[C_{20}H_{26}B_{11}]^-$ present in the asymmetric unit of the unit cell. The Cs and CH11B11-group were modeled with disordered (disordered site occupancy ratio was 79%/21%). The molecule is a polymeric structure. The cation-anion polymeric chains form a plane along the b-axis and the n-glide direction. The B level alert is probably due to the disorder of the Cs and CH11B11-group.

Atomic coordinates, isotropic and anisotropic displacement parameters of all the non-hydrogen atoms were refined by means of a full matrix least-squares procedure on F^2. The H-atoms were included in the refinement in calculated positions riding on the atoms to which they were attached, except H1, H1D, H3A, H4A, H6A and H7A bonded to C1, C1D, C3, C4, C6, and C7, respectively were refined with DFIX restraints. The refinement converged at R1 = 0.0315, wR2 = 0.0708, with intensity I>2□ (I). The largest peak/hole in the final difference map was 0.999/-0.490 e/$Å^3$.

Table 5-2 Crystal data and structure refinement for **51[Cs^+]**.

Identification code	vL266JKr2-20_0m	
Empirical formula	C20 H26 B11 Cs	
Formula weight	518.23	
Temperature	100(2) K	
Wavelength	0.71073 Å	
Crystal system	Monoclinic	
Space group	P 21/n	
Unit cell dimensions	a = 13.7371(4) Å	a= 90°.
	b = 10.4955(3) Å	b= 108.6604(5)°.
	c = 17.4166(5) Å	g = 90°.
Volume	2379.08(12) $Å^3$	
Z	4	
Density (calculated)	1.447 Mg/m^3	
Absorption coefficient	1.563 mm^{-1}	
F(000)	1024	
Crystal size	0.434 x 0.273 x 0.126 mm^3	
Theta range for data collection	1.654 to 31.528°.	
Index ranges	-20<=h<=19, -15<=k<=15, -25<=l<=25	
Reflections collected	57635	
Independent reflections	7865 [R(int) = 0.0234]	
Completeness to theta = 25.242°	100.0 %	
Absorption correction	Semi-empirical from equivalents	
Refinement method	Full-matrix least-squares on F^2	
Data / restraints / parameters	7865 / 329 / 413	
Goodness-of-fit on F^2	1.140	

Final R indices [I>2sigma(I)]	R1 = 0.0315, wR2 = 0.0708
R indices (all data)	R1 = 0.0372, wR2 = 0.0732
Extinction coefficient	n/a
Largest diff. peak and hole	0.999 and -0.490 e.Å^{-3}

X-Ray Structure of **3'[HNMe$_3$]$^+$**:

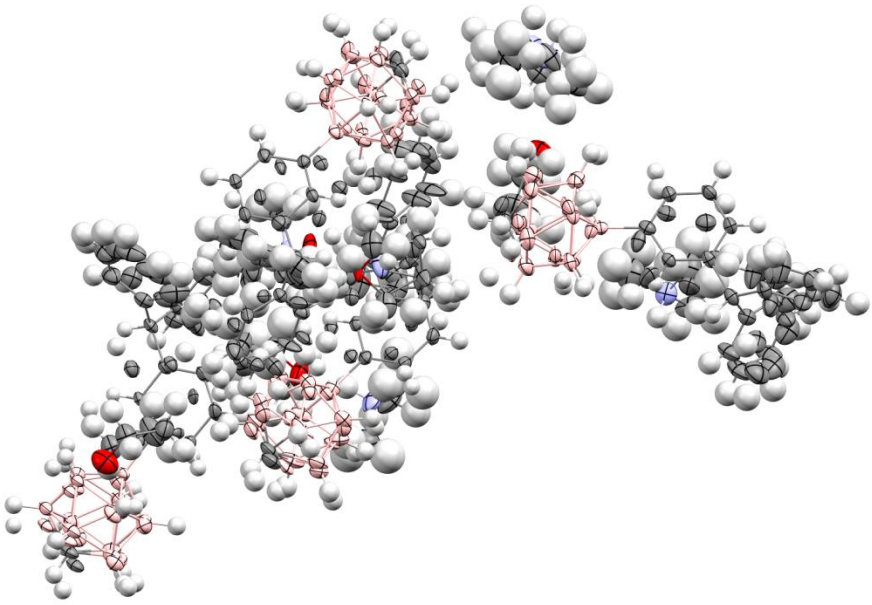

Figure 5-22 Crystal structure of **51'[HNMe$_3^+$]**. Color code = H = white, B = pink, C = gray, N = blue, O = red.

A colorless prism fragment (0.542 x 0.303 x 0.123 mm^3) was used for the single crystal x-ray diffraction study of $[C_3H_{10}N]^+.[C_{20}H_{26}B_{11}]^-.C_4H_8O$ (sample vL266JKr_0m). The crystal was coated with paratone oil and mounted on to a cryo-loop glass fiber. X-ray intensity data were collected at 100(2) K on a Bruker APEX2 platform-CCD x-ray diffractometer system (fine focus Mo-radiation, λ = 0.71073 Å, 50KV/30mA power). The CCD detector was placed at a distance of 5.0600 cm from the crystal.

A total of 3600 frames were collected for a sphere of reflections (with scan width of 0.3^o in ω, starting ω and 2θ angles of –30^o, and ϕ angles of 0^o, 90^o, 120^o, 180^o, 240^o, and 270^o for every 600 frames, 80 sec/frame exposure time). The frames were integrated using the Bruker SAINT software package and using a narrow-frame integration algorithm. Based on a monoclinic crystal system, the integrated frames yielded a total of 136026 reflections at a maximum 2θ angle of 58.260^o (0.73 Å resolution), of which 32906

were independent reflections (R_{int} = 0.0447, R_{sig} = 0.0353, redundancy = 4.1, completeness = 99.9%) and 26149 (79.5%) reflections were greater than 2σ(I). The unit cell parameters were, **a** = 8.5424(3) Å, **b** = 21.3147(7) Å, **c** = 33.6589(11) Å, **β** = 90.2206(6)°, V =6128.5(4) $Å^3$, Z = 8, calculated density D_c = 1.122 g/cm^3. Absorption corrections were applied (absorption coefficient μ = 0.060 mm^{-1}; max/min transmission = 0.993/0.968) to the raw intensity data using the SADABS program.

The Bruker SHELXTL software package was used for phase determination and structure refinement. The distribution of intensities (E^2-1 = 0.741) and systematic absent reflections indicated two possible space groups, Pc and P2/c. The space group Pc (#7) was later determined to be correct. Direct methods of phase determination followed by two Fourier cycles of refinement led to an electron density map from which most of the non-hydrogen atoms were identified in the asymmetric unit of the unit cell. With subsequent isotropic refinement, all of the non-hydrogen atoms were identified. There were four cations of $[C_3H_{10}N]^+$, four meta/para disordered-anions of $[C_{20}H_{26}B_{11}]^-$, and four solvent molecules of THF (where one of the four THF was modeled with 50%/50% site occupancy disorder) present in the asymmetric unit of the unit cell. The four meta/para anion-disordered site occupancy ratios were 83%/17%, 81%/19%, 73%/27%, and 61%/39%. The two cation-disordered site occupancy ratios were 73%/27% and 50%/50%. There was space group ambiguity between Orthorhombic Pca2(1) and monoclinic Pc. The final structure refinement was based on the monoclinic Pc space group. The structure was refined as a pseudo-merohedral twin (twin law 1 0 0, 0 -1 0, 0 0 -1) and the major/minor component twin ratio was 76%/24%. Using Pca2(1) space group, data reduction and refinement gave a much higher R_{int} = 0.0829, R_{sig} = 0.0285 and R1 = 0.0768 at 0.81 Angstroms resolution, respectively in comparision to Pc space group (R_{int} = 0.0447, R_{sig} = 0.0353, R1 = 0.0768 at 0.73 Angstroms resolution). The B level Alert of the C-C bond precession is probably due to the cations, THF, and the four whole molecule-anion meta/para disorders where restraints were used to allow the refinement to converge.

Atomic coordinates, isotropic and anisotropic displacement parameters of all the non-hydrogen atoms were refined by means of a full matrix least-squares procedure on F^2. The H-atoms were included in the refinement in calculated positions riding on the atoms to which they were attached, except the H1A, H1B, H1C, H1D, H1E, HIF, HIG and H1H atoms bonded to C1A, C1B, C1C, C1D, C1E, C1F, C1G and C1H, respectively were refined with DFIX restraints. The refinement converged at R1 = 0.0768, wR2 = 0.2054, with intensity I>2σ (I). The largest peak/hole in the final difference map was 0.724/-0.543 e/$Å^3$.

Table 5-3 Crystal data and structure refinement for **51'[$HNMe_3^+$]**.

Identification code	vL266JKr_0m	
Empirical formula	C27 H44 B11 N O	
Formula weight	517.54	
Temperature	100(2) K	
Wavelength	0.71073 Å	
Crystal system	Monoclinic	
Space group	P c	
Unit cell dimensions	a = 8.5424(3) Å	a= 90°.
	b = 21.3147(7) Å	b= 90.2206(6)°.
	c = 33.6589(11) Å	g = 90°.
Volume	6128.5(4) $Å^3$	
Z	8	
Density (calculated)	1.122 Mg/m^3	
Absorption coefficient	0.060 mm^{-1}	
F(000)	2208	
Crystal size	0.542 x 0.303 x 0.123 mm^3	

Theta range for data collection	1.542 to 29.130°.
Index ranges	-11<=h<=11, -29<=k<=29, -46<=l<=46
Reflections collected	136026
Independent reflections	32906 [R(int) = 0.0447]
Completeness to theta = 25.242°	100.0 %
Absorption correction	Semi-empirical from equivalents
Refinement method	Full-matrix least-squares on F^2
Data / restraints / parameters	32906 / 7534 / 2333
Goodness-of-fit on F^2	1.013
Final R indices [I>2sigma(I)]	R1 = 0.0768, wR2 = 0.2054
R indices (all data)	R1 = 0.0976, wR2 = 0.2262
Absolute structure parameter	-0.1(3)
Extinction coefficient	n/a
Largest diff. peak and hole	0.724 and -0.543 e.$Å^{-3}$

5.5 References

1. R. N. Grimes, *Dalton Transactions*, 2015, **44**, 5939-5956.
2. J. Zhang ,Z. Xie, *Accounts of Chemical Research*, 2014, **47**, 1623-1633.
3. A. R. Popescu, F. Teixidor ,C. Viñas, *Coordination Chemistry Reviews*, 2014, **269**, 54-84.
4. C. Douvris ,J. Michl, *Chemical Reviews*, 2013, **113**, PR179-PR233.
5. A. Spokoyny, *Pure and Applied Chemistry*, 2013, **85**, 903-919.
6. P. Farràs, E. J. Juárez-Pérez, M. Lepšík, R. Luque, R. Núñez ,F. Teixidor, *Chemical Society Reviews*, 2012, **41**, 3445-3463.
7. M. Scholz ,E. Hey-Hawkins, *Chemical Reviews*, 2011, **111**, 7035-7062.
8. C. A. Reed, *Accounts of Chemical Research*, 2010, **43**, 121-128.
9. R. N. Grimes, *Carboranes*, Academic Press, New York, 2016.
10. N. S. Hosmane, *Handbook of Boron Science : with Applications in Organometallics, Catalysis, Materials and Medicine*, World Scienific, Hackensack, New Jersey, 2019.
11. C. Douvris ,O. V. Ozerov, *Science*, 2008, **321**, 1188-1190.
12. B. Shao, A. L. Bagdasarian, S. Popov ,H. M. Nelson, *Science*, 2017, **355**, 1403.
13. O. Allemann, S. Duttwyler, P. Romanato, K. K. Baldridge ,J. S. Siegel, *Science*, 2011, **332**, 574.
14. T. Klis, D. R. Powell, L. Wojtas ,R. J. Wehmschulte, *Organometallics*, 2011, **30**, 2563-2570.
15. S. Cummings, H. P. Hratchian ,C. A. Reed, *Angewandte Chemie International Edition*, 2016, **55**, 1382-1386.
16. Y. Shoji, N. Tanaka, K. Mikami, M. Uchiyama ,T. Fukushima, *Nature Chemistry*, 2014, **6**, 498.
17. E. S. Stoyanov, I. V. Stoyanova, F. S. Tham ,C. A. Reed, *Journal of the American Chemical Society*, 2010, **132**, 4062-4063.
18. T. Kato ,C. A. Reed, *Angewandte Chemie International Edition*, 2004, **43**, 2908-2911.
19. K.-C. Kim, C. A. Reed, D. W. Elliott, L. J. Mueller, F. S. Tham, L. Lin ,J. B. Lambert, *Science*, 2002, **297**, 825-827.
20. R. Núñez, M. Tarrés, A. Ferrer-Ugalde, F. F. de Biani ,F. Teixidor, *Chemical Reviews*, 2016, **116**, 14307-14378.
21. I. Krossing ,I. Raabe, *Angewandte Chemie International Edition*, 2004, **43**, 2066-2090.

22. S. H. Strauss, *Chemical Reviews*, 1993, **93**, 927-942.

23. S. P. Fisher, A. El-Hellani, F. S. Tham ,V. Lavallo, *Dalton Transactions*, 2016, **45**, 9762-9765.

24. A. L. Chan, J. Estrada, C. E. Kefalidis ,V. Lavallo, *Organometallics*, 2016, **35**, 3257-3260.

25. J. C. Axtell, K. O. Kirlikovali, P. I. Djurovich, D. Jung, V. T. Nguyen, B. Munekiyo, A. T. Royappa, A. L. Rheingold ,A. M. Spokoyny, *Journal of the American Chemical Society*, 2016, **138**, 15758-15765.

26. M. Hailmann, N. Wolf, R. Renner, T. C. Schäfer, B. Hupp, A. Steffen ,M. Finze, *Angewandte Chemie International Edition*, 2016, **55**, 10507-10511.

27. J. Estrada, D. H. Woen, F. S. Tham, G. M. Miyake ,V. Lavallo, *Inorganic Chemistry*, 2015, **54**, 5142-5144.

28. J. Estrada, S. E. Lee, S. G. McArthur, A. El-Hellani, F. S. Tham ,V. Lavallo, *Journal of Organometallic Chemistry*, 2015, **798**, 214-217.

29. M. J. Asay, S. P. Fisher, S. E. Lee, F. S. Tham, D. Borchardt ,V. Lavallo, *Chemical Communications*, 2015, **51**, 5359-5362.

30. A. El-Hellani ,V. Lavallo, *Angewandte Chemie International Edition*, 2014, **53**, 4489-4493.

31. V. Lavallo, J. H. Wright Ii, F. S. Tham ,S. Quinlivan, *Angewandte Chemie International Edition*, 2013, **52**, 3172-3176.

32. A. El-Hellani, C. E. Kefalidis, F. S. Tham, L. Maron ,V. Lavallo, *Organometallics*, 2013, **32**, 6887-6890.

33. A. Himmelspach, M. Finze ,S. Raub, *Angewandte Chemie International Edition*, 2011, **50**, 2628-2631.

34. R. D. Kennedy, C. L. Stern ,C. A. Mirkin, *Inorganic Chemistry*, 2013, **52**, 14064-14071.

35. Z. Yinghuai, K. Carpenter, C. C. Bun, S. Bahnmueller, C. P. Ke, V. S. Srid, L. W. Kee ,M. F. Hawthorne, *Angewandte Chemie International Edition*, 2003, **42**, 3792-3795.

36. F. Šembera, J. Plutnar, A. Higelin, Z. Janoušek, I. Císařová ,J. Michl, *Inorganic Chemistry*, 2016, **55**, 3797-3806.

37. V. Ďorďovič, Z. Tošner, M. Uchman, A. Zhigunov, M. Reza, J. Ruokolainen, G. Pramanik, P. Cígler, K. Kalíková, M. Gradzielski ,P. Matějíček, *Langmuir*, 2016, **32**, 6713-6722.

38. B. Ringstrand ,P. Kaszynski, *Accounts of Chemical Research*, 2013, **46**, 214-225.

39. J. Pecyna, D. Pociecha ,P. Kaszyński, *Journal of Materials Chemistry C*, 2014, **2**, 1585-1591.

40. J. Pecyna, B. Ringstrand, S. Domagała, P. Kaszyński ,K. Woźniak, *Inorganic Chemistry*, 2014, **53**, 12617-12626.

41. S. G. McArthur, R. Jay, L. Geng, J. Guo ,V. Lavallo, *Chemical Communications*, 2017, **53**, 4453-4456.

42. S. G. McArthur, L. Geng, J. Guo ,V. Lavallo, *Inorganic Chemistry Frontiers*, 2015, **2**, 1101-1104.

43. R. T. Boeré, C. Bolli, M. Finze, A. Himmelspach, C. Knapp ,T. L. Roemmele, *Chemistry – A European Journal*, 2013, **19**, 1784-1795.

44. Z. Xie, T. Jelinek, R. Bau ,C. A. Reed, *Journal of the American Chemical Society*, 1994, **116**, 1907-1913.

45. R. J. Wiersema ,M. F. Hawthorne, *Inorganic Chemistry*, 1973, **12**, 785-788.

46. A. Himmelspach, G. J. Reiss ,M. Finze, *Inorganic Chemistry*, 2012, **51**, 2679-2688.

47. M. J. Ingleson, G. Kociok-Köhn ,A. S. Weller, *Inorganica Chimica Acta*, 2005, **358**, 1571-1580.

48. N. J. Bullen, A. Franken, C. A. Kilner ,J. D. Kennedy, *Chemical Communications*, 2003, 1684-1685.

49. A. Franken, C. A. Kilner, M. Thornton-Pett ,J. D. Kennedy, *Journal of Organometallic Chemistry*, 2002, **657**, 176-179.

50. B. Grüner, Z. Janoušek, B. T. King, J. N. Woodford, C. H. Wang, V. Všetečka ,J. Michl, *Journal of the American Chemical Society*, 1999, **121**, 3122-3126.

51. T. Jelinek, P. Baldwin, W. R. Scheidt ,C. A. Reed, *Inorganic Chemistry*, 1993, **32**, 1982-1990.

52. Z. Janoušek, U. Lehmann, J. Častulík, I. Císařová ,J. Michl, *Journal of the American Chemical Society*, 2004, **126**, 4060-4061.

Chapter 6: Playing with Charges: In Pursuit of a Carbenoid Carbocation Ion Pair

6.1 Introduction

In 1902, Norris[1, 2] and Kehrman[3] reported that triphenylmethanol reacts with concentrated sulfuric acid to produce deep-yellow solutions of an unknown compound. The following year Adolf von Baeyer recognized that the isolated material possessed salt-like character.[4] Although they did not recognize the exact structure of the compound, these pioneers had inadvertently discovered one of the first isolable carbocations, namely the triphenyl methyl cation (trityl cation) **50** (Figure 6-1). While stable, the trityl cation is a potent electrophile that can participate in a variety of addition, oxidation, and abstraction reactions.[5, 6]

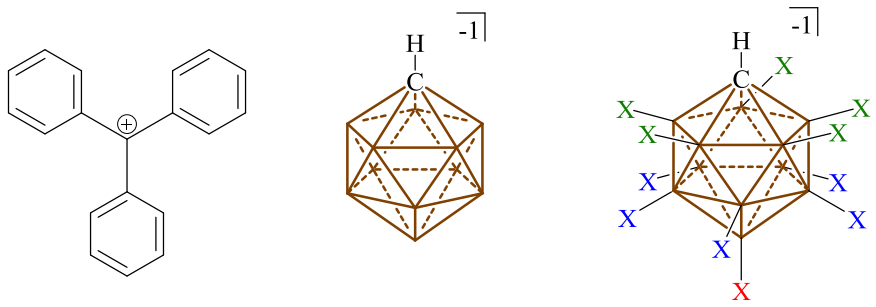

Figure 6-1 Triphenyl methyl cation **52** (left), 12 vertex icosahedral carborane anion **3** (middle) and halogenated 12 vertex icosahedral carborane (right). Different substation patterns shown in different colors; green = substitution of the upper pentagonal belt (B2-B7), blue = substitution of the lower pentagonal belt (B6-B11), red = substitution of the antipodal boron (B12). Unlabeled vertices = B-H.

Another fascinating branch of carbon chemistry is carbenes.[7-11] Carbenes feature a divalent carbon center with two nonbonding electrons and typically are transient reactive intermediates. However, in the late 20th century Bertrand and Arduengo reported the first isolable versions of carbenes, namely the phosphinosilyl[12, 13] and N-heterocyclic carbenes (NHCs),[14] respectively. Due to the presence of a lone pair

of electrons and an accessible p-orbital, carbenes display ambident nucleophilic and electrophilic character at the carbon center.

A third class of unusual carbon containing molecules are carborane clusters, which feature hypercoordinate carbon atoms that can achieve a maximum coordination number of 6 at carbon.[15-17] Unlike carbocations and carbenes, certain carboranes are extraordinarily unreactive, particularly the 12-vertex icosahedral carborane anion $[HCB_{11}H_{11}]^{-1}$ **3** and its polyhalogenated derivatives (Figure 6-1). As exemplified independently by Reed,[18] Siegal,[19] Ozerov[20-22] and most recently Nelson,[23, 24] such carborane anion derivatives can be utilized to stabilize transient high energy carbocations that normally are not persistent. Over the last few years we have designed various ligand frameworks, including N-carboranyl NHCs **30**[25] and **35[Li$^+$]**[26] (formally carbenoids, Li^+ is coordinated to carbene carbon), that feature covalently linked *closo*-carborane anions. The charge of the carborane anions renders the NHC ligands anionic, which opens up the possibility of designing unusual electrostatically tethered ion pairs of both fundamental and practical importance. Herein we report our efforts to electrostatically link two classic organic reactive species, namely carbenes and carbocations.

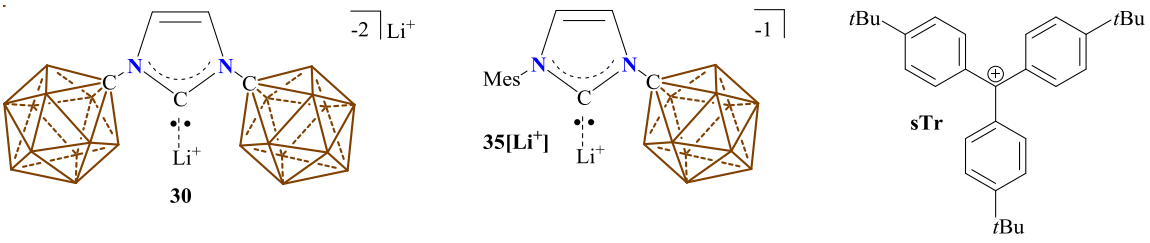

Figure 6-2 Structures of **30**, **35[Li+]** and super trityl (**sTr**).

Attack of trityl cations with nucleophiles such as phopshines is known[27, 28] and it has been demonstrated that phosphines attack the tertiary central carbon of the trityl cation[29, 30] as well as the *para* position of one of the benzene rings of the trityl cation.[31, 32] In 2009, Stephan and coworkers demonstrated that the bulky *t*-butyl NHC **53** reacts with **52[B(C$_6$F$_5$)$_4$]**$^-$ forming an adduct where the nucleophile NHC has

attacked a *para*-position of one of the benzene rings of the trityl cation forming **54**, Scheme 6-1.[33] We hypothesized that by kinetically protecting the *para*-position of the benzene rings, we could prevent this type of reactivity. To achieve this, we thought to block the *para*-position with a sterically encumbering substituent such as *tert*-butyl. Therefore, we decided to implement the tris(*para*-(*tert*-butyl)phenyl)methyl cation **sTr** (super trityl) with a BF_4^- counter anion.[34] Next, we envisioned that it might be possible to generate a carbene/carbocation ion pair if the carbene was anionic and contained enough steric pressure to prevent approach of the nucleophile to the electrophile. To perform such a reaction, we imagined a salt metathesis reaction with our dianionic or monoanionic NHC **30** or **35[Li$^+$]** respectively, and a trityl salt, Figure 6-2.

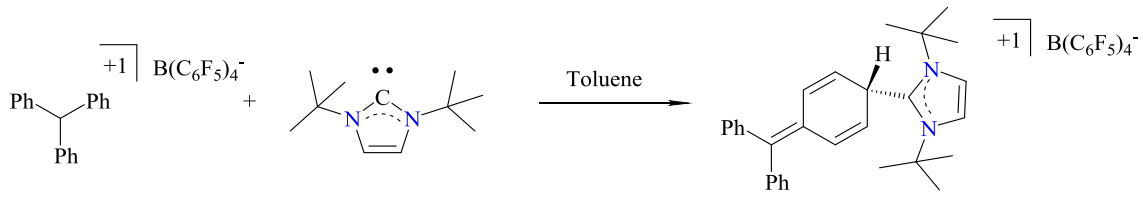

52[B(C$_6$F$_5$)$_4^-$] **53** **54**

Scheme 6-1 Work by Stephan and coworkers outlining the reactivity of bulky NHC and $[Ph_3C]^+$ $[B(C_6F_5)_4]^-$.

6.2 Reactivity of an Anionic Imidazolium **29** with **sTr**.

Knowing that trityl cation **52** undergoes electrophilic aromatic substitution "like" reactions with **3[Li$^+$]** or **3[Ag$^+$]**, and forms *para* and *meta* substituted products, we sought to test the reactivity of **sTrCl** with imidazolium **29**.[35] If the carborane clusters of **29** undergoes electrophilic aromatic substitution "like" reactions with **sTrCl**, the probability of forming a carbene/carbocation ion pair would likely be unsuccessful.

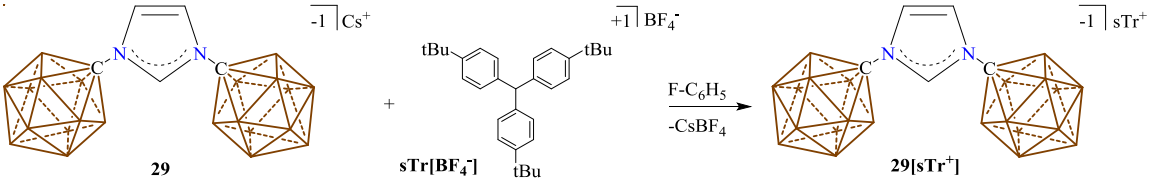

Scheme 6-2 Synthesis of **29[sTr$^+$]**.

To probe the reactivity of **29**, a 1:1 reaction of **29** with **sTr[BF$_4^-$]** in methylene chloride was performed, however this reaction proved fruitless as imidazolium **29** is almost completely insoluble in methylene chloride. In an effort to overcome the solubility issue the solvent was changed to F-C_6H_5 and **sTrCl** to **sTr[BF$_4^-$]**. Upon adding a suspension of **29** to a suspension of **sTr[BF$_4^-$]** the heterogeneous mixture remained highly colored, Scheme 6-2. ^{11}B NMR analysis of the crude reaction mixture showed three resonances in a 1:5:5 ratio that each split into doublets, indicating the carborane cluster retained its C_{5v} symmetry. After working up the reaction by filtering off the $CsBF_4$, the ^{13}C NMR spectrum showed the expected tertiary carbon of the trityl cation at 204 ppm. The ^{1}H NMR spectrum showed no singlets near 4.5 ppm as the methine proton of the tertiary carbon for triphenylmethyl appears in this region, corroborating the compatibility of **29** and **sTr**$^+$. Moving downfield, the aromatic region of the ^{1}H NMR spectrum displays four unique resonances, the imidazolium protons display two resonances at 8.27 (t, ^4J = 1.8 Hz) and 7.17 (d, ^4J = 1.8) ppm and the **sTr** cation displays two doublets at 7.87 and 7.61 (^3J = 8.4 Hz) ppm.

To unambiguously determine the structure of **29[sTr$^+$]** a single crystal X-ray diffraction study was undertaken. Suitable crystals were grown by vapor diffusion of pentane into a methylene chloride solution containing **29[sTr$^+$]**. The solid-state structure confirmed the proposed the structure of **29[sTr$^+$]**, Figure 6-3. In the solid-state, the nitrogen carbene bond lengths for N1-C2 and C2-N3 are 1.330(2) and 1.332(2) Å respectively and show no deviation from reported imidazolium **29**.[25] Both N1 and N3 are planar with a sum of C-N-C angles = 360°, indicating both nitrogen atoms are sp^2 hybridized, the same is seen in **29**. The sum of internal angles of the imidazolium core = 540° which suggest the core is perfectly planar and not at all disturbed by the cation. The average N-$C_{cluster}$ distance is 1.460(2) Å and the average $C_{cluster}$-B distance is 1.710(3) Å, similar to **29** who has an average N-$C_{cluster}$ distance of 1.455 Å and $C_{cluster}$-B distance of 1.718

Å.[25] The closest approach of **sTr**$^{+}$ and **29** are 3.81 Å, which is well out of the range for any type of interaction and further emphasizes the weakly coordinating nature of the carborane anion. The structure of **29[sTr**$^{+}$**]** is unique as no example of hydridic **3** has ever been isolated with a trityl cation.

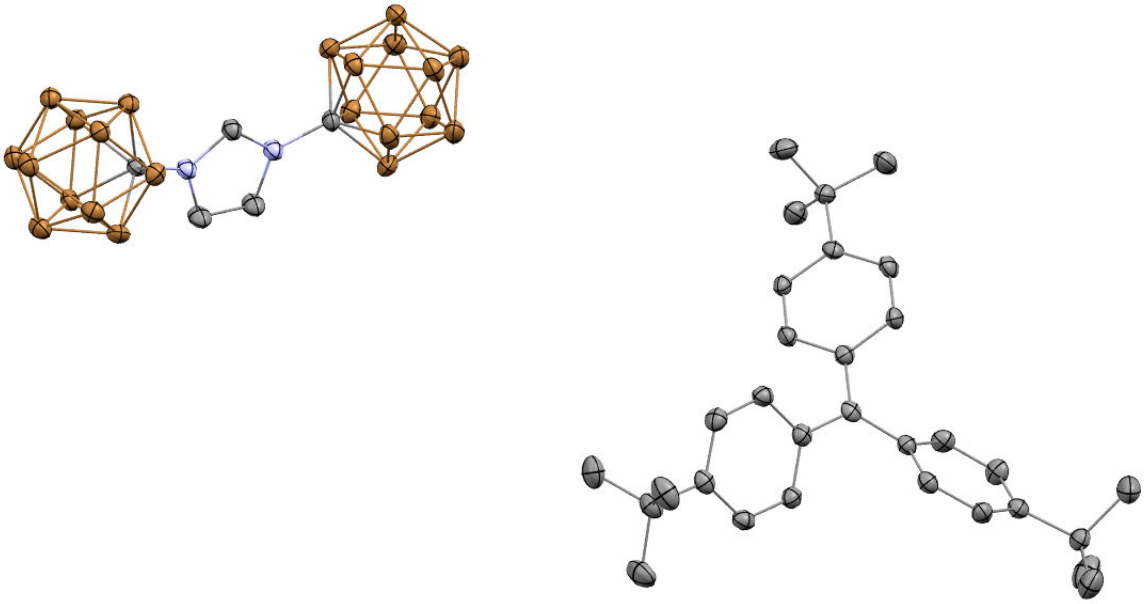

Figure 6-3 Solid state structure of **29[sTr**$^{+}$**]**. The closest contact to the trityl cation is 3.81Å away. Hydrogen atoms have been omitted for clarity. Color code: B = brown, C = gray, N = blue.

6.3 Reactivity of an Anionic Mesityl/Carboranyl N-bound Carbenoid with **sTr**

Knowing that the **sTr** cation is compatible with the N-bound carborane anion, we now wanted to see if it was possible to generate a carbene carbocation ion pair. To achieve this we chose to react monoanionic NHC, **35[Li**$^{+}$**]**, with **sTr[BF4**$^{-}$**]** in a 1:1 ration using F-C_6H_5 solvent. We chose to test this molecule first; compared to **30**, as the steric pressure associated with the carbene carbon of **35[Li**$^{+}$**]** is less than that associated with the carbene carbon of **30**. Another advantage of using **35** is that it is a mono anion

whereas NHC **30** is a dianion, thus **35** will only be able to have one trityl cation where as **30** could have one or two trityl cations.

Upon mixing a 1:1 ratio of non-colored **35[Li$^+$]** and highly-colored **sTr[BF$_4^-$]** in F-C_6H_5 solvent a slow loss of color was observed. After optimizing the conditions, the reaction was found to be much quicker when using **sTrCl** and **35[K$^+$]** in C_6H_6 solvent as **35[K$^+$]** has better solubility than **35[Li$^+$]**. Thus, by monitoring a 1:1 reaction of **35[K$^+$]** and **sTrCl** in C_6D_6 solvent in a J-Young tube, the reaction was found to be complete within minutes, however it generated a multitude of signals in the ^{1}H NMR spectrum, Figure 6-20. The ^{1}H NMR spectrum displayed six upfield aliphatic signals (0 – 3 ppm) and eight downfield olefinic and aromatic signals (5 – 8 ppm). Upon integration of the six aliphatic signals, the singlets at 0.96, 1.12 and 1.43 each integrated to nine protons while the remaining three singlets at 1.38, 1.86 and 2.03 each integrated to three protons. Interpreting these singlets as three non-equivalent *tert*-butyl methyls and three non-equivalent methyl suggested the formation of single product.

Careful analysis of the signals between 5 – 6 ppm in methylene chloride-d_2 revealed a doublet at 5.52 ppm with an integration of 1H and a coupling constant of 10.3 Hz indicative of a vicinal proton with the classical cis coupling constant.[36] The other proton of the *cis* system was located at 5.23 ppm and displayed a doublet of doublets with an integration of 1H. One of the coupling constants was the expected 10.3 Hz and the other was found to be 1.0 Hz, which is typical for a ^{4}J "W coupling" suggesting that this proton was adjacent to the *tert*-butyl position on the **sTr** ring. The coupled proton that was found to be "W coupling" with a coupling constant of 1 Hz was located at 5.73 ppm and integrated to 1H as well. The splitting pattern for this proton was a doublet of doublets with a coupling constant of 1 Hz and 5.5 Hz. The 5.5 Hz coupling constant raised the question of whether this coupling was due to vicinal *cis* coupling. This did not seem likely as the classical vicinal *cis* coupling constant is around 10 Hz ± 4 Hz.[36] A plausible interpretation of this coupling constant would be a proton that was no longer part of an sp^2 hybridized system and perhaps attached to a sp^3 hybridized carbon. Indeed a ^{1}H-^{13}C HSQC NMR experiment found this proton to be attached to a carbon appearing at 37 ppm confirming the sp^3 hybridization of the carbon atom. This evidence suggests that an attack by the NHC nucleophile had occurred at the *ortho*-position of

one of the aryl rings of the **sTr** ring system. This was unexpected and seemed unlikely given the steric congestion associated with **sTr** and **35**, however unlikely, this was consistent with the given NMR data and we proposed **55**, scheme 6-3.

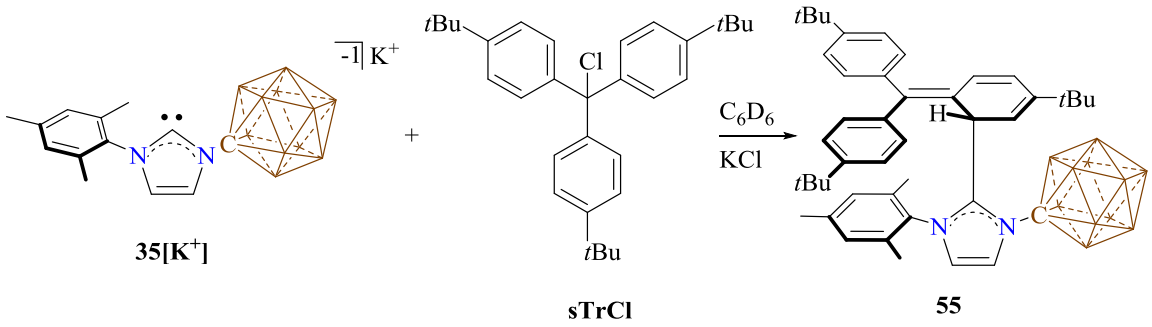

Scheme 6-3 Reaction of **35[K$^+$]** and **sTrCl** furnishing **55**. *t*Bu = *tert*-butyl, Mes = 1,3,5-trimethylphenyl.

To substantiate this claim, we decided to perform a single crystal X-ray diffraction study on **55**. Single crystals suitable for X-ray diffraction were grown by heating a saturated NMR tube containing **55** in benzene to reflux then letting the tube cool to room temperature. The solid-state structure confirmed the connectivity of **55** and thus the proposed structure, Figure 6-4. The bond lengths of the attacked ring system are 1.5208(19) for C1-C2, 1.336(2) for C2=C3, 1.464(2) for C3-C4, 1.345(2) for C4=C5, 1.4599(19) for C5-C6 and 1.528(2) for C6-C1 confirming the broken aromaticity of the ring, average C-C bond lengths for other two rings is 1.391 Å where C-C max and C-C min is 1.398 and 1.382 Å respectively. The C6-C7 bond length is in range for a typical C-C double bond with a length of 1.3572(19) Å which is drastically shorter than the other two C7-C_{Ar} bond lengths (avg = 1.491(2) Å). Surprisingly the C1-C8 bond length is in range for a common C-C single bond at 1.5086(18) Å. To the best of our knowledge this is the first example of a non-radical based *ortho*-addition to a trityl cation.[37]

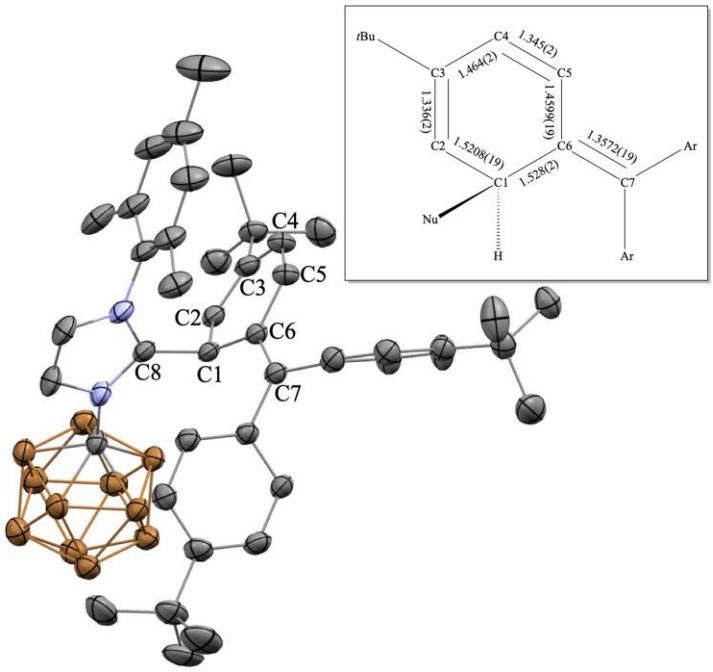

Figure 6-4 X-ray structure of **55**. Hydrogen atoms have been omitted for clarity. Color code: B = brown, C = gray, N = blue. Inset bond lengths are in Å. Ar = 4-*tert*-butylphenyl.

6.4 Reactivity of a Dianionic Bis Carboranyl N-bound Carbenoid with **sTr**$^+$

Increasing the steric pressure of the nucleophile we now wanted to test dianionic lithium NHC **30**. Thinking about the reactivity of **30** with **sTr[BF$_4^-$]**, one could imagine two possible products, the mixed salt **30[Li$^+$][sTr$^+$]** and the pure salt **30[2sTr$^+$]**. In this case we choose to target the mixed salt **30[Li$^+$, sTr$^+$]** because the Li$^+$ cation should further help protect the nucleophilic carbene carbon by coordination to the lone pair, Scheme 6-4. This coordination is evident in the crystal structure of **30** where one of the Li$^+$ ions is bound to the carbene carbon (2.110(2) Å). The coordination of Li$^+$ to the carbene carbon even persist in the solution-state, this is evident by an upfield shift in the ^{7}Li NMR spectrum at -0.52 ppm.[25]

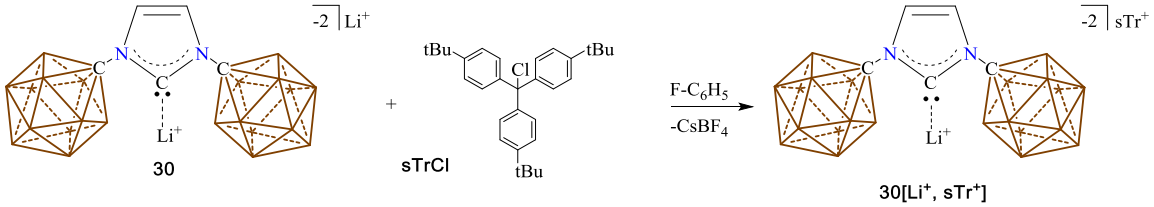

Scheme 6-4 Reaction of **30** and **sTrCl** generating proposed **30[Li$^+$, sTr$^+$]**.

Mixing a 1:1 mixture of **30** with **sTr[BF$_4^-$]** in F-C_6H_5 solvent the reaction mixture begins highly colored (yellow-orange) but over time fades to a brownish suspension resulting in the formation of imidazolium **29**. When **sTr[BF$_4^-$]** is switched to **sTrCl** the reaction remains highly colored for a longer period of time. In an attempt to analyze the highly colored reaction mixture, ^{1}H NMR spectroscopy was employed in F-C_6D_5 solvent. However, the resonances in the ^{1}H NMR spectrum did not corroborate the solid-state structure, instead suggested imidazolium **29** and **sTrCl**.

In an attempt to understand the highly colored reaction mixture, crystals were grown of the highly colored filtrate (F-C_6H_5 filtrated was saturated with pentane and cooled to -30°C), which were suitable for a single crystal X-ray diffraction study. Multiple low-quality crystal structures suggested that, in the solid state, the desired carbene carbocation ion pair was being formed, Figure 6-5.

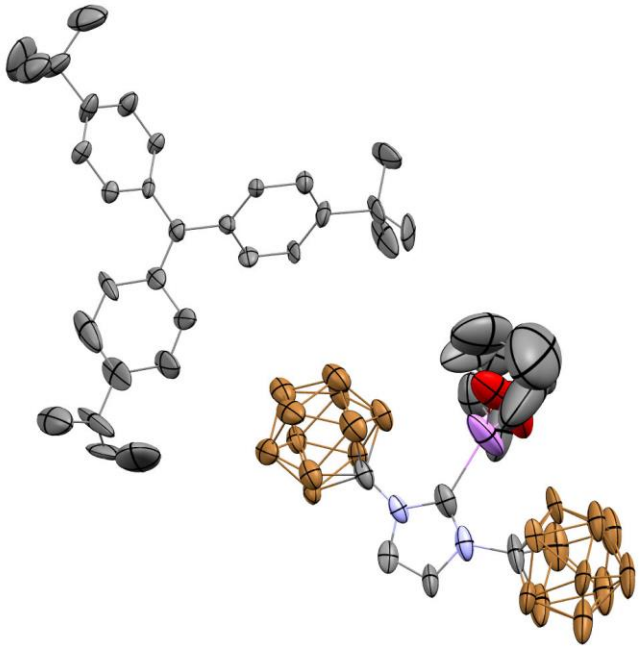

Figure 6-5 Low quality solid state structure of **30[Li$^+$, sTr$^+$]**.] Color code: Li = pink, B = brown, C = gray, N = blue, O = red.

Despite the crystallographic evidence, no conclusive solution state NMR data supported this structure. The ^{1}H-NMR spectrum displays a broad singlet at 8.70 (1H) and 7.00 (2H) which corresponds to the iminium and backbone protons of **29** respectively, meanwhile **sTrCl** displays a large singlet at 1.36 corresponding to the *tert*-butyl methyls and two downfield resonances at 7.37 and 7.35 ppm corresponding to the aryl protons. To ensure the deuterated solvent was anhydrous a ^{1}H NMR spectrum was taken of the NHC **30** in F-C_6D_5 which displayed one downfield (other than signals corresponding to protio fluorobenzene) singlet at 6.94 ppm corresponding to the backbone protons of the imidazolylidene core and no trace of imidazolium **29**, Figure 6-43 & Figure 6-45. Meaning if protons were introduced, they must have come from **sTrCl** or the reaction itself. Interestingly, if the mixture is cooled at -30°C for 24 hours new peaks corresponding to the trityl cation appears at 7.77, 7.45 and 1.44 ppm in the ^{1}H NMR spectrum and in the ^{13}C NMR spectrum at 36.55 and 30.18 ppm, Figure 6-33 & Figure 6-34, respectively. The signals corresponding to the trityl cation explain the highly colored nature of the mixture and are likely seen due to the decreased solubility of the imidazolium **29** and **sTrCl** mixture.

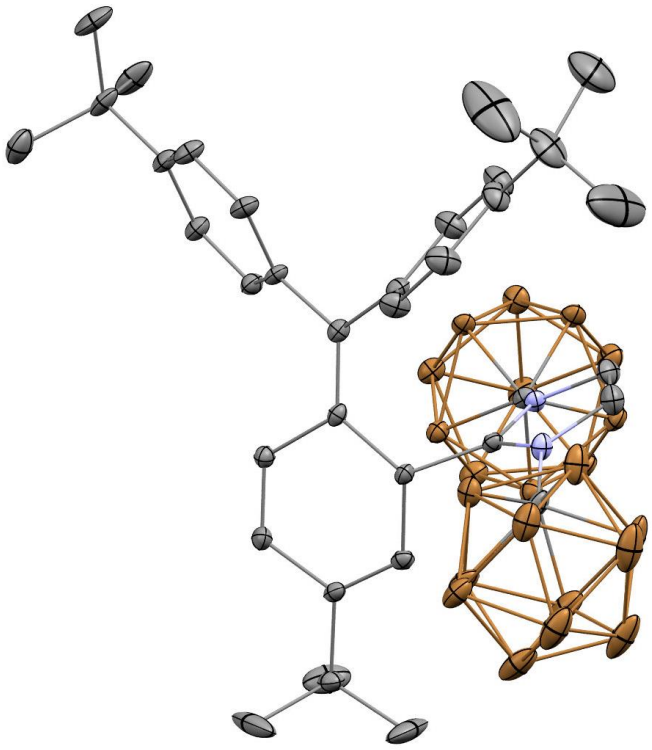

Figure 6-6 Solid state structure of **56**. Hydrogen atoms and **sTr**$^{+}$ counter ion omitted for clarity. Color code: B = brown, C = gray, N = blue.

When the same reaction was performed in *ortho*-difluorobenzene the crystals contained a few morphologically distinct green plates, these plates were manually separated from the crystal mass. Upon diffraction these crystalline plates displayed the same phenomena as **55** where the carbene carbon had attacked the *ortho*-position of one of the aryl rings of the trityl cation forming **56**, Figure 6-6. To corroborate this structure the remaining isolated crystals were analyzed by multinuclear NMR spectroscopy. The ^{1}H NMR spectrum of **56** displays similar characteristic resonances as **55** (6.43 ppm (d, ^{3}J = 2.5 Hz), 6.43 ppm (d, ^{3}J = 10.8 Hz), 6.08 ppm (d, ^{3}J = 10.8 Hz), 3.35 ppm (d, ^{3}J = 2.5 Hz)) but does not show the ^{4}J "W coupling" across the *tert*-butyl substituted carbon atom and the *ortho*-substituted carbon shows a small coupling of 2.5 Hz vs 5.5 Hz for **56** vs **55** respectively. This coupling was confirmed though a ^{1}H-^{1}H COSY NMR experiment which displayed two cross peaks at [5.35, 6.43] and [6.43, 5.35] ppm, Figure 6-42. The

^{1}H-^{13}C HSQC NMR spectrum displays the characteristic peak at [6.43, 39.0] ppm corresponding to the *ortho*-substituted carbon atom of the aryl ring, Figure 6-41. Interestingly the local C2v symmetry of the imdazolium core has been broken and two unique doublets (6.96 ppm, $^{3}J(H,H)$ = 2.4 Hz; 6.90 ppm, $^{3}J(H,H)$ = 2.4 Hz) are seen in the ^{1}H NMR spectrum as well as the ^{13}C NMR spectrum were two carborane carbons are located at 81 and 80 ppm. To arrive at such a product, suggest that the NHC **30** undergoes a halide abstraction from **sTrCl** and forms an ion pair with **sTr**$^{+}$ and then reacts further to generate **54**, Scheme 6-5. One plausible cause of protonation of NHC **30** to imidazolium **29** is if NHC **30** deprotonates the hydrogen atom on the sp^{3} hybridized carbon restoring aromaticity to the ring.

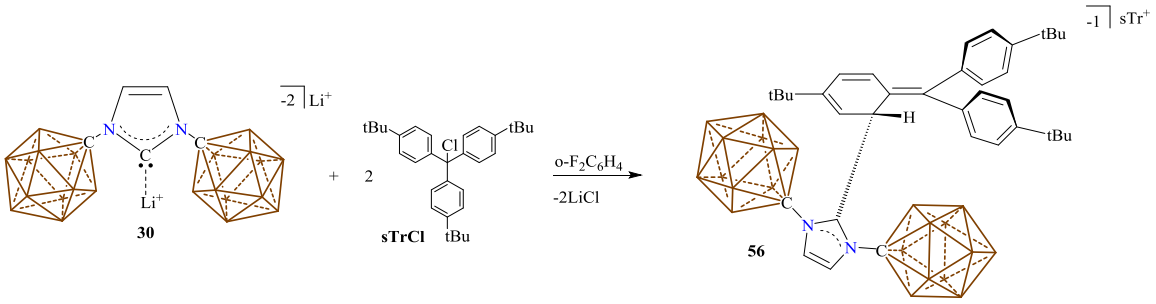

Scheme 6-5 Formation of **56**.

6.5 Conclusion

In conclusion we have demonstrated that it is possible to generate a stable trityl cation with the hydridic carborane anion **3** in the form of **29[sTr**$^{+}$**]**. Upon reaction of mono anionic NHC **35[K**$^{+}$**]** with **sTrCl** we have fully characterized a new *ortho*-substituted adduct **55**. Investigating the reaction of dianionic NHC **30** with **sTrCl** we have identified a similar *ortho*-substituted product **56**. We are currently investigating the potential of forming a carbenoid carbocation ion pair by utilizing the halogenated variants of the 12 vertex carborane **3** and ten vertex carborane **4**.

6.6 Experimental

General Considerations:

All manipulations were carried out using standard Schlenk or glovebox techniques under an argon or dinitrogen atmosphere unless otherwise stated. Dry solvents were obtained via distillation under argon from potassium (benzene-d_6), phosphorus pentoxide (fluorobenzene, fluorobenzene-d_5) or calcium hydride (methylene chloride-d_2). Benzene, toluene, pentane and hexane were collected from a solvent purification system by SG Waters USA, LLC utilizing a fifteen-minute argon sparge followed by passage though activated aluminum. Cesium 1-amino-1-carba-*closo*-undecaborate **3[Cs$^+$]** was prepared following the procedure by Jelínek and co-works.[38] The dianionic carbene **30** and anionic carbene **35** was prepared via the El-Hellani[25] and Asay[26] route respectively. Super trityl chloride, 1-[Bis(4-*tert*-butylphenyl)(chloro)methyl]-4-*tert*-butylbenzene, was prepared via the Bosset route.[34] Super trityl BF_4, tris(4-(*tert*-butyl)phenylmethylium tetrafluoroborate, was prepared via modified Arnett route, *vide infra*, for convenience the spectra are reproduced.[39] Unless specifically stated, reagents were purchased from commercial vendors and used without further purification. Nuclear magnetic resonance (NMR) spectroscopy was carried out using: Bruker Avance 300 MHz, Bruker NEO 400 MHz, Bruker Avance 600 MHz, Varian Inova 300 MHz, Varian Inova 400 MHz or Varian Inova 500 MHz spectrometers. NMR chemical shifts are reported in parts per million (ppm) with ^{1}H and ^{13}C chemical shifts referenced to the residual non-deutero solvent. The ^{11}B NMR chemical shifts were externally referenced to BF_3•OEt_2. The ^{11}B-^{1}H coupling constants from ^{11}B spectra are reported when possible. High-resolution mass spectrometry (HRMS) was collected on an Agilent Technologies 6210 (TOF LC/MS) featuring a multimode ESI/APCI with direction injection. Fourier transform infrared spectroscopy was recorded on a Bruker ALPHA interferometer in a glove box under an Argon atmosphere.

Modified Synthesis of Super Trityl Tetrafluoroborate, **sTr[BF_4^-]**:

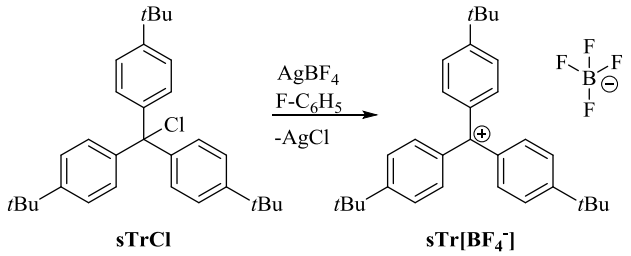

sTrCl **sTr[BF_4^-]**

Scheme 6-6 Modified synthesis of **sTr[BF_4^-]**.

A glass scintillation vial was equipped with a stir bar and loaded with crystalline super trityl chloride **sTrCl** (564 mg, 1.26 mmol) and fluorobenzene (10 mL). The stirring suspension was boiled until all the super trityl chloride had dissolved. The solution was cooled until a precipitate started to form at which point a solution of silver tetrafluoroborate (246 mg, 1.26 mmol) in fluorobenzene (2 mL) was added dropwise yielding an orange suspension containing a white precipitate. The suspension was stirred for thirty minutes at room temperature, at which point solid silver chloride was filtered off. The solid was washed with fluorobenzene (2 x 1 mL) and the combined filtrates were pumped down to dryness. The orange solid was washed with benzene (3 x 5 mL), furnishing super trityl tetrafluoroborate, tris(4-(*tert*-butyl)phenyl)methylium tetrafluoroborate, **sTr[BF_4^-]**, (550 mg, 87 % yield). The NMR data matched that reported in the literature.[39] ^{1}H NMR (400 MHz, methylene chloride-d_2, 25°C): δ = 7.87 (m, 2H), 7.61 (m, 2H), 1.48 (s, 27H). ^{13}C[^{1}H] NMR (100 MHz, acetonitrile-d_3, 25°C): δ = 206.2, 169.2, 143.1, 138.6, 128.4, 37.4, 30.9 ppm. ^{11}B NMR (96 MHz, acetonitrile-d_3, 25°C): δ = -0.9 ppm. ^{19}F NMR (376 MHz, acetonitrile-d_3, 25°C): δ = -152.3.

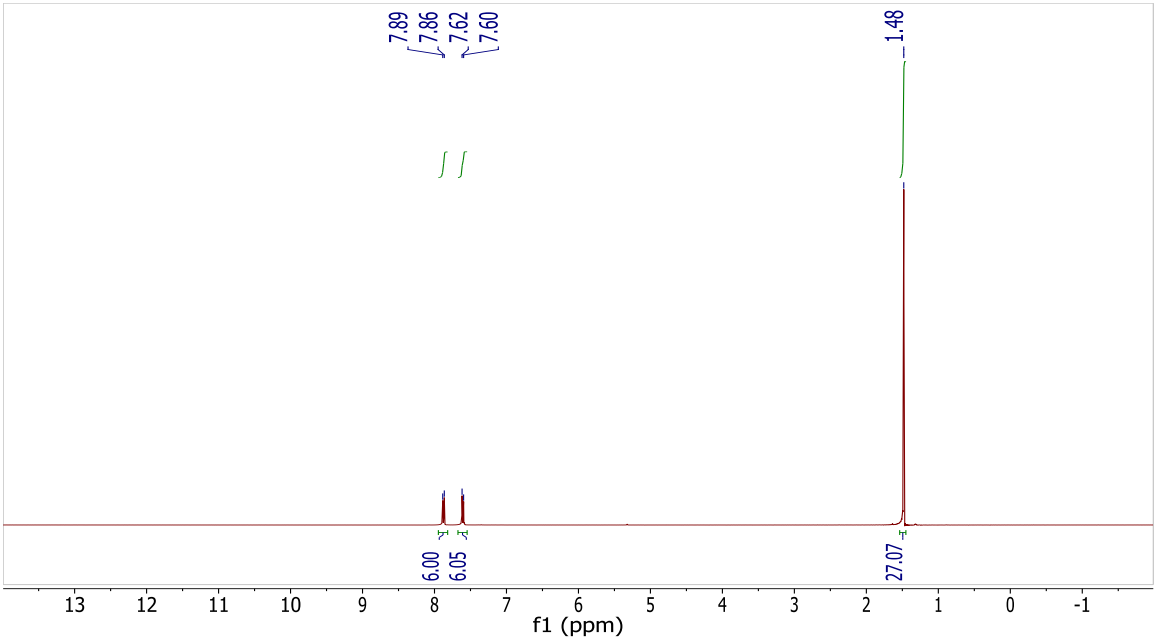

Figure 6-7 ^{1}H-NMR spectrum of **sTr[BF_4^-]** in dry methylene chloride-d_2.

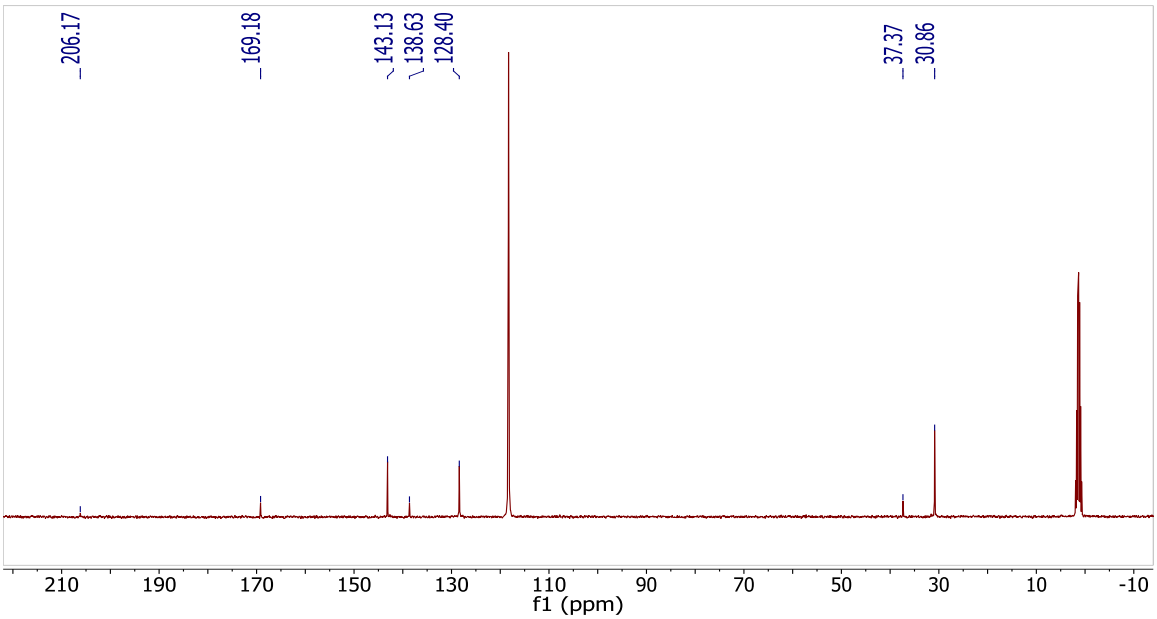

Figure 6-8 ^{13}C[^{1}H]-NMR spectrum of **sTr[BF_4^-]** in dry acetonitrile-d_3.

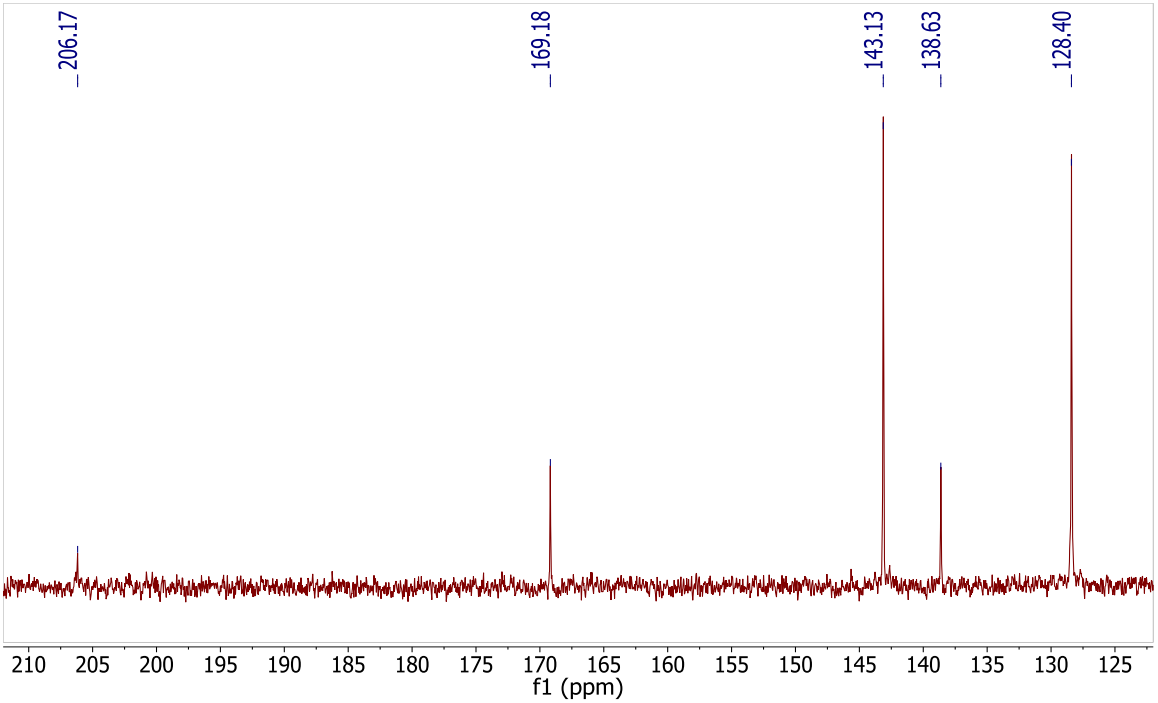

Figure 6-9 An expansion of the $^{13}C[^{1}H]$-NMR spectrum showing the downfield signals of **sTr[BF_4^-]**, the super trityl cation appears at 206 ppm.

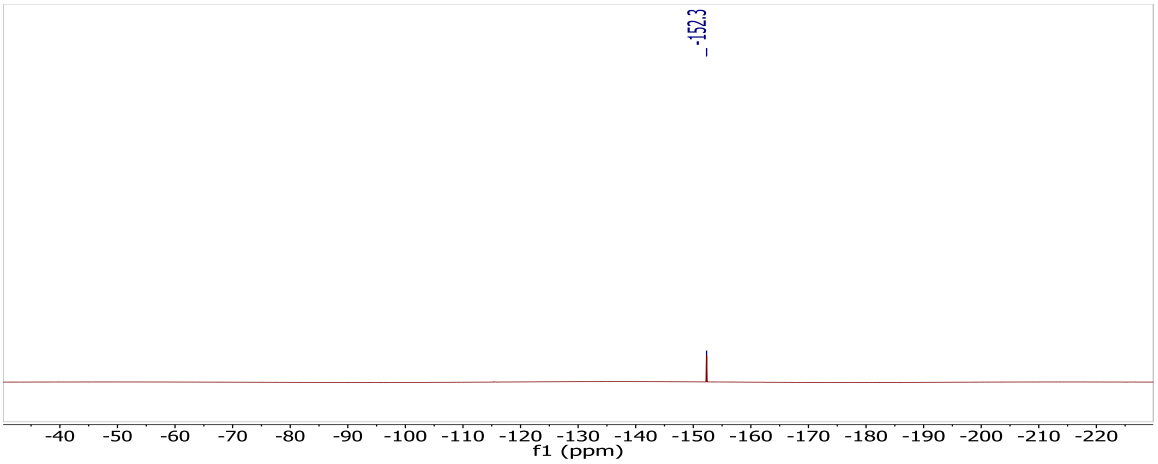

Figure 6-10 ^{19}F-NMR spectrum of **sTr[BF_4^-]** in dry acetonitrile-d_3.

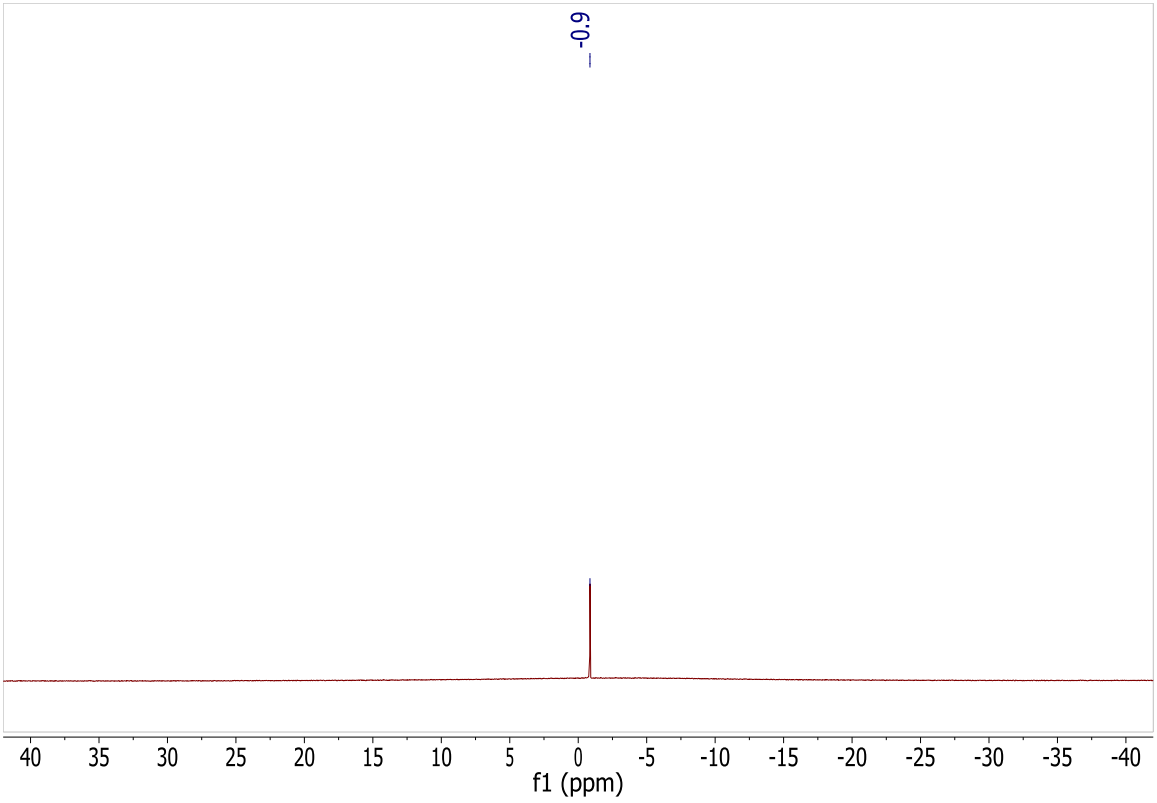

Figure 6-11 ^{11}B-NMR spectrum of **sTr[BF_4^-]** in dry acetonitrile-d_3.

Synthesis of Super Trityl Symmetrical Imidazolium, **29[sTr^+]:**

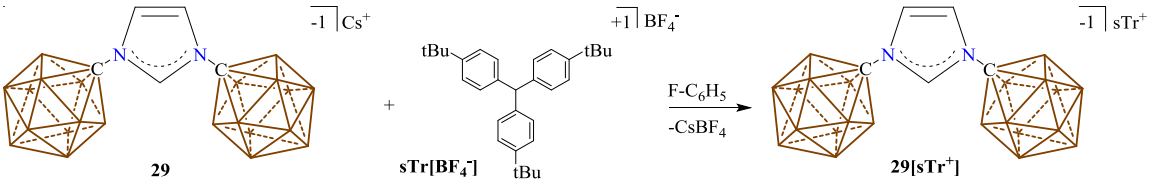

Scheme 6-7 Synthesis of **29[sTr^+]**.

A glass scintillation vial was loaded with cesium imidazolium **29** (51.4 mg, 106 μmol) and super trityl tetrafluoroborate, **sTr[BF_4^-]** (52.9 mg, 106 μmol) and the solids were suspended in fluorobenzene (2 mL). The reaction was stirred for 30 minutes then filtered. The highly colored, bright orange filtrate was pumped down to dryness, furnishing the title compound, **29[sTr^+]**, as an orange solid (78.6 mg, 97% yield). ^{1}H NMR (500 MHz, chloroform-d_1, 25°C): δ = 8.26 (t, $^3J(H,H)$ = 1.7 Hz, 1H), 7.86 (d, $^3J(H,H)$ = 8.5 Hz,

2H), 7.60 (d, $^{3}J(H,H)$ = 8.5 Hz, 2H), 7.17 (d, $^{3}J(H,H)$ = 1.7 Hz, 2H), 2.56-1.07 (bm, 22H, B-H), 1.48 (s, 27H). $^{1}H[^{11}B]$ NMR (300 MHz, chloroform-d_1, 25°C): δ = 8.26 (1H), 7.86 (2H), 7.60 (2H), 7.17 (2H), 1.97 (B-H), 1.67 (B-H), 1.48 (27H). $^{11}B[^{1}H]$ NMR (96 MHz, chloroform-d_1, 25°C): δ = -5.1, -9.6, -10.6 ppm. ^{11}B NMR (160 MHz, chloroform-d_1, 25°C): δ = -5.1 (d, $^{1}J(H,B)$ = 119.0 Hz), -9.6 (d), -10.6 (d). $^{13}C[^{1}H]$ NMR (126 MHz, chloroform-d_1, 25°C): δ = 203.6, 169.2, 142.0, 137.4, 133.7, 128.12, 121.9, 75.2, 37.1, 30.1 ppm. IR (KBr pellet, 25°C): ~2600 cm^{-1} (B-H stretch).

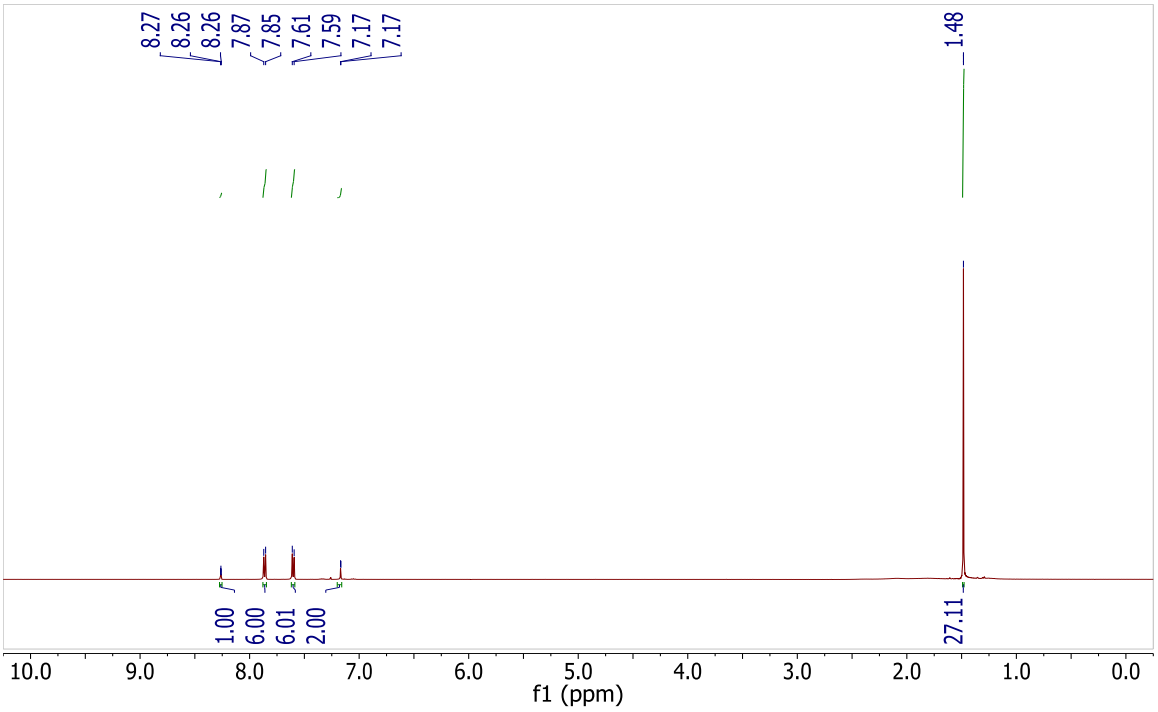

Figure 6-12 ^{1}H-NMR spectrum of **29[sTr^{+}]** in dry chloroform-d_1.

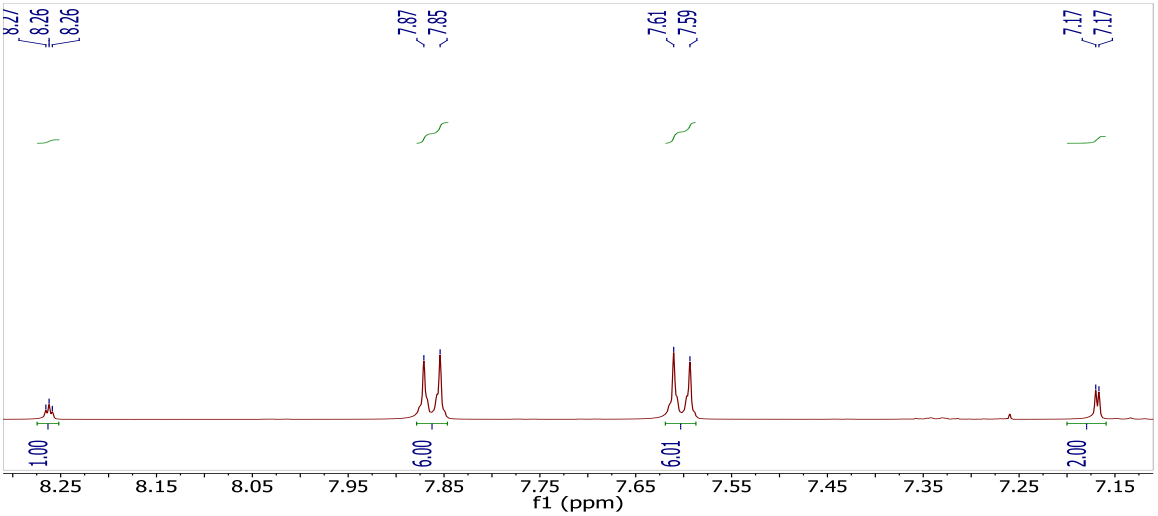

Figure 6-13 An expansion of the aromatic region in the ^{1}H-NMR of compound **29[sTr^{+}]** showing the J coupling. *Note: the small peak at 7.26 is chloroform-h_1 from the deuterated solvent.*

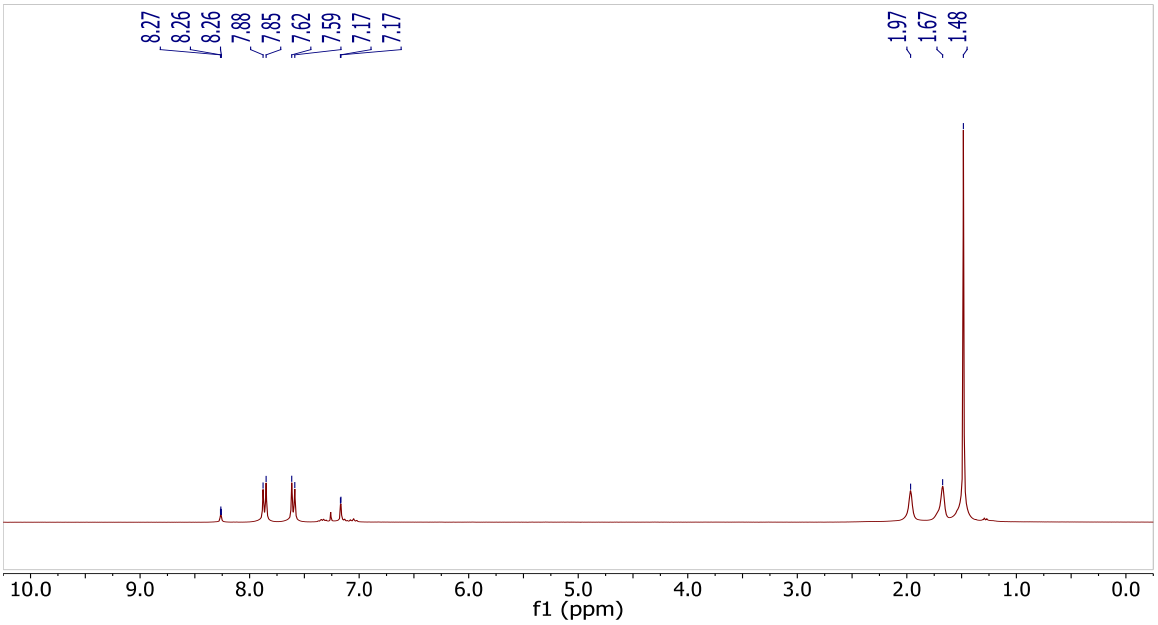

Figure 6-14 ^{1}H[^{11}B]-NMR spectrum of **29[sTr^{+}]** in dry chloroform-d_1. The boron hydrides appear at 1.97 and 1.67 ppm.

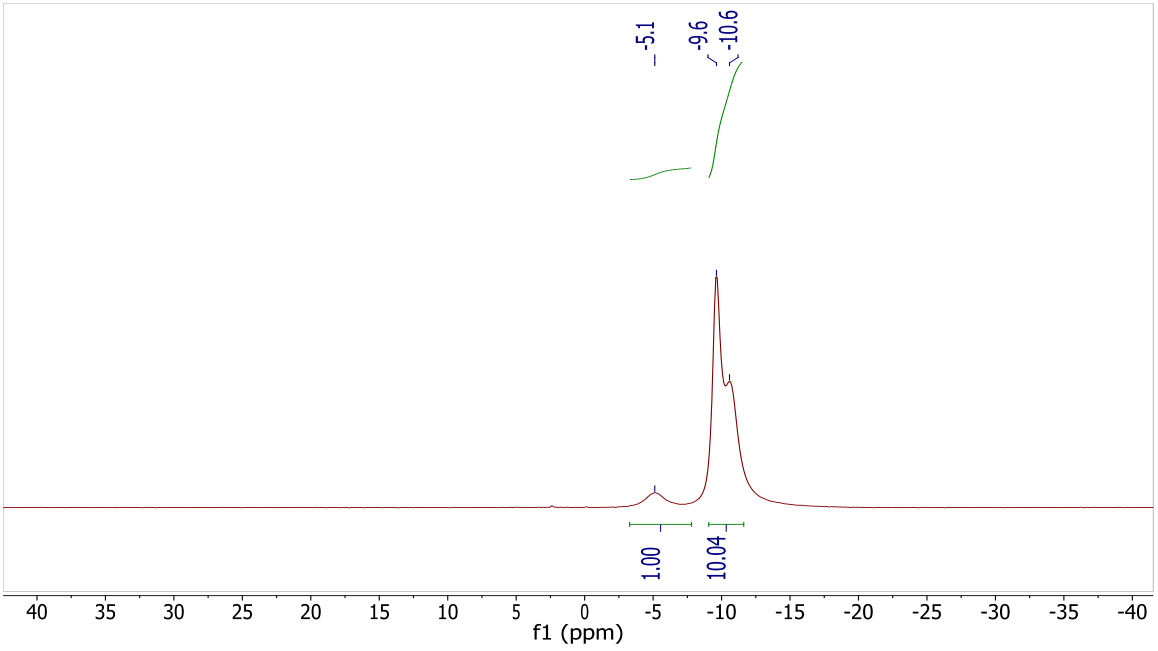

Figure 6-15 $^{11}B[^{1}H]$-NMR spectrum of 29[sTr^{+}] in dry chloroform-d_1.

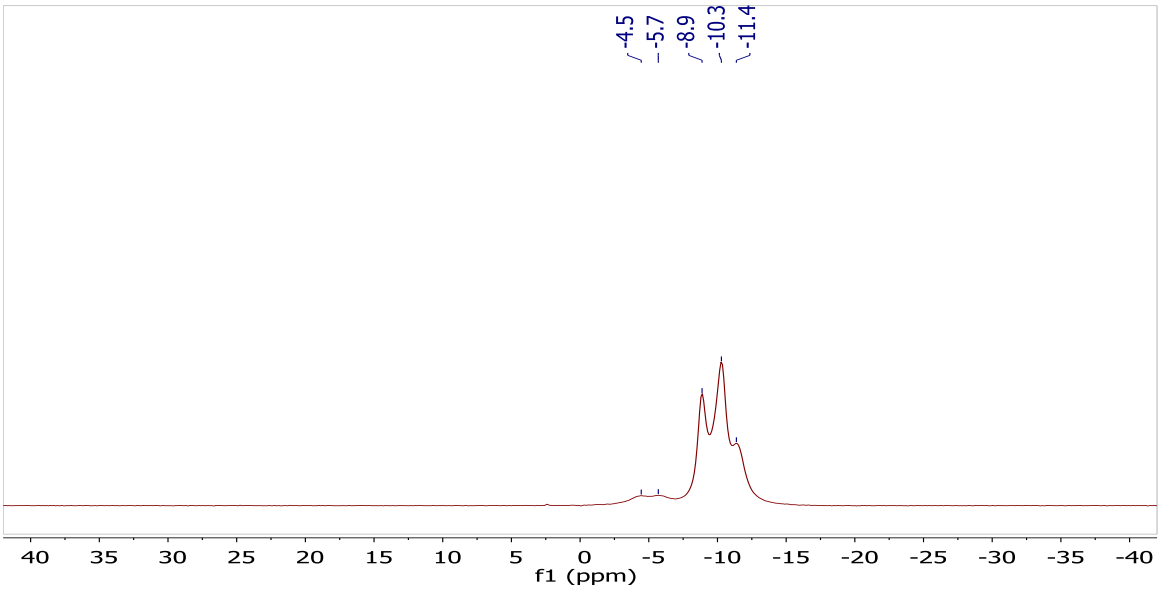

Figure 6-16 ^{11}B-NMR spectrum of **29[sTr^{+}]** in dry chloroform-d_1.

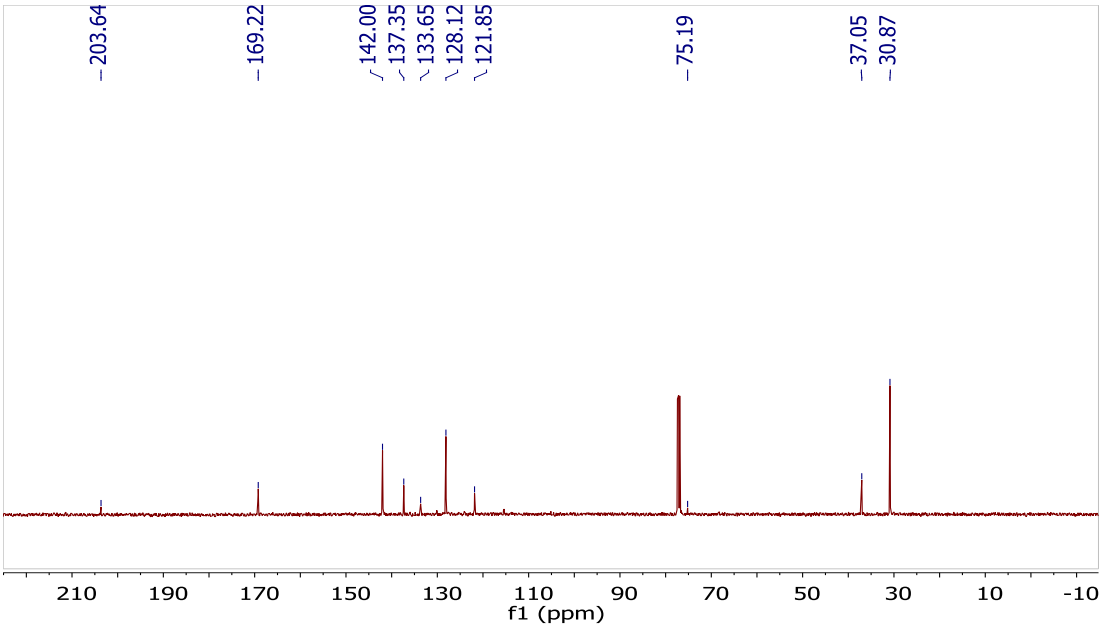

Figure 6-17 $^{13}C[^{1}H]$-NMR spectrum of **29[sTr^{+}]** in dry chloroform-d_1.

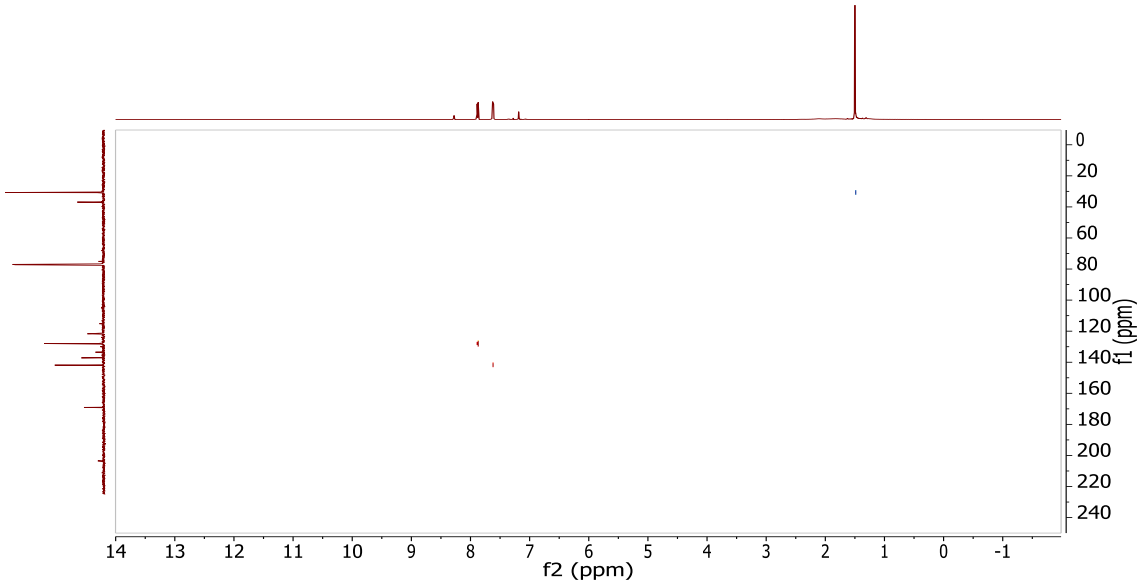

Figure 6-18 ^{13}C-^{1}H gHSQC-NMR spectrum of **29[sTr^{+}]** in dry chloroform-d_1.

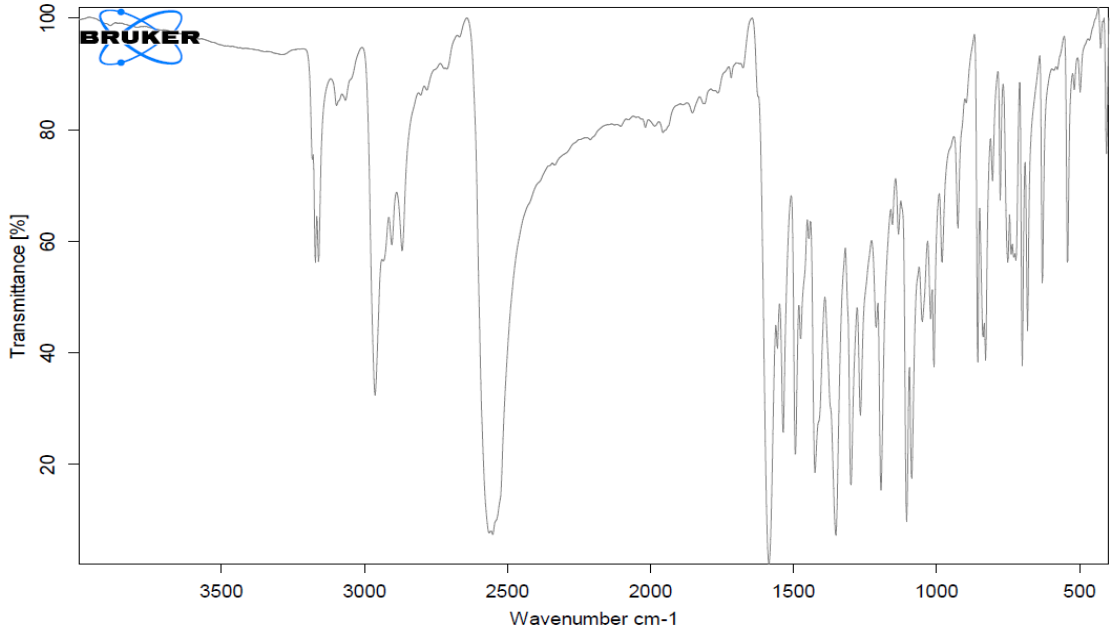

Figure 6-19 IR spectrum of **29[sTr$^+$]** in dry chloroform-d_1. The B-H stretches appear around 2600 wavenumbers.

Synthesis of *ortho* substituted adduct, **55:**

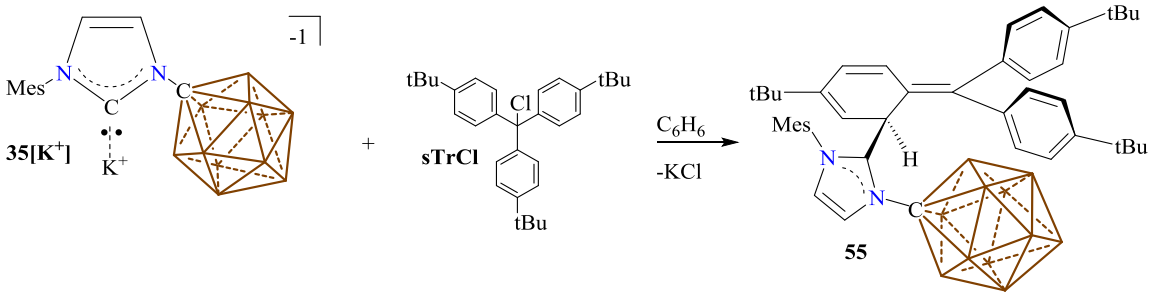

Scheme 6-8 Synthesis of **55**.

Method A:

A J-young tube was loaded **35[K$^+$]** (20.0 mg, 30.5 μmol), finely ground **sTrCl** (13.7 mg, 30.5 μmol) and dry deuterated benzene. The J-young tube was sealed then heated with a heat gun until all the

solids dissolved (*note: crystalline super trityl chloride dissolves in benzene upon heating*). The reaction was complete upon heating (quantitative yield by NMR).

Method B:

A glass scintillation vial was loaded with **35[K^+]** (265 mg, 405 μmol) and equipped with a stir bar and dry benzene (2 mL). A separate vial was loaded with **sTrCl** (181 mg, 405 μmol) and suspended in benzene (2 mL). The suspension of super trityl chloride was transferred to the carbene solution and the vial containing the super trityl chloride was washed with benzene (2 x 1 mL) and transferred to the carbene as well. The reaction was stirred for 1 hour at room temperature. After one hour the benzene solution was concentrated down to about 2 mL and toluene (8 mL) was added which dissolved all the solid (*note: no precipitation of KCl was noted*). The solution was concentrated down to about 3 mL and cooled to -30°C for 24 hours which furnished crystals suitable for X-ray diffraction. ^{1}H NMR (400 MHz, benzene-d_6, 25°C): δ = 7.65 (s, 1H), 7.31 (d, $^{3}J(H,H)$ = 7.9 Hz, 2H), 7.13 (d, $^{3}J(H,H)$ = 8.0 Hz, 2H), 6.97 (d, $^{3}J(H,H)$ = 8.0 Hz, 2H), 6.40 (d, $^{3}J(H,H)$ = 7.9 Hz, 2H), 6.39 (s, 1H), 6.13 (s, 1H), 6.10 (d, $^{3}J(H,H)$ = 4.8 Hz, 1H), 6.04 (d, $^{3}J(H,H)$ = 4.8 Hz, 1H), 5.73 (s, 1H), 5.67 (d, $^{3}J(H,H)$ = 10.1 Hz, 1H), 5.04 (d, $^{3}J(H,H)$ = 10.1 Hz, 1H), 3.38-0.91 (bm, 11H, B-H), 2.03 (s, 3H), 1.86 (s, 3H), 1.43 (s, 9H), 1.38 (s, 3H), 1.12 (s, 9H), 0.96 (s, 9H). ^{1}H NMR (400 MHz, methylene chloride-d_2, 25°C): δ = 7.93 (d, $^{3}J(H,H)$ = 2.3 Hz, 1H), 7.73 (m, 2H), 7.27 (m, 2H), 6.88 (s, 2H), 6.87 (m, 2H), 6.85 (d, 1H), 6.48 (m, 2H), 5.78 (d, $^{3}J(H,H)$ = 5.5 Hz, 1H), 5.73 (dd, $^{3}J(H,H)$ = 5.5 Hz, $^{4}J(H,H)$ = 1.0 Hz, 1H), 5.52 (d, $^{3}J(H,H)$ = 10.3 Hz, 1H), 5.23 (dd, $^{3}J(H,H)$ = 10.3 Hz, $^{4}J(H,H)$ = 1.0 Hz, 1H), 2.37-1.40 (bm, 11H, B-H), 2.28 (s, 3H), 2.26 (s, 3H), 1.67 (s, 3H), 1.37 (s, 9H), 1.30 (s, 9H), 1.06 (s, 9H). ^{13}C[^{1}H] NMR (125 MHz, methylene chloride-d_2, 25°C): δ = 152.6, 151.7, 151.4, 147.0, 142.2, 139.5, 138.5, 136.8, 134.9, 131.4, 131.0, 130.8, 129.1, 128.6, 127.3, 126.4, 125.6, 121.8, 120.4, 113.0, 79.8, 37.0, 35.3, 31.8, 28.9, 21.5, 19.8, 18.8, 17.9 ppm. ^{11}B[^{1}H] NMR (160 MHz, methylene chloride-d_2, 25°C): δ = -4.6, -11.0 ppm. ^{11}B NMR (160 MHz, methylene chloride-d_2, 25°C): δ = -4.6 ($^{1}J(H,B)$ = 147.7 Hz), -11.0 ($^{1}J(H,B)$ = 124.0 Hz). HRMS (negative mode ESI/APCI) $[M]^{-}$ m/z calc'd = 737.6093 : Found = 737.62228.

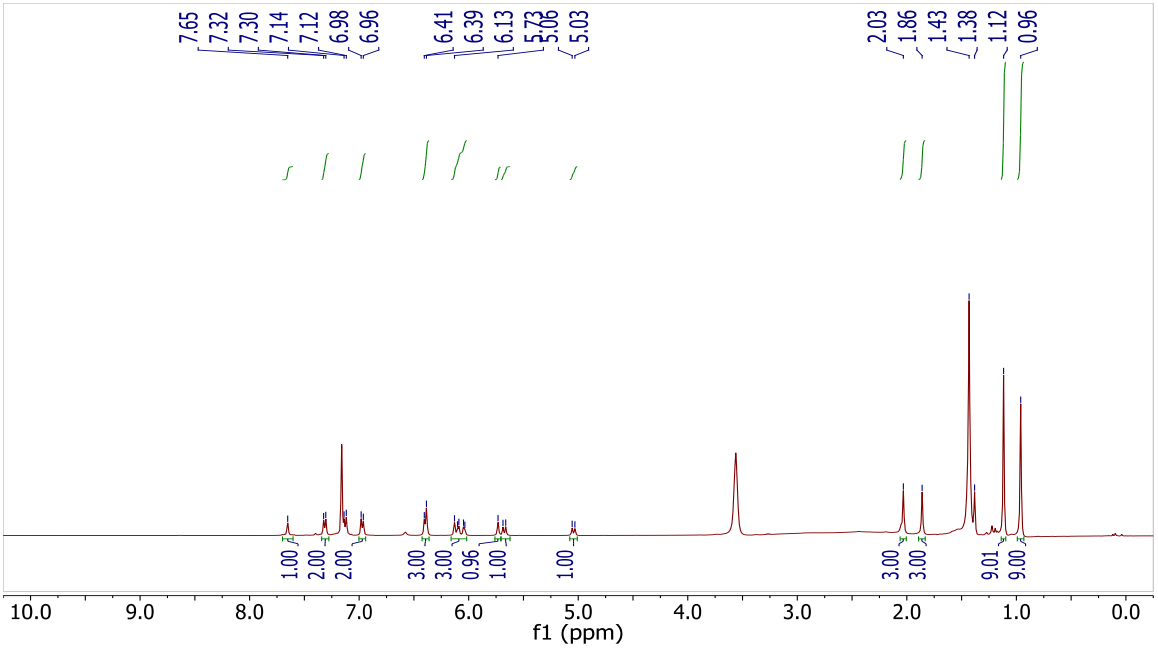

Figure 6-20 Crude ^{1}H-NMR spectrum of **55** in dry benzene-d_6. The peak at 3.6 and 1.4 ppm is due to THF coordinated to the potassium cation of NHC **35[K^{+}]**.

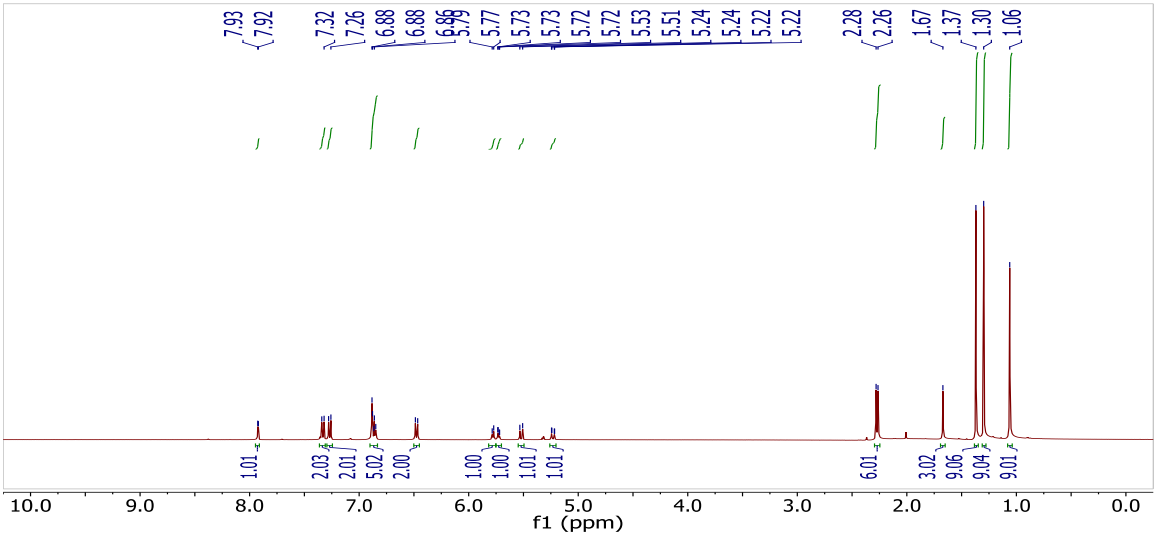

Figure 6-21 ^{1}H-NMR spectrum of **55** in dry methylene chloride-d_2.

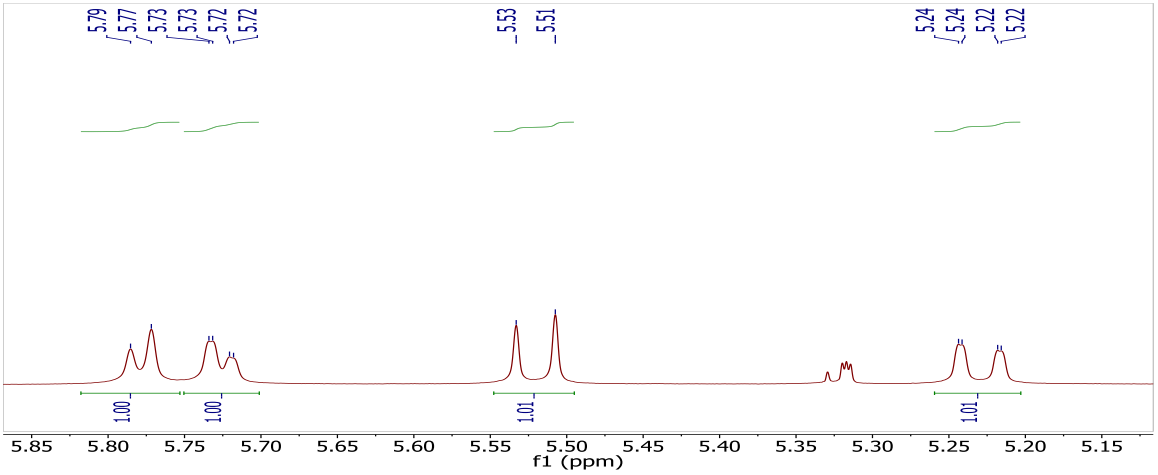

Figure 6-22 An expanded view of the olefin region of the ^{1}H-NMR of **55** in dry methylene chloride-d_2, showing the large cis coupling and the small long range coupling of the dearomatized protons. *Note: the peaks at 5.33 and 5.32 ppm are methylene chloride-h_2 and methylene chloride-d_1h_1 respectively.*

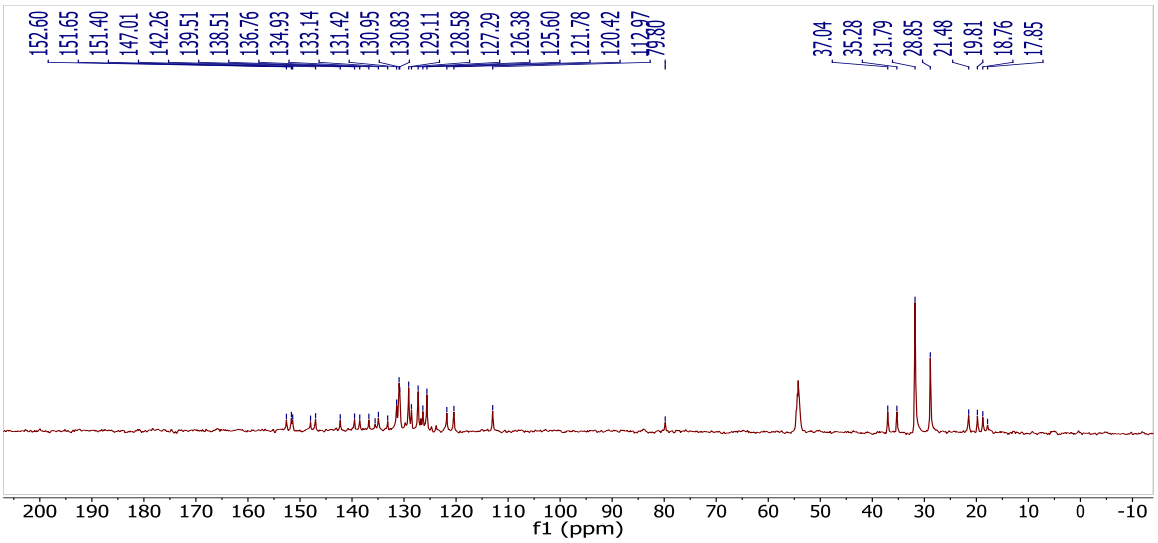

Figure 6-23 ^{13}C[^{1}H]-NMR spectrum of compound **55** in dry methylene chloride-d_2.

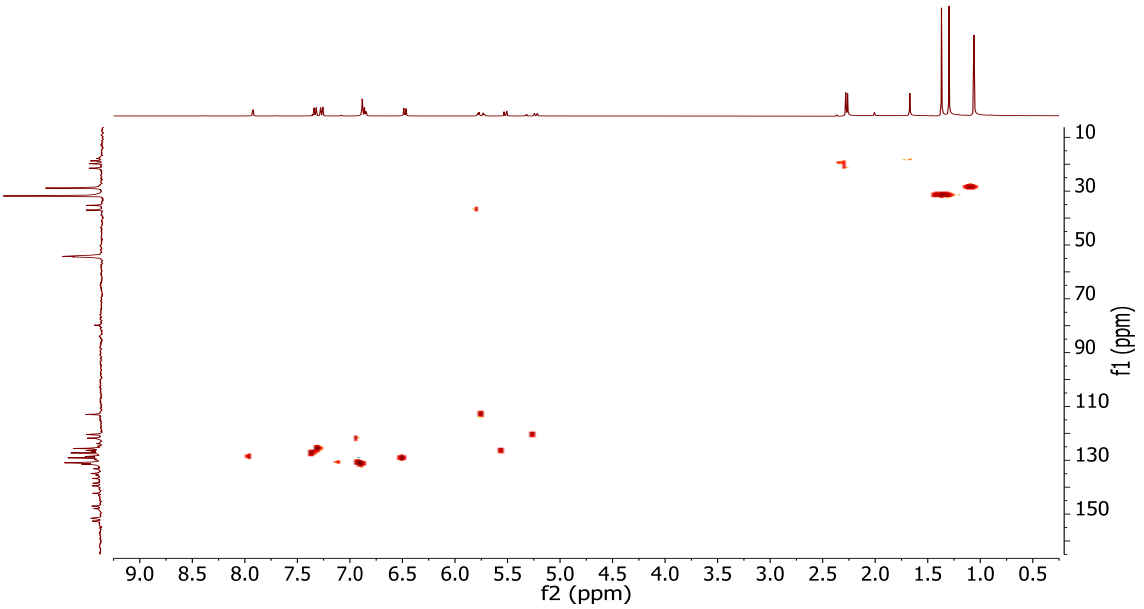

Figure 6-24 ^{13}C-^{1}H HSQC-NMR spectrum of compound **55** in dry methylene chloride-d_2. Note: the cross peak at (7.1 ppm, 130 ppm) is due to a trace amount of imidazolium.

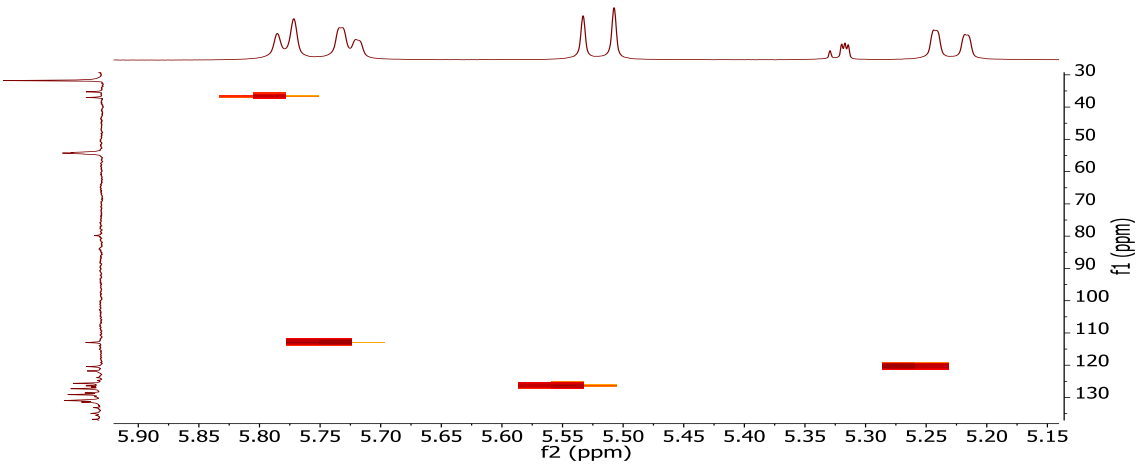

Figure 6-25 Expanded view of the olefin region of the ^{13}C-^{1}H HSQC-NMR spectrum of compound **55** in dry methylene chloride-d_2.

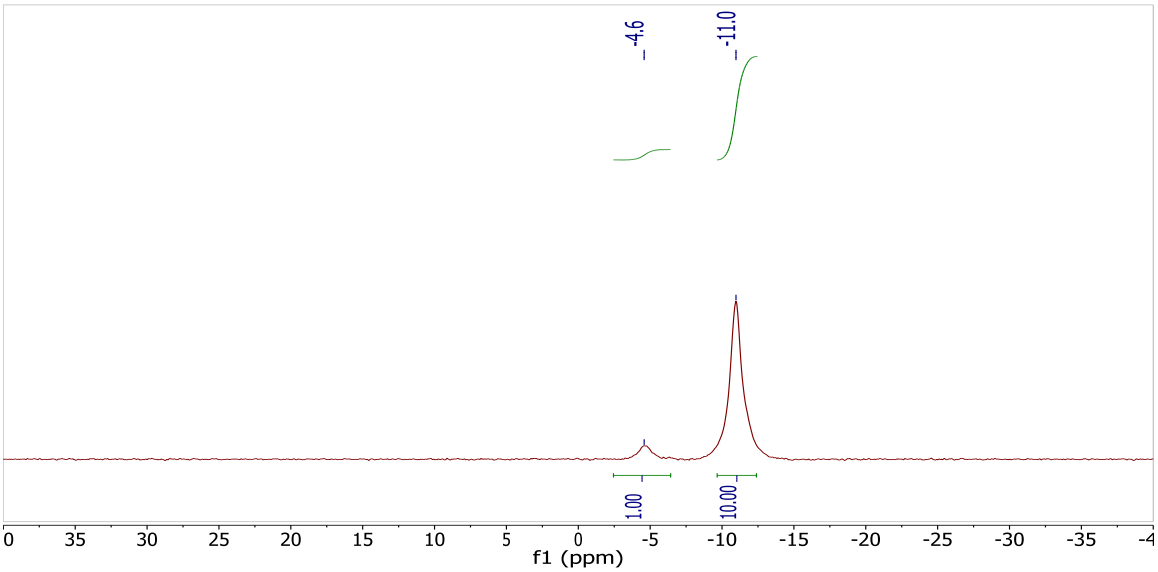

Figure 6-26 $^{11}B[^{1}H]$-NMR spectrum of compound **55** in dry methylene chloride-d_2.

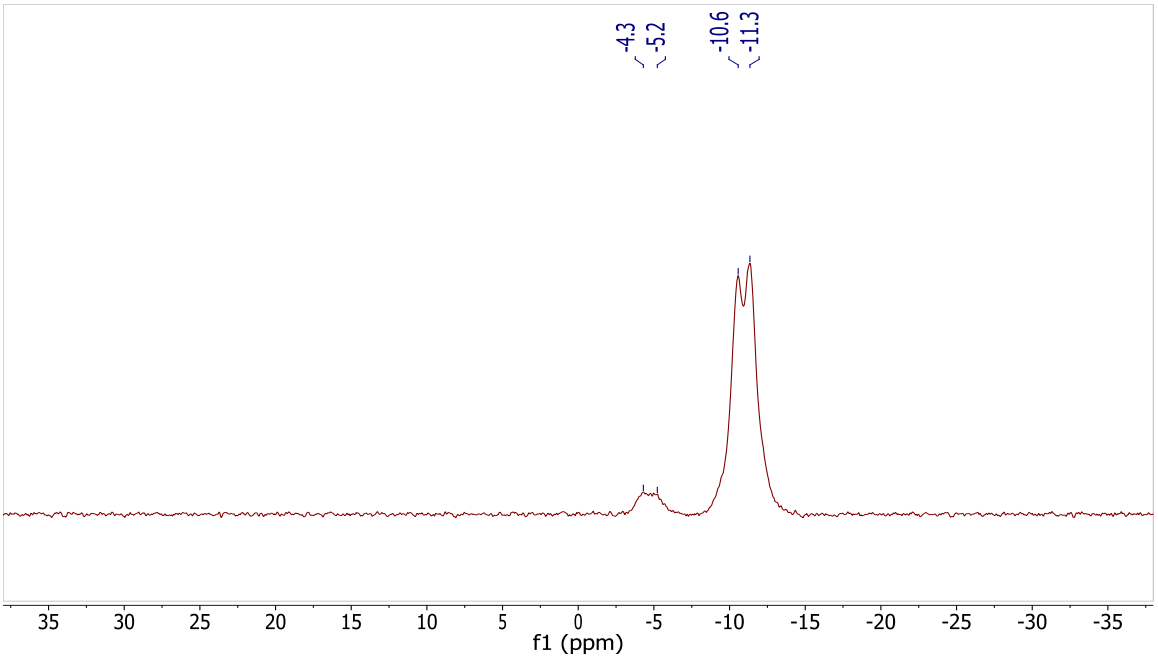

Figure 6-27 ^{11}B-NMR spectrum of compound **55** in dry methylene chloride-d_2.

Synthesis of crystalline **30[Li$^+$, sTr$^+$]:**

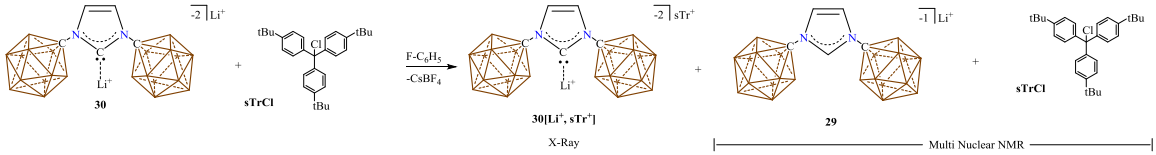

Scheme 6-9 Synthesis of the mixture **30[Li+, sTr+]** + **29** + **sTrCl**.

A glass scintillation vial was equipped with a stir bar and loaded with **30** (100 mg, 197 µmol) and suspended in F-C_6H_5. A separate scintillation vial was loaded with **sTrCl** (88 mg, 197 µmol) and suspended in F-C_6H_5 and added dropwise during which an immediate color change to yellow occurred. The reaction was stirred at room temperature for 15 minutes then the suspension was filtered and placed in the freezer. The resulting crystals were decanted and some were used for X-ray crystallography while others were used for NMR analysis. *NOTE: the crystals were separated to two containers, one for X-ray and the other for NMR analysis.* ^{1}H NMR (600 MHz, fluorobenzene-d_5, 25°C): δ = 8.70 (s, 1H), 7.37 (s, 6H), 7.35 (s, 6H), 7.00 (bs, 2H), 1.36 (s, 27H), 3.25-1.25 (bs, 22H) ppm. ^{11}B NMR (160 MHz, Fluorobenzene-d_5, 25°C): δ = -6.4, -10.9, -12.0. ^{13}C[^{1}H] NMR (125 MHz, Fluorobenzene-d_5, 25°C): δ = 151.3, 144.0, 134.2, 128.4, 125.7, 122.2, 83.8, 76.2, 34.9, 31.5 ppm.

NMR after cooling J-Young tube at -30°C for 24 hours: ^{1}H NMR (400 MHz, fluorobenzene-d_5, 25°C): δ = 8.70 (s, 1H), 7.77 (s), 7.45 (s), 7.37 (s), 7.35 (s), 7.00 (s), 1.44 (s), 1.36 (s), 3.25-1.25 (bs) ppm.

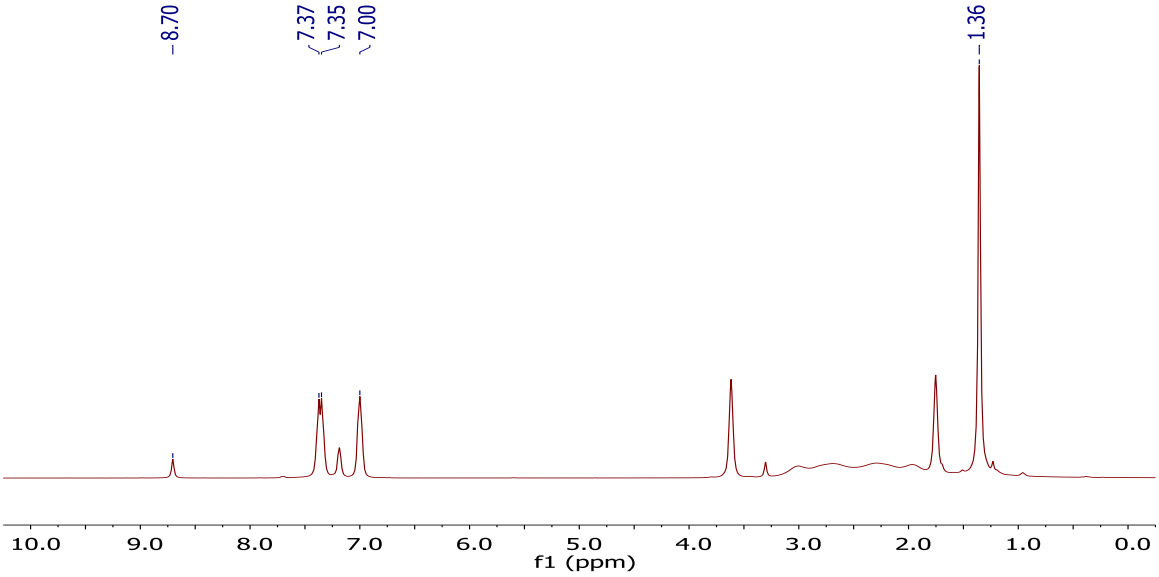

Figure 6-28 ^{1}H-NMR spectrum of crystalline mixture **29** and **sTrCl** in fluorobenzene-d_5. Note: the backbone protons of the imidazolium core overlap with the F-C_6D_5 solvent at 7.00 ppm.

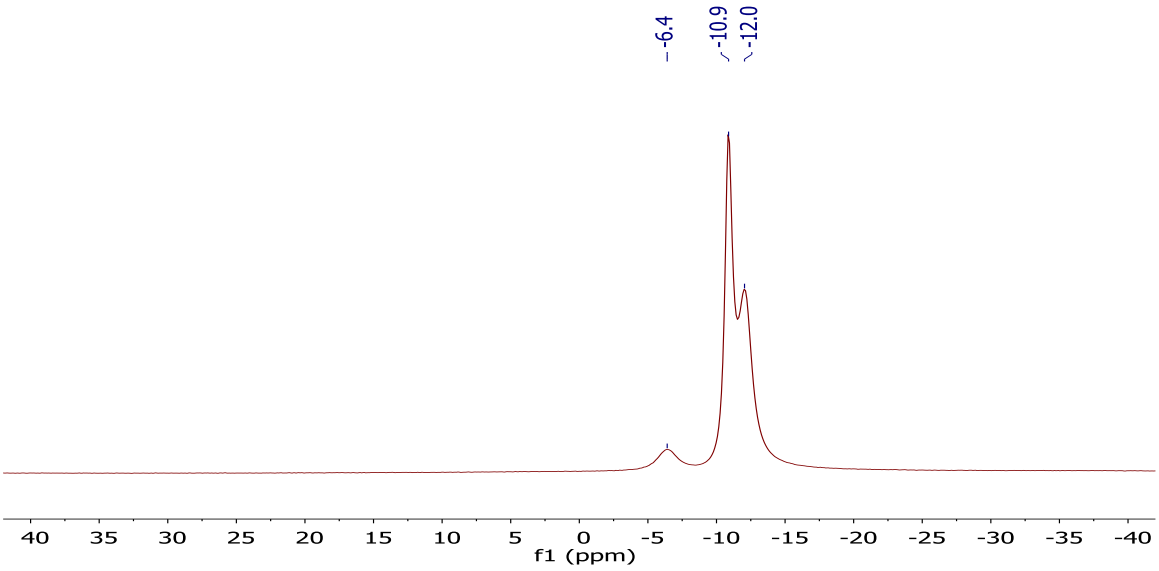

Figure 6-29 ^{11}B[^{1}H]-NMR spectrum of crystalline mixture **29** and **sTrCl** in fluorobenzene-d_5.

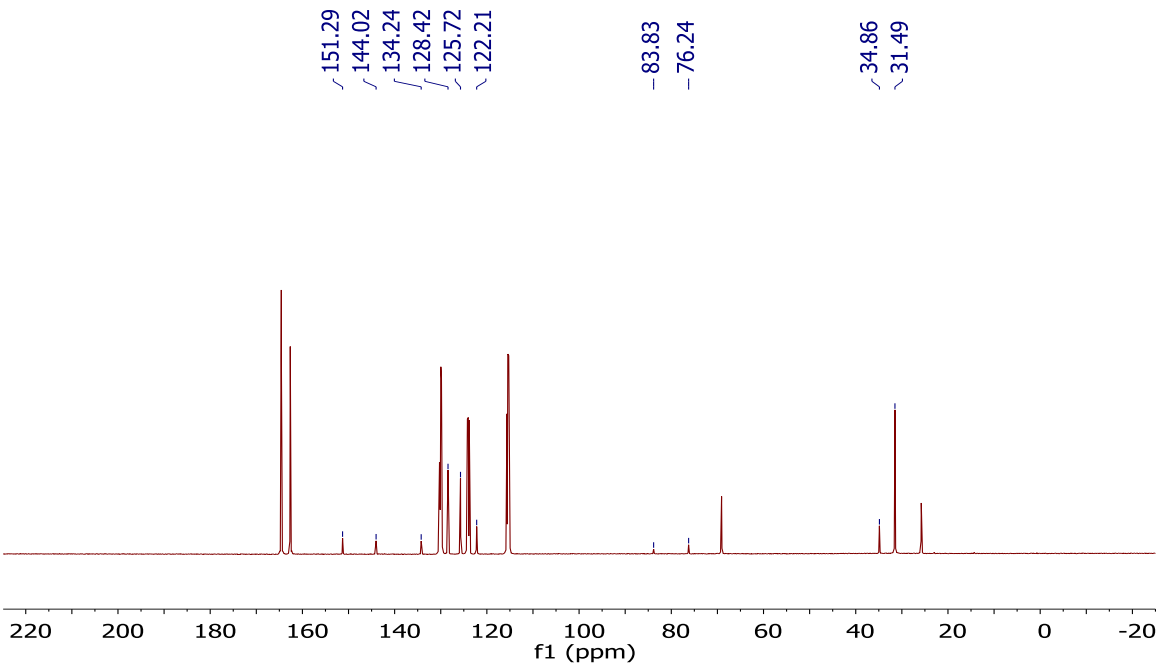

Figure 6-30 ^{13}C-NMR spectrum of crystalline mixture **29** and **sTrCl** in fluorobenzene-d_5. *Note: number of scans = 17,000.*

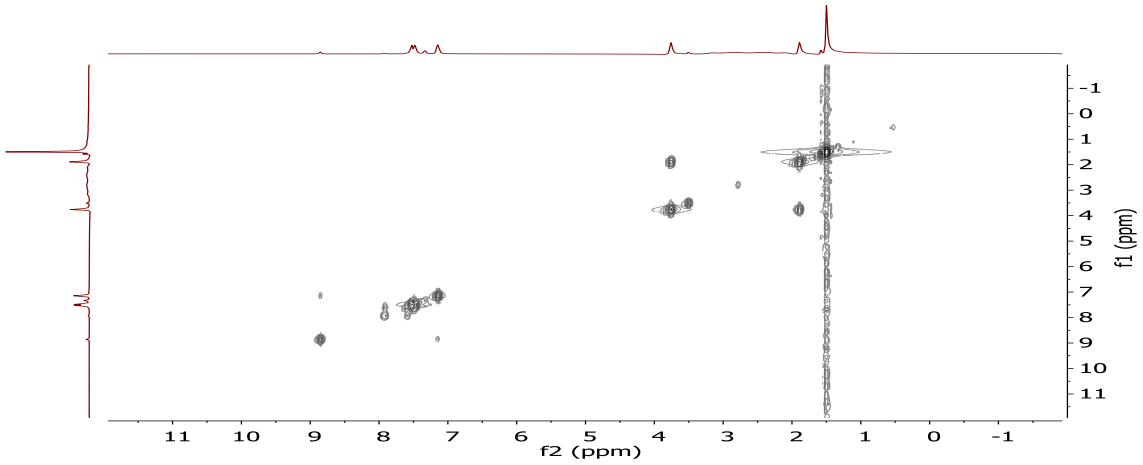

Figure 6-31 ^{1}H-^{1}H COSY-NMR spectrum of crystalline mixture **29** and **sTrCl** in fluorobenzene-d_5. Note: the cross peak at [8.70, 7.00] ppm and vice versa correspond to the imidazolium protons.

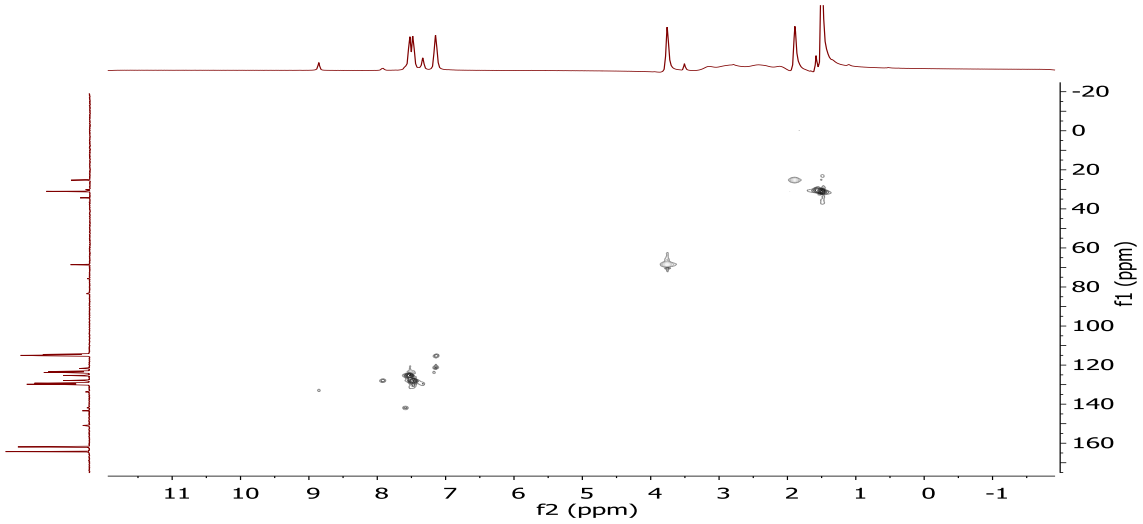

Figure 6-32 ^{13}C-^{1}H HSQC-NMR spectrum of crystalline mixture **29** and **sTrCl** in fluorobenzene-d_5. Note: the peak at [7.0, 122] ppm corresponds to the imidazolium backbone protons overlapping with the F-C_6D_5 solvent.

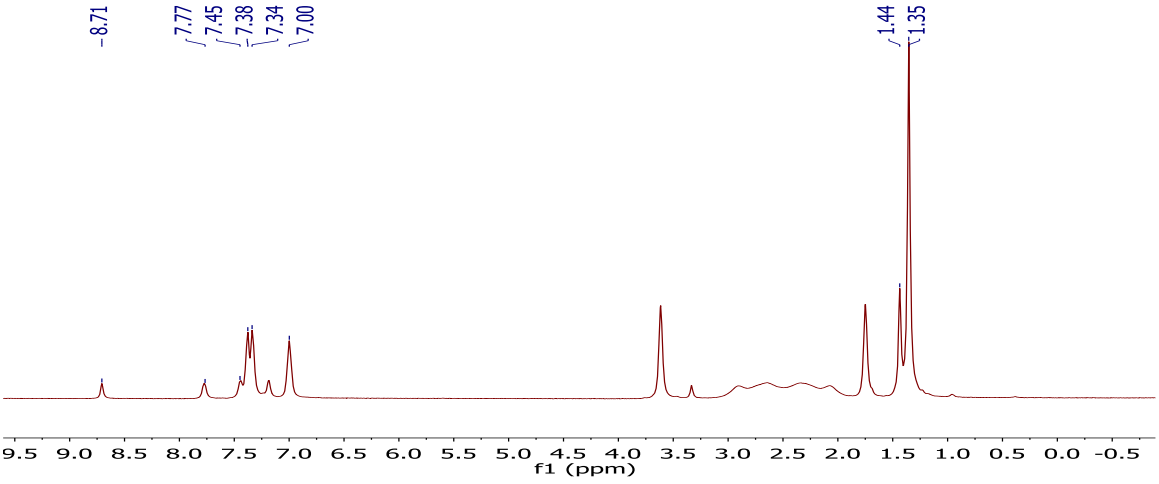

Figure 6-33 ^{1}H-NMR spectrum of crystalline mixture **29** and **sTrCl** with some potential **30[Li^+, sTr^+]** in fluorobenzene-d_5 after being in the freezer for 24 hours. *Note: new peaks appear at 7.77, 7.45 and 1.44 ppm.*

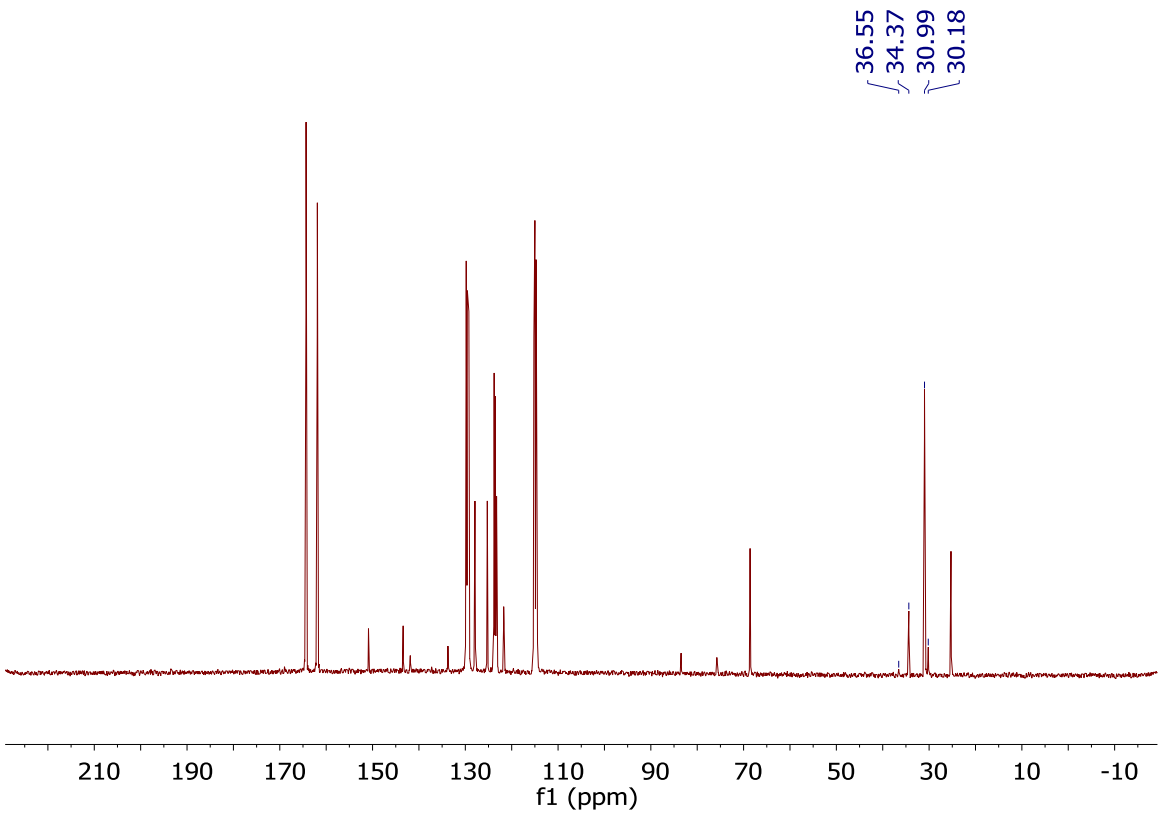

Figure 6-34 ^{13}C-NMR spectrum of crystalline mixture **29** and **sTrCl** with some potential **30[Li$^+$, sTr$^+$]** in fluorobenzene-d_5 after cooling at -30 °C for 24 hours showing potential trityl cation at 36.55 and 30.18 ppm and non trityl cation at 34.37 and 30.99 ppm.

Isolation of *ortho* substituted adduct, **56:**

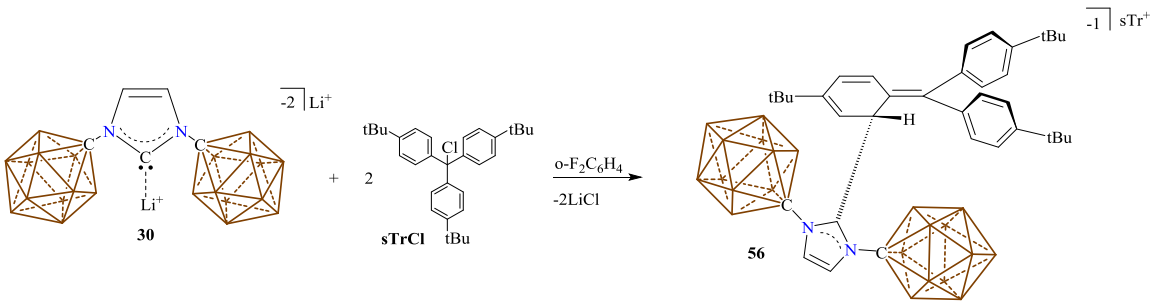

Scheme 6-10 Isolation of crystalline **56** from the reaction mixture.

A glass scintillation vial was equipped with a stir bar and loaded with **30** (100 mg, 197 µmol) and suspended in *o*-$F_2C_6H_4$. A separate scintillation vial was loaded with **sTrCl** (88 mg, 197 µmol) suspended in *o*-$F_2C_6H_4$, the suspension of **sTrCl** was added dropwise to NHC **30** which underwent an immediate color change to yellow. The reaction was stirred at room temperature for 15 minutes then the suspension was filtered and placed in the freezer. The crystals were examined under a microscope and green plates were manually separated from the crystal mass, yield estimated as less than 30 mg (<17%). ^{1}H NMR (600 MHz, methylene chloride-d_2, 25°C): δ = 7.87 (d, $^{3}J(H,H)$ = 8.1 Hz, 6H), 7.60 (d, $^{3}J(H,H)$ = 8.1 Hz, 6H), 7.15 (d, $^{3}J(H,H)$ = 7.8 Hz, 4H), 7.00 (d, $^{3}J(H,H)$ = 7.8 Hz, 4H), 6.96 (d, $^{3}J(H,H)$ = 2.4 Hz, 1H), 6.90 (d, $^{3}J(H,H)$ = 2.4 Hz, 1H), 6.43 (d, $^{3}J(H,H)$ = 1.8 Hz, 1H), 6.42 (d, $^{3}J(H,H)$ = 10.7 Hz, 1H), 6.08 (d, $^{3}J(H,H)$ = 10.7 Hz, 1H), 5.35 (d, $^{3}J(H,H)$ = 1.8 Hz, 1H), 1.49 (s, 27H), 1.31 (s, 9H), 1.26 (s, 9H), 1.15 (s, 9H), 2.5-1.1 (bs, 22H) ppm. ^{1}H[^{11}B] NMR (600 MHz, methylene chloride-d2, 25°C): δ = 7.88 (d), 7.60 (d), 7.15 (d), 7.00 (d), 6.96 (d), 6.89 (d), 6.43 (d), 6,42 (d), 6.08 (d), 5.36 (d), 2.21 (bs, B-H), 1.65 (bs, B-H), 1.60 (bs, B-H), 1.50 (s), 1.32 (s), 1.27 (s), 1.16 (s) ppm. ^{11}B[^{1}H] NMR (192 MHz, methylene chloride-d_2, 25°C): δ = -6.8, -7.0, -13.5, -14.2 ppm. ^{11}B NMR (192 MHz, methylene chloride-d_2, 25°C): δ = -6.8, -7.0, -13.5, -14.2 ppm. ^{13}C[^{1}H] NMR (151 MHz, methylene chloride-d_2, 25°C): δ = 203.6, 168.9, 151.3, 149.8, 149.0, 141.5, 140.0, 138.0, 137.2, 136.7, 130.5, 130.0, 129.5, 129.2, 127.8, 125.5, 124.8, 123.3, 123.2, 116.7, 114.9, 80.7, 80.0, 38.6, 34.3, 34.2, 33.7, 31.0, 30.8, 30.4, 27.3 ppm.

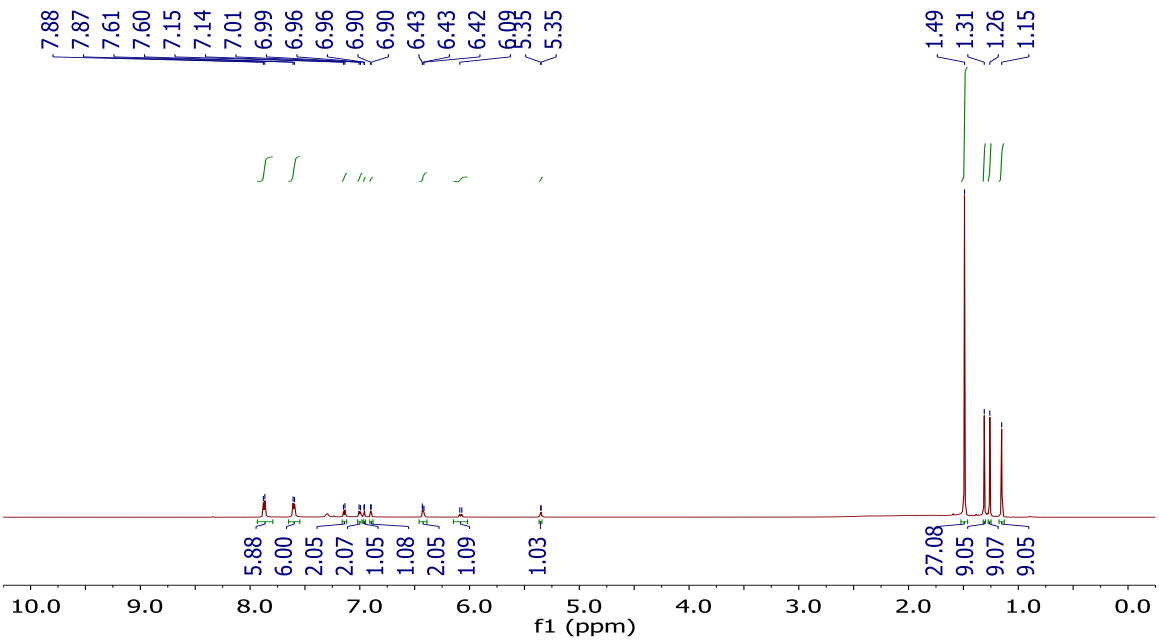

Figure 6-35 ^{1}H-NMR spectrum of **56** in methylene chloride-d_2.

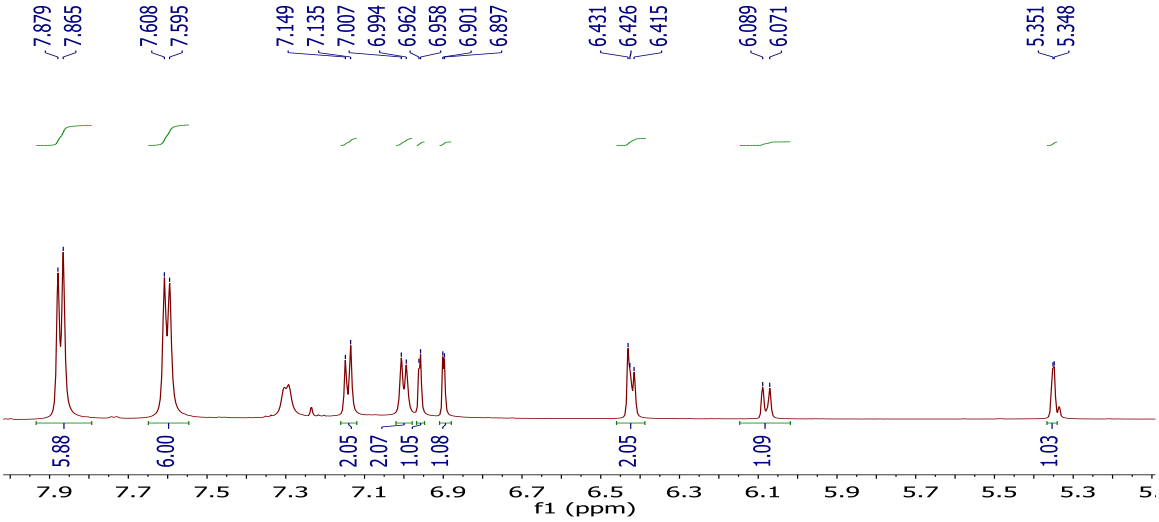

Figure 6-36 An expansion of the ^{1}H-NMR spectrum of **56** in methylene chloride-d_2 showing the aromatic region. *Note: the small peak to the right of 5.39 is $CHDCl_2$.*

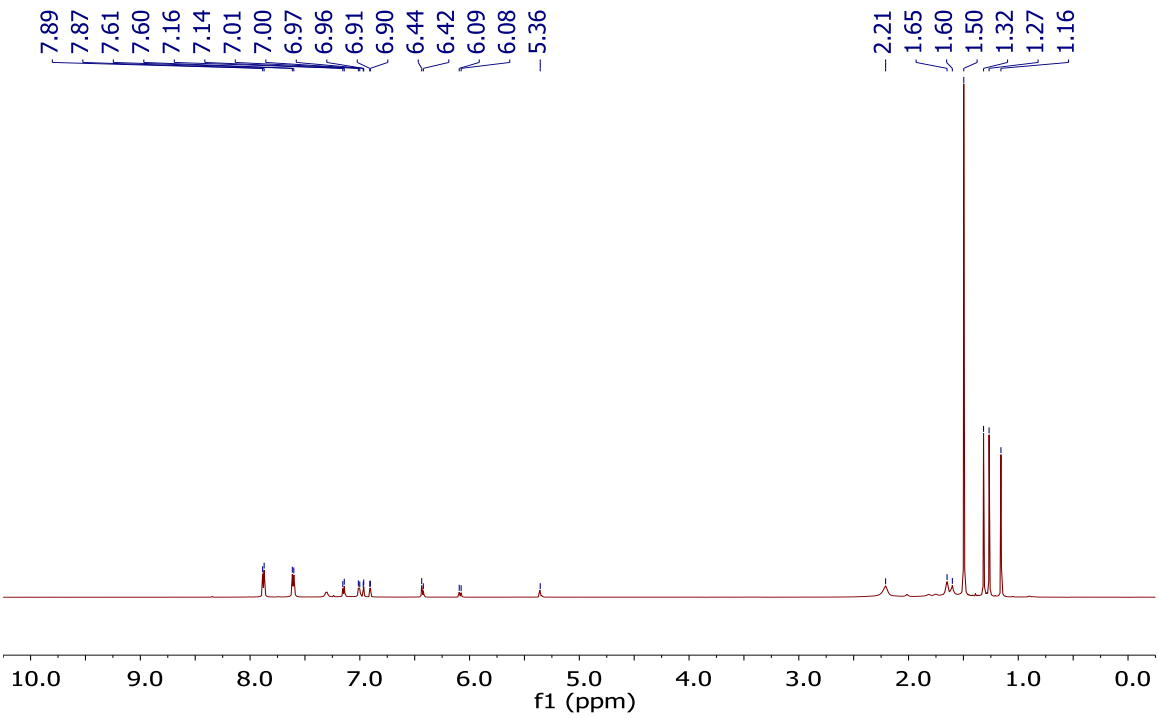

Figure 6-37 $^{1}H[^{11}B]$-NMR spectrum of **56** in methylene chloride-d_2. *Note: the B-H resonances appear at 2.21, 1.65 and 1.60 ppm.*

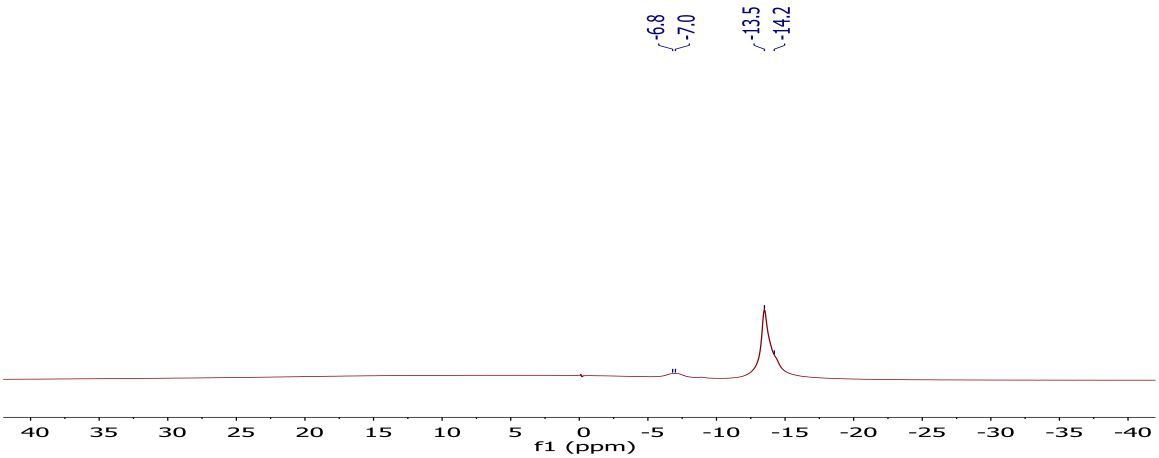

Figure 6-38 $^{11}B[^{1}H]$-NMR spectrum of **56** in methylene chloride-d_2.

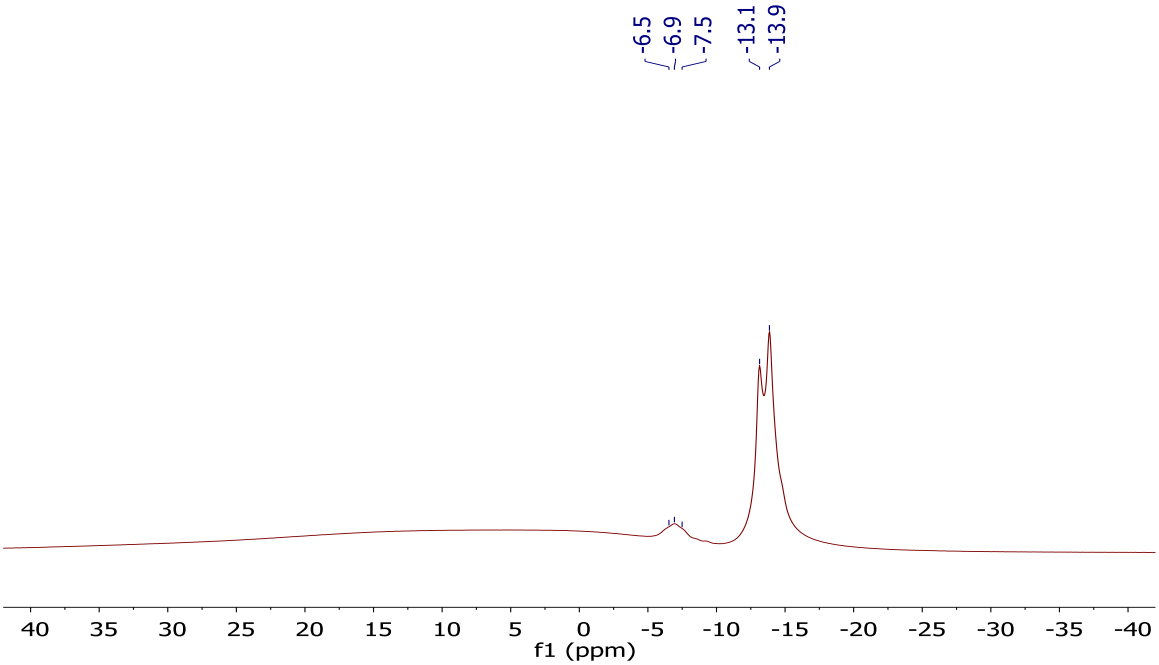

Figure 6-39 ^{11}B-NMR spectrum of **56** in methylene chloride-d_2.

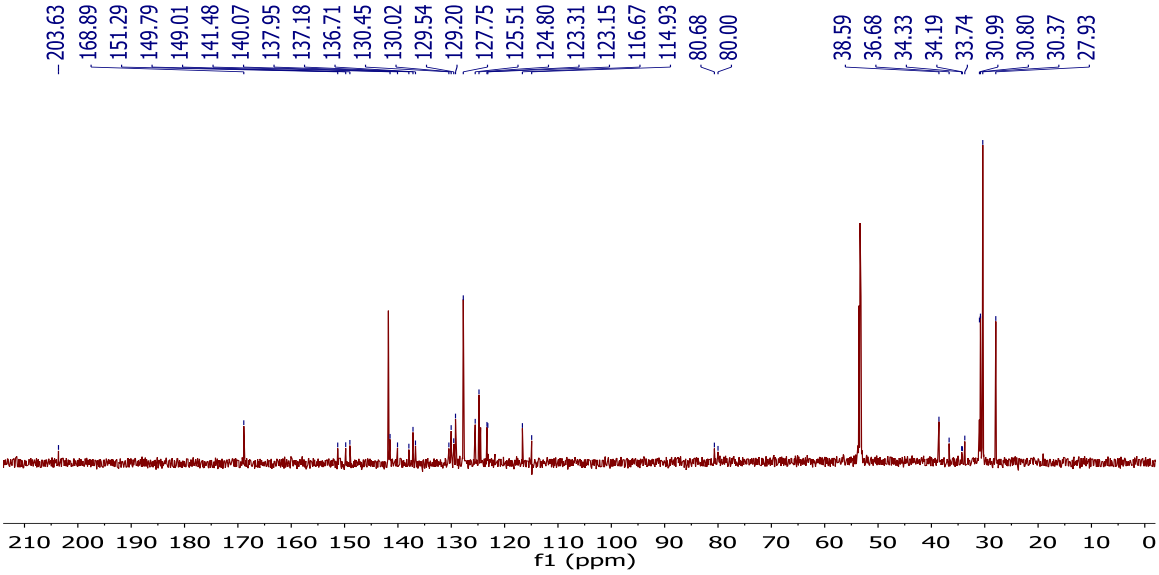

Figure 6-40 ^{13}C[^{1}H]-NMR spectrum of **56** in methylene chloride-d_2.

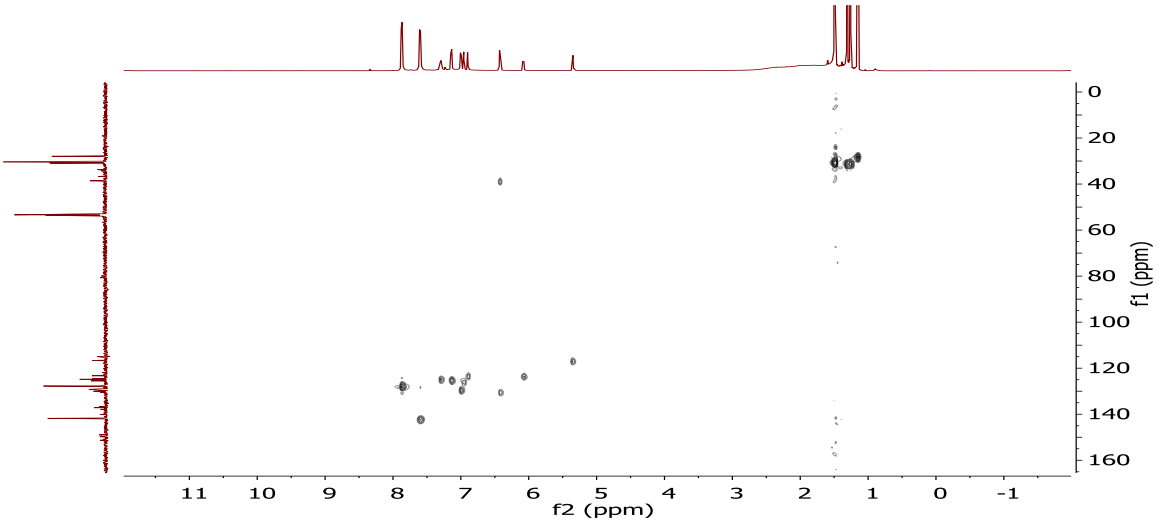

Figure 6-41 ^{13}C-^{1}H HSQC-NMR spectrum of **56** in methylene chloride-d_2. *Note: the peak at [6.42, 39.0] ppm is the aryl C attached to NHC **30**.*

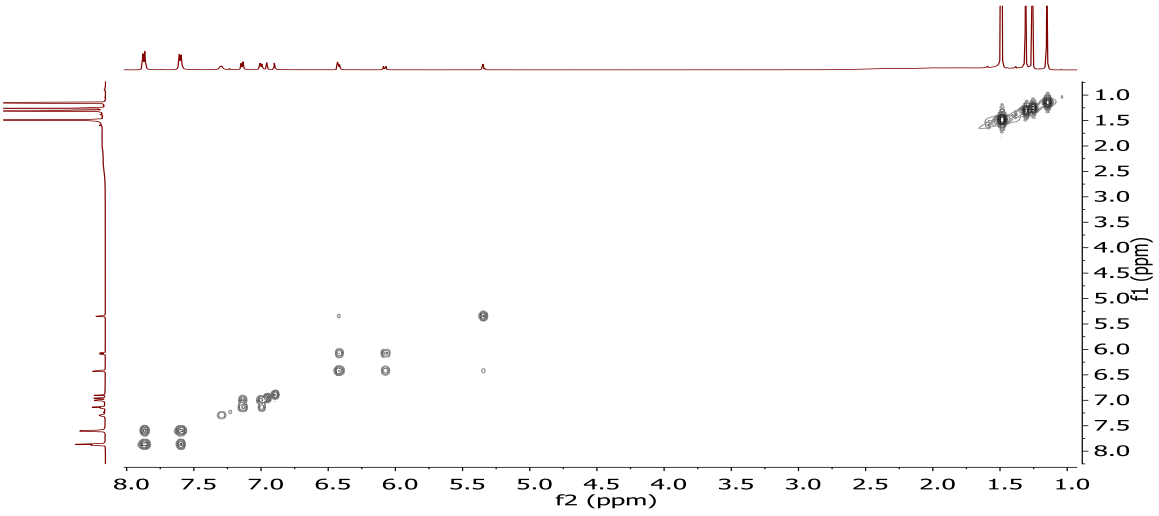

Figure 6-42 ^{1}H-^{1}H COSY-NMR spectrum of **56** in methylene chloride-d_2.

Miscellaneous NMR Spectrum:

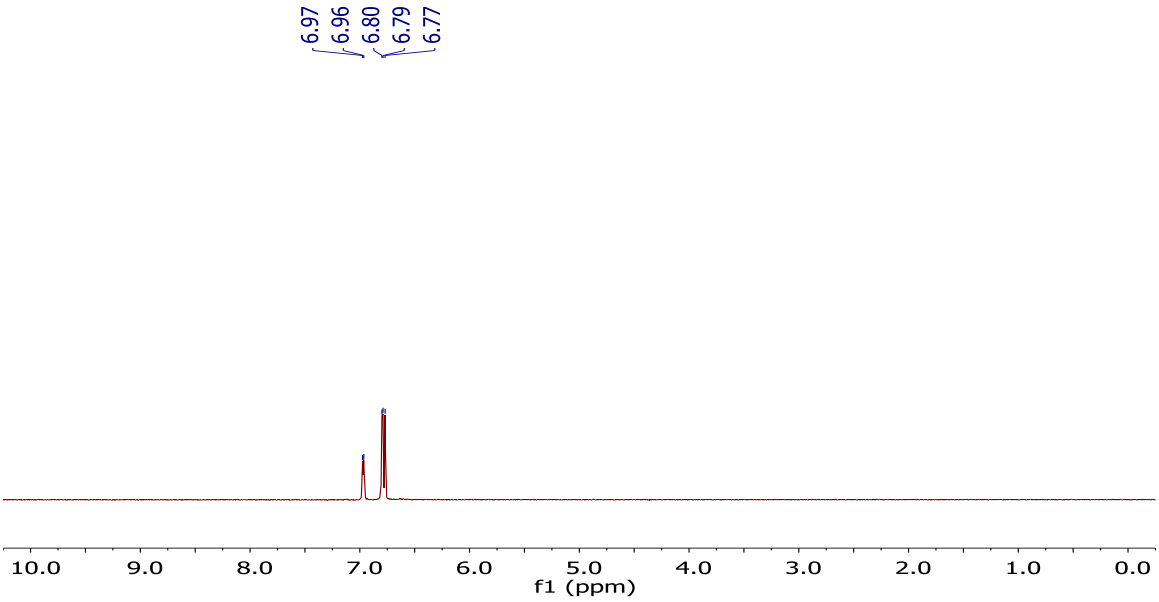

Figure 6-43 ^{1}H-NMR spectrum of neat anhydrous F-C_6D_5.

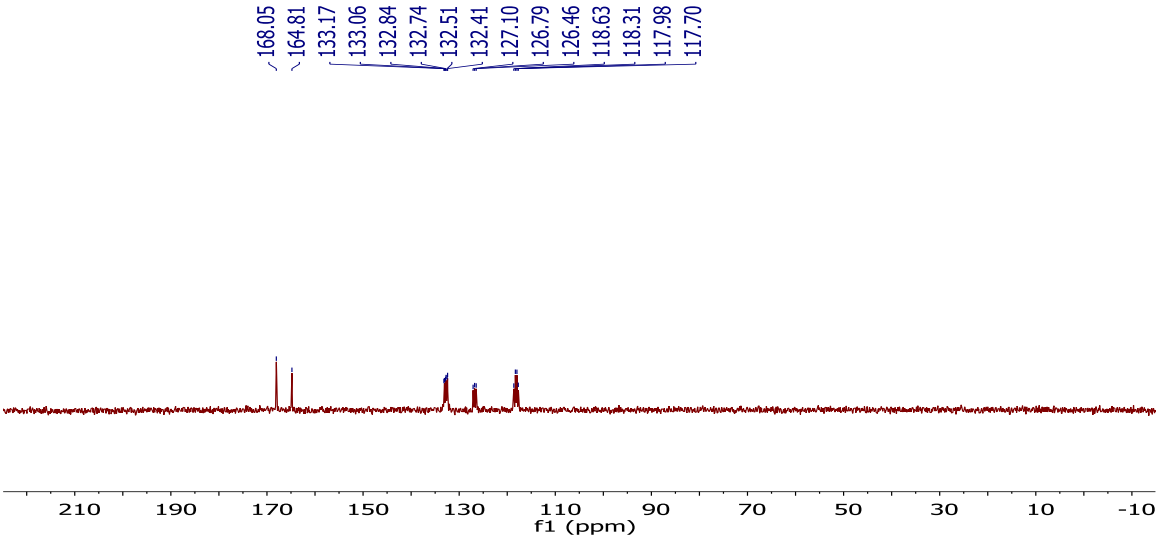

Figure 6-44 ^{13}C-NMR spectrum of neat anhydrous F-C_6D_5.

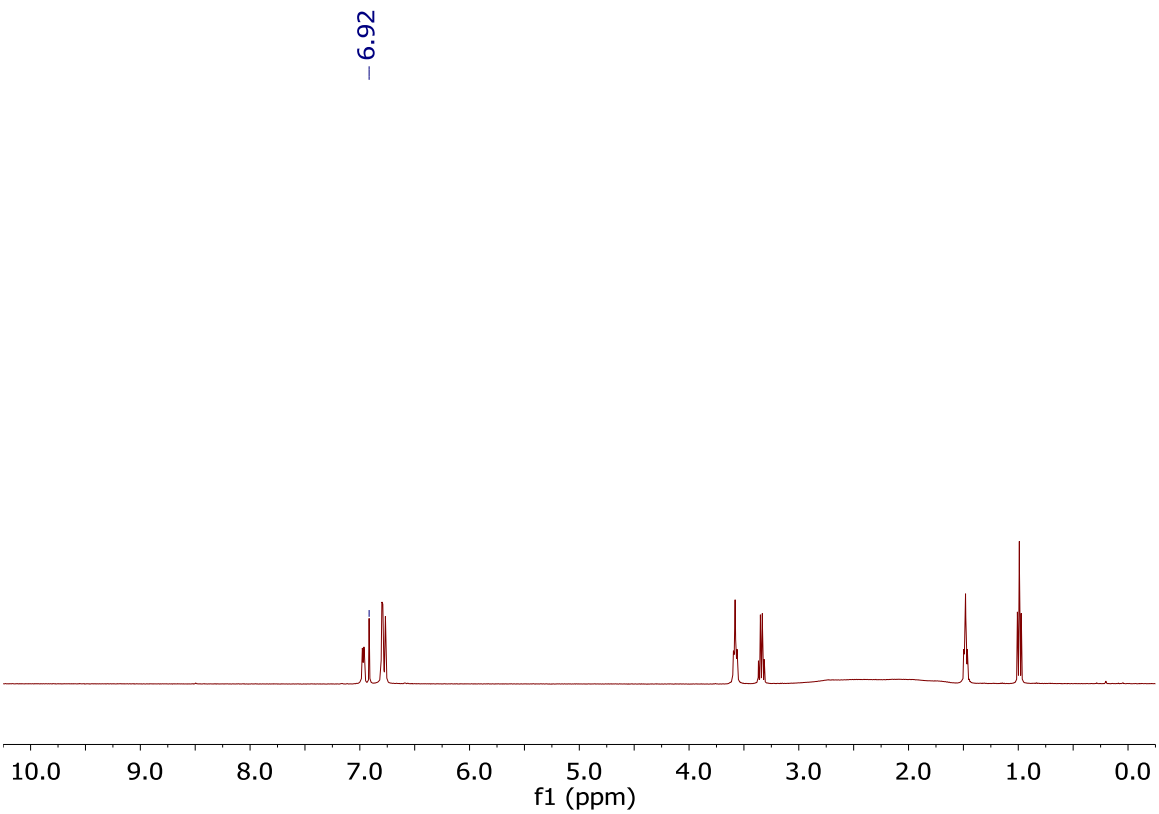

Figure 6-45 ^{1}H-NMR spectrum of **30** in anhydrous F-C_6D_5. Note: the backbone protons of the imidazolylidene are at 6.92 ppm.

X-Ray Structures

Solid State Structure of **29[sTr$^+$]:**

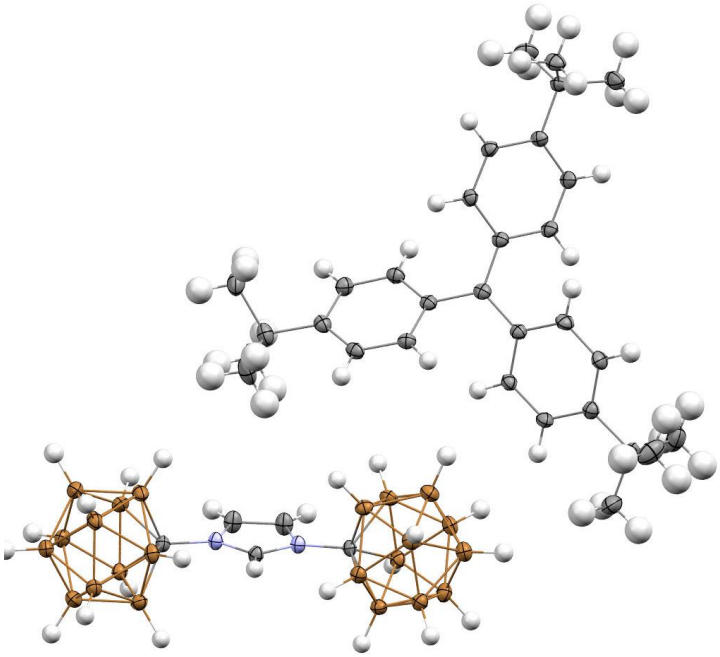

Figure 6-46 Solid state structure of **29[sTr$^+$]**. Color code: H = white, B = brown, C = gray, N = blue.

A yellow plate-needle fragment (0.589 x 0.312 x 0.044 mm^3) was used for the single crystal x-ray diffraction study of $[C_{31}H_{39}]^+.[C_5H_{25}B_{22}N_2]^-$ (sample vL288SF_0m). The crystal was coated with paratone oil and mounted onto a cryo-loop glass fiber. X-ray intensity data were collected at 100(2) K on a Bruker APEX2 platform-CCD x-ray diffractometer system (fine focus Mo-radiation, λ = 0.71073 Å, 50KV/30mA power). The CCD detector was placed at a distance of 5.0600 cm from the crystal.

A total of 3000 frames were collected for a sphere of reflections (with scan width of 0.3^o in ω, starting ω and 2θ angles of –30^o, and ϕ angles of 0^o, 90^o, 120^o, 180^o, and 270^o for every 600 frames, 120 sec/frame exposure time). The frames were integrated using the Bruker SAINT software package and using a narrow-frame integration algorithm. Based on a monoclinic crystal system, the integrated frames yielded

a total of 83245 reflections at a maximum 2θ angle of 58.260^{o} (0.73 Å resolution), of which 12452 were independent reflections (R_{int} = 0.0496, R_{sig} = 0.0334, redundancy = 6.7, completeness = 100%) and 9219 (74.0%) reflections were greater than 2σ(I). The unit cell parameters were, **a** = 18.1340(5) Å, **b** = 12.0884(3) Å, **c** = 22.7027(6) Å, **β** = 111.6302(5)^{o}**,** V = 4626.2(2) Å^{3}, Z = 4, calculated density D_c = 1.095 g/cm^{3}. Absorption corrections were applied (absorption coefficient μ = 0.055 mm^{-1}; max/min transmission = 0.998/0.968) to the raw intensity data using the SADABS program.

The Bruker SHELXTL software package was used for phase determination and structure refinement. The distribution of intensities (E^2-1 = 0.959) and systematic absent reflections indicated one possible space group, P2(1)/n. The space group P2(1)/n (#14) was later determined to be correct. Direct methods of phase determination followed by two Fourier cycles of refinement led to an electron density map from which most of the non-hydrogen atoms were identified in the asymmetric unit of the unit cell. With subsequent isotropic refinement, all of the non-hydrogen atoms were identified. There was one cation of $[C_{31}H_{39}]^{+}$ and one anion of $[C_5H_{25}B_{22}N_2]^{-}$ present in the asymmetric unit of the unit cell.

Atomic coordinates, isotropic and anisotropic displacement parameters of all the non-hydrogen atoms were refined by means of a full matrix least-squares procedure on F^2. The H-atoms were included in the refinement in calculated positions riding on the atoms to which they were attached. The refinement converged at R1 = 0.0517, wR2 = 0.1269, with intensity I>2σ (I). The largest peak/hole in the final difference map was 0.344/-0.243 e/Å^{3}.

Table 6-1 Crystal data and structure refinement for **29[sTr$^+$]**.

Identification code	vL288SF_0m	
Empirical formula	C36 H64 B22 N2	
Formula weight	762.71	
Temperature	100(2) K	
Wavelength	0.71073 Å	
Crystal system	Monoclinic	
Space group	P 21/n	
Unit cell dimensions	a = 18.1340(5) Å	α = 90°.
	b = 12.0884(3) Å	β = 111.6302(5)°.
	c = 22.7027(6) Å	γ = 90°.
Volume	4626.2(2) Å^3	
Z	4	
Density (calculated)	1.095 Mg/m^3	
Absorption coefficient	0.055 mm^{-1}	
F(000)	1616	
Crystal size	0.589 x 0.312 x 0.044 mm^3	
Theta range for data collection	1.803 to 29.130°.	
Index ranges	-24<=h<=24, -16<=k<=16, -31<=l<=31	
Reflections collected	83245	
Independent reflections	12452 [R(int) = 0.0496]	
Completeness to theta = 25.242°	100.0 %	
Absorption correction	Semi-empirical from equivalents	
Refinement method	Full-matrix least-squares on F^2	
Data / restraints / parameters	12452 / 0 / 550	
Goodness-of-fit on F^2	1.031	

Final R indices [I>2sigma(I)]	R1 = 0.0517, wR2 = 0.1269
R indices (all data)	R1 = 0.0776, wR2 = 0.1410
Extinction coefficient	n/a
Largest diff. peak and hole	0.344 and -0.243 e.Å^{-3}

Solid State structure of **54**:

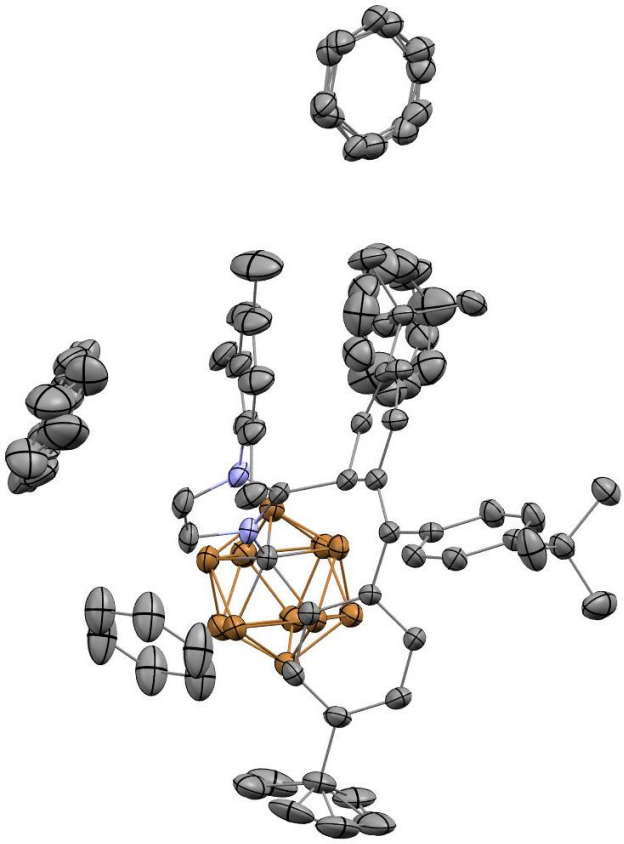

Figure 6-47 Solid state structure of **55** showing the lattice bound C_6H_6 molecules. Hydrogen atoms are omitted for clarity. Color code: B = brown, C = gray, N = blue.

A colorless prism fragment (0.548 x 0.253 x 0.118 mm^3) was used for the single crystal x-ray diffraction study of $[C_{44}H_{63}B_{11}N_2].[C_6H_6]_4$ (sample vL274SF_0m). The crystal was coated with paratone oil

and mounted on to a cryo-loop glass fiber. X-ray intensity data were collected at 100(2) K on a Bruker APEX2 platform-CCD x-ray diffractometer system (fine focus Mo-radiation, λ = 0.71073 Å, 50KV/30mA power). The CCD detector was placed at a distance of 5.0600 cm from the crystal.

A total of 3000 frames were collected for a sphere of reflections (with scan width of 0.3^o in ω, starting ω and 2θ angles of –30^o, and ϕ angles of 0^o, 90^o, 120^o, 180^o, and 270^o for every 600 frames, 60 sec/frame exposure time). The frames were integrated using the Bruker SAINT software package and using a narrow-frame integration algorithm. Based on a monoclinic crystal system, the integrated frames yielded a total of 109008 reflections at a maximum 2θ angle of 58.260^o (0.73 Å resolution), of which 16211 were independent reflections (R_{int} = 0.0446, R_{sig} = 0.0299, redundancy = 6.7, completeness = 100%) and 11187 (69.0%) reflections were greater than 2σ(I). The unit cell parameters were, **a** = 21.2057(7) Å, **b** = 13.3683(4) Å, **c** = 21.2750(7) Å, **β** = 94.2342(6)^o**,** V = 6014.7(3) Å^3, Z = 4, calculated density D_c = 1.072 g/cm^3. Absorption corrections were applied (absorption coefficient μ = 0.058 mm^{-1}; max/min transmission = 0.993/0.969) to the raw intensity data using the SADABS program.

The Bruker SHELXTL software package was used for phase determination and structure refinement. The distribution of intensities (E^2-1 = 0.952) and systematic absent reflections indicated two possible space groups, P2/c and Pc. The space group P2/c (#13) was later determined to be correct. Direct methods of phase determination followed by two Fourier cycles of refinement led to an electron density map from which most of the non-hydrogen atoms were identified in the asymmetric unit of the unit cell. With subsequent isotropic refinement, all of the non-hydrogen atoms were identified. There was one molecule of [$C_{44}H_{63}B_{11}N_2$] and four C_6H_6 solvent molecules present in the asymmetric unit of the unit cell. One of the three T-butyl-groups of $C_{44}H_{63}B_{11}N_2$ was modeled with disordered (disordered site occupancy ratio was 50%/50%). One partially occupied (95% occupied) benzene was located at the inversion center. Two disordered and partially occupied (25% occupied) benzene were located at the 2-fold rotation axis

parallel to the b-axis. Two other disordered benzene were in general positions (disordered site occupancy ratios were 76%/24% and 54%/46%).

Atomic coordinates, isotropic and anisotropic displacement parameters of all the non-hydrogen atoms were refined by means of a full matrix least-squares procedure on F^2. The H-atoms were included in the refinement in calculated positions riding on the atoms to which they were attached. The refinement converged at R1 = 0.0587, wR2 = 0.1501, with intensity $I>2\sigma$ (I). The largest peak/hole in the final difference map was 0.402/-0.245 e/$Å^3$.

Table 6-2 Crystal data and structure refinement for **55**.

Identification code	vL274SF_0m	
Empirical formula	C61.84 H80.84 B11 N2	
Formula weight	971.08	
Temperature	100(2) K	
Wavelength	0.71073 Å	
Crystal system	Monoclinic	
Space group	P 2/c	
Unit cell dimensions	a = 21.2057(7) Å	α = 90°.
	b = 13.3683(4) Å	β = 94.2342(6)°.
	c = 21.2750(7) Å	γ = 90°.
Volume	6014.7(3) $Å^3$	
Z	4	
Density (calculated)	1.072 Mg/m^3	
Absorption coefficient	0.058 mm^{-1}	
F(000)	2083	

Crystal size	0.548 x 0.253 x 0.118 mm^3
Theta range for data collection	1.523 to 29.130°.
Index ranges	-29<=h<=29, -18<=k<=18, -29<=l<=29
Reflections collected	109008
Independent reflections	16211 [R(int) = 0.0446]
Completeness to theta = 25.242°	100.0 %
Absorption correction	Semi-empirical from equivalents
Refinement method	Full-matrix least-squares on F^2
Data / restraints / parameters	16211 / 675 / 851
Goodness-of-fit on F^2	1.038
Final R indices [I>2sigma(I)]	R1 = 0.0591, wR2 = 0.1504
R indices (all data)	R1 = 0.0903, wR2 = 0.1694
Extinction coefficient	n/a
Largest diff. peak and hole	0.403 and -0.247 $e.Å^{-3}$

6.7 References

1. J. F. Norris ,W. W. Sanders, *American Chemical Journal*, 1901, **25**, 54-56.
2. J. F. Norris, *American Chemical Journal*, 1901, **25**, 117-122.
3. F. Kehrmann ,F. Wentzel, *Berichte der deutschen chemischen Gesellschaft*, 1901, **34**, 3815-3819.
4. A. Baeyer ,V. Villiger, *Berichte der deutschen chemischen Gesellschaft*, 1902, **35**, 1189-1201.
5. G. A. Olah, *Journal of the American Chemical Society*, 1972, **94**, 808-820.
6. R. R. Naredla ,D. A. Klumpp, *Chemical Reviews*, 2013, **113**, 6905-6948.
7. F. E. Hahn ,M. C. Jahnke, *Angewandte Chemie International Edition*, 2008, **47**, 3122-3172.
8. F. E. Hahn, *Chemical Reviews*, 2018, **118**, 9455-9456.
9. D. Bourissou, O. Guerret, F. P. Gabbaï ,G. Bertrand, *Chemical Reviews*, 2000, **100**, 39-92.
10. H. V. Huynh, *Chemical Reviews*, 2018, **118**, 9457-9492.
11. M. N. Hopkinson, C. Richter, M. Schedler ,F. Glorius, *Nature*, 2014, **510**, 485.
12. A. Igau, A. Baceiredo, G. Trinquier ,G. Bertrand, *Angewandte Chemie International Edition in English*, 1989, **28**, 621-622.
13. A. Igau, H. Grutzmacher, A. Baceiredo ,G. Bertrand, *Journal of the American Chemical Society*, 1988, **110**, 6463-6466.
14. A. J. Arduengo, R. L. Harlow ,M. Kline, *Journal of the American Chemical Society*, 1991, **113**, 361-363.
15. C. Douvris ,J. Michl, *Chemical Reviews*, 2013, **113**, PR179-PR233.
16. N. S. Hosmane, *Handbook of Boron Science : with Applications in Organometallics, Catalysis, Materials and Medicine*, World Scienific, Hackensack, New Jersey, 2019.
17. S. P. Fisher, A. W. Tomich, S. O. Lovera, J. K. Kleinsasser, J. Guo, M. J. Asay, H. M. Nelson ,V. Lavallo, *Chemical Reviews*, 2019.
18. C. A. Reed, *Accounts of Chemical Research*, 2010, **43**, 121-128.
19. O. Allemann, S. Duttwyler, P. Romanato, K. K. Baldridge ,J. S. Siegel, *Science*, 2011, **332**, 574.
20. R. Ramírez-Contreras, N. Bhuvanesh, J. Zhou ,O. V. Ozerov, *Angewandte Chemie International Edition*, 2013, **52**, 10313-10315.

21. C. Douvris, C. M. Nagaraja, C.-H. Chen, B. M. Foxman ,O. V. Ozerov, *Journal of the American Chemical Society*, 2010, **132**, 4946-4953.

22. C. Douvris ,O. V. Ozerov, *Science*, 2008, **321**, 1188-1190.

23. S. Popov, B. Shao, A. L. Bagdasarian, T. R. Benton, L. Zou, Z. Yang, K. N. Houk ,H. M. Nelson, *Science*, 2018, **361**, 381.

24. B. Shao, A. L. Bagdasarian, S. Popov ,H. M. Nelson, *Science*, 2017, **355**, 1403.

25. A. El-Hellani ,V. Lavallo, *Angewandte Chemie International Edition*, 2014, **53**, 4489-4493.

26. M. J. Asay, S. P. Fisher, S. E. Lee, F. S. Tham, D. Borchardt ,V. Lavallo, *Chemical Communications*, 2015, **51**, 5359-5362.

27. H. Hoffmann ,P. Schellenbeck, *Chemische Berichte*, 1966, **99**, 1134-1142.

28. J. B. Lambert ,J. H. So, *The Journal of Organic Chemistry*, 1991, **56**, 5960-5962.

29. R. A. Jones, G. Wilkinson, M. B. Hursthouse ,K. M. A. Malik, *Journal of the Chemical Society, Perkin Transactions 2*, 1980, 117-120.

30. X. Fang, B. L. Scott, K. D. John, G. J. Kubas ,J. G. Watkin, *New Journal of Chemistry*, 2000, **24**, 831-833.

31. G. Bidan ,M. Genies, *Tetrahedron Letters*, 1978, **19**, 2499-2502.

32. L. Cabrera, G. C. Welch, J. D. Masuda, P. Wei ,D. W. Stephan, *Inorganica Chimica Acta*, 2006, **359**, 3066-3071.

33. P. A. Chase, A. L. Gille, T. M. Gilbert ,D. W. Stephan, *Dalton Transactions*, 2009, 7179-7188.

34. C. Bosset, R. Coffinier, P. A. Peixoto, M. El Assal, K. Miqueu, J.-M. Sotiropoulos, L. Pouységu ,S. Quideau, *Angewandte Chemie International Edition*, 2014, **53**, 9860-9864.

35. J. F. Kleinsasser, S. P. Fisher, F. S. Tham ,V. Lavallo, *European Journal of Inorganic Chemistry*, 2017, **2017**, 4417-4419.

36. H. Guenther ,G. Jikeli, *Chemical Reviews*, 1977, **77**, 599-637.

37. Y. Uchimura, T. Takeda, R. Katoono, K. Fujiwara ,T. Suzuki, *Angewandte Chemie International Edition*, 2015, **54**, 4010-4013.

38. T. Jelínek, J. Plešek, S. Hermanek ,S. Bohumil, *Collection of Czechoslovak Chemical Communications*, 1986, **51**, 819-829.

39. E. M. Arnett, R. A. Flowers, R. T. Ludwig, A. E. Meekhof ,S. A. Walek, *Journal of Physical Organic Chemistry*, 1997, **10**, 499-513.

Chapter 7: Old Cations Making New Friends, One is Li and the Other Au.

7.1 Introduction

Carborane anions are an unusual class of boron cluster compounds that contain at least one atom of hypercoordinate carbon.[1-6] Since their discovery in the late 1960's these molecules have been known for their chemical stability and weakly coordinating abilities.[7] The last thirty years is a testament to these claims as these clusters have allowed for the isolation of potent electrophiles such as anhydrous H^+,[8] protonated carbon dioxide,[9] dialkyl alumenium cation,[10] fullerene cations,[11] trityl cation,[12-14] isopropyl cation,[15] benzenium cation,[16] *tert*-butyl cation[17] and the first report of a free silylium ion.[18] The isolation of these cations was only possible with polyfunctionalized variants of anion **3**.[6] Functionalization of these clusters typically takes on two forms, the hexafunctionalized $\mathbf{3X_6}$ and the perfunctionalized $\mathbf{3X_{11}}$, Figure 7-1.

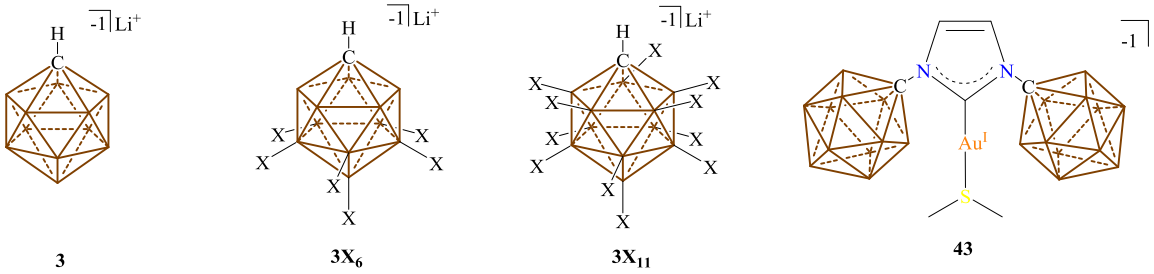

3 $\mathbf{3X_6}$ $\mathbf{3X_{11}}$ **43**

Figure 7-1 Structure of icosahedral carborane anion **3** as well as its hexafunctionalized form $\mathbf{3X_6}$ and perfunctionalized derivative $\mathbf{3X_{11}}$. The structure on the far right is the anionic Au complex **43**.

Recently we have reported an anionic Au(I) complex that bears an anionic NHC ligand featuring two N-bound carborane anions **43**, Figure 7-1 right.[19] We were curious to see if the lithium counter cation which stabilized the charge of complex **43** in the previous synthesis, could be replaced with a more reactive counter ion, *ut supra*.[19] The steric bulk associated with the N-bound carborane anions should protect the Au center from reaction with bulky cations, thus we chose to target the trityl cation and then perhaps a silylium

ion. These ions contain bulky aryl and alkyl groups which will further protect the cation from reacting at the Au center. However, the NHC ligands are susceptible to reactions with these cations, specifically the B-H bonds of the carborane are known to react with the trityl cation and undergo electrophilic aromatic substitution "like" reactions forming *meta* and *para* arylated products.[14] Another plausible reaction is the abstraction of the labile SMe_2 ligand by the silyl ion, this has been demonstrated by Oestreich and coworkers who has shown that silyl ions can be trapped with diphenylsulfide.[20]

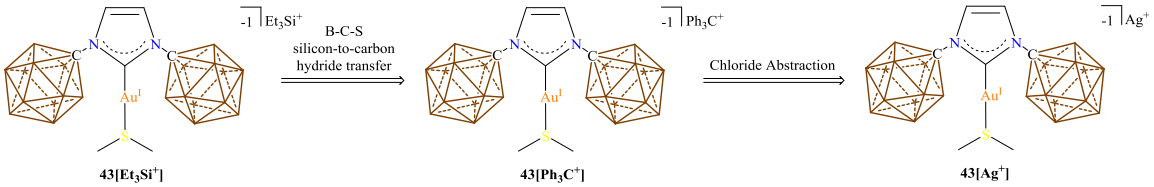

Figure 7-2 Retrosynthetic analysis leading to the silylium ion **43[Et_3Si^+]** from **43[Ag^+]**. B-C-S = Bartlett-Condon-Schneider.

With these challenges in mind, we began our retrosynthetic analysis for **43[Et_3Si^+]**. The most common method used to achieve a silylium ion is through the Bartlett-Condon-Schneider silicon-to-carbon hydride transfer using a trityl salt, such as **43[Ph_3C^+]**. To gain access to **43[Ph_3C^+]** a halide abstraction from trityl chloride would be performed using a silver salt such as **43[Ag^+]**. The bimetallic reagent **43[Ag^+]** was described in chapter 4 and will be used as an access point to **43[Ph_3C^+]**, Figure 7-2.

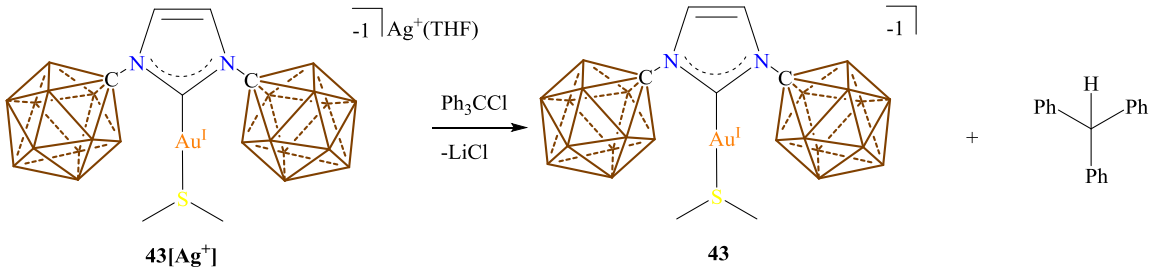

Scheme 7-1 Attempted synthesis of anionic Au(I) complex with a trityl cation. The cation of anionic Au(I) complex is unknown but believed to be a cationic THF species.

7.2 Synthesis of a Zwitterionic Au(III) complex

The reaction of **43[Ag$^+$]** with trityl chloride in a F-C_6H_5 suspension lead to an immediate color change to yellow-orange which then darkened to brown, Scheme 7-1. The suspension was filtered (removal of AgCl) and the brown filtrate was analyzed by multinuclear NMR spectroscopy. The filtrate did not contain the expected aryl resonances for a trityl cation. Further investigation of this material, by washing with diethyl ether, lead to the separation of a residue, which contained **43**, and the supernatant, which contained triphenylmethane. ^{1}H NMR analysis of the residue displayed singlets at 7.42 and 2.80 ppm corresponding to the anionic Au(I) fragment as well as a triplet and doublet at 8.44 and 7.56 ppm respectively corresponding to imidazolium **29**. It should be noted that the cation for **43** was not identified but it is believed to be either a cationic THF species from the hydride abstraction with the trityl cation or an H^+ as indicated by a large bump in the ^{1}H NMR spectrum at 11.35 ppm. In the supernatant, triphenylmethane was unambiguously identified using a combination of ^{1}H, ^{13}C and ^{13}C-^{1}H HSQC NMR experiments, the ^{1}H NMR spectrum showed a distinct singlet (1H) at 5.57 ppm with the expected doublet (6H), triplet (3H), triplet (6H) at 7.14, 7.22 and 7.32 respectively. The ^{13}C NMR spectrum shows four resonances, three aromatic signals at 129.6, 128.4 and 126.4 as well as a characteristic methine signal at 56.0 ppm. The ^{13}C-^{1}H HSQC spectrum revealed a cross peak at [5.6, 56] ppm unambiguously identifying the tertiary methine of triphenylmethane.

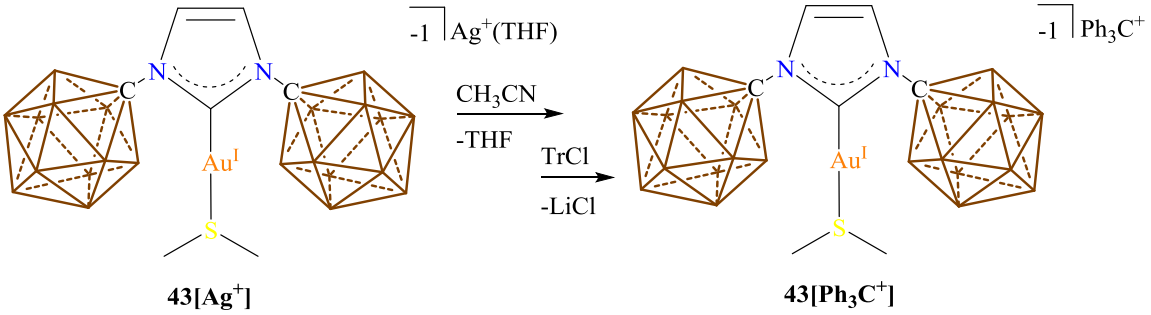

Scheme 7-2 Synthesis of 43 with a trityl cation. Acetonitrile is used to remove THF coordinated to the Ag^+ cation.

Baffled by the presence of triphenylmethane, we closely considered the reaction and realized that the Ag^+ cation was coordinated to THF which is known to decompose trityl cations. Thus acetonitrile was used to remove all THF coordinated to the Ag^+ cation, Scheme 7-2. When **43[Ag^+]** with no coordinated THF was reacted with trityl chloride the crude reaction mixture showed the expected aryl resonances for a trityl cation, ^{1}H NMR spectrum has signals for a trityl cation at 8.36 (t, 3H), 7.96 (t, 6H) and 7.77 (d, 6H) ppm. Upon filtering off the AgCl and washing with benzene to remove excess trityl chloride, the desired trityl salt **43[Ph_3C^+]** was obtained. The trityl salt was confirmed by multinuclear NMR analysis, the ^{11}B NMR spectrum revealed that the C_{5v} symmetry of the cluster had been preserved. The ^{1}H NMR spectrum displays the downfield aryl C-H signals at 8.36 (t, 3H), 7.96 (t, 6H) and 7.77 (d, 6H) ppm while the Au(I) complex displays the backbone protons of the imidazolylidene at 7.35 (s, 2H) ppm and ligated dimethylsulfide protons at 2.84 (s, 6H) ppm. The ^{13}C NMR spectrum displayed the signature downfield signal for the carbocation at 210.5 ppm.

Upon trying to obtain a suitable ^{13}C NMR spectrum of **43[Ph_3C^+]**, we occasionally observed extra signals in the aromatic region, accompanied by a brown solid. The ^{1}H NMR spectrum now revealed the consumption of the trityl resonances (8.36, 7.96 and 7.7 ppm) and multiple upfield aryl resonances that were not there previously, there were also multiple new singlets between 4 and 5 ppm suggestive of methine protons from triphenylmethane like compounds. We postulated that these methine protons were coming from electrophilic aromatic substitution “like” reactions occurring between the carborane clusters

and trityl cation with corresponding rearrangement of the non-aromatized C-H proton to the tertiary C as previously reported by Kleinsasser and coworkers.[14]

In an attempt to identify the decomposition products of **43[Ph_3C^+]**, we performed multiple decomposition studies where pure **43[Ph_3C^+]** was decomposed by prolonged exposure to halogenated solvents (F-C_6H_5, $CHCl_3$, CH_2Cl_2) or aromatic hydrocarbon solvents (C_6H_6, CH_3-C_6H_5). During these experiments we noticed a new signal in the ^1H NMR spectrum at 3.2 ppm which was slightly upfield from the dimethylsulfide methyl protons at 2.8 ppm, this new peak appeared to increase in intensity as the peak at 2.8 decreased in intensity. The compound giving rise to the signal at 3.2 ppm was also found to be soluble in aromatic hydrocarbon solvents. To us, this suggested the presence of a new Au complex where the dimethylsulfide protons were in a more deshielding environment and that the complex was now zwitterionic which is why it was soluble in aromatic hydrocarbon solvents. Indeed, on one occasion we were able to isolate the compound giving rise to the signal at 3.2 ppm.

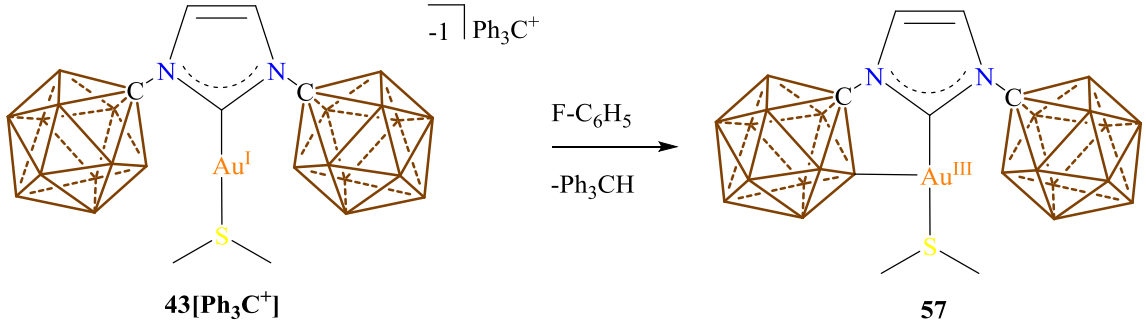

43[Ph_3C^+] **57**

Scheme 7-3 Synthesis of cyclometalated Au(III), **57**.

During a decomposition study of **43[Ph_3C^+]** in a F-C_6H_5 solvent, a noticeably high conversion of the peak at 2.8 ppm to the peak at 3.2 ppm was observed. Extraction of the residue with 3:1 toluene to hexane allowed for the isolation of the signal at 3.2 ppm in the supernatant. Multinuclear NMR analysis gave the following results. The ^{11}B NMR spectrum displayed seven resonances suggesting the symmetry of one of the clusters had been broken. The $^1H[^{11}B]$ NMR spectrum corroborated the broken symmetry of one

of the carborane clusters by giving rise to seven smaller B-H signals at 3.23 3.05, 2.86, 2.77, 2.44, 2.18 and 1.36 ppm as well as two larger signals at 2.50 and 2.30 ppm. The $^{1}H[^{11}B]$ spectrum only displayed two downfield doublets at 6.13 and 5.70 ppm with a coupling constant of 2.1 Hz. The lack of aryl resonances in the $^{1}H[^{11}B]$ NMR spectrum eliminated the possibility of a trityl substituent attached to the carborane cluster and supported the hypothesis of two distinct N-bound carboranyl clusters. The ^{13}C NMR spectrum substantiates the two distinct carborane clusters by displaying two distinct carborane carbon atoms at 78.7 and 75.7 ppm along with two chemically inequivalent imidazolylidene backbone carbon atoms at 122.9 and 119.6 ppm. With this data, we suggested that the Au complex must have formed a metallocycle with one of neighboring boron atoms of the carborane cluster, Scheme 7-3. To rationalize this, we hypothesized a heterolytic oxidative addition via cooperative ion paring where the Au center helps the trityl abstract a hydride from the upper pentagonal belt of the carborane cluster giving rise to a borenium ylide which undergoes an oxidative addition at Au, Figure 7-3.

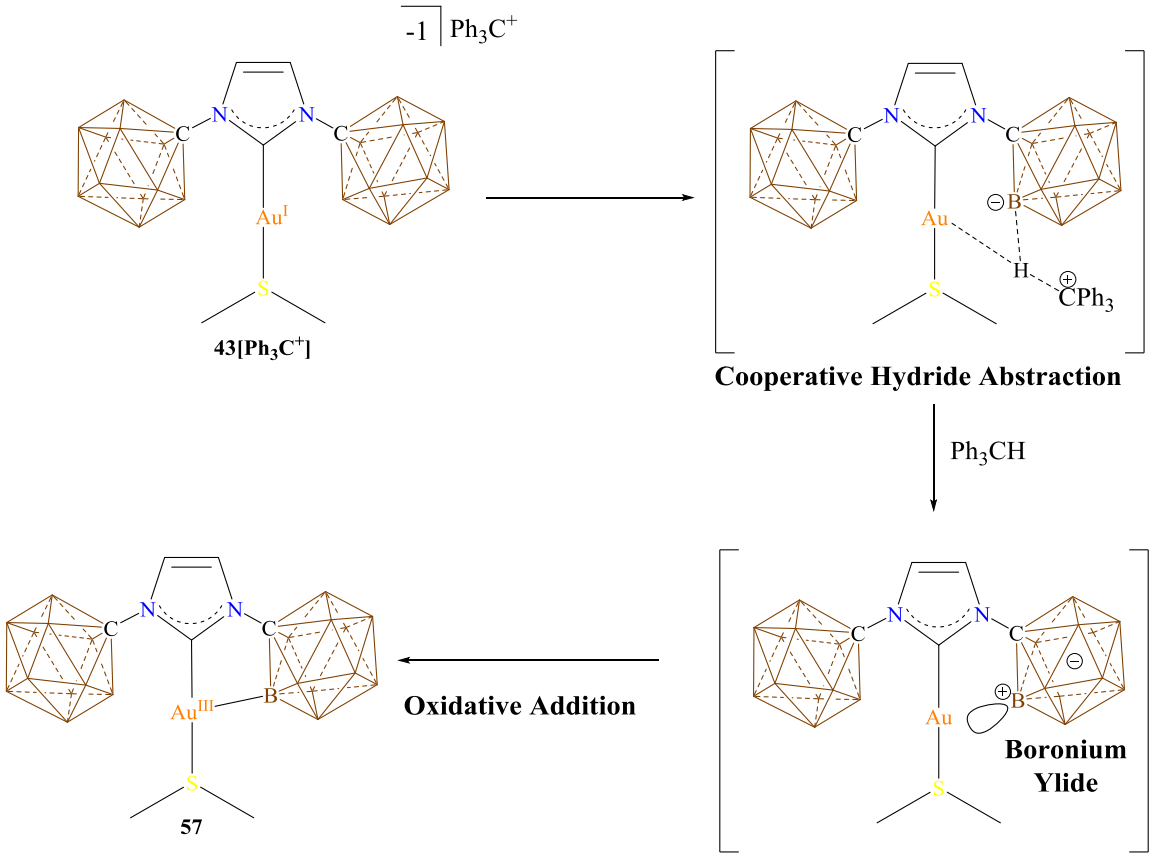

Figure 7-3 Hypothesis leading to formation **57**.

Crystals suitable for a single crystal X-ray diffraction study were grown by layering a methylene chloride solution containing **57** with hexane. The solid state structure revealed a pseudo T-shaped Au(III) complex. In the solid state, the structure is disordered over two positions and the structure with higher population (88%) will be discussed. The Au-B1 bond distance is 2.208(5) Å and the Au-B2 bond distance is 2.746(5) Å. The closest B-H contact occurs between B2-H and the Au center with a bond length of 1.734 Å which is well within range for an agostic interaction, however we see no evidence for this kind of interaction by room temperature NMR studies. Due to the aforementioned bonding, the NHC ligand is canted with a mild yaw distortion of 13.18°.[21, 22] This distortion is also evident in the non-linear geometry of the ∠C2-Au-S of 172°. This deviation from linearity is due to the formation of the Au-B1 bond and the

congestion associated with the crystal packing. This is seen in the larger crystal density of **57**, 1.640 Mg/m^3 compared to **43[Li$^+$]**, 1.394 Mg/m^3. The C2-Au bond length is 2.008(3) Å which is slightly shorter than that of **43[Li$^+$]**, 2.030(3) Å,[19] and within range for other reported NHC Au(III) complexes.[23-25] What is unique about complex **57** is that the Au(III) center contains two *cis*-accessible coordination sites; the first site is occupied by the agostic like interaction between the Au center and **57** the H-B bond, and the second site becomes available when the SMe_2 ligand dissociates from the Au center. Despite many attempts we were never able to isolate this complex again.

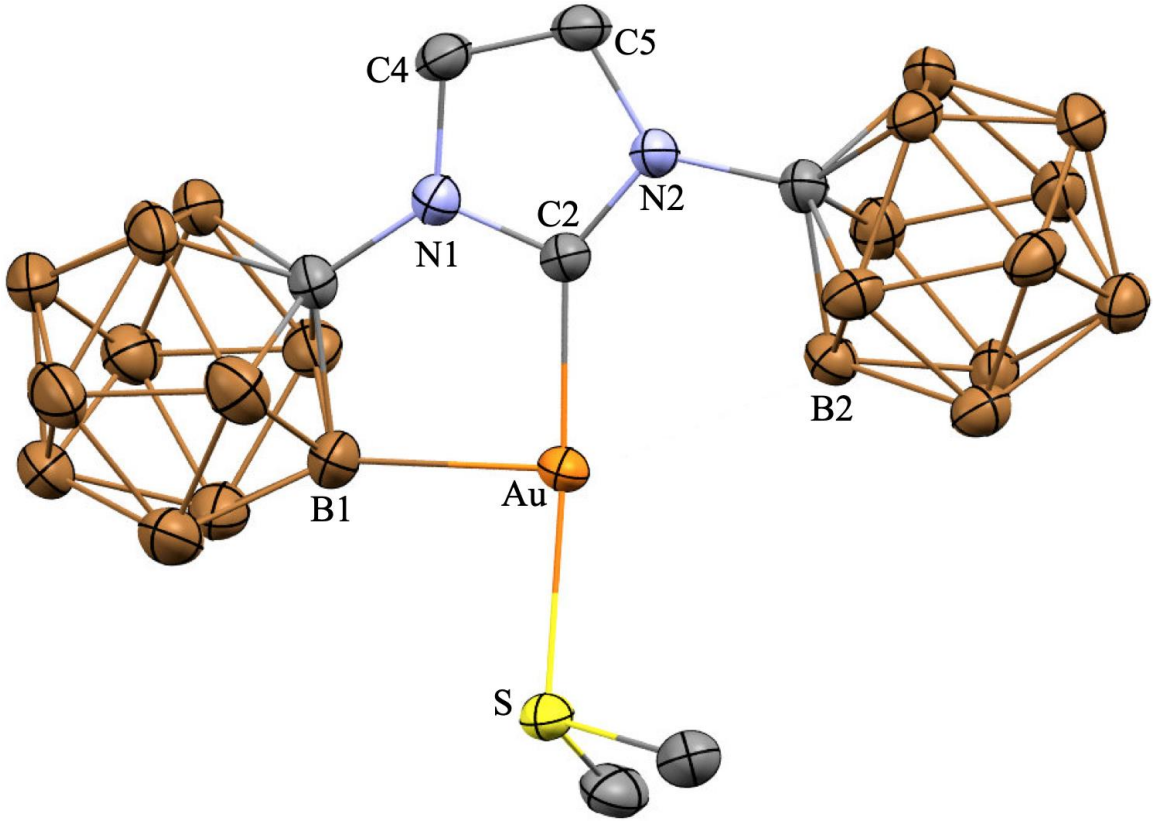

Figure 7-4 Solid state structure of **57**. Hydrogen atoms are omitted for clarity. Color code: B = brown, C = gray, N = blue, S = yellow, Au = orange.

Understanding the decomposition product **57** gave us insights to what molecular modifications had to be made to **43[Ph_3C^+]** in order to generate a stable anionic Au(I) complex with a trityl cation. This led us to two soluitons: 1) stabilize the trityl cation or 2) stabilize the anionic Au(I) fragment. To achieve the former, we hypothesized that by appending a *tert*-butyl group to the *para* positions of each aromatic ring of the trityl, we could avoid unwanted electrophilic aromatic substitution "like" reactions from occurring.[6, 14] The electron donating effects of the *tert*-butyl group would help stabilize the trityl cation, potentially eliminating the hydride abstraction leading to the formation of **57**. To stabilize the Au(I) fragment **43**, we would need to prevent the B-H bonds of the carborane from undergoing hydride abstraction with the trityl cation. To achieve this, we decided to hexahalogenate the antipodal and lower pentagonal belt of the carborane clusters. We choose to only hexahalogenate as perhalogenation (fully halogenated) could lead to steric issues associated with the deprotonation of the corresponding imidazolium or coordination issue with the Au(I) center. We also wanted to see if the halide abstraction could be performed with the lithium salt, **43[Li^+]** instead of **43[Ag^+].** This would eliminate the loss of a precious metal biproduct AgCl.

7.3 Stabilization of the Trityl Cation and the Formation of **43[sTr^+]**

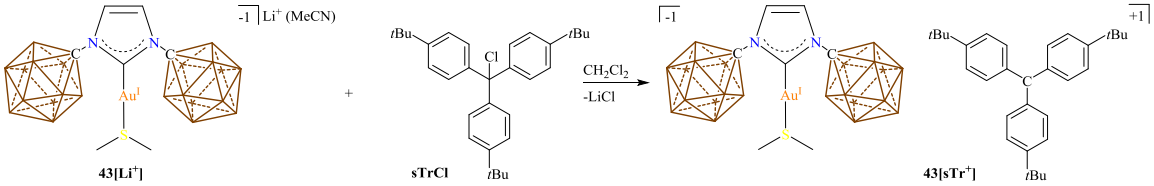

Scheme 7-4 Synthesis of **43[sTr^+]**. **sTr^+** = super trityl cation = 4',4',4'-tri-(*tert*-butyl)-trityl) cation.

To test our hypothesis regarding the stabilization of the trityl cation, we reacted a 1:1 mixture of super trityl (**sTrCl**, super trityl = 4',4',4'-tri-(*tert*-butyl)-trityl) chloride[26] and **43[Li^+]** in methylene chloride, Scheme 7-4. Upon addition of **sTrCl** to **43[Li^+]**, an immediate color change from brownish to yellow accompanied by a precipitate was observed. These observations were consistent with the formation of a

carbenium ion and suggested that the use of a silver salt was not necessary. The crude reaction mixture was filtered to remove LiCl and the highly colored filtrate was analyzed by multinuclear NMR spectroscopy. The ^{1}H NMR spectrum did not show any signals between 4 to 5 ppm suggesting that no electrophilic aromatic substitution "like" reactions followed by hydride migration had occurred. The anionic Au(I) fragment, **43**, was located at 7.26 (s, 2H) and 2.67 (s, 6H) ppm and displayed no major shift in ppm from the starting complex **43[Li^{+}]**. The only three remaining resonances in the ^{1}H NMR spectrum did not correspond to **sTrCl** and the downfield shift of the aryl doublets at 7.86 (d, 6H, $^{3}J_{(H,H)}$ = 8.5 Hz) and 7.59 (d, 6H, $^{3}J_{(H,H)}$ = 8.5 Hz) ppm suggested the formation of **sTr^{+}** **(sTr^{+}** = super trityl cation = 4',4',4'-tri-(*tert*-butyl)-trityl cation**)**. Indeed, the ^{13}C NMR spectrum corroborated the presence of the **sTr^{+}** ion with a downfield resonance at 204 ppm. These results are consistent with the formation of **43[sTr^{+}]**. To test the stability of this complex the NMR tube was heated to 100°C and no decomposition was observed.

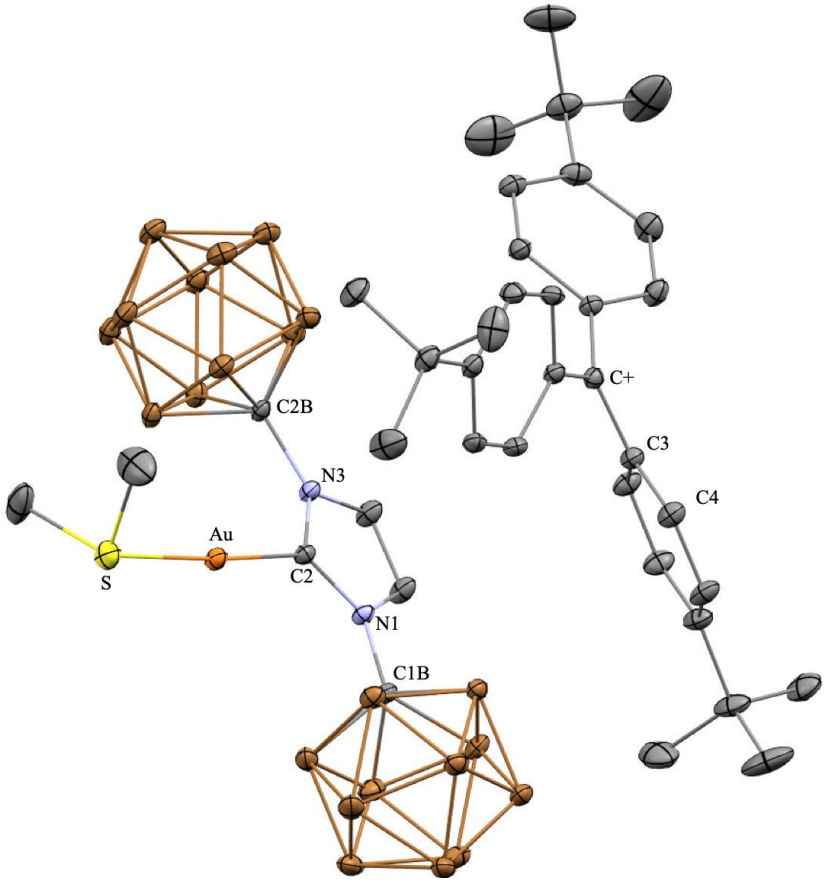

Figure 7-5 Solid state structure of **43[sTr$^+$]**. Hydrogen atoms have been omitted for clarity. Color code: B = brown, C = carbon, N = blue, S = yellow, Au = orange.

The structure of **43[sTr$^+$]** was unambiguously confirmed by a single-crystal X-ray diffraction study, Figure 7-5. In the solid state, the **sTr$^+$** ion displays no interaction at the tertiary carbocation (C+). However, there are multiple close contacts between the aryl groups of **sTr$^+$** and neighboring carborane anions. Not counting the many close contacts containing hydrogen atoms, the closest C_{aryl} ••• $B_{carborane}$ distance is 3.692 Å. The C-C bond lengths of the aryl substituents for the **sTr$^+$** ion vary between 1.377(2) and 1.414(2) Å, where the shortest bond lengths are consistently found between the *ortho* and *meta* C-C bonds (with respect to C+) with an average distance of 1.382(2) Å. The sum of the three $\angle C_{ipso}$-C$^+$-C_{ipso} (where C_{ipso} is an aryl C attached to C+) is 360° indicating the C+ carbocation is sp^2 hybridized. The Au-C2 distance is 2.0273(14) Å which is similar to **43[Li$^+$]** with a respective Au-C2 distance of 2.030(3) Å.[19] The

carborane carbon-nitrogen bond lengths are 1.4661(17) and 1.4642(17) for N1-C1B and N2-C2B respectively. These distances are in the range for normal C-N single bonds, thus there is no evidence for *exo*-π-conjugation between the cluster and heterocycle.[22, 27-29]

7.4 Stabilization of the Carborane Anion by Hexahalogenation of the Cluster

To address the issue of stabilizing the carborane anion we opted to hexahalogenate the clusters. The halogenated carborane clusters are even more stable then their corresponding B-H variants. The reason for this is that the longer B-X bonds help screen the negative charge and thus render the cluster even more weakly coordinating. Here we choose to hexahalogenate the clusters because perhalogentaion would likely render the deprotonation of the imidazolium troublesome as well as making the coordination chemistry of the corresponding NHC difficult or impossible.[30] The hexahalogenated imidazoliums and corresponding NHC-Au-Cl complexes were developed by a former lab mate, Dr. Scott McArthur, and the synthesis of these compounds can be found elsewhere.[30] The following sections will pick up with the synthesis of the NHC-Au-SMe2 complexes.

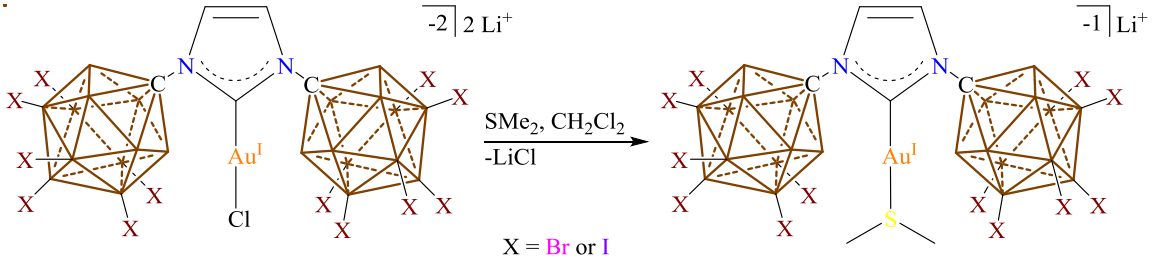

Scheme 7-5 Synthesis of **43X$_{12}$[Li$^+$]**. X = bromine or iodine.

To exchange the chloride ligand of **43(Cl)X$_{12}$[2Li$^+$]** (X = Br or I) for SMe_2 the complex was stirred in methylene chloride in the presence of an excess of SMe_2, Scheme 7-5. Over a 12-hour period, both reactions precipitate LiCl and the filtrate gives **43X$_{12}$[Li$^+$]**. The ^{1}H NMR spectrum of **43Br$_{12}$[2Li$^+$]** and **43I$_{12}$[2Li$^+$]** show the presence of the dimethylsulfide ligand at 2.93 and 2.97 ppm respectively as well

as the imidazolylidene backbone protons at 7.37 and 7.41 ppm respectively. The two-step synthesis (NHC to NHC-Au-Cl to NHC-Au-SMe_2) is preferred over a single step synthesis (NHC to NHC-Au-SMe_2) reported by Fisher and coworkers because of the improved yields.[19] Another advantage of the two step synthesis is all the NHC is converted to the corresponding **$43X_{12}[Li^+]$**, whereas the single step synthesis generates **$43X_{12}[2Li^+]$** as an unwanted side product.

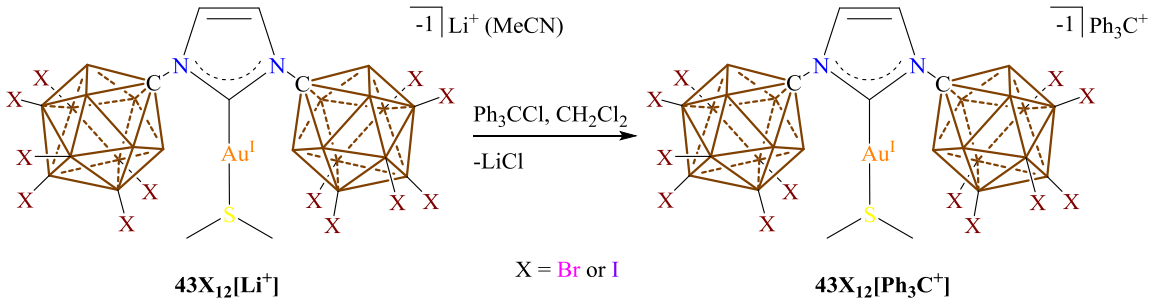

Scheme 7-6 Synthesis of **$43X_{12}[Ph_3C^+]$**. X = bromine or iodine.

Next was to test the reactivity of the halogenated compounds **$43X_{12}[Li^+]$** with the trityl cation. A solution of trityl chloride was added to a solution of **$43X_{12}[Li^+]$** (X = Br or I) in methylene chloride which gave an immediate precipitate and color change to yellow. After filtration of the LiCl the filtrate was analyzed by multinuclear NMR spectroscopy. ^{1}H NMR of both **$43Br_{12}[Li^+]$** and **$43I_{12}[Li^+]$** displayed no singlets between 4 to 5 ppm indicating that electrophilic aromatic substitution "like" reactions were not present in the bulk material. Both **$43Br_{12}[Li^+]$** and **$43I_{12}[Li^+]$** displayed the expected downfield triplet, triplet, doublet at 8.31, 7.93, and 7.70 ppm corresponding to the aryl protons of the trityl cation. The only difference in the ^{1}H NMR spectrum of **$43Br_{12}[Li^+]$** and **$43I_{12}[Li^+]$** was the location of the imidazolylidene protons which were located at 7.35 and 7.39 ppm respectively along with the dimethylsulfide methyl protons at 2.92 and 2.97 ppm. Both of the ^{13}C NMR spectrums showed a downfield resonance at 211 ppm which corresponds to the formal carbocation of the trityl cation. This data supported the formation of the

ion pair **43X$_{12}$[Ph$_3$C$^+$]** (X = Br or I). As expected, these compounds are also resistant to hydride abstraction and do not decompose in prolonged exposure to aryl hydrocarbon or alkyl halide solvents.

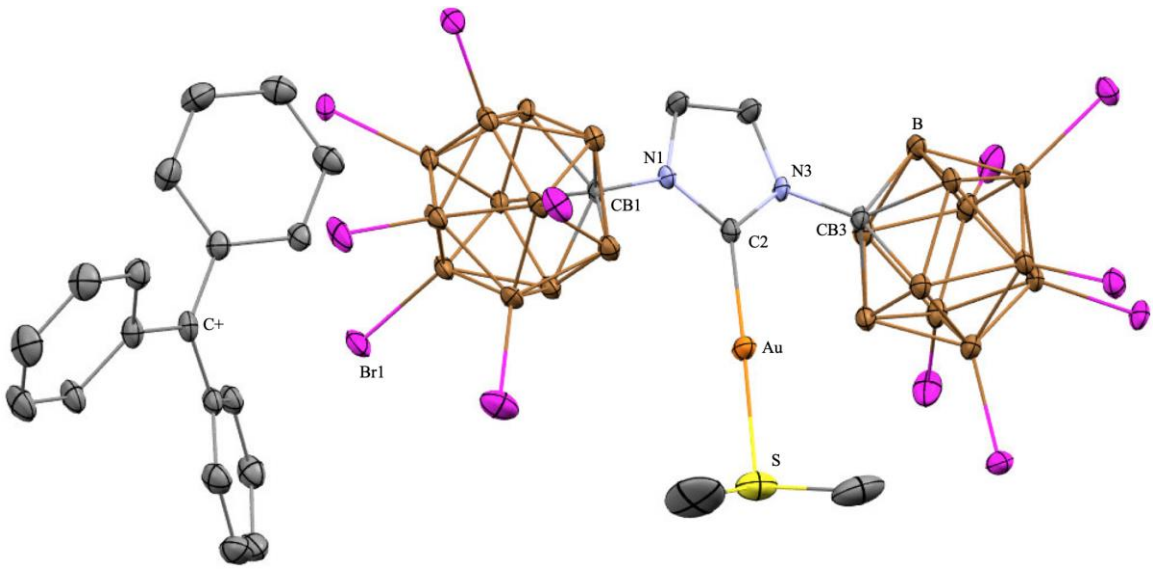

Figure 7-6 Solid state structure of **43Br$_{12}$[Ph$_3$C$^+$]**. Hydrogen atoms have been omitted for clarity. Color code: B = brown, C = gray, N = blue, S = yellow, Br = magenta.

To see if there were any interactions between the trityl cation and the anionic Au(I) complexes we wanted to grow crystals suitable for single-crystal X-ray diffraction studies. Both compounds crystallize from a mixture of methylene chloride and hexane, however only **43Br$_{12}$[Ph$_3$C$^+$]** gave sufficient data to discuss accurate bond metrics, Figure 7-6. In the solid-state the trityl cation of **43Br$_{12}$[Ph$_3$C$^+$]** shows 4 close contacts with the bromine atoms of carborane anion. The closest of these interactions is the Br1-C+ interaction at 3.473 Å. The bond lengths of aryl C-C bonds of the trityl cation are substantially sorter then those of **43[sTr$^+$]**, the average aryl C-C bond length is 1.394 Å. The longest aryl C-C bonds are bonds between the C_{ipso}-C_{ortho} carbon atoms (with respect to C+) with an average distance of 1.414 Å. The sum of the $\angle C_{ipso}$-C$^+$-C_{ipso} is 360° indicating the tertiary carbocation C+ is sp^2 hybridized. The C2-Au bond distance is 2.016(3) Å which is standard for these types of complexes. The ∠C2-Au-S angle is nearly linear at 176°. The N1-CB1 and N3-CB2 bond distances are 1.464(4) and 1.461(4) Å respectively,

indicating that there is no *exo*-π-conjugation between the cluster and the heterocycle.[22, 27-29] The low quality structure of **43I$_{12}$[Ph$_3$C$^+$]** confirms the existence of the ion pair, however the low quality data does not allow for a bond metric discussion, Figure 7-7.

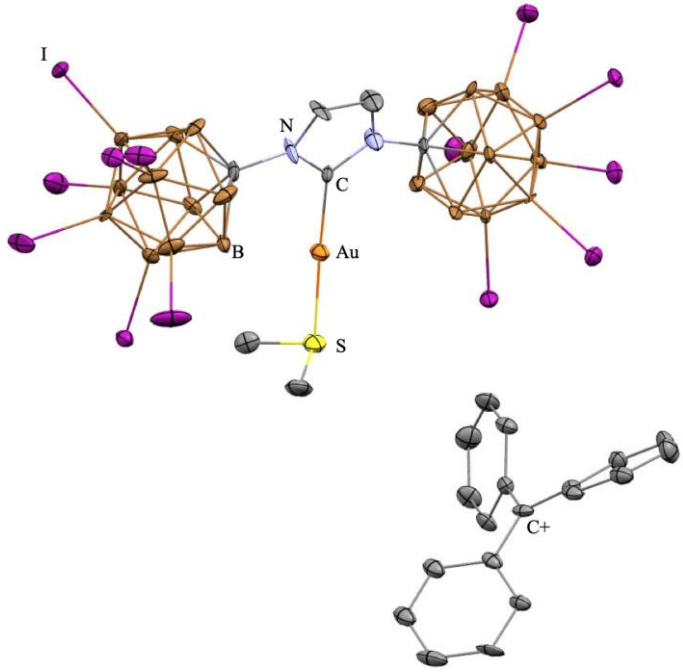

Figure 7-7 Low-quality solid-state structure of **43I$_{12}$[Ph$_3$C$^+$]**. Hydrogen atoms omitted for clarity. Color code: B = brown, C = gray, N = blue, Au = orange, S = yellow, I = purple.

7.5 Synthesis of a Anionic Au(I) Complex with a Silylium Ion

With **43X$_{12}$[Ph$_3$C$^+$]** in hand, we wanted to see if we could generate the ion pair **43[Et$_3$Si$^+$]**. To perform this reaction, we decided to react **43X$_{12}$[Ph$_3$C$^+$]** (X = Br or I) with Et_3SiH in *o*-$Cl_2C_6H_4$. Upon mixing a solution of **43Br$_{12}$[Ph$_3$C$^+$]** with Et_3SiH a color change from yellow to white is observed over a 30-minute period. The reaction is then filtered into hexane which precipitate outs a white solid. Analysis of this solid by multinuclear NMR spectroscopy gives the following results: a disappearance of the H-Si bond at 3.90 ppm in the ^{1}H NMR spectrum, a downfield shifted resonance in the ^{1}H-^{29}Si HSQC at 66.1 and 61.3

ppm, three peaks at 0.8, -8.3, --15.9 ppm with a 1:5:5 ratio in the ^{11}B NMR spectrum. With this data in mind we can conclude that the Bartlett-Condon-Schneider silicon-to-carbon hydride transfer was successful, and we propose the formation of **43Br$_{12}$[Et$_3$Si$^+$]**, Scheme 7-7. When a similar reaction is performed with **43I$_{12}$[Ph$_3$C$^+$]** we observe the loss of triphenylmethane but run into solubility issues trying to dissolve the white insoluble material post washing. The decreased solubility of this material complicates its structural elucidation, for this reason we will discuss **43Br$_{12}$[Et$_3$Si$^+$]** in greater detail. Despite solubility setbacks we believe **43I$_{12}$[Ph$_3$C$^+$]** gives a similar product which we will tentatively assign **43I$_{12}$[Et$_3$Si$^+$]**. If the same reaction is tried with **43[sPh$_3$C$^+$]**, no single major product is formed.

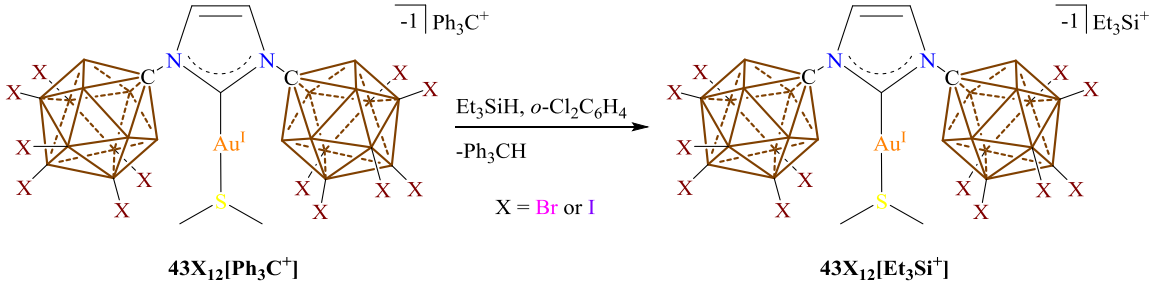

Scheme 7-7 Synthesis of **43Br$_{12}$[Et$_3$Si$^+$]**

With the current data of **43[Et$_3$Si$^+$]**, we are unable to comment on the coordination mode of the Si$^+$ ion. We can conclude that the silyl ion is far from free due to its upfield shift. Calculations suggest that free Et$_3$Si$^+$ should have a ^{29}Si NMR signal greater than 200 ppm.[31-33] Despite the experimental prediction, Nava and Reed have shown that free Et$_3$Si$^+$ is impossible to generate.[34] If the Et$_3$Si$^+$ ion does not form a Et$_3$Si(solvent)$^+$ adduct the Et$_3$Si$^+$ ion will dimerize, even under stoichiometric conditions it form a [Et$_3$Si-H-SiEt$_3$]$^+$ adduct.[34] This dimer could explain why Reed and coworkers observed two resonances at 111.8 and 106.2 ppm, in the solid state ^{29}Si NMR spectrum of proposed [Et$_3$Si$^+$][**3Br$_6$**].[35] Since this dimer does not exist when the Et$_3$Si$^+$ ion is coordinated to solvent, the chemical shift of the Si atom moves upfield. The highest reported chemical shift for a Et$_3$Si(solvent)$^+$ adduct is at 92.3 ppm in benzene.[36] Since

$43Br_{12}[Et_3Si^+]$ contains two chemical shifts, one may propose that a $[Et_3Si\text{-}H\text{-}SiEt_3]^+$ dimer had formed. We do not believe this is the case. Instead, we believe that the upfield resonance suggest two $Et_3Si(solvent)^+$ adducts. One is likely the $Et_3Si(o\text{-}Cl_2C_6H_4)^+$ adduct formed because $o\text{-}Cl_2C_6H_4$ is the reaction solvent and NMR solvent. The other is likely due to the Et_3Si^+ ion coordinating to the dimethylsulfide ligand of the anionic Au(I) complex. In support of this claim, Oestreich and coworkers have reported the trapping of an R_3Si^+ ion with diphenylsulfide and this $R_3Si(Ph_2S)^+$ adduct has a ^{29}Si chemical shift of 58.8 (R = *i*Pr) ppm. We are currently working on elucidating the structure of **$43I_{12}[Et_3Si^+]$** as well as the coordination environment of the Et_3Si^+ ion of **$43Br_{12}[Et_3Si^+]$**.

7.8 Experimental

General Considerations:

All manipulations were carried out using standard Schlenk or glovebox techniques under a dinitrogen atmosphere (industrial grade, glovebox) or purified elemental argon (99.995%, Schlenk line) unless otherwise stated. Dry solvents were obtained via distillation under argon from calcium hydride (acetonitrile, fluorobenzene, methylene chloride), sodium-potassium alloy (diethyl ether), potassium (benzene) or potassium utilizing benzophenone ketyl radical as an indicator (tetrahydrofuran). Pentane and toluene were collected from a solvent purification system by SG Waters USA, LLC utilizing a fifteen-minute argon sparge followed by passage though activated aluminum. Compounds **$3[Cs^+]$** and **$43[Li^+]$** were prepared according to the literature. Unless specifically stated, reagents were purchased from commercial vendors and used without further purification. Nuclear magnetic resonance (NMR) spectroscopy was carried out using: Bruker Avance 300 MHz, Bruker Avance 600 MHz, and Bruker NEO 400 MHz (CryoProbe), Varian Inova 500 MHz. NMR chemical shifts are reported in parts per million (ppm) with ^1H and ^{13}C chemical shifts referenced to the residual non-deutero solvent. The $^{11}B\text{-}^1H$ coupling constants from ^{11}B spectra are reported when possible. Infrared spectroscopy was recorded on a Bruker ALPHA FTIR Spectrometer or Thermo Fisher Nicolet FTIR Spectrometer. High-resolution mass spectrometry (HRMS) was collected on an Agilent Technologies 6210 (TOF LC/MS) featuring a direct injection with multimode

electrospray ionization/atmospheric-pressure chemical ionization (ESI/APCI). Melting points were obtained on a Büchi Model B-545.

General Decoordination Procedure of $3H_{12}[Li^+(MeCN)]$:

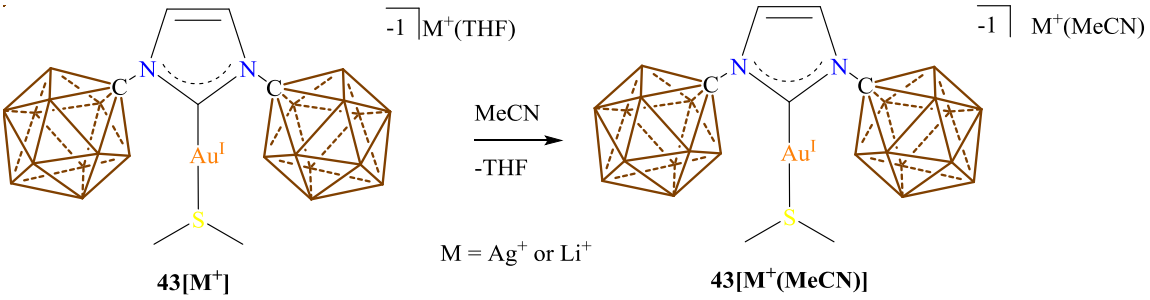

Scheme 7-8 Generic Synthesis of **43[M$^+$(MeCN)]** where M = Li^+ or Ag^+.

The following is a generic procedure for switching THF coordinated to Ag^+ or Li^+ to acetonitrile coordinated to Ag^+ or Li^+. As an example, **43[Li$^+$]** was dissolved in acetonitrile and placed under vacuum until all volatiles were removed. This process was repeated until no THF was detectable by NMR, typically three processes was required to removal all THF, **43[Li$^+$(MeCN)]** was recovered in quantitative yield. Other yields are quantitative as well. *Note: **43I_{12}[Li$^+$]** is not very soluble in acetonitrile but the process still works*. ^{1}H NMR (400 MHz, methylene chlroide-d_2, 25°C): δ = 7.35 (s, 2H), 2.78 (s, 6H), 3.28-0.90 (bm, 22H, B-H). ^{1}H[^{11}B] NMR (400 MHz, methylene chloride-d_2, 25°C): δ = 7.35 (s, 2H), 2.78 (s, 6H), 2.58 (s, 10H, B-H), 1.72 (s, 2H, B-H), 1.61 (s, 10H, B-H). ^{11}B[^{1}H] NMR (128 MHz, methylene chloride-d_2, 25°C): δ = -8.8, -13.9 ppm. ^{11}B NMR (128 MHz, methylene chloride-d_2, 25°C): δ = -8.8 (^{1}*J(H,B)* = 128.4 Hz), -13.8 (^{1}*J(H,B)* = 136.8 Hz). ^{13}C[^{1}H] NMR (101 MHz, methylene chloride-d_2, 25°C): δ = 174.3, 122.3, 79.8, 25.1 ppm. IR (Solid, ATR, 25°C): B-H stretch appears near 2500 cm^{-1}.

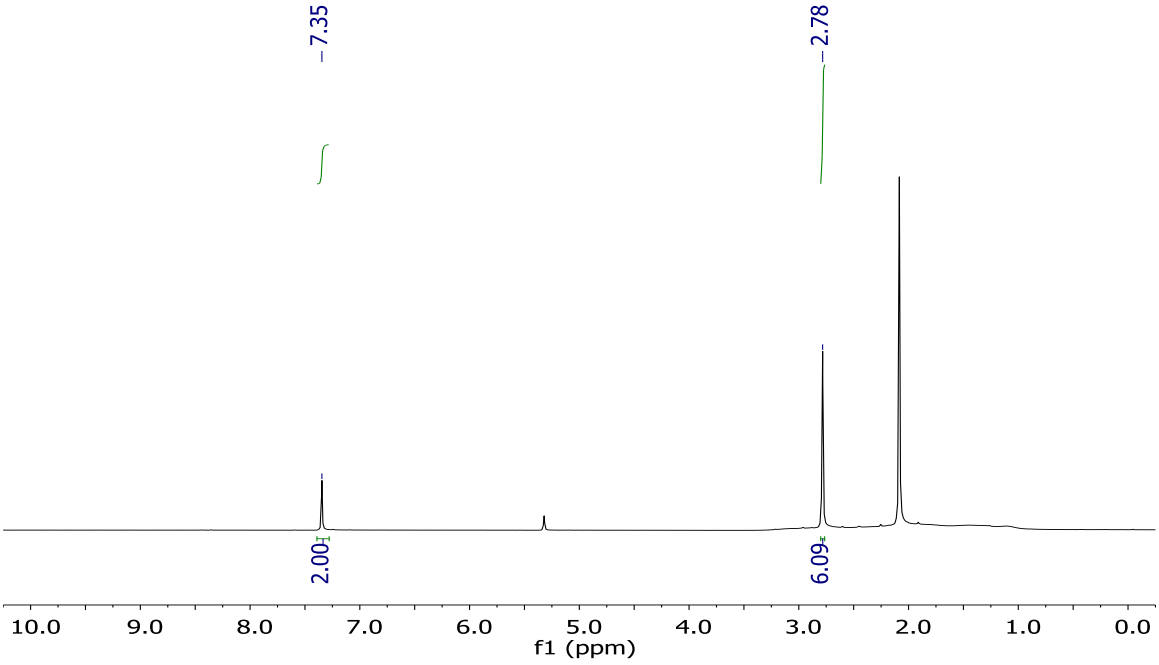

Figure 7-8 ^{1}H NMR-spectrum of **43[Li^{+}(MeCN)]** in methylene chloride-d_2. *Note: acetonitrile can be seen at 2.1 ppm.*

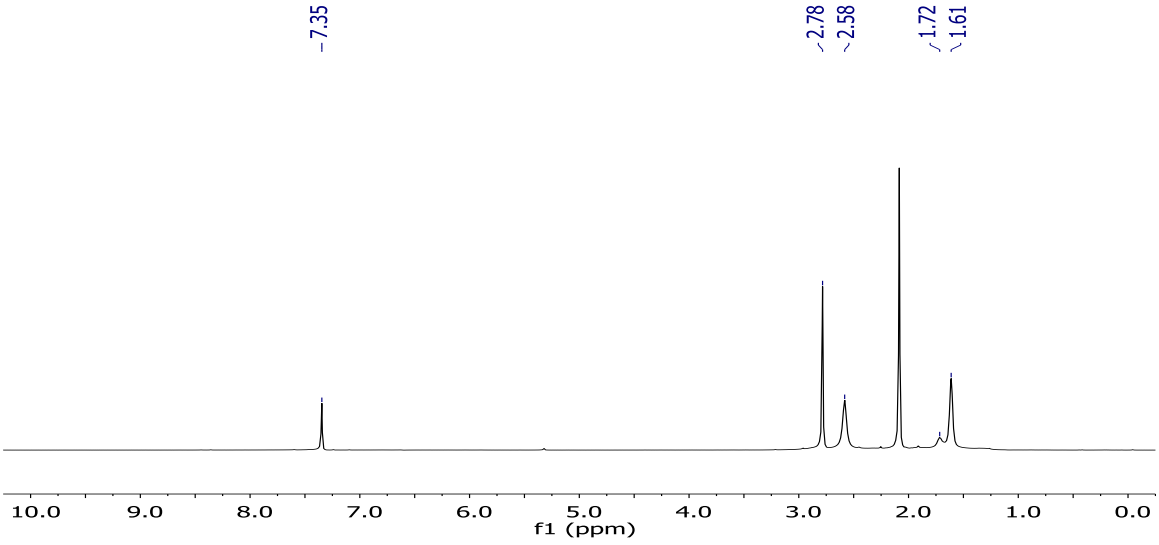

Figure 7-9 ^{1}H[^{11}B] NMR-spectrum of **43[Li^{+}(MeCN)]** in methylene chloride-d_2. *Note: acetonitrile can be seen at 2.1 ppm.*

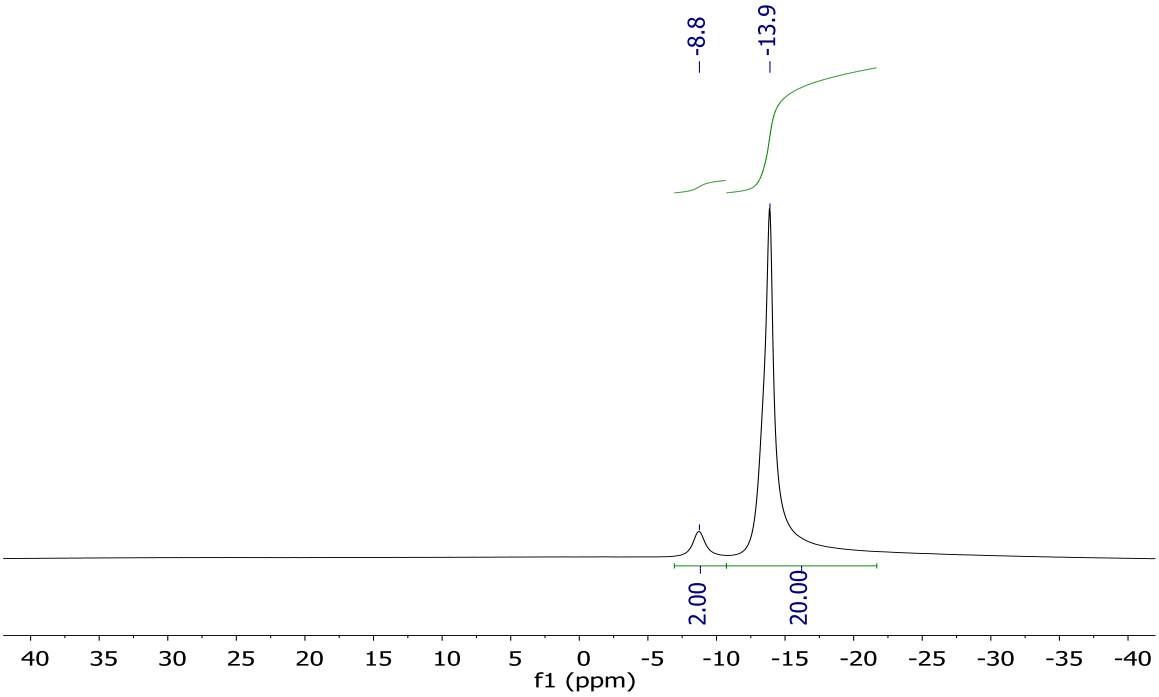

Figure 7-10 $^{11}B[^{1}H]$ NMR-spectrum of **43[Li^{+}(MeCN)]** in methylene chloride-d_2.

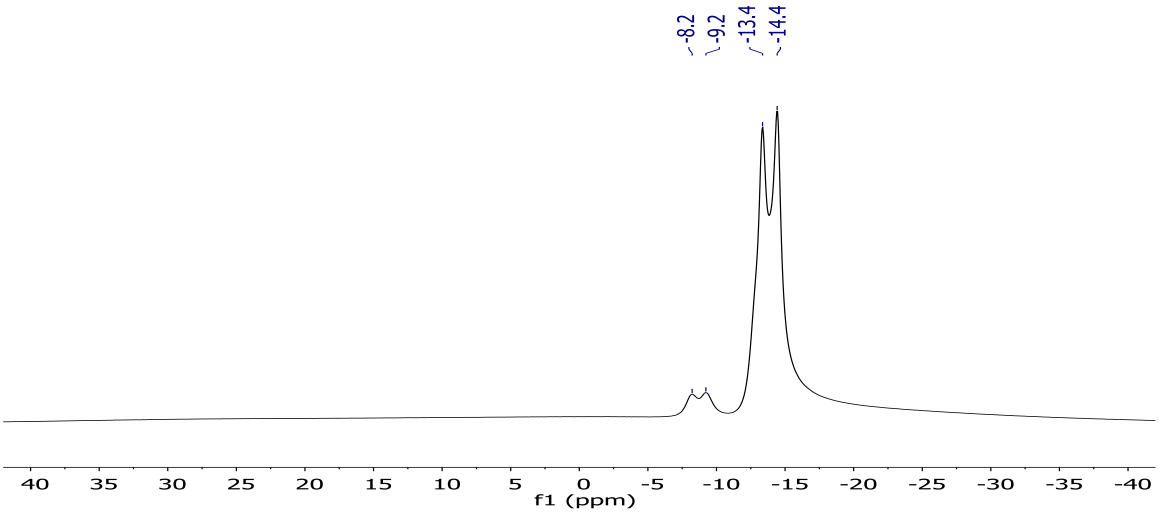

Figure 7-11 ^{11}B NMR-spectrum of **43[Li^{+}(MeCN)]** in methylene chloride-d_2.

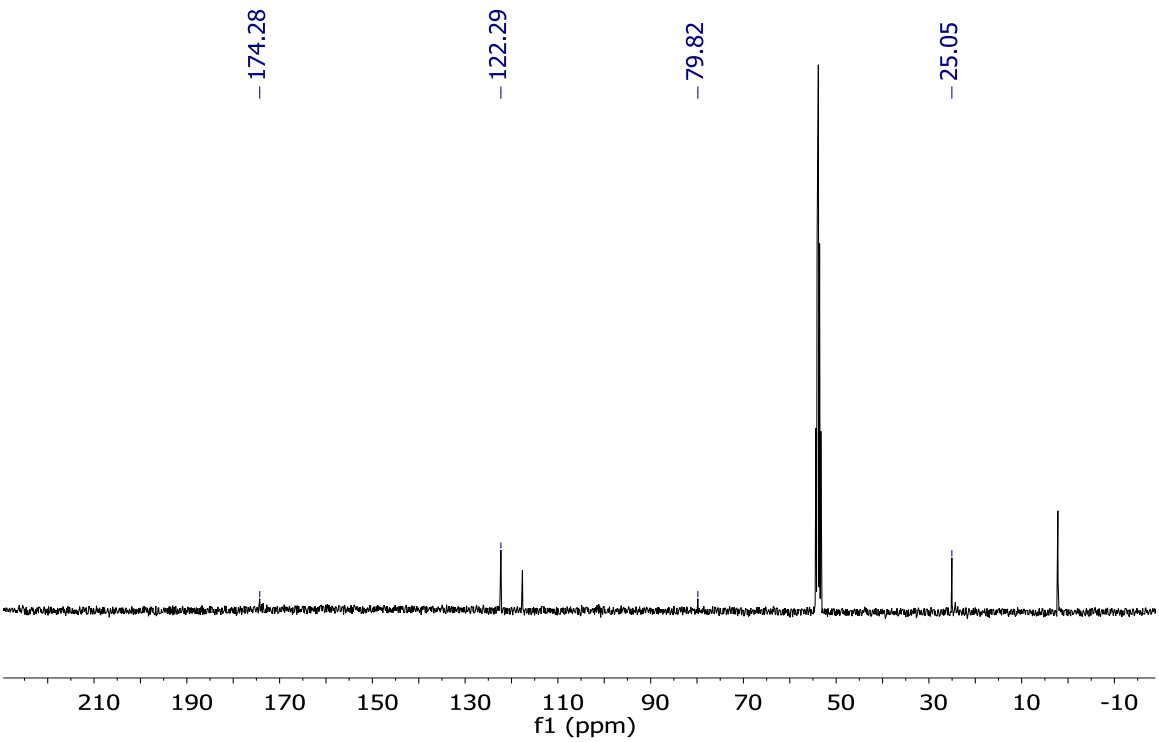

Figure 7-12 $^{13}C[^{1}H]$ NMR-spectrum of **43[Li^{+}(MeCN)]** in methylene chloride-d_2. *Note: acetonitrile can be seen at 118 and 2 ppm.*

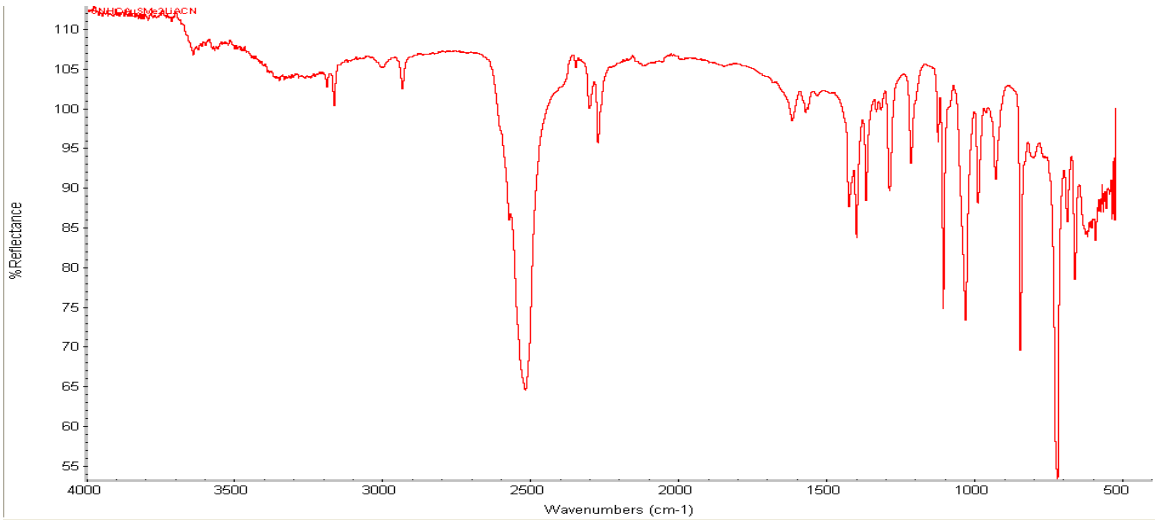

Figure 7-13 IR spectrum of **43[Li^{+}(MeCN)]** in the solid state showing the B-H stretches near at 2500 cm^{-1}.

Synthesis of 43[Ph_3C^+]:

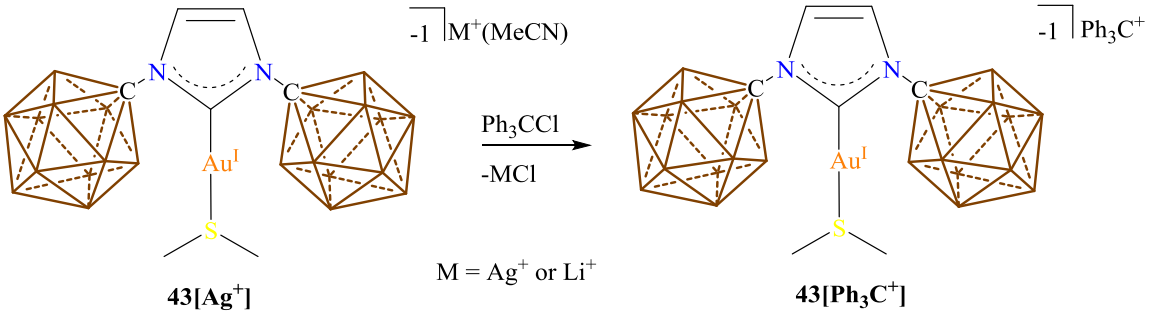

Scheme 7-9 Synthesis of **43[Ph_3C^+]**.

The following was done in a glovebox under a dinitrogen atmosphere with the Li^+ cation, the same procedure works for the Ag^+ cation. A glass scintillation vial was loaded with **Ph_3CCl** (1.2 equivalents) and dissolved in 5 mL of methylene chloride. **Ph_3CCl** was added dropwise to a stirring solution of **43[Li^+]** (*note: THF cannot be coordinated to the M^+ cation otherwise the reaction will fail!)* dissolved in 5 mL of methylene chloride. The vial containing the **Ph_3CCl** was washed twice with methylene chloride (5 mL each) and added to the reaction. The reaction progressed for 1 hour at 25°C during this time the reaction darkened and a precipitate formed. The reaction was filtered through a Büchner funnel equip with an oven dried medium – fine plain paper filter then a pipette filter containing an oven dried glass microfiber filter. The filtrate was evaporated to dryness yielding 578 mg of the desired complex (99% yield). If further purification is required the complex can be dissolved in dry acetonitrile and pumped down on the high vacuum until a precipitate crashes out of solution. The mother liquor is decanted off and placed in the freezer at -32°C forming more precipitate. The collected precipitate was washed with cold acetonitrile giving **43[Ph_3C^+]** (412 mg, yield 71%). ^{1}H NMR (300 MHz, chloroform-d_1, 25°C): δ = 8.36 (m, 3H), 7.99 (m, 6H), 7.76 (m, 6H), 7.35 (s, 2H), 2.84 (s, 6H), 3.57-0.83 (bm, 22H, B-H). ^{1}H[^{11}B] NMR (300 MHz, chloroform-d_1, 25°C): δ = 8.36 (m, 3H), 7.98 (m, 6H), 7.76 (m, 6H), 7.35 (s, 2H), 2.84 (s, 6H), 2.63 (bs, 10H), 1.82 (bs, 2H), 1.70 (bs, 6H). ^{13}C[^{1}H] NMR (125 MHz, acetonitrile-d_3, 25°C): δ = 211.8, 175.1, 144.0, 141.1, 131.1, 128.4, 123.4, 80.2, 24.1 ppm. ^{11}B[^{1}H] NMR (96 MHz, chloroform-d_1, 25°C): δ = -8.9, -13.8

ppm. ^{11}B NMR (96 MHz, chloroform-d_1, 25°C): δ = -8.9 ($^1J(H,B)$ = 124.1 Hz), -13.8 ($^1J(H,B)$ = 135.7 Hz). IR (KBr pellet, 25°C): B-H stretch = 2539 cm^{-1}.

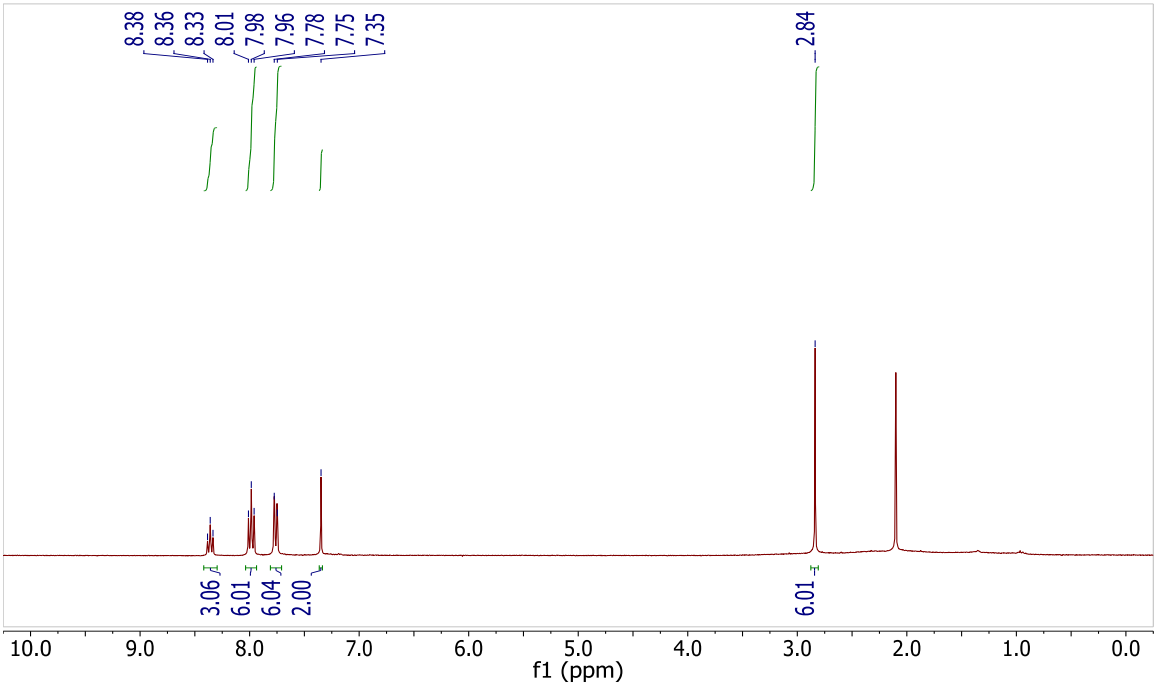

Figure 7-14 ^{1}H-NMR spectrum of **43[Ph_3C^+]** in chloroform-d_1. *Note: the peak at 2.1 ppm is due to acetonitrile.*

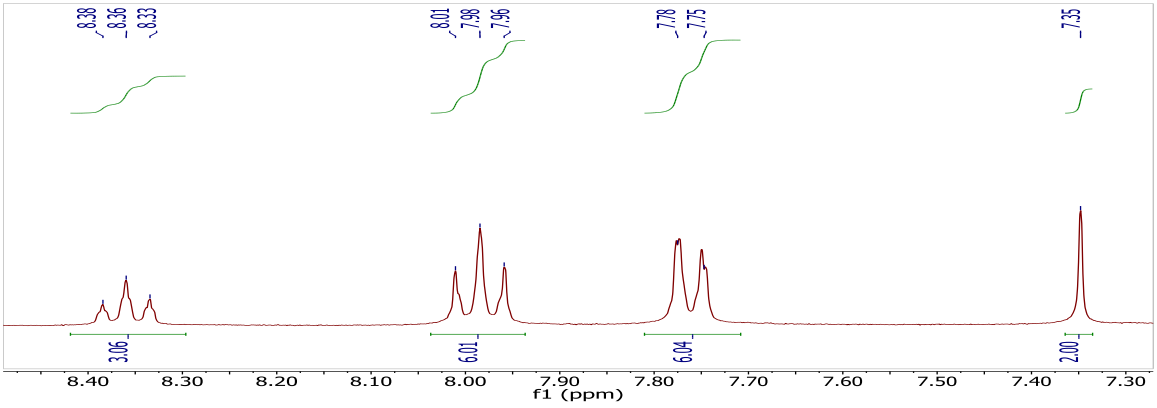

Figure 7-15 An expansion of the ^{1}H NMR spectrum featuring the aromatic region of **43[Ph_3C^+]**.

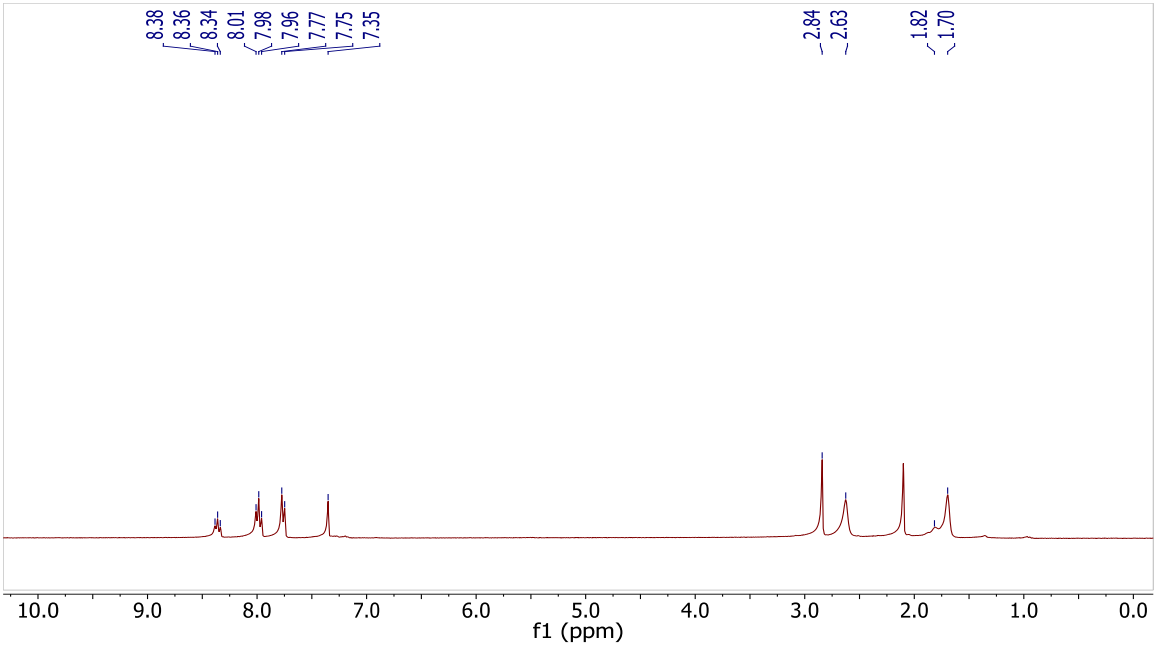

Figure 7-16 $^{1}H[^{11}B]$ NMR spectrum of **43[Ph_3C^+]** in chloroform-d_1. *Note: the boron hydrides appear at 2.63, 1.82 and 1.70 ppm. Acetonitrile is seen at 2.1 ppm.*

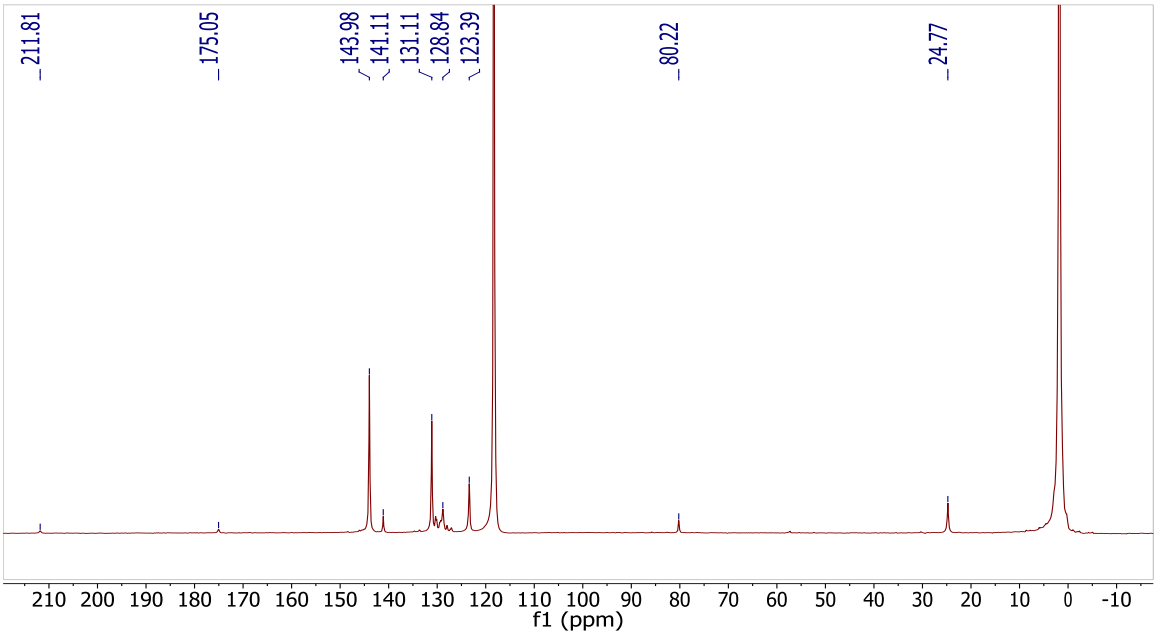

Figure 7-17 $^{13}C[^{1}H]$ NMR of **43[Ph_3C^+]** in acetonitrile-d_3. *Note: Acetonitrile-d_3 is seen at 1.3 and 118 ppm.*

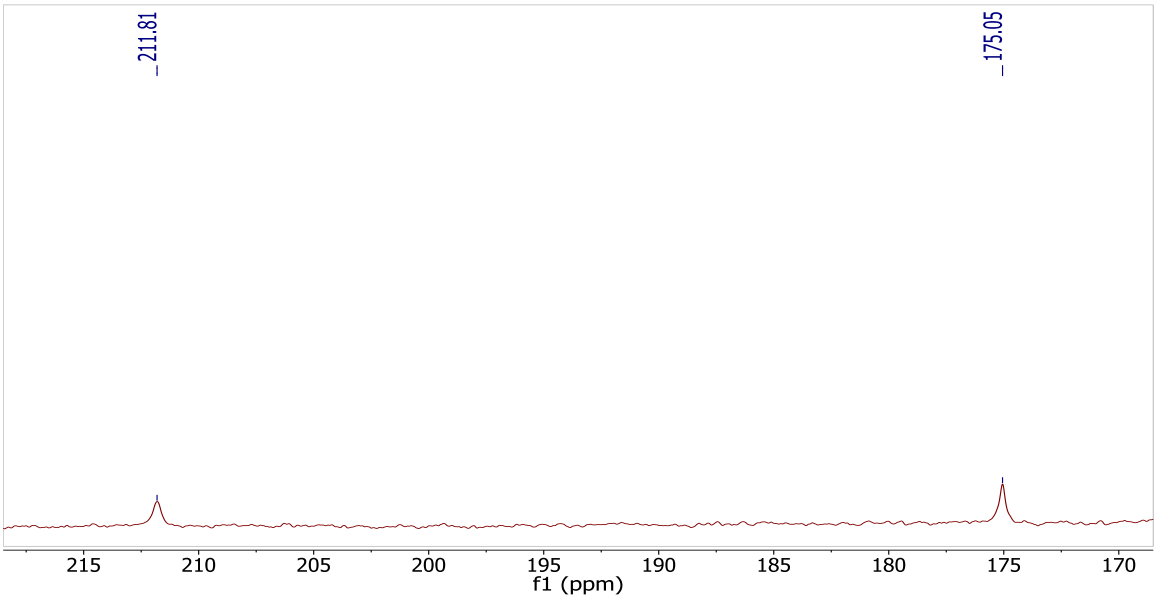

Figure 7-18 An expansion of the far downfield region of the $^{13}C[^{1}H]$ NMR of **43[Ph_3C^+]** showing the formal carbocation of the trityl cation along with the carbene carbon.

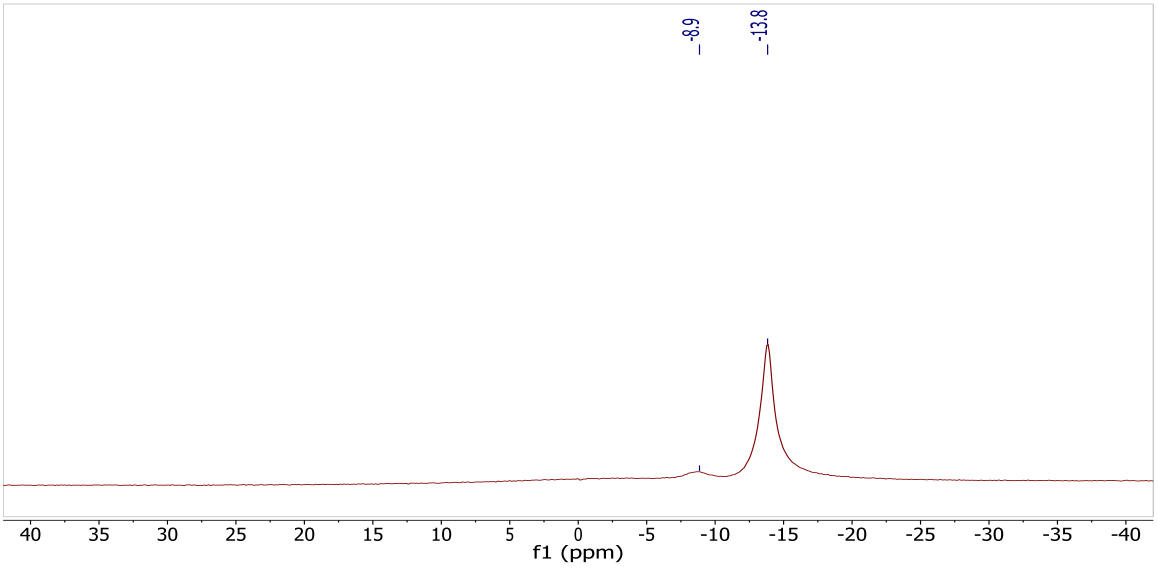

Figure 7-19 $^{11}B[^{1}H]$ NMR spectrum of **43[Ph_3C^+]** in Chloroform-d_1.

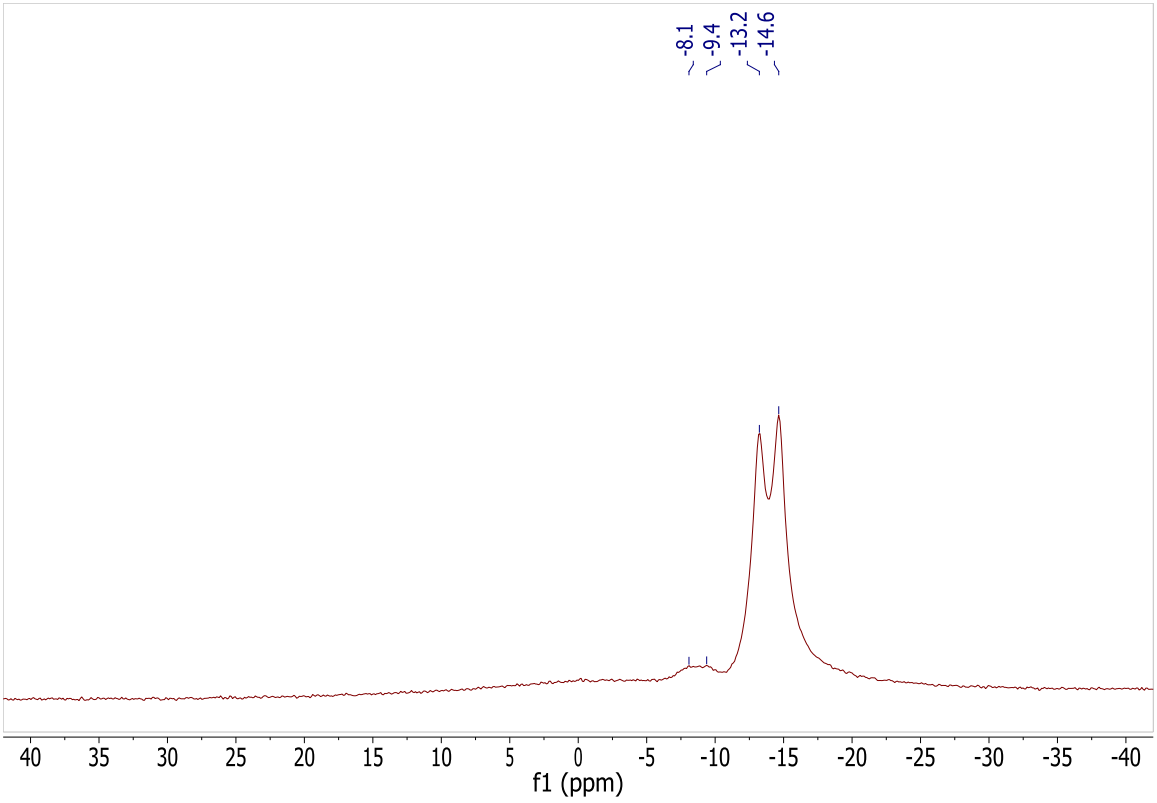

Figure 7-20 ^{11}B NMR of **43[Ph_3C^+]** in chloroform-d_1 showing the ^{1}J B-H coupling.

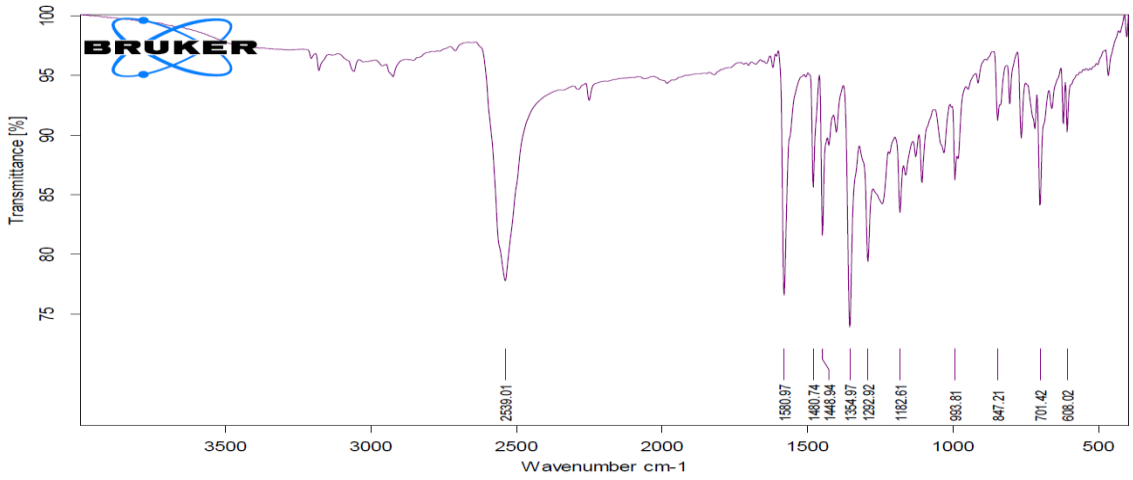

Figure 7-21 IR spectrum of solid **43[Ph_3C^+]**. *Note: the B-H stretches appear at 2539 cm^{-1}.*

Synthesis of 57:

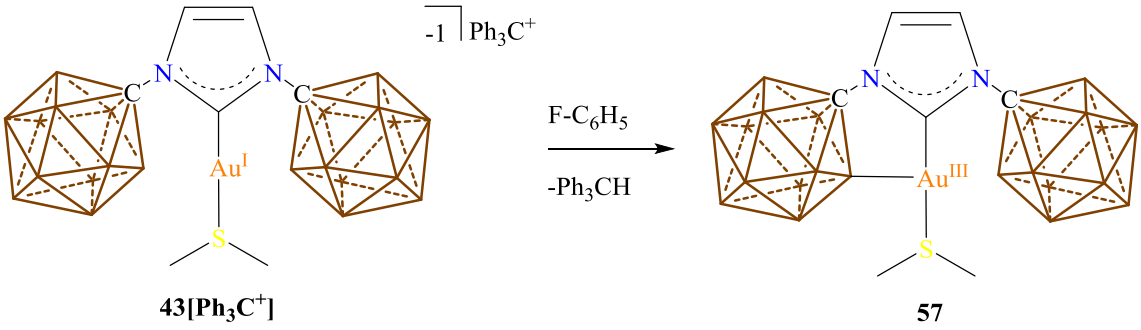

Scheme 7-10 Synthesis for the isolation of **57** which worked exactly once.

In a glove box under dinitrogen atmosphere a glass scintillation vial was equipped with a stir bar and loaded with **43[Ph_3C^+]** (558.0 mg, 650 μmol) and suspended in 5 mL of benzene. The reaction was stirred overnight and then the supernatant was carefully removed. The supernatant was evaporated to dryness and the solid was dissolved in 3 mL of toluene and added to a 18 mL of stirring pentane. The supernatant surprisingly contained **57** and upon removal of solvents *in vacuo* gave the title compound (45 mg, 12 % yield). Crystals suitable for X-ray diffraction were grown by layering an NMR tube with methylene chloride and pentane. *Note: this experiment was not reproducible.* ^{1}H NMR (300 MHz, benzene-d_6, 25°C): δ = 6.11 (d, $^{3}J(H,H)$ = 2.1 Hz, 1H), 5.69 (d, $^{3}J(H,H)$ = 2.1 Hz, 1H), 1.33 (s, 6H), 3.50 – 1.70 (bm, 22H, B-H). ^{1}H[^{11}B] NMR (300 MHz, Benzene-d_6, 25°C): δ = 6.13 (d, $^{3}J(H,H)$ = 2.1 Hz, 1H), 5.71 (d, $^{3}J(H,H)$ = 2.1 Hz, 1H), 3.23 (s, 1H, B-H), 3.05 (s, 1H, B-H), 2.86 (s, 1H, B-H), 2.77 (s, 2H, B-H), 2.72 (s, 5H, B-H), 2.50 (s, 2H, B-H), 2.44 (s, 5H, B-H), 2.40 (s, 1H, B-H), 2.30 (s, 2H, B-H), 2.18 (s, 2H, B-H), 1.36 (s, 6H). ^{13}C[^{1}H] NMR (125 MHz, Benzene-d_6, 25°C): δ = 169.0, 122.9, 119.6, 78.7, 75.8, 23.81 ppm. ^{11}B[^{1}H] NMR (192.5MHz, Benzene-d_6, 25°C): δ = -4.0, -8.1, -9.2, -10.0, -10.8, -12.5 ppm.

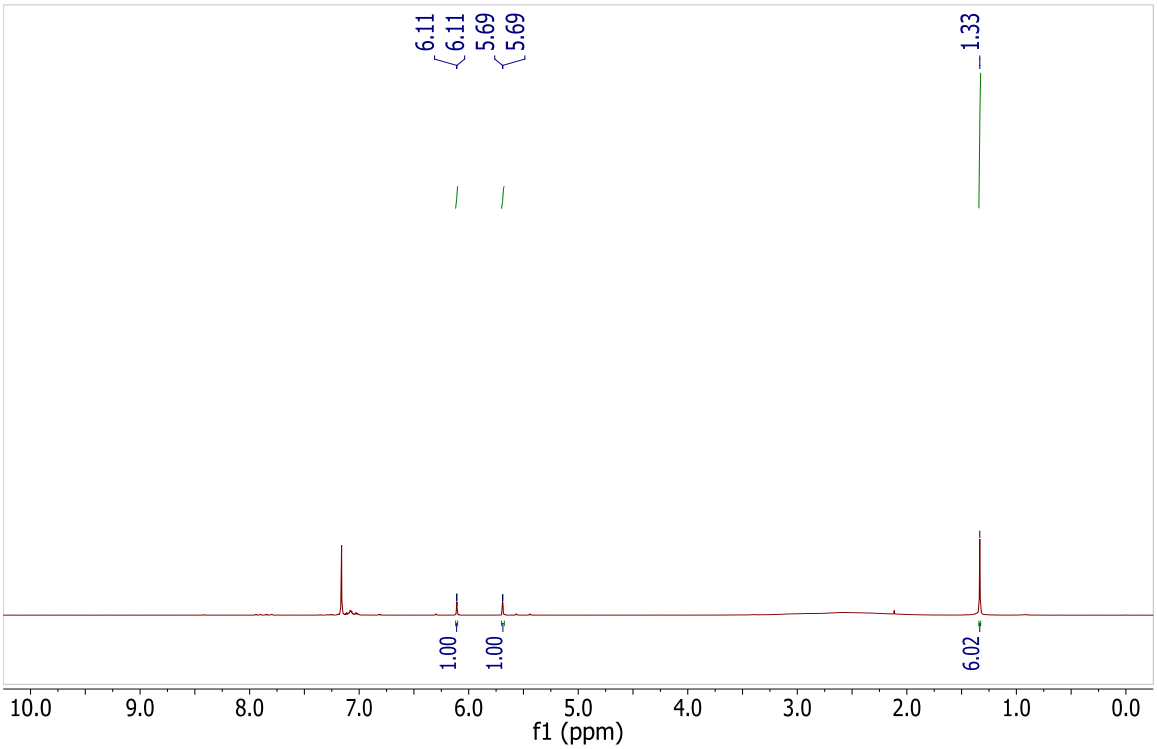

Figure 7-22 ^{1}H-NMR spectrum of **57** in benzene-d_6. *Note: trace toluene can be seen near 7.1 and 2.1 ppm.*

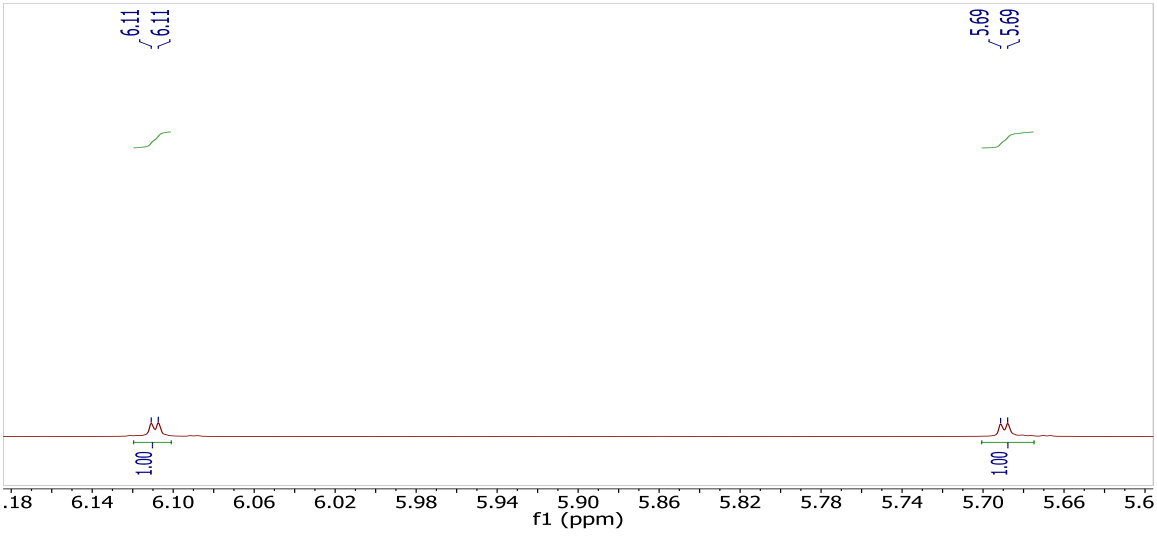

Figure 7-23 An expanded view of the aromatic region of the ^{1}H-NMR of **57** in benzene-d_6, showing the small ^{3}J-coupling of the imidazolylidene protons.

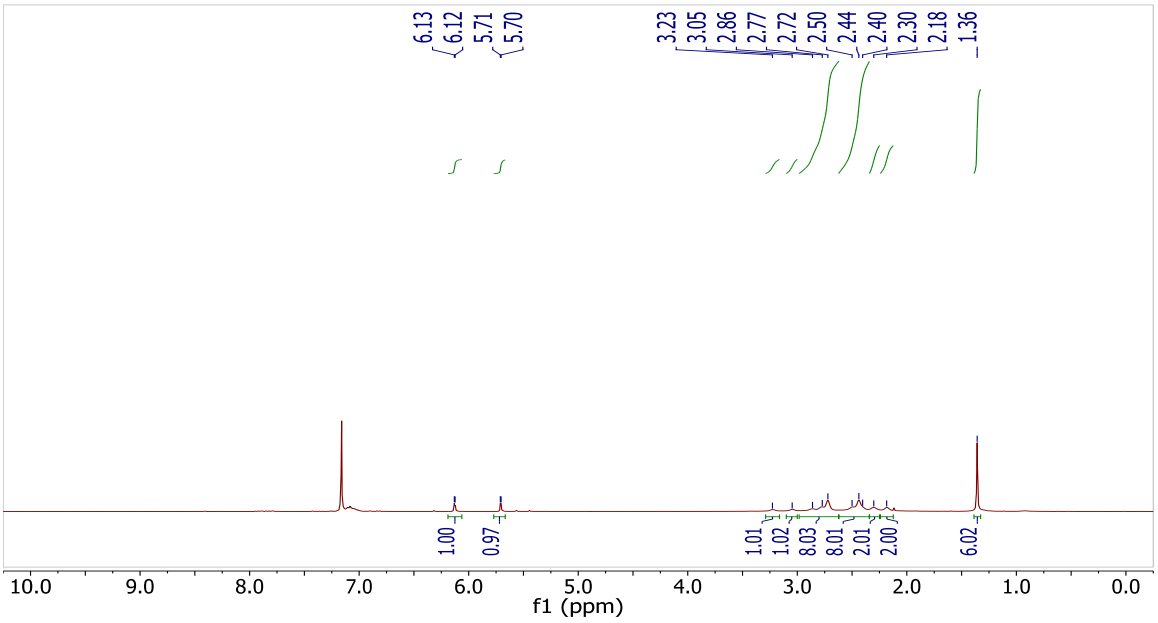

Figure 7-24 $^{1}H[^{11}B]$-NMR spectrum of **57** in benzene-d_6. The borohydrides are found between 3.23 to 2.18 ppm. *Note: trace toluene can be seen near 7.1 and 2.1 ppm.*

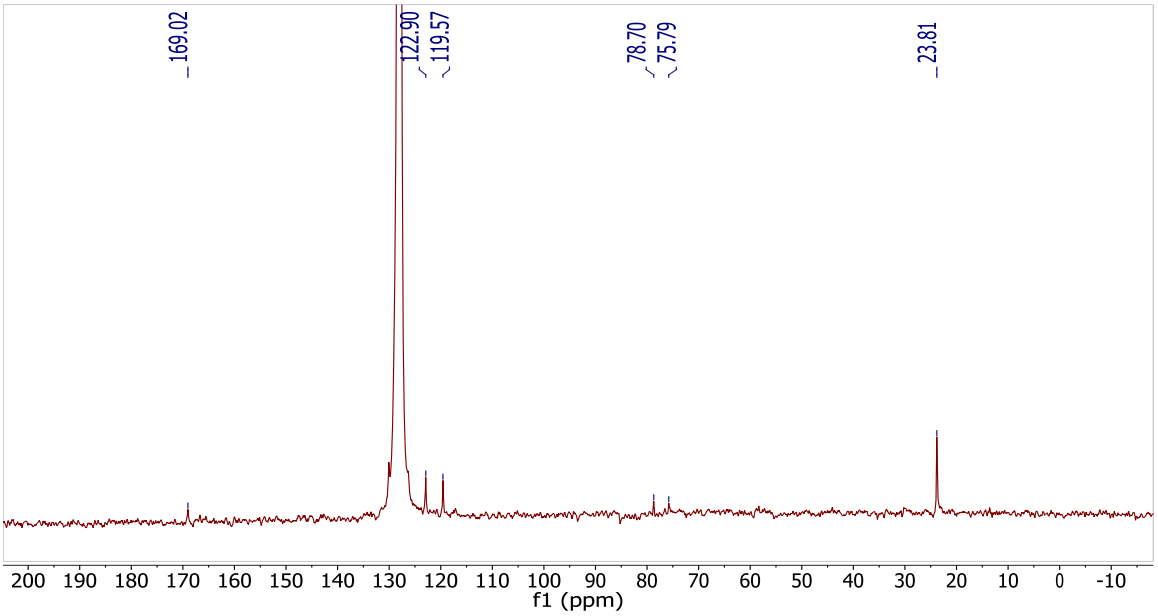

Figure 7-25 $^{13}C[^{1}H]$-NMR spectrum of **57** in benzene-d_6. *Note: The large peak at 128.0 is benzene-d_6 and the small one to the left is benzene-h_6 (128.6 ppm).*

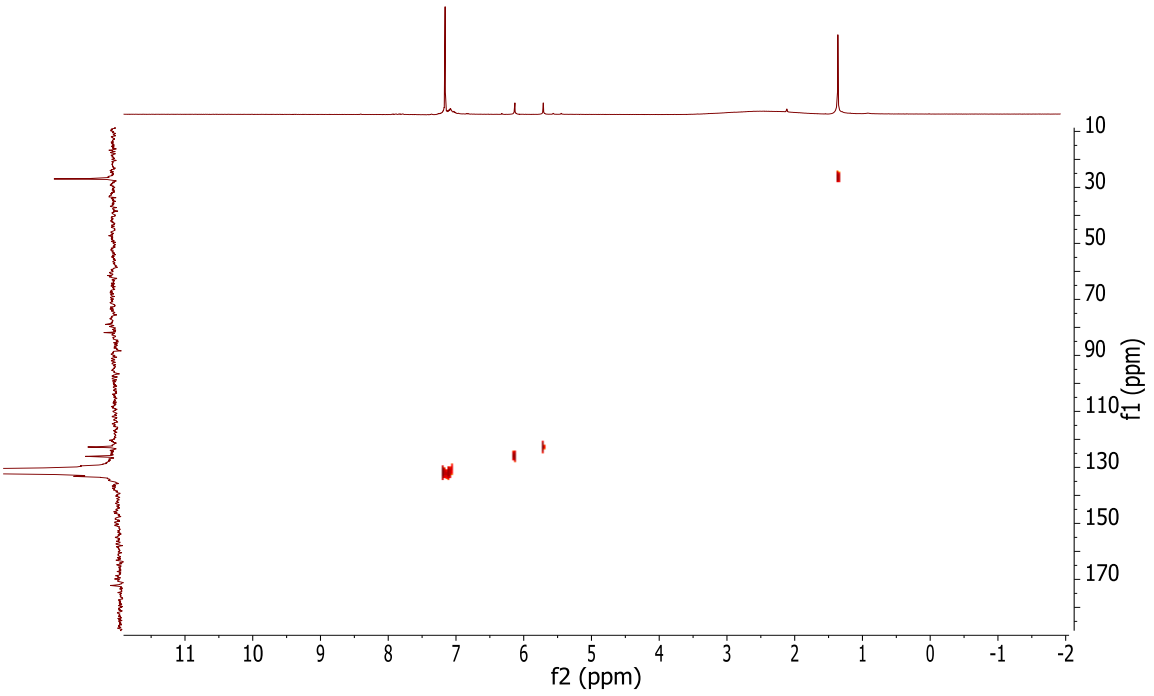

Figure 7-26 ^{1}H-^{13}C HSQC-NMR spectum of **57** in benzene-d_6.

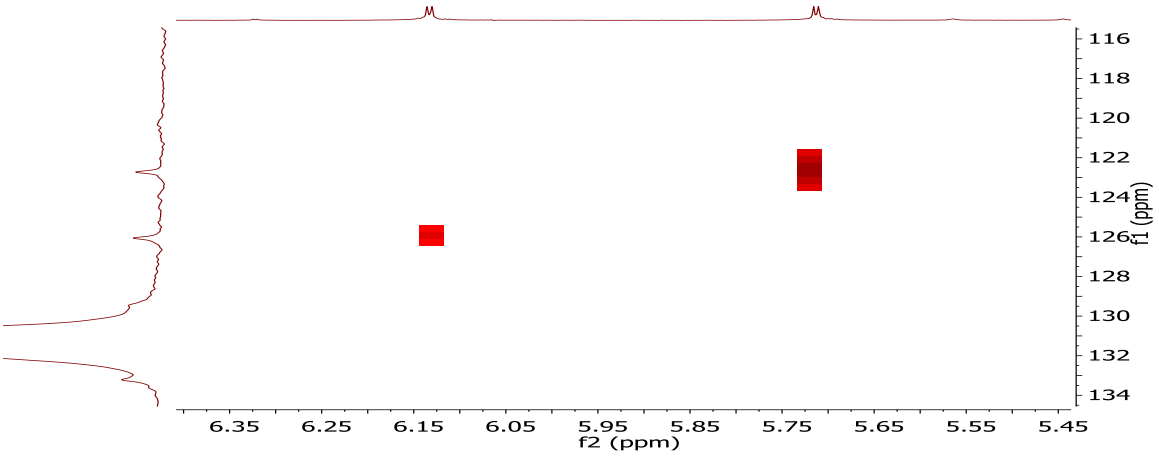

Figure 7-27 An expansion of the ^{1}H-^{13}C HSQC-NMR spectrum of **57** showing the correlation between the two non-equivalent backbone protons of the imidazolylidene ring with their corresponding carbon resonances.

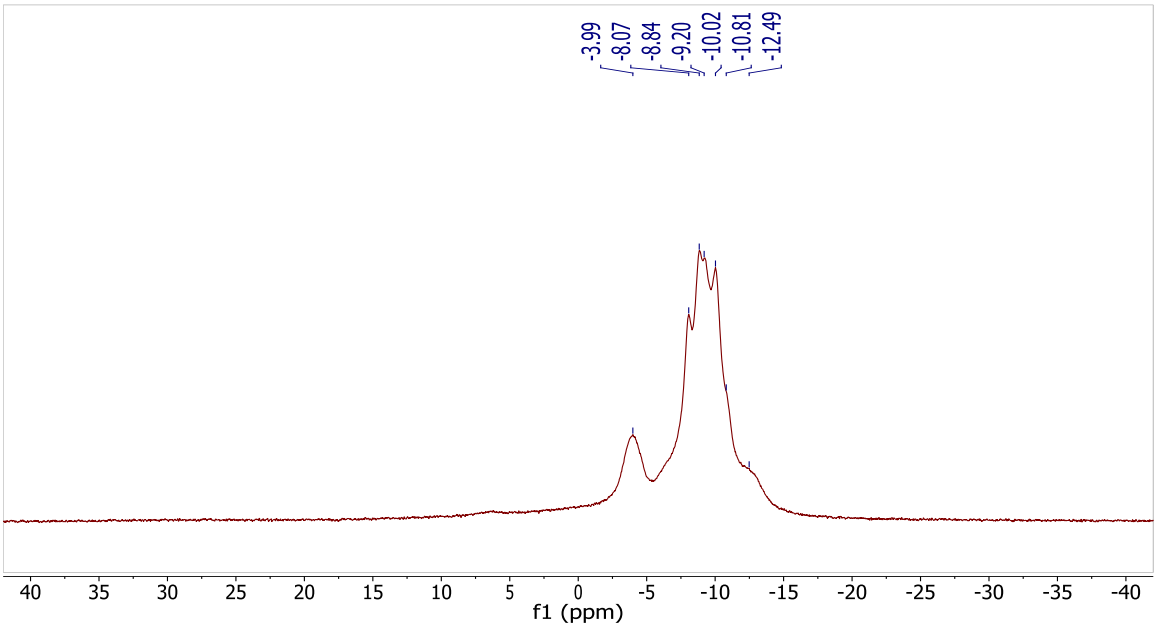

Figure 7-28 $^{11}B[^{1}H]$-NMR spectrum of **57** in benzene-d_6.

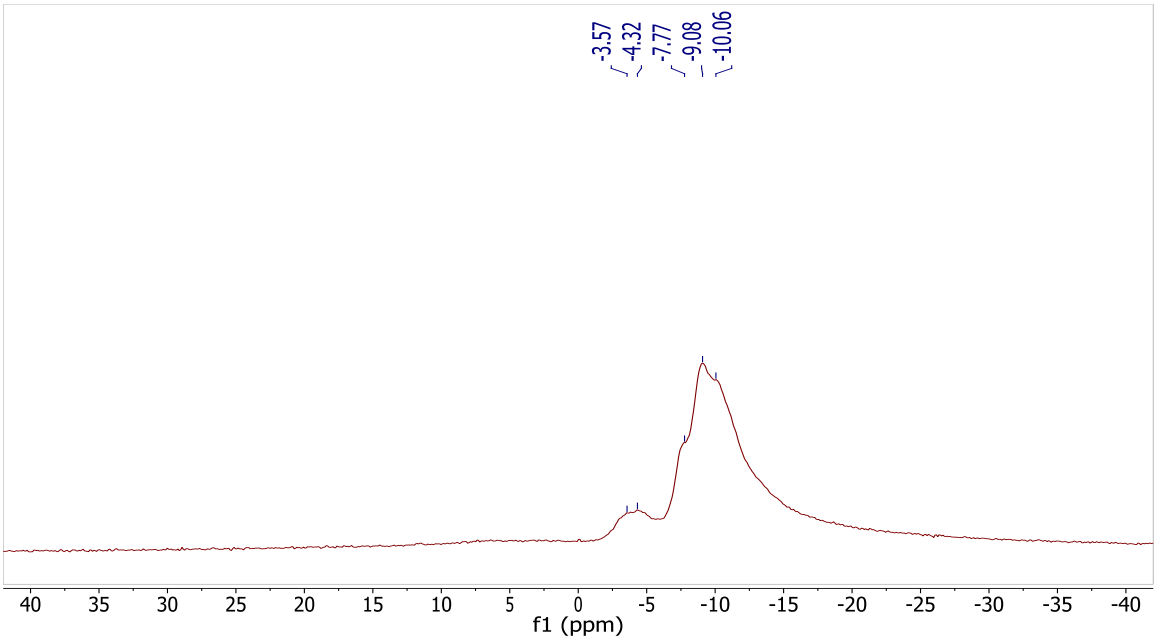

Figure 7-29 ^{11}B-NMR spectrum of **57** in benzene-d_6.

Synthesis of 43[sTr$^+$]:

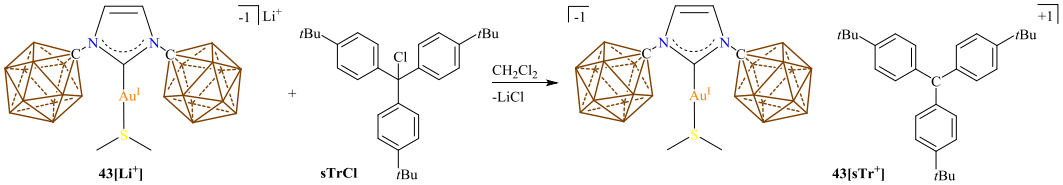

Scheme 7-11 Synthesis of **43[sTr$^+$]**.

The following was done in a glovebox under a dinitrogen atmosphere. A glass scintillation vial was equipped with a stir bar and loaded with **43[Li$^+$]** (100.0 mg, 111.1 μmol) and the complex was dissolved in DME (DME = 1,2-dimethoxyethane, 3 x 2mL) and the solvent removed *in vacuo* (the purpose of this is to displace any THF coordinated to Li$^+$). Once the THF was removed, **sTrCl** (49.7 mg, 111.1 μmol) was added to the same vial containing the Au complex. The solids were suspended in 3 mL of methylene chloride and stirred for 30 minutes at room temperature. The yellow highly colored suspension was filtered to remove insoluble materials (mostly LiCl). The filtrate was substantially pure but contained DME (see ^{1}H NMR Figure 7-30), yield quantitative. To remove a majority of the DME, the compound was dissolved in a minimal amount of methylene chloride and pentane was added dropwise until the solution turned cloudy. At this point the suspension was placed in a freezer at -30 °C until a yellow microcrystalline material formed, yield 57% of **43[sTr$^+$]**. ^{1}H NMR (400 MHz, methylene chloride-d_2, 25°C): δ = 7.86 (2, 6H), 7.59 (d, 6H), 7.31 (s, 2H), 2.77 (s, 6H), 1.48 (s, 27H), 3.3-0.9 (bm, 22H, B-H). ^{1}H[^{11}B] NMR (300 MHz, methylene chloride-d_2, 25°C): δ = 7.86 (2, 6H), 7.59 (d, 6H), 7.31 (s, 2H), 2.77 (s, 6H), 2.55 (s, 10H, B-H), 1.68 (s, 2H, B-H), 1.58 (s, 10H, B-H), 1.48 (s, 27H). ^{11}B[^{1}H] NMR (128 MHz, methylene chloride-d_2, 25°C): δ = -8.6, -13.8 ppm. ^{11}B NMR (128 MHz, methylene chloride-d_2, 25°C): δ = -8.6 (^{1}*J(H,B)* = 131.6 Hz), -13.8 (^{1}*J(H,B)* = 135.4 Hz). ^{13}C[^{1}H] NMR (125 MHz, methylene chloride-d_2, 25°C): δ = 204.1, 174.2, 169.4, 142.3, 137.6, 128.2, 122.2, 79.8, 37.1, 30.8, 25.1 ppm. IR (ATR, 25°C): B-H stretch = 2533 cm^{-1}.

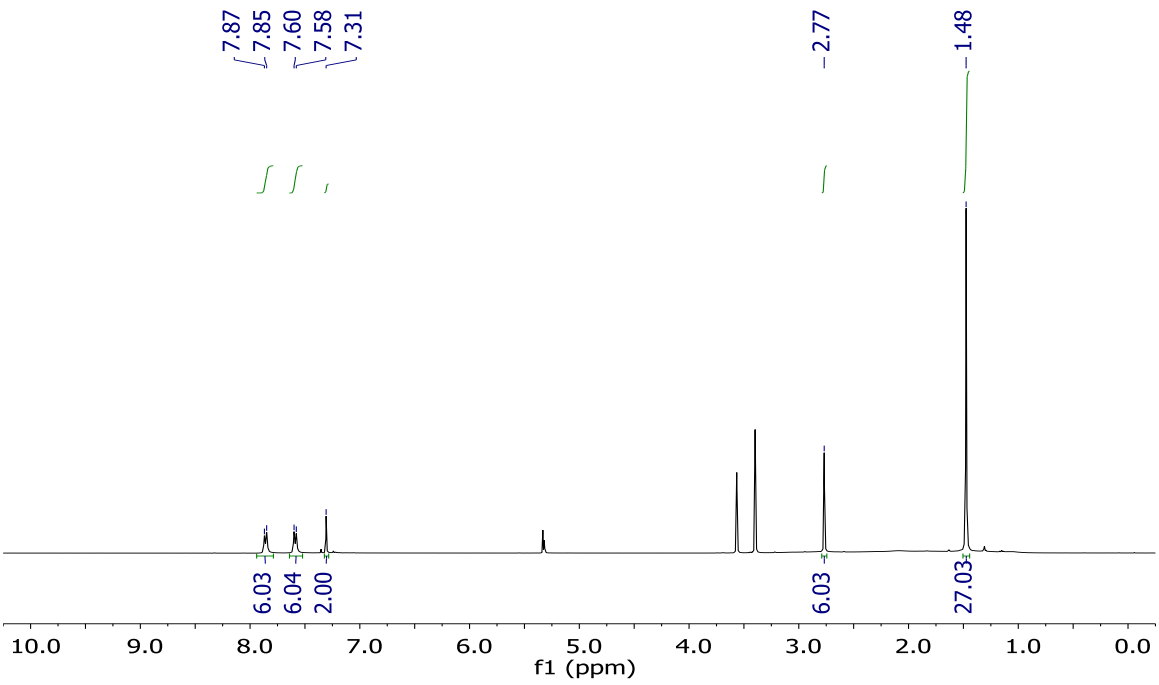

Figure 7-30 ^{1}H-NMR of **43[sTr^{+}]** in methylene chloride-d_2. *Note: DME can be seen at 3.40 and 3.57 ppm.*

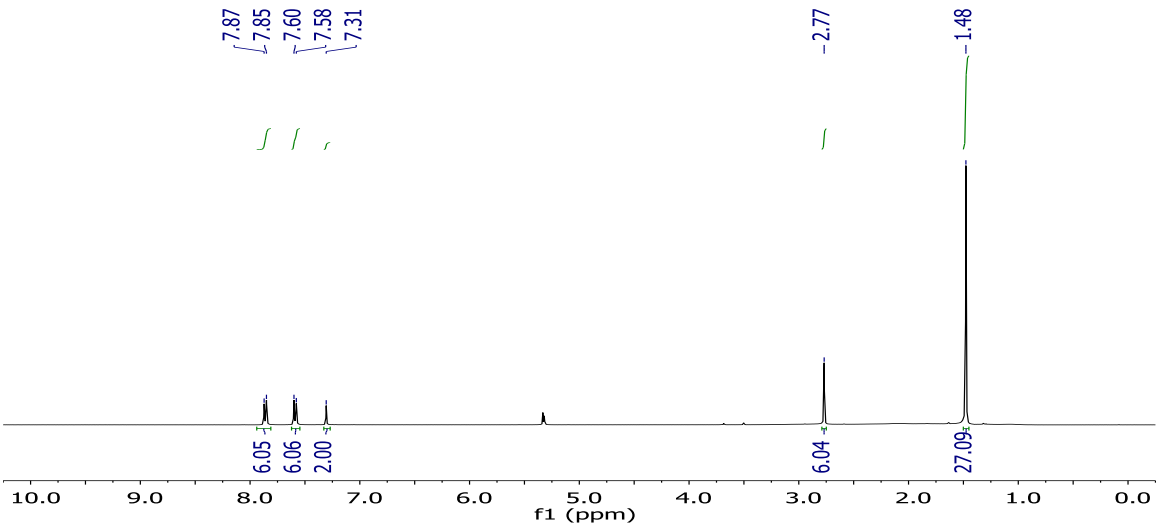

Figure 7-31 ^{1}H-NMR of **43[sTr^{+}]** in methylene chloride-d_2.

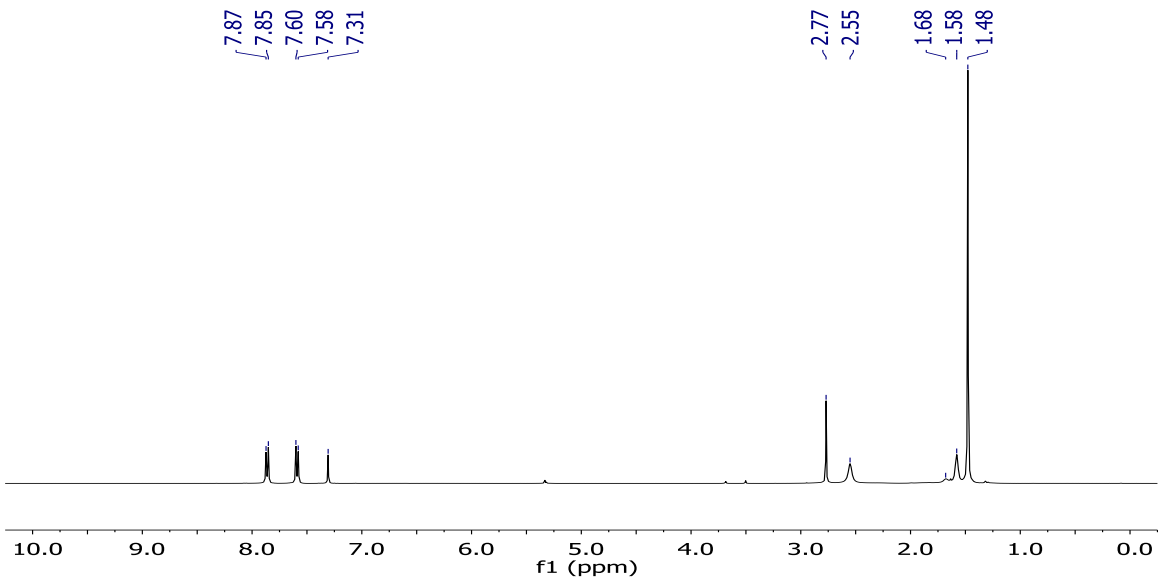

Figure 7-32 $^{1}H[^{11}B]$-NMR of **43[sTr^{+}]** in methylene chloride-d_2. *Note: the B-H's can be seen at 1.58, 1.68 and 2.55 ppm.*

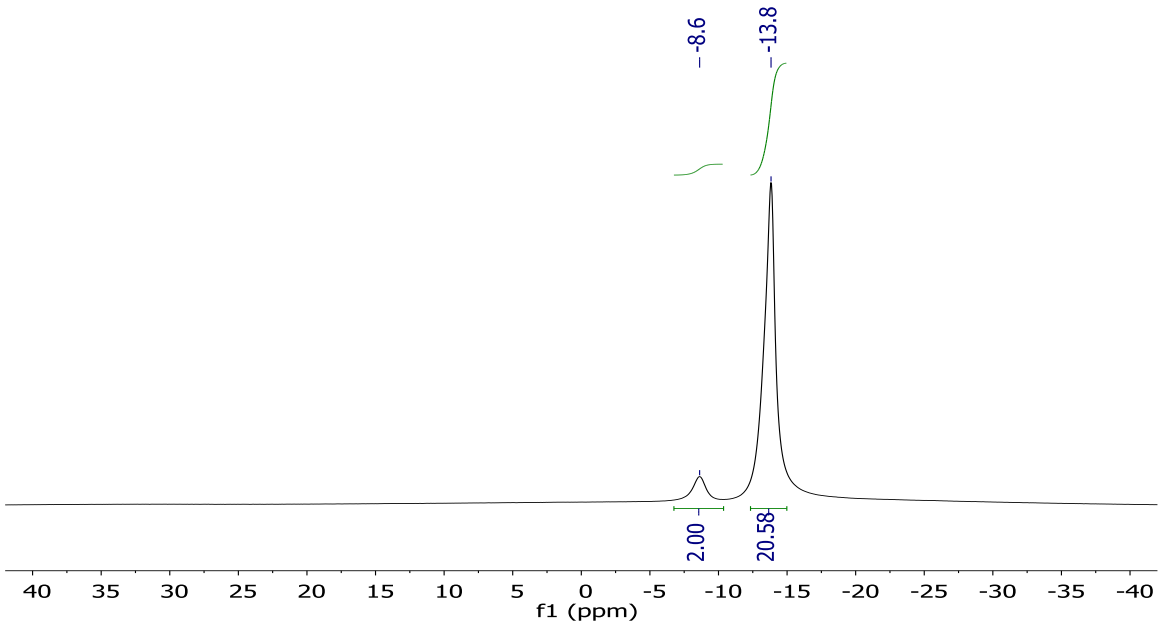

Figure 7-33 $^{11}B[^{1}H]$-NMR of **43[sTr^{+}]** in methylene chloride-d_2.

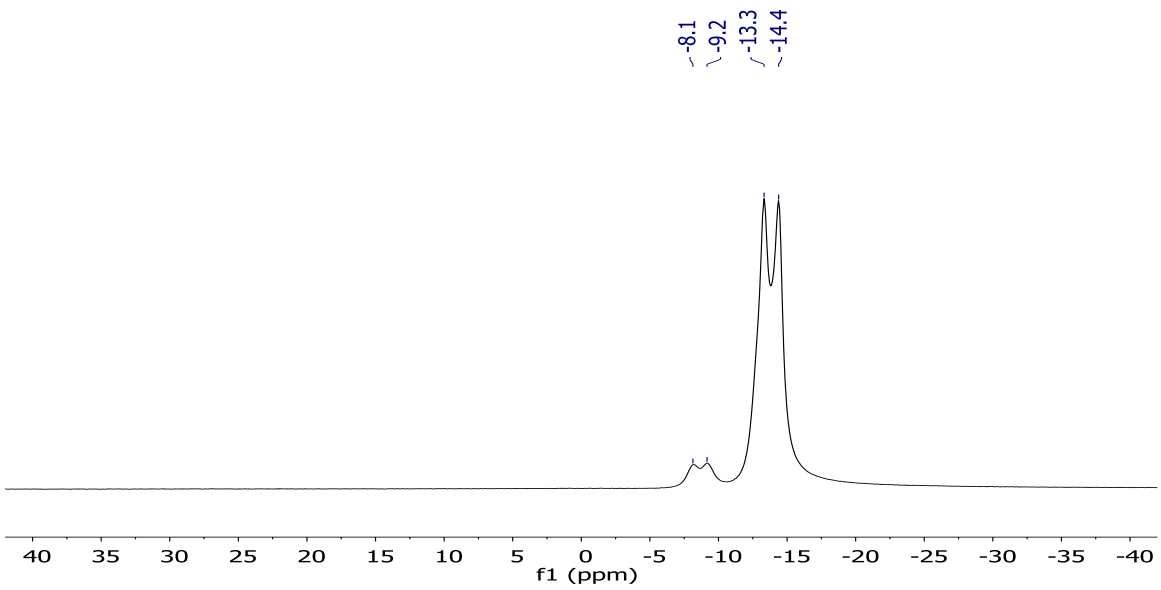

Figure 7-34 ^{11}B-NMR of **43[sTr$^+$]** in methylene chloride-d_2.

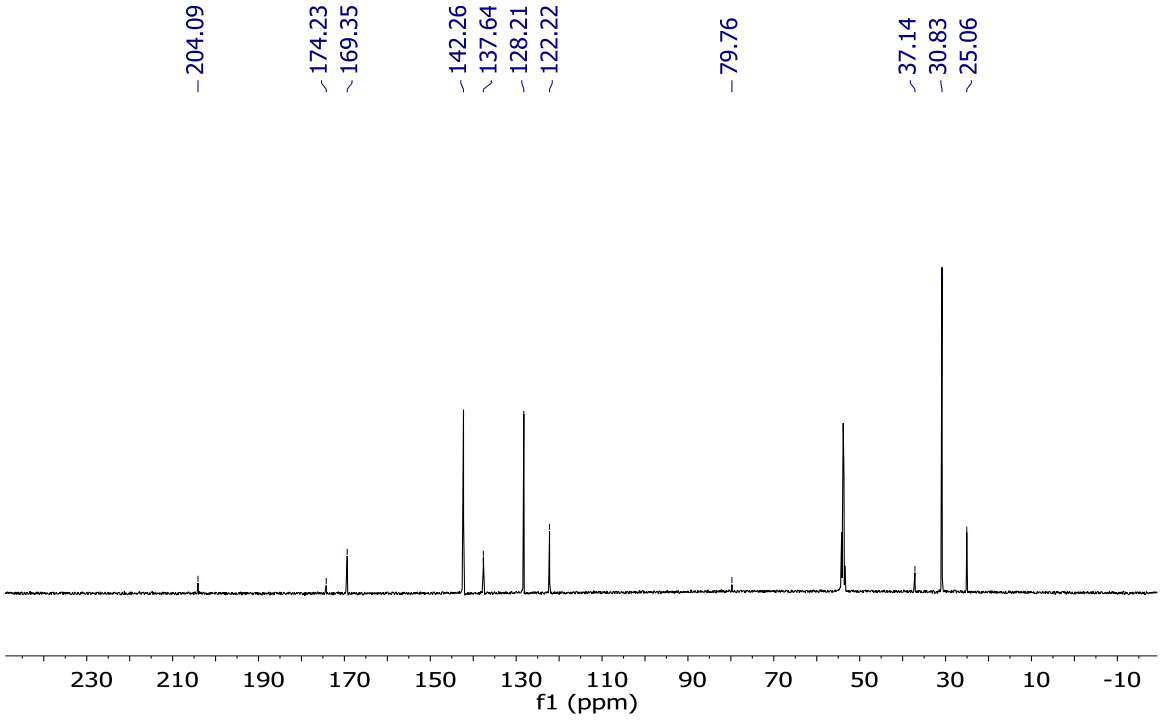

Figure 7-35 ^{13}C[^{1}H]-NMR spectrum of **43[sTr$^+$]** in methylene chloride-d_2.

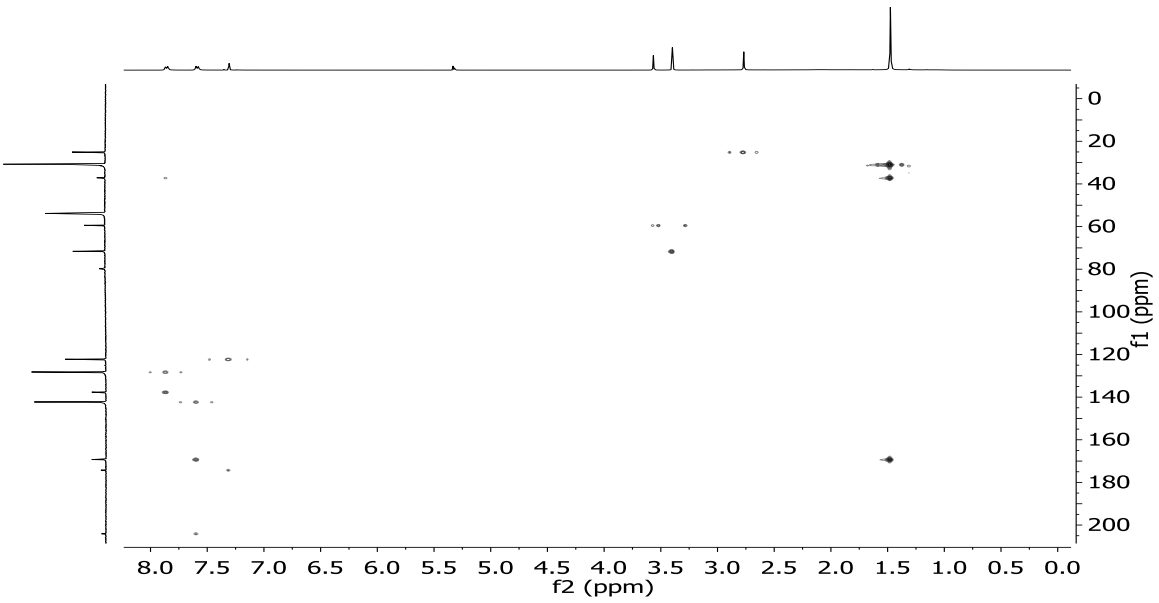

Figure 7-36 $^{1}H,^{13}C$-HMBC-NMR spectrum of **43[sTr^{+}]** in methylene chloride-d_2. *Note: DME is present in the spectrum at (3.4, 72) and (3.6, 60) ppm.*

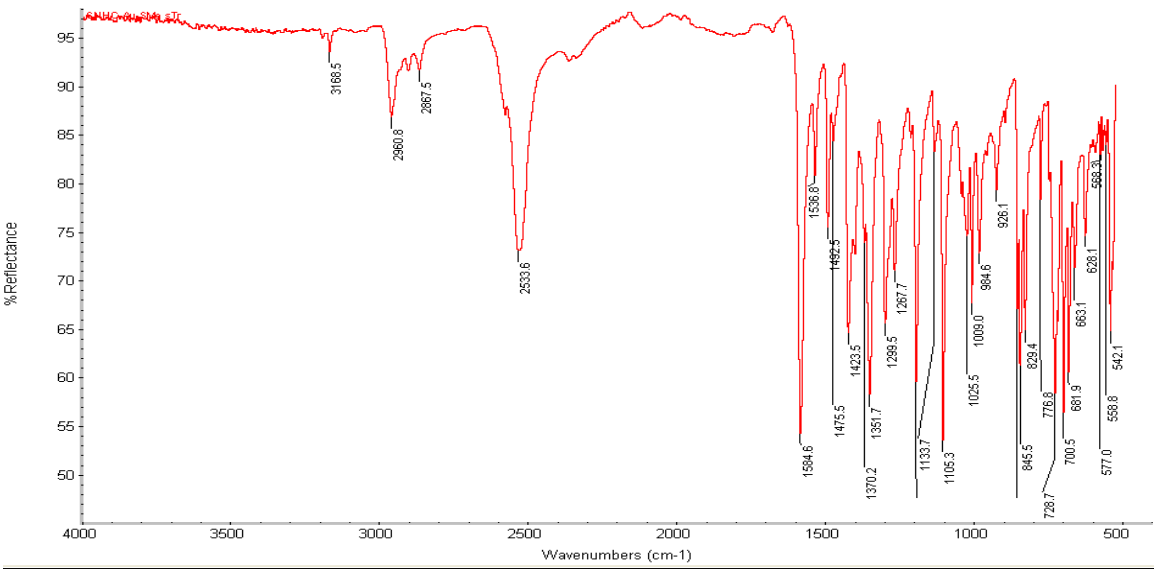

Figure 7-37 IR spectrum of **43[sTr^{+}]** in the solid state. *Note: the borohydrides of the cluster can be seen at 2533.6 cm^{-1}.*

Synthesis of $43Br_{12}[Li^+]$:

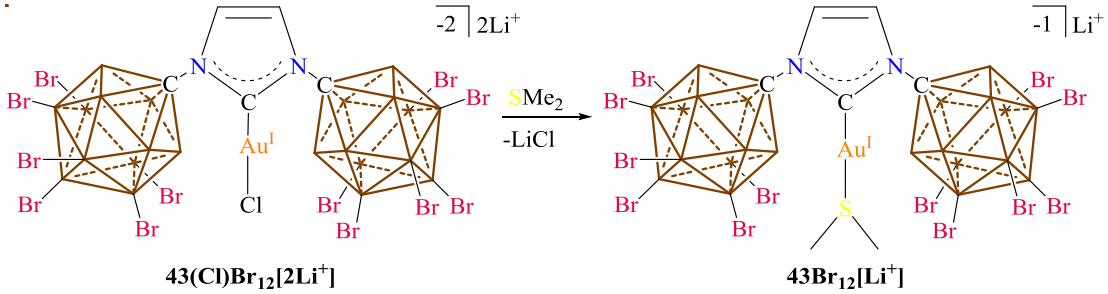

Scheme 7-12 Synthesis of **$43Br_{12}[Li^+]$**.

A glass scintillation vial was equipped with a stir bar and loading with **$43(Cl)Br_{12}[2Li^+]$** (200 mg, 0.097 mmol) and the compound was suspended in methylene chloride (5 mL). To the suspension freshly distilled dimethylsulfide (1 mL, excess) was added and the suspension stirred overnight at room temperature. The next morning the suspension was pumped to dryness and solid extracted with methylene chloride (2 x 10 mL), the liquid extract was pumped down to dryness furnishing the title compound **$43Br_{12}[Li^+]$** (0.165 g, 85% yield). ^{1}H NMR (500 MHz, methylene chloride-d_2, 25°C): δ = 7.37 (2H, s), 2.93 (6H, s), 3.8 – 2.2 (bs, 10H, B-H) ppm. ^{1}H[^{11}B]-NMR spectrum (300 MHz, methylene chloride-d_2, 25°C): δ = 7.37 (2H, s), 3.29 (10H, bs), 2.93 (6H, s) ppm. ^{11}B[^{1}H] NMR (128 MHz, methylene chloride-d_2, 25 °C): δ = -1.4, -10.3, -17.8 ppm. ^{11}B NMR (128 MHz, methylene chloride-d_2, 25 °C): δ = -1.3, -10.3, -17.8 (broad) ppm. ^{13}C[^{1}H] NMR (126 MHz, methylene chloride-d_2, 25 °C): δ = 176.9, 123.7, 71.5, 25.0 ppm. ^{7}Li[^{1}H] NMR (233 MHz, chloroform-d_1, 25 °C): δ = -0.61 ppm. IR (solid, ATR, 25 °C): 2598.7 cm^{-1}. Melting point: 104 – 106 °C.

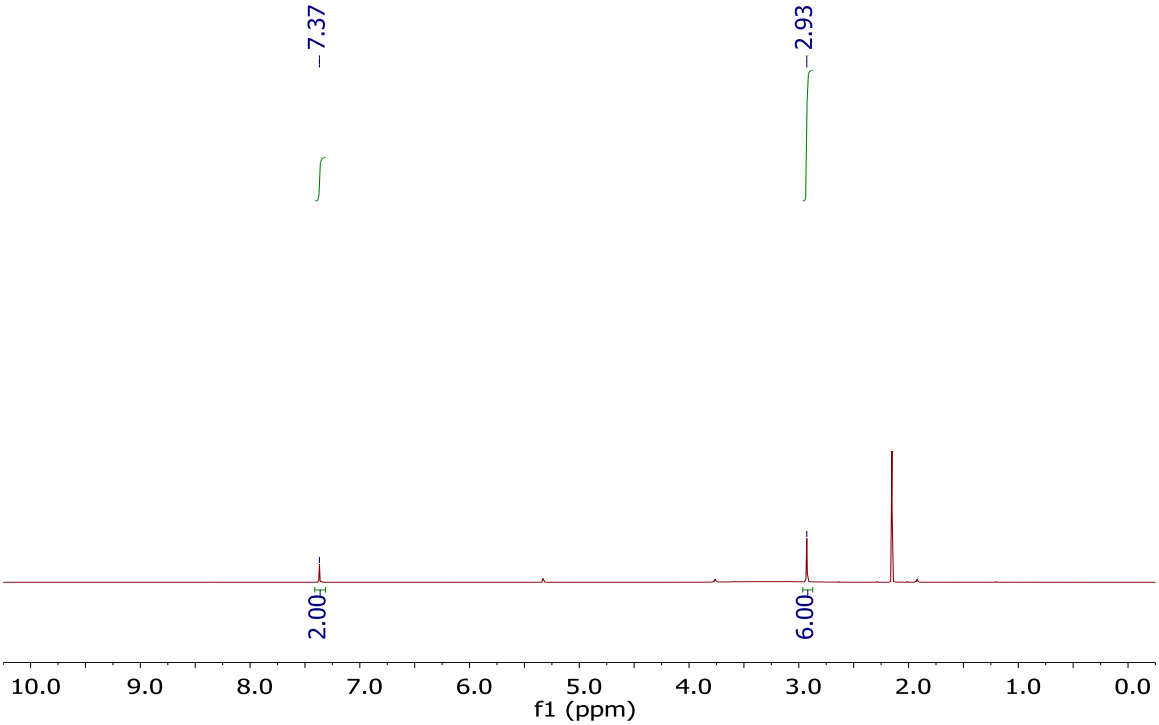

Figure 7-38 ^{1}H NMR-spectrum of **43Br$_{12}$[Li^{+}]** in methylene chloride-d$_2$. *Note: acetonitrile and THF are coordinated to the Li^{+} counter cation at 2.2, 3.8 and 1.9 ppm respectively.*

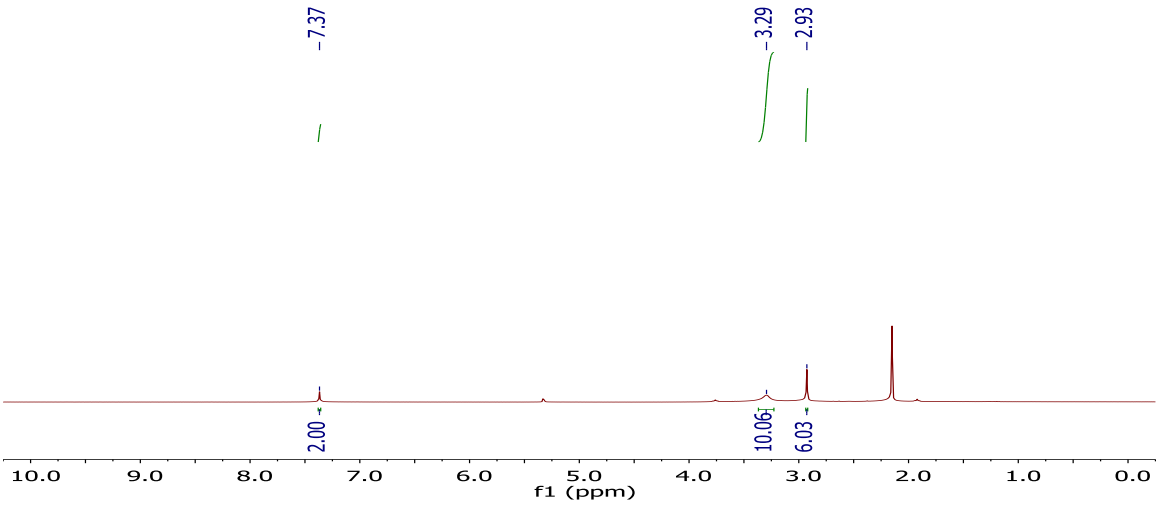

Figure 7-39 ^{1}H[^{11}B] NMR-spectrum of **43Br$_{12}$[Li^{+}]** in methylene chloride-d$_2$. *Note: acetonitrile and THF are coordinated to the Li+ counter cation at 2.2, 3.8 and 1.9 ppm respectively.*

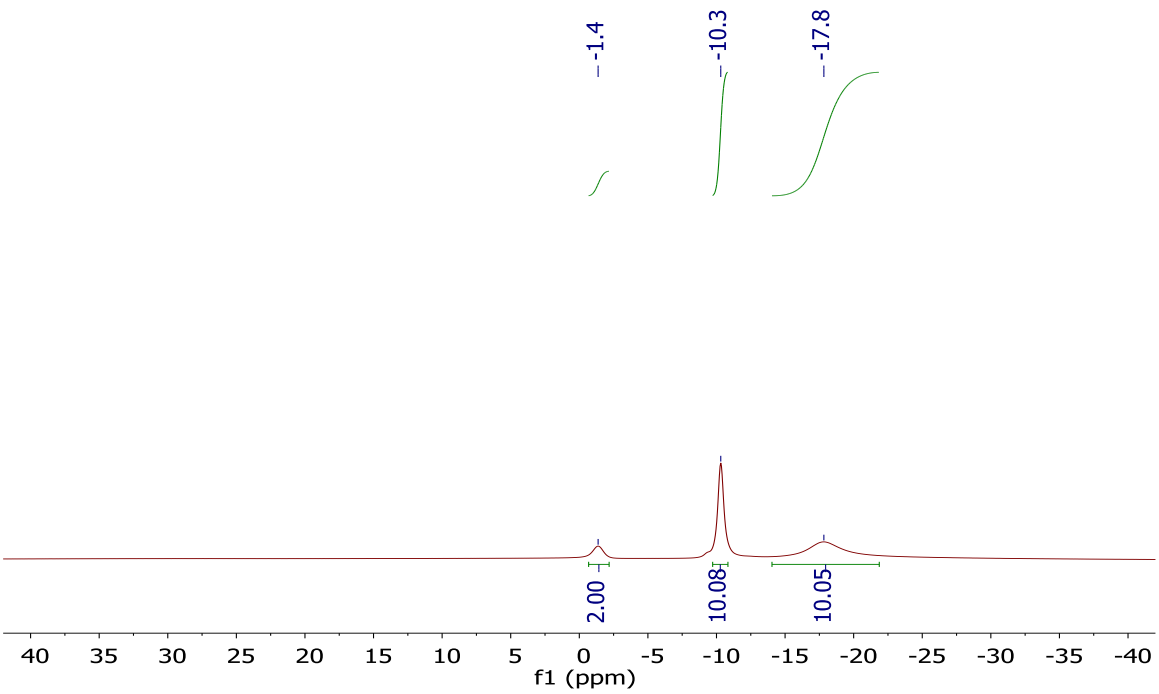

Figure 7-40 $^{11}B[^{1}H]$ NMR-spectrum of **43Br$_{12}$[Li^{+}]** in methylene chloride-d$_2$.

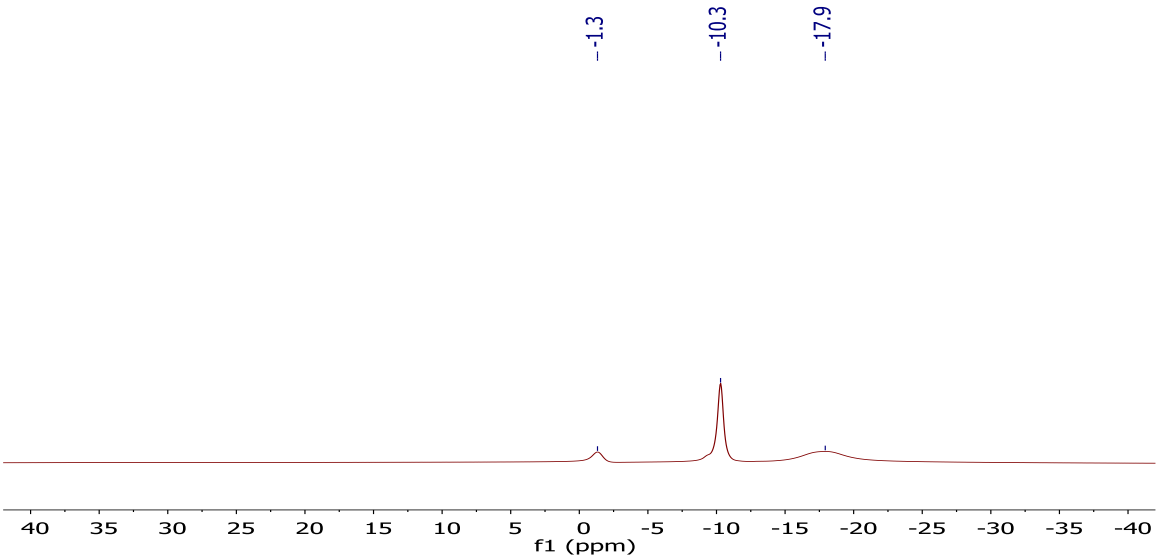

Figure 7-41 ^{11}B NMR-spectrum of **43Br$_{12}$[Li^{+}]** in methylene chloride-d$_2$.

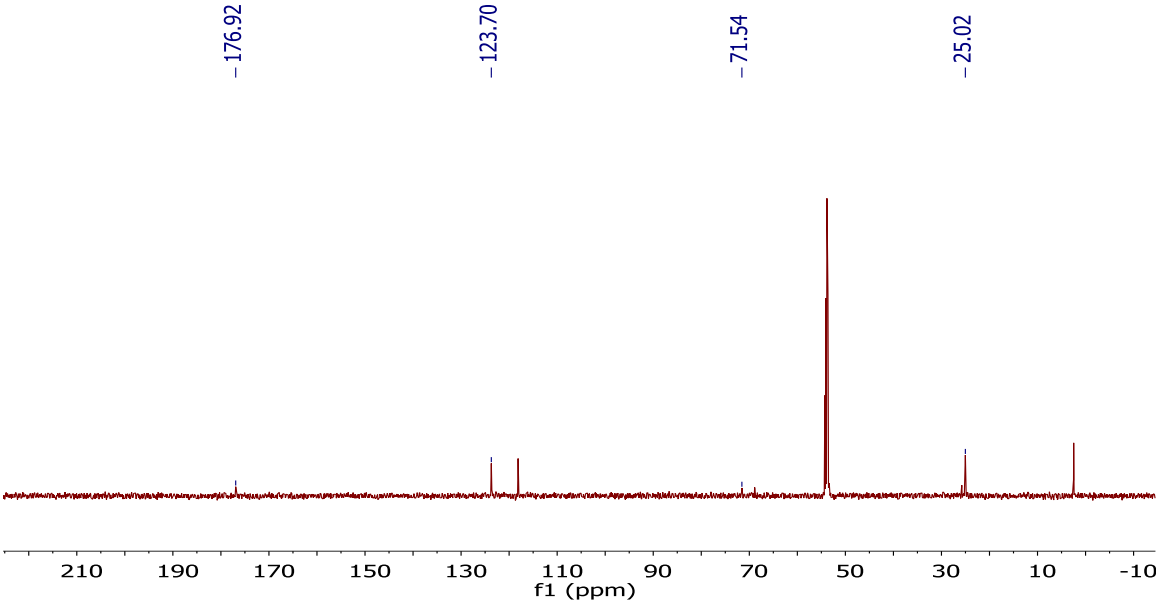

Figure 7-42 $^{13}C[^{1}H]$ NMR-spectrum of **43Br$_{12}$[Li^{+}]** in methylene chloride-d$_2$. *Note: acetonitrile and THF coordinated to the Li^{+} counter cation can be seen at 3, 118 and 26, 69 ppm respectively.*

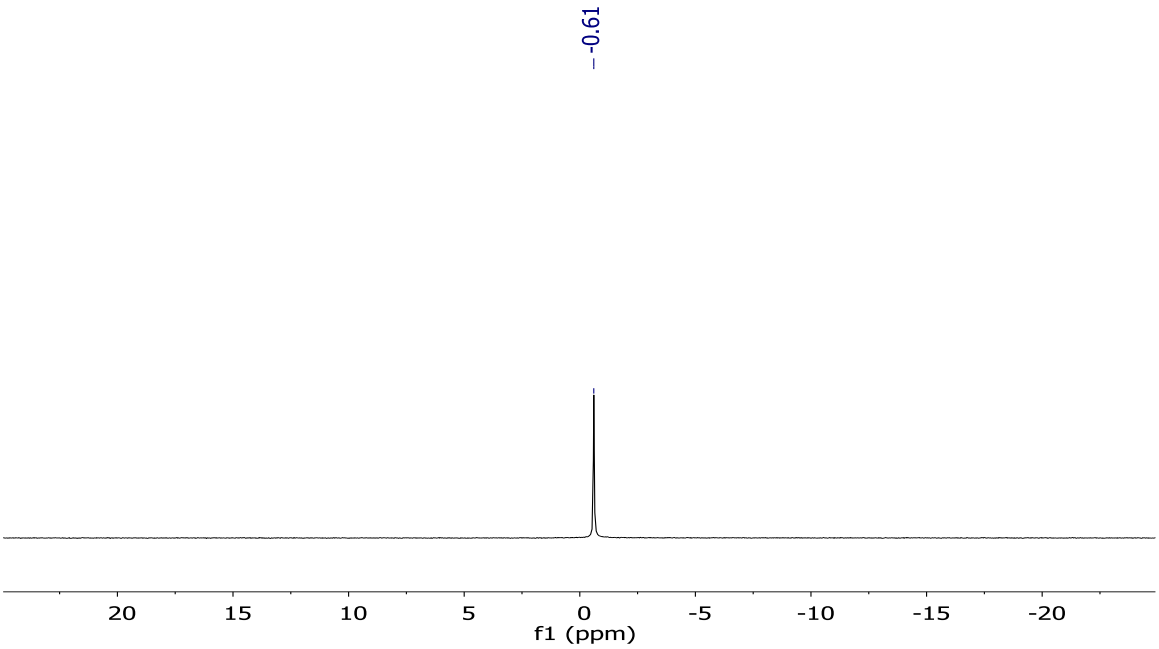

Figure 7-43 $^{7}Li[^{1}H]$ NMR-spectrum of **43Br$_{12}$[Li^{+}]** in chloroform-d$_1$.

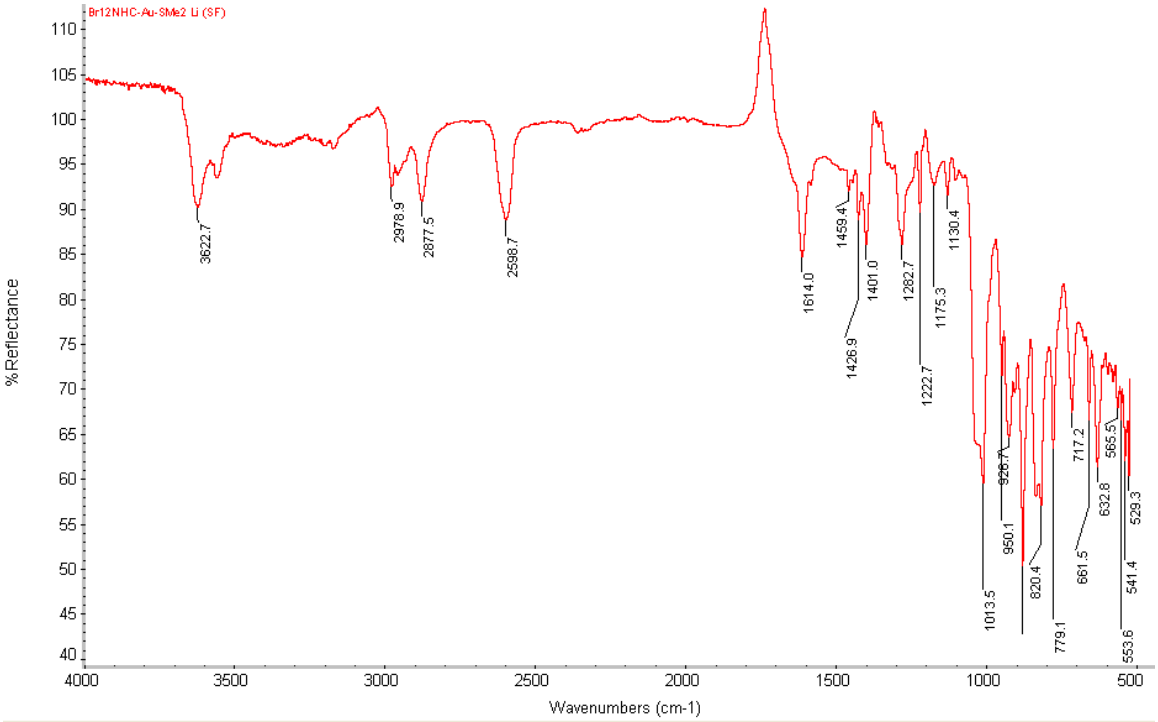

Figure 7-44 IR spectrum of **43Br$_{12}$[Li$^+$]** showing the B-H stretches at 2598.7 cm^{-1}.

Synthesis of 43Br$_{12}$[Ph$_3$C$^+$]:

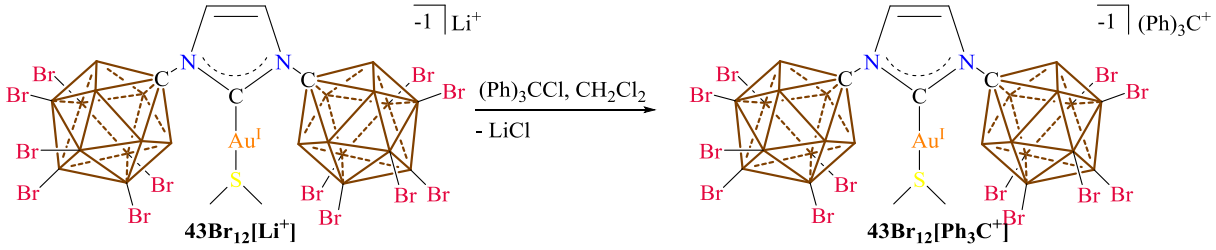

Scheme 7-13 Synthesis of **43Br$_{12}$[Ph$_3$C$^+$]**.

A glass scintillation vial was equipped with a stir bar and loaded with **43Br$_{12}$[Li$^+$]** (*Note: the lithium counter cation is coordinated to MeCN)* (0.550 g, 0.311 mmol) and the solid was suspended in

methylene chloride (5 mL). Trityl chloride dissolved in methylene chloride (3 mL) was added to the suspension and the reaction changed colors from pale yellow to bring yellow. The reaction as stirred for one hour at room temperature then filtered. The filtrate was concentrated down to 3 mL then added dropwise to a stirring benzene solution (16 mL) which forms a yellowish top layer and red bottom layer. After stirring for 15 minutes the upper benzene layer was removed and the remaining oil was pumped down to dryness furnishing the title compound **43Br$_{12}$[Ph$_3$C$^+$]** quantitatively. ^{1}H NMR (600 MHz, methylene chloride-d$_2$, 25°C): δ = 8.31 (3H, t, $^3J(H,H)$ = 7.5 Hz), 7.93 (6H, t, $^3J(H,H)$ = 7.5 Hz), 7.69 (6H, d, $^3J(H,H)$ = 7.5 Hz), 7.35 (2H, s), 2.92 (6H, s), 4.2 – 2.2 (bs, 10H, B-H) ppm. ^{1}H[^{11}B]-NMR spectrum (300 MHz, methylene chloride-d$_2$, 25°C): δ = 8.31 (3H, t, $^3J(H,H)$ = 7.5 Hz), 7.92 (6H, t, $^3J(H,H)$ = 7.5 Hz), 7.70 (6H, d, $^3J(H,H)$ = 7.5 Hz), 7.36 (2H, s), 3.28 (10H, bs), 2.92 (6H, s) ppm. ^{11}B[^{1}H] NMR (96 MHz, methylene chloride-d$_2$, 25 °C): δ = -1.4, -10.3, -17.7 ppm. ^{11}B NMR (96 MHz, methylene chloride-d$_2$, 25 °C): δ = -1.3, -10.3 (broad), -17.7 ppm. ^{13}C[^{1}H] NMR (126 MHz, methylene chloride-d$_2$, 25 °C): δ = 211.0, 176.9, 144.0, 143.2, 140.3, 131.2, 123.7, 71.5, 25.0 ppm. Melting Point: 130 - 150 °C then decomposed at 155 – 160°C.

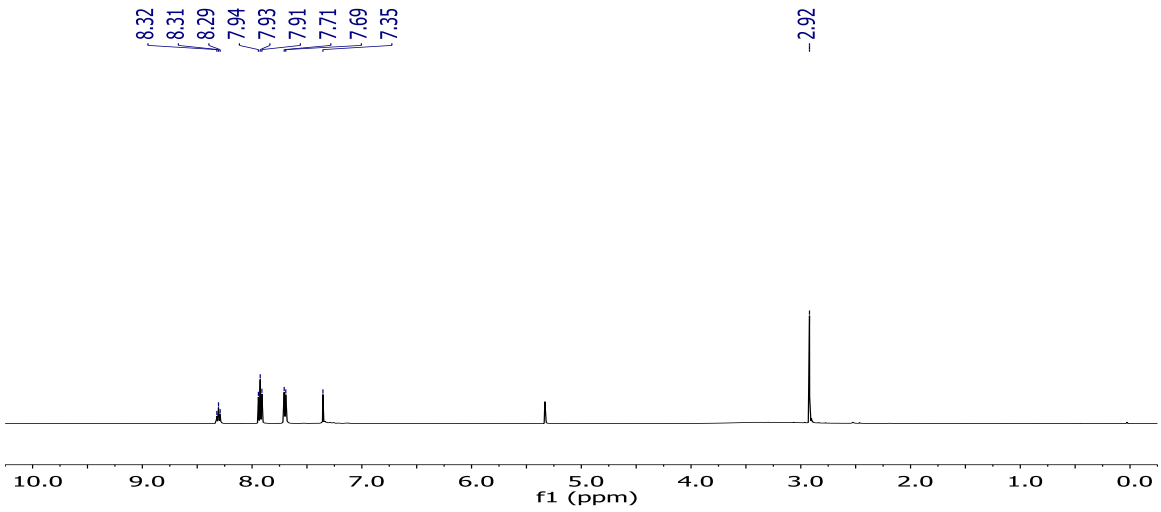

Figure 7-45 ^{1}H NMR-spectrum of **43Br$_{12}$[Ph$_3$C$^+$]** in methylene chloride-d$_2$. *Note: Benzene (7.35 ppm) from the wash overlaps with the backbone protons of the NHC ligand.*

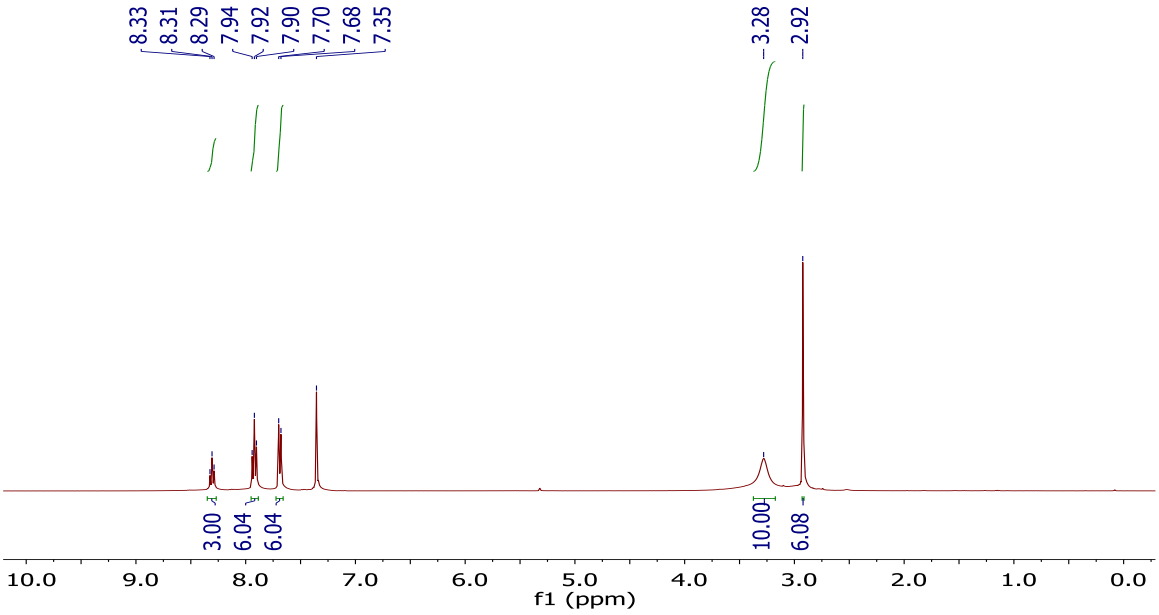

Figure 7-46 $^{1}H[^{11}B]$ NMR-spectrum of **$43Br_{12}[Ph_3C^+]$** in methylene chloride-d_2. *Note: benzene (7.35 ppm) from the wash overlaps with the backbone protons of the NHC ligand.*

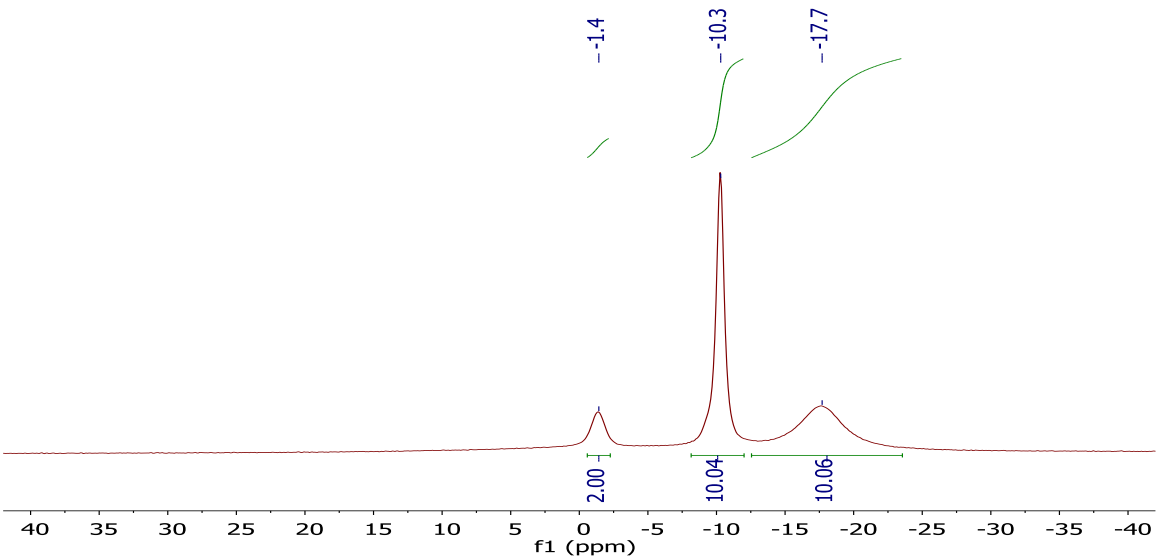

Figure 7-47 $^{11}B[^{1}H]$ NMR-spectrum of **$43Br_{12}[Ph_3C^+]$** in methylene chloride-d_2.

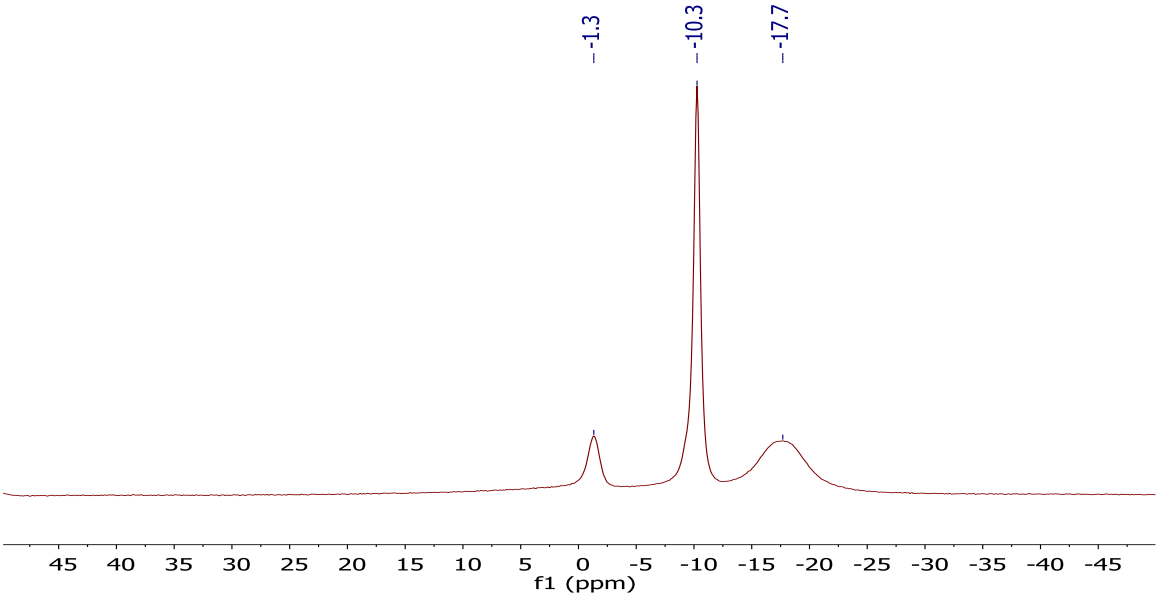

Figure 7-48 ^{11}B NMR-spectrum of **43Br$_{12}$[Ph$_3$C$^+$]** in methylene chloride-d$_2$.

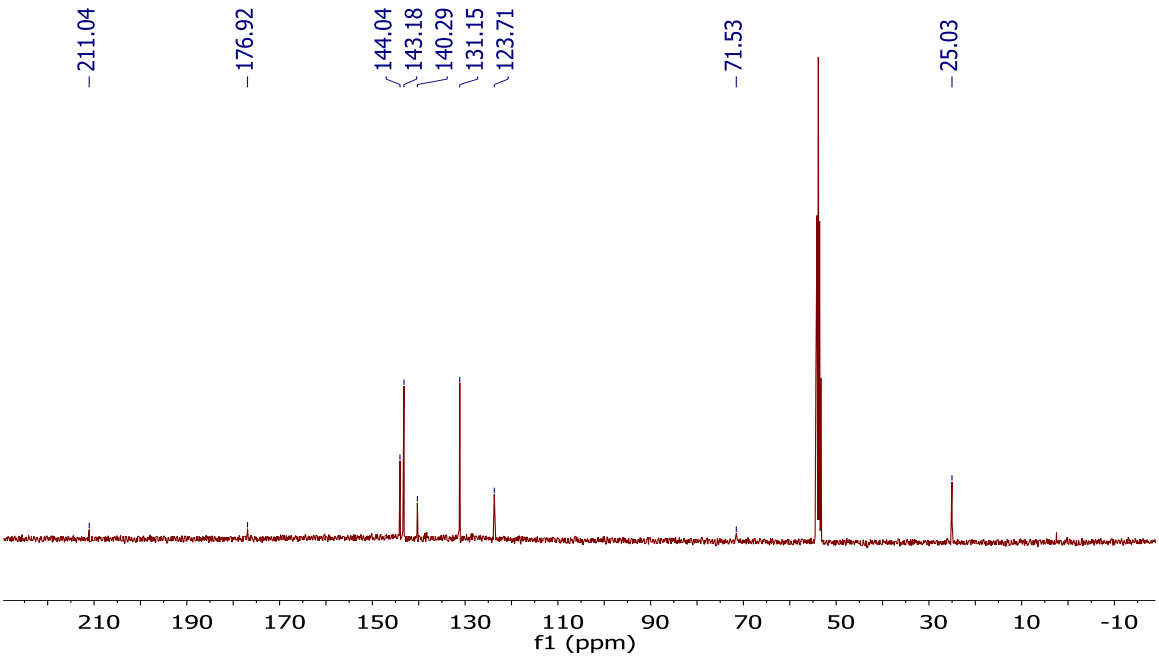

Figure 7-49 ^{13}C[^{1}H] NMR-spectrum of **43Br$_{12}$[Ph$_3$C$^+$]** in methylene chloride-d$_2$. *Note: the carbene carbon of the NHC ligand appears at 176.9 ppm.*

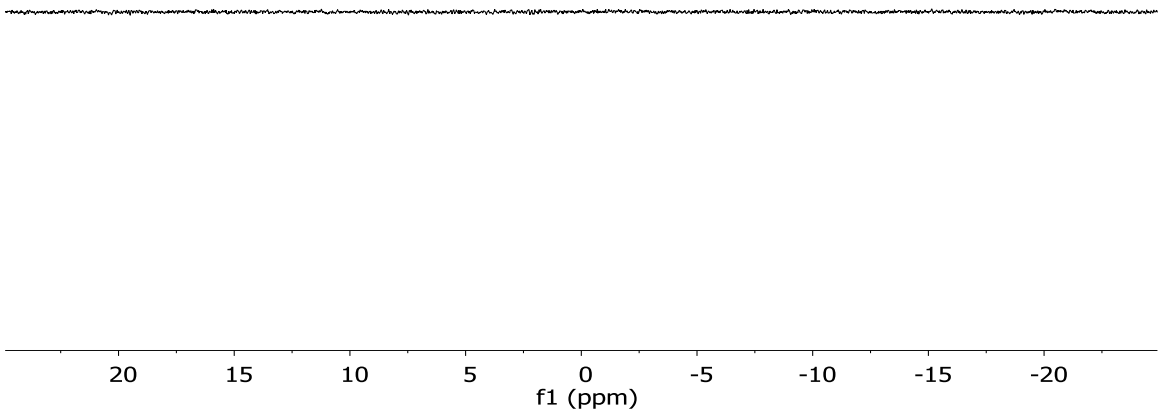

Figure 7-50 ^{7}Li NMR-spectrum of **$43Br_{12}[Ph_3C^+]$** in methylene chloride-d_2. NMR showing the presence of no Li^+ in the sample.

Synthesis of $43I_{12}[Li^+]$:

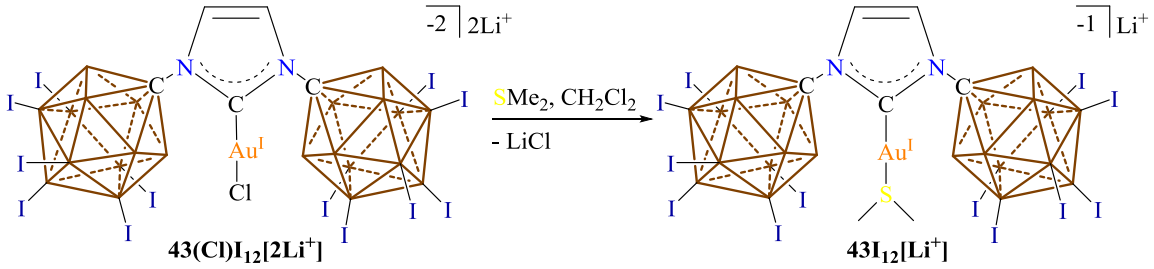

Scheme 7-14 Synthesis of **$43I_{12}[Li^+]$**.

A glass scintillation vial was equipped with a stir bar and loading with **$43(Cl)I_{12}[2Li^+]$** (300 mg, 158 µmol) and the compound was suspended in methylene chloride (5 mL). To the suspension freshly distilled dimethylsulfide (1 mL, excess) was added and the suspension stirred overnight at room temperature. The next morning the suspension was pumped to dryness and solid extracted with methylene chloride (2 x 10 mL), the liquid extract was pumped down to dryness furnishing the title compound, **$43I_{12}[Li^+]$** (250 mg, 89% yield). ^{1}H NMR (400 MHz, methylene chloride-d_2, 25°C): δ = 7.41 (2H, s), 2.97 (6H, s) ppm. ^{1}H[^{11}B]-NMR spectrum (300 MHz, methylene chloride-d_2, 25°C): δ = 7.41 (2H, s), 3.86 (10H, bs), 2.97 (6H, s) ppm. ^{11}B[^{1}H] NMR (128 MHz, methylene chloride-d_2, 25 °C): δ = -6.1, -12.1, -20.0 ppm. ^{11}B NMR (128 MHz, methylene chloride-d_2, 25 °C): δ = -6.2, -12.3 (broad), -20.0 ppm. ^{13}C[^{1}H] NMR (126 MHz, methylene chloride-d_2, 25 °C): δ = 176.0, 123.5, 85.0, 25.2 ppm. ^{7}Li NMR (233 MHz, methylene chloride-d_2, 25 °C): δ = 0.63 ppm. IR (solid, ATR, 25 °C): 2591.9 cm^{-1}. Melting point: decomposed at 160 °C.

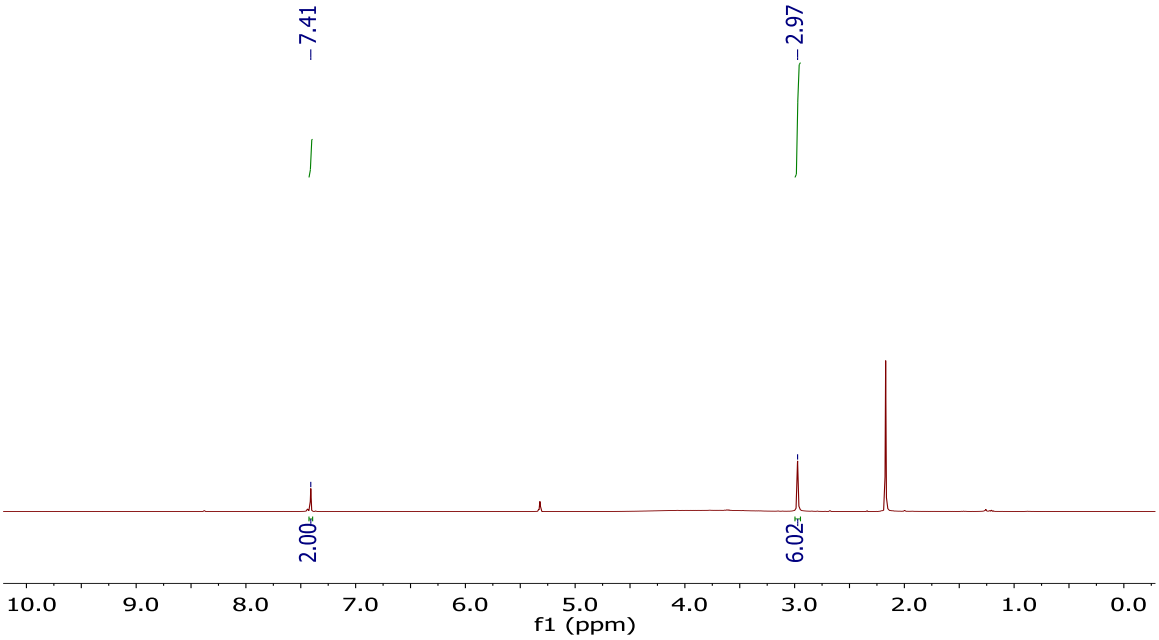

Figure 7-51 ^{1}H-NMR spectrum of compound **43I$_{12}$[Li^{+}]** in methylene chloride-d$_2$. *Note: acetonitrile coordinated to the lithium cation can be seen at 2.17 ppm.*

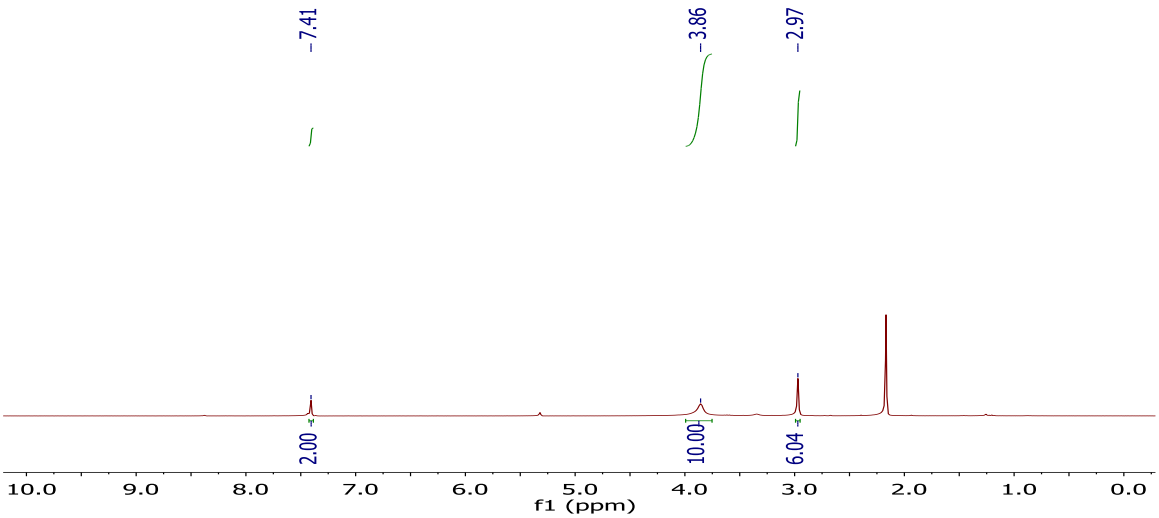

Figure 7-52 ^{1}H[^{11}B]-NMR spectrum of compound **43I$_{12}$[Li^{+}]** in methylene chloride. *Note: the borohydrides show up at 3.86 ppm.*

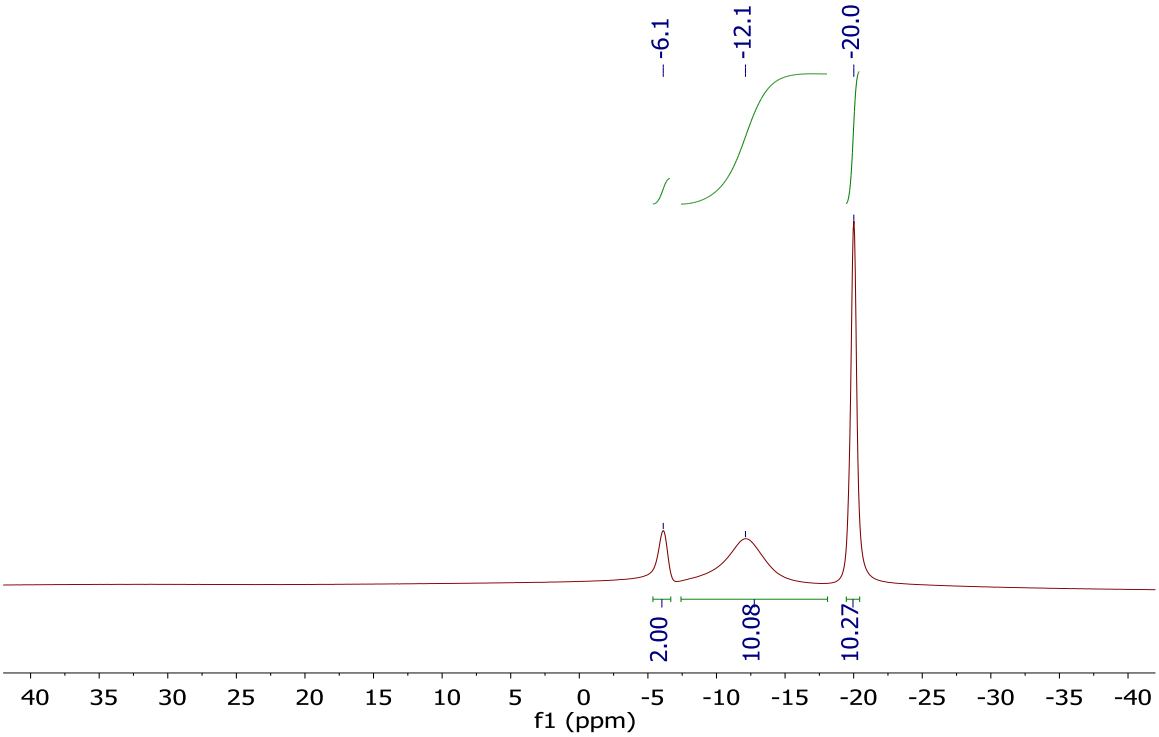

Figure 7-53 $^{11}B[^{1}H]$-NMR spectrum of compound **$43I_{12}[Li^{+}]$** in methylene chloride-d_2.

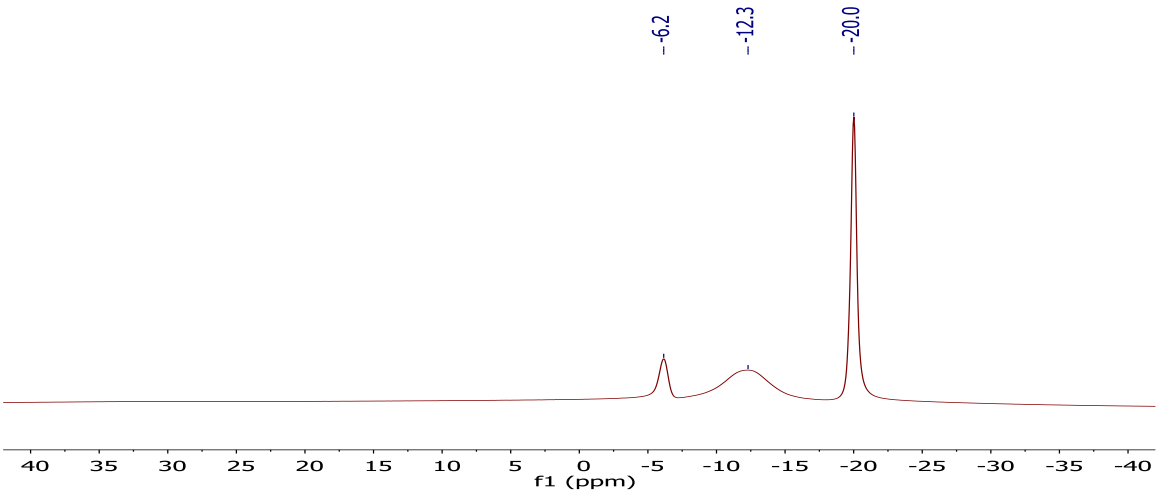

Figure 7-54 ^{11}B-NMR spectrum of compound **$43I_{12}[Li^{+}]$** in methylene chloride-d_2.

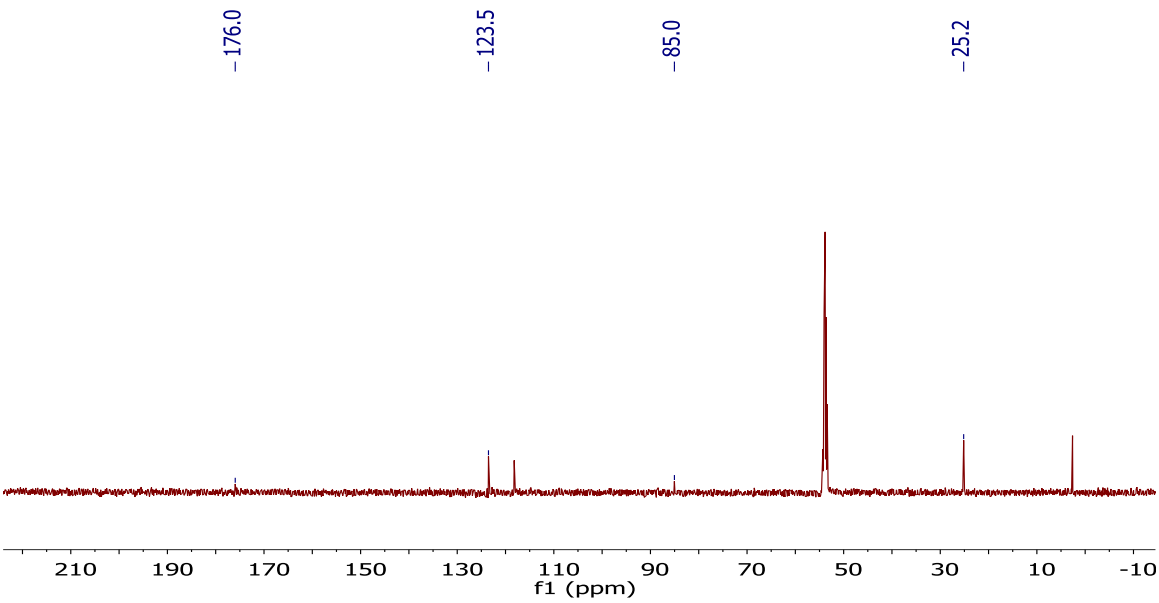

Figure 7-55 $^{13}C[^{1}H]$-NMR spectrum of compound **$43I_{12}[Li^{+}]$** in methylene chloride-d_2. *Note: coordinated acetonitrile can be seen at 2.6 and 118 ppm.*

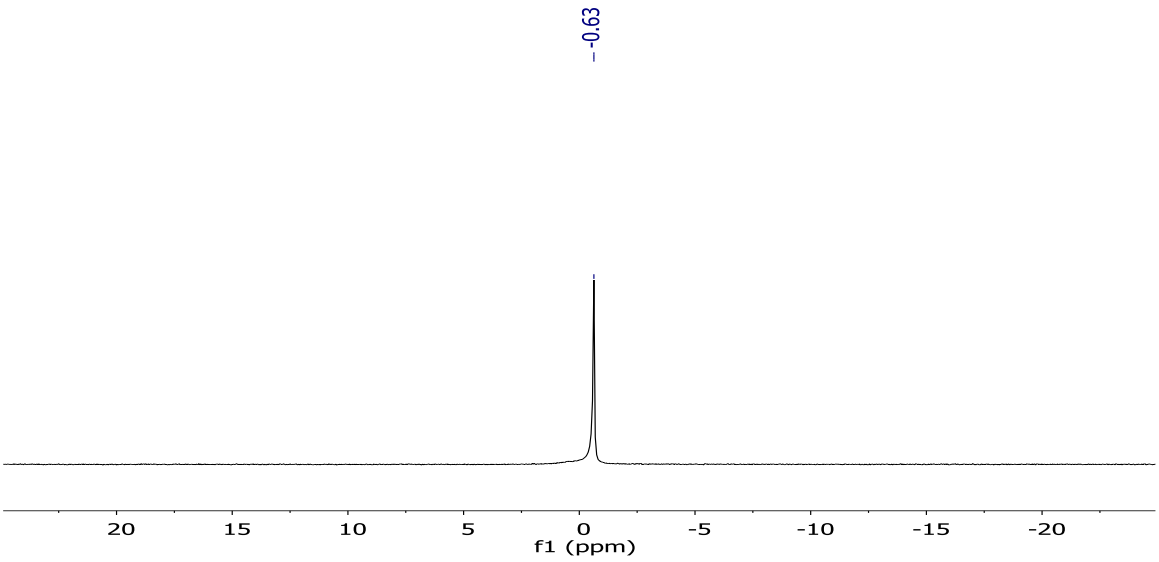

Figure 7-56 ^{7}Li-NMR spectrum of compound **$43I_{12}[Li^{+}]$** in methylene chloride-d_2.

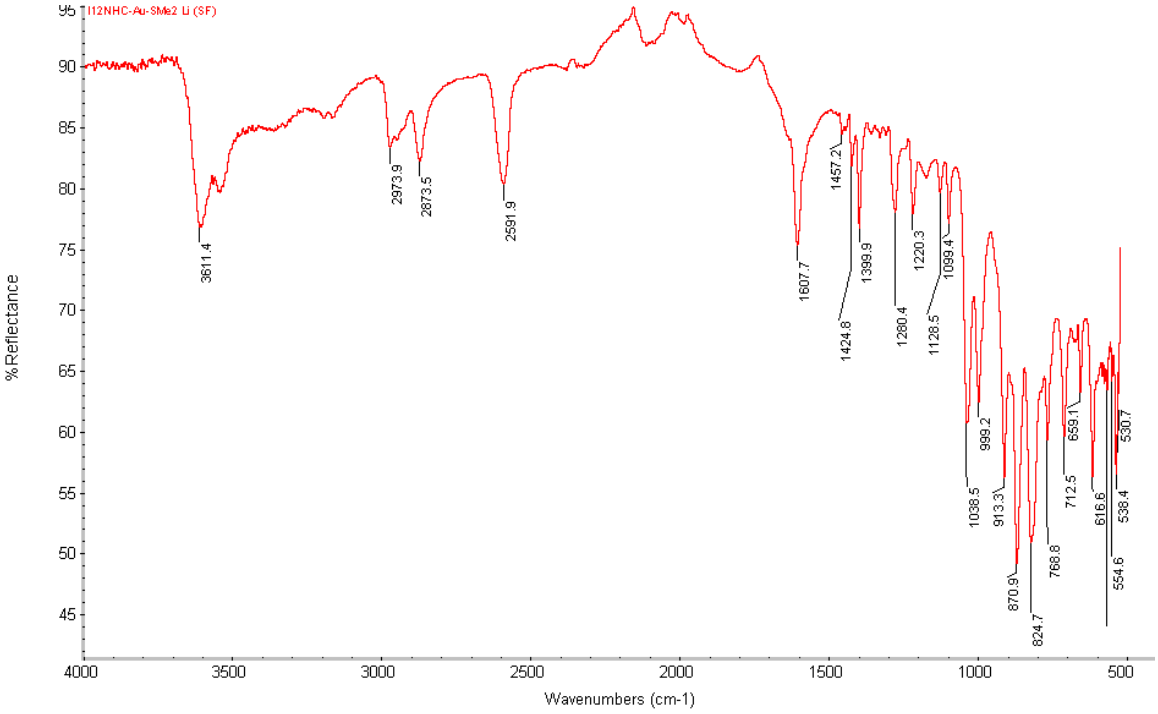

Figure 7-57 IR spectrum of **$43I_{12}[Li^+]$** showing the B-H stretches at 2591.9 cm^{-1}.

Synthesis of $43I_{12}[Ph_3C^+]$:

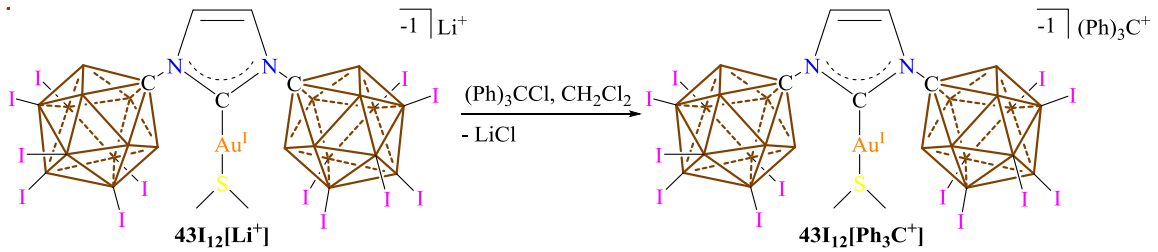

Scheme 7-15 Synthesis of **$43I_{12}[Ph_3C^+]$**.

A glass scintillation vial was equip with a stir bar and loaded with **$43I_{12}[Li^+]$** (*Note: the lithium counter cation should be coordinated to MeCN prior to starting this reaction)* (200 mg, 87 µmol) and the solid was suspended in methylene chloride (5 mL). Trityl chloride dissolved in methylene chloride (3 mL)

was added to the suspension and the reaction changed colors from pale yellow to bring yellow. The reaction as stirred for one hour at room temperature then filtered. The filtrate was concentrated down to 3 mL then added dropwise to a stirring benzene solution (16 mL) which forms a yellowish top layer and red bottom layer. After stirring for 15 minutes the upper benzene layer was removed and the remaining oil was pumped down to dryness furnishing the title compound, **$43I_{12}[Ph_3C^+]$**, quantitatively. ^{1}H NMR (600 MHz, methylene chloride-d_2, 25°C): δ = 8.32 (3H, t, $^3J(H,H)$ = 7.5 Hz), 7.93 (6H, m), 7.70 (6H, d, $^3J(H,H)$ = 7.1 Hz), 7.40 (2H, s), 2.97 (6H, s) ppm. ^{1}H[^{11}B]-NMR spectrum (600 MHz, methylene chloride-d_2, 25°C): δ = 8.31 (3H, t, $^3J(H,H)$ = 7.5 Hz), 7.93 (6H, t, $^3J(H,H)$ = 7.5 Hz), 7.70 (6H, d, $^3J(H,H)$ = 7.5 Hz), 7.40 (2H, s), 3.84 (10H, bs), 2.97 (6H, s) ppm. ^{11}B[^{1}H] NMR (96 MHz, methylene chloride-d_2, 25 °C): δ = -6.1, -12.5, -20.0 ppm. ^{11}B NMR (96 MHz, methylene chloride-d_2, 25 °C): δ = -6.2, -12.4 (broad), -20.0 ppm. ^{13}C[^{1}H] NMR (126 MHz, methylene chloride-d_2, 25°C): δ = 211.0, 176.0, 144.1, 143.2, 140.3, 131.2, 123.5, 85.0, 25.2 ppm.

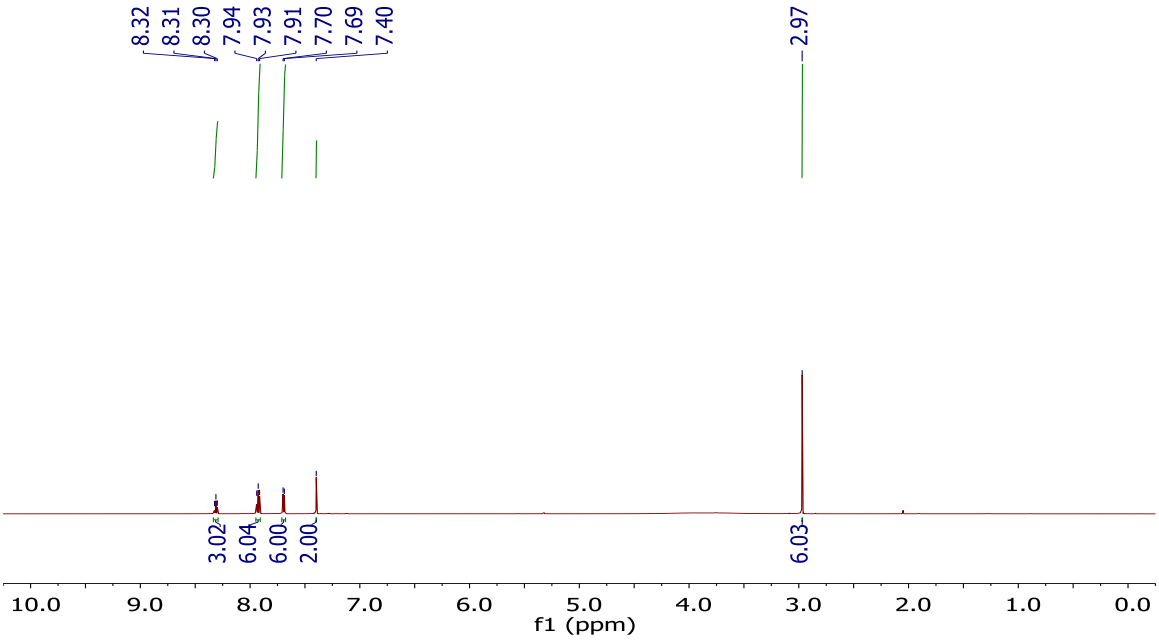

Figure 7-58 ^{1}H-NMR spectrum of compound **$43I_{12}[Ph_3C^+]$** in methylene chloride-d_2.

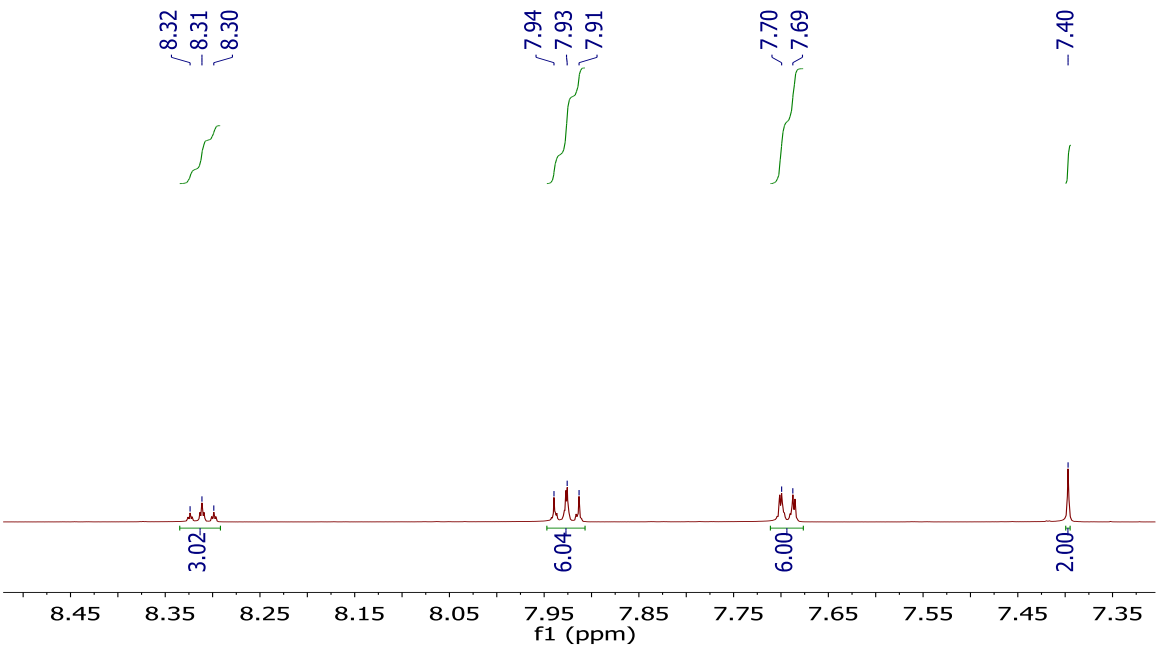

Figure 7-59 An expansion of the ^{1}H-NMR spectrum showing aromatic region of compound **43I$_{12}$[Ph$_3$C$^+$]** in methylene chloride-d$_2$.

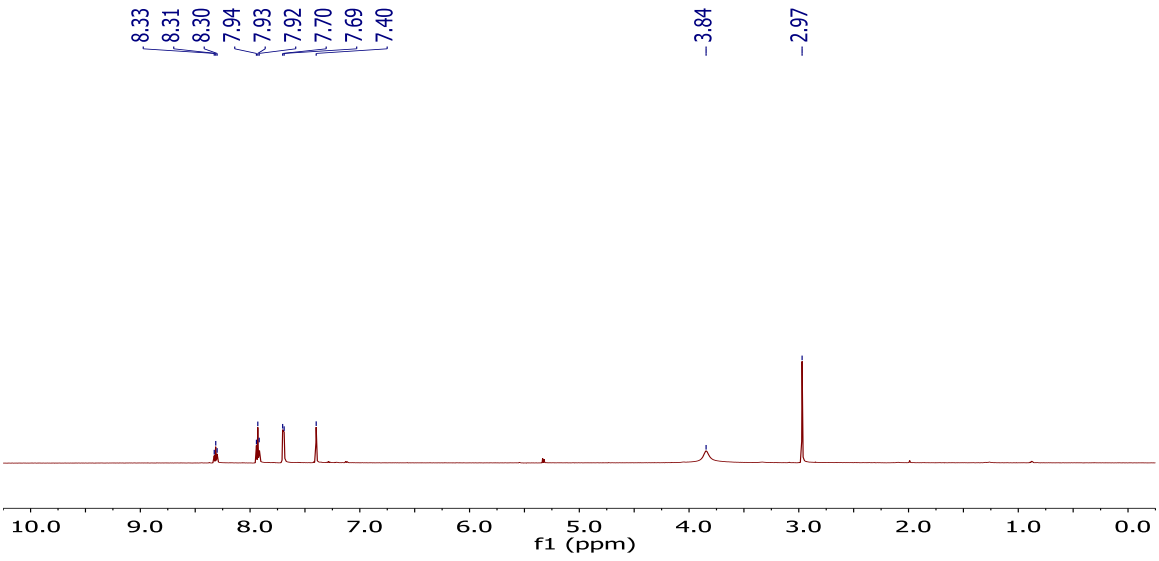

Figure 7-60 ^{1}H[^{11}B]-NMR spectrum of compound **43I$_{12}$[Ph$_3$C$^+$]** in methylene chloride-d2. *Note: the borohydrides appear at 3.84 ppm.*

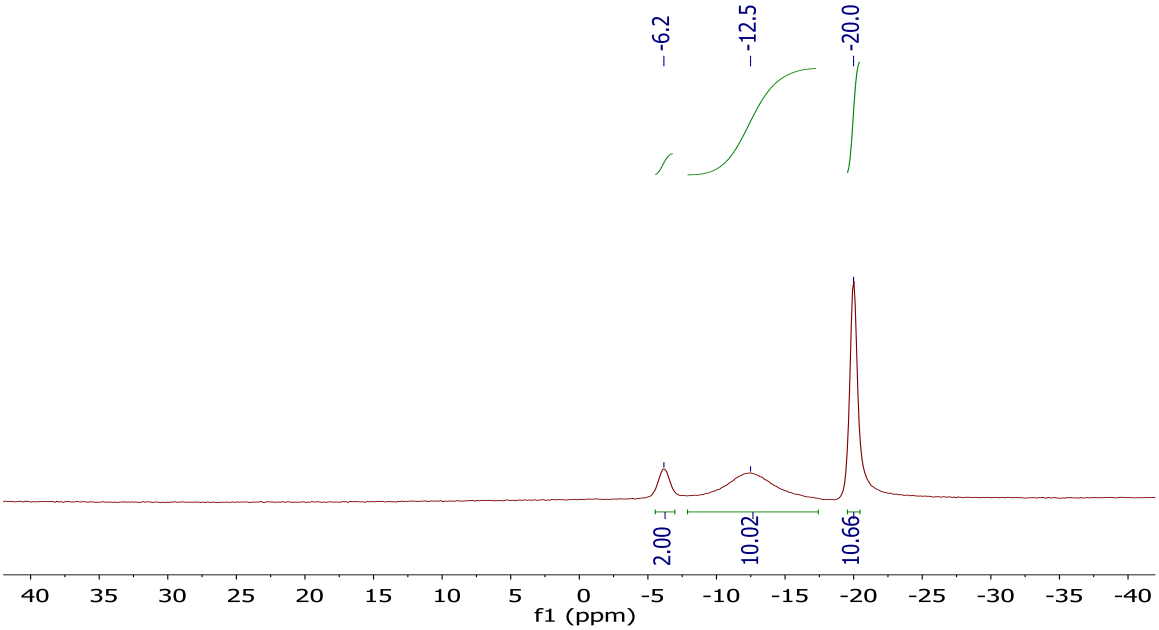

Figure 7-61 $^{11}B[^{1}H]$-NMR spectrum of compound **$43I_{12}[Ph_3C^+]$** in methylene chloride-d_2.

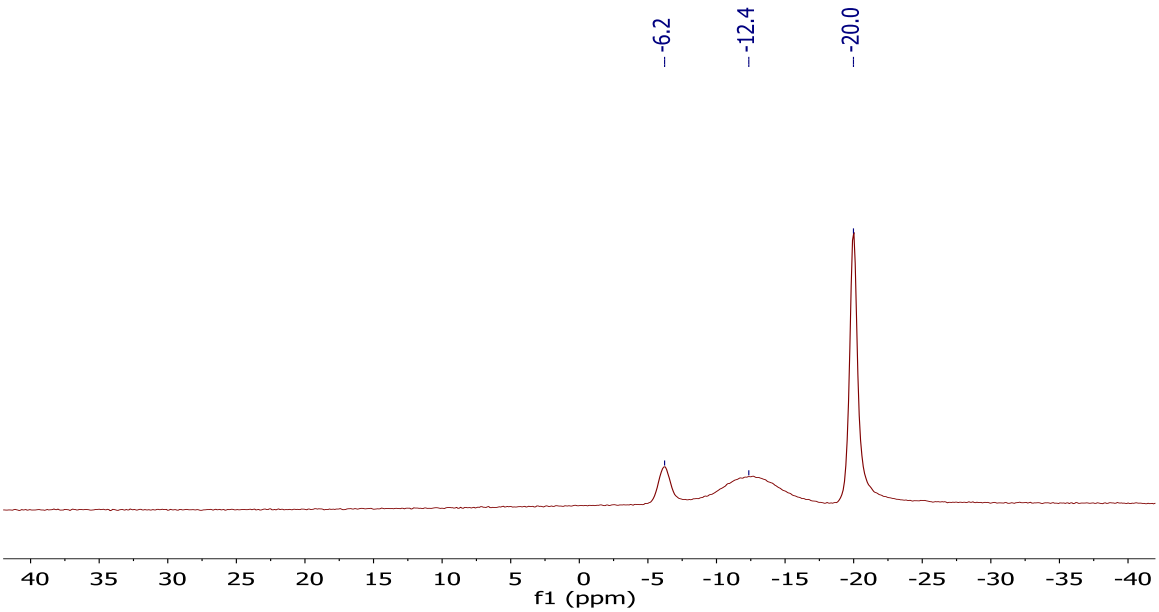

Figure 7-62 ^{11}B-NMR spectrum of compound **$43I_{12}[Ph_3C^+]$** in methylene chloride-d_2.

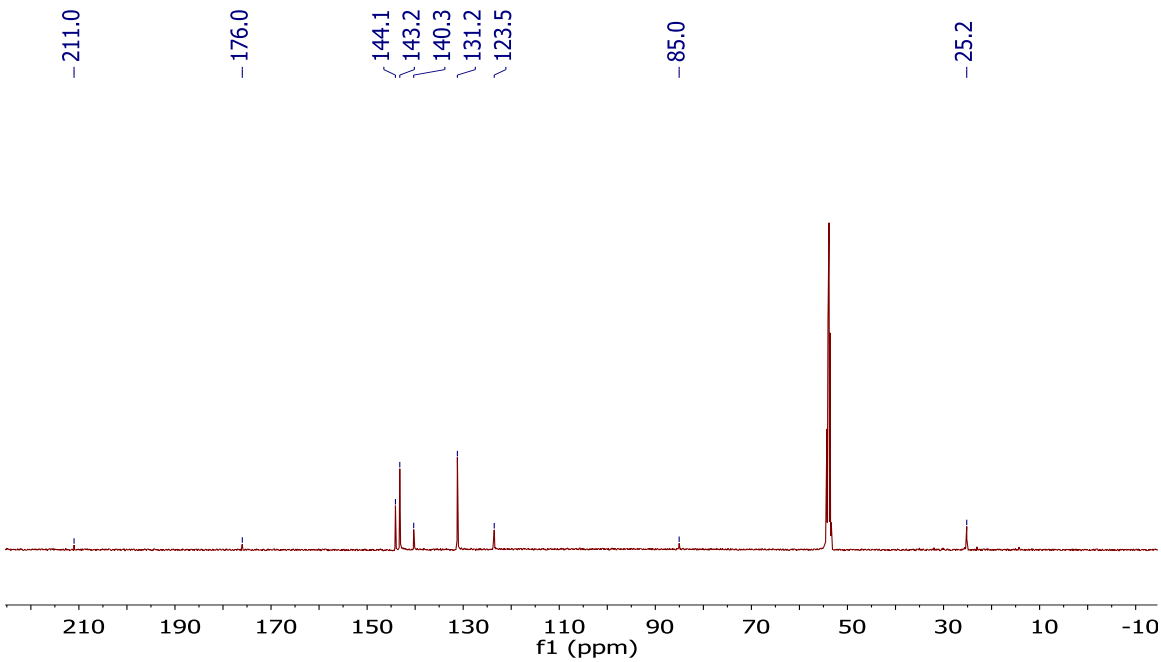

Figure 7-63 $^{13}C[^{1}H]$-NMR spectrum of compound **$43I_{12}[Ph_3C^+]$** in methylene chloride-d_2.

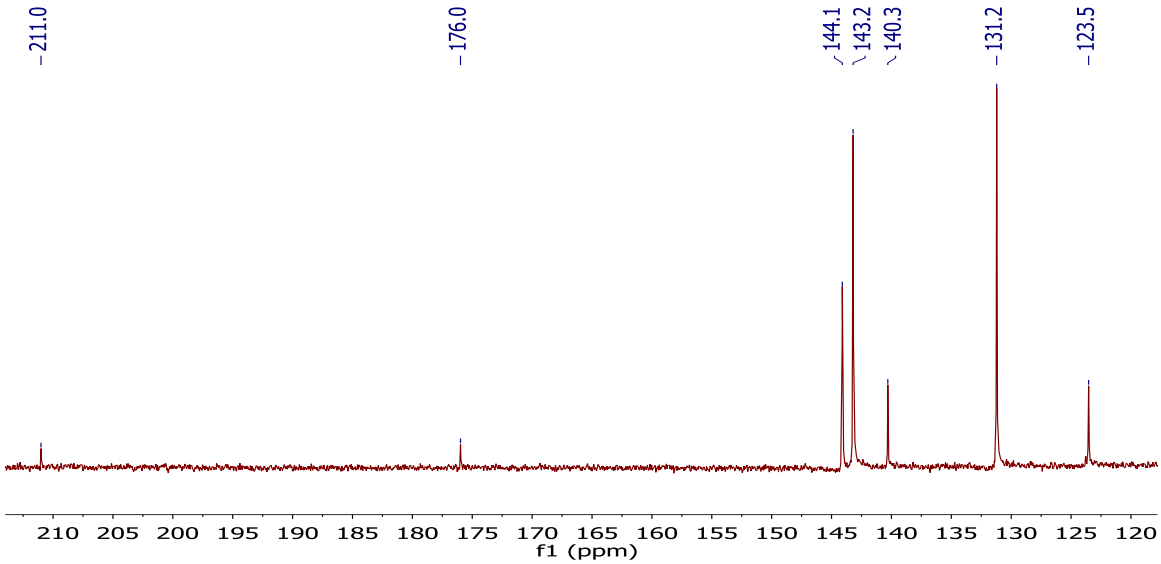

Figure 7-64 $^{13}C[^{1}H]$-NMR spectrum showing the down field region of **$43I_{12}[Ph_3C^+]$** with the trityl cation appearing at 211.0 ppm.

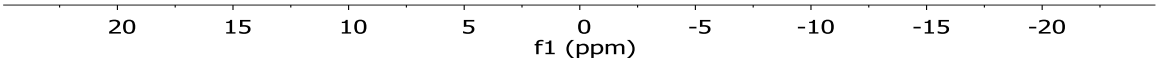

Figure 7-65 ^{7}Li-NMR spectrum of **43I$_{12}$[Ph$_3$C$^+$]** in methylene chloride-d$_2$.

Synthesis of 43Br$_{12}$[Et$_3$Si$^+$]:

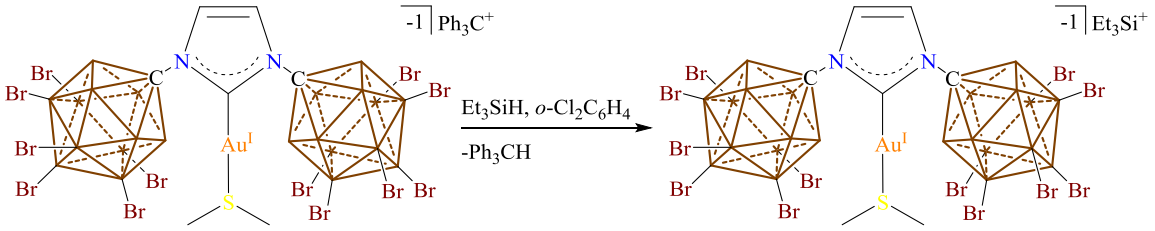

43Br$_{12}$[Ph$_3$C$^+$] **43Br$_{12}$[Et$_3$Si$^+$]**

Scheme 7-16 Synthesis of **43Br$_{12}$[Et$_3$Si$^+$]**.

A 20 mL glass scintillation vial was equip with a stir bar and loaded with **43Br[Ph$_3$C$^+$]** (277 µmol, 500 mg) and suspended in *o*-Cl$_2$C$_6$H$_4$ (3 mL). To the stirring solution triethylsilane (277 µmol, 44 µL) was added in a slight excess and the reaction stirred until the reaction was no longer colored (approximately 30

minutes to an hour). At this point the reaction was filtered and the filtrate added to a stirring solution of pentane (17 mL). After stirring for 30 minutes the pentane was removed and the solid washed with pentane (4 x 15 mL), *note: if the o-$Cl_2C_6H_4$ is not completely removed the compound will go from an off white solid to a dark purple oil upon drying under vacuum*. After decanting the last pentane wash, the off white solid was place under vacuum furnishing **43Br[Et_3Si^+]** as an off white solid (403.7 mg, 87% yield). ^{1}H NMR (600 MHz, *o*-$Cl_2C_6D_4$, 25 °C): δ = 8.64 (s, 2H), 5.4 – 4.6 (bs, 10H, B-H), 4.04 (s, 6H), 2.37 (m, 15H) ppm. ^{1}H[^{11}B] NMR (600 MHz, *o*-$Cl_2C_6D_4$, 25 °C): δ = 8.65 (s, 2H), 4.96 (bs, 10H, B-H), 4.05 (s, 6H), 2.38 (m, 15H) ppm. ^{11}B[^{1}H] NMR (192 MHz, *o*-$Cl_2C_6D_4$, 25 °C): δ = 1.0, -8.1, -15.9 ppm. ^{11}B NMR (192 MHz, *o*-$Cl_2C_6D_4$, 25 °C): δ = 1.0, -8.1, -15.9 ppm. ^{13}C[^{1}H] NMR (151 MHz, *o*-$Cl_2C_6D_4$, 25 °C): δ = 178.0, 124.5, 73.0, 25.6, 7.2, 7.0, 6.9, 6.1 ppm.

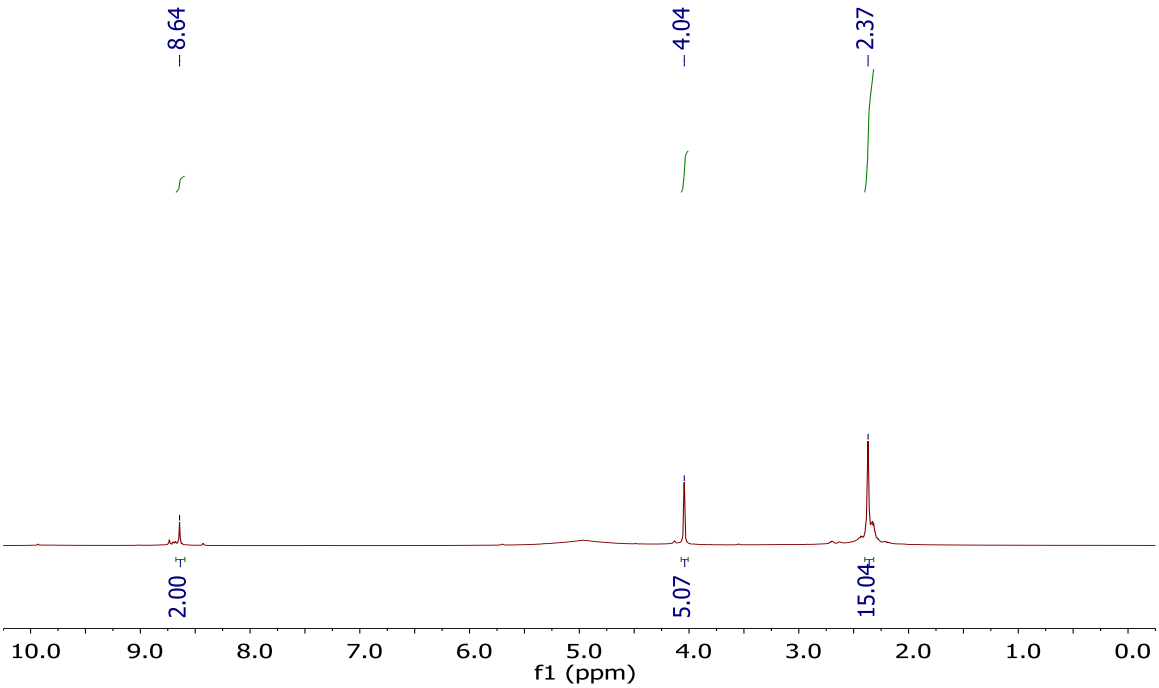

Figure 7-66 ^{1}H-NMR spectrum of **43Br$_{12}$[Et_3Si^+]** in *ortho*-dichlorobenzne-d_4.

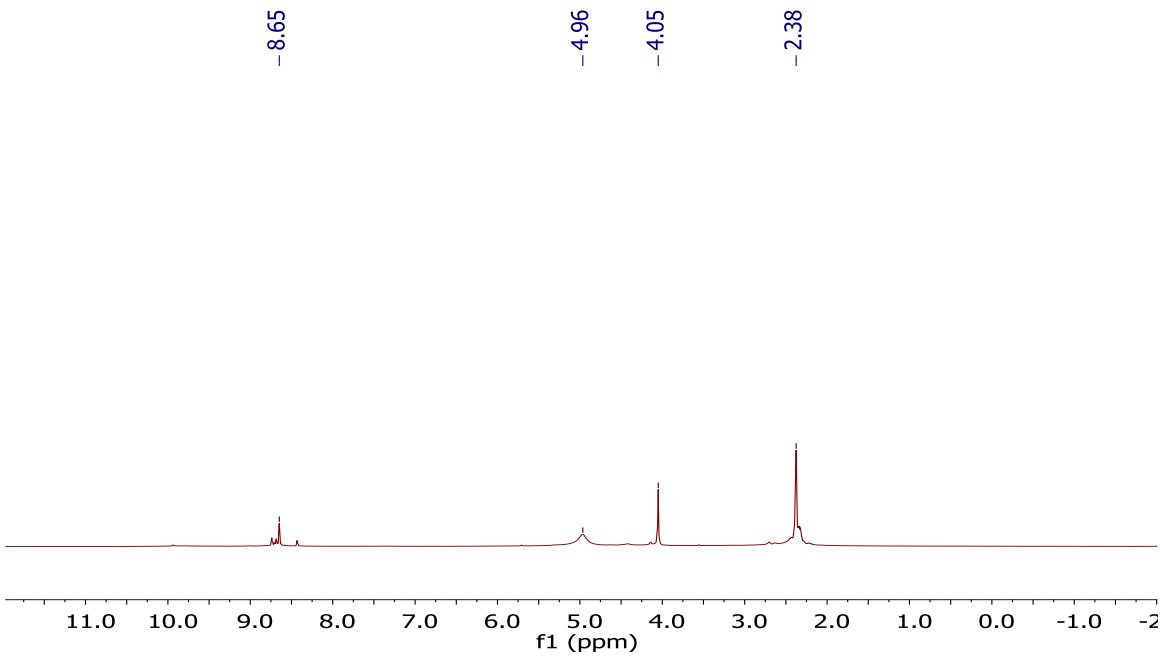

Figure 7-67 $^{1}H[^{11}B]$-NMR spectrum of **$43Br_{12}[Et_3Si^+]$** in *ortho*-dichlorobenzne-d_4.

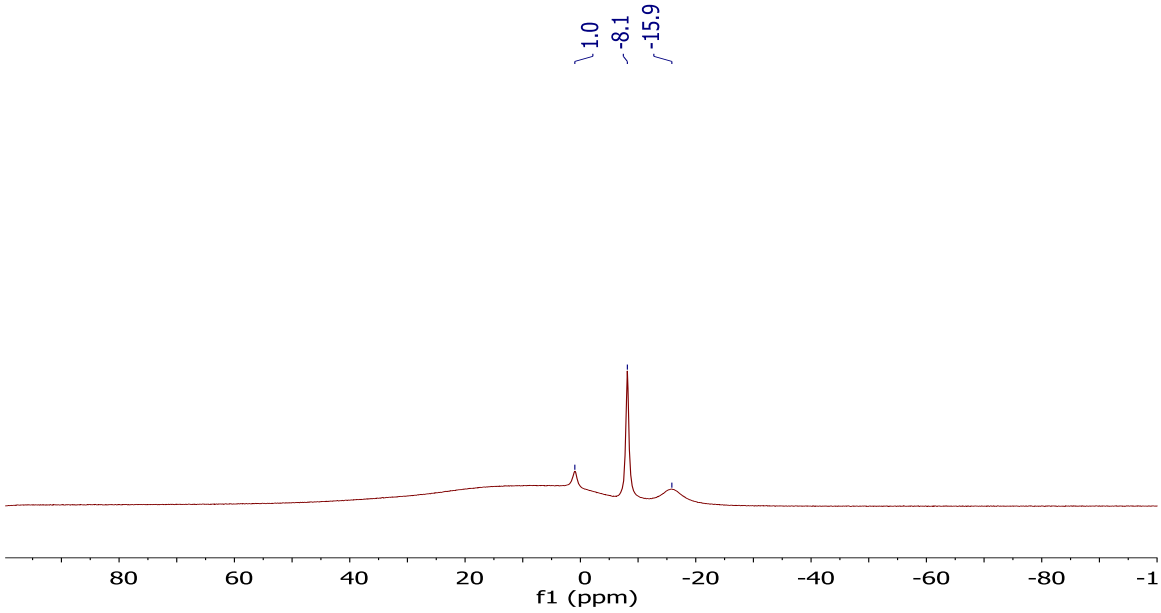

Figure 7-68 $^{11}B[^{1}H]$-NMR spectrum of **$43Br_{12}[Et_3Si^+]$** in *ortho*-dichlorobenzne-d_4.

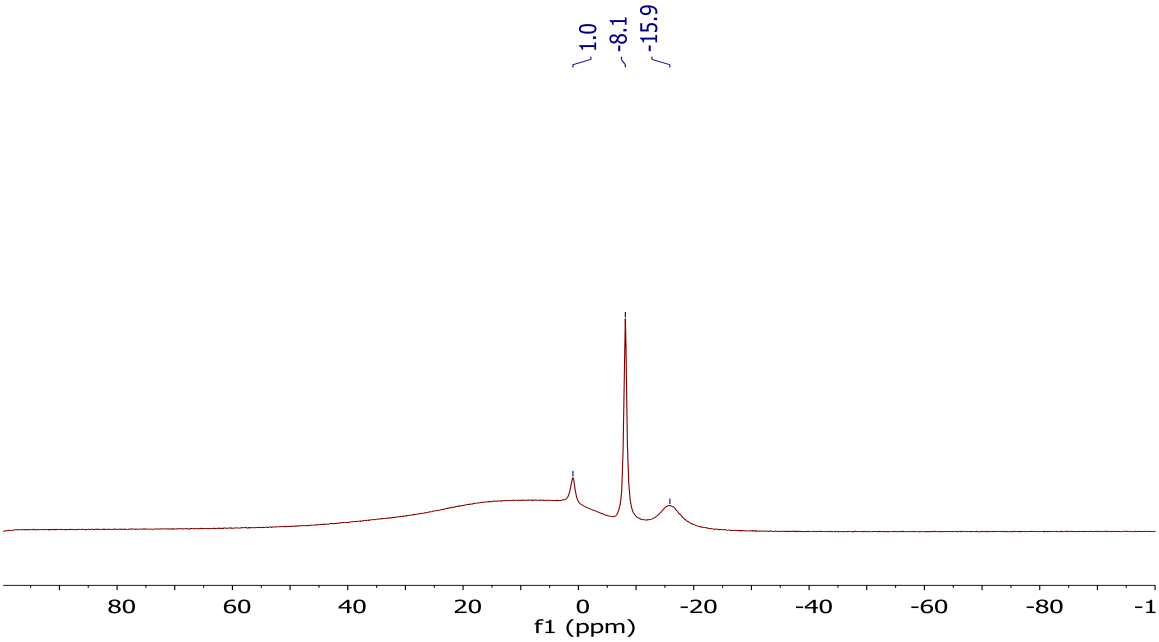

Figure 7-69 ^{11}B-NMR spectrum of **43Br$_{12}$[Et$_3$Si$^+$]** in *ortho*-dichlorobenzne-d$_4$.

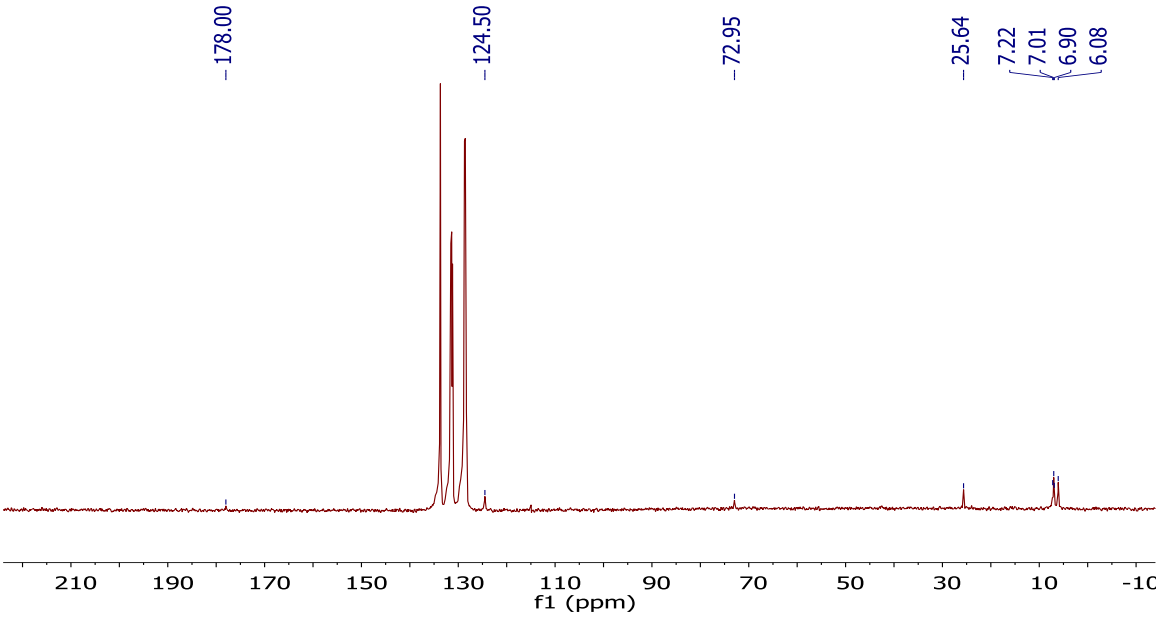

Figure 7-70 ^{13}C[^{1}H]-NMR spectrum of **43Br$_{12}$[Et$_3$Si$^+$]** in *ortho*-dichlorobenzne-d$_4$.

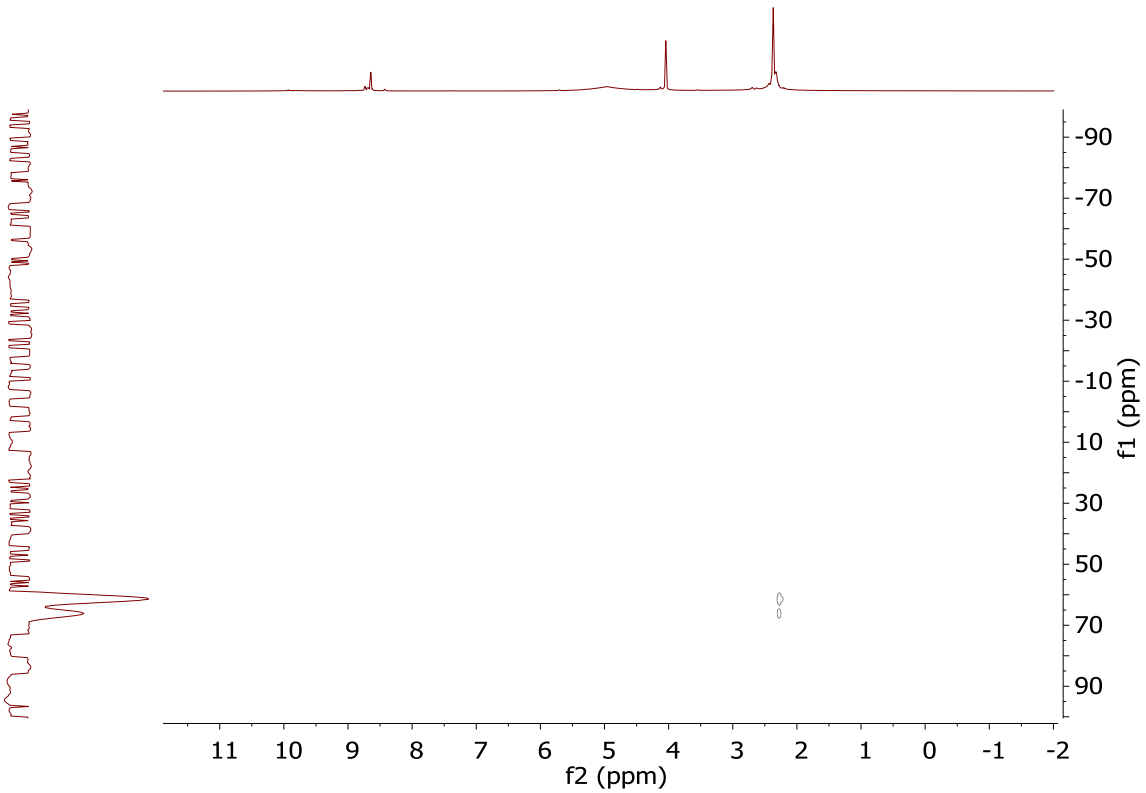

Figure 7-71 ^{1}H-^{29}Si HSQC-NMR spectrum of **43Br$_{12}$[Et$_3$Si$^+$]** in *ortho*-dichlorobenzne-d$_4$. *Note: the vertical axis, ^{29}Si axis, is an internal projection "maximum".*

X-Ray Structure Determination

Crystal Structure of 57:

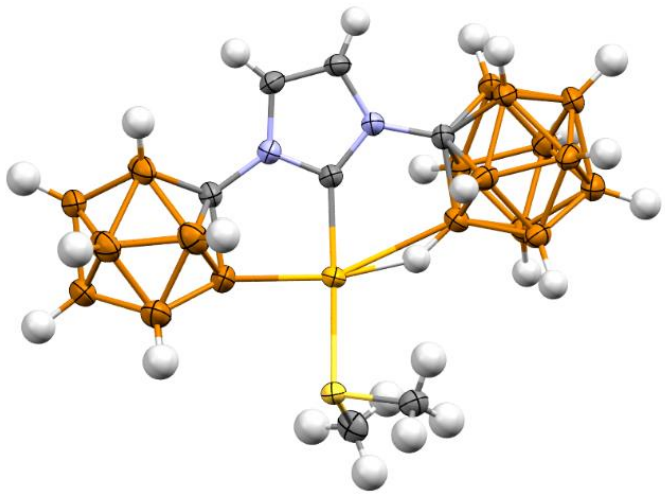

Figure 7-72 Solid state structure of **57**. Color code: Au = orange, B = brown, C = gray, N = blue, S = yellow, hydrogen = white.

A colorless prism fragment (0.565 x 0.333 x 0.155 mm^3) was used for the single crystal x-ray diffraction study of $C_7H_{29}B_{22}N_2SAu.[CH_2Cl_2]_{1.35}$ (sample vL249SF_0m). The crystal was coated with paratone oil and mounted on to a cryo-loop glass fiber. X-ray intensity data were collected at 100(2) K on a Bruker APEX2 platform-CCD x-ray diffractometer system (fine focus Mo-radiation, λ = 0.71073 Å, 50KV/30mA power). The CCD detector was placed at a distance of 5.0600 cm from the crystal.

A total of 3600 frames were collected for a sphere of reflections (with scan width of 0.3^o in ω, starting ω and 2θ angles of -30^o, and ϕ angles of 0^o, 90^o, 120^o, 180^o, 240^o, and 270^o for every 600 frames, 20 sec/frame exposure time). The frames were integrated using the Bruker SAINT software package and using a narrow-frame integration algorithm. Based on a monoclinic crystal system, the integrated frames yielded a total of 69305 reflections at a maximum 2θ angle of 61.016^o (0.70 Å resolution), of which 8956

were independent reflections (R_{int} = 0.0346, R_{sig} = 0.0186, redundancy = 7.7, completeness = 100%) and 8142 (90.9%) reflections were greater than 2σ(I). The unit cell parameters were, **a** = 29.2447(15) Å, **b** = 14.0197(7) Å, **c** = 14.3142(7) Å, **β** = 93.2313(7)°**,** V = 5859.5(5) $Å^3$, Z = 8, calculated density D_c = 1.640 g/cm^3. Absorption corrections were applied (absorption coefficient μ = 5.348 mm^{-1}; max/min transmission = 0.491/0.152) to the raw intensity data using the SADABS program.

The Bruker SHELXTL software package was used for phase determination and structure refinement. The distribution of intensities (E^2-1 = 0.904) and systematic absent reflections indicated one possible space group, C2/c. The space group C2/c (#15) was later determined to be correct. Direct methods of phase determination followed by two Fourier cycles of refinement led to an electron density map from which most of the non-hydrogen atoms were identified in the asymmetric unit of the unit cell. With subsequent isotropic refinement, all of the non-hydrogen atoms were identified. There was one disordered molecule of $C_7H_{29}B_{22}N_2SAu$ and seven partially occupied disordered solvent molecules of CH_2Cl_2 present in the asymmetric unit of the unit cell. The disordered site occupancy ratio of $C_7H_{29}B_{22}N_2SAu$ was 89%/11%. The percentage of the seven partial occupied CH_2Cl_2 sites were 31%, 29%, 21%, 18%, 17%, 15%, and 4%. The checkcif Alert Levels B, C and G are probably due to other possible disorder of the Au-atom position and CH_2Cl_2 disorder positions, which can not be modeled properly, and absorption correction errors.

Atomic coordinates, isotropic and anisotropic displacement parameters of all the non-hydrogen atoms were refined by means of a full matrix least-squares procedure on F^2. The H-atoms were included in the refinement in calculated positions riding on the atoms to which they were attached. The refinement converged at R1 = 0.0333, wR2 = 0.850, with intensity I>2σ (I). The largest peak/hole in the final difference map was 2.592/-1.062 e/$Å^3$. The large difference electron density peak/hole near the Au-atom is

probably due to the absorption correct errors and other possible disorder of Au-atom position which can not be modeled properly.

Table 7-1 Crystal data and structure refinement for **57**.

Identification code	vL249SF_0m	
Empirical formula	C8.36 H31.71 Au B22 Cl2.71 N2 S	
Formula weight	723.20	
Temperature	100(2) K	
Wavelength	0.71073 Å	
Crystal system	Monoclinic	
Space group	C 2/c	
Unit cell dimensions	a = 29.2447(15) Å	α= 90°.
	b = 14.0197(7) Å	β= 93.2313(7)°.
	c = 14.3142(7) Å	γ = 90°.
Volume	5859.5(5) $Å^3$	
Z	8	
Density (calculated)	1.640 Mg/m^3	
Absorption coefficient	5.348 mm^{-1}	
F(000)	2775	
Crystal size	0.565 x 0.333 x 0.155 mm^3	
Theta range for data collection	1.611 to 30.508°.	

Index ranges	-41<=h<=41, -20<=k<=20, -20<=l<=20
Reflections collected	69305
Independent reflections	8956 [R(int) = 0.0346]
Completeness to theta = 25.242°	100.0 %
Absorption correction	Semi-empirical from equivalents
Refinement method	Full-matrix least-squares on F^2
Data / restraints / parameters	8956 / 461 / 517
Goodness-of-fit on F^2	1.166
Final R indices [I>2sigma(I)]	R1 = 0.0333, wR2 = 0.0850
R indices (all data)	R1 = 0.0375, wR2 = 0.0871
Extinction coefficient	n/a
Largest diff. peak and hole	2.592 and -1.062 e.$Å^{-3}$

Crystal Structure of 43[sPh3C+]:

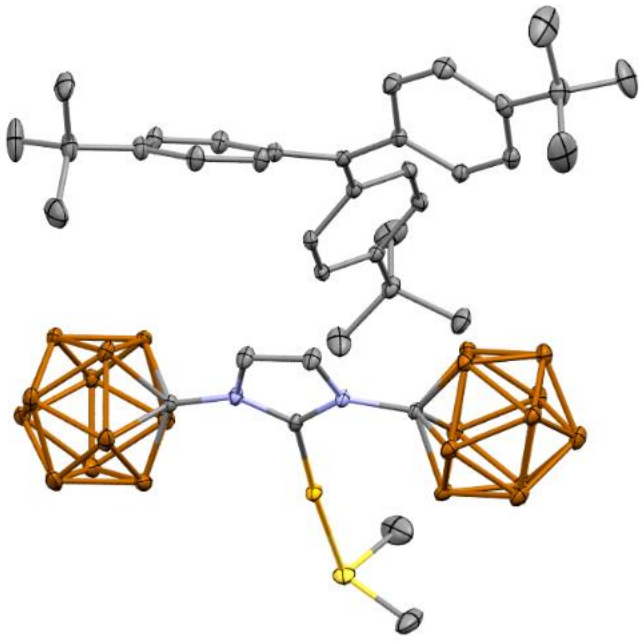

Figure 7-73 Solid state structure of **43[sPh3C+]**. Hydrogen atoms omitted for clarity. Color code: Au = orange, B = brown, C = gray, N = blue, S = yellow, hydrogen = white.

Diffraction data were collected on a Bruker-AXS Apex II diffractometer with an Apex II CCD detector using Mo K_α radiation (λ = 0.71073 Å) from a fine-focus sealed tube source. Data were collected at 100 K by performing 0.5° ω-scans, integrated using SAINT[1], and absorption corrected using SADABS[2]. The structure was solved by direct methods using SHELXT[3] and refined against F^2 on all data by full-matrix least squares with SHELXL-2018/3[4] following established refinement strategies[5]. All non-hydrogen atoms were refined anisotropically. All hydrogen atoms were included into the model at geometrically calculated positions and refined using a riding model. The isotropic displacement parameters of all hydrogen atoms were fixed to 1.2 times the U value of the atoms they are linked to (1.5 times for methyl groups). Crystal and data quality details, as well as a summary of the residual refinement values, are listed in the accompanying table.

Compound **43[sPh3C+]** crystallizes in the triclinic centrosymmetric space group *P-1* with one molecule of **43[sPh3C+]** one molecule of para-*t*-butyl-substituted trityl, and one molecule of dichloromethane per asymmetric unit. One *t*-butyl group of the substituted trityl exhibited disorder that was modeled over two positions; the disorder ratio was refined freely and converged at 70:30. This disorder was refined with the help of similarity restraints on 1,2- and 1,3- distances.

Table 7-2 Crystal data and structure refinement for vl339sf.

Identification code	vl339sf	
Empirical formula	C39 H71 Au B22 Cl2 N2 S	
Formula weight	1105.72	
Temperature	100(2) K	
Wavelength	0.71073 Å	
Crystal system	Triclinic	
Space group	P-1	
Unit cell dimensions	a = 12.6767(8) Å	α = 114.344(2)°.
	b = 15.2969(9) Å	β = 95.526(3)°.
	c = 16.0865(10) Å	γ = 104.140(2)°.
Volume	2686.6(3) $Å^3$	
Z	2	
Density (calculated)	1.367 Mg/m^3	
Absorption coefficient	2.908 mm^{-1}	

F(000)	1116
Crystal color	yellow
Crystal size	0.245 x 0.167 x 0.151 mm^3
Theta range for data collection	1.699 to 29.575°
Index ranges	-17 <= *h* <= 17, -21 <= *k* <= 21, -22 <= *l* <= 22
Reflections collected	97858
Independent reflections	15078 [R(int) = 0.0313]
Completeness to theta = 25.242°	100.0 %
Absorption correction	Semi-empirical from equivalents
Refinement method	Full-matrix least-squares on F^2
Data / restraints / parameters	15078 / 45 / 640
Goodness-of-fit on F^2	1.062
Final R indices [I>2sigma(I) = 14168 data]	R1 = 0.0174, wR2 = 0.0430
R indices (all data, 0.72 Å)	R1 = 0.0197, wR2 = 0.0439
Largest diff. peak and hole	1.035 and -0.667 $e.Å^{-3}$

Crystal Structure of 43Br$_{12}$[Ph3C+]:

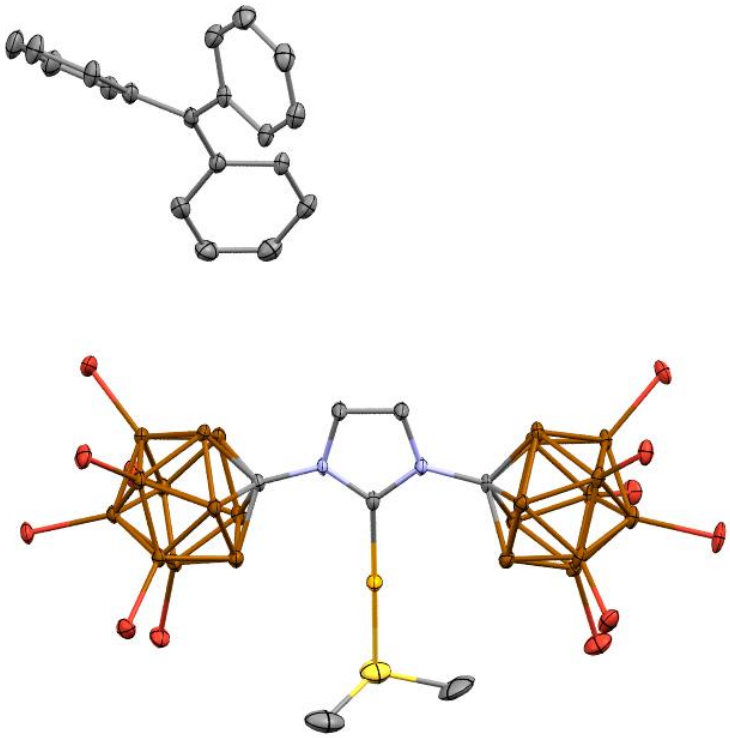

Figure 7-74 Solid state structure of **43Br$_{12}$[Ph3C+]**. Hydrogen atoms omitted for clarity. Color code: B = brown, C = gray, N = blue, Au = orange, S = yellow, Br = ruby red.

A yellow prism fragment (0.482 x 0.463 x 0.122 mm^3) was used for the single crystal x-ray diffraction study of $[C_{19}H_{15}]^+.[C_7H_{18}B_{22}Br_{12}N_2SAu]^-.[C_6H_5F]_{0.77}[CH_2Cl_2]_{0.23}$ (sample vL301SF_0m). The crystal was coated with paratone oil and mounted on to a cryo-loop glass fiber. X-ray intensity data were collected at 100(2) K on a Bruker APEX2 platform-CCD x-ray diffractometer system (fine focus Mo-radiation, l = 0.71073 Å, 50KV/30mA power). The CCD detector was placed at a distance of 5.0600 cm from the crystal.

A total of 3600 frames were collected for a sphere of reflections (with scan width of 0.3^{o} in w, starting w and 2q angles of –30^{o}, and f angles of 0^{o}, 90^{o}, 120^{o}, 180^{o}, 240^{o}, and 270^{o} for every 600 frames, 10 sec/frame exposure time). The frames were integrated using the Bruker SAINT software package and using a narrow-frame integration algorithm. Based on a triclinic crystal system, the integrated frames yielded a total of 58734 reflections at a maximum 2q angle of 56.564 (0.75 Å resolution), of which 13945 were independent reflections (R_{int} = 0.0310, R_{sig} = 0.0255, redundancy = 4.2, completeness = 99.9%) and 12422 (89.1%) reflections were greater than 2s(I). The unit cell parameters were, **a** = 9.0627(5) Å, **b** = 17.1820(9) Å, **c** = 18.6821(10) Å, α = 87.7680(9) β = 88.6994(8)^{o}, γ = 75.7526(8) V = 2817.2(3) Å^{3}, Z = 2, calculated density D_c = 2.231 g/cm^{3}. Absorption corrections were applied (absorption coefficient m = 11.213 mm^{-1}; max/min transmission = 0.342/0.074) to the raw intensity data using the SADABS program.

The Bruker SHELXTL software package was used for phase determination and structure refinement. The distribution of intensities (E^2-1 = 0.937) and no systematic absent reflections indicated two possible space groups, P-1and P1. The space group P-1 (#2) was later determined to be correct. Direct methods of phase determination followed by two Fourier cycles of refinement led to an electron density map from which most of the non-hydrogen atoms were identified in the asymmetric unit of the unit cell. With subsequent isotropic refinement, all of the non-hydrogen atoms were identified. There was one cation of $[C_{19}H_{15}]^{+}$, one anion of $[C_7H_{18}B_{22}Br_{12}N_2SAu]^{-}$ where the two CH3-groups bonded to the S-atom were modeled with disorder (disordered site occupancy ratio was 71%/29%), one partially occupied disordered C_6H_5F (disordered site occupancy ratio was 40%/37%), and one partially occupied CH_2Cl_2 (23% occupied) present in the asymmetric unit of the unit cell. .

Atomic coordinates, isotropic and anisotropic displacement parameters of all the non-hydrogen atoms were refined by means of a full matrix least-squares procedure on F^2. The H-atoms were included in the refinement in calculated positions riding on the atoms to which they were attached. The refinement converged at R1 = 0.0265, wR2 = 0.0606, with intensity I>2s (I). The largest peak/hole in the final

difference map was 2.079/-1.877 e/Å^3. The high peak/hole in the difference electron density map near the Au and Br atoms are probably due to absorption corrections error.

Table 7-3 Crystal data and structure refinement for **43Br$_{12}$[Ph3C+]**.

Identification code	vL301SF_0m	
Empirical formula	C30.84 H37.31 Au B22 Br12 Cl0.47 F0.77 N2 S	
Formula weight	1892.89	
Temperature	100(2) K	
Wavelength	0.71073 Å	
Crystal system	Triclinic	
Space group	P -1	
Unit cell dimensions	a = 9.0627(5) Å	α= 87.7680(9)°.
	b = 17.1820(9) Å	β= 88.6994(8)°.
	c = 18.6821(10) Å	γ = 75.7526(8)°.
Volume	2817.2(3) Å^3	
Z	2	
Density (calculated)	2.231 Mg/m^3	
Absorption coefficient	11.213 mm^{-1}	
F(000)	1752	
Crystal size	0.482 x 0.463 x 0.122 mm^3	
Theta range for data collection	1.667 to 28.282°.	

Index ranges	-12<=h<=12, -22<=k<=22, -24<=l<=24
Reflections collected	58734
Independent reflections	13945 [R(int) = 0.0310]
Completeness to theta = 25.242°	100.0 %
Absorption correction	Semi-empirical from equivalents
Refinement method	Full-matrix least-squares on F^2
Data / restraints / parameters	13945 / 424 / 714
Goodness-of-fit on F^2	1.039
Final R indices [I>2sigma(I)]	R1 = 0.0265, wR2 = 0.0606
R indices (all data)	R1 = 0.0322, wR2 = 0.0626
Extinction coefficient	n/a
Largest diff. peak and hole	2.079 and -1.877 e.$Å^{-3}$

7.7 References

1. S. P. Fisher, A. W. Tomich, S. O. Lovera, J. K. Kleinsasser, J. Guo, M. J. Asay, H. M. Nelson ,V. Lavallo, *Chemical Reviews*, 2019.

2. S. P. Fisher, A. W. Tomich, J. Guo ,V. Lavallo, *Chemical Communications*, 2019, **55**, 1684-1701.

3. R. N. Grimes, *Carboranes*, Academic Press, New York, 2016.

4. N. S. Hosmane, *Handbook of Boron Science : with Applications in Organometallics, Catalysis, Materials and Medicine*, World Scienific, Hackensack, New Jersey, 2019.

5. A. Spokoyny, *Pure and Applied Chemistry*, 2013, **85**, 903-919.

6. C. Douvris ,J. Michl, *Chemical Reviews*, 2013, **113**, PR179-PR233.

7. W. H. Knoth, *Journal of the American Chemical Society*, 1967, **89**, 1274-1275.

8. E. S. Stoyanov, S. P. Hoffmann, M. Juhasz ,C. A. Reed, *Journal of the American Chemical Society*, 2006, **128**, 3160-3161.

9. S. Cummings, H. P. Hratchian ,C. A. Reed, *Angewandte Chemie International Edition*, 2016, **55**, 1382-1386.

10. K.-C. Kim, C. A. Reed, G. S. Long ,A. Sen, *Journal of the American Chemical Society*, 2002, **124**, 7662-7663.

11. C. A. Reed, K.-C. Kim, R. D. Bolskar ,L. J. Mueller, *Science*, 2000, **289**, 101.

12. Z. Xie, D. J. Liston, T. Jelínek, V. Mitro, R. Bau ,C. A. Reed, *Journal of the Chemical Society, Chemical Communications*, 1993, 384-386.

13. Z. Xie, T. Jelinek, R. Bau ,C. A. Reed, *Journal of the American Chemical Society*, 1994, **116**, 1907-1913.

14. J. F. Kleinsasser, S. P. Fisher, F. S. Tham ,V. Lavallo, *European Journal of Inorganic Chemistry*, 2017, **2017**, 4417-4419.

15. T. Kato, E. Stoyanov, J. Geier, H. Grützmacher ,C. A. Reed, *Journal of the American Chemical Society*, 2004, **126**, 12451-12457.

16. C. A. Reed, K.-C. Kim, E. S. Stoyanov, D. Stasko, F. S. Tham, L. J. Mueller ,P. D. W. Boyd, *Journal of the American Chemical Society*, 2003, **125**, 1796-1804.

17. T. Kato ,C. A. Reed, *Angewandte Chemie International Edition*, 2004, **43**, 2908-2911.

18. K.-C. Kim, C. A. Reed, D. W. Elliott, L. J. Mueller, F. S. Tham, L. Lin ,J. B. Lambert, *Science*, 2002, **297**, 825-827.

19. S. P. Fisher, A. El-Hellani, F. S. Tham ,V. Lavallo, *Dalton Transactions*, 2016, **45**, 9762-9765.

20. A. Simonneau, T. Biberger ,M. Oestreich, *Organometallics*, 2015, **34**, 3927-3929.

21. M. Poyatos, J. A. Mata ,E. Peris, *Chemical Reviews*, 2009, **109**, 3677-3707.

22. J. Estrada ,V. Lavallo, *Angewandte Chemie International Edition*, 2017, **56**, 9906-9909.

23. M. Blaya, D. Bautista, J. Gil-Rubio ,J. Vicente, *Organometallics*, 2014, **33**, 6358-6368.

24. A. V. Zhukhovitskiy, I. J. Kobylianskii, C.-Y. Wu ,F. D. Toste, *Journal of the American Chemical Society*, 2018, **140**, 466-474.

25. N. P. Mankad ,F. D. Toste, *Chemical Science*, 2012, **3**, 72-76.

26. C. Bosset, R. Coffinier, P. A. Peixoto, M. El Assal, K. Miqueu, J.-M. Sotiropoulos, L. Pouységu ,S. Quideau, *Angewandte Chemie International Edition*, 2014, **53**, 9860-9864.

27. A. El-Hellani ,V. Lavallo, *Angewandte Chemie International Edition*, 2014, **53**, 4489-4493.

28. M. J. Asay, S. P. Fisher, S. E. Lee, F. S. Tham, D. Borchardt ,V. Lavallo, *Chemical Communications*, 2015, **51**, 5359-5362.

29. M. Etienne ,A. S. Weller, *Chemical Society Reviews*, 2014, **43**, 242-259.

30. S. G. McArthur, Ph.D., UC Riverside, 2018.

31. G. A. Olah ,L. D. Field, *Organometallics*, 1982, **1**, 1485-1487.

32. M. Arshadi, D. Johnels, U. Edlund, C.-H. Ottosson ,D. Cremer, *Journal of the American Chemical Society*, 1996, **118**, 5120-5131.

33. G. A. Olah, G. Rasul, L. Heiliger, J. Bausch ,G. K. S. Prakash, *Journal of the American Chemical Society*, 1992, **114**, 7737-7742.

34. M. Nava ,C. A. Reed, *Organometallics*, 2011, **30**, 4798-4800.

35. Z. Xie, R. Bau, A. Benesi ,C. A. Reed, *Organometallics*, 1995, **14**, 3933-3941.

36. J. B. Lambert, S. Zhang ,S. M. Ciro, *Organometallics*, 1994, **13**, 2430-2443.

Chapter 8: Efforts Towards an Anionic Au(I) Complex with a Borenium Counter Cation and its Potential for Tandem Catalytic Hydroamination-Hydrogenation.

8.1 Introduction

The chemistry of boron is surrounded by its intrinsic Lewis acidity which arises from its electron deficient nature.[1] Since boron is a second-row element, it still expected to meet the octet rule despite the fact that it only has three valence electrons. To achieve an octet, boron typically follows two bonding motifs; in the first classification the boron forms three covalent bonds and one dative bond. In the second classification, the boron forms four covalent bonds and becomes anionic. Within the first classification exist Frustrated Lewis Pairs (FLPs),[2-4] this is a class of compounds that possesses both a Lewis acidic and Lewis basic fragment that are unable to combine due to steric constraints. These molecules have gained popularity due to their ability to heterolytically cleave small molecules such as dihydrogen. An example of this is shown on the top of Scheme 8-1 which displays FLP **58** splitting dihydrogen and forming a zwitterionic species **59**.

Building upon the foundation developed by FLP chemistry, borenium catalysts has begun to emerge.[5, 6] In these systems, the Lewis pairs are not attached to the same compound but are still capable of activating small molecules such as dihydrogen.[5, 6] Shown in Scheme 8-1 bottom is a borenium catalyst **BF_4[60]** splitting dihydrogen with the help of imine **61** forming the borohydride **H[60]** and cationic iminium **62** (in this context compound **60** is the cationic boron containing molecule with a hydrogen atom **H[60]** or with a BF_4^- counter anion **BF_4[60]**).[6] If the Lewis basic component is an imine, such as **61**, the hydrogenation of the imine has been reported with extremely low H_2 pressure (1 atm).[6]

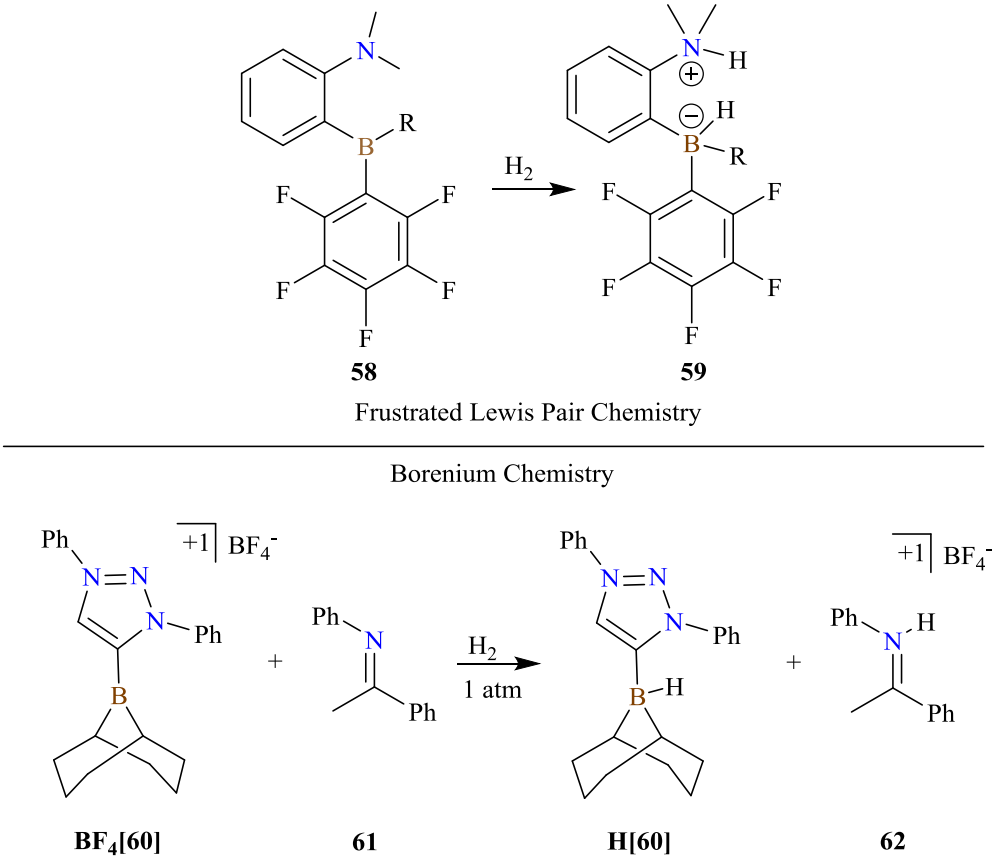

Scheme 8-1 Top: a frustrated Lewis pair **58** and its ability to split dihydrogen forming the zwitterionic complex **59**. Pre-catalyst R = C_6F_5, catalytically active species R = substrate. Bottom: A borenium catalyst **BF_4[60]** undergoing dihydrogen splitting at 1 atm with imine **61**.

The second classification encompasses weakly coordinating anions such as BF_4^-, $B(C_6F_5)_4^-$, and $B[3,5\text{-}(CF_3)C_6H_3]_4^-$.[7, 8] These anions have been used to isolate reactive cations such as $Et_3Si\text{-}H\text{-}SiEt_3^+$,[9] $H(OEt_2)_2^+$,[10] and Ta caitons.[11, 12] Another class of weakly coordinating anions that also contain boron are carborane anions (Figure 8-1, left).[13-16] Functionalized carborane anions have been used to isolate reactive species where the following anions have failed such as the first report of a free silylium ion.[17-19] Building on this work, a bastion of carborane chemistry has emerged. In this respect, Lavallo and coworkers have begun building organometallic complexes that bear a carboranyl substituent tethered to the ligand framework.[20-25] Along these lines, Fisher and coworkers have reported an anionic Au(I) complex that bears two carborane anions **43**.[22] We have also demonstrated that the carboranes of complex **43** can be

halogenated which render the cluster even more robust and were able to isolate reactive cations such as the trityl cation, Ph_3C^+, (**43Br$_6$[Ph$_3$C$^+$]**) and silylium ion, **43Br$_6$[Et$_3$Si$^+$]**, Figure 8-1 right (see Chapter 7).

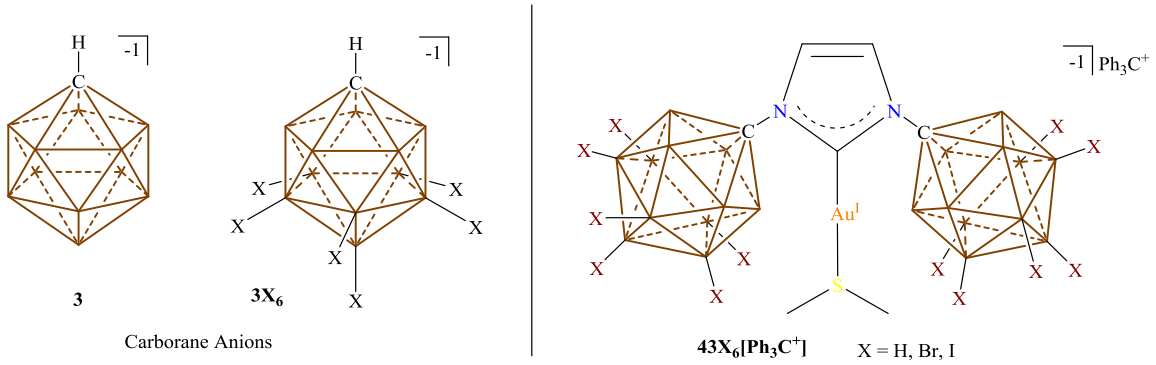

Figure 8-1 Left: Carborane anion **3** and hexafunctionalized carborane anion **3X$_6$**. Right: Anionic Au(I) complex displaying the hexahalogenation pattern on each carborane cluster, X = bromine or iodine. Unlabeled vertices = B-H.

Returning to the idea of tandem hydroamination-hydrogenation reactions, we envisioned pairing our anionic Au(I) fragment **43** with a borenium cation. In this reaction, the anionic Au(I) fragment would perform the hydroamination and the borenium cation would undertake the hydrogenation. It turns out that borenium catalyst **BF$_4$[60]** is the most active borenium hydrogenation catalyst capable of hydrogenating imines at 1 atm of H_2 pressure. There are also not examples of borenium catalyst hydrogenating alkynes to olefins or alkanes. With this in mind, we set out to investigate the ion pair of **43** with borenium cation **60**.

Reactivity of Anionic Au(I) complexes with a Borenium Hydride **H[60]**.

The most common way to prepare borenium cations, such as **BF$_4$[60]**, is to perform a hydride abstraction from the corresponding trityl salt and borohydride. To obtain a borenium cation ionically paired with our anionic Au(I) fragment, we reacted a 1:1 mixture of **43[Ph$_3$C$^+$]** with **H[60]** in methylene chloride solvent. The reaction immediately goes from highly colored to colorless suggesting the

trityl cation had been quenched and that the abstraction from the borohydride was complete. Indeed ^{1}H NMR analysis of the crude reaction mixture displayed complete conversion of the trityl cation to triphenylmethane. After washing away the triphenylmethane with pentane, the remaining solid was analyzed by multinuclear NMR spectroscopy. The ^{1}H NMR spectrum showed the anionic Au(I) fragment **43** was intact; singlet at 7.32 (NHC backbone protons) and 2.78 (Au-S(CH_3)$_2$) ppm. The former borohydride **H[60]** displayed a substantial shift in the backbone proton of the 1,2,3-triazolium substituent from 8.13 to 8.44 ppm along with a slight downfield shift (0.71 to 0.88 ppm) of the methine protons adjacent to the B atom. These chemical shifts are in line with the abstraction of the hydrogen atom from **H[60]**. The anionic Au(I) fragment **43** displayed its characteristic peaks in the ^{1}H NMR spectrum at 7.32 (NHC backbone protons) and 2.78 (Au-S(CH_3)$_2$) ppm. Lastly the ^{1}H NMR spectrum contained an unknown singlet at 2.63 ppm that integrated to 3H. The ^{11}B NMR spectrum did not corroborate the existence of a borenium cation and showed no signs of a resonance near 80.6 ppm where the reported borenium resonance appears.[6] Inspection of the ^{13}C NMR spectrum revealed all the expected peaks with the addition of two peaks at 116.2 and 3.66 ppm. After scrutinizing the NMR data, we realized that cationic boron compound **60** was coordinated to a molecule of acetonitrile and likely formed **43[60^{+}(MeCN)]**, Scheme 8-2. The acetonitrile is likely from **43[Ph_3C^{+}]**, it turns out acetonitrile is extremely difficult to remove from **43[Ph_3C^{+}]**. This is likely due to the presence of Li^{+} ions present in **43[Ph_3C^{+}]**. Indeed, attempting to remove acetonitrile from **43[Li^{+}]** is extremely difficult and requires high heat for multiple days. This suggest that something is coordinated to acetonitrile and we believe it to be **43[Li^{+}]** as LiCl should be removed via filtration from methylene chloride. At the time ^{7}Li NMR was not used to check **43[Ph_3C^{+}]** for complete cation exchange.

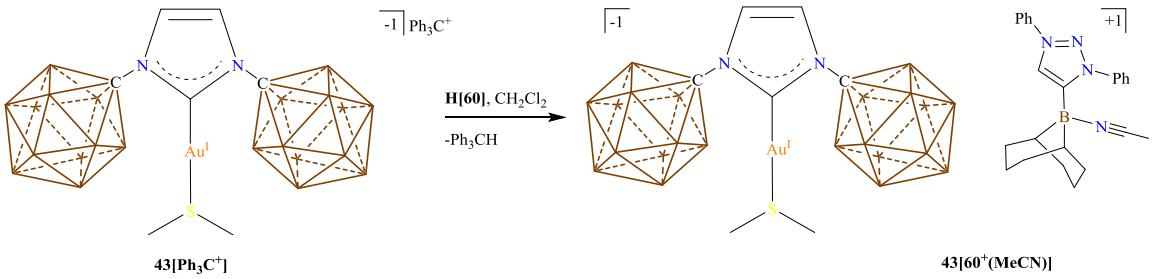

Scheme 8-2 Reaction of **43[Ph_3C^+]** with borohydride **H[60]** and the presumed product **43[60^+(MeCN)]**. There are likely trace amounts of **43[Li^+]** still present in **43[Ph_3C^+]** where the Li^+ ion is coordinated to MeCN.

Unaware of the issue with acetonitrile, we decided to move to the hexahalogenated clusters starting with **43Br_6[Ph_3C^+]**. When a 1:1 ratio of **43Br_6[Ph_3C^+]** was reacted with **H[60]** and immediate color change from yellow to colorless was observed. Analysis of the ^{1}H NMR spectrum of the crude reaction allowed us to pick out peaks corresponding to triphenylmethane. There were also two downfield singlets at 8.90 and 8.46 ppm for the backbone proton of the 1,2,3-triazolium substituent of the presumed boroenium cation and one singlet at 7.39 relating to the backbone protons of the NHC. The ^{11}B[^{1}H] NMR spectrum displayed a small resonance at 58.4 ppm as well as three upfield resonance for the carborane anion at -1.4, -10.2 and -17.8 ppm. The triphenylmethane was washed away with pentane washes but the other resonances at 8.90, 8.46, and 7.39 ppm remained along with the resonances in the ^{11}B NMR spectrum. The two resonances at 8.90 and 8.46 ppm were puzzling because they both corresponded to the backbone proton of 1,2,3-triazolium. Eventually we realized that these resonances corresponded to a 50:50 mixture of three coordinate borenium **43Br_6[60^+]** and four coordinate boronium **43Br_6[60^+(MeCN)]** ions in solution, Scheme 8-3.

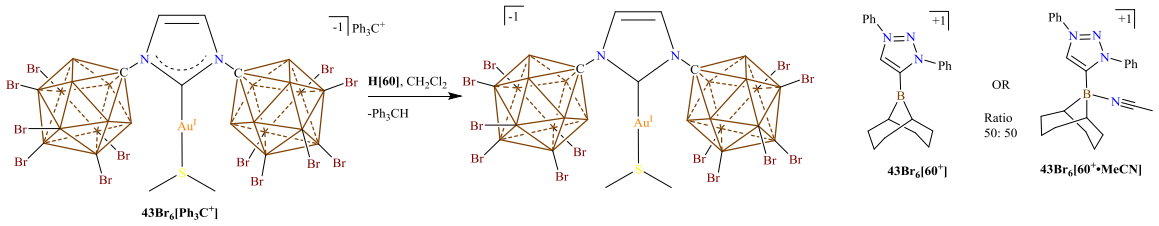

Scheme 8-3 Synthesis of **43Br$_6$[60]** and **43Br$_6$[60•MeCN]**.

Still unaware of the issue we acetonitrile, we moved onto test the reaction of a 1:1 mixture **43I$_6$[Ph$_3$C$^+$]** and **H[60]** in methylene chloride. Surprisingly, the ^{11}B NMR spectrum of the crude reaction mixture did display the a small borenium peak at 81.8 ppm. After washing away the trity chloride in pentane, the ^{1}H NMR spectrum displayed the expected downfield shift for the 1,2,3-triazolium backbone proton at 8.98 ppm in good agreement with the reported value suggestion the formation of **43I$_6$[60$^+$]**.[6] Close inspection of the aromatic region displayed what appear to be multiple aryl resonances supportive of some adduct formation, indeed there is a small peak at 2.79 ppm suggestive of a small amount of acetonitrile adduct **43I$_6$[60$^+$(MeCN)]** (less than 5%), Scheme 8-4. Layering a methylene chloride solution of mostly **43I$_6$[60$^+$]** with benzene gave poor quality crystals which were suitable for an ID using single crystal X-ray diffraction. The ID confirmed the structure of **43I$_6$[60$^+$]**, Figure 8-2.

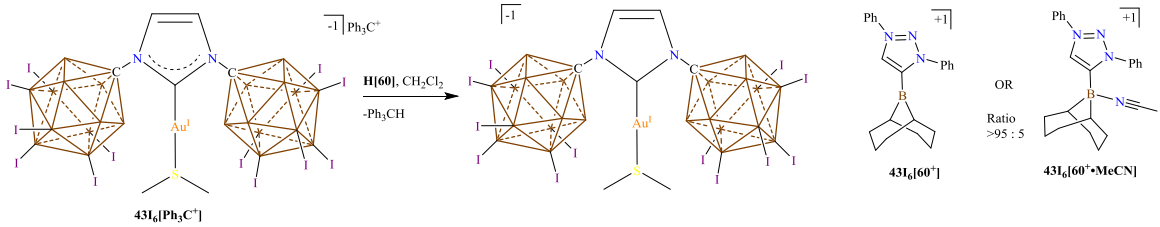

Scheme 8-4 Synthesis of **43I$_6$[60$^+$]** with a small amount of **43I$_6$[60$^+$(MeCN)]**.

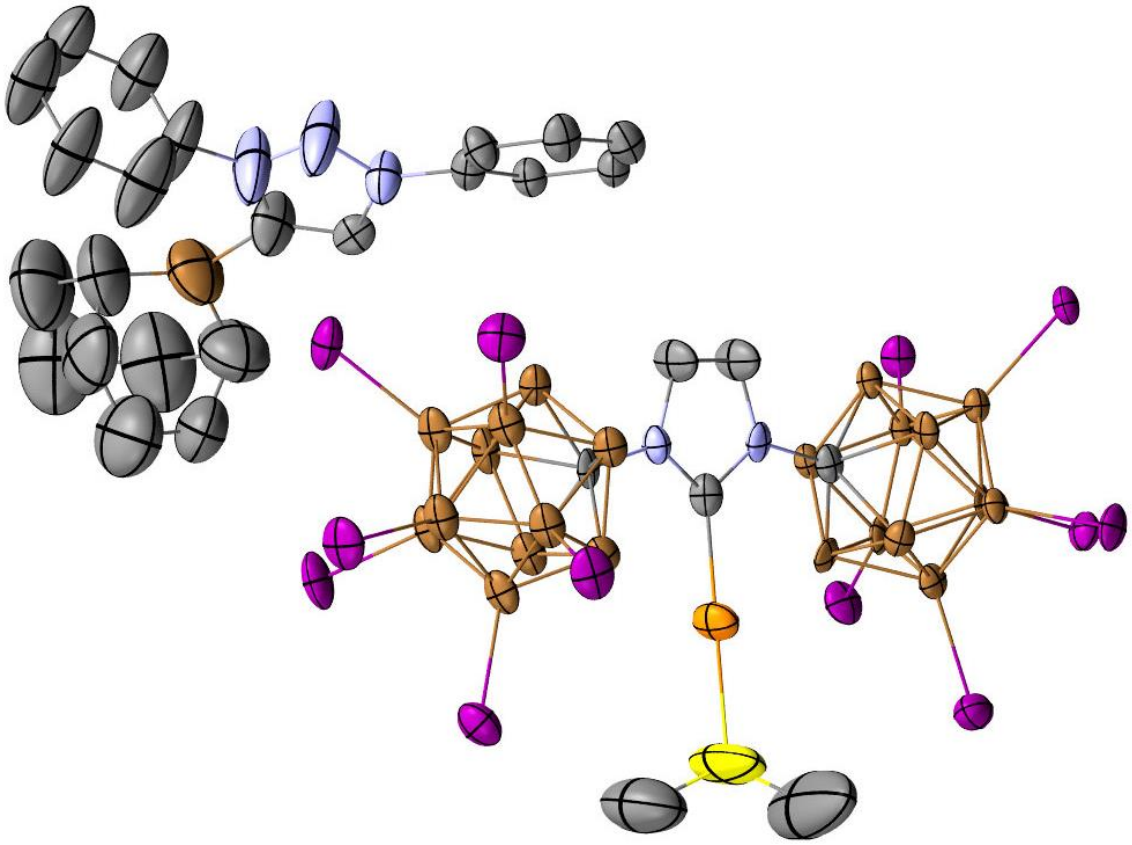

Figure 8-2 Solid state structure of **43I$_6$[60$^+$]**. Hydrogen atoms omitted for clarity. Color code: B = brown, C = gray, N = blue, S = yellow, Au = orange, I = magenta.

8.3 Catalytic Tandem Hydroamination-Hydrogenation reaction.

With **43[60(MeCN)]**, the 50:50 mixture of **43Br6[60$^+$]**:**43Br$_6$[60$^+$(MeCN)]** and **43I$_6$[60$^+$]** (**43I$_6$[60$^+$]** is actually a mixture of >95:5, see above) in hand we wanted to test the catalytic tandem hydroamination-hydrogenation of aniline, phenylacetylene and H_2, Scheme 8-5. A Teflon Schlenk was loaded with 10 mol% **43X$_6$[60$^+$]** (X = H, Br, I; *note some X variants are mixtures of **[60$^+$]** and **[60$^+$(MeCN)]**)*, aniline, phenylacetylene and less than one mL of methylene chloride. To the solution H_2 gas was added over three freeze pump thaw cycles. However, all three systems only produced the hydroamination product (imine) and no hydrogenation product. Baffled by this reactivity, we tested the hydrogenation of imine **61** with **43I$_6$[60$^+$]** and H_2 gas using the same protocol described above and found

the hydrogenation took substantially longer then reported,[6] reported **BF_4[60]** = 18 hours, unreported **$43I_6[60^+]$** = 48 hours, where **$43I_6[60^+]$** only produced trace amounts of amine **63**, Scheme 8-5. Concerned about the hydrogenation of **BF_4[60]** we attempted to reconstruct the hydrogenation conditions reported.[6] In our hands, we were unable to successfully hydrogenate imine **61** with **BF_4[60]** using 1 atm of hydrogen atmosphere. We were however, able to perform the hydrogenation slightly above 1 atm of H_2, this was achieved by adding 1 atm of H_2 gas to a submerged Teflon Schlenk in liquid nitrogen. However, even this technique did not lead to a successful hydroamination-hydrogenation reaction with **$43I_6[60^+]$**. Thus, we thought to test poisoning experiments with catalyst **BF_4[60]** and found that the catalyst was poisoned by amines.

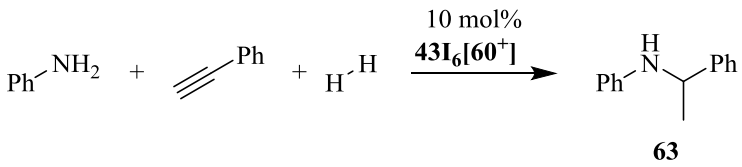

63

Scheme 8-5 Desired tandem catalytic hydroamination-hydrogenation using catalyst **$43I_6[60^+]$** containing less than 5% of **$43I_6[60^+$(MeCN)]**.

8.4 Experimental

General Considerations:

All manipulations were carried out using standard Schlenk or glovebox techniques under a dinitrogen atmosphere (industrial grade, glovebox) or purified elemental argon (99.995%, Schlenk line) unless otherwise stated. Dry solvents were obtained via distillation under argon from calcium hydride (acetonitrile, fluorobenzene, methylene chloride), sodium-potassium alloy (diethyl ether), potassium (benzene) or potassium utilizing benzophenone ketyl radical as an indicator (tetrahydrofuran). Pentane and toluene were collected from a solvent purification system by SG Waters USA, LLC utilizing a fifteen-minute argon sparge followed by passage though activated aluminum. Compounds **$3[Cs^+]$** and **$43[Li^+]$** were prepared

according to the literature. Unless specifically stated, reagents were purchased from commercial vendors and used without further purification. Nuclear magnetic resonance (NMR) spectroscopy was carried out using: Bruker Avance 300 MHz, Bruker Avance 600 MHz, and Bruker NEO 400 MHz (CryoProbe), Varian Inova 500 MHz. NMR chemical shifts are reported in parts per million (ppm) with ^{1}H and ^{13}C chemical shifts referenced to the residual non-deutero solvent. The ^{11}B-^{1}H coupling constants from ^{11}B spectra are reported when possible.

Synthesis of 43[60^{+}(MeCN)]:

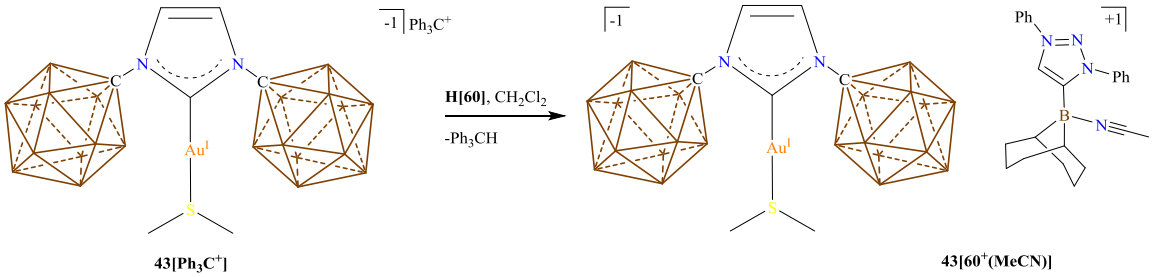

Scheme 8-6 Synthesis of **43[60^{+}(MeCN)]**.

A glass scintillation vial was equipped with a stir bar and loaded with **43[Ph$_3$C^{+}]** (200 mg, 224 µmol, *likely contaminated with* ***43[Li^{+}(MeCN)]***) which was dissolved in methylene chloride (1 mL). To the stirring solution **H[60]** (76.8 mg, 224 µmol)in methylene chloride (3 mL) was added dropwise and the reaction stirred for 30 minutes. The reaction was filtered, and the filtrate was added to a vigorously stirring solution of pentane (15 mL). The residue was washed twice more with pentane (20 mL) and the tan solid was pumped down to dryness furnishing **43[60^{+}(MeCN)]** (95% yield, 202 mg). ^{1}H NMR (400 MHz, methylene chloride-d$_2$, 25 °C) ∂ = 8.44 (s, 1H), 7.93 – 7.62 (10 H, m), 7.32 (s, 2H), 2.78 (s, 6H), 2.63 (s, 3H), 1.84 – 1.46 (bs x 5, 12H), 0.88 (s, 2H), 3.75 – 0.90 (bs, 22H) ppm. $^{1}H[^{11}B]$ NMR (400 MHz, methylene chloride-d$_2$, 25 °C) ∂ = 8.43 (s, 1H), 7.93 – 7.61 (10 H, m), 7.32 (s, 2H), 2.78 (s, 6H), 2.63 (s, 3H), 2.59 (s, 10H, B-H), 1.91 – 1.46 (m, 24 H), 0.88 (s, 2H) ppm. $^{11}B[^{1}H]$ NMR (128 MHz, methylene chloride-d$_2$, 25 °C) ∂ = -8.7, -13.9 ppm. ^{11}B NMR (128 MHz, methylene chloride-d$_2$, 25 °C) ∂ = -8.7 (^{1}J*(B-*

H) = 121.2 Hz), -13.9 (^{1}J*(B-H)* = 136.1 Hz) ppm. ^{13}B NMR (151 MHz, methylene chloride-d_2, 25 °C) ∂ = 174.2, 155.1, 136.7, 135.0, 132.7, 131.4, 131.0, 130.3, 129.7, 128.5, 126.2, 122.2, 121.9, 116.2, 79.6, 30.7, 25.0, 23.9, 21.6, 3.7 ppm.

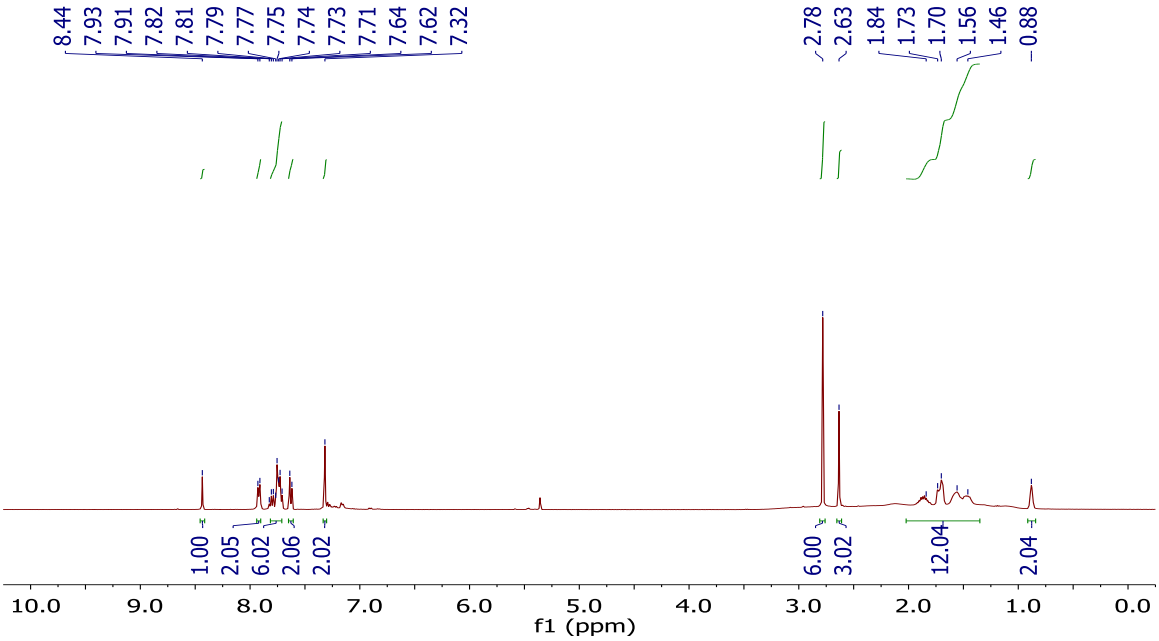

Figure 8-3 ^{1}H-NMR spectrum of **43[60^{+}(MeCN)]** in methylene chloride-d_2.

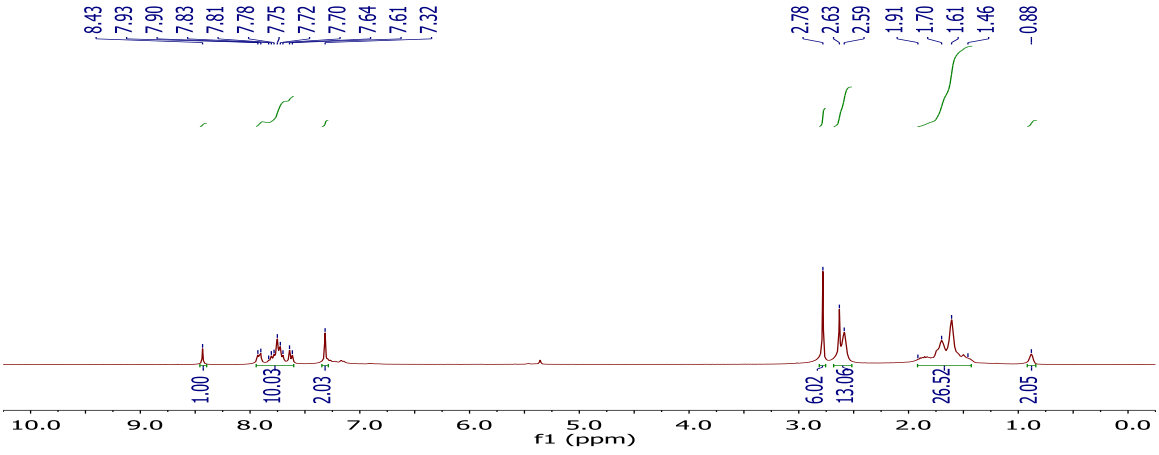

Figure 8-4 ^{1}H[^{11}B]-NMR spectrum of **43[60^{+}(MeCN)]** in methylene chloride-d_2.

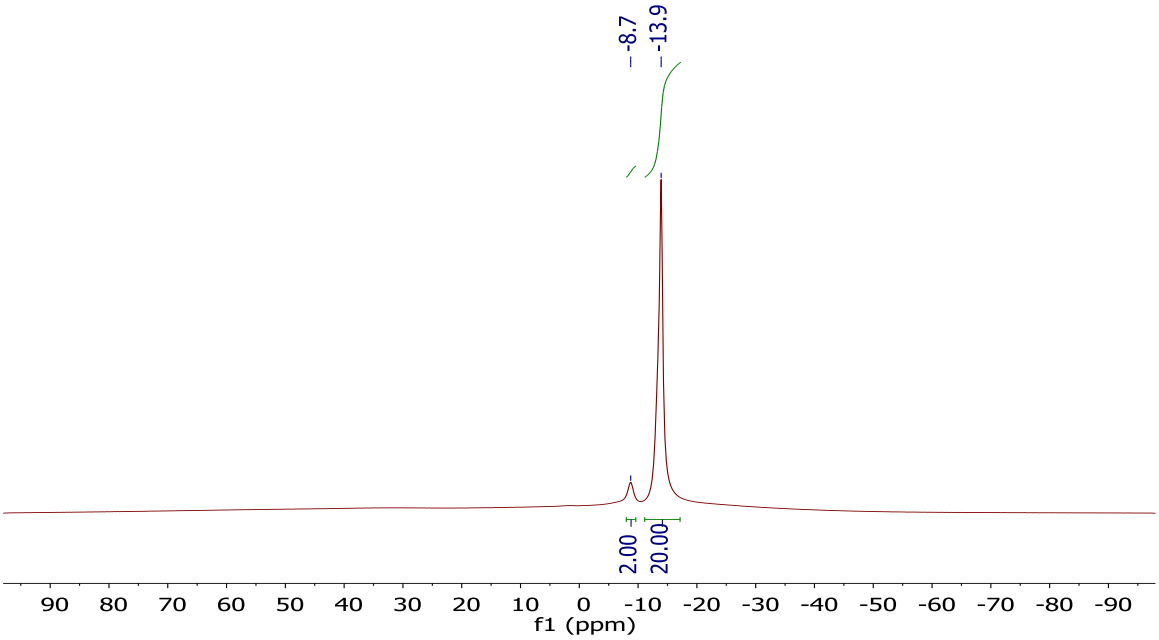

Figure 8-5 $^{11}B[^{1}H]$-NMR spectrum of **43[60^{+}(MeCN)]** in methylene chloride-d_2.

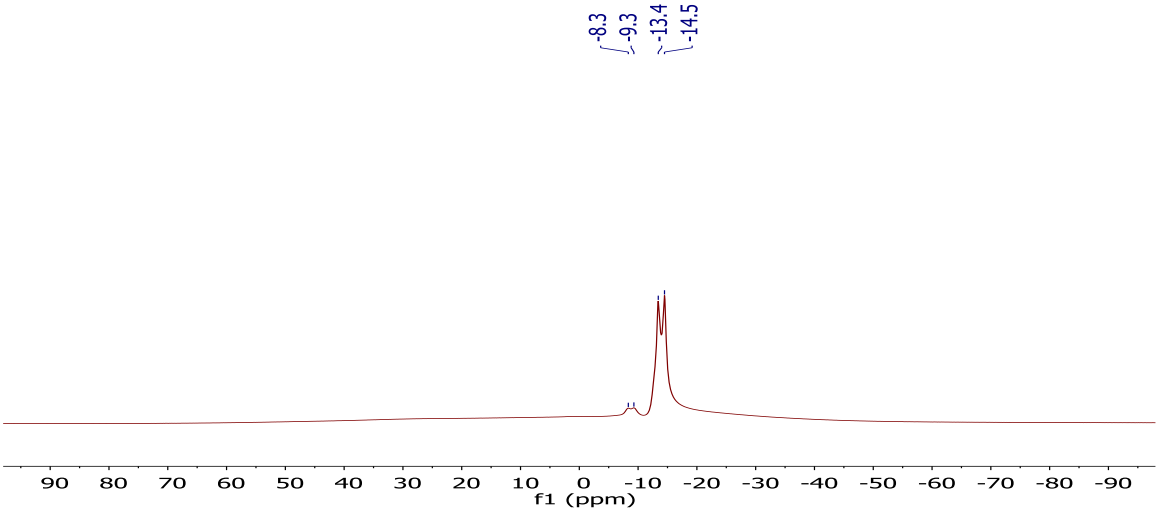

Figure 8-6 ^{11}B-NMR spectrum of **43[60^{+}(MeCN)]** in methylene chloride-d_2.

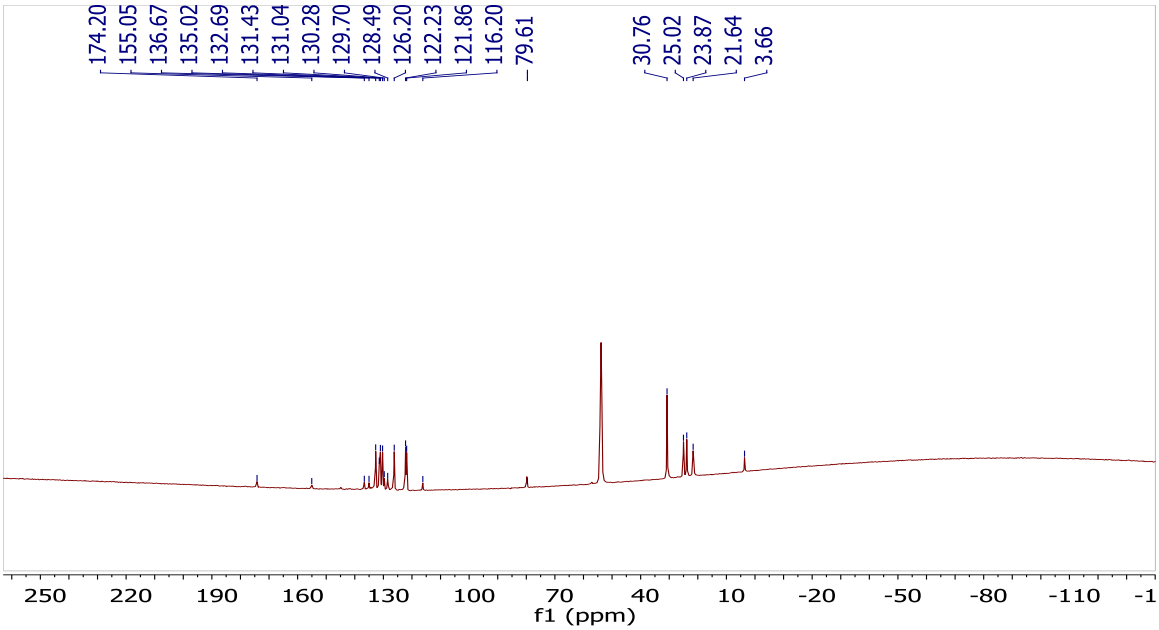

Figure 8-7 ^{13}C-NMR spectrum of **43[60^{+}(MeCN)]** in methylene chloride-d_2.

Synthesis of 50:50 Mixture of 43Br$_6$[60^{+}] and 43Br$_6$[60^{+}(MeCN)]:

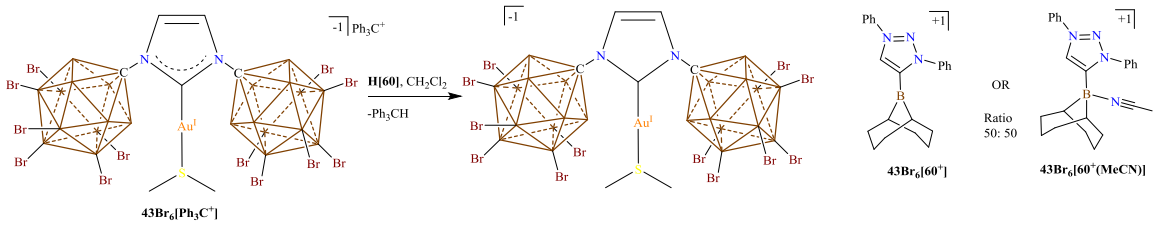

Scheme 8-7 Synthesis of the mixture **43Br$_6$[60^{+}]** and **43Br$_6$[60^{+}MeCN]**.

A glass scintillation vial was equipped with a stir bar and loaded with **43Br$_6$[Ph$_3$C^{+}]** (300 mg, 167 µmol, *likely contaminated with **43Br$_6$[Li^{+}(MeCN)]***) which was dissolved in methylene chloride (1 mL). To the stirring solution **H[60]** (57.4 mg, 167 µmol) in methylene chloride (3 mL) was added dropwise and the reaction stirred for 30 minutes. The reaction was filtered, and the filtrate was added to a vigorously stirring solution of pentane (15 mL). The residue was washed twice more with pentane (20 mL) and the tan solid was pumped down to dryness furnishing a 50:50 ratio of **43Br$_6$[60^{+}]** and **43Br$_6$[60^{+}(MeCN)]**. ^{1}H NMR

(400 MHz, methylene chloride-d_2, 25 °C) ∂ = 8.90 (s), 8.46 (s), 7.96 – 7.61 (10 H, m), 7.35 (s, 2H), 4.0 – 2.8 (bs, 10H, B-H), 2.92 (s, 6H), 2.71 (s), 1.82 – 1.42 (m, 12H), 0.93 (s, 2H) ppm. $^{11}B[^{1}H]$ NMR (128 MHz, methylene chloride-d_2, 25 °C) ∂ = 59.3, -8.7, -13.9 ppm.

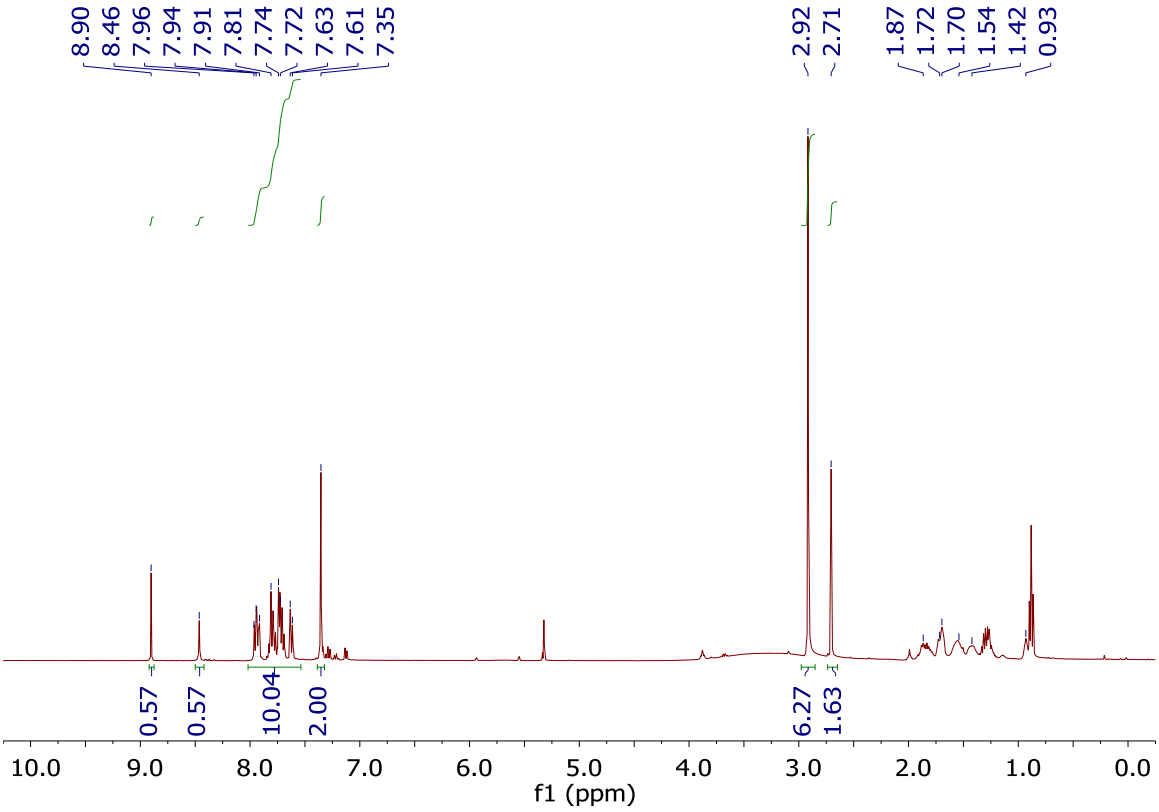

Figure 8-8 ^{1}H-NMR spectrum of the 50:50 mixture containing **43Br$_6$[60$^+$]** and **43Br$_6$[60$^+$(MeCN)]** in methylene chloride-d_2. *Note: the peak at 8.90 and 8.46 represent the 1,2,3-triazolium backbone protons of* ***43Br$_6$[60$^+$]*** *and* ***43Br$_6$[60$^+$(MeCN)]*** *respectively.*

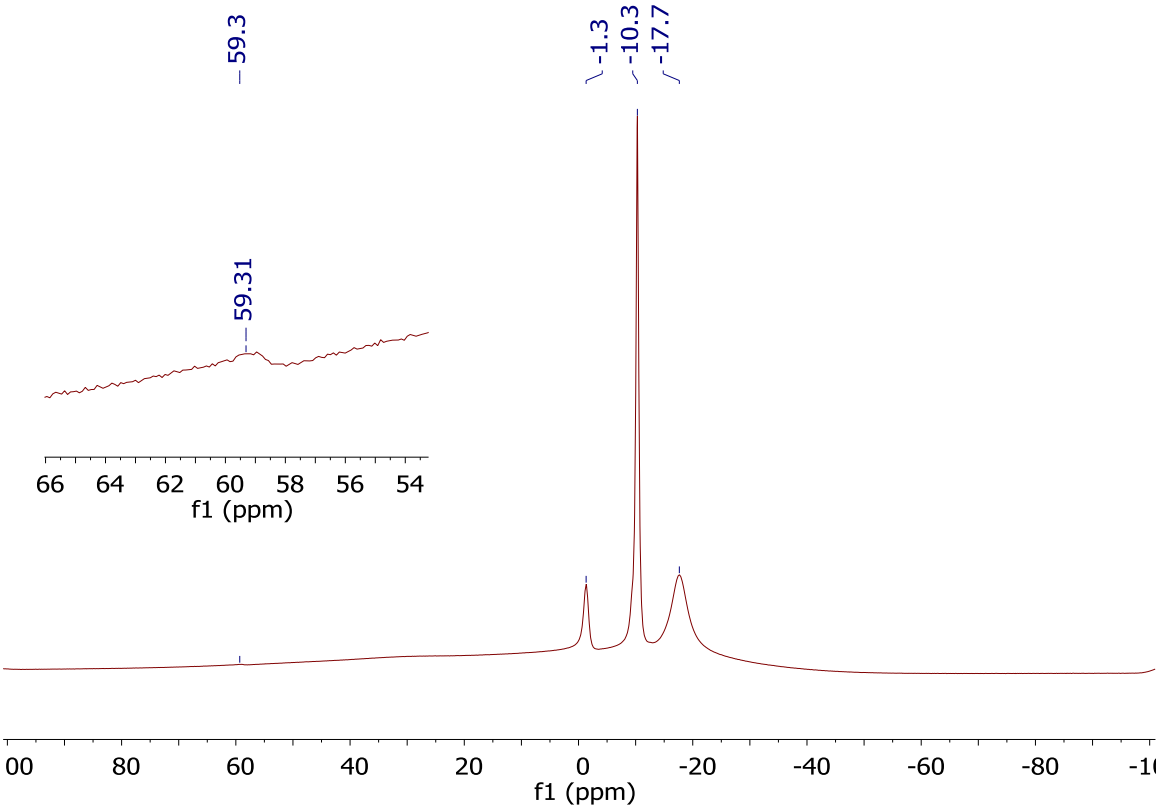

Figure 8-9 $^{1}H[^{11}B]$-NMR spectrum of the 50:50 mixture containing **43Br$_6$[60$^+$]** and **43Br$_6$[60$^+$(MeCN)]** in methylene chloride-d$_2$. The insert shows a blowup of the downfield boron resonance.

Synthesis of >95:5 mixture of 43I$_6$[60$^+$] and 43I$_6$[60$^+$(MeCN)] Respectively:

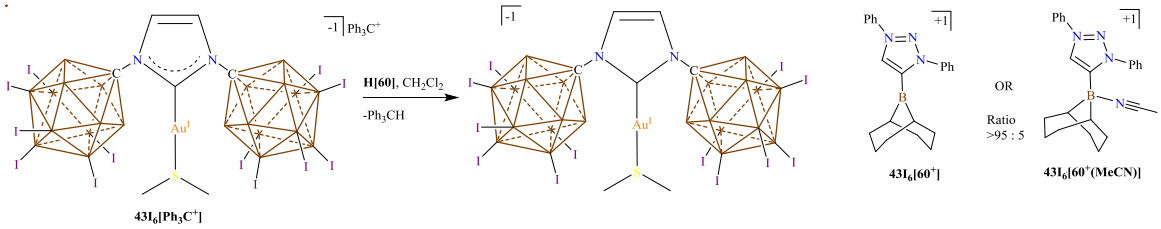

A glass scintillation vial was equipped with a stir bar and loaded with **43I$_6$[Ph$_3$C$^+$]** (300 mg, 167 µmol, *likely contaminated with* ***43I$_6$[Li$^+$(MeCN)]***) which was dissolved in methylene chloride (1 mL). To the stirring solution **H[60]** (57.4 mg, 167 µmol) in methylene chloride (3 mL) was added dropwise and the reaction stirred for 30 minutes. The reaction was filtered, and the filtrate was added to a vigorously stirring

solution of pentane (15 mL). The residue was washed twice more with benzene (5 mL) and the tan solid was pumped down to dryness furnishing a > 95:5 ratio of **43I$_6$[60$^+$]** and **43I$_6$[60$^+$(MeCN)]** respectively. ^{1}H NMR (400 MHz, methylene chloride-d$_2$, 25 °C) ∂ = 8.98 (s, 1H), 8.02 – 7.68 (10 H, m), 7.37 (s, 2H), 4.2 – 3.4 (bs, 10H, B-H), 2.98 (s, 6H), 2.79 (s), 2.03 (s, 6H) 1.81 (s, 4H), 1.41 (s, 2H), 0.87 (s, 2H) ppm. ^{11}B[^{1}H] NMR (128 MHz, methylene chloride-d$_2$, 25 °C) ∂ = 81.0, -6.1, -12.0, -20.0 ppm. ^{11}B NMR (128 MHz, methylene chloride-d$_2$, 25 °C) ∂ = 81.8, -6.1, -12.2, -20.0 ppm.

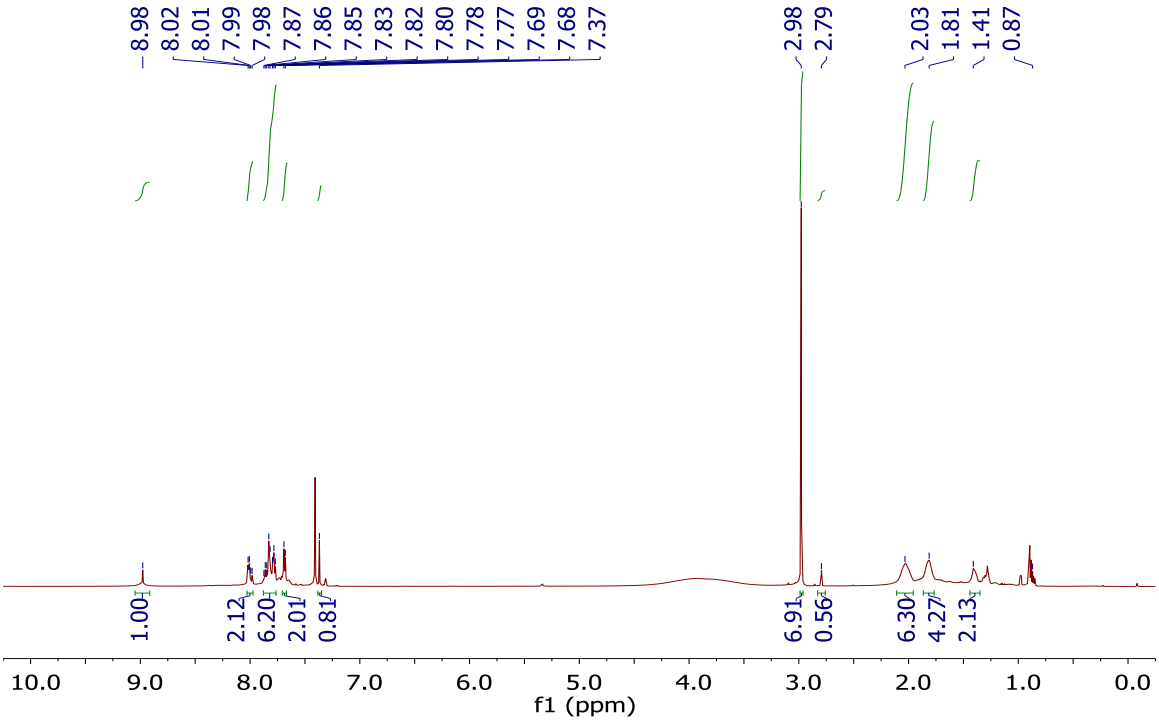

Figure 8-10 ^{1}H-NMR spectrum of the >95:5 mixture containing **43I$_6$[60$^+$]** and **43I$_6$[60$^+$(MeCN)]** in methylene chloride-d$_2$.

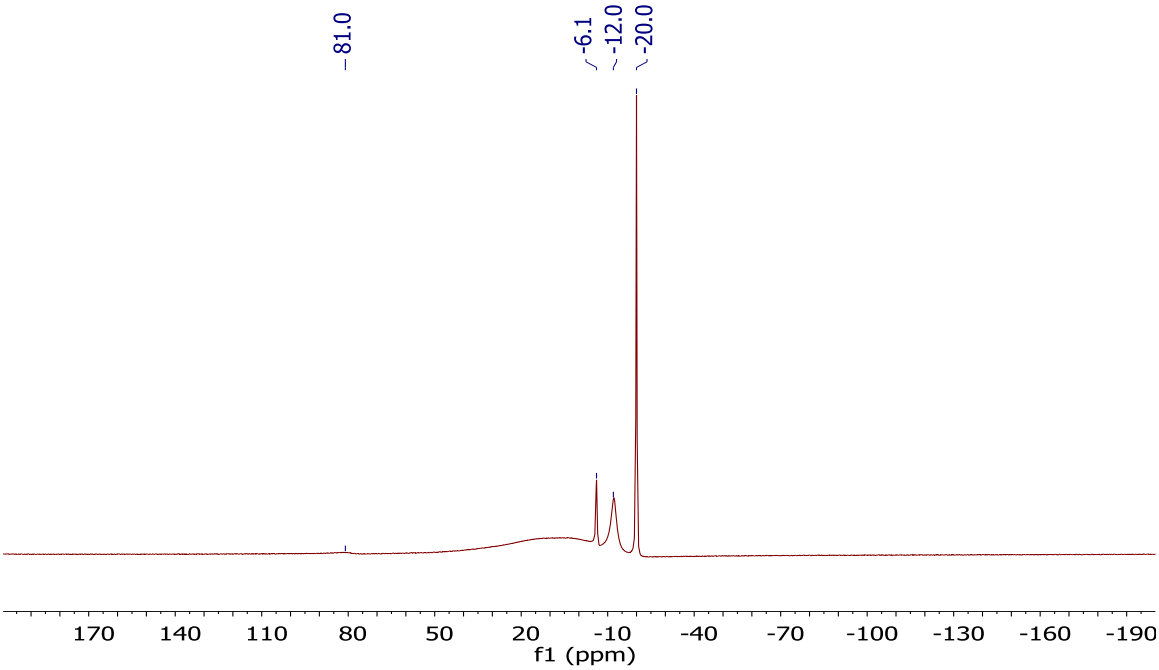

Figure 8-11 $^{11}B[^{1}H]$-NMR spectrum of the >95:5 mixture containing **$43I_6[60^+]$** and **$43I_6[60^+(MeCN)]$** in methylene chloride-d_2.

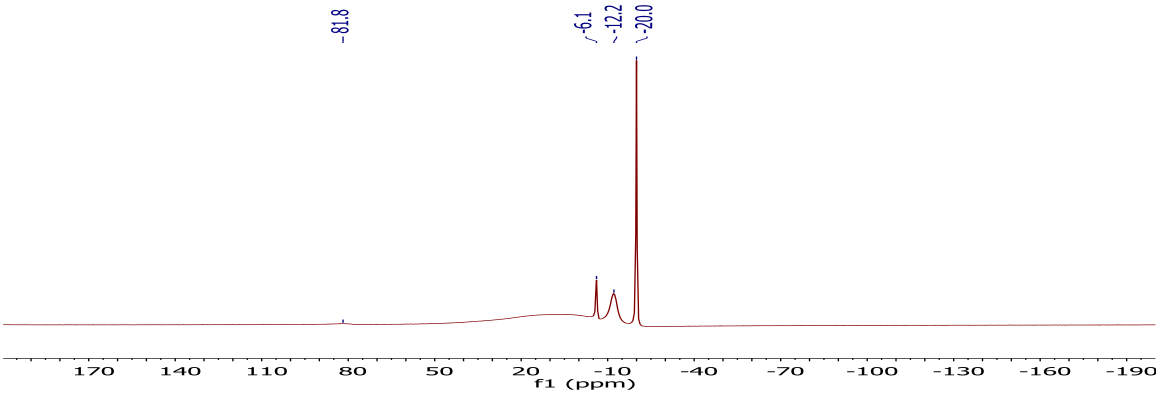

Figure 8-12 ^{11}B-NMR spectrum of the >95:5 mixture containing **$43I_6[60^+]$** and **$43I_6[60^+(MeCN)]$** in methylene chloride-d_2.

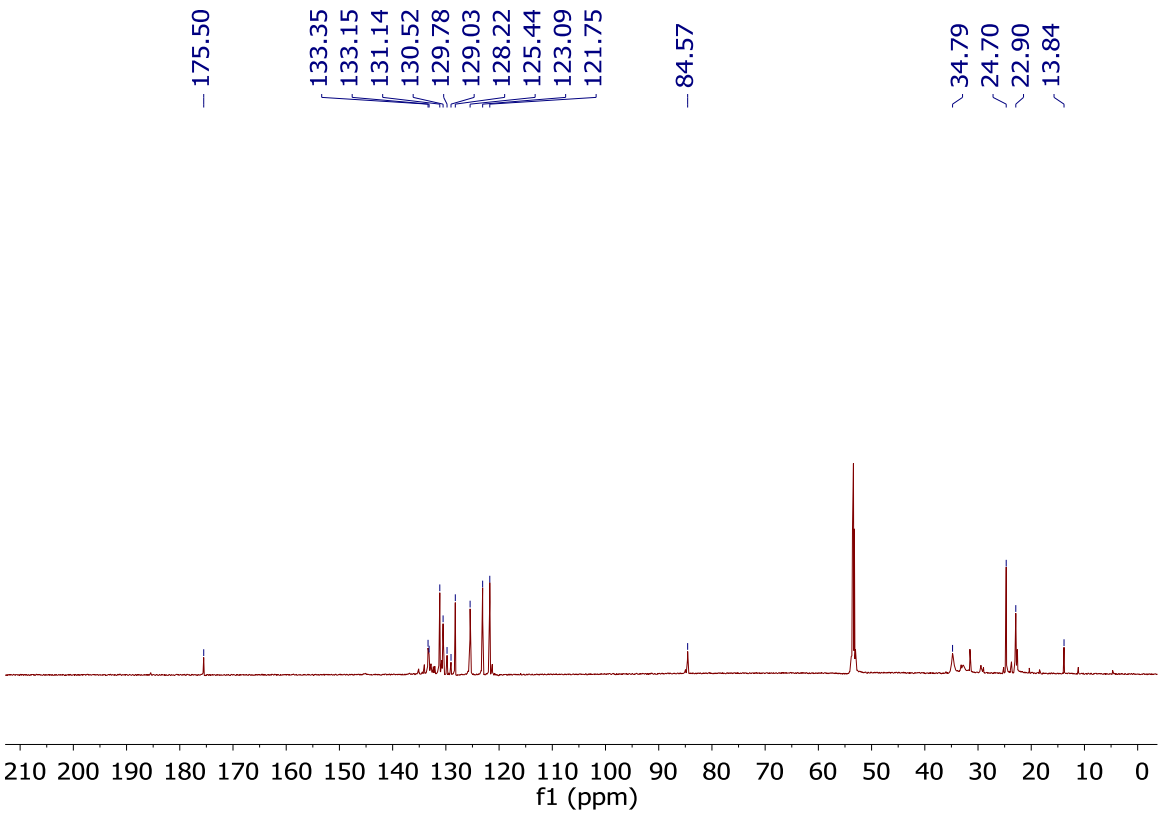

Figure 8-13 ^{13}C-NMR spectrum of the >95:5 mixture containing **43I$_6$[60$^+$]** and **43I$_6$[60$^+$(MeCN)]** in methylene chloride-d$_2$.

8.5 References

1. W. E. Piers, S. C. Bourke ,K. D. Conroy, *Angewandte Chemie International Edition*, 2005, **44**, 5016-5036.

2. D. W. Stephan ,G. Erker, *Angewandte Chemie International Edition*, 2015, **54**, 6400-6441.

3. D. W. Stephan, *Science*, 2016, **354**, aaf7229.

4. A. R. Jupp ,D. W. Stephan, *Trends in Chemistry*, 2019, **1**, 35-48.

5. P. Eisenberger, A. M. Bailey ,C. M. Crudden, *Journal of the American Chemical Society*, 2012, **134**, 17384-17387.

6. P. Eisenberger, B. P. Bestvater, E. C. Keske ,C. M. Crudden, *Angewandte Chemie International Edition*, 2015, **54**, 2467-2471.

7. S. H. Strauss, *Chemical Reviews*, 1993, **93**, 927-942.

8. I. Krossing ,I. Raabe, *Angewandte Chemie International Edition*, 2004, **43**, 2066-2090.

9. M. Nava ,C. A. Reed, *Organometallics*, 2011, **30**, 4798-4800.

10. M. Brookhart, B. Grant ,A. F. Volpe, *Organometallics*, 1992, **11**, 3920-3922.

11. H. C. Strauch, G. Erker ,R. Fröhlich, *Organometallics*, 1998, **17**, 5746-5757.

12. H. C. Strauch, B. Wibbeling, R. Fröhlich, G. Erker, H. Jacobsen ,H. Berke, *Organometallics*, 1999, **18**, 3802-3812.

13. C. Douvris ,J. Michl, *Chemical Reviews*, 2013, **113**, PR179-PR233.

14. N. S. Hosmane, *Handbook of Boron Science : with Applications in Organometallics, Catalysis, Materials and Medicine*, World Scienific, Hackensack, New Jersey, 2019.

15. S. P. Fisher, A. W. Tomich, J. Guo ,V. Lavallo, *Chemical Communications*, 2019, **55**, 1684-1701.

16. C. A. Reed, *Accounts of Chemical Research*, 2010, **43**, 121-128.

17. K.-C. Kim, C. A. Reed, D. W. Elliott, L. J. Mueller, F. S. Tham, L. Lin ,J. B. Lambert, *Science*, 2002, **297**, 825-827.

18. J. B. Lambert, S. Zhang ,S. M. Ciro, *Organometallics*, 1994, **13**, 2430-2443.

19. J. B. Lambert ,S. Zhang, *Journal of the Chemical Society, Chemical Communications*, 1993, 383-384.

20. J. F. Kleinsasser, E. D. Reinhart, J. Estrada, R. F. Jordan ,V. Lavallo, *Organometallics*, 2018, **37**, 4773-4783.

21. J. F. Kleinsasser, S. E. Lee, C. A. Lugo, V. Tej, S. G. McArthur ,V. Lavallo, *Polyhedron*, 2018, **156**, 245-248.

22. S. P. Fisher, A. El-Hellani, F. S. Tham ,V. Lavallo, *Dalton Transactions*, 2016, **45**, 9762-9765.

23. J. Estrada, D. H. Woen, F. S. Tham, G. M. Miyake ,V. Lavallo, *Inorganic Chemistry*, 2015, **54**, 5142-5144.

24. J. Estrada, S. E. Lee, S. G. McArthur, A. El-Hellani, F. S. Tham ,V. Lavallo, *Journal of Organometallic Chemistry*, 2015, **798**, 214-217.

25. V. Lavallo, J. H. Wright Ii, F. S. Tham ,S. Quinlivan, *Angewandte Chemie International Edition*, 2013, **52**, 3172-3176.

Chapter 9: Additional Compounds

9.1 Phosphine Amine

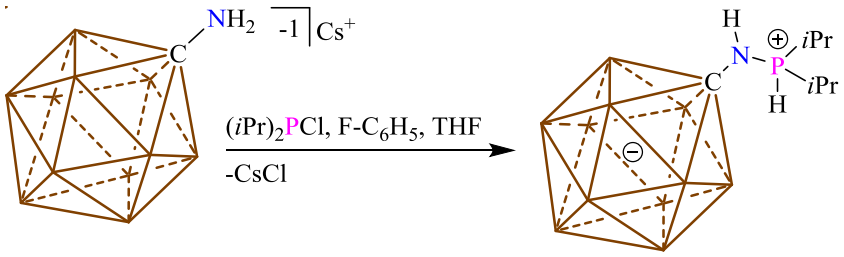

1NH$_2$[Cs] **PAH**

Neat chlorodiisopropylphosphine (0.173 mL, 1.1 mmol) was added to a stirring solution of **1NH2[Cs]** (316.5 mg, 1.1 mmol) in Ph-F/THF (1:1 ratio). The mixture was stirred overnight at room temperature. The next morning the solution was placed in the freezer. Less than 2 hours later the persuing crystals were collected by vacuum filtration giving crytaline **PAH**. ^{1}H NMR (400 MHz, THF-d$_8$, 25 °C) ∂ = 6.98 (ddt, 1H, $^{1}J(P,H)$ = 510.3 Hz, $^{3}J(H,H_{methine})$ = 9.9 Hz, $^{3}J(H, H_{methine})$ = 4.7 Hz), 5.79 (t, 1 H, $^{1}J(H,N)$ = 11.2 Hz), 2.52 (dtd, 2H, $^{3}J(H,H_{Phos})$ = 9.9 Hz, $^{3}J(H,H_{methyl})$ = 7.2 Hz, $^{3}J(H,H_{phos})$ = 4.7 Hz), 1.34 (dd, 6H, $^{3}J(H,H)$ = 13.4 Hz, $^{3}J(H,H)$ = 6.4 Hz), 1.29 (dd, 6H, $^{3}J(H,H)$ = 12.2 Hz, $^{3}J(H,H)$ = 6.4 Hz), 2.3-0.9 (bm, 11H, B-H) ppm. ^{1}H[^{11}B] NMR (300 MHz, THF-d$_8$, 25 °C) ∂ = 6.98 (m, 1H), 5.79 (t, 1H),1.90 (s, 5H, B-H), 1.56 (s, 5H, B-H) 1.51 (s, 1H, B-H) 2.52 (m, 2H), 1.34 (m, 6H), 1.29 (m, 6H) ppm. ^{11}B[^{1}H] NMR (96 MHz, THF-d$_8$, 25 °C) ∂ = -11.4, -13.9 ppm. ^{11}B NMR (96 MHz, THF-d$_8$, 25 °C) ∂ = -11.4 (d, 1H), -13.9 (d, 10H, $^{1}J(B,H)$ = 141.9 Hz) ppm. ^{13}C[^{1}H] NMR (126 MHz, MeCN-d$_8$, 25 °C) ∂ = 78.1, 23.0, 22.5, 15.6, 14.8 ppm. IR (solid, ATR, 25 °C) = ~2600 (B-H), ~3400 (N-H) cm^{-1}.

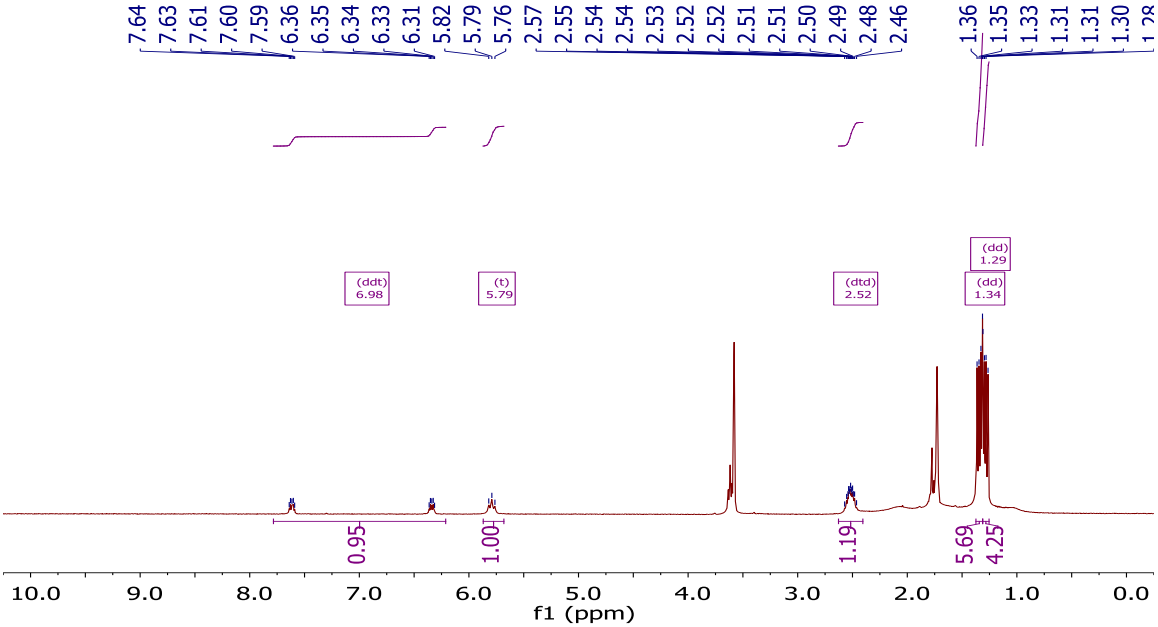

Figure 9-1. ^{1}H-NMR spectrum of **PAH** in THF-d_8. *Note: the peaks at 3.6 and 1.8 ppm are due to THF coordinated to the Li counter cation.*

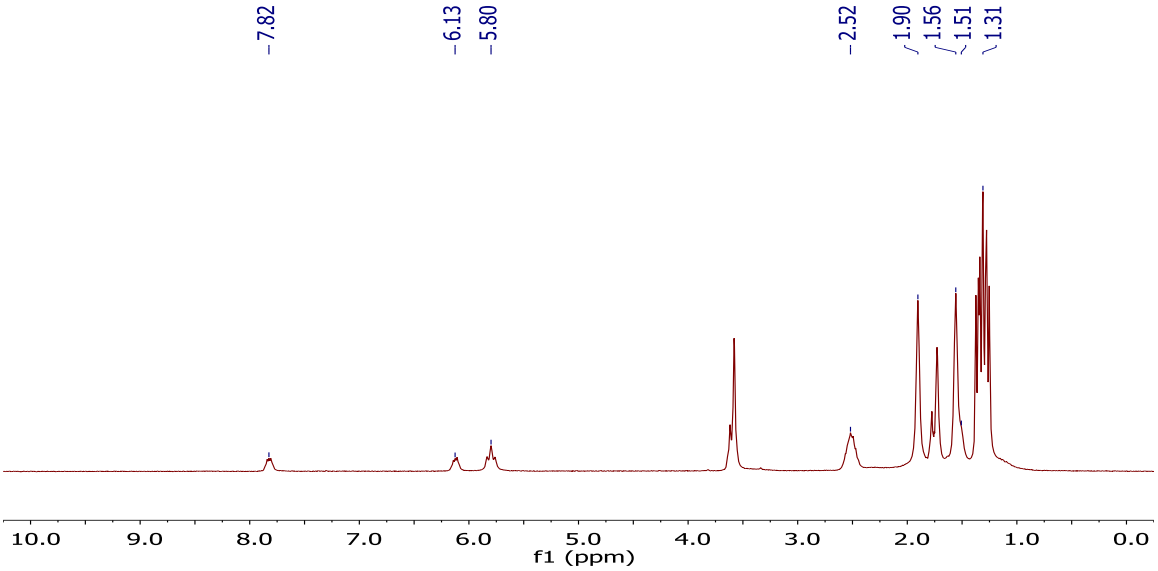

Figure 9-2. ^{1}H[^{11}B]-NMR spectrum of **PAH** in THF-d_8. *Note: the B-H protons appear at 1.9, 1.56 and 1.51 ppm.*

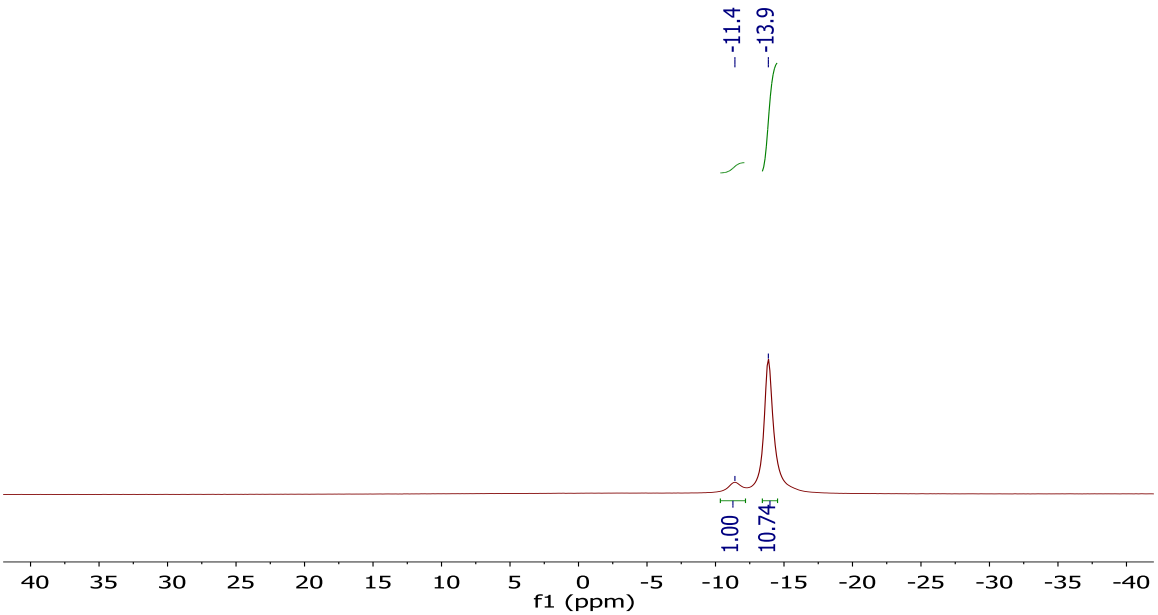

Figure 9-3. $^{11}B[^{1}H]$-NMR spectrum of **PAH** in THF-d_8.

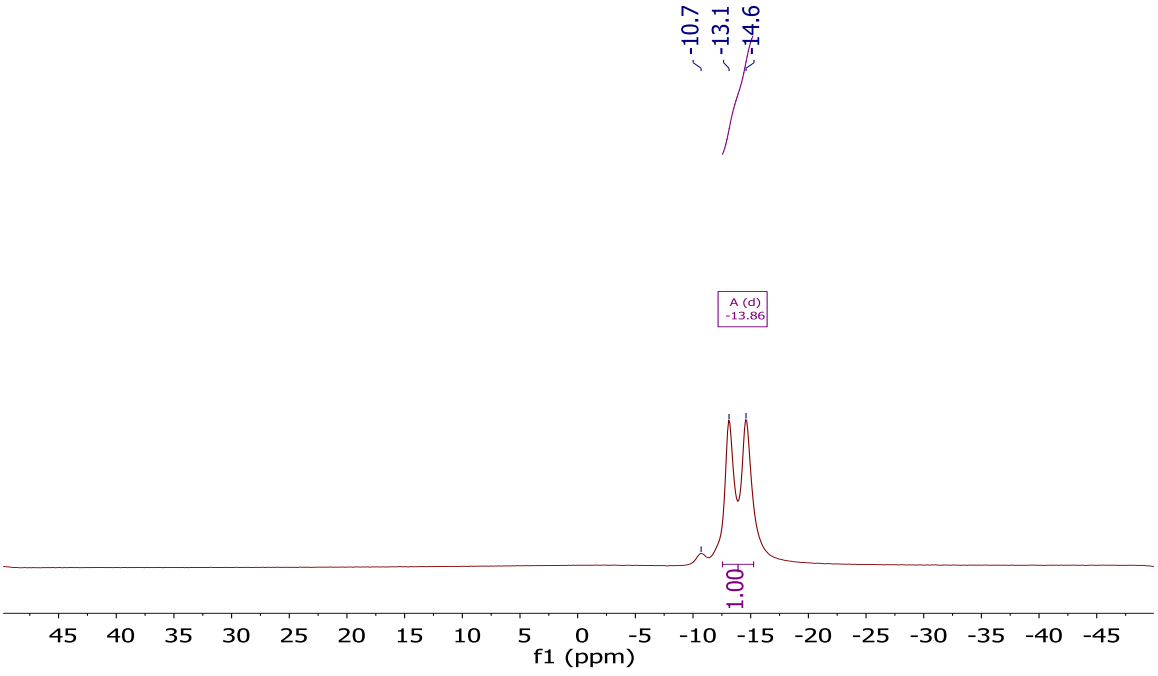

Figure 9-4. ^{11}B-NMR spectrum of **PAH** in THF-d_8.

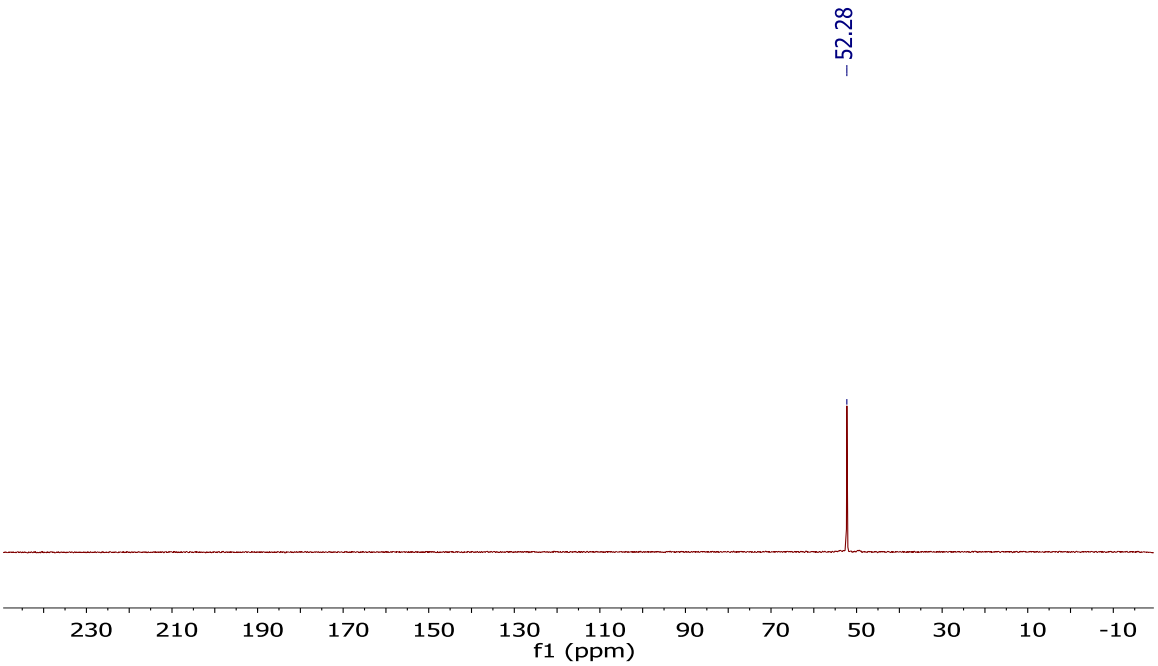

Figure 9-5. $^{31}P[^{1}H]$-NMR spectrum of **PAH** in THF-d_8.

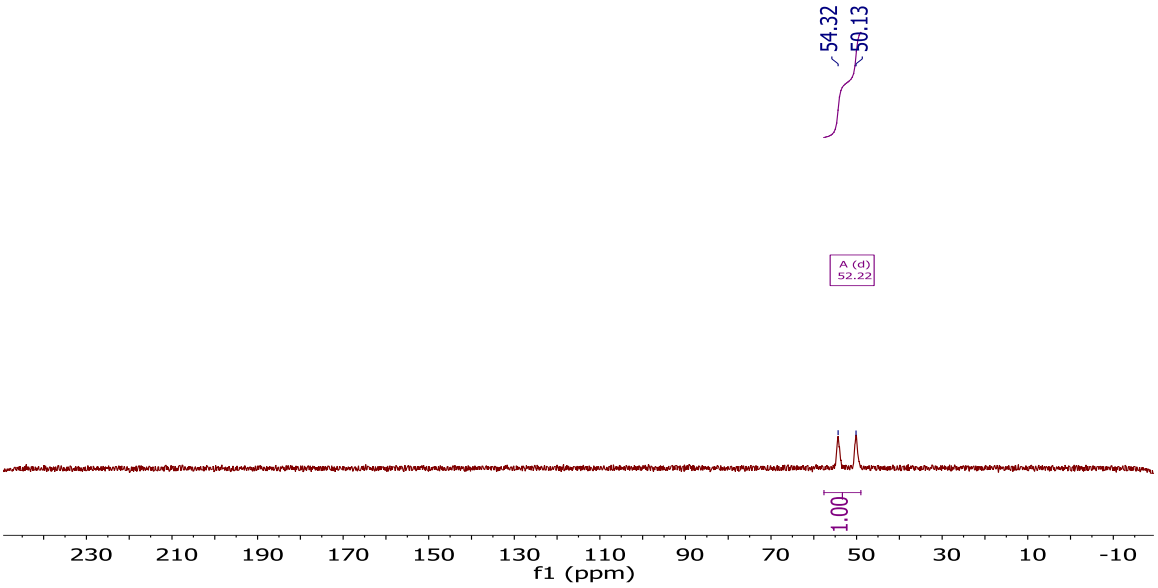

Figure 9-6. ^{31}P-NMR spectrum of **PAH** in THF-d_8.

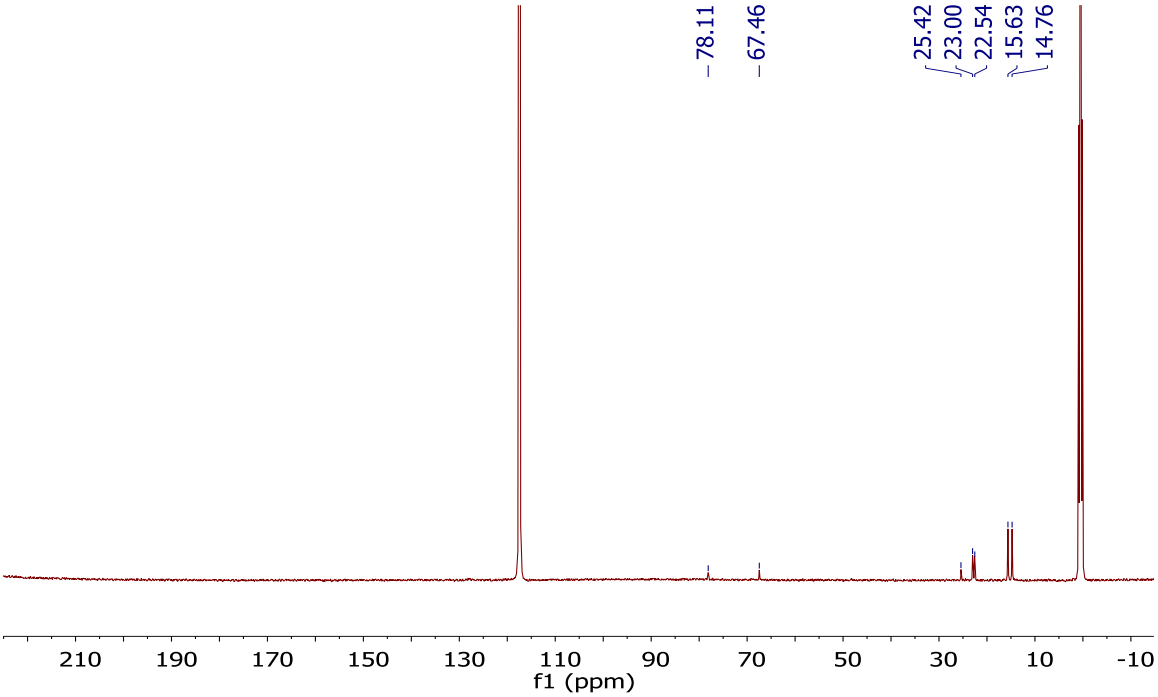

Figure 9-7. $^{13}C[^{1}H]$-NMR spectrum of **PAH** in acetonitrile-d_3. *Note: THF can be seen at 67.46 and 25.42 ppm.*

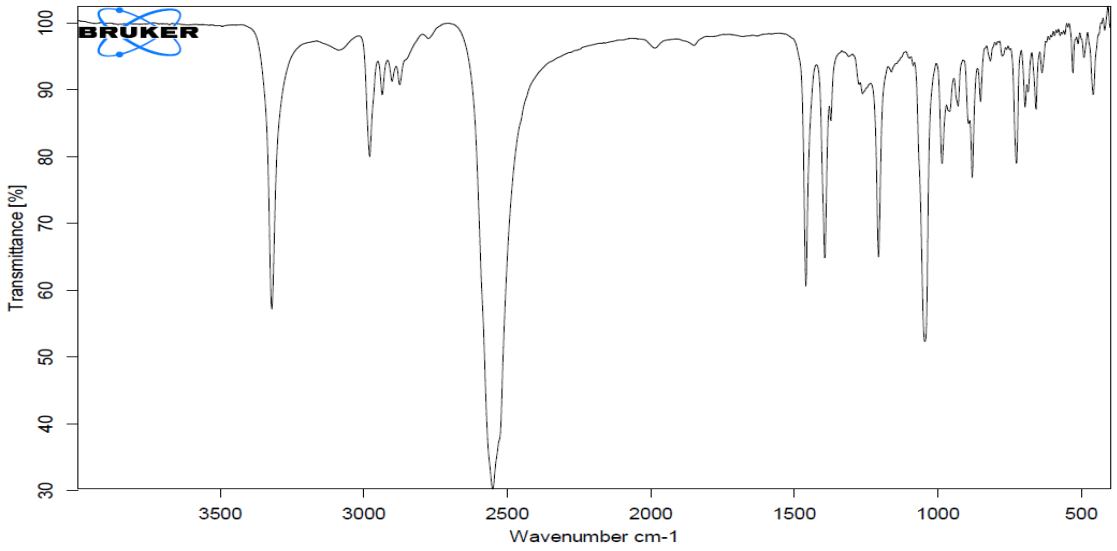

Fiugre 9-8. FT-IR spectrum of **PAH** in the solid state.

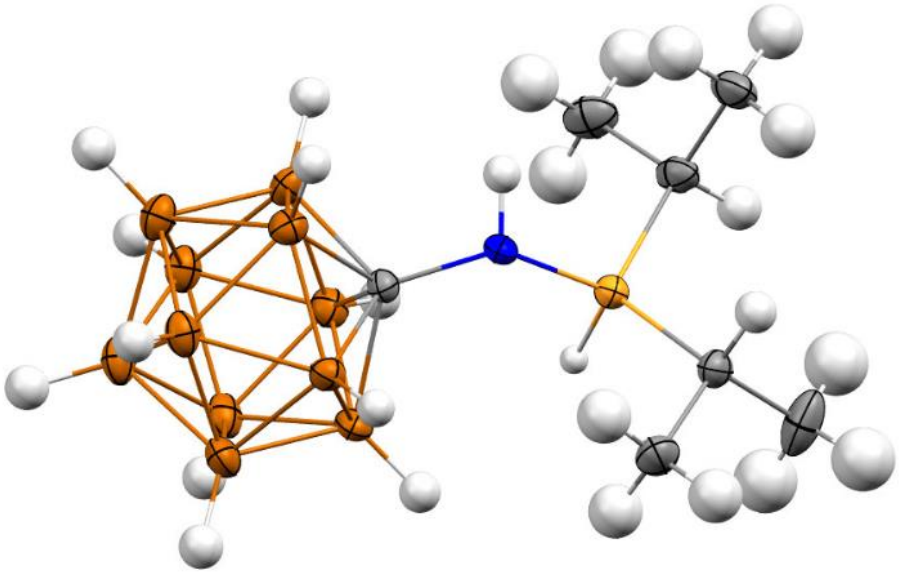

Figure 9-9. Solid state structure of **PAH**. Color code: H = white, B = brown, C = gray, N = blue, P = orange.

Table 9-1. Crystal data and structure refinement for PAH (lavallo30_0m_a, Dr. Rheingold UCSD).

Identification code	SF1	
Empirical formula	C7 H27 B11 N P	
Formula weight	275.17	
Temperature	100.0 K	
Wavelength	0.71073 Å	
Crystal system	Monoclinic	
Space group	P 21/n	
Unit cell dimensions	a = 8.6518(10) Å	α= 90°.
	b = 14.172(2) Å	β= 94.137(5)°.
	c = 13.5228(16) Å	γ = 90°.
Volume	1653.7(4) $Å^3$	
Z	4	
Density (calculated)	1.105 Mg/m^3	
Absorption coefficient	0.145 mm^{-1}	
F(000)	584	

Crystal size	0.12 x 0.08 x 0.05 mm^3
Theta range for data collection	2.084 to 24.996°.
Index ranges	-10<=h<=10, -16<=k<=16, -16<=l<=15
Reflections collected	10307
Independent reflections	2904 [R(int) = 0.0472]
Completeness to theta = 24.996°	99.9 %
Absorption correction	Semi-empirical from equivalents
Max. and min. transmission	0.2602 and 0.2349
Refinement method	Full-matrix least-squares on F^2
Data / restraints / parameters	2904 / 0 / 189
Goodness-of-fit on F^2	1.053
Final R indices [I>2sigma(I)]	R1 = 0.0599, wR2 = 0.1552
R indices (all data)	R1 = 0.0757, wR2 = 0.1661
Extinction coefficient	n/a
Largest diff. peak and hole	0.947 and -0.655 e.$Å^{-3}$

Conclusion

The novel ligands and ions pairs reported have a combination of potentially meaningful synthetic uses in both organic and inorganic chemistry. The explotation of the carborane amine has lead to new NHC salts which were found to be suitable ligands for Au(I) chemistry. Bimetallic complexes where briefly investigated. The utilization of halogenated carborane clusters was key to the isolation of the trityl salts while the non-halogenated cluster lead to decomposition. Investigation of this decomposition lead to the discovery of a rare Au(III) cyclometallated complex that contained an Au-B bond. The first instance of a hydridic carborane cluster paired with a cationic trityl derivative is reported. This was achieved by using the electron rich super trityl, 4',4',4'-tri-(*tert*-butyl)-trityl. A new method of creating trityl salts was discovered using Li^+ in place of Ag^+. This eliminates wasteful AgCl and removes a synthetic step from the synthsis. Tandem hydroamination/hydrogenation chemistry with a borenium cation was investigated.

We are currently investigating the trityl salts in Bartlett-Condon-Schneider silicon-to-carbon hydride transfer reactions. The goal of this chemistry is to generate ion pairs with the extremely potent silylium ion electrophile. The future goal of this chemistry is to create bimetallic complexes containing cationic transition metal complexes and metallic complexes containing reactive main group cations that will be useful in novel catalytic reactions.